IAEA TECDOC SERIES

IAEA-TECDOC-2004

IAEA-TECDOC-2004

Fuel Failure in Normal Operation of Water Reactors: Experience, Causes and Mitigation

Proceedings of a Technical Meeting

IAEA
International Atomic Energy Agency

FUEL FAILURE IN NORMAL OPERATION OF WATER REACTORS: EXPERIENCE, CAUSES AND MITIGATION

The following States are Members of the International Atomic Energy Agency:

AFGHANISTAN
ALBANIA
ALGERIA
ANGOLA
ANTIGUA AND BARBUDA
ARGENTINA
ARMENIA
AUSTRALIA
AUSTRIA
AZERBAIJAN
BAHAMAS
BAHRAIN
BANGLADESH
BARBADOS
BELARUS
BELGIUM
BELIZE
BENIN
BOLIVIA, PLURINATIONAL STATE OF
BOSNIA AND HERZEGOVINA
BOTSWANA
BRAZIL
BRUNEI DARUSSALAM
BULGARIA
BURKINA FASO
BURUNDI
CAMBODIA
CAMEROON
CANADA
CENTRAL AFRICAN REPUBLIC
CHAD
CHILE
CHINA
COLOMBIA
COMOROS
CONGO
COSTA RICA
CÔTE D'IVOIRE
CROATIA
CUBA
CYPRUS
CZECH REPUBLIC
DEMOCRATIC REPUBLIC OF THE CONGO
DENMARK
DJIBOUTI
DOMINICA
DOMINICAN REPUBLIC
ECUADOR
EGYPT
EL SALVADOR
ERITREA
ESTONIA
ESWATINI
ETHIOPIA
FIJI
FINLAND
FRANCE
GABON
GEORGIA
GERMANY
GHANA
GREECE
GRENADA
GUATEMALA
GUYANA
HAITI
HOLY SEE
HONDURAS
HUNGARY
ICELAND
INDIA
INDONESIA
IRAN, ISLAMIC REPUBLIC OF
IRAQ
IRELAND
ISRAEL
ITALY
JAMAICA
JAPAN
JORDAN
KAZAKHSTAN
KENYA
KOREA, REPUBLIC OF
KUWAIT
KYRGYZSTAN
LAO PEOPLE'S DEMOCRATIC REPUBLIC
LATVIA
LEBANON
LESOTHO
LIBERIA
LIBYA
LIECHTENSTEIN
LITHUANIA
LUXEMBOURG
MADAGASCAR
MALAWI
MALAYSIA
MALI
MALTA
MARSHALL ISLANDS
MAURITANIA
MAURITIUS
MEXICO
MONACO
MONGOLIA
MONTENEGRO
MOROCCO
MOZAMBIQUE
MYANMAR
NAMIBIA
NEPAL
NETHERLANDS
NEW ZEALAND
NICARAGUA
NIGER
NIGERIA
NORTH MACEDONIA
NORWAY
OMAN
PAKISTAN
PALAU
PANAMA
PAPUA NEW GUINEA
PARAGUAY
PERU
PHILIPPINES
POLAND
PORTUGAL
QATAR
REPUBLIC OF MOLDOVA
ROMANIA
RUSSIAN FEDERATION
RWANDA
SAINT KITTS AND NEVIS
SAINT LUCIA
SAINT VINCENT AND THE GRENADINES
SAMOA
SAN MARINO
SAUDI ARABIA
SENEGAL
SERBIA
SEYCHELLES
SIERRA LEONE
SINGAPORE
SLOVAKIA
SLOVENIA
SOUTH AFRICA
SPAIN
SRI LANKA
SUDAN
SWEDEN
SWITZERLAND
SYRIAN ARAB REPUBLIC
TAJIKISTAN
THAILAND
TOGO
TONGA
TRINIDAD AND TOBAGO
TUNISIA
TÜRKİYE
TURKMENISTAN
UGANDA
UKRAINE
UNITED ARAB EMIRATES
UNITED KINGDOM OF GREAT BRITAIN AND NORTHERN IRELAND
UNITED REPUBLIC OF TANZANIA
UNITED STATES OF AMERICA
URUGUAY
UZBEKISTAN
VANUATU
VENEZUELA, BOLIVARIAN REPUBLIC OF
VIET NAM
YEMEN
ZAMBIA
ZIMBABWE

The Agency's Statute was approved on 23 October 1956 by the Conference on the Statute of the IAEA held at United Nations Headquarters, New York; it entered into force on 29 July 1957. The Headquarters of the Agency are situated in Vienna. Its principal objective is "to accelerate and enlarge the contribution of atomic energy to peace, health and prosperity throughout the world''.

IAEA-TECDOC-2004

FUEL FAILURE IN NORMAL OPERATION OF WATER REACTORS: EXPERIENCE, CAUSES AND MITIGATION

PROCEEDINGS OF A TECHNICAL MEETING

INTERNATIONAL ATOMIC ENERGY AGENCY
VIENNA, 2022

COPYRIGHT NOTICE

For further information on this publication, please contact:

Nuclear Fuel Cycle and Materials Section
International Atomic Energy Agency
Vienna International Centre
PO Box 100
1400 Vienna, Austria
Email: Official.Mail@iaea.org

Printed by the IAEA in Austria
July 2022

IAEA Library Cataloguing in Publication Data

Names: International Atomic Energy Agency.
Title: Fuel failure in normal operation of water reactors : experience, causes and mitigation / International Atomic Energy Agency.
Description: Vienna : International Atomic Energy Agency, 2022. | Series: IAEA TECDOC series, ISSN 1011–4289 ; no. 2004 | Includes bibliographical references.
Identifiers: IAEAL 22-01518 | ISBN 978–92–0–126022–2 (paperback : alk. paper) |
ISBN 978–92–0–125922–6 (pdf) |
Subjects: LCSH: Water cooled reactors. | Water cooled reactors — Fuel. | Water cooled reactors — Inspection. | Nuclear power plants. | Nuclear industry.

FOREWORD

There is a high level of interest in the analysis of fuel failure data from Member States' water cooled reactors, even though the actual rate of fuel failure in this type of reactor is low. Nuclear power plants are seeking to streamline the operaton of their plants while increasing the reliability of their nuclear fuel.

Since the 1970s, following suggestions of the Technical Working Group on Fuel Performance and Technology, the IAEA has overseen the analysis of fuel failure data from Members States' water cooled reactors. Two publications were subsequently published in the area of fuel failure: IAEA Nuclear Energy Series No. NF-T-2.1, Review of Fuel Failures in Water Cooled Reactors and IAEA Nuclear Energy Series No. NF-T-2.5, Review of Fuel Failures in Water Cooled Reactors (2006–2015).

Recognizing the importance of this area, the Technical Working Group on Fuel Performance and Technology requested to continue its research and organized a Technical Meeting in December 2020 entitled Fuel Failure in Normal Operation of Water Reactors: Experience, Causes and Mitigation. The participants of the meeting provided relevant and valuable material in five technical sessions: the status and experience regarding fuel failures during normal operation; detection, management and monitoring of fuel failures; the impact of plant operation on failures and degradation, and possible mitigation actions by plant operation; the mitigation of failures by design and manufacturing; post-irradiation examinations, experimental studies and modelling of leaking fuel behaviour.

At the meeting, participants exchanged views on national experience and perspectives, and progress and results from research and development through paper presentations and discussion forums.

The objective of this publication is to provide an up-to-date review of data, experience and knowledge in the area of fuel failure during the operation of water cooled reactors.

The IAEA wishes to thank all participants for their contributions. The IAEA officer responsible for this publication was M. Veshchunov of the Division of Nuclear Fuel Cycle and Waste Technology.

EDITORIAL NOTE

This publication has been prepared from the original material as submitted by the contributors and has not been edited by the editorial staff of the IAEA. The views expressed remain the responsibility of the contributors and do not necessarily represent the views of the IAEA or its Member States.

Neither the IAEA nor its Member States assume any responsibility for consequences which may arise from the use of this publication. This publication does not address questions of responsibility, legal or otherwise, for acts or omissions on the part of any person.

The use of particular designations of countries or territories does not imply any judgement by the publisher, the IAEA, as to the legal status of such countries or territories, of their authorities and institutions or of the delimitation of their boundaries.

The mention of names of specific companies or products (whether or not indicated as registered) does not imply any intention to infringe proprietary rights, nor should it be construed as an endorsement or recommendation on the part of the IAEA.

The authors are responsible for having obtained the necessary permission for the IAEA to reproduce, translate or use material from sources already protected by copyrights.

The IAEA has no responsibility for the persistence or accuracy of URLs for external or third party Internet web sites referred to in this publication and does not guarantee that any content on such web sites is, or will remain, accurate or appropriate.

CONTENTS

MITIGATION OF FAILURES BY DESIGN AND MANUFACTURING (Session 4)

PIES, EXPERIMENTAL STUDIES AND MODELLING OF LEAKING FUEL BEHAVIOUR (Session 5)

1. INTRODUCTION

1.1. BACKGROUND

In spite of the low fuel failure rate in currently operating water cooled nuclear power reactors, there is a continued high level of interest in fuel failures, for two reasons. First, the problems and inconvenience caused by fuel failures can still be important for nuclear power plants' operation. Second, the generally accepted goal of achieving a zero failure rate requires a detailed knowledge of existing failure mechanisms, their root causes and remedies.

Fission products and actinides released from fuel elements into the primary coolant depend on their behavior inside the rods. During the operation of the reactor, the initial inventory of radionuclides in fresh fuel gradually increases due to nuclear fission and neutron capture reactions. This inventory is usually located inside the rods, but part of this amount can be released into the primary coolant in the event of a fuel element failure. Operational feedback shows that the number of fuel failures is limited. However, despite efforts to reduce the risk of fuel defects, it is not yet possible to completely eradicate them.

In the past decades, the IAEA has fostered, via Technical Meetings, the exchange of information on the analysis of fuel failures, that has been compiled in several technical documents:

— INTERNATIONAL ATOMIC ENERGY AGENCY, Atomic Energy Review, Vol. 17 (1979), No. 4, IAEA, Vienna.
— INTERNATIONAL ATOMIC ENERGY AGENCY, Fuel Failure in Normal Operation of Water Reactors: Experience, Mechanisms and Management, 26-29 May 1992), IAEA-TECDOC-709, IAEA, Vienna (1993).
— INTERNATIONAL ATOMIC ENERGY AGENCY, Review of Fuel Failures in Water Cooled Reactors, Technical Reports Series No. 388, IAEA, Vienna (1998).
— INTERNATIONAL ATOMIC ENERGY AGENCY, Fuel Failure in Water Reactors: Causes and Mitigation, IAEA-TECDOC-CD-1345, IAEA, Vienna (2003).
— INTERNATIONAL ATOMIC ENERGY AGENCY, Review of Fuel Failures in Water Cooled Reactors, Nuclear Energy Series No. NF-T-2.1, IAEA, Vienna (2010).
— INTERNATIONAL ATOMIC ENERGY AGENCY, Water Chemistry and Clad Corrosion/Deposition Including Fuel Failures, IAEA-TECDOC-CD-1692, IAEA, Vienna (2013).
— INTERNATIONAL ATOMIC ENERGY AGENCY, Review of Fuel Failures in Water Cooled Reactors (2006–2015), Nuclear Energy Series No. NF-T-2.5, IAEA, Vienna (2019).
— INTERNATIONAL ATOMIC ENERGY AGENCY, Foreign Material Management in NPPs and Projects, IAEA-TECDOC-1970, IAEA, Vienna (2021).

Following the recommendation of the IAEA Technical Working Group on Fuel Performance and Technology and considering the importance of information exchange and co-ordination of national efforts in this area, a TM bringing together specialists from Member States was organized to share data, experience and knowledge on fuel failure during the operation of water cooled reactors, and to facilitate the preparation of the IAEA Technical Document provisionally entitled Fuel Failure in Normal Operation of Water Reactors: Experience, Causes and Mitigation.

The IAEA Technical Meeting (TM) on Fuel Failure in Normal Operation of Water Reactors: Experience, Causes and Mitigation was held virtually on 14-18 December 2020.

Fourty one (41) experts representing 15 Member States and 1 International organization (OECD/NEA) attended the meeting. The TM was divided in 5 technical sessions:

— Overview of status and experience regarding fuel failures during normal operation.
— Detection, management and monitoring of fuel failures.
— Impact of plant operation on failures/degradation and possible mitigation actions by plant operation.
— Mitigation of failures by design and manufacturing.
— PIEs, experimental studies and modelling of leaking fuel behaviour.

A total of 21 papers compiled in the present document were presented and discussed at the meeting. The main conclusions and recommendations were summarized by the session chairs.

1.2. OBJECTIVES

The main objective of the publication is to provide an up-to-date review on data, experience and knowledge in the area of fuel failure during the normal operation of water reactors on the base on results of Technical Meeting on "Fuel Failure in Normal Operation of Water Reactors: Experience, Causes and Mitigation" (14-18 December 2020).

1.3. SCOPE

In line with the objective described in Section 1.2, this publication provides information on fuel failure in Normal Operation of Water Reactors and covers:

- Overview of status and experience regarding fuel failures during normal operation.
- Mitigation of failures by design and manufacturing.
- Mitigation of failures/degradation (due to debris, crud, water chemistry, etc.) by plant operation.
- Detection and monitoring of failures.
- Performing experimental studies of fuel failure and degradation mechanisms.
- Performing modelling and code development for analysis of fuel failures under normal operation conditions, accidental conditions, potential impact on fuel handling.

1.4. STRUCTURE

This publication addresses decision makers and senior managers involved in the organization of fuel related activities at different national or company levels, as well as specialists in R&D institutions, fuel vendor organizations, nuclear utilities and safety regulatory authorities interested in global approach to improve fuel reliability and performance.
Section 2 provides extended Summary of the Technical Meeting:

- Technical Session 1: Overview of status and experience regarding fuel failures during normal operation
- Technical session 2: Detection, management and monitoring of fuel failures
- Technical session 3: Impact of plant operation on failures/degradation and possible mitigation actions by plant operation
- Technical session 4: Mitigation of failures by design and manufacturing
- Technical session 5: PIEs, experimental studies, and modelling of leaking fuel behaviour.

Section 3 provides conclusion for each technical session and Technical Meeting as a whole.
The second part of the publication represents full papers collected during the Technical Meeting.

2. SUMMARY OF THE TECHNICAL SESSIONS

2.1. TECHNICAL SESSION 1: OVERVIEW OF STATUS AND EXPERIENCE REGARDING FUEL FAILURES DURING NORMAL OPERATION

The first session was chaired by Mr. R. Lewis (Bruce Power, Canada). The Session provided a high-level overview of some of the recent experience at various NPPs related to observation of fuel defects, efforts to understand the defect causes. The Session also provided insight into the techniques available in Canada for post-irradiation examination of fuel. The Session included four presentations based on submitted papers, summarized below.

2.1.1. Status and experience regarding fuel failures at Ringhals NPP (K.M. Carling, Sweden)

As stated in the presentation to the TM, Sweden has three nuclear reactors in operation. These units reportedly produce approximately 15% of the power demanded by Sweden. The Ringhals Unit 1 is a BWR while the Units 2 to 4 are PWRs. The Ringhals NPP Units 3 and 4 have approximately 6 to 9 more years of potential operation. Between 1990 and 2019, just under half of the fuel defects observed at Ringhals have occurred in Unit 3.

It is worth mentioning that Pellet-Cladding Interactions (PCI) have affected both BWR and PWR units historically. Efforts to address this via manufacturing have helped reduce the observed frequency of this type of defect. Although manufacturing defects have also been observed historically, they are observed at much lower frequencies than debris fretting defects.

In the period 1990 to 1997 there was some variability in the number of fuel defects observed, however post 1997 there was a consistent trend of about 1 defect per year across the fleet, up to about 2005. Since 2006, the units have performed well with only one defect observed in 2014.

The improvements in fuel performance are attributable to a much more focused commitment to manging foreign material exclusion, promoting awareness of its importance, and reducing the number of manufacturing related defects.

Ringhals remains dedicated to preventing or minimizing the long-term contamination that may occur due to fuel defects through their fuel failure management practices. These practices are aligned with industry best practices. For example, online monitoring is used to provide early warning of failed fuel, added to which chemistry monitoring is enhanced if defects are suspected, plus active efforts are made to minimize degradation of the existing failures by operating the unit in such a manner as not to exacerbate the defect(s).

In addition to this a forced outage may be undertaken if the fuel failure degrades beyond acceptable limits and as a strategy, all fuel assemblies (FAs) undergo sipping during outages to ensure a defect-free restart of the unit.

To further enhance the understanding of fuel condition, the Ringhals NPP staff also perform visual fuel inspections on unloaded fuel assemblies and in the event defect fuel is identified (whether via sipping or inspection) these can be prioritized for post-irradiation examinations in hot cells; consistent with best practices identified by INPO and WANO.

2.1.2. Fuel failures recent experience and their mitigation: a US perspective (C. Faulkner, USA)

Like other NPPs around the world, the focus of the US industry has been to eliminate debris fretting defects and adopt a prevention-based model. Overall, the US fleet has managed to steadily increase safety performance indicators, reduce the number of fuel failures, and achieve record output (e.g., 20% in 2019).

In the US, there are 94 operating reactors. One third are BWR and the remainder PWR. In general, most recent failures, consistent with the overall industry, are due to debris fretting. A higher incidence rate (4-5x) is noted in units that have limited feedwater straining capability (due to lack of pumped forward drains). Other defect causes may be present but have not been proven conclusively. Duty-related failures include PCI and missing pellet surface (MPS) assisted non-classical PCI.

In the period 2013 to 2018 (inclusive), debris fretting was the dominant failure mechanism for cores with failed fuel, excepting for 2013 and 2014. It is accepted that certain metallic foreign material can be introduced

during maintenance work, because of component / fuel degradation or as a result of inadvertent injection from interfacing systems. It is not uncommon for the debris (or foreign material) that caused the defect to be absent during inspection/examination. These observations align well with those made by other utilities, e.g., CANDUs.

Typically, debris in PWRs will become trapped between spacer grids and fuel rods while in BWRs fretting is promoted in the upper portion of the bundle due to boiling/voids.

Although recently have seen an all-time low for the number or fuel defects and although there is a historical trend downwards, there is still a low-level persistence. The US plants remain committed to addressing this. Developments in 3D printing technology may soon make more advanced filter designs possible, which may facilitate another method to reduce the debris or foreign material burden within the core/interfacing systems.

In the interim, the refuelling process may afford an indirect method of reducing at least some of the debris / foreign material burden as trapped pieces are removed with unloaded assemblies.

In terms of detecting defects, the data suggests that there is no clear pattern as to when a defect may present itself following the ingress of debris. The range is potentially going from a week to four years. The time between in-service related component degradation and its contribution to debris/foreign material that causes a defect to present itself is less easily inferred.

Consistent with industry best practices, efforts are in place to implement an effective foreign material exclusion programme. As such, efforts are taken to identify potential sources of debris and to proactively address them. Efforts are also taken to retrieve debris where possible. If debris cannot be retrieved, analysis should be performed to confirm that expected impacts remain acceptable and that performance will not be affected.

In the interest of continuous improvement, further actions have been identified to develop a new approach to debris prevention, detection, and correction. As part of this a comprehensive long-term strategy aimed at prevention is needed, standards of excellence required (for implementation purposes), gaps in knowledge/skills required closure and self-awareness/correction of existing conditions needed to be improved.

It should be noted that while the focus remains heavily on preventing debris fretting related failures, work has also been done to provide power ramp rate guidelines to prevent PCI failures (via rod conditioning), mitigation of baffle jetting by conversion of downflow baffle barrel configurations to upflow configurations, and by introducing new spacer grid designs to eliminate or reduce bundle self-excitation to levels that would minimize potential for grid-to-rod fretting. One-off manufacturing defects may occur sporadically and are addressed on a case-by-case basis.

2.1.3. Recent Canadian fuel performance (W. Grant, Canada)

There are currently 19 operating power reactors in Canada, all of which are of the CANDU design. These reactors make use of horizontal fuel channels within a core filled with heavy water and connected to headers with piping called feeders (inlet/outlet). On-power refuelling is performed, and adjacent channels are bi-directionally fuelled. The cores are fuelled with small bundle assemblies. The bundles are composed of either 28 or 37 elements (arranged in concentric rings), containing stacks of fuel pellets, enclosed at their ends with endcaps. The elements are then constrained within a geometry using endplates and appendages to provide the required separation between fuel elements/pencils. The sheathing of the elements is made of Zircaloy.

There is some variation in the equipment or methods used to detect and locate failed fuel across the Canadian CANDU fleet. The variance is primarily related to the age of the plants and the technologies that were prevalent at the time. All plants have access to chemistry monitoring via grab samples. Some plants also have gaseous fission product monitoring systems which allow for online monitoring. Systems such as the delayed neutron monitoring system and feeder scanning systems are primarily intended to be used for location of fuel failures, with the former being an online system and the latter only being used offline during outages.

Debris fretting remains the main cause of fuel defects across the Canadian fleet. This is consistent with the industry experience captured in INPO IER 19-6. It is not uncommon for debris fretting to trend upwards following initial construction or major refurbishment activities. This is a lesson learned and efforts are well underway to limit this in current and future refurbishment activities. The core mitigation strategy focuses on 1) prevention via foreign material exclusion and 2) rapid location and removal once defected fuel is detected.

Since CANDU units may refuel specific fuel channels while online, without needing to take the entire core offline, the removal of suspected defect-containing fuel strings from a given fuel channel can be easily accomplished. The ability to refuel in a timely manner limits the extent to which fuel degradation can occur.

In the recent past, most debris have been small, wire-like or swarf-like pieces. This is based on review of visual fuel inspection data of discharged fuel. Although not ideal, sometimes debris trapped in fuel bundles is removed from the core when these bundles are discharged. This helps lower the debris /foreign material burden in the system.

In cases where refurbishment has led to elevated defect rates, the operating experience has shown that an elevated rate may persist for up to 5 years after the initial introduction of debris. In this time, a downward trend does develop as the defect rates return to their pre-elevated rate. In recent years, the regulator has also supported the addition of a foreign material exclusion programme inspection to the standard refurbishment inspection suite of activities.

The main mode of fuel failure is that of debris fretting or debris-induced failures. Occasionally, one-off manufacturing issues may also present themselves, but these are not a norm. On-site irradiated fuel inspections and off-site hot-cell post-irradiation examinations form an integral part of determining the defect causes.

From the perspective of the Canadian regulator, there have been limited fuel performance issues across the Canadian fleet. There has been effective oversight and fuel condition management by licensees and effective oversight of licensee programmes by the regulator. Fuel defect rates remain acceptable.

2.1.4. Review of defect root-cause post-irradiation examination (PIE) of PHWR fuels at CNL, and related developments in PIE at CNL to support defect root cause examinations for Canadian PHWR utilities (S. Corbett, Canada)

Canadian Nuclear Laboratories (CNL) is Canada's only hot-cell laboratory. Other facilities maintain warm cells. The different being the level of radioactive material they are licensed to handle and the capability of their "cells" to accept high active materials or not.

Work done at CNL is diverse, but their portfolio includes routine examination of failed fuel submitted by nuclear generating stations in Canada when the defect cause cannot be elucidated from initial on-site in-bay fuel inspections or disassembly. CNL also provides storage and disposal services for irradiated fuel material sent by the various utilities. It is normal practice to keep samples for at least one year, in retrieval storage, before eventual disposal (in the event follow-up is requested by the client).

When fuel is shipped from a utility to the hot cells, the examination process begins with the non-destructive examination of the fuel. Work is done to assess non-defected reference elements (where applicable) using profilometers and gamma scans. Work may also be done using stereomicroscopes to confirm features that were observed during the poolside inspections at the respective utility. It is not uncommon for artefacts to present differently when dry and in-air, versus when inspected wet and under water.

Profilometry is a useful source of data as it provides information on fuel element bowing, ovality and allows for calculation of residual sheath strain. These can give indirect evidence of challenges to fuel performance. Bowing for example could be indicative of axial load conditions that were not ideal while sheath strain could reflect power ramping that was becoming excessive.

Gamma scanning looks at gross gamma energy distributions and provides information on the axial flux shape, end-flux peaking, axial power gradients that may have existed during operation and insights into whether there may be missing pellet surfaces or gaps in the pellet stack. However, to date, no CANDU fuel discharged from a Canadian unit has failed due to a missing pellet surface (or depression in the sheathing).

Supplementary information may also be acquired by performing gas volume collection and helium leak testing. Gas volumes will give an estimate of what sort of actual operation the element underwent based on the amount of fission gas trapped in the fuel-to-sheath gap and the helium leak test can help isolate areas on the element that may be home to an otherwise visually indistinct leak path.

Since destructive activities may be required to further understand the nature of the defect or potential cause, CNL is also has facilities where metallography, ceramography, microscopy, macroscopy, etc. can be performed. Samples to be evaluated using these techniques will often need to be sized for mounting and activity purposes. To accomplish this, the hot cells are equipped with longitudinal fuel cutting tools and other implements. Built-in water cooling prevents overheating of these tools.

Key information obtained following destructive exams typically include identification of defects, inclusions, incomplete welds, other anomalies not seen during in-bay onsite visual inspections at the utility, enhanced dimensional measurements, oxide and deposit thickness / distribution, fuel / cladding grain structure and morphology as well as fuel / cladding hydride concentration / distribution.

In general, for CANDU fuel, whenever the ratio of hydrogen to deuterium is heavily in favour of one radioisotope over the other it is usually a good sign that you either have a primary hydriding defect or a secondary hydriding defect (specifically a deuteride rich defect site) respectively. Primary defects tend to present themselves because of pre-existing contaminants such as hydrogenous material within the element, introduced during manufacturing and which results in conditions within the element that cause blistering and loss of hermetic integrity during in-core operation. This is disambiguated from a primary defect site which is simply the first defect site that appears on a failed element, and which could be due to debris fretting or some other mechanism.

Consistent with a focus on continuous improvement, CNL is looking at developing ultrasonic testing capability to help in small defect detection, frequency scanning eddy current techniques (mainly for LWR fuel), and focused ion beam (FIB) for ablation of very small surfaces/areas when doing detailed examinations.

A new hot-cell and laboratory area is planned, called the Advanced Nuclear Materials Research Centre (ANMRC) and there is a new federally funded project looking at "Development of Novel PIE Techniques for Innovative Fuels that power SMRs and Advanced Reactors".

2.2. TECHNICAL SESSION 2: DETECTION, MANAGEMENT AND MONITORING OF FUEL FAILURES

The session was chaired by Mr. I.A. Evdokimov (TRINITI, Russian Federation). The Session was devoted to current NPP experience in application of various techniques for identification of fuel failures both during reactor operation and during the maintenance outage after the end of cycle. Some new approaches and methods being under development for detection of fuel failures were presented as well. The Session included six presentations based on submitted papers, summarized below.

2.2.1. Experience in Detection of WWER Fuel Failures by Activity of ^{133}Xe and ^{135}Xe during Reactor Operation (P.M. Kalinichev, Russian Federation)

At present time, according to regulations, iodine activities are used to detect fuel failures in WWERs during reactor operation. The main indicator of a fuel failure is a spiking of primary coolant activity during power transients. Under steady-state operation conditions, the ratio of normalized release rates between ^{131}I and ^{134}I is used.

However, based on iodine activity, it is not always possible to detect the fuel failure or correctly identify the moment of the failure occurrence. This situation may happen in case of a small defect in cladding or for high-burnup fuel if the defect in cladding is overlapped by the surface of the fuel pellet. This problem is aggravated if solid fuel pellets are used in fuel rods. If it is so, fuel deposits can make the dominant contribution to iodine activity, and the fuel failure may not be noticeable.

For more reliable identification of fuel failures at WWERs, a technique based on the analysis of ^{133}Xe and ^{135}Xe activity ratio was developed. The advantage of noble gas is that it is not surfactant like iodine and does not adsorb at cladding inner surface. So, Xe may be released more easily from the leaking fuel rod than iodine. The main idea of using the ratio of ^{133}Xe and ^{135}Xe activities is that its value is limited by a certain threshold for the failure-free core. If there is a fuel failure, the more long-lived ^{133}Xe is released from a leaking fuel rod at a higher rate than the more short-lived ^{135}Xe. So, the ratio between the measured activities of ^{133}Xe and ^{135}Xe becomes above the threshold.

It is worth noting that the ratio between the two Xe radionuclides has low sensitivity to partial loss of gas from the coolant samples with the existing sampling procedures at WWERs. Thus, no additional measurements are required to apply this technique in practice besides the existing routine measurements performed at WWER power units. The proposed technique was applied for analysis of coolant activity data at several WWERs in course of the last 3 years. It demonstrates the capability to reveal fuel failures during steady-state reactor operation even if it is not possible by iodine activities. Analysis of Xe activities also provides a proper identification of the moment of a fuel failure.

2.2.2. Monitoring, Prediction, and Identification of Fuel Failures during 17th Campaigns on Each Unit of Temelín NPP and Overview of all Fuel Failures since 2010 (J. Raindl, Czech Republic)

Temelín NPP experiences an elevated rate of fuel failures. Most of the failures are characterized as a ‘gaseous type’ failure. It is so because in many cases ^{131}I activity remains below the minimum detectable level and the failure occurrence is identified only by ^{133}Xe activity.

Temelín NPP implements the following approach to evaluation of fuel failures during reactor operation. The number of fuel failures is estimated by drastic variations in activity evolution such as a stepwise increase in iodine and xenon activity or changes in the activity ratios for $^{133}Xe/^{135}Xe$ and $^{85m}Kr/^{135}Xe$. The average burnup of leaking fuel is estimated by activity of ^{134}Cs and ^{137}Cs during the spiking events. Evolution of the ratio between ^{85m}Kr and ^{135}Xe activities is also used for burnup assessment. Even if there are several leakers during a fuel cycle, this approach provides a good agreement with the results of sipping tests in the mast of the refuelling machine after the reactor shutdown.

Majority of leaking fuel assemblies at Temelín NPP spent 2 or 3 fuel cycles in reactor. The root cause of the failures has not been reliably identified. But it is worth noting, that introduction of a new type of fuel (TVSA-T mod.2 design) at Temelín-2 led to decrease of the failure rate in this power unit over the last two years.

2.2.3. Application of an Improved Technique for Burnup Evaluation of WWER Leaking Fuel Based on the Data on Spiking Events (O.V. Vilkhivskaya, Russian Federation)

A conventional approach to evaluation of burnup of the leaking fuel assemblies at operating WWER power units is to use a burnup correlation of $^{134}Cs/^{137}Cs$ activity ratio in the primary coolant during spiking events. However, from 2000s, analysis of spiking events and PIE data have shown this technique to be rather inaccurate in some cases. In this regard, development of improved techniques for better evaluation of burnup for leaking fuel is of high importance to the NPPs. Improvement is possible by better estimation of cesium inventories as they evolve in each fuel rod, for a particular fuel type and a particular fuel loading pattern in the core, during the fuel cycle.

Currently, a standard pin-by-pin neutronic calculation for the evolution of linear heat generation rates and fuel burnup is required before every fuel cycle at WWERs. However, these calculations do not provide data on Cs inventory in the fuel pellets. Thus, additional methods should be utilized to account for Cs build-up rates in different fuel rods/FAs in each fuel cycle.

An improved technique was introduced previously for express calculation of build-up of Cs isotopes in fuel pellets for every fuel rod in the core. This approach employs the NPPs results of routine neutronic calculations of actual pin-by-pin linear heat generation rate for each fuel cycle with a particular core loading pattern. The activity ratios $A(^{134}Cs)/A(^{137}Cs)$ in fuel calculated in the framework of this technique show good agreement with the available NPP data. Some successful comparison was also made with recent PIE data.

In general, the proposed technique provides better results in estimation of leaking fuel burnup by analysis of Cs spiking during operation of WWER power units.

2.2.4. Studying the Effect of Operating Parameters on Response of the Fuel-Cladding Failure Monitoring System in MTRs (A.H. Elhefnawy, Egypt)

Most monitoring and detection systems for nuclear fuel failure during reactor operation depend on measuring the gamma activity released from radioactive fission products that diffused from the fuel element using gamma spectrometry. In contrast, the typical MTR research reactors monitor the ‘activity’ of delayed neutrons released from the delayed neutron precursors escaping from the reactor core.

Because of the relatively big difference in half-lives for the six groups of these delayed neutrons precursors, the measured delayed neutrons count-rate depends mainly on the time that water takes to transfer from the reactor core to the neutron detector of the monitoring system. The calibration process of this monitoring system was based on a nominal flow rate of water (≈ 7 Litre/min) that limits the detection probability to the first two groups of delayed neutrons precursors (^{87}Br and ^{137}I in particular).

During reactor operation, two operating parameters are noticed to affect the readings of the detector which was not considered in the calibration process before. The first parameter is the disturbance of water flow rate from the reactor core to the detector by the effect of the reactor’s main cooling system. It decreases the probability of the other four groups of delayed neutron precursors to be included in the measuring process. The second parameter is the dependence of diffusion of delayed neutron precursors on the burnup rate of the fuel elements. Because of discarding these effects, high fluctuations in the response of the detector occur causing a false alarm to be recorded. Therefore, it became necessary to redesign the calibration process of the fuel-cladding failure monitoring system calculating a new calibration constant that compensates the effect of these operating parameters.

2.2.5. WANO Fuel Reliability Indicator for CANDU Fuel (B.J. Lewis, Canada)

A fuel reliability indicator (FRI) has been proposed by the World Association of Nuclear Operators (WANO) to monitor industry progress in achieving and maintaining high fuel integrity. This WANO methodology was revised in respect to CANDU fuel operation conditions and integrity assessment.

This analysis specifically accounts for different mechanisms of fission product release based on a Booth diffusion model and recoil theory. In this treatment, the coolant activity concentration of ^{131}I provides for an assessment of defective fuel in the reactor. This quantity is corrected for tramp uranium effects using a measured coolant activity concentration of ^{134}I.

The proposed treatment includes the development of a common power-scaling correlation for the higher-powered CANDU fuel. A methodology is outlined for correcting coolant activities for the effects of coolant purification and identifies requirements for normalization of the fuel reliability indicator to a reference purification rate constant and average fuel rating. This analysis is further extended with the possible use of the isotope, ^{133}Xe, for common analysis among various CANDU reactor types since this isotope is not affected by ion-exchange purification effects, coolant chemistry or fuel defect size. This latter isotope can be used to predict the number of fuel defects and the average linear power of the defective elements that are present in the core. The isotope, ^{134}I, can also be used to estimate the amount of in-core tramp uranium.

The complete model provides a CANDU-specific fuel reliability indicator as a suggested means of standardization for defective fuel analysis for comparison across the nuclear industry.

2.2.6. Experience in Detection of Fuel Washout from Leaking Fuel Rods during Operation of WWER Power Units (P.M. Kalinichev, Russian Federation)

One of the possible and most severe consequences of a fuel failure is that fragments of fuel pellets or fuel grains may be washed out from the leaking fuel rod into the coolant. Radiological consequences of fuel washout may persist for a long period of time up to 10 years – in the form of high background activity for on-power units.

Detection of fuel washout is possible during evaluation of primary coolant activity during reactor operation. The amount of fuel deposits on surfaces of the in-core structures is evaluated using activities of the most short-lived radionuclides that can be detected in the primary coolant. In WWERs, activity of ^{134}I is traditionally used for this purpose.

However, observed ^{134}I activity may increase during operation even in cases when leaking fuel in the core is absent, and fuel deposits are the only source of the fission products release. The reason is that in fuel deposits, plutonium builds up faster and up to higher concentrations compared to its average concentration in fuel pellets. This behaviour is due to lower self-shielding effect for the resonance neutron captures by ^{238}U in fuel deposits on the outer cladding surface. Intensive plutonium build-up leads to increase in the fission rate in fuel deposits resulting in gradual increase in the background ^{134}I activity during reactor operation.

Recently, a criterion was proposed to distinguish between cases when the increase in activity of short-lived radionuclides is due to fission products release from the existing fuel deposits in the core or it is due to washout of fuel particles from leaking fuel. Practical applications at NPPs and comparison with the available PIE data show this criterion to be an effective tool for detection of fuel washout from leaking fuel.

2.3. TECHNICAL SESSION 3: IMPACT OF PLANT OPERATION ON FAILURES/DEGRADATION AND POSSIBLE MITIGATION ACTIONS BY PLANT OPERATION

The session was chaired by Mr. I. Arimescu (Framatome Inc., USA). Four presentations were made during this session, in which the theme was about the role and impact of plant operation on fuel failures or degradation processes and mitigating actions that have been taken in plant operation to prevent or limit fuel failures.

2.3.1. Fuel failure in normal operation of ANGRA 2 Brazilian nuclear power plant (Nelbia Lapa, Nuclear Energy Commission, Brazil)

The paper is mainly focused on describing an observation of localized enhanced corrosion at the top of some fuel rods in bundles from a certain manufacturing batch. This observation was made during visual examination (VE), after one fuel bundle was identified by sipping as failed and a flurry of white particles (identified as oxide flakes) followed manipulation of that bundle.

The observed enhanced corrosion (larger than typical, but not exceeding design thresholds) did not cause the observed fuel rod failure, but it was treated as a potential issue and design analyses coupled with additional thorough VE of all fuel assemblies were carried out to identify all affected fuel bundles and to take conservative, precautionary measures.

This singular localized enhanced corrosion event was also observed in a few other cases in the past in other plants and the current event in ANGRA 2 is still being investigated as part of the root-cause analysis (RCA). Some preliminary conclusions are nevertheless emerging, e.g., this localized enhanced corrosion appears to only affect cladding behaviour during the first cycle and doesn't evolve afterwards. With regards to root causes, several tracks are being followed as multiple causes are possible, solely or in combination, from surface contamination to local T/H conditions, coolant chemistry, etc. as mentioned before only a certain group of fuel rods at a specific location was affected and thus the operational conditions seem to play an important role.

In conclusion, it was reiterated that no primary or secondary crack was identified by VE of peripheral rods, which were affected by localized enhanced corrosion during the first cycle and therefore, while the fuel rod failure RCA is still underway. The fuel failure is clearly not related to the corrosion event, and the current working hypothesis is that the failure mode is most likely debris fretting (3 out of the 5 failures in Angra-2, since 2002, were by debris fretting).

2.3.2. Fuel Failure in Krško Nuclear Power Plant – Causes and Corrective Measures (T. Nemec, Slovenia)

The fuel leaker Operational Excellence (OE) of the Krško NPP was introduced by a brief description of the plant, which is in operation since 1983, currently its lifetime being extended to 2043, not in the least due to safety upgrades that have been implemented in the period 2013-2021.

It was emphasized in the paper the relevance of the correlation between the occurrence of GTRF fuel failures and the increase of cycle length; it is remarked that this correlation was also observed by EDF (see paper 1 in Session 4). It was also highlighted that the latest failures that were caused by baffle jetting have received a lot of media attention and public interest because of the severe fuel rod damage whereby some of the failed fuel rods had broken pieces detached from them.

In all cases root cause analyses have been performed and corrective actions at all levels have been reviewed and implemented as necessary and to the extent possible. With respect to plant operation, the following actions have been described in the paper:

Failed fuel action plan, which established I-134 coolant activity thresholds.

Mitigation for baffle jetting: up flow conversion in 2015.

In addition, it was mentioned that design changes have been identified with regards to mitigation of GRTF failures and after their implementation in 2015 no GTRF fuel failure has occurred.

Finally, it was stated that full public transparency was adopted in recent years with respect to latest baffle jetting leakers and that contributed significantly to regaining public confidence.

2.3.3. Inspection and Repair of Damaged Fuel Assembly (An Na, China)

The paper describes the leaker experience during the first cycle of operation of Unit 2 of the Hainan Changjiang NPP, which was started in June 2016 and high coolant activity was detected at beginning of cycle. Hainan NPP units have only on-line sipping equipment, which in the Chinese LWR fleet experience is not always capable of detecting small break leakers. Also, most of the plants in China don't have ultrasound inspection and repair equipment. The actions taken to remedy this lack of equipment on site in the case of Hainan NPP are described and the successful outcome presented.

From the operation point of view, the paper describes the operational restrictions taken after the radiochemistry indicated that leakers are present in the core, by setting activity limits for operating conditions, followed by higher threshold for strengthened supervision and culminating with a bounding threshold that triggers shutdown within 48 h. It was remarked that following the above-mentioned operational measures the activity remained within operational set limits during the remainder of the first cycle of Hainan Unit 2.

The paper also summarized the Chinese NPP fleet leaker statistics: from 2010 to 2016, 34 units accumulated a total of 102 cycles with failures in 24 cycles, again stressing the lack of off-line inspection and repair of fuel assemblies with leakers.

Because fuel inspection onsite was not available, accelerated development and implementation of ultrasonic equipment beside the off-line sipping device took place in 2016. This ultrasonic system was able to detect two failed bundles in Hainan Unit 2 and thorough visual inspection (under water video equipment) showed that one rod was damaged beyond repair (broken into two pieces), while the other one was less damaged, so that it was possible to be replaced by a dummy and the bundle returned to the core.

The experience gained at Hainan NPP with the leaker detection ultrasonic system and the developed repair equipment has been documented in procedures and management guidelines and it was shared with the other NPP's in China. Operational guidelines have also been refined for the situation of cores with leakers in terms of monitoring the leaker evolution, supervision thresholds and actions to be taken for these conditions.

2.3.4. Measures to Improve Fuel Reliability (V. Mecir, Czech Republic)

The paper provides the status of the measures investigated to improve fuel reliability in general and specifically in the case of the Temelín NPP during period of the most recent cycles of operation. These measures are categorized as Design, Manufacturing and Operational with prime focus on Design and Operation.

With regards to the last category, the Temelín NPP operational measures consist in:

— Observing fuel design limits in operation, such as Rod Cluster Control Assembly (RCCA) movement restrictions.
— Core design with or without FA rotation, for various reasons, but primarily in order to avoid radial power distribution anomaly and axial offset (AO).

The OE was summarized as follows: coolant activity spikes occurred shortly after startup in Cy 4 and in following cycles in both Temelín units. Investigations were undertaken to determine whether debris fretting or proximity to RCCA correlation to failures; also detailed neutronic, thermal hydraulic and thermomechanical calculations were performed for OE with failed fuel.

The fuel behaviour of the failed fuel rods was thus assessed to identify potential trends for local rod AO and core-wide AO, as no clear-cut conclusions could be drawn with respect to debris fretting or core power distribution control being the root cause of the failures. CFD calculations were performed to evaluate assembly deformation impact on fuel performance, considering the potential impact of increased void fraction. Previous OE T/M calculations showed failed rods were not limiting wrt. cladding stress magnitude.

Finally, operation evaluation focused on foreign material exclusion (FME) assessment and some weaknesses have been identified, which were followed up by actions to improve FME requirement implementation, such as:

— Pipelines flushing before core loading.
— Scheduled special FME search - inspections in the following outage stages:
    — S1: Before FA unloading (shortly after upper internals removal) from reactor.
    — S2: After FA unloading from reactor.
    — S3 Before FA loading into reactor.
    — S4 After FA loading (shortly before upper internals and vessel lid installation.

2.4. TECHNICAL SESSION 4: MITIGATION OF FAILURES BY DESIGN AND MANUFACTURING

The session was chaired by Mr. I. Arimescu (Framatome Inc., USA). In this session, three presentations were made.

2.4.1. Failed Fuel Assemblies in EDF PWRS over the Last 25 Years: Main Causes, Mitigation, and Failed Fuel Evacuation (M. Moatti, France)

The paper is a comprehensive review of EDF's Operational Excellence (OE) over the last 25 years of operating its 58 NPPs (in December 2020 down to 56 NPPs, as Fessenheim 1 and 2 have been permanently shut down in 2020) at 18 sites in France. In summary, the EDF French fleet has experienced approximately 400 failed FAs over the last 25 years, with varying annual failure rates, with an average around 0.2% for fuel assemblies, but with transient peaks of up to 0.6% in two occasions. In the last five years a decreasing trend was established with an assembly failure rate close to 0.1%.

The paper identifies two major failure causes, namely, grid-to-rod fretting, and exogenous or fuel-related debris (which may involve fuel fabrication processes).

Grid-to-rod fretting (GTRF), one of the two major failure mechanisms led to a flurry of failures in 2001 (28 FAs in Cattenom 3) and in 2002 (22 failed FAs in Nogent 2). The salient observations on GRTF were:

— Located at bottom grid level in last cycle of operation and in mid radial core cells, where cross flow is largest.
— Transition from 12 to 18 months for the 1300 MWe NPPs cycle correlated with GTRF occurrence (N.B. same observation as for Krsko NPP in paper 2 of session 3).

Thorough analysis identified the root cause of GTRF mechanism by the evolution of spacer-to-rod contact force evolution during operation, namely, grid springs relaxation induced by irradiation decreases rods holding forces in the bottom grid, leading to an increase of the rods vibration, up to the point of failure by cladding wear; increased cycle length from 12 months to 18 months, which was implemented also increased the propensity of GTRF by allowing more time for the vibration-induced wear after relaxation of the rod-to-spring contact force.

The identification of the GTRF mechanism led to design/manufacturing changes in order to mitigate GTRF, namely introduction of an additional grid and more robust spacer design. These design changes have been verified by design analysis and ultimately confirmed by OE; the efficacy of the design/manufacturing changes was considered demonstrated after upgraded FAs underwent three 18-month cycles of operation, which were completed by 2006. No GTRF failure has occurred after implementation of these design changes (some difference between 900 MWe and 1300 MWe plants).

The other major failure mechanism was debris fretting either exogenous or from damage of FA itself. Despite significant mitigation in the 90's with the introduction of debris filters in all fuel assembly designs, debris fretting is still a potential cause for fuel assemblies' failure; this is, in no small part, due to debris originating in the fuel assembly itself, such as rupture of Inconel springs by Assisted Stress Corrosion Cracking (IASCC). Material changes to prevent IASCC of spacers and grids were the solution to this problem. With regards to exogenous debris, FME measures were and are reinforced at all NPPs and manufacturing sites, such as:

— Actions on FME hazard work areas: establishment of boundaries, maintenance of a clean and tidy work area.
— Inspection performed to ensure that no foreign material ingress has occurred.
— Securing tools and personal protection equipment.
— FME requirements systematically considered in risk analysis of operations in NPP.

Finally, the paper mentioned some actions which were taken in manufacturing, such as: end plug welding, rod insertion in FA, to mitigate some minor fabrication-related fuel failure mechanisms, such as end-plug shear break.

The paper ends by describing progress made in failed fuel transportation, an important end-of-cycle activity. Specifically, upgraded transportation casks relived the licensing concern regarding hydrogen flammability risk and this led to a significant decrease of failed fuel inventory in spent fuel pools on the NPP sites.

2.4.2. Sanmen Nuclear Power Plant (AP1000) Fuel Management (T. Hao, China)

This paper describes the fuel management strategy adopted by Sanmen Nuclear Power Plant in order to assure a high likelihood of leaker-free operation; this is considered to be providing a reference for other nuclear power plants in China in order to improve operating performance across the whole Chinese NPP fleet.

Sanmen NPP (1st AP1000 gen III PWR), was started in 2018 and the first cycle was successfully completed on December 3, 2019. The design cycle length of the first cycle was 450 effective fuel power days (EFPD). Actually, the cycle length is extended to 471.4 EFPD by reducing power operation at the end of life and improves the fuel utilization ratio of discharge assembly in the first cycle. During the whole first cycle, all monitored radionuclides' activities in the primary loop were lower than the detection limit. There was no iodine spike during large power changes. The monthly fuel reliability index (FRI) of the whole cycle was no more than 0.037 Bq/ g, indicating that fuel integrity was maintained.

The good operation performance of Sanmen Nuclear Power Plant Unit 1 reflects the comprehensive fuel management strategy. The paper describes the activities undertaken by Sanmen NPP to ensure fuel reliability from three aspects: fuel assembly manufacturing, foreign material prevention management and reactor operation control.

2.4.3. Overview of Status and Experience Regarding Fuel Failures at NPP Temelín for 20 Years of Operation (D. Ernst, Czech Republic)

The paper presents an outline of the Operational Excellence (OE) of the Temelín NPP with respect to fuel failures, which was summarized as follows: during the 17 cycles from 2000 to 2020, two fuel types have been used and relatively significant numbers of leakers have occurred for both (relatively uniform distribution over time).

Temelín NPP has 2 units of the VVER-1000 type and the fuel was supplied by WEC until 2009 and by TVEL afterwards. The plant is equiped with on-line and off-line sipping systems and also currently has a fully operational fuel inspection and repair system.

The WEC fuel (VVANTAGE-6) was first time loaded in 2000 and during the following 8 cycles in both units, 72 leaking FAs were recorded. The main failure mode for VVANTAGE-6 fuel was identified as GTRF.

TVEL's fuel, TVSA-T, was used from 2010 until 2020 and during the 10 cycles in Unit 1 and 9 cycles in Unit 2, 49 leakers were recorded. Initially, end-plug manufacturing issues were identified as the root cause of three leakers, namely pores in the end-plug material. This issue was resolved by changes in end-plug material and manufacturing process.

Afterwards, fuel rod bow was suspected as the root cause of the following 46 leakers, because of the observation made during PIE of higher axial elongation of some fuel rods. This postulated enhanced rod bow can lead to a severe interaction with the upper tie plate or cause increased flow-induced vibration at spacer grids.

Consequently, a design change was introduced by TVEL, namely the number of grids increased from 8 to 12 in the TVSA-T mod 2 FA, which boosted FA resistance to fuel rod bow. Operation of this new fuel design started in 2018 as a first batch and by 2021 Unit 2 will have a full core with TVSA-T mod 2.

2.5. TECHNICAL SESSION 5: PIES, EXPERIMENTAL STUDIES, AND MODELLING OF LEAKING FUEL BEHAVIOUR

The session was chaired by Mr. N. Waeckel (France). The objective of this session is to show how modelling, associated to proper validation experiments, can help the nuclear operators dealing with in-reactor leaking fuel rods. The Session included four presentations from France and Russia based on submitted papers, summarized below.

2.5.1. Fuel Failure Mitigation is a Key Challenge for the Nuclear Operator (Nicolas Waeckel, France)

Changes in fuel managements schemes are often followed by fuel design modifications which, in turn, may result in unexpected fuel failures. The author showed, through two examples how modelling and experiments are good tools to anticipate in-reactor behaviour of new types of fuel and prevent nuclear industry from bad surprises.

In the first example it was shown that an engineering approach enables understanding and solving a major Fuel Assembly (FA) design issue (which led to tens of fuel rod failures by Grid-To-Rod-Fretting (GTRF) in one French 1300MWe power plant in 2001). The proposed engineering approach combines (i) analytical mechanical/dynamic calculations to assess the evolution under irradiation of the fuel rods contact in the grid cells of a complete fuel assembly structure (to confirm the hypothetical failure scenario) and (2) parametric full-scale experiments, in an out-of-pile thermal hydraulic loop, HERMES P, (to reproduce the in-reactor by simulating various levels of cross flows and to validate/qualify the design modification proposed by the fuel vendor to mitigate the GTRF issue). Based on this approach, the French industry demonstrated, in less than 15 months, that the failure scenario was indeed identified, and that the mitigation option was robust (the modification did not generate other problems elsewhere, within the FA).

The second example dealt with the behaviour of leaking fuel rods during a rapid power transient (Reactivity Initiated Accident RIA). Since in-reactor leaking fuel rods usually exhibit secondary degradation which makes them much more fragile, they can fail prematurely and generate detrimental physical phenomena which are not covered by the usual safety design limit. To answer a question asked by the regulator, the French Industry studied in detail the consequences of the premature failure of a leaker during an RIA transient. In this case, the early rod failure generates a series of violent pressure pulses (due to fuel particles dispersal, fuel-coolant interaction (FCI), and vaporization / collapse of the overheated area of the coolant). As a result, it must be demonstrated that these successive pressure pulses do not damage the neighbour fuel rods (i.e., no domino effect) and do not damage the

Reactor Pressure Vessel (RPV) inner wall (i.e., integrity of the second barrier). Comprehensive analytical calculations clearly demonstrate that the pressure pulses dampen quickly within the fuel bundles and have no detrimental effects on the failed fuel rod environment.

2.5.2. Short-Term Drop of The Reactor Power as a Potential Remedy against Secondary Degradation of Leaking Fuel (I. Evdokimov, Russian Federation)

This paper was a useful attempt to define what kind of mitigation actions could be implemented in commercial Nuclear Power Plant (NPP) to minimize the secondary degradation of a leaking fuel rod, right after the primary leak is identified.

Based on mechanistic simulations (using the RTOP-CA code) and on separate effect tests (performed in HALDEN test reactor where the fuel rods were connected to an external feed line to simulate the water ingress and in MIR test reactor where the fuel rods where the primary leak was artificially created prior to the irradiation), the approach aimed at better simulating the various physical phenomena which appear in a fuel rod exhibiting a primary leak. The objective was to show that appropriate power reductions enable substituting steam with water in the fuel pellet-cladding gap and thus preventing secondary degradation of the fuel rods.

Additional research would be helpful, including simulations and small-scale experiments before providing complete guidelines.

2.5.3. Capabilities of the RTOP-CA Code to Simulate Leaking Fuel Behaviour and Release of Radioactive Fission Products into Primary Coolant of Light-Water Reactors (A. Sorokin, Russian Federation)

This paper presented the simulation capabilities of the extended version of the RTOP-CA fuel performance code regarding leaking fuel behaviour, including fission products release into WWER primary coolant and cladding diameter evolutions.

Models were valuably validated on dedicated experiments in MIR research reactor and were used to reproduce in-pile behaviour of leaking fuel rods.

The extended version is able to simulate the behaviour of WWER fuel (hollow and solid pellet designs), including U-Gd fuel. Code validation includes commercial NPP coolant activity records, experimental results on artificially defected fuel rodlets tested in MIR reactor, PIEs on WWER fuel rods, test results on small-scale experiments in research reactors and neutron code simulations.

2.5.4. Modelling of Radioactive Fission Gas Release from Defective PWR Fuel Rod by MFPR/R Code (V. Tarasov, Russian Federation)

The paper described a new mechanistic model to better evaluate Fission Gas / Fission Products releases out of an experimental defective fuel (i.e., AECL tests).

The long-term vision is to implement this mechanistic model in fuel performance codes (e.g., SFPR code) to better address leaking fuel issues within a commercial nuclear reactor. They could enable to better detect/identify leaking fuel rods within a commercial NPP fuel core or to help the operators implement the right mitigation actions to maintain the leakage under control.

Nevertheless, models assumptions still need to be improved. The studies foreseen in the near future include the elimination of uncertainties in the temperature and geometry of the fuel element during irradiation, a more accurate simulation of iodine deposits on the inner cladding surface, a more realistic modelling of the kinetics of fuel oxidation due to radiolysis, further improvements of the proposed hydrogen model and, extension of the model to transient regimes.

3. CONCLUSIONS

In this Technical Meeting, participants exchanged their views on national perspectives, R&D progress and results via paper presentations and discussion forums. The key points were as follows.

3.1. TECHNICAL SESSION 1:

As expected, the presentations reiterated the understanding and industry position that debris fretting is the single greatest barrier to defect free operation and the achievement of a zero-defect goal.

The discussion showed that the importance of foreign material exclusion and the need for vigilance given the potential for debris to be introduced during maintenance work (during outages), in-service degradation of components and inadvertent introduction from interfacing systems cannot be overstated.

The US provided a very good example of forward thinking and willingness to take the initiative to develop an effective long-term strategy.

There was some interest in understanding whether the fuel that leaves the CANDU plants is fully integral, only being dismantled at the hot cell. It was clarified that the stations are equipped with tooling to effect disassembly of the required defected elements from the main carcass of the bundle. It is these elements that are shipped to the hot-cells and further manipulated during examinations.

During the presentation by the Canadian regulator, there were a few fuel damage modes (unrelated to debris fretting) that were presented. Although these do not normally result in fuel failure, the potential, albeit very low, does still exist. A question was posed by the audience, building on the concept of fuel damage that does not necessarily result in defects.

The question posed, referred to crossflow conditions in the CANDUs. In a CANDU plant, the fuel enters the fuel channel at an inlet region and leaves at an outlet. At the inlet and outlet, there are connections to the feeders. The points at which the connections are made result in flow entering the channel at a right angle. Bundles during the fuelling in or fuelling out process will encounter this crossflow for a brief period. It is not uncommon for some bundles to spend longer than normal; however, it is relatively infrequent that these will result in significant fuel damage that could predispose the fuel elements to sheath breaches. This contrasts with other utilities (non-CANDUs) where crossflow is an issue.

3.2. TECHNICAL SESSION 2:

It is helpful for nuclear operator to have a variety of different methods and techniques for failure monitoring and evaluations. It is an advantage if available methods are based on different measurable values either physical or chemical (like iodine or noble gas activity). In this case, different methods complement each other and provide a better insight into what happens with leaking fuel. Some new techniques of failure detection and analysis are under development or improvement in the IAEA Member States. This is a positive factor for the industry.

Accurate detection of the moment of the failure occurrence may be important for assessment of the failure mechanisms. It may be possible to correlate the failure with some changes of the operational parameters, such as power transients or changes in water chemistry. It is also possible to estimate how long time does it take for a particular mechanism to lead to a fuel failure (e.g., grid-to-rod fretting or debris fretting). Sensitive methods for detection of failure occurrence are also urgent for implementation of corrective measures aimed at mitigation of fuel failures.

Information collected in the framework of detection and monitoring of fuel failures may be also used for making decisions on handling of leaking fuel after it is discharged from the reactor.

3.3. TECHNICAL SESSIONS 3 AND 4:

The papers in sessions 3 and 4 were dedicated to PWR Operational Excellence (OE) and fuel failure mitigation actions. With respect to plant operation the main mitigating actions were presented as follows:

- Change to baffle up flow at baffle core plate locations to mitigate baffle jetting.
- Foreign material exclusion (FME) implementation in all stages, including the construction phase, to prevent to the maximum extent possible debris fretting.
- Power limitations/restrictions to prevent challenging conditions for fuel rod thermo-mechanical behavior.

With regards to design/manufacturing preventing actions, the following were mentioned:

— Design changes to increase structure robustness, such as additional grid(s), mainly in order to limit the magnitude of fuel rod bow, but also to prevent GTRF at FA bottom.
— Improved spacer design to address GRTF; rods with autoclaved bottom part and debris filters in order to mitigate debris fretting failure mode.

A common thread for all fuel types and NPPs was the occurrence of failure mechanisms caused by structure-flow interaction; the resulting flow-induced vibrations (see also similar example for CANDU OE presented in session 1) lead to fretting wear that eventually could cause a localized cladding breach.

A salient feature of the reliability actions described in the papers was that the cycle from an improvement idea to engineering studies, tests, implementation in manufacturing, confirmatory lead test assemblies (LTAs) and culminating with the implementation in production is rather long (spanning several years at least). Accomplishing this process requires focus and perseverance combined with coordination of several engineering, manufacturing and plant operations organizations and qualified staff. It was also remarked that such a long and complex research and development programme also requires flexibility to account and accommodate intermediate findings, which could lead to a change of course if needed, by adopting back up options, or variants of the main candidate change.

In order to complete the above discussion and include the BWR OE, reference can be made to paper 2 from Session 1, which mentioned that the dominant failure mode in BWRs, especially in last 10 years was debris fretting (similar to PWR statistics) and that preventive measures similar to PWRs have been taken.

Several papers described actions to develop or upgrade onsite equipment for monitoring or poolside fuel examination/repair, which is important to assure a clean and safe operation of NPPs.

Finally, an underlying methodological approach was emphasized during discussions, namely the use of Root Cause Analysis (RCA), as a diagnostic tool for fuel leakers and as a basis for future actions to prevent to the maximum extent possible re-occurrence of such events. In summary, the following features were mentioned as needed with respect to a successful application of RCA, as part of a structured approach in the nuclear fuel performance and reliability:

— Good monitoring and leaker detection system.
— Good poolside PIE capabilities (provide symptoms and OE feedback).
— Understand the failure mechanism - without a good diagnostic, no remedy is possible.
— Good RCA (don’t just check boxes, dig deeper), analyze major dependencies (address multi-variable and potential confounding factors).
— Identify corresponding corrective actions at all levels, including operation, design, fabrication.
— Define the problem very well – a well formulated question contains the answer.
— Don’t allow the temporary quick fixes to become permanent, as they might not work in all conditions.

3.4. TECHNICAL SESSION 5:

In Session 5 mechanistic simulations of in-reactor leaking fuel behaviours have been proposed by several contributors. These simulations are based on correlations or mechanistic models. When available, the models are partially validated using in-pile experiments on short leaking fuel rodlets. The various physical phenomena to deal with include:

— Physical/empirical models describing fuel oxidation phenomena and degradation of the thermophysical properties of UO_{2+x}:

The thermophysical properties include the specific heat, fuel thermal conductivity and density of the oxidized fuel – these properties are needed for fuel temperature calculations of the defective fuel rod. The fuel oxidation models need to predict the stoichiometry deviation of the fuel radially, axially, and azimuthally (near and remote of the defect site). The fuel oxidation model would presumably consider multi-phase transport including normal diffusion and thermo-diffusion for interstitial oxygen migration in the solid, as well as gas-phase (steam/hydrogen) transport in the fuel pellet cracks. A reduced thermal conductivity in the fuel will also lower the incipient melting temperature of the oxidized fuel making it more prone to centreline melting. Higher temperatures result in enhanced fission product diffusion as well as a higher intrinsic diffusivity in the oxidized fuel matrix.

— Hydriding/fuel-rod degradation model for defective fuel:

The hydriding model needs to be coupled to a fuel performance code accounting for stresses on the brittle cladding, initiation of sunbursts and hydride blisters, and migration of the hydrogen through the clad wall (to initiate a crack with thermal expansion of the zirconium hydride and oxidized fuel expansion), as well as axially in the cladding with the temperature gradient to cooler regions of the clad at the end caps (depending on the axial power distribution in the rod).

— Sources of hydrogen in the fuel-to-clad gap by radiolysis, clad oxidation, and fuel oxidation:

It is noted that the kinetics of these reactions are important.

— Gap transport:

The determination of the oxygen potential in the gap is essential to understand fuel oxidation and hydriding phenomena. The critical hydrogen-to-steam ratio is needed to account for the location of hydriding/hydride blisters in the cladding at a given location in the fuel rod. The transport of outgoing fission products and hydrogen/helium, and incoming steam, through the breach and along the gap (Stefan-Maxwell multi-component diffusion) needs to be discussed. Effect of iodine chemistry on the escape rate/empirical diffusion coefficient in the gap accounting for iodine adsorption on the fuel/clad surfaces (i.e., including the effect of the water-steam ratio for dissolution of cesium iodide salt localized around the defect site). Effect of the physical path length for radioactive noble gas release depending on the breach location(s) and rod length (Chapman-Enskog diffusion theory). The mass transfer/boundary conditions for the transport equation at the breach location. The gap heat transfer coefficient which will change as steam and hydrogen replace the helium fill gas.

— Tramp uranium characterization:

Fuel loss, deposition and transport should be studied more thoroughly to help nuclear operators defining the best approaches to remove the fuel fragments from the heat transport system (uranium contamination led to alpha exposure during refurbishment activities in commercial NPPs).

In general, the Technical Meeting provided the basis for the preparation of an IAEA TECDOC compiling the papers presented during the event. It also provided discussions for future activities to support the collection of Member States' knowledge and expertise on fuel failure during the operating conditions of water-cooled reactors.

OVERVIEW OF STATUS AND EXPERIENCE REGARDING FUEL FAILURES DURING NORMAL OPERATION

(Session 1)

Chairperson

R. LEWIS
Canada

STATUS AND EXPERIENCE REGARDING FUEL FAILURES AT RINGHALS NPP

K.M. CARLING, J. LYBARK, M. DAVIDSSON
Ringhals AB,
Väröbacka, Sweden

Abstract

The status and experience regarding fuel failures at Ringhals NPP will be presented. The scope is from year 1990 until today. Ringhals NPP consists of one BWR and three PWR units which were connected to the grid from 1975 to 1983. The authors will discuss some aspects from our experience regarding fuel failures with the focus on the last few fuel failures which also are the ones that have occurred during the last years.

1. INTRODUCTION

Ringhals Nuclear Power Plant (Ringhals NPP) is located on the west-coast of Sweden. It consists of four units, one BWR unit and three PWR units, see Table 1 for data describing the units. In December 2019, one of the PWR units was taken off the grid for the last time. The BWR unit will be taken off the grid for the last time in December 2020. Thus, there will be two PWR units remaining in power production from January 2021, Unit 3, and Unit 4.

TABLE 1. DATA RINGHALS NPP

	Unit 1 (R1)	Unit 2 (R2)	Unit 3 (R3)	Unit 4 (R4)
Type of reactor	BWR	PWR	PWR	PWR
Start of production	1976	1975	1981	1983
Net electric power (MW)	881	(1)	1063	1123

Unit 2, 904 MW electric power, was taken off the grid permanently at the end of December 2019.

2. METHOD

Data about fuel failures at Ringhals NPP for the years from 1990 to 2019 has been collected and compiled. A fuel failure has been defined as one fuel assembly with one or more leaking fuel rods. The focus has been the number of fuel failures, when the fuel failure happened, and the cause of the fuel failure. Information has been sourced from Ringhals' NPP internal documents and records.

3. RESULTS

After the introduction of the accident modules in DIONISIO, several complex experiments were simulated, all of them taken from the IAEA database.

3.1 Number of fuel failures

In Fig. 1 below, the number of fuel failures at Ringhals NPP is presented on a per year and per unit basis. During the period from 1990-1997, there were several fuel failures every year, and they occurred at more than one unit for each year. Between 1998 and 2005, there were fewer fuel failures, one every year and only at one unit at a time. During the last period, from 2006 until 2019, there was only one fuel failure, i.e., there has been only one fuel failure during the last ten years period and extending some additional years historically. The total number of fuel failures during the whole period, from 1990 to 2019, was 40.

.

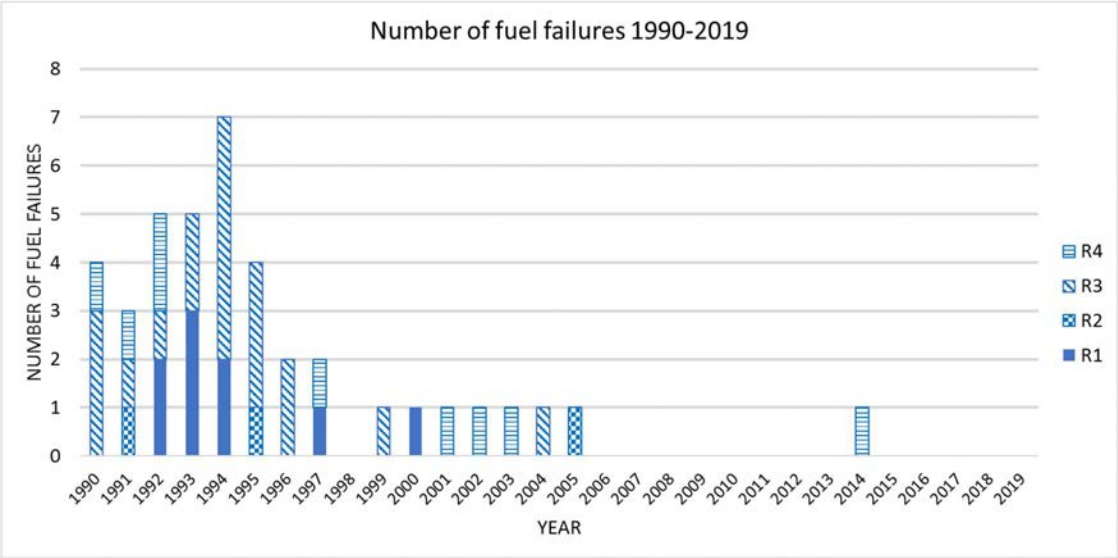

FIG. 1. The number of fuel failures for each unit at Ringhals NPP during the years 1990-2019.

3.2 Root causes of fuel failures

In Fig. 2 below, the statistics for the fuel failures have been further broken down by their root causes. As has been noted in the industry, debris fretting is the most common root cause of fuel failures. For Ringhals NPP, manufacturing defects is the next most common root cause. The third most common root cause during the period 1990-2019 has been PCI-failures at the BWR unit that occurred until approximately 1994. The PCI-type failures have been a cause for fuel failures from the initial core of the reactor. The PCI-type fuel failure mechanism was eliminated at Ringhals NPP Unit 1 with the introduction of fuel rods with an internal liner with the continuation of conservative operating guidelines. In the end, there will always be the possibility of the odd incident, known but not representative for the usual root cause of fuel failures, which is marked “other” in the pie chart.

If the root causes are summarized based on the most common causes identified for failed fuel in the BWR and the three PWRs respectively, the following facts are found. For the BWR, Unit 1, PCI and debris fretting are the most common root causes for fuel failure. For the three PWRs, Unit 2 to 4, debris fretting, and manufacturing defects have been the most common fuel failure mechanisms. Thus, the most common failure mechanism, for the units at Ringhals NPP, is debris fretting, especially if we focus on the last fifteen years of operation.

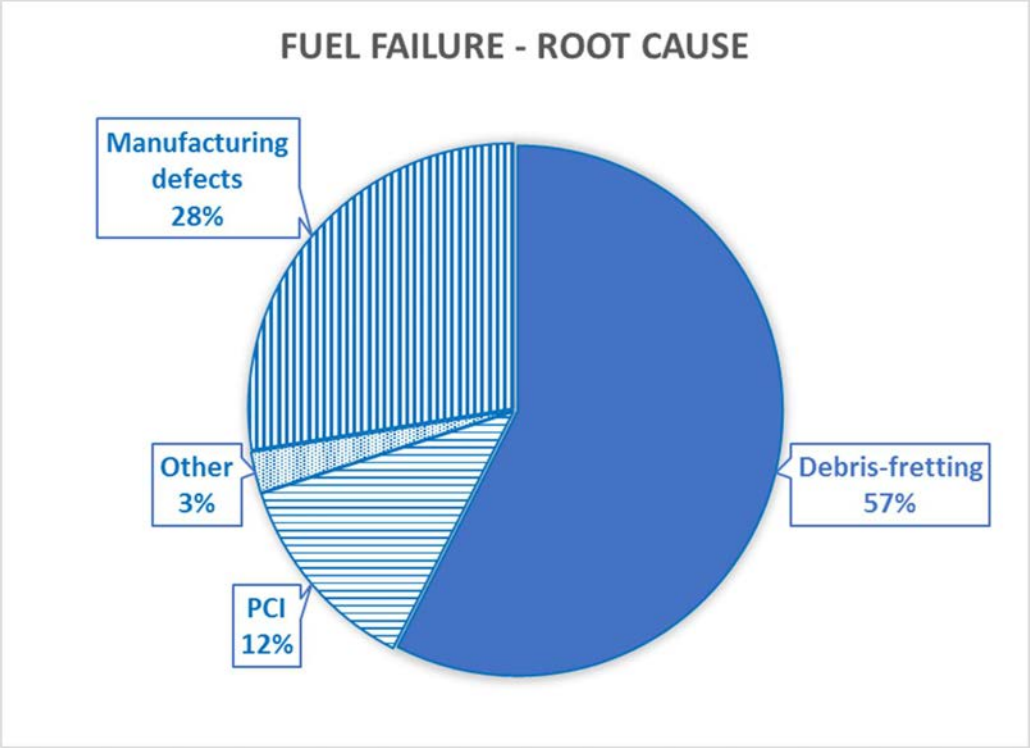

FIG. 2. Pie chart overview of the root cause of fuel failures at Ringhals NPP during the years 1990-2019.

3.3 Managing of fuel failures

The goal of managing of fuel failures at Ringhals NPP is to prevent or minimize the long-term potential for contamination of the units, as this would increase the risk of higher doses to personnel.

When a fuel failure is first detected, the response per procedure [1] is to monitor the relevant parameters to assess the characteristics of the fuel failure. In so doing, it is possible to understand the properties of the fuel failure and the likely extent of damage.

Fuel failure monitoring is available at all units. Monitoring is primarily performed with online equipment and supplemented by daily and weekly monitoring of samples (taken by the chemistry and radiophysicis departments).

According to plant procedure [1], the core operation will be adjusted to minimize the risk of making the fuel failure worse. Using the monitoring information, assessment of the propagation of the fuel failure can be performed on a continuous basis. This assessment can be used to minimize the risk that the fuel failure will degrade too much. These procedures [1] are put in place to be able to assess whether it is necessary to have an outage immediately to identify and unload the damaged fuel assembly. Finally, no unit is to be started without full sipping scan of all the fuel assemblies to make sure that all fuel assemblies with fuel failures has been removed from the core. The core shall not have any fuel failures present when it is re-started.

3.4 Example of a fuel failure event

Between 2004-2005, Unit 2 at Ringhals NPP was run at full power with a confirmed fuel failure for a period of approximately five months. The fuel failure was discovered on October 8th, 2004, through the detection of Xe-133 in the chimney. This observation led to initiation of further analyses and the presence of a fuel failure was later confirmed. Also, analysis showed that the amount of free fissile material (FFM, i.e., tramp uranium) was low, below the detection limit.

To keep the fuel failure under control, power ramp restrictions were put in place, as well as expanded monitoring through chemistry and radiophysics analyses. An analysis group was formed to follow the fuel failure. Safety evaluations of the fuel failure, to assess the possibility of continued operation, were regularly performed. During the five-months after the fuel failure was detected, there was two scrams which put strain on the fuel failure,

but no indication of increasing amounts of FFM. The unit was shutdown February 15th, 2005, and the planned outage started.

When the fuel was unloaded from the reactor, all fuel assemblies were sipped to identify leaking rods. One fuel assembly indicated that it contained leaking fuel rods. The fuel assembly was taken aside to be repaired with individual fuel rods being checked for leaks. Two fuel rods were found to be potentially leaking. During visual inspection, one of the fuel rods clearly had defects caused by debris fretting (primary and secondary defects in nature). Fig. 3 provides an example of a secondary defect observed on the failed assembly removed from Unit 2. Both rods were sent to a hot-cell laboratory where it was confirmed that one of the fuel rods was leaking due to debris fretting while the other was intact.

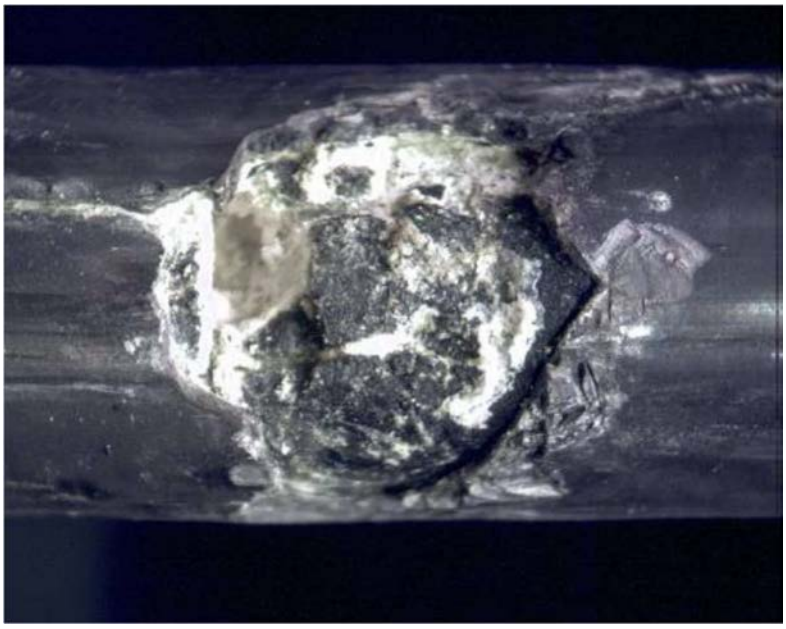

FIG. 3. Damage to the leaking fuel rod at the height of the fifth spacer. The damage is of the secondary fuel rod failure type.

4. DISCUSSION

Since most of the fuel failures arise from debris fretting, the most important, proactive work at Ringhals NPP is the work with Foreign Material Exclusion (FME) - which has been in place at the plant since 2011. If there is no debris, there will be no fuel failures due to debris fretting. As such, when working on any system present at the plant, the workforce actively applies the applicable FME procedures as part of their daily activities.

Another important aspect of the effort to reduce the number of fuel failures has been the fuel inspection program. The intention of this program is to monitor the condition of unloaded fuel assemblies to assess, to as large an extent as possible, the soundness of them. Among the fuel inspection program activities for the PWR-units is the four-sided visual screening and recording of the fuel assemblies when as they are loaded into and unloaded from the core during outages. The recorded movies of the fuel assemblies during unloading are assessed more closely shortly after unloading is completed. If any questions arise, the appointed fuel assembly will be assessed through new, close-up and more detailed, filming process that renders a movie with higher resolution of the full fuel assembly.

Part of lessons learned about fuel failures is to identify the cause of the fuel failure, both through poolside examination activities and by sending the failed fuel rods offsite to a hot-cell laboratory for post-irradiation examination (PIE). This is particularly important when the cause of the fuel failure cannot be identified during onsite, poolside, fuel inspections.

Presently, the amount of free fissile material (FFM) has decreased, see the example from Unit 1 in Fig. 4. The reduction in FFM can be seen for all the units at Ringhals NPP. Although not shown here, it is worth mentioning that the fuel failures at Unit 4 in 2014 and at Unit 2 in 2004 did not increase the amount of FFM due

to the reducing water chemistry of the PWR-units. The low amount of FFM is one of the key contributors to the low dose to personnel.

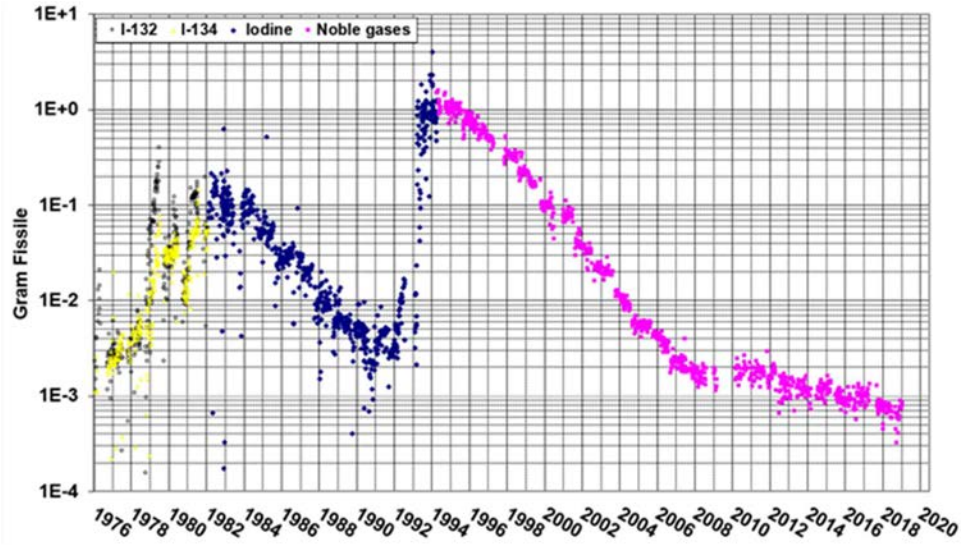

FIG. 4. Example of decrease of FFM Ringhals NPP, Unit 1.

4.1 CONCLUSIONS

At Ringhals NPP the number of fuel failures has decreased from the previous ten-year period to one fuel failure during the last ten years of operation. The main root cause of the confirmed fuel failures during the last twenty years is debris fretting. In order to minimize and mitigate the potential occurrence of debris fretting related fuel failures, a comprehensive effort on FME has been undertaken by the plant (management and working level). One of the primary benefits of having a low number of fuel failures has been the reduced dose to plant personnel. There will also be the benefit of reducing the burden on engineers and analysts to deal with fuel failures. In the end, few fuel failures also reduce the efforts needed to decontaminate the unit during decommissioning.

ACKNOWLEDGMENTS

The main author, K.M. Carling, would like to acknowledge the efforts made by Å. Henning on Fig. 4. Also, the work of the FME-group at Ringhals NPP is appreciated and hereby acknowledged.

REFERENCES

[1] WINGE, F. DAVIDSSON, M., Instruktion – Bränsleskadestrategi för R1-4, internal report, Ringhals AB, Väröbacka, Sweden, 2019.

FUEL FAILURES RECENT EXPERIENCE AND THEIR MITIGATION: A US PERSPECTIVE

C. FAULKNER (INPO), I. ARIMESCU (Framatome Inc.), S. MAZURKIEWICZ (Framatome Inc.), R. SCHNEIDER (GNF), M. O'CAIN (Westinghouse)

Abstract

As part of the Tractebel contribution to the IAEA FUMAC project, Tractebel has used the updated FRAPTRAN-TE-1.5 code for simulation of selected Halden LOCA tests IFA-650.9 and IFA-650.10, together with the improvement in the thermal hydraulic modelling by using the imposed thermal hydraulic boundary conditions from SOCRAT calculations and in the thermal boundary conditions (axial power profile, plenum temperature). In particular, the impacts of the model improvements such as the Quantum Technologies' axial relocation model and errors corrections in the adapted FRAPTRAN-TE-1.5 version on the calculation results were identified and discussed. In addition, the statistical uncertainty and sensitivity analysis has been performed on the FRAPTRAN-TE-1.5 modelling of the selected Halden LOCA test IFA-650.10, which helped the identification of significant input parameters for LOCA fuel Behaviour modelling. The final objective is to apply the qualified fuel rod transient analysis codes FRAPCON/FRAPTRAN to develop an efficient methodology for assessing the performance and quantifying the margins for advanced technology fuel (ATF) designs under design basis accident conditions (in particular LOCAs).

1. INTRODUCTION

Fuel failures consist of some form of cladding breach, which leads to a partial loss of the fission product barrier function of the fuel cladding, intact cladding being the first protective barrier and thus, an important feature of the nuclear operating plant's defense-in-depth (DID) philosophy. One important undesired outcome of fuel failures is the release of fission products into the primary coolant system which, in severe cases, can lead to increased worker dose, reactor systems contamination and could even result in the increased risk of radioactive material being released to the environment. However, the radiological impact of a few fuel rod failures can be accommodated by the primary coolant system, with negligible effect on onsite staff and offsite population radioactive exposure. The operational impact of fuel failures can be high in both BWRs and PWRs as fuel failures result in economic consequences including additional outage scope, core design rework, and more complicated dry fuel storage requirements.

Therefore, the nuclear industry in the US and globally has endeavored from the early days to identify fuel failure causes and to adopt measures to prevent to the maximum extent possible fuel failures in normal operation. The countermeasures to fuel failures encompassed all stages from the design/manufacturing of nuclear fuel to its operation in nuclear power reactors. In addition, mitigation of severe degradation of failed fuel was another objective that was incorporated in core operating guidelines.

2. INDUSTRY FAILURE TRENDS IN THE LAST 5-10 YEARS – US STATISTICS

Fuel failures in the US PWR and BWR fleets are at an all-time low for the current year, namely two failed cores presently. Both leakers are in BWRs with pumped forward drains, which have historically been more susceptible to debris failures, since ~35% of the feedwater flow does not pass through the condensate treatment system. In the last five years there were some excursions in failures, more so in BWRs than in PWRs. This is illustrated in Figure 1 and Table 1 in the context of the broader time interval going back to 2010. Note that the failure data refer to the year when the failed rods were discharged, which is not always the year when failure occurred, because of the time delay from fuel failure identification and economic considerations regarding the timing of an outage start following a failure event.

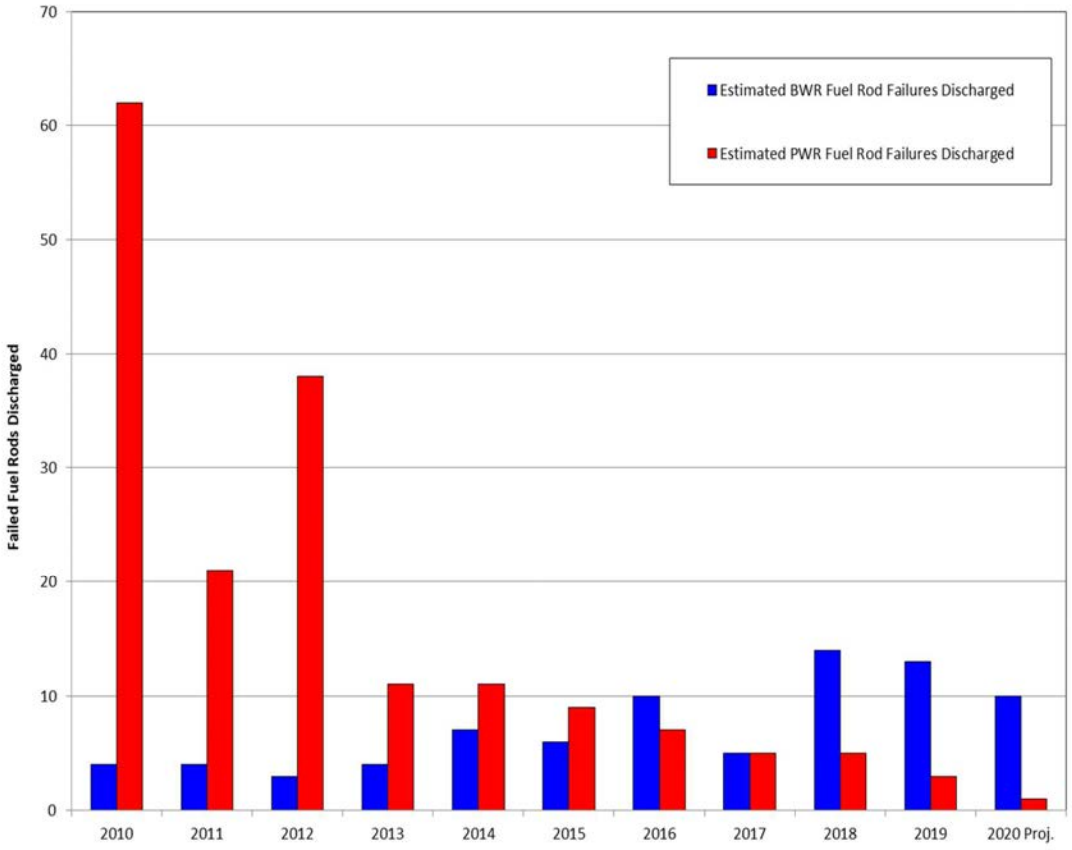

FIG. 1. Fuel failure statistics for US LWRs in the 2010–2020-time interval.

TABLE 1: PARAMETRIC STUDIES ON FRAPTRAN-TE-1.5 MODEL OPTIONS

	BWR		PWR	
	# Failed Cores	# Rods	# Failed Cores	# Rods
2014	5	7	5	11
2015	4	6	3	9
2016	4	10	5	7
2017	4	5	3	5
2018	5	14	4	5
2019	7	13	2	3

Within the BWR fleet most plants have had no failures, a few have had 1-2 failures, while a few others have had multiple consecutive cycles with one or more failures.

The bulk of the fuel failures in US LWRs were due to the debris fretting mechanism, as illustrated in Figure 2 for all LWRs in US for the 2013–2018-time interval. Actions taken by utilities and fuel vendors in the past 2-3 years have apparently had some success in arresting and turning around the upward trend that was noticed for this failure mechanism during 2016 to present day, as can be observed from the data presented in Table 1, more noticeably for PWRs.

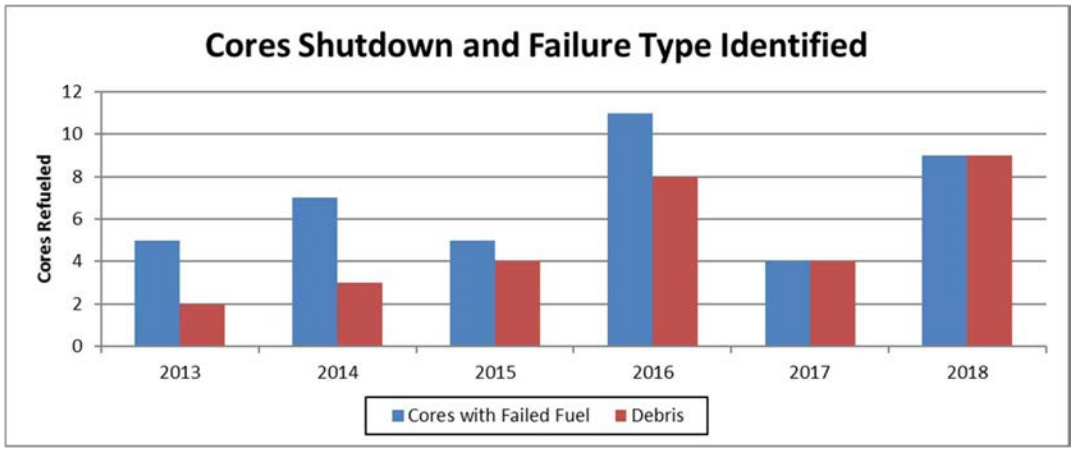

FIG. 2. Comparison of total failed cores and cores with debris-related failures.

In the case of BWRs there are only 2 plants with leakers in operation at the present time, which would represent 2 or 3 potential failed rods. With no additional industry BWR failures (Westinghouse and Framatome are currently leaker-free in PWRs), the US industry is projected to remain on track to achieve the leaker-free status by spring of 2021.

3. US INDUSTRY DEBRIS-RELATED FUEL FAILURE TRENDS

As noted in the previous section, the dominant fuel failure mechanism for both BWRs and PWRs in the last 10 years was debris fretting. This is illustrated for the two reactor types in Figure 3, which indeed shows that debris-related failures are a majority for BWRs, and practically half of the failures reported for PWRs.

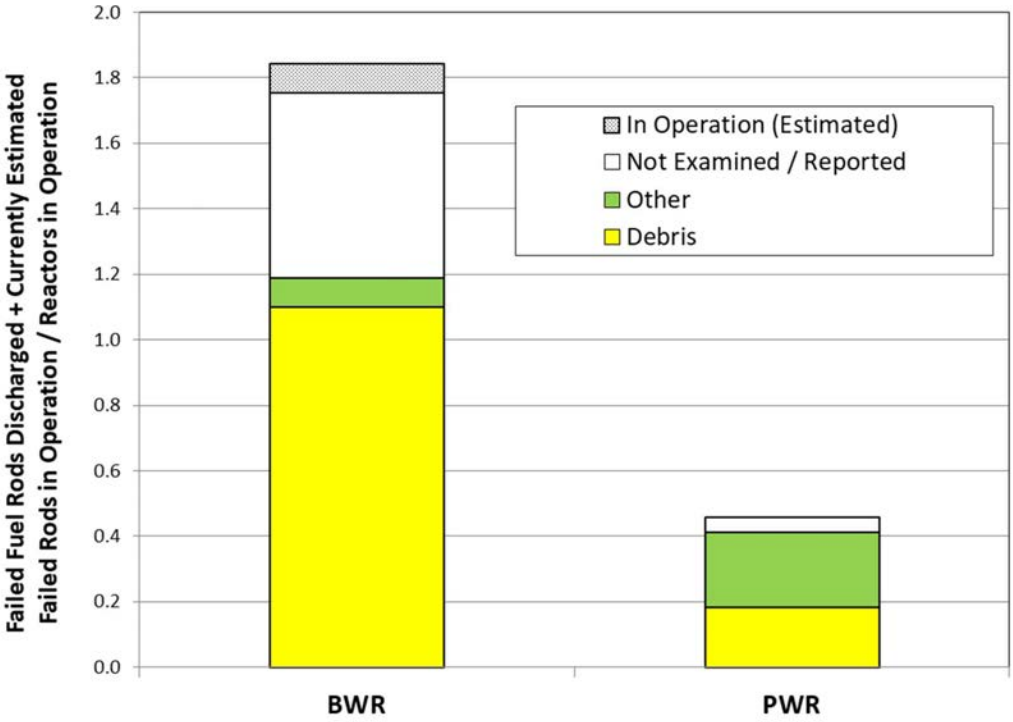

FIG. 3. Leaker cause breakdown for the 2014–2020-time interval.

4. DEBRIS FRETTING FAILURE MECHANISM

The debris fretting failure mechanism originates when certain metallic foreign material, generically called "debris", which can be introduced in the primary coolant system during outages from maintenance work or during operation from component/fuel degradation, and afterwards can potentially become trapped between the spacer grids and a fuel rod. This trapped debris vibrates under the action of the coolant flow and can wear (or fret, through repeatedly wiping away the oxide layer) through the cladding, eventually creating a through-wall perforation.

After a through-wall debris fretting perforation occurs, loss of inert helium and ingress of steam initiates secondary degradation processes internal to the fuel rod (temperature increase, fuel rod inner diameter oxidation, pellet oxidation and swelling), similar to the progression from other primary failure causes. The debris fretting primary defect site is generally still recognizable by visual inspection because of the characteristic indentation features of the debris fretting wear mechanism. The debris that caused the failure is often not visible or still present during follow-on leaking fuel inspections.

In BWRs, with fuel channels, there is a large increase in coolant velocity with elevation due to boiling/voids; relative to single-phase water at the entrance to the bundle, at higher elevations the same mass flow rate is maintained at upwards of ~80% void fraction. It has long been observed that debris fretting perforations are strongly skewed to the spacers in the upper ~1/3 to 1/2 of the bundle. Nevertheless, debris fretting failures can occur in the lower part of a fuel rod in BWRs, when the piece of debris is trapped at a lower elevation spacer grid; however, this has not been observed after the introduction in production of modern debris filters. It was observed that debris can enter the fuel channel from either the bottom (in the flow direction), but also from the top during shutdowns (potentially debris carried upward through the bypass region between fuel channels).

Nevertheless, it is considered that most of the debris that is causing failures entered the fuel channel through the lower tie plates (LTPs) filters, based on the following main arguments:

— Correlations of multi-failure cycles with major steam plant modifications work (piping and heat exchanger replacements).
— The tendency for fuel to "clean up" the debris in the core – typically after a debris ingress event, reloads present in-core at the time incur most of the failures; fuel loaded in subsequent cycles experiences far fewer, if any, failures.
— Correlations of multi-failure cycles with component failures in service (pump impellers, valves, on-line repairs, spiral wound gaskets, condensate demineralizer resin trap screen failures, etc.).
— Observations of debris on the LTP filters of the fuel in these same cycles.
— Debris collected from LTP filters by HE-UFC (high-efficiency ultrasonic fuel cleaning) campaigns – logically, plants with no failures have had the least debris, plants with 1-2 failures in the preceding cycle have some debris, and plants with multiple failures and/or debris failures in consecutive cycles have generally seen the most debris. Since this cleaning occurs in the spent fuel pool or cask pit area, it has provided the best evidence that debris does not routinely fall from filters into other bundles. In some campaigns hundreds of pieces of debris, including pieces of metal debris up to several inches in length (that would have been expected to fall out based on mass) have been removed by this cleaning equipment.
— Flow through the bundles during normal power operation is in the upward direction and the tiny pieces of wire or wire-like material that cause most debris fretting failures (Figure 3) are not likely to enter against this flow (except during shutdown with the lower flow rates due to natural circulation and shutdown cooling).
— Plants with pumped forward drains (where up to ~35-40% of feedwater is untreated for chemistry and not strained for debris removal) have experienced debris failures at rates 4 to 5 times higher than in cascaded-drains plants – true in all countries operating BWRs and for all vendors' fuel.
— The debris that is occasionally found trapped in spacers is very small in size, in many cases 1 cm or less in length, and the perforations that are found behind spacers are also very small (often apparently because of the tips of wires or wire-like material) and these are the only pieces able to enter the bundles through LTP filters.
— With generally strong focus on foreign material exclusion (FME) controls on most refuel floors, as well as the compelling evidence that debris does not fall from filters during X-Y direction fuel moves in pools, it is very rare for debris to be sighted atop the upper tie plate filters of fuel bundles during core verifications.

The time to failure by debris fretting after a debris ingress event has varied from the fastest of just one to two weeks in a fresh (new) bundle, to up to ~four years. It is easier to estimate the time to failure if the suspected cause is due to outage-related maintenance or modifications; however, in recent years more failures have been suspected

to be linked to equipment failures in service during operation, for which the time elapsed between ingress and failure is more elusive.

One important observation has been that nearly all failures in 24-month cycle BWRs occur in first or second cycle fuel which operates at relatively high powers and flows, in central core areas. Shuffling bundles out to low power locations during the third or fourth cycle rarely results in debris-related failure in these locations, even for bundles known to have been through debris excursion events in previous cycles, with several debris failures within the reload. This is part of the operating experience and considerations regarding the flow-induced vibration conditions necessary to initiate the debris failure mechanism.

Figure 4 provides examples of modern debris fretting failures and the challenge presented by very small pieces of metallic foreign material. Non-metallic debris such as lint, threads, fibrous material, paint chips, or clumps of friable material such as rust flakes or chunks, are not a threat to fuel integrity via fretting.

Wire sticking out of fuel rod – later removed with a plier tool – very small through-wall perforation (with bubbles present).

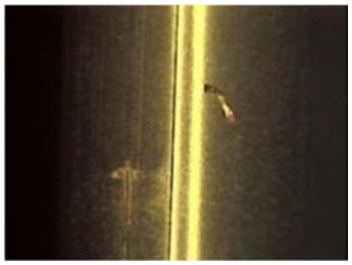

Typical small debris fretting perforation at spacer grid area – debris no longer present.

FIG. 4. Debris Fretting Examples.

With PWR cores, many of the same fundamental debris-related issues exist as with the BWR discussion above. In PWRs, as previously noted, the number of debris leakers has historically trended downward, but in recent years has stabilized as a persistent problem. Over time, with the development of better debris trapping fuel features at the bottom of the fuel (debris filtering bottom nozzles, debris trapping grids and fuel rod coatings), defenses against fuel failures have grown more robust. Developments in additive manufacturing (3D-printing) could point to more advanced debris filtering designs in the coming years. Note, however, that debris traveling between bundles will continue to present a challenge to prevent debris leakers higher up in PWR bundles, where debris resistant features are not present. Continued reinforcement of operating plant FME programs will assist in mitigating those and other debris-related leakers.

Likewise, with BWRs, cleaning and debris retrieval services exist for PWR cores to identify, and removal debris found in the core or in the fuel prior to core restart.

5. MEASURES TO MITIGATE DEBRIS FRETTING FAILURES

Fuel vendors have traditionally focused on LTP filters for debris mitigation and on spacer geometry to attempt to reduce capture. Oxide coating of the bottom portion of fuel rods also provides additional debris mitigation. In recent years several concepts for hardened, fret-resistant coatings on cladding, which have been proposed and researched in the past, have been introduced into reactors in lead test bundles. In addition, fuel vendors and nuclear steam supply system (NSSS) vendors have teamed up to provide feedwater system strainers to attempt to reduce debris inputs from the steam-plant side of BWRs.

Cleanup activities that have been effective include removing all debris identified during in-vessel visual inspections which is a normal/standard practice and cleaning out the bottom head drain (BHD) lines in plants where they have been found to be clogged with foreign material and thus unable to perform one of the desired functions. BHD line cleaning restores one of the removal paths for small debris items to reactor water cleanup system filters. Condensate storage tanks and suppression pools are also potential sources of debris, when emergency core cooling systems and shutdown cooling systems are run for surveillance testing or briefly inject to the vessel after plant transients.

One US BWR had ~17 total failures across three cycles, from late 2015 to 2019. The current cycle has an estimated one failure. Utility and nuclear fuel vendor actions that all appear to have contributed to improved reliability include:

- Identification and replacement of plant components (metal gaskets) in secondary system valves that were prone to failure.
- Extensive plant flushing and cleaning operations of low point drains, feedwater heaters, etc.
- Installation of full-flow debris strainers in the feedwater system, very close to the reactor (after the high-pressure feedwater heaters and after pumped-forward drains are added to the feedwater).
- Ultrasonic fuel cleaning to remove debris inventory from LTP filters of bundles.
- Implementation of bundles with advanced debris resistant features including LTP filter improvements and spacer modifications to eliminate or reduce debris capture sites based on operating experience.

6. OTHER FAILURE CAUSES

Duty-related failures include PCI, missing pellet surface (MPS)-assisted non-classical PCI, a.k.a. MPS-PCI and hydride-assisted PCMI failures at high residence time. These different forms of duty-related failures can be differentiated fairly accurately based on the operational characteristics of the events including the terminal powers and exposures at the time of the power ramp that triggered the duty-related failure. Classic PCI failures are rare in either barrier (liner) or non-barrier (for current optimized Zry-2 cladding material and modern fuel rod designs) fuel and generally have occurred in the ~20-30 MWd/kgU exposure range, in leading-duty rods/nodes in maneuvers that increased powers to well above the plant experience base and the fuel's conditioned history. Duty-related failures are most likely to be attributed to MPS issues at the fuel vendors if the rods/nodes failed immediately after a power-increase maneuver but were not necessarily leading in power or stress relative to many others that saw similar or higher duty. Another variant has been a small number of failed rods exposed to step changes in power very late in life, such as in 3rd-cycle fuel in 24-month cycles in the final 1-2 months during the approach to all-rods out. Most higher power density or uprated cores do not load or operate cores in such a way as to experience this type of duty; lower power density plants with smaller batch fractions may have more fuel of this age in central core areas. Core operating guidelines providing ramp rate guidance are also used to mitigate the PCI failure mechanism via rod conditioning.

As PWR plants age, issues with baffle bolt breakage and baffle jetting have been observed in the US. Baffle bolt breakage in the US has manifested itself in debris leakers either via debris created by the loose lock bars or bolt heads. Inspection programs of bolts have resulted in significant bolt replacements in impacted plants with mitigation of any recurring debris leakers. Baffle jetting, either due to baffle bolt deterioration or general plant aging occurs in PWR plants with a downflow baffle barrel configuration. In those plants that have experienced baffle jetting, converting to an upflow baffle barrel configuration has resolved the jetting issue, while also providing more GTRF margin for third cycle fuel on core peripheries.

Manufacturing-related leakers are historically infrequent and random in nature. There "signature" is typically difficult to confirm, with failures being flagged as due to manufacturing when all other leaker mechanisms have been ruled out. When they occur, typically due to a weld or cladding defect, they are more likely to occur early in the life of a fuel bundle. In some isolated cases hydrogenous contamination of the fuel rod during manufacturing led to a primary hydriding failure. Fuel vendors, via leaker root cause assessments, customer audits, general process improvements and effective FME programs, continue to maintain and monitor fuel performance.

GTRF-related failures since 2014 have become less and less frequent as plants have moved to new fuel designs with new spacer grid designs eliminating fuel bundle self-excitation. Albeit the GTRF mechanism is nearly extinct, continued attention should be paid to the introduction of new cladding material to ensure that the grid-to-rod wear-couple retains sufficient operational margin (i.e., do not place a low oxide cladding in marginal GTRF grid designs).

7. CONCLUSIONS

The US fleet of reactors has done a good job recently of reducing fuel failures to much more easily manageable levels in most plants, Fig. 5. This accomplishment is particularly noteworthy given the current economic climate for most plants, with extreme cost pressures for shorter outages, deferral of maintenance work, as well as pressure to extract the maximum possible energy from each reload and bundle, with smaller thermal

limit margins. These pressures are brought on mainly by competition with low-cost natural gas, but also to some extent in some areas from wind or hydro energy. Several older, smaller plants have been permanently shut down each year, while several plants in the US fleet are still struggling to maintain economic viability. Nevertheless, it was remarked that the US nuclear power plant fleet has achieved a record output (20 % of US electricity annual production in 2019 and 55% of all carbon-free electricity sources) and production efficiency (capacity factor of 93.4% in 2019). At the same time, the safety performance indicators of all LWRs in the US have steadily increased over time, reaching their highest levels in the last 5-10 years; this is also correlated with the continuous decrease of fuel failures, except the debris-related failures, which are now the focus of the whole industry from fuel vendors to power plants. The overall fuel failure trends in the US in the last ten years are illustrated in Figure 5, showing a continuous reduction in both multiple-cycle failures and an increase in the number of clean cores: 56% of US cores have operated for more 5 cycles without a fuel failure. During the 2nd and 3rd quarter of this year and continuing into this last quarter of 2020, no PWR cores operated with a fuel failure. Barring any new failures, at the end of 2020, only 2 cores will have active fuel failures, scheduled for removal in the first quarter of 2021, which is the lowest level since 2012.

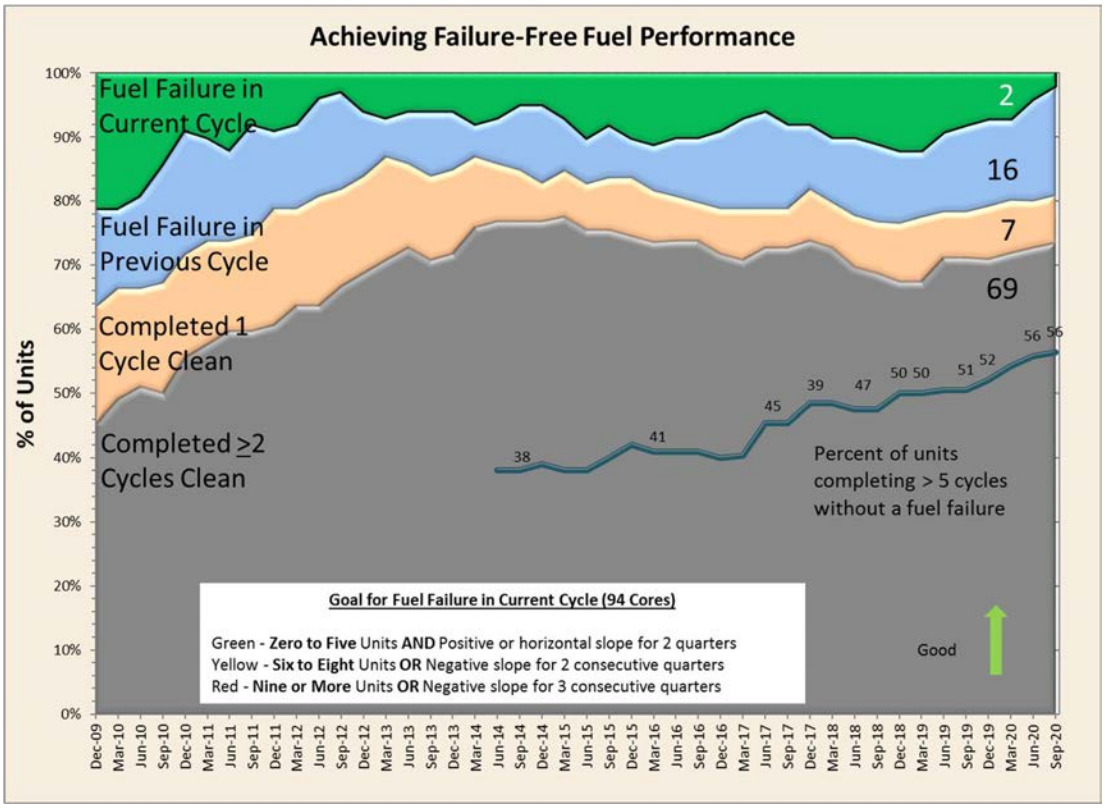

FIG. 5. Failure trends in the US nuclear power plant fleet in the last ten years.

RECENT CANADIAN FUEL PERFORMANCE

W.A. GRANT, M. SECOR
Canadian Nuclear Safety Commission,
Ottawa, Canada

Abstract

The paper summarizes the CANDU fuel design and operating environment, describes recent fuel performance challenges experienced by the Canadian industry and discusses the regulatory response and perspective of the CNSC. A review and status update on the specific fuel condition issues related to post-refurbishment debris fretting excursions, endplate cracking and fuel deposits is included. Fuel performance trending, defect detection capabilities/effectiveness and defect root cause investigations are also be discussed in a limited capacity.

1. INTRODUCTION

In Canada, there are 19 operating nuclear power reactors across six licensed stations. All existing power reactors are based on the Canadian Deuterium Uranium (CANDU) design and are regulated by the Canadian Nuclear Safety Commission (CNSC). The paper outlines the regulatory perspective on the efficacy of the Canadian industry in overseeing fuel condition and managing fuel safety issues. First, a generic background on the CANDU reactor, fuel design and defect detection capabilities are provided to frame the readers understanding of the technology. Next, a brief explanation of the importance of fuel safety is provided before moving into recent and historic fuel performance challenges. The paper concludes with a summary of the regulators position on the fuel performance programs across the Canadian reactor fleet.

2. CANDU TECHNOLOGY

2.1 CANDU Design Overview

The generic CANDU design presented in Figure 1 is a pressurized heavy water reactor that separates the partitioned primary coolant circuit loops from the secondary steam circuit. The primary heat transport system (PHTS) is generally divided into two coolant loops, each comprised of a lattice of horizontal, pressurized fuel channels suspended in a low-pressure heavy water moderator. A string of natural uranium fuel bundles is positioned within each fuel channel and is cooled by heavy water driven by a set of large heat transport system (HTS) pumps. The number of fuel channels varies with reactor design but ranges from 360 to 480, each containing 12 or 13 fuel bundles. For a generic reactor, this amounts to more than 5000 fuel bundles being in the core at any given time. The use of natural uranium fuel necessitates on-power fueling to maintain criticality. This is accomplished by pairs of fueling machines that can service each fuel channel to simultaneously deliver new fuel to one side of a channel while accepting irradiated fuel at the other. Generally, a total of 12 to 16 bundles in groups of four or eight bundles per visited channel are fueled each day to maintain normal operations. Defueled bundles are transported to an on-site irradiated fuel pool (IFP) where they are stored in light water for many years before being transferred to dry-storage canisters.

2.2 CANDU Fuel Design

Modern CANDU fuel bundles consist of 37 fuel elements, which have a collapsible Zircalloy-4 sheath, arranged in concentric rings of 6, 12 and 18 elements around a single central element. Fuel elements are capped at both ends and suspended in place by welds to a pair of thin webbed endplates that bookend the fuel bundles. Contact between elements within a fuel bundle or between an element and the fuel channel is prohibited by the inter-element Zircalloy spacer pads and outward-facing Zircalloy bearing pads, respectively. Within each fuel element lies a string of roughly 30 ceramic, high-density natural uranium fuel pellets, all shaped to accommodate thermal expansion and fission gas production. Finally, to promote heat transfer and prevent stress-induced cracking, a thin graphite-based compound is applied to the inside of the elements and the elements are back filled with Helium gas. Each bundle is assigned a unique serial number that is imprinted by the manufacturer on the endplates. The serial numbers identify the manufacturer and fuel type and are used to track fuel position during operations and in storage.

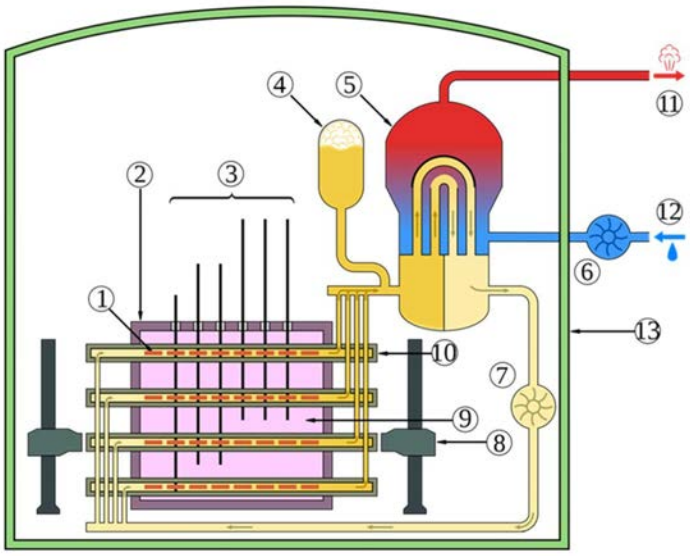

1	Fuel bundle
2	Calandria
3	Control rods
4	Pressurizer
5	Steam generator
6	Feedwater pump
7	PHTS pump
8	Fuelling machine
9	Moderator
10	Fuel channels
11	Steam
12	Feedwater
13	Containment structure

FIG. 1. Cross section of CANDU Reactor (Inductiveload, 2007).

2.3 Failed fuel detection

In addition to manual chemistry grab sample analysis that can detect the presence of a defect within a PHTS loop, there are three systems linked to the CANDU reactor design that are able to detect the presence of defected fuel: the gaseous fission product (GFP) system, the delayed neutron (DN) system and feeder scans.

The GFP system provides continuous sampling and monitoring of the reactor core and can detect elevated levels of radioactivity in a particular loop but is not able to identify the channel containing the defected fuel nor the burnup of the defected fuel. In some cases, the GFP system can estimate the severity of the defect using a ratio of Xenon to Krypton isotopes.

The DN system can be used at-power and may be run routinely or following an indication of a fuel defect from another system. The system draws a sample of the coolant coming from the outlet of a fuel channel and diverts the flow to a sampling room where short-lived fission-products can be detected. The resolution of the DN system can detect bundles with small defect sites and can accurately identify the channel containing the defect.

Feeder scans may be used to detect severely defected fuel after the unit has been shut down. This is done through measuring the presence of fission products by passing a gamma-sensitive detector across the downstream feeders. The effectiveness of this method is diminished over the operating life of the reactor as noise becomes introduced into the signal owing to the fields that build up on the outlet feeders after long periods of operation.

3. FUEL PERFORMANCE MANAGEMENT

The fuel pellet and fuel sheath act as the first and second physical barriers against the release of radioactive fission products. Protection of the fuel through robust design, controlled operations and an effective monitoring program are crucial to operational fuel safety and are the essential means of ensuring the fuel condition remains within the design envelope. In support of the CNSC mandate to protect the health and safety of Canadians and the environment; at the time of first licensing, all licensees are issued a set of dose limits, to which they are accountable. Deviations from the fuel's normal operating conditions can lead to degradations in the fuel condition that may have the potential to challenge the site dose limits under certain accident conditions. An extensive but not necessarily complete list of fuel degradation mechanisms associated with CANDU fuel can be found in Table 1. The primary heat transport fission product inventory and in particular iodine-131 levels affect the safety case, specifically in a theoretical containment bypass accident. As such, regulatory limits and the safe operating envelope define limits which the operator must adhere to. Generally individual defects are not a threat to the overall safety case of the plants. Due to the iodine spiking phenomena the concern is many small defects that will

simultaneously ‘wash out’ upon a unit shutdown. As such removal of even small defect is considered important to maintain safety margins.

Both the licensee and the regulator have important roles in overseeing fuel safety.

2.4 The role of the licensee

The accountability for on-site fuel safety lies with the holder of the power reactor operating license. To ensure that the fuel condition remains within the design and qualification envelope, the license holders are required to restrict the fuel operating environment to a defined safe operating envelope (SOE) that, through supporting analyses, has been proven to prohibit unsafe fuel conditions. Operational fuel safety is complimented by the establishment and oversight the fuel design program, quality assurance program and foreign material exclusion practices as well as the fuel handling, fuel management and fuel surveillance programs. Routine inspections of recently discharged fuel acts as a surrogate for in-core fuel inspections and are used as a basis to verify the active fuel’s fitness-for-duty. In-bay inspections are performed post-discharge in the IFP and are generally limited to observations of deposits, evidence of material interactions and other visual indications. The capability for visual indications is typically limited to the peripheral rods but when warranted, in-bay or off-site bundle deconstruction and testing may be performed. The licensee records and trends the inspection findings and reviews the data periodically to identify and address developing threats to the bulk fuel condition.

When the defect detection system(s) annunciate that a defect may be present in-core or, when in-bay inspections reveal an unanticipated fuel condition that may be a precursor to fuel defects, actions are taken relative to the incremental risk introduced by the degradation in fuel condition. Local defects are targeted and defueled from the core while the reactor is on-power whereas issues impacting the general fuel condition prompt assessments to determine the appropriate path forward. If a bundle has been identified as having a defect but the root cause isn’t able to be determined during inspection in the IFP, the bundle, element, and/or component is often shipped off-site for a post irradiation examination (PIE) at a qualified hot cell.

2.5 The role of the regulator

The regulator is responsible for verifying compliance with licensing requirements, assessing licensee fuel programs and evaluating industry fuel performance. REGDOC-3.1.1, *Reporting Requirements for Nuclear Power Plants* [2], requires licensees to report to the CNSC using event reports for situations or events of higher safety significance and that may require short-term action by the CNSC, and to submit routine scheduled reports on fuel monitoring and inspections. These reports are used by the regulator to verify that the licensee has effectively controlled the environment of the fuel to within the accepted limits. In situations where the regulator believes that the fuel condition is no longer bounded by the existing licensing envelope, they may impose operating restrictions or constraints proportional to the safety issue, such as enhanced monitoring or power derates, until fuel safety can be re-affirmed. Trending of licensee and industry fuel performance is also performed to allow for pro-active actions to be taken to counter negative trends. In addition to the specific and annual reporting, periodic inspections of the fuel programs are carried out alongside intermittent checks to ensure that the safety analyses and safety analysis tools are maintained and updated within reasonable timeframes.

TABLE 1. KEY DEGRADATION MECHANISMS AFFECTING CANDU FUEL CONDITION [2]

Degradation category	Observable effect	Key influencing parameters	Impacts relevant to safety
Deformation without material loss	Sheath collapse and ridging	Coolant pressure, Temperature	Mechanical strength, Heat transfer
	Sheath ballooning (uniform) or bulging (non uniform)	Internal gas pressure, Temperature	Mechanical strength, Heat transfer, Loss of sheath integrity
	Pellet/clad mechanical interaction	Power ramps	Loss of sheath integrity
	Element bowing	Loads, Temperature	Mechanical strength, Heat transfer
	Endplate deformation	Loads	Mechanical strength, Heat transfer
	Bundle drooping, sagging	Loads	Mechanical strength, Heat transfer
	Athermal sheath strain	Loads	Loss of sheath integrity
Deformation with material loss	Fretting	Interaction with debris	Loss of sheath integrity
	Bearing pad wear	Interaction with pressure tubes	Heat transfer, Impact on PT condition
	Spacer wear	nteraction between elements	Heat transfer
	Scratching, nicks	Interaction with in-reactor components	Loss of sheath integrity
Change in material properties	Sheath oxidation	Temperature, Coolant chemistry	Mechanical strength, Heat transfer
	Hydriding	Coolant chemistry	Mechanical strength, Sheath temperature
	Stress corrosion	Power ramps, internal gas composition	Loss of sheath integrity
	Crevice corrosion	Coolant chemistry	Impact on PT condition
	Material phase transitions	Temperature, irradiation	Mechanical strength
	Fuel grain growth	Temperature, irradiation	Heat transfer
	Internal gas pressure and composition change	Burn-up, Temperature	Heat transfer, stress corrosion
Integrity failures	Endcap to sheath weld failures	Manufacturing defects, Loads	Loss of sheath integrity
	Endcap to endplate weld breaks	Manufacturing defects, Loads, fatigue	Mechanical strength
	End-plate cracks	Vibration, Loads, fatigue	Mechanical strength

4. RECENT AND HISTORIC FUEL PERFORMANCE CHALLENGES

4.1 Post-Refurbishment Debris Fretting

CANDU reactors may undergo a life-extension refurbishment after roughly 30-40 years of operations. A key activity undertaken during a refurbishment is the replacement of primary heat transport components, specifically pressure tubes and feeder pipes. All licensees in Canada have a foreign material exclusion program to prevent contamination of the primary heat transport system, but the scope of the refurbishment activities has in some circumstances, resulted in debris entering the system.

Since 2012 four units have been refurbished in Canada, with two more units currently undergoing refurbishments. Most restarted units have experienced an elevated number of defects due to debris fretting with the magnitude being a measure of the success of their foreign material exclusion program. In the limiting case, up to three defects per month were observed followed by the defect rate slowly reducing over the course of several years.

Removal of debris from the coolant circuit has proven to be difficult with historical attempts to introduce strainers resulting in their degradation and generation of additional debris. The current strategy is to rely upon the fuel to catch the debris and be discharged or settle out. Additionally, the action of the main pumps has been shown to reduce the debris to a smaller less damaging size.

Detection, location, and removal of defect fuel bundles after a refurbishment has proven to be an important activity to ensure that iodine-131 regulatory limits are respected. Fortunately, on power fueling facilitates the prompt removal of defect bundles when the plant systems locate the defect. Typically, the time from detection to removal is on the order of several weeks. Prevention is the most effective risk management strategy as such the CNSC has updated its standard refurbishment inspection suite to include a review of the foreign material exclusion program.

4.2 Endplate Cracking

Figure 2 shows a diagram of an endplate for a CANDU Fuel bundle. The endplate provides the primary structural component that keeps the fuel elements aligned into the bundle structure. The fuel elements are resistance welded to the endplate on each end. If the endplate is significantly damaged, the bundle will lose its structural integrity and disassemble.

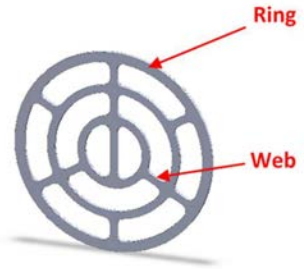

FIG. 2. Endplate structure.

'Endplate Cracking' is damage that produces a through wall crack or break of a web or ring section of an end plate. A single through wall crack or break will weaken the structural integrity of a bundle. Two or more cracks or breaks can, depending on the relative locations, allow a fuel element (FE) to become free and move into contact with another fuel element or the pressure tube (PT). FE/FE or FE/PT contact may eventually lead to a failure of one of the components.

Endplate cracking is believed to be caused by acoustic vibrations created by the main pump in the primary heat transport system. The passing frequency of the pump impellors is close to the natural frequency of the fuel bundles for CANDU reactors, and some feeder pipe designs are unable to adequately dissipate these pressure waves before they reach the connected fuel channel. The degree of damage has varied by plant.

The regulatory perspective of endplate cracking is that it is evidence that the bundle design is not qualified for the operating environment. Thus, it is a level one defence in depth issue. Deviations from the bundle design geometry are not typically accounted for in the safety case for plants and thus endplate cracking needs to be addressed for plants that exhibit this phenomenon.

Several solutions have been implemented to address the issue. One plant, which on initial start-up had significant issues with endplate cracking, resolved the problem by employing a seven-vane impellor pump design (instead of the original five-vane design) to move the acoustic frequency out of the bundle's natural frequency range. Another station in Canada which has been experiencing a much lower level of endplate cracking over its lifetime are presently looking into a bundle redesign to enhance bundle mechanical strength to resolve the issue.

4.3 Fuel Deposits

Fuel deposits are commonly seen on fuel bundles in every CANDU reactor. Carbon steel feeder pipes are the primary source of the iron oxide deposit material. The frequency and magnitude of deposits are managed by tightly controlled chemistry practices and typically, they are limited to small, localized flecks of iron oxide about the size of a piece of ground pepper. These small deposits have not posed any hazard to the fuel sheaths.

The Primary Heat Transport (PHT) system has several sources of iron oxide such as the feeders and headers. Flow assisted corrosion of these components introduces iron into the system. Lower operating pH levels have been shown to reduce feeder corrosion however they also inverse the solubility dependence on temperature in some ranges resulting in the iron oxide deposits forming on hot surfaces such as the fuel.

Recently there have been two instances of fuel deposits which raised regulatory interest. The first instance resulted from an operator changing the normal operating chemistry pH to decrease feeder thinning rates and led to thick iron oxide deposits near the bundle bearing pads. In the second instance, a chemistry control issue during the hot conditioning of the PHT system, led to thin deposits covering the entire fuel sheath. During commissioning, the PHT system is hot conditioned to develop a protective magnetite layer on the feeders to resist and reduce corrosion during subsequent operations. Typically, this activity is done with fuel in the core, but not used as heat source, however in this case the fuel was used as the heat source. A loss of control of pH happened during the hot conditioning, leading to deposits of magnetite not only on the feeders but also over the fuel sheath surface.

Both iron oxide deposits observed were porous and mostly magnetite or hematite. The deposits act as a thermal insulator, increasing the local temperature underneath. The thicker deposits were porous in nature and allowed water to still reach the sheath through channels. This phenomenon, known as wick boiling, is common in BWRs but was formerly unseen at CANDU plants. It is effective at cooling unless the pores get blocked, creating a trapped steam bubble against the sheath. Blocked pores occurred at the plant with thick deposits. Those deposits compacted and became adherent and insulating, leading to elevated sheath temperatures and the transformation of some of the sheath material to zirconium oxide. A sheath oxide layer (ZrO_2) naturally exists between the fuel sheath (Zircaloy Metal) and the deposit. Small pores in the CRUD layer can extend to the sheath oxide layer and form the channels needed for wick boiling.

All fuel sheaths experience some level of sheath oxidation (formation of a ZrO_2 layer) during their operational life. At the normal operating temperatures for CANDU fuel, the oxidation rate is very slow and results in typical sheath oxide thicknesses of roughly five microns on spent fuel.

The oxide layers observed under thick deposits were more than the fitness for service limits. A return to the previous PHT system pH levels and an extensive monitoring program was able to resolve the issue and ensure safe operations until the deposit formation reversed, and the oxidized bundles were removed from the core through normal fuelling.

The second fuel deposit event which occurred as part of commissioning activities of units following a refurbishment had only thin deposits and didn't produce significant zirconium oxide layers. The concern centered on the thermal cooling capabilities during a hypothetical accident situation, such as a loss of coolant or loss of flow event. The deposits were slowly removed by operations, but the regulatory action was to preclude the operator from performing additional hot conditioning activities until they could demonstrate they could do so within the safety case.

The two instances identified the need to better document chemistry challenges with respect to prevention of fuel deposits for PHWR reactors. The 'Technical Meeting on the Control and Monitoring of Coolant Chemistry and Related Issues on Fuel Reliability in Pressurized Heavy Water Reactors T1-TM-1804474' was held in November 2019 to discuss this recent OPEX with the aim of developing an IAEA report on the subject. The

industry has also performed some experiments on better understanding the hot conditioning chemistry control requirements to prevent further reoccurrences.

5. INDUSTRY-WIDE FUEL PERFORMANCE REVIEW

All the recent and historic fuel performance challenges noted in section 4 have been localized in time and to specific units. In each case, investigations into the issues were launched, the factors contributing to the abnormal fuel condition were identified and actions to resolve the fuel safety issue(s) were taken. In most cases, on-power refuelling assisted the operators to quickly identify the issue as well as to gauge the effectiveness of the corrective actions. Residual performance issues have been judged to have a negligible impact on operational fuel safety.

Across the Canadian industry, the management of fuel performance has generally met the CNSC expectations with respect to yearly defect rate and defect residency time. Safe fuel performance in Canada has been assured by the licensee and the regulator through vigilance in the oversight of the fuel operating environment, responsiveness in detecting and arresting abnormal fuel conditions and through the trending of fuel inspection observations to pro-actively identify and arrest negative conditions.

6. SUMMARY

The industry and the regulator both contribute to ensuring fuel safety and safeguarding the public from the harmful effects of radiation. The fuelling and defect detection systems at CANDU plants support the prompt detection and removal of defects and enable the level of operational risk to be identified and controlled. Recent refurbishment activities have introduced debris causing fuel fretting, chemistry issues have created fuel deposits and a historical design weakness has damaged endplates. In each case, the effects of the fuel safety issue were observed, the cause was identified, and risk-informed actions were taken to restore the fuel condition. Generally, infrequent operating issues and low defect rates from Canadian reactors are evidence of a robust design and effective fuel oversight.

REFERENCES

[1] Inductiveload, “CANDU Reactor Schematic,” 08 10 2007. https://commons.wikimedia.org/w/index.php?curid=2872419. [Accessed 18 09 2020].

[2] VIKTOROV, A., COUTURE, M., SUK, H. C., Application of "Fitness for Service" Concept to Evaluation of CANDU Fuel Performance, SMiRT, Toronto, 2007.

REVIEW OF DEFECT ROOT-CAUSE POST-IRRADIATION EXAMINATION (PIE) OF PHWR FUELS AT CNL, AND RELATED DEVELOPMENTS IN PIE AT CNL TO SUPPORT DEFECT ROOT-CAUSE EXAMINATIONS FOR PHWR UTILITIES

S. CORBETT
Canadian Nuclear Laboratories (CNL),
Chalk River, Canada

Abstract

Canadian Nuclear Laboratories (CNL) has extensive experience conducting post-irradiation examination (PIE) of both intact and defected Pressurized Heavy Water Reactor (PHWR) fuel. Defect root-cause examinations are challenging when a primary defect cannot be located or positively identified. PHWR fuel element/bundle manufacturing and nuclear plant operations have improved over the last few decades with gained experience (including more robust quality assurance practices), along with improved conditions in-core, resulting in lower defect rates. Concurrently, in-core defect detection methods have improved, enabling detection of fuel defects earlier. With fewer, more quickly identified and removed defects, it is difficult to diagnose root causes not attributable to debris fretting. The paper summarizes several recent fuel element failure investigations conducted at the Chalk River Laboratories (CRL), including methods used, some key performance results, and some of the technical challenges faced. Also discussed are some newer CNL PIE tools and techniques to improve locating and investigating primary defect causes to increase the likelihood of positively identifying the root cause of fuel element failures.

1. INTRODUCTION

Canadian Nuclear Laboratories (CNL) has extensive experience conducting post-irradiation examination (PIE) of intact and defected fuel elements for Canadian Pressurized Heavy Water Reactor (PHWR) utilities (i.e., CANDU fuel elements/bundles). This includes examination of experimental fuel elements (with planned an unplanned defects) irradiated in the National Research Universal (NRU) and National Research Experimental (NRX) research reactors at the Chalk River Laboratories (CRL). Although infrequent, defects can have a significant effect on overall health, safety, and economics of an operating reactor. Related work previously published by the CANDU Owners Group (COG) compiled historical data on defected PHWR power reactor fuels [1]. The work presented here includes a summary of more recent PHWR fuel element defect root-cause examinations performed at CNL from 2002-2018. A brief overview of how defect root-cause examinations are conducted is provided in Section 2. Section 3 includes a review of recent defect root-cause examinations (from ~2002-2018). Emphasis is given to fuel elements where the root cause of failure could not be determined, highlighting some of the technical challenges faced during such examinations, and improvements made to related PIE activities during recent years. Some ongoing developments expected to support defect root-cause and other PIE projects at CNL are briefly discussed in Section 4.

A fuel element defect (for the purpose of the paper) is defined as a through-wall path in the sheath (i.e., cladding) or endcap regions created during manufacturing or irradiation, that led to heavy water coolant ingress into the element but is not attributed to wear-related failure modes. Primary defects are associated with regions where coolant (heavy water in PHWRs) initially enters a fuel element. If this occurs, the dissociation of oxygen and hydrogen (deuterium in the case of heavy water reactors) can lead to "secondary" damage at locations remote of the primary defect, including additional through-wall defects, the extent of which is dependent on the size of the initial defect and its incubation time at a given element linear power. Primary defects such as those associated with internal hydrogen (H) contamination (e.g., from under-baked CANLUB or excess pellet moisture) [2] can result in high H concentrations in sheath or endcap regions, referred to as "hydriding" or "primary hydriding" defects. Through-wall defects with very high deuterium (D) and low hydrogen content suggest the defect was the direct result of subsequent exposure to heavy water coolant (i.e., a secondary defect), referred to as "deuteriding" or "secondary deuteriding" defects. Both primary and secondary defects lead to sheath hydrogen/deuterium (H/D) embrittlement in one more region of a fuel element. It can be difficult to determine if an observed defect is primary or secondary in nature; more recently, H/D analysis is performed using High-Vacuum Extraction Mass Spectrometry (HVEMS) to help differentiate between primary and secondary defects (discussed further below).

In PHWR fuel, primary defect mechanisms are attributed to three major failure modes: 1) fabrication-related defects such as incomplete end-closure welds, porosity within endcap barstock or primary hydriding from under-baked CANLUB coating with excess hydrogen; 2) operational-related defects such as debris fretting, abnormal

fuel handling, or acoustic resonance within the fuel channels; and 3) design-related defects that can be created during operation, such as stress-corrosion cracking (SCC) during high-power operation or circumferential end-cap cracking [1]. No additional failure modes have been positively identified in recent years. The most common primary failure mode in PHWRs is related to fretting wear from small foreign materials inadvertently introduced into the primary heat transport system (PHTS); such failures are not discussed here. In some cases, positive identification of a primary defect can be difficult, and visual clues along the element surfaces may not be present or entirely apparent. Furthermore, secondary damage that occurs after the formation of the primary defect could potentially mask evidence of the primary defect. An intact fuel bundle in a PHWR reactor will typically reside to an average bundle burnup of about 7500-9200 MWd/tM (180-220 MWh/kgU) before discharge (approximately a one-year residency period); therefore, high-burnup related defects are not a major concern for Canadian PHWR fuel.

2. DEFECT ROOT-CAUSE EXAMINATION METHODOLOGY

The main objective of a defect root-cause examination is to deduce the mode of fuel element failure, using a methodology that begins with non-destructive examinations (NDE) followed by destructive examinations (DE). Following defect detection and discharge from the core, the cause of failure is initially examined underwater via remote camera system in an irradiated/spent fuel bay at the reactor site. If the observed defects cannot be easily attributed to a specific failure mode (e.g., debris fretting), the defected elements (possibly including an intact "control" element) may be removed from the bundle shipped to CNL for non-destructive and destructive examinations (NDE, DE) to determine the root cause of failure. Other information such as the bundle's power, burnup and refuelling shift histories are provided by the utility to compare the NDE and DE results against fuel performance baselines.

2.1 Non-Destructive Examination (NDE)

2.1.1 Visual Examination

At CNL, defected fuel elements first undergo a detailed visual examination in a hot cell at four planes (0, 90, 180, and 270 degrees) using an in-cell macroscope (up to 27x magnification) and USB-3 colour cameras Fig. 3 includes examples of the typical high-magnification resolution that can be achieved during NDE. These images also illustrate the difficulty in positively identifying possible defect locations. Although usually flagged as "areas of interest", it is not always practical to destructively examine every anomalous feature observed during NDE, mainly due to cost and facility time associated with doing so.

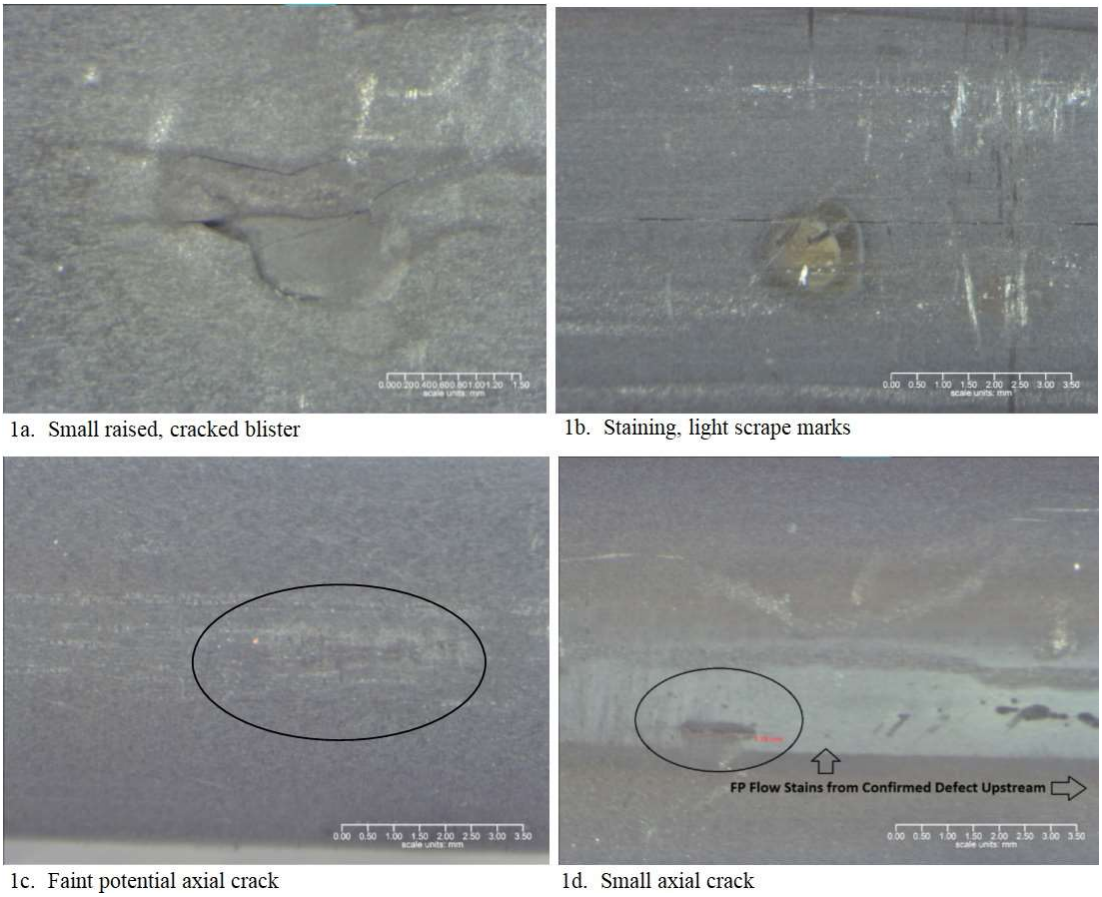

1a. Small raised, cracked blister

1b. Staining, light scrape marks

1c. Faint potential axial crack

1d. Small axial crack

FIG. 3. Fuel Element Features Observed During NDE.

2.1.2 Profilometry and Gas Puncture

During a defect root-cause examination only intact control elements can undergo profilometry to measure residual sheath strain; defected elements can pose contamination/dose concerns during maintenance and storage of the profilometer. Sheath strain in a normally operated fuel element is usually benign, ranging from slightly compressive to slightly tensile, with highest strains observed at pellet interface regions (forming sheath ridges). Control elements are also typically punctured to collect and measure total gas volume within the free element. Gas volumes under 10 mL suggest benign fuel operation, and subsequent gas composition analysis is usually not required (the gas overpressure low-probability defect threshold for 37-element PHWR fuel elements is ~100 mL [3]). Gas compositional analysis includes a measured inventory of Xe and Kr isotopes, the main constituents of fission-gas to determine the percent of fission-gas release (FGR) from the fuel. Higher %FGR is typically correlated with higher-power and/or higher-temperature operation, increasing the likelihood of observing SCC-related defects.

In Fig. 4 the black line shows the average diameter profile of a control element from a PHWR power reactor, irradiated under normal operating conditions (NOC) irradiated to a burnup of ~5000 MWd/tM (~120 MWh/kgU). The plot suggests the element reference end (RE) experienced slightly higher powers than the non-reference end (NRE) that led to slightly larger sheath ridging. This element had negligible residual sheath strain and very low gas volume, and element outer diameters remained close to nominal (as-fabricated) diameters. In contrast, the red line in Fig. 4 shows the profile of an experimental (NRU-irradiated) fuel element that experienced very high beginning-of-life (BOL) powers (>65 kW/m) and high burnup (about three times greater than nominal PHWR discharge burnup). Very high sheath strains and gas volumes were measured for this element; through-wall stress corrosion cracking (SCC) defects were observed on similarly operated elements from the same bundle. Both elements shown in the plot had similar pre-irradiation element diameters and pellet geometries.

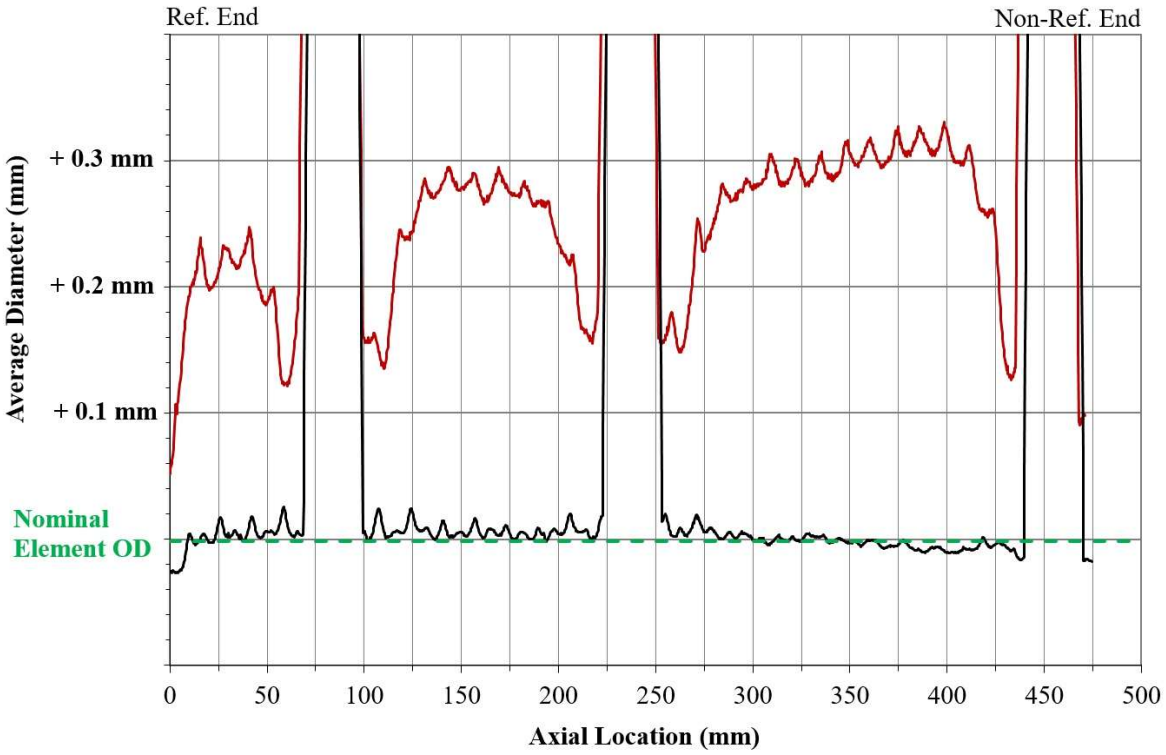

FIG. 4. Two different PHWR fuel element OD profiles (average of three planes) superimposed onto the same plot. Black line is an intact power reactor control element during NOC. Red line is an experimental (NRU) element irradiated at high power to high burnup.

2.1.3 Gamma Scanning

Both defected and intact fuel elements are gamma scanned at 1 mm intervals as part of NDE activities. Based on gross Cs-137 behaviour across a fuel element, gamma scanning can reveal local and gradual power/flux gradients and potential defects along a fuel element. Fig. 5 shows the gamma scan plot of an intact control element and a defected element from the same bundle. The slight gradient observed suggests the left/RE side of the element/bundle experienced slightly higher powers than the NRE. No obvious anomalies are observed in the intact element plot (green line). In the defected fuel element (black line), large Cs-137 peaks can be observed at defect regions, most likely caused by water ingress. The defect region near the element NRE shows an overall dip in Cs-137, indicating some fuel erosion/loss from that region. A large Cs-137 spike was also observed in the gamma scan at the RE endcap region, later confirmed to be defected.

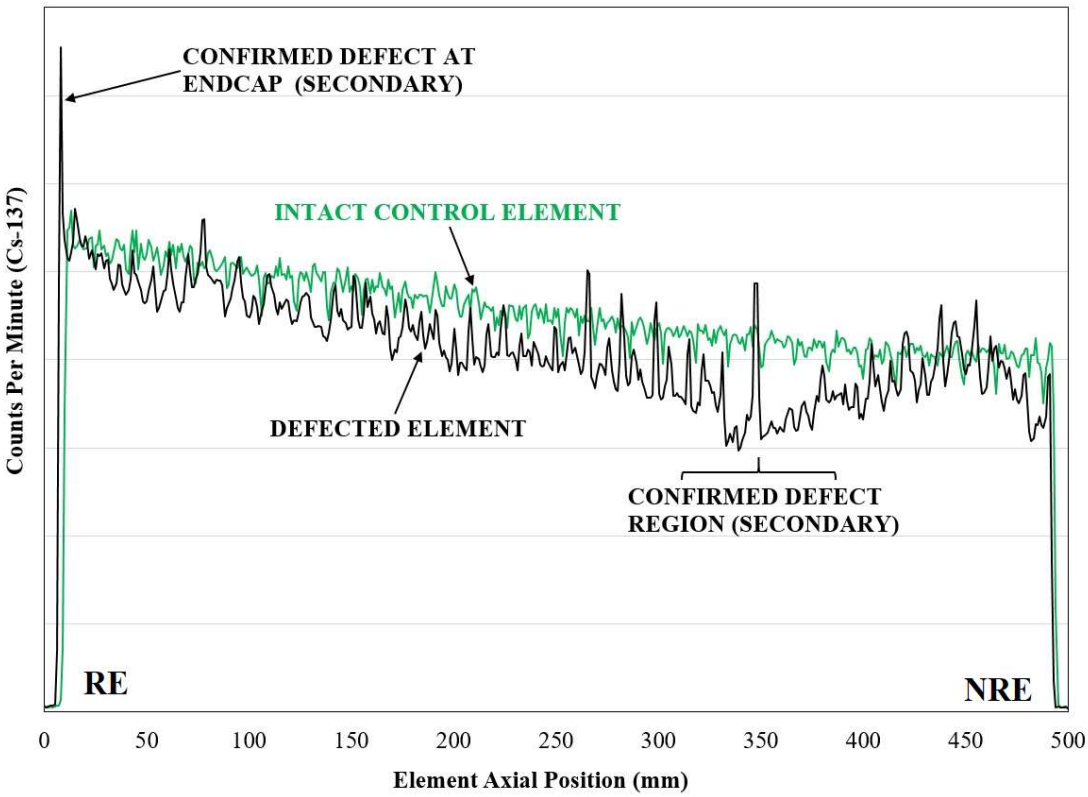

FIG. 5. Gamma scans of an intact control element (green) and defected element (black).

2.2 Destructive Examination (DE)

The information obtained during NDE is used to determine which regions of the fuel element to examine during DE, including potential locations for subsequent metallography and H/D analysis (described further below). Examination of various locations using more than one method (e.g., metallography combined with H/D analysis), allows one to more definitively confirm if a defect is primary or secondary. In the section below, only the major hot cell activities are described; other analytical and optical methods can be employed during defect root-cause exams, including (but not limited to): macroscopy, scanning-electron microscopy (SEM/EDX/WDX), X-Ray Diffraction, hardness testing (although not yet employed during defect examinations), immersion density, oxygen/metal ratio analysis, alpha/beta autoradiography, cladding inner diameter (ID) examinations, and endplate distortion measurements (an NDE technique). The shielded SEM in Chalk River allows for sample access from the hot cell directly to the SEM via a sample elevator, uniquely suited for examination of very high-dose and/or larger sized fuel or material samples. A shielded Focused Ion Beam (FIB) facility is also being commissioned at CNL's Chalk River campus, to assist with micro sample preparation for material property analysis of both fuel and material samples.

2.2.1 Helium Leak Testing

The first destructive activity is usually helium leak testing, where previously selected sections of an element are cut from the element and sealed with Swagelok fittings, then pressurized under water to high internal pressures. Any through-wall defects are identified by gas bubbles streaming from the defect location, as the gas pressure is slowly increased. Some element sections cannot be sealed to perform a leak test, being too close in proximity to confirmed defects, appendages, or other features. Applying the fittings to an element section can be difficult using manipulators; occasionally a fitting has to be re-applied, resulting in a loss of approximately 10 mm of fuel section encompassed around the fitting. In addition, fittings may leak, slip or partially defected endcaps may separate under high pressure, which interfere with visual observations of potential smaller defects. Areas with potential through-wall defects are referenced for potential metallography. Incipient SCC cracks or blisters may also be

forced open by the internal gas pressure, thus revealing their location. There is also potential for oxide to block the through-wall path of a small defect, preventing leaks, even under very high internal pressures.

2.2.2 Metallography (Sheath) and Ceramography (Fuel)

Following leak testing, metallographic samples may be prepared for optical microscopy, concentrating on regions expected to have the greatest likelihood of finding a primary defect. For examination of fuel sheath defects such as axial cracks and blisters, the metallographer grinds to the area of interest and characterizes the defect location under the microscope. For endcap regions, the endcaps are first sectioned along with the weld and some fuel/cladding where possible, then mounted endcap side down. The endcap is first optically examined for piping porosity in the as-polished (AP) condition (and more recently in the hydride etch (HE) condition) by grinding through the endcap spigot weld until the entire back face of the endcap is revealed. The left image in Fig. 6 shows the back of a RE endcap from a defected PHWR fuel element. A heavy distribution of hydrides is revealed around the entire endcap periphery, no hydriding within the central portion of the endcap and no porosity. The anomalous regions appearing as stains were confirmed to be hydrides at high magnification. The endcap is then cut longitudinally in half or quartered to reveal the inside surface of the endcap. The right image in Fig. 6 is a representative cross-section of an endcap. Initially, examination of endcaps is performed in: a) the AP condition to characterize any weld anomalies/defects and the oxide growth; b) the microstructure etch (ME) condition to reveal the overall endcap cladding grain microstructure; and c) the HE conditions to reveal hydride/deuteride concentrations and preferential orientation, if any. The sections are then ground through at set intervals to look for signs of through-wall defects.

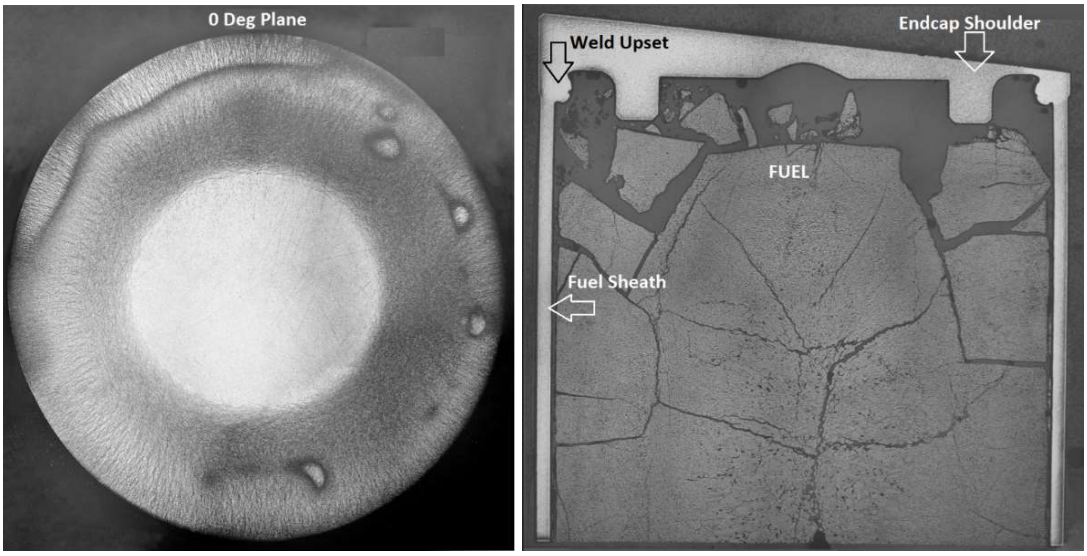

FIG. 6. Left: Endcap showing significant H/D around entire circumference. Right: Example of an endcap cross-section cut longitudinally in half (endcap shoulder also referred to as pellet stop).

More recently, other optical methods of defect examination have been utilized to better assess failure modes, such as fractography of defect sites in the shielded SEM facility. For example, the fracture face of an axial crack was recently imaged under the SEM, shown in Fig. 7. Two distinct failure modes are observed: the embrittled H/D blister region encompassing the sheath OD, and a portion of ductile cladding closer to the sheath ID, where eventual shear failure occurred. The bottom image in Fig. 7 is a metallographic sample of the same defect region (HE condition), confirming the presence of a large H/D blister in the region.

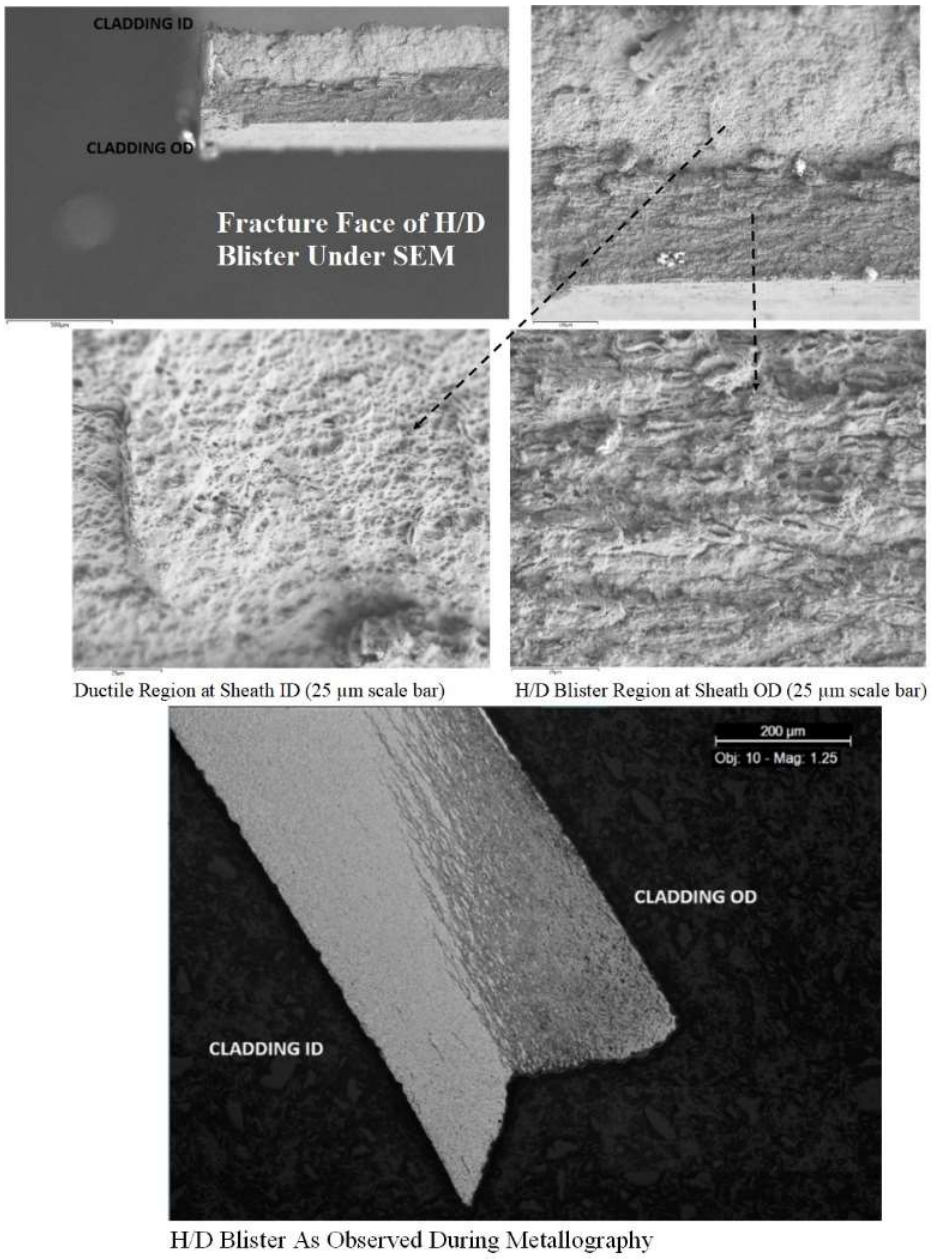

FIG. 7. SEM images showing the cross-section of a defect fracture face. Bottom image shows the defect region via metallography.

2.2.3 Hydrogen/Deuterium (H/D) Analysis

Sections of cladding or endcap regions may be examined for hydrogen (H) and deuterium (D) content. Primary hydride blisters (from excessive internal hydrogen contamination in the element) [2] can have very similar metallographic and visual properties as a secondary deuteride blister (from internal exposure to heavy water). Currently at CNL, High-Vacuum Extraction Mass Spectrometry (HVEMS) is used to measure the content of hydrogen and deuterium (in µg/g or ppm), and the results are used to help discern between a primary hydriding and secondary hydriding (i.e., deuteriding) defect, based on the respective H and D concentrations measured. The hydrogen content specification for as-fabricated fuel is 25 µg/g (maximum), with nominal pre-irradiated concentrations of about 15 µg/g [4]. During irradiation, additional hydrogen pickup (from CANLUB coating and fuel pellets) occurs, and historically observed concentrations have been shown to range from 10 to 80 µg/g [4]. Deuterium content in intact elements has been historically observed up to about 350 µg/g [4].

3. SURVEY OF RECENT DEFECTS EXAMINED AT CNL

This section is a survey of several recent defect root-cause examinations performed at CNL from 2002 to 2018. A summary of each investigation is provided, focusing on fuel elements where the primary defect was not found or positively identified. As previously defined in this paper, a defect is as a through-wall path in the sheath (i.e., cladding) or endcap regions, either developed during irradiation or manufactured, that led to heavy water coolant ingress into the element (not attributed to wear-related failure modes). Typically, the initially observed defects are the result of secondary damage, requiring the primary defect site to be located.

In 2002, three outer-ring elements (06, 15 and 18[1]) and 1 inner-ring element (33), all from different bundles, were shipped to CNL for defect root-cause examination. Through-wall defects included H/D blisters, axial cracks, an element broken in two, and a missing endcap, all concluded to be secondary damage. The root cause of failure for elements 06, 15, and 18 was confirmed to be incomplete endcap closure welds (see Fig. 8). For elements 06 and 15, the primary defect site was found based on leaks observed at the endcap-sheath interface during leak testing. The incomplete closure weld found at the endcap of element 18 initially passed leak testing and was verified as defected by metallography only. The presence of oxide within the discontinuity in the element 18 endcap indicated that it was part of a larger discontinuity that allowed for coolant exposure and therefore oxidize the region. Experience had shown that the leak path can become plugged with oxide and cannot be detected by leak testing, expected to be the reason the endcap passed leak testing. For inner-ring element 33, although visible sheath defects were observed that appeared to be secondary deuteriding, no primary defect site was found. The endcaps were cut into quarters for metallographic examination of the quartered planes, which suggested they were both intact. No evidence of debris fretting, endcap porosity/piping, incomplete welds or SCC was found, and all observed defects appeared to be the result of secondary deuteriding. One defect scenario that could not be ruled out was primary hydriding, which could occur from contamination of the sheath or fuel pellet from a hydrocarbon (e.g., oil, grease, under-baked CANLUB, etc.), but this could not be positively confirmed. At the time, CNL did not have a means for measuring H/D ratios, with HVEMS to be introduced later.

[1] PHWR elements are numbered from 1 to 37 (or 28, depending on the bundle design) for each position in the bundle.

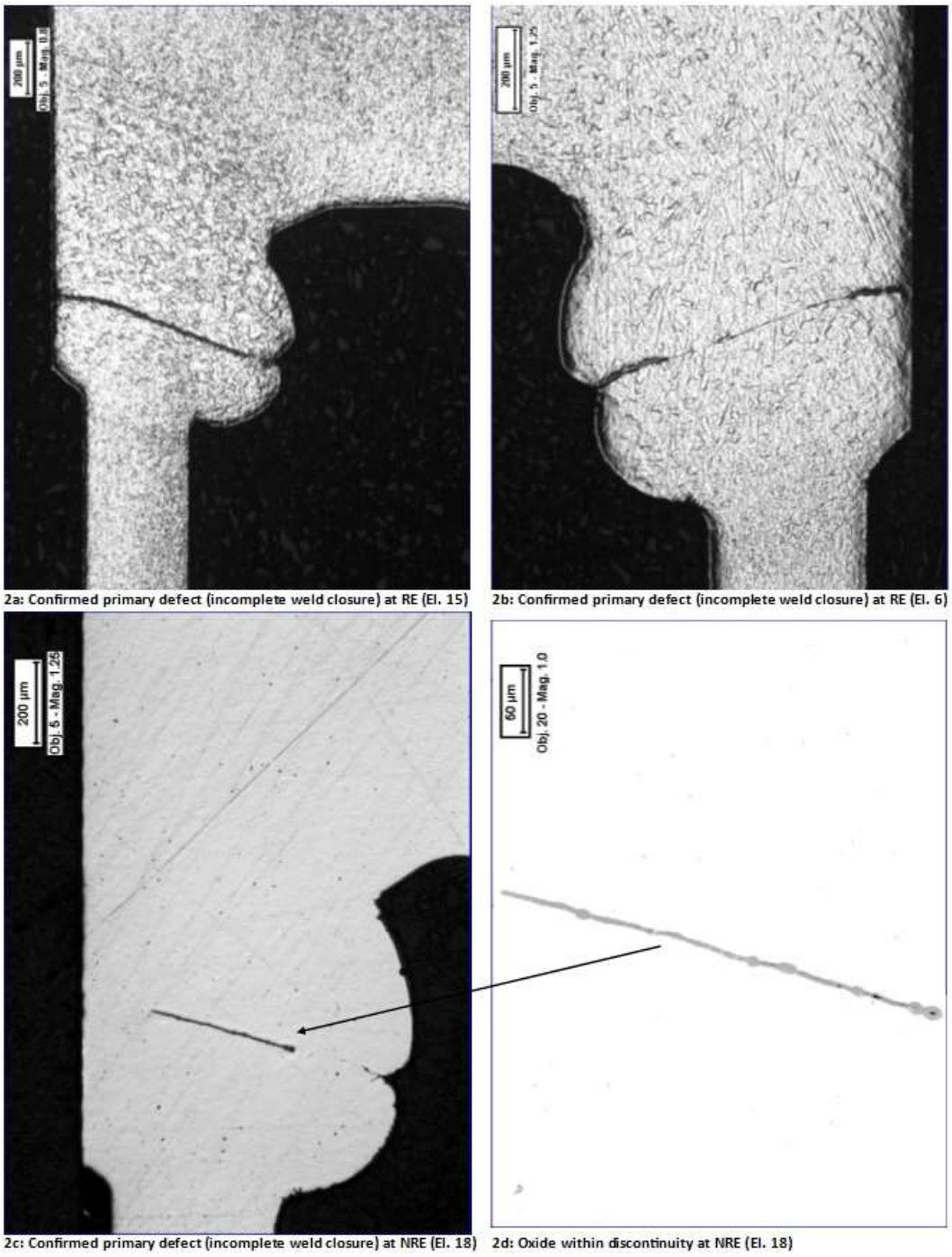

FIG. 8. Confirmed primary defects (incomplete weld closures), elements 15, 06, and 18.

Also in 2002, one outer-ring element (15) was shipped to CNL for defect root-cause examination. The observed defect is shown in Fig. 9 (top image), located between the element centre and NRE. No leaks were found at the element RE. Two other defects were found at the element Non-Reference End (NRE) during leak testing on other side of the NRE BP. There was no evidence of endcap damage or incomplete welds. Metallographic examination revealed H/D blisters at all defect sites. Residual sheath strain and gas volumes for the intact control elements were within the expected range. As a result, the defect root-cause mechanism could not be determined. As H/D analysis was not available at this time, testing for primary hydriding could not be performed.

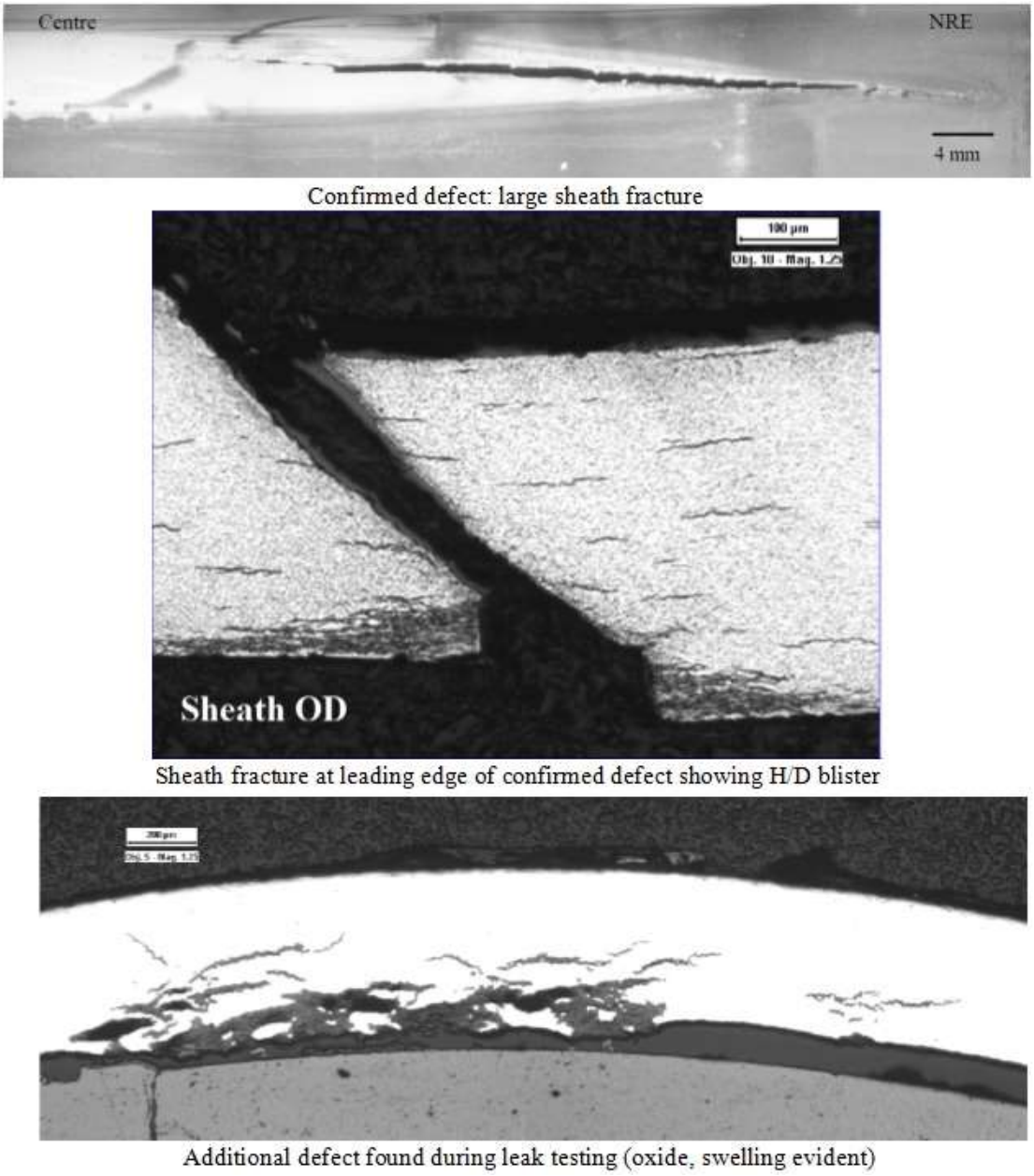

FIG. 9. Defects observed on element 15 (no primary root cause mechanism found).

In 2005, four outer-ring elements (04, 14, 17, and 18), each from a different bundle, were shipped to CNL for defect-root cause examination. Element 04, shipped for having a suspect defect, was confirmed to have been intact following leak testing, and element 17 failed by debris fretting. The root causes of failure for elements 14 and 18 were not determined. Element 14 had a separated endcap that broke off during in-bay dismantling, concluded to be the result of secondary deuteriding. The left images in Fig. 10 are from the separated endcap region, where massive hydriding was observed on the adjacent sheath examined by metallography. Element 18 was observed to have several defects along the sheath, including visible axial splits, cracks, hydride blister near an endcap, and fission product staining, all concluded to be the result of secondary deuteriding. Leak testing and metallographic examination of the endcaps did not reveal any defects. The right images in Fig. 10 show a typical intact weld closure region at the endcap ID. For elements 14 and 18, all endcap closure welds appeared to be acceptable, and examination revealed no evidence of debris fretting, endcap porosity, or SCC. Measured gas volumes from intact control elements were low, and therefore high FGR was not suspected to be a contributing factor. As H/D analysis was not available at this time, testing for primary hydriding could not be performed.

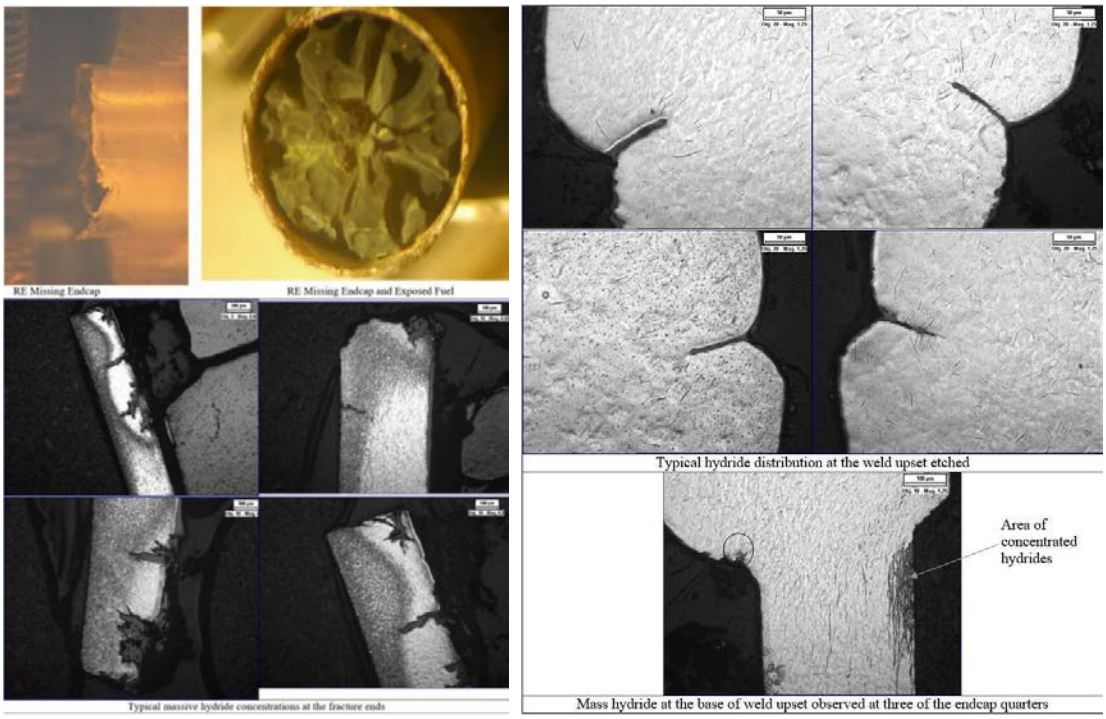

FIG. 10. Left: Secondary damage to RE endcap (element 14); Right: A typical intact weld upset (element 18).

In 2006, two outer-ring elements (09 and 12) were shipped to CNL for defect root-cause examination. Element 12 failed because of debris fretting. Element 9 was concluded to have failed because of a manufacturing flaw or a large load inadvertently applied to the element at the NRE bearing pad location; the defect was located during leak testing. Damage to endcap weld closure regions, including separation of the RE endcap, was concluded to be secondary damage. Metallographic examination revealed a through-wall crack at the base of the bearing pad that was undetected during NDE. The sheath ID 180 degrees from the fracture was damaged (see Fig. 11 for representative images). One scenario was that a load was applied to the bearing pad region during fabrication (before welding the element to the bundle), which cracked the fuel pellets and deformed the sheath surface 180 degrees from the bearing pad. This damage was found to be more likely to occur during manufacture when the element was handled by itself; once welded to a bundle, such large forces were deemed less likely since the element would have significant flexibility and be expected to bend. Additionally, it would be very difficult to damage the opposite side of the sheath (180 degrees from the BP), once the element was welded to the bundle. The other scenario is that the fuel sheath had an incipient crack at the NRE BP region, which may have contained braze eutectic material, creating an environment for crevice corrosion that eventually led to mechanical failure from the applied stresses. In either case, the bearing pad region was concluded to be the primary defect location, but the exact failure mechanism was not determined.

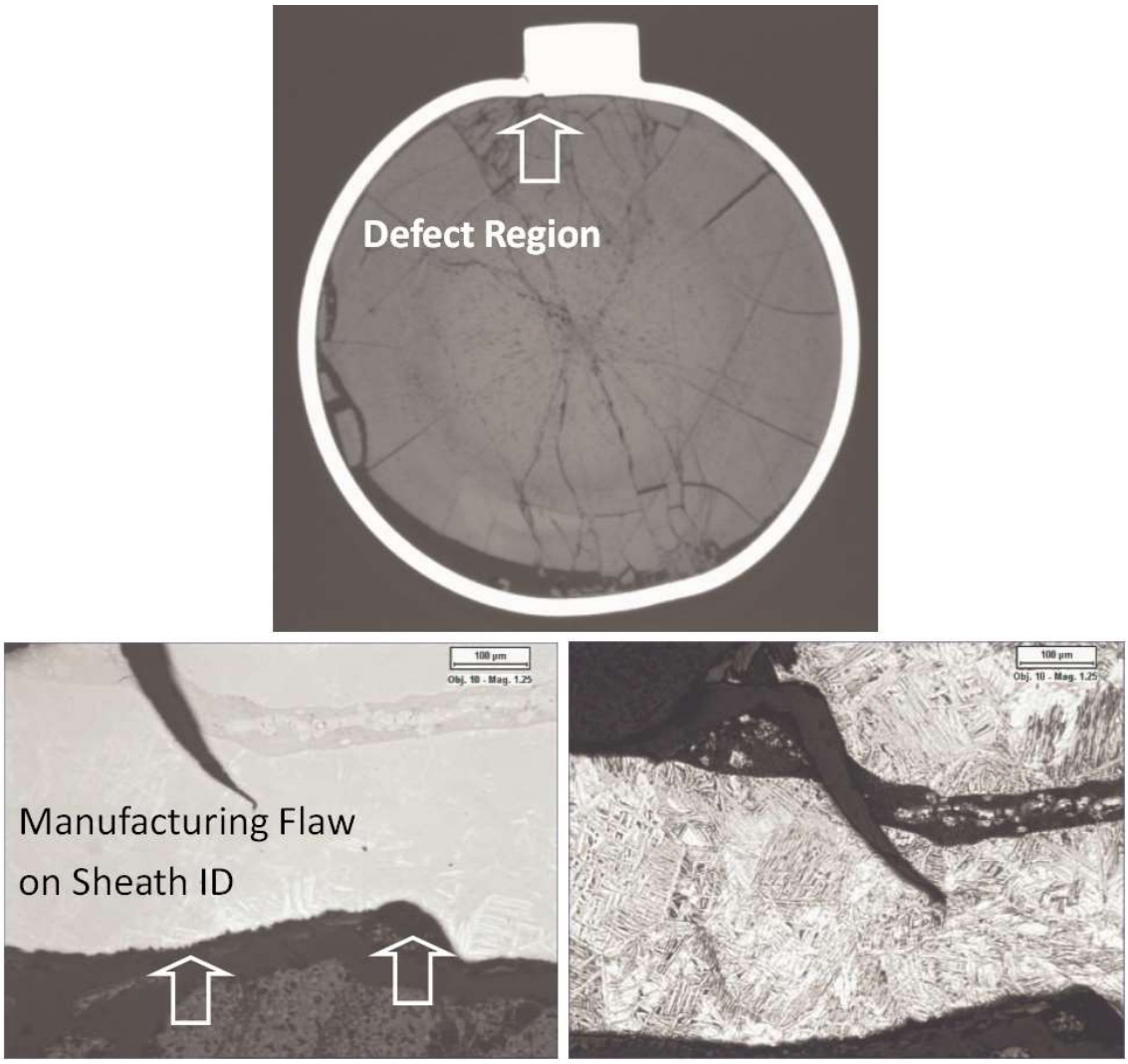

FIG. 11. Manufacturing flaw detected at NRE BP region, element 09.

In 2007, one inner-ring element (32) was shipped to CNL for defect root-cause examination. The observed defect is shown in Figs 12 and 13. No excessive hydriding or closure weld damage was observed at the endcap regions. Adjacent control elements had normal element fission-gas volumes, and no unusual sheath strain, ridging or bowing was observed, ruling out overpower-related defects. No other failures were observed during leak testing. Endcap weld regions appeared intact, and no signs of SCC were observed. Severe hydriding was found at the defect site and the crack regions, suggesting the cause of failure was a large hydride blister at the confirmed defect site. Hydrogen content around the defect site at ~400 µg/g, significantly higher than the manufacturing limit of 25 µg/g and beyond the range of 10-80 µg/g historically observed in irradiated fuel sheath [4]. Deuterium content was approximately 150 µg/g, below the 350 µg/g concentration historically observed in intact fuel sheath. The primary defect mechanism was ultimately concluded to be hydrogen contamination from excessive moisture, following an investigation after the PIE results were issued. Potential sources of excess H include lower-density fuel pellets with higher moisture content, under-baked CANLUB coating, or contamination with hydrogenous organic contaminants (e.g., grease, oil, etc.)

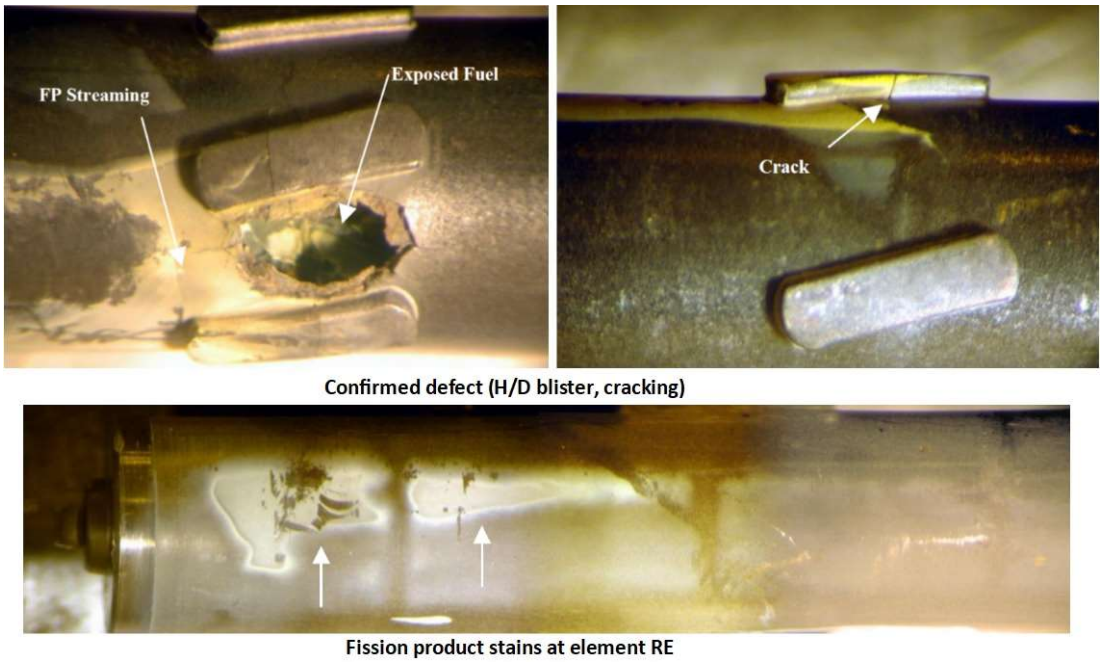

FIG. 12. Open H/D Blister observed between two spacer pads, FP streaming at NRE BP, element 32.

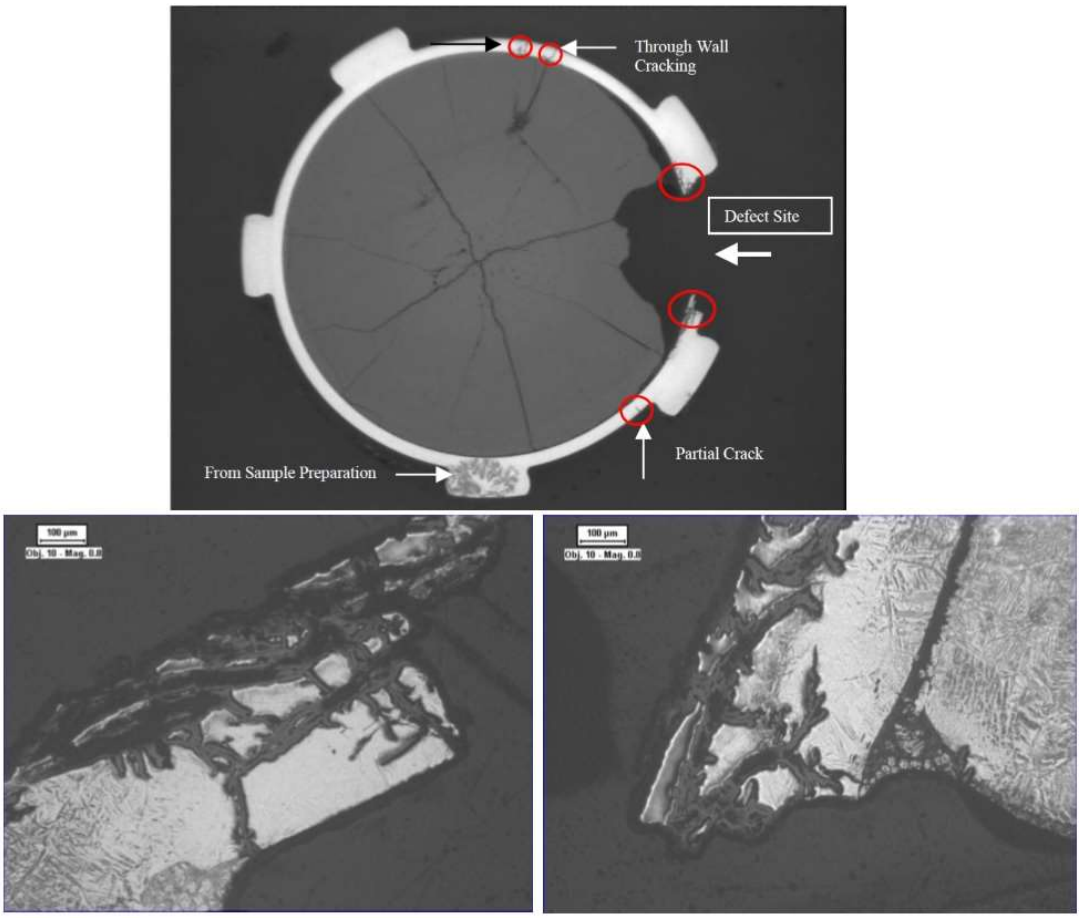

FIG. 13. Location of defect due to primary hydriding, element 32.

Also in 2007, four outer-ring elements were shipped to CNL for defect root-cause examination. The RE endcap from element 07 broke off while removing the endplate piece attached to it during NDE, and no leaks were observed in the remaining fuel element. H/D content was measured in the sheath adjacent to the RE endcap, and a piece of the endcap. The high H content in the sheath (~250 µg/g) and endcap (~2400 µg/g) confirmed that the failure was likely the result of primary hydriding (which occurred during irradiation). For element 09, bubbles were observed coming from the NRE endcap region during in-bay inspection; otherwise, no defects or anomalies were observed along the element. Metallographic examination found a through-wall crack in the closure weld region, which was also heavily hydrided. At 180 degrees from the failed weld region the closure weld was found to be acceptable, with only light hydriding (see Fig. 14). Hydrogen content at the sheath fracture was found to be higher (~70 µg/g) than the deuterium content (~30 µg/g). Primary hydriding was concluded to be the root cause of failure. Similarly, element 10 was shipped with a missing RE endcap. The H content in the sheath adjacent to the endcap was very high (>1000 µg/g), confirming primary hydriding. For element 18, both endcaps had broken off during initial in-bay inspections and were not shipped to CRL. H/D content of the sheath fracture regions adjacent to the missing endcap regions were very high (~1500 µg/g H; ~3500 µg/g D), suggesting the element likely failed as a result of primary hydriding, but some secondary deuteride damage also occurred. Primary hydriding was confirmed to be the cause of failure upon further investigation.

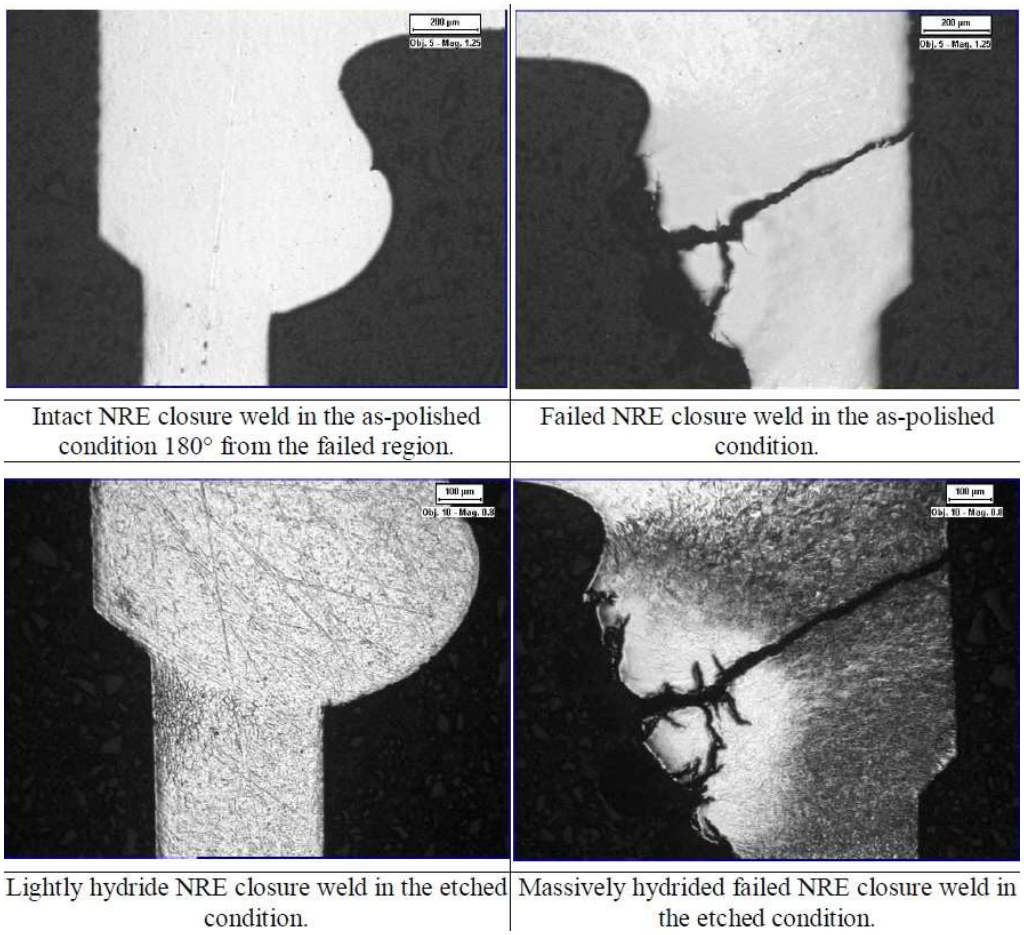

FIG. 14. Defected end-closure weld at the NRE endcap, element "9".

In 2008, six elements from six different bundles were shipped to CNL for defect root-cause examination. The defected elements from one of the bundles failed because of primary hydriding. The defect on a second bundle was the result of debris fretting. The defected elements from two other bundles failed because of incomplete closure welds. For intermediate-ring element 23, the exact defect mechanism could not be determined. This element was observed with a ruptured blister near the element NRE; H/D analysis indicated the blister region had

higher D and typical H content and was concluded to be secondary damage. No leaks were detected at any other location along the element. Metallography of endcap weld closure regions showed they were intact and in good condition. Despite metallography, H/D analysis and leak testing, the primary defect site could not be located.

In 2010, two fuel elements from separate bundles were shipped to CNL for defect root-cause examination. Intermediate-ring element 25 failed because of debris fretting. Inner-ring element 30 failed because of an unknown defect mechanism, and PIE activities ruled out debris fretting, incomplete welds, endcap porosity, gas overpressure, and SCC. Only one small section (120 mm) at the element NRE could be leak tested, because the rest of the element was too brittle from H/D contamination and ruptured H/D blisters to pressurize. Hydrogen contamination (primary hydriding) was not completely ruled out as a possible root cause of failure; the H content taken from two of the defected sheath blister locations was slightly elevated (~90 µg/g H; ~3000 D at one location; ~60 µg/g H; ~3500 µg/g D at the other). The source of hydrogen could not be positively determined, or if it was introduced pre- or post-defect.

In 2012, three elements (9, 13 and 14) from separate bundles were shipped to CNL for defect root-cause examination. Element 9 was determined to have failed by debris fretting. The primary defect site for element 13 could not be identified; PIE confirmed the element did not fail from gas over-pressurization, primary hydriding, incomplete closure welds, or SCC. For element 14, the primary defect site was not located, but sheath irregularities (deep gouges) were observed at one leak site (shown in Fig. 15) up to 40 µm wide and 10 to 90 µm deep, which did not meet the technical specification for Zr sheathing at this location. These were suspected to be manufacturing anomalies that played a role in element failure, where a deep gouge resulted in propagation of through-wall cracking during irradiation that led to coolant ingress, resulting in secondary deuteriding damage and plugging of the primary crack site with oxide. It is important to note that metallography up to 2016 was usually conducted at one planar surface only (including end-cap regions); in 2016 CNL developed and adopted a technique to perform exploratory grinding and imaging to find through-wall flaws. For element 14, primary hydriding could not be ruled out as a possible root cause, observing elevated H (~130 ppm) and also a high D content (~1400 ppm) in the region of the sheath irregularities. The element was suspected to contain an unknown manufacturing defect that could be associated with a primary hydriding failure, or sheath ID flaws that led to the development of a through-wall defect during irradiation.

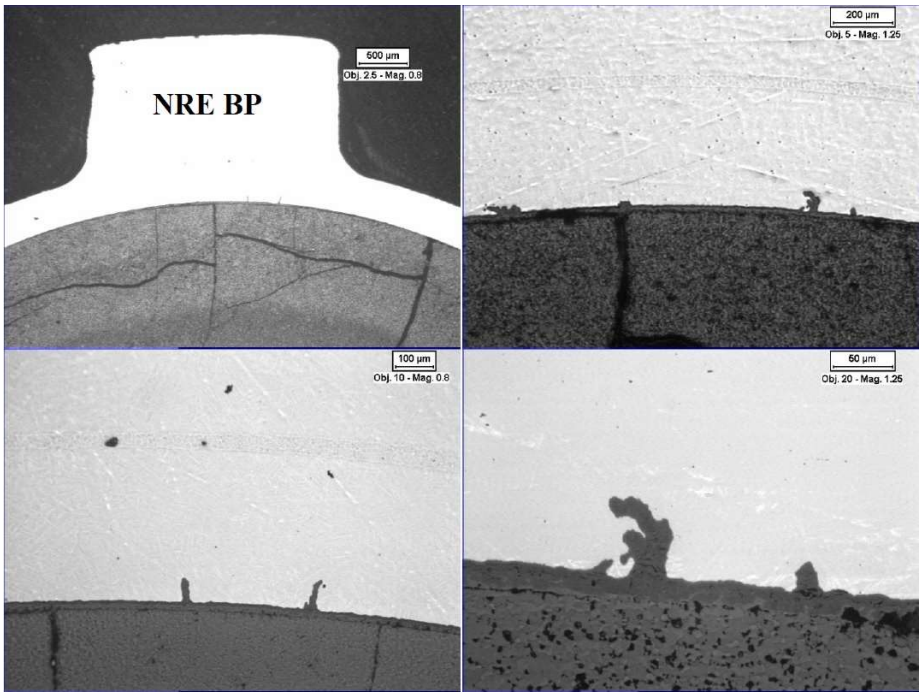

FIG. 15. Oxide-filled sheath ID "irregularities" below the NRE BP, element 14.

In 2014, five defected fuel elements from five separate bundles were shipped to CNL for defect root-cause examination. Element 01 was concluded to have failed by debris fretting. The primary defect site for elements 04,

09, 13, and 15 could not be identified by visual examination, leak testing, sheath H/D analysis or metallographic examination. Primary hydriding, incomplete endcap welds and endcap porosity were ruled out, as well as high-power related defects. In the sheath blister region adjacent to the RE endcap in element 15, elevated H (>350 ppm) and D (>7000 ppm) were measured. The blister was suspected to be a secondary defect, but the source of the elevated H remained unknown, like the 2010 and 2012 defects previously discussed. As suspected during previous defect root-cause PIE, in the presence of a small pre-existing flaw made during fabrication, the bundles would have resided in-core for sufficient time for a through-wall secondary defect to occur.

In 2016, four defected fuel elements were shipped from three bundles to CNL for defect root-cause examination. Element 13 was observed with two defects: an axial crack between the RE and element mid-plane, and an H/D blister near the NRE BP. Both endcaps were observed to be intact and in good condition. The cause of the axial crack was not determined but suspected to be the result of secondary deuteriding. H/D analysis of the crack region (in an as-received zone) indicated approximately 60 µg/g H and 250 µg/g D. Similar to previously observed defects, the blister region (in a heat-affected zone) had a relatively high H content (~250 µg/g) and a very high D content (~5600 µg/g) and concluded to be secondary damage based on the very high D content. The defect root-cause for element 13 was not identified. The examination was not able to rule out possible small manufacturing flaws not detected during leak testing, mechanical damage during pre-irradiation handling of the bundle, or defects associated with the inclusion of a non-hydrogenous material. This was also the first root-cause examination that included optical and metallographic examinations of cladding ID surfaces after defueling and cleaning. No through wall defects were found, even after dye-penetrant testing of the remaining sheath sections. Fig. 16 shows a feature of interest near a pellet-pellet interface region, revealing only oxide deposit at the locations examined. A separate assessment of this element concluded that the axial split region could be the primary failure site, in the form of a pre-existing flaw that occurred during manufacturing, handling, or by debris fretting. During the irradiation, it was suspected that crevice corrosion and oxidation occurred, leading to erosion of the material at the flaw.

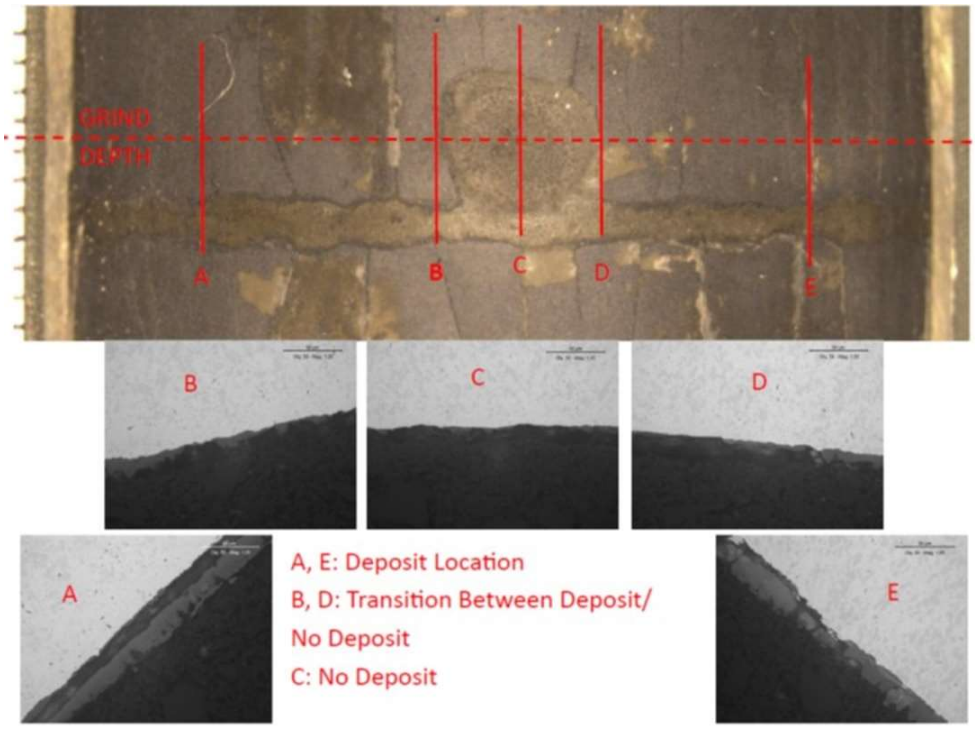

FIG. 16. Area of interest during Cladding ID examination revealing oxide, but no obvious or incipient defects (element 13).

Also in 2016, fifteen defected and seven control elements from a total of ten bundles were shipped to CNL for PIE. Of these fifteen elements, four were concluded to be fretting defects (2, 6, 16, 17), and one element had an incomplete weld (3), shown in Fig. 17. For the other nine confirmed-defected elements shipped (including eight outer-ring elements and one intermediate ring element), the root cause of failure could not be determined. The

endcaps from the nine elements were not observed to leak under high internal pressures during leak testing. The possibility of small weld incompletions (similar, but smaller than that observed for element 3) was not ruled out. Previous experience indicated that through-wall pores can allow for heavy water ingress before plugging up with oxide, allowing secondary deuteriding to occur. These ingress paths typically range from 20-100 µm in diameter and can exist in groups. Considering that element 03 had a high leak pressure and the defect was small, it is possible that smaller weld incompletions could have plugged with oxide during operation, and thus not leaked at high pressure. Also, during this examination, improvements to endcap metallography were developed that included multiple grinds through each endcap quarter to locate through-wall defects (see left image of Fig. 17). Although more time-consuming, this examination method was able to successfully find the defect shown in the right image of Fig. 17. Furthermore, custom modification of fittings used during leak testing were used during this examination, which successfully reduced the amount of leakage at the fittings and the frequency of slippage at high pressures.

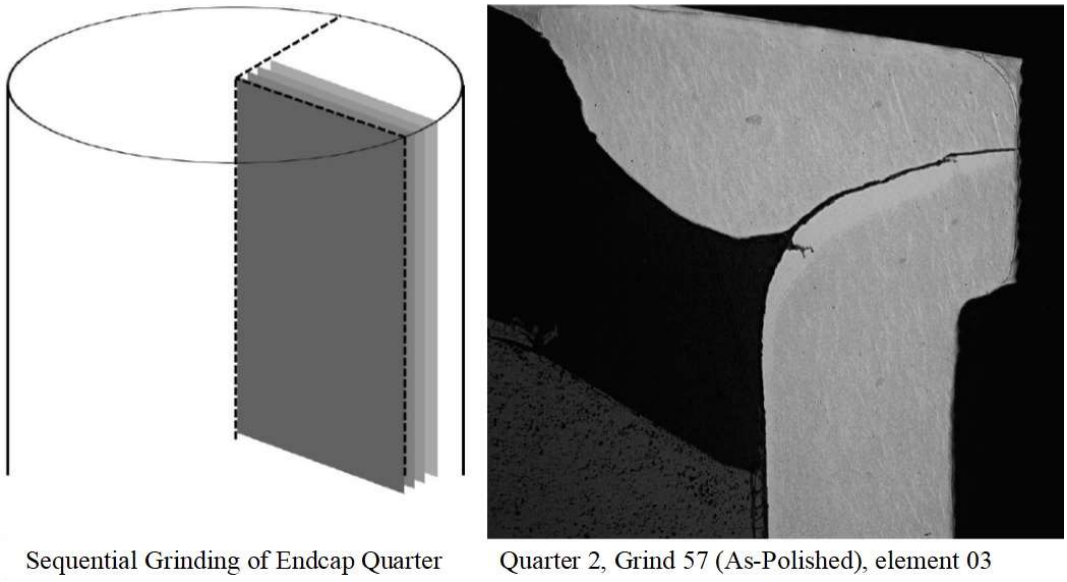

FIG. 17. Incomplete weld closure found during in-depth metallographic examination, element 3.

In 2018, four defected fuel elements from 4 separate bundles were shipped to CNL for PIE; during the preparation of this paper, the examination is ongoing. Element 18 has completed most of its examination and is described here. This element was observed during in-bay inspection to have two cracked, raised blisters near the NRE endcap (as a result the NRE endcap could not be leak tested). The larger observed blister is shown in the top image of Fig. 18. H/D analysis of the sheath from the defect region confirmed the blister was secondary damage, with ~60 µg/g H and >5000 µg/g D. The element's power history did not suggest overpower-related defects would be present, since maximum element powers remained within normal operating conditions during a refuelling shift at a burnup ~2100 MWd/tM (~50 MWh/kgU). Endcap weld closure regions appeared to be intact and in good condition (see bottom images in Fig. 18). During this examination, the endcaps were cut longitudinally in half rather than quartered, with subsequent grinding at set intervals to look for defects (none were found). Leak testing of element 18 revealed a through wall H/D blister about 220 mm from the element RE which was concluded to be secondary damage, shown in Fig. 19.

Observed Defect (Secondary Deuteride Blister)

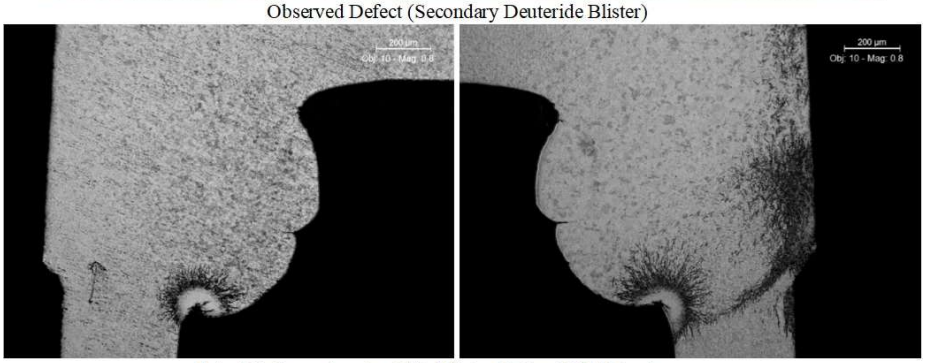

Intact Endcaps showing H/D Blisters Below Weld Upset

FIG. 18. Top: Observed defect (raised H/D blister confirmed to be likely secondary damage. Bottom: NRE Endcap showing hydride/deuteride concentrations, but no weld incompletions.

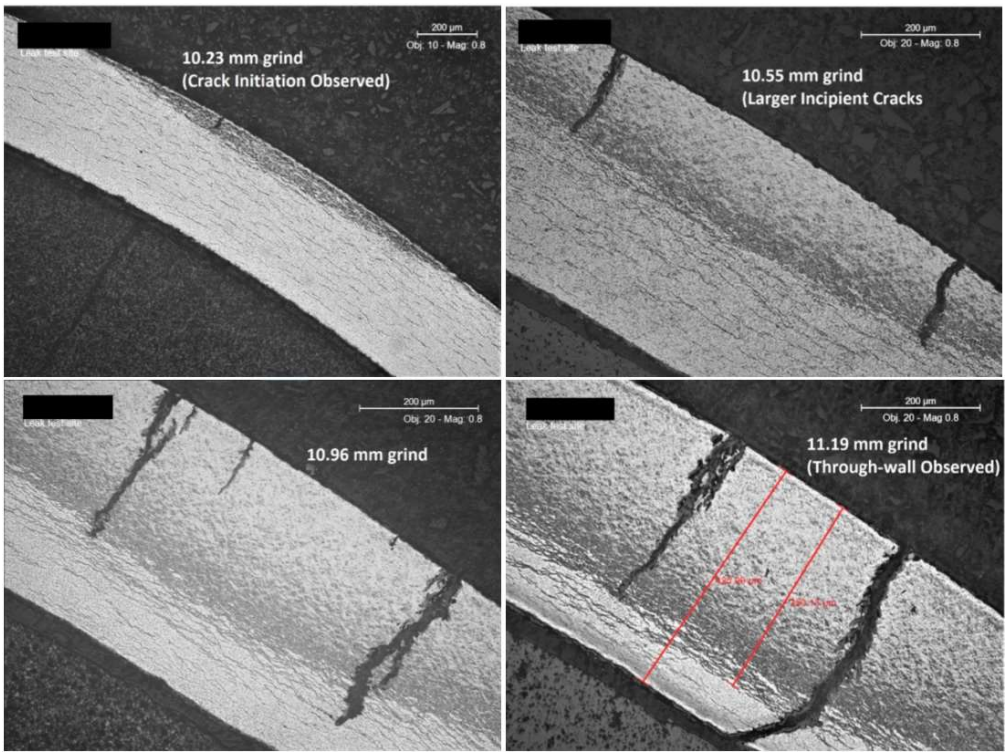

FIG. 19. Evolution of a suspect secondary deuteride blister during a metallographic exam to locate the through-wall defect and located during leak testing (element 18).

4. DEVELOPMENTS AT CNL TO SUPPORT DEFECT ROOT-CAUSE PIE

As highlighted in Section 3, there remain challenges in locating and positively identifying the root cause of fuel element failures. Additional techniques such as SEM imaging and cladding ID surface examinations have been applied to defect root-cause PIE in recent years, with varying degrees of success. Ongoing improvements of routine PIE activities such as element leak testing and metallography have been made in recent years, including exploratory grinding at set intervals entire endcaps to find the through-wall defect location, compared to historical examinations at only one planar surface.

Ultrasonic testing (UT) has been identified as a NDE technique that can be applied to identify locations for potential DE, including at the endcap regions, to assist with locating small flaws that may not be observed during PIE. UT testing has shown promise during development stages (using un-irradiated sheath), including detection of prefabricated endcap and sheath flaws (see Fig. 20). Future work will include UT testing on un-irradiated fuel element samples with oxide. Although metallographic examination of endcap regions is quite successful at locating flaws such as incomplete weld closures, there is still a concern that smaller weld flaws might be overlooked at the grind intervals endcaps are examined during grinding/polishing stages. However, examining samples at small intervals (e.g., 20-100 microns) is not always practical, given the overall time required to examine a complete a typical endcap examination.

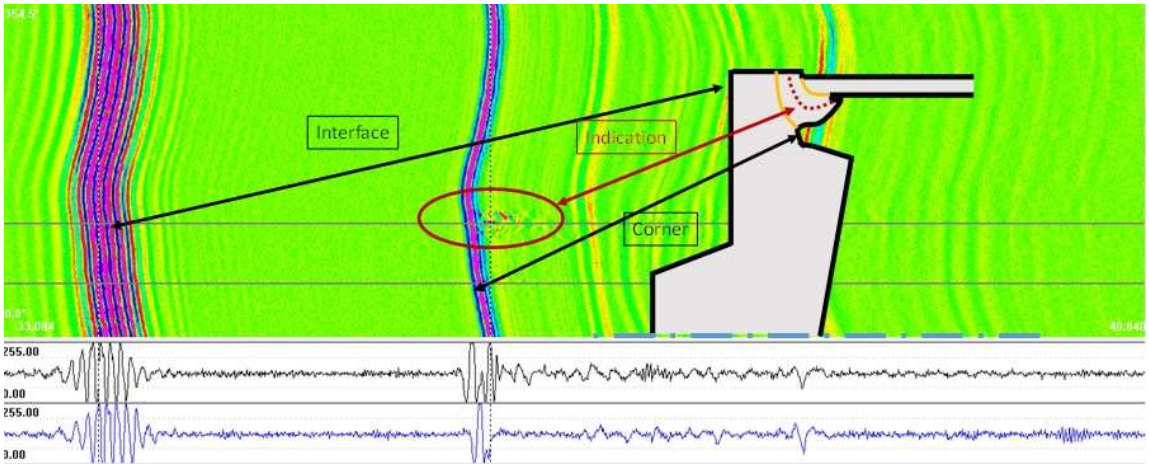

FIG. 20. Ultrasonic Testing results from out-of-cell testing on laboratory-produced weld flaws, showing indication of flaw.

5. DISCUSSION

The in-service performance of Canadian PHWR fuel bundle assemblies is excellent, with very low defect rates. This is partially attributed to gradual improvements and lessons learned during decades of bundle manufacturing and reactor operating experience, as well as robust quality assurance practices at all stages of the fuel cycle. For example, in earlier years of Canadian PHWR fuel development, the application of a carbon-based coating (i.e., CANLUB, or DAG-154) to the inner bore of the Zircaloy sheathing resulted in significant reduction in stress-corrosion cracking (SCC) related defects attributed to refuelling power ramps. An example of manufacturing improvements is related to an endcap failure mode detected in Canada as early as the 1980s, resulting from porosity in the manufactured Zr barstock [2]. Thanks to improved manufacturing and inspection practices, such failures have not been positively confirmed at CNL for over two decades (endcap porosity examinations are still conducted on elements with unknown primary defects).

Although foundational activities during a defect root-cause examination remain similar, developments have been made to routine examination activities, progress has been made to utilize novel examination methods where possible, and efforts to develop new techniques to allow for more accurate defect root-cause assessments. The radiological nature of irradiated fuel elements introduces technical challenges and limitations, the major impediment being the need for remote handling in specialized facilities. Not every anomalous feature along a fuel element can be examined in detail during a defect root-cause examination, which can add uncertainty to conclusions on the primary failure mode. Some of the more commonly observed primary defects are associated with incomplete end closures at endcap regions, and primary hydriding, the latter being more difficult to positively

identify and characterize. Although not always the case, it is common to find the primary defect remote of the initially observed defect. Therefore, if an observed defect is confirmed to be secondary, it is typical for an examination to begin at the endcap region remote of the confirmed defect, followed by examination of subsequent locations of interest, based on decreasing likelihood of finding the primary defect region.

The number of fuel elements described in Section 3 with undetermined primary failure mechanisms highlights the difficulty in locating and deducing the most probable failure mode, based on evidence obtained through PIE and provided by the utility. Heavy secondary damage can mask the ability to locate or fully characterize a primary defect. In the absence of neutron radiographic techniques at CRL, HVEMS is the only technique available to determine the difference between a primary hydriding and secondary deuteriding defect. Improvements in PIE techniques that focus on distinguishing between primary and secondary defects, or to locate incipient cracks and other small flaws more expediently, would help to streamline subsequent destructive activities. Traditional metallography remains the most-used technique to characterize defects, but it is time-consuming and relevant resources are limited. Less obvious/rarely observed primary defect mechanisms, such as of crevice corrosion on cladding surfaces as a catalyst to the formation of through-wall sheath defects, are more difficult to correlate with historically observed fuel element failure modes. Further study is recommended to confirm these are legitimate and potentially recurring performance concerns.

6. CONCLUSION

As novel PIE analysis techniques and equipment are developed under relevant projects at CNL, they will be increasingly applied to defect root-cause examinations, including development of small and very small sample preparation techniques using FIB technology. Such advancements in PIE are expected to streamline activities, in an effort to reduce time performing exploratory activities such as searching for potential defect sites, while offering additional performance data for consideration. Longer-term plans at CNL include the construction of the Advanced Nuclear Materials Research Centre (ANMRC), a new suite of hot cells dedicated to irradiated fuel and materials PIE expected to be commissioned in this decade.

ACKNOWLEDGEMENTS

Acknowledgements are given to several retired CNL PIE Staff, whose past work significantly contributed to this document, including (but not limited to): A.M. Manzer, J. Montin, Z. He, W.R. Richmond, S. Abate, M.R. Floyd, P.J. Valliant, I.A. Lusk, and K. Vaillancourt. CNL Hot Cell Staff are acknowledged for their unique expertise, and CNL Fuel Development Staff are thanked for their expertise and their timely review of this document, including S.J. Livingstone, N.F. Harrison, and J. Armstrong. Also acknowledged are the Canadian power reactor utilities, which have worked with CNL for decades to ensure safe and reliable operation of PHWR reactors. Lastly, IAEA staff are acknowledged for providing a forum to discuss fuel failures during normal operating conditions with other experts in the international nuclear community.

REFERENCES

[1] LIVINGSTONE, S., SUK, E., LEWIS, B. and YATABE, S., State-of-the-Art-Report on Defected Fuel, CANDU Owners Group (COG) Report COG-08-2075, 2010.

[2] MANZER, A.M., Post Defect Deterioration of CANDU Fuel: What Have we Learned? Proceedings of the 4th International Conference on CANDU Fuel, Pembroke, ON, Canada, 1995.

[3] FLOYD, M.R., Extended Burnup CANDU Fuel Performance, Proceedings from the 7th International Conference on CANDU Fuel, Kingston, Ontario, Canada, 2001.

[4] MONTIN, J., JUDAH, J. and SCOTT, R., OPG Fuel Surveillance Program, Proceedings from the 9th International Conference on CANDU Fuel, 2005.

DETECTION, MANAGEMENT AND MONITORING OF FUEL FAILURES

(Session 2)

Chairperson

I.A. EVDOKIMOV
Russian Federation

EXPERIENCE IN DETECTION OF WWER FUEL FAILURES BY ACTIVITY OF ^{133}XE AND ^{135}XE DURING REACTOR OPERATION

P.M. KALINICHEV, I.A. EVDOKIMOV
SRC RF TRINITI,
Troitsk, Russian Federation,

V.V. LIKHANSKII
NRC "Kurchatov Institute",
P.N. Lebedev Physical Institute,
Moscow, Russian Federation.

Abstract

Fuel failures may occur during operation of Nuclear Power Plants. This may lead to substantial financial losses. Negative effects of reactor operation with leaking fuel in the core may be reduced if fuel failures are detected in due time of the cycle. At present time, the ratio of the normalized release rates of ^{131}I and ^{134}I is used to detect fuel failures in WWERs during steady state operation. However, based on iodine activity, it is not always possible to detect the fuel failure. This situation may occur in case of a small defect in cladding of a leaking fuel rod or for high-burnup fuel if the defect in cladding is overlapped by the surface of the fuel pellet. This problem is aggravated if solid fuel pellets are used in fuel rods. If it is so, fuel deposits can make the dominant contribution to iodine activity, and the fuel failure may not be noticeable. For more reliable identification of fuel failures at WWERs, a technique based on the analysis of ^{133}Xe and ^{135}Xe activity ratio was previously developed. The paper is a summary of experience with this technique for revealing of fuel failures during operation of commercial WWER power units. It is shown that noble gases activity can be a more reliable indicator of fuel failure than iodine activities.

1. INTRODUCTION

Fuel failures may occur during operation of Nuclear Power Plants (NPPs). Monitoring and analysis of primary coolant activity is used to ensure the radiation safety of power units and to mitigate the adverse effects of fuel failures [1-8]. The key objective of coolant activity analysis is prompt identification of fuel failures.

At present time, iodine activities are used to detect fuel failures in WWERs during reactor operation [9]. The main indicator of a fuel failure is activity spiking in primary coolant during power transients. Under steady-state operation conditions, the ratio between the normalized release rates of ^{131}I and ^{134}I is used in WWERs (the release rate is normalized to the cumulative fission yield). If this ratio exceeds the threshold value, it indicates the presence of a leaking fuel rod in the core. For WWER-1000 reactors, this value is 5. However, based on iodine activity, it is not always possible to clearly identify the fuel failure. Such situation may occur in case of a small defect in fuel cladding, or when fuel burnup is high (so that the pellet-to-cladding gap is closed near the defect and in the adjacent area). These issues are more urgent for fuel rods with solid fuel pellets. If the rate of iodine release into coolant is low the main contribution to iodine activity may come from fuel deposits residing on the in-core surfaces (or tramp uranium). As a result, a fuel failure may be obscured by the background activity.

Activities of ^{133}Xe and ^{135}Xe are used for more reliable detection of fuel failures in PWR reactors [10]. But this technique cannot be used as such for WWER reactors for the following reasons. First, both the absolute values and the ratios of noble gases' activities depend on the rate of gas removal from the coolant (the rate of coolant degassing). The coolant degassing parameters are different for PWR and WWER reactors. Moreover, the rate of noble gas removal from the coolant may differ markedly among WWER power units. Second, unlike PWR reactors, WWER power units do not currently use the practice of coolant sampling at the reactor pressure. The gases are partially lost from the coolant samples with the existing sampling procedures, and the data on absolute noble gas activity may not be representative. However, these difficulties may be overcome if the ratio of ^{133}Xe to ^{135}Xe activity is handled in a certain way. The corresponding method was proposed recently [11].

The paper briefly outlines the technique [11] for detection of fuel failures by ^{133}Xe and ^{135}Xe activities. The focus is on made on current experience in practical application of the developed technique during operation of WWER power units.

2. METHOD OF FUEL FAILURE IDENTIFICATION

If there is a leaking fuel in the core, the source of each radionuclide (R_c) can be written as

$$R_c = R + \boldsymbol{R} = R + \frac{\mu}{\lambda+\mu} R_f \quad (1)$$

Here R is the rate of fission product release from fuel deposits to primary coolant (s^{-1}), **R** is the rate of fission product release from the leaking fuel rod (s^{-1}), λ is the decay constant (s^{-1}), R_f is the rate of fission product release from fuel pellets to fuel rod internal volume (s^{-1}), and μ is the escape rate coefficient for the given radionuclide from fuel rod into the coolant (s^{-1}). The escape rate coefficient relates the rate of release into the coolant to the total inventory of fission product inside the leaking fuel rod [11]. The value μ depends on the characteristics of leaking fuel, the decay constant, and the radionuclide's chemical properties. For surfactant species (iodine, in particular), μ can be much smaller than for noble gases in the same leaking fuel rod.

It follows from Eq. (1) that contribution of leaking fuel to the cumulative fission product source in the coolant is defined by the ratio between the decay constant λ and the escape rate coefficient μ. The decay constants for ^{133}Xe and ^{131}I are close [13]. With the chemical properties of xenon and iodine being similar, marked deviations of ^{133}Xe and ^{131}I activities from the background level after fuel failure would be observed simultaneously. However, due to iodine adsorption on inner cladding surface it is possible (in a certain range of 'small' failures[2]) that ^{131}I activity is still governed by release from fuel deposits, while ^{133}Xe activity would exceed the background level by a great extent. The more iodine is adsorbed inside the leaking fuel rod, the wider this range of the 'small' failures is[3]. This issue becomes important when hydraulic resistance of the leaking fuel rod is high. High hydraulic resistance is typical to small cracks in cladding or high-burnup fuel (when pellet-to-cladding gap is collapsed). Hydraulic resistance also increases if solid fuel pellets are used in fuel rods. Owing to these factors, noble gas activity may be a more sensitive failure indicator than iodine activity.

To ensure reliable detection of a fuel failure by noble gas activities it is necessary to use a pair of gaseous fission products with the following properties:

— The lifetime of the two fission products should differ significantly. In this case, much of the short-lived isotope will decay having no time to leave the leaking fuel rod, while activity of the long-lived isotope will increase markedly after the failure. So, the selected radionuclides' activity ratio will be much higher after the fuel failure, than in case of a clean core.
— The radiation yields of the selected radionuclides are expected to depend weakly on the fissile nuclide composition. Fuel burnup in fuel deposits is normally unknown. Consequently, strong dependence of radiation yields on fuel nuclide inventory may lead to wide uncertainties. In particular, this is the reason for ^{85m}Kr and ^{88}Kr not being suitable for analysis.
— The nuclides used should be isotopes of one chemical element. Coolant samples in WWERs cannot be taken at reactor pressure, as in PWRs. In WWERs, samples are taken from a pipeline with lower pressure and temperature than in the primary circuit. The sampling container is filled with water at atmospheric pressure. This procedure leads to partial degassing of water and some portion of dissolved noble gases is lost. Since gases have different solubility, the gas losses during sampling vary for different chemical elements, e.g., for Xe and Kr.

Among the noble gas radionuclides available for monitoring at NPPs the above requirements are met by the pair of ^{133}Xe and ^{135}Xe.

---

[2] Sometimes, a 'small' failure is used in a sense of a small defect in the fuel cladding with ensuing low rate of fission products release. Actually, the release rate depends not only on the size of the defect. The size of hydraulic channels inside the leaking fuel rod is important, too. It may happen that the defect itself is not small (e.g., a noticeable hole or a long crack) but the release rate is low due to the closed pellet-to-cladding gap in the leaking fuel rod. So, the 'small' failure should be better associated with the high hydraulic resistance of the leaking fuel rod.

[3] If the defect in cladding is in the 'cold' zone and is covered with water, iodine can dissolve in it and be released from the leaking fuel rod rather quickly.

Fig. 1 shows the threshold ratio of ^{133}Xe and ^{135}Xe activities as a function of the rate of coolant cleaning from noble gases [12]. The threshold is an upper estimate for ^{133}Xe and ^{135}Xe activity ratio if fuel deposits are the only source of fission products release into the primary coolant. The dotted line corresponds to the 'monolayer' approximation [9] (when fuel is assumed to be deposited on the outer cladding surface as a monatomic layer). The solid line corresponds to fuel deposits consisted of 'coarse' particles (size more than the range of fission fragments in UO_2 ~ 5 microns) with a developed open surface. If the ratio of xenon activities in primary coolant appears to be higher than the solid line in Fig. 1, it means that a leaking fuel rod is present in the core. In the area below the solid line, no clear conclusion on fuel failure can be drawn only based on the ratio between ^{133}Xe and ^{135}Xe activities.

The fuel failure detection by noble gas activities in WWERs is as follows [11]:

a. The rate of the xenon removal from the coolant η_{Xe} is determined (see below).
b. With the diagram in Fig. 1 (solid line), the threshold ratio of ^{133}Xe and ^{135}Xe activities corresponding to the η_{Xe} value is determined.
c. The threshold is compared to the ratio of actual ^{133}Xe and ^{135}Xe activities in primary coolant. If the actual data exceed the threshold, this indicates a fuel failure in the core.

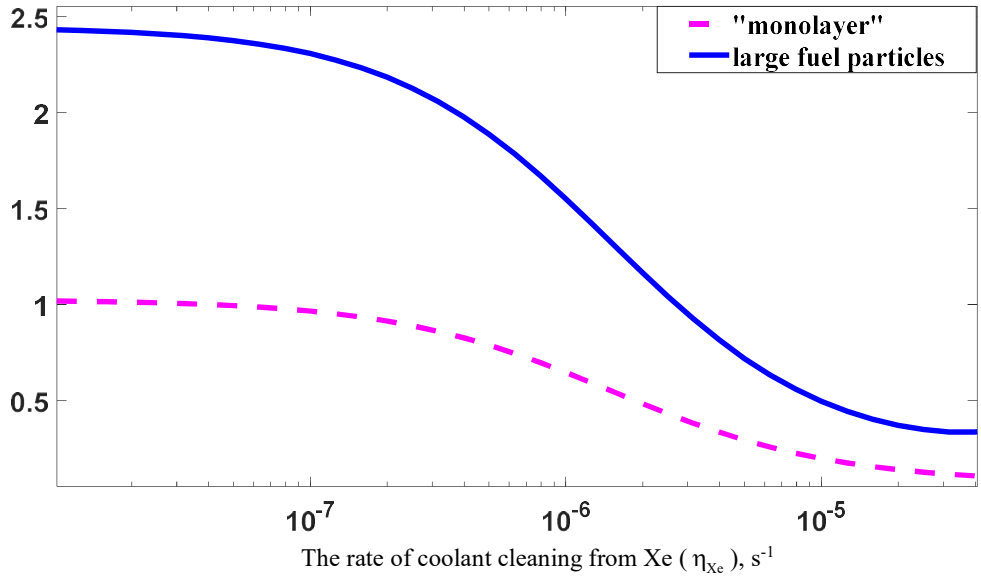

FIG. 1. The threshold ratio of ^{133}Xe and ^{135}Xe activities for WWER-1000 reactors: - - – for 'monolayer' fuel deposits, ——– for fuel deposits in the form of 'coarse' fuel particles.

Current regulations for WWERs do not require to monitor the rate of noble gas removal from primary coolant. Nevertheless, the coolant degassing parameters can be determined by measuring noble gas activities before and after the degasser of the feed water. In this case, the degassing rate could be calculated using the equation

$$\eta_{Xe} = \frac{Q}{M}\left[1 - \frac{A^2_{Xe}}{A^1_{Xe}}\right] \quad (2)$$

where A^1_{Xe}, A^2_{Xe} are the xenon activities before and after the degasser, respectively; Q is the coolant flow rate to the degasser and M is the mass of primary coolant.

Such measurements are performed at some WWER power units. If the xenon removal rate is not measured, it is possible to adopt a conservative approach by using the maximum threshold value of 2.48 which corresponds to η_{Xe}= 0 (see Fig. 1).

3. EXAMPLES OF APPLICATIONS FOR WWER-1000 POWER UNITS

Some practical examples below demonstrate the advantages of fuel failure detection by the ratio of ^{133}Xe and ^{135}Xe activities.

3.1 Example 1. Cycle H-1

Figs 2-3 show an example of WWER-1000 fuel cycle. During the cycle, the reactor operated under steady-state conditions. Activity of ^{131}I was low. The ratio of the normalized release rates for ^{131}I and ^{134}I was low (did not exceed the threshold value of 5). No spike effect was detected during reactor shutdown in course of power reduction. According to the regulations, it was possible to stop activity monitoring and conclude that there was no leaking fuel in the core.

Despite the absence of fuel failure indicators according to regulatory document [9], the NPP personnel continued monitoring of coolant activity. The rationale was an increase in ^{133}Xe activity detected approximately 250 days from the beginning of the cycle. A sharp spike in ^{131}I activity was recorded after the pressure relief in the primary circuit.

Subsequent analysis by the above teachnique [11] showed that starting from 250th day of the cycle, the ratio of ^{133}Xe and ^{135}Xe activities significantly exceeded the 'conservative' threshold value of 2.48. It clearly confirms the appearance of leaking fuel in the core from this moment.

One leaking fuel assembly (FA) after 4 years of operation was found during the reactor outage. If the only basis for making a decision was iodine activity, then the leaking FA after cycle H-1 would not be detected.

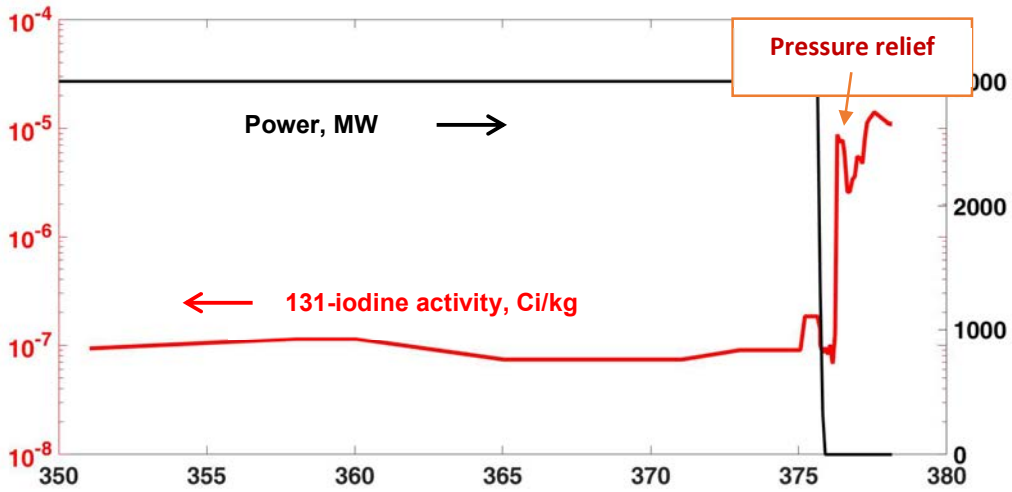

FIG. 2. Reactor power and ^{131}I activity during cycle H-1.

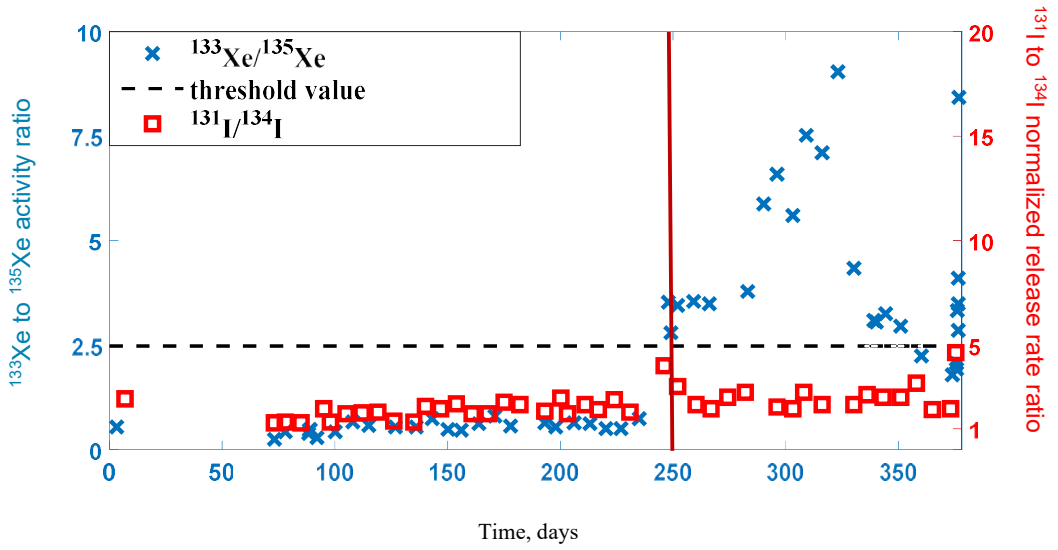

FIG. 3. Ratio of ^{133}Xe and ^{135}Xe activities (the vertical axis on the left) and ratio of the normalized iodine release rates (the vertical axis on the right) during cycle H-1. The red vertical line shows the moment of the fuel failure.

3.2 Example 2. Cycle G-1

Another case is illustrated in Figs. 4-5. During cycle G-1 there were no signs of a fuel failure until August 1, 2018, on the basis of iodine activity [9], (Fig. 4). However, since June 19, ^{133}Xe activity has been detected in direct spectrometric samples. The ratio of ^{133}Xe and ^{135}Xe activities was greater than 4 (Fig. 5). This is above the maximum (conservative) threshold (see section 2). Thus, in this case the fuel failure was detected by noble gas activity 45 days earlier than by iodine activity. If the fuel failure occurred later (close to the end of the cycle) it could remain if only iodine activity was evaluated in the frame of fuel integrity analysis.

One leaking FA was found after cycle G-1 by the failed fuel detection system (FFDS).

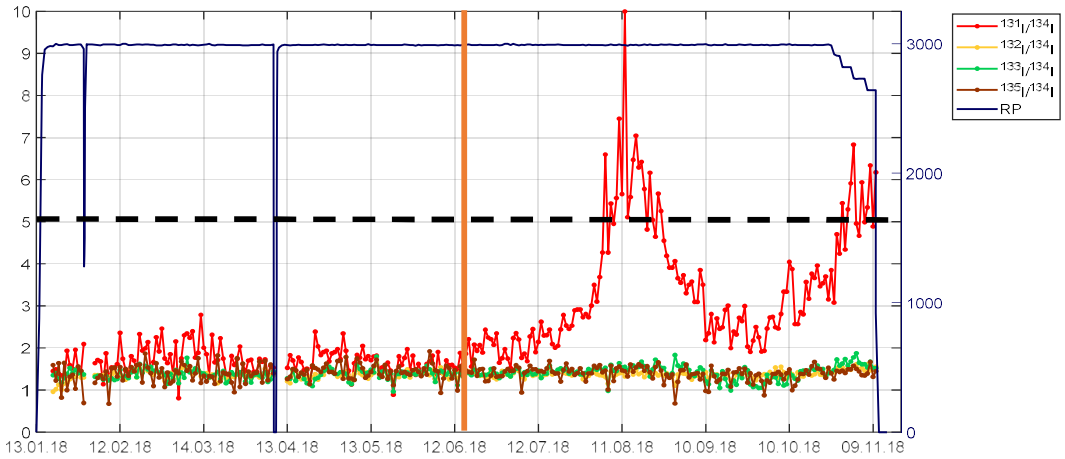

FIG. 4. Ratio of iodine normalized release rates during cycle G-1. The red vertical line shows the moment of the fuel failure. The black dotted line is the threshold for the ratio of ^{131}I to ^{134}I normalized release rates.

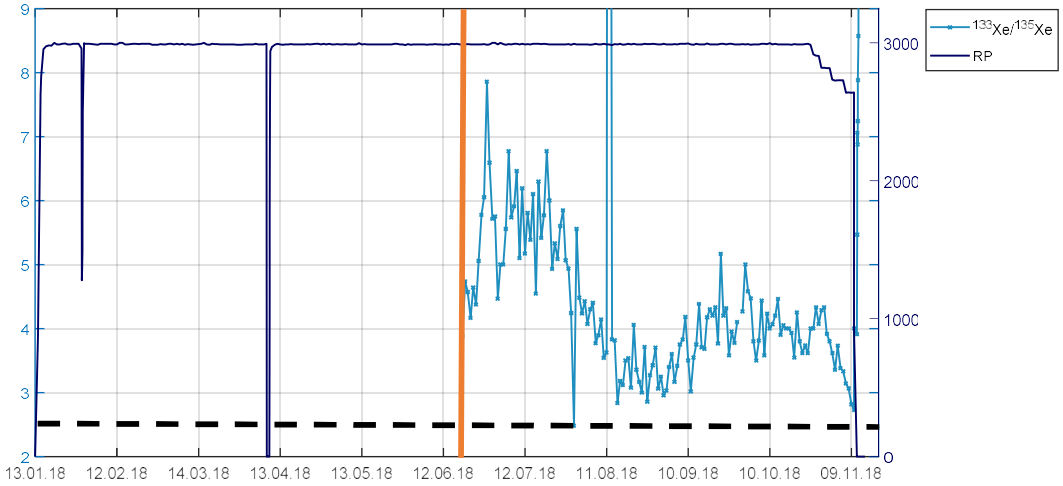

FIG. 5. Ratio of xenon activities during cycle G-1. The red vertical line shows the moment of the fuel failure. The black dotted line is the conservative threshold for the ratio of 133Xe to 135Xe activity.

3.3. Example 3. Cycle F-4

In the initial period of cycle F-4, ^{131}I activity was below the minimum detectable level during direct spectrometry of taken coolant samples (Fig. 6).

The coolant degassing rate was controlled at this power unit. The value of η_{Xe} was found to be about 3×10^{-5} s^{-1}. The corresponding threshold ratio of ^{133}Xe to ^{135}Xe activity is ~ 0.4 (see Fig. 1). This value was exceeded almost from the beginning of the cycle (Fig. 7). So, the leaking fuel was in the core from the moment when the reactor reached its nominal power. Spiking of ^{131}I activity confirmed the fuel failure 20 days after. Note that the ratio of the normalized release rates for ^{131}I and ^{134}I during steady-state reactor operation were below the threshold value of 5 up to the end of cycle F-4.

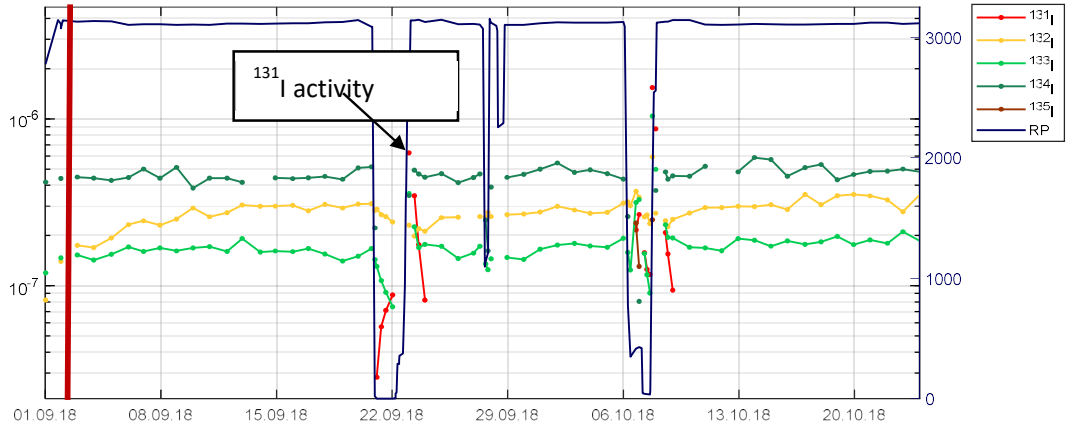

FIG. 6. Iodine activity (Ci/kg) during cycle F-4. The red vertical line shows the moment of the fuel failure.

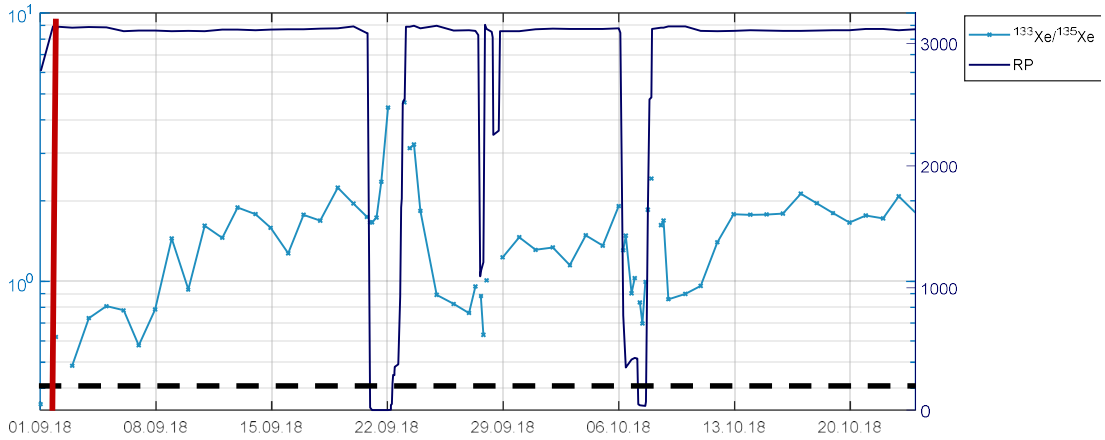

FIG. 7. Ratio of xenon activities during cycle F-4. The red vertical line shows the moment of the fuel failure. The black dotted line is the threshold ratio of ^{133}Xe to ^{135}Xe activity.

Three leaking FAs were found during the outage after cycle F-4.

3.4 Example 4. Cycle C-3

For the first 80 days of cycle C-3, there were no signs of fuel failure based on iodine activity. The ratio of the normalized release rates for ^{131}I and ^{134}I was well below the threshold value of 5 (Fig. 8). The degassing rate was controlled. According to the measurements, the threshold ratio of ^{133}Xe to ^{135}Xe activity was 0.4. This value was exceeded one week after the reactor was put into full power (Fig. 9). Gradual increase in the ratio of ^{133}Xe to ^{135}Xe activity indicated presence of leaking fuel in the core from the very beginning of cycle. The fuel failure was confirmed by activity spiking 80 days after the beginning of the cycle (Fig. 10). The ratio of iodine normalized release rates under steady state operation conditions exceeded the threshold value 5 only 40 days later the spiking event.

One FA was confirmed to be leaking after the end of cycle C-3.

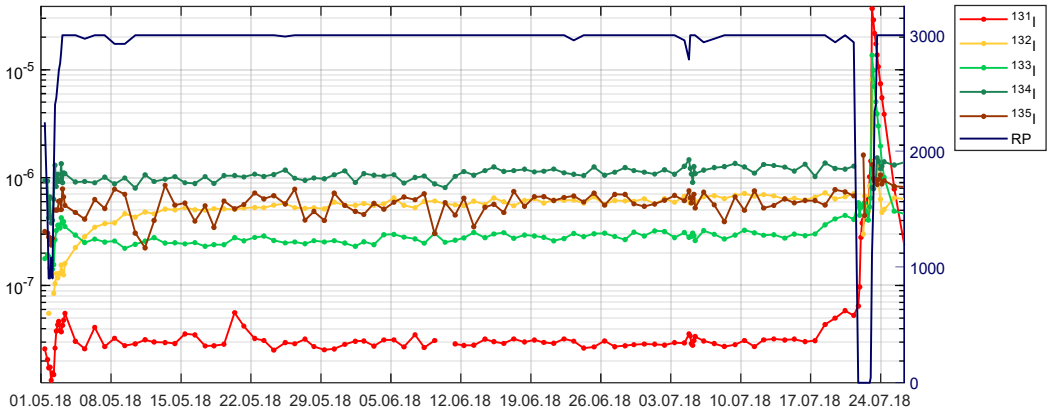

FIG. 8. Iodine activities (Ci/kg) during cycle C-3.

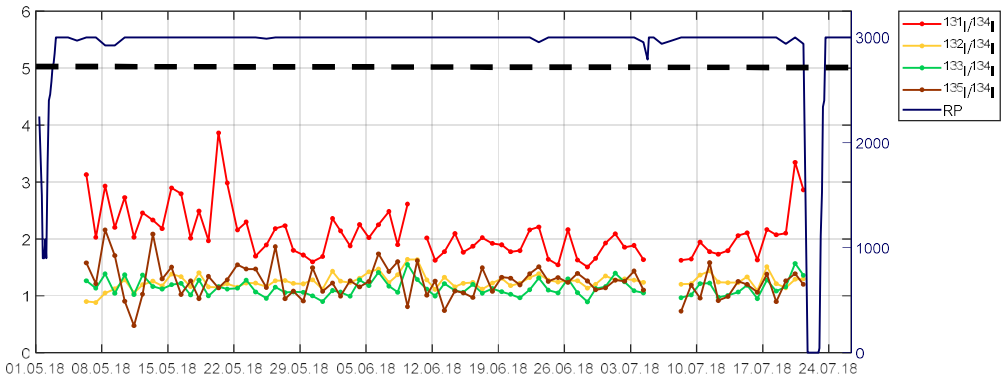

FIG. 9. Ratio of iodine normalized release rates during cycle C-3. The black dotted line is the threshold value for $^{131}I/^{134}I$.

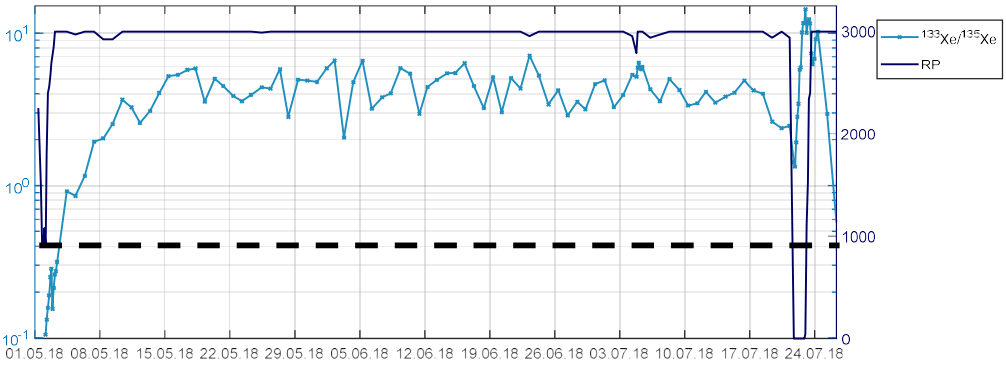

FIG. 10. Ratio of xenon activities during cycle C-3. The black dotted line is the threshold for a fuel failure.

3.5 Example 5. Cycle E-4

For the first 75 days during the cycle E-4, ^{131}I activity was below the minimum detectable level for direct spectrometric samples (Fig. 11). According to monitoring of the coolant degassing rate, the threshold ratio of ^{133}Xe to ^{135}Xe activity was 0.4. This value was exceeded 4 days after the beginning of the cycle (Fig. 12). Activity of ^{131}I was first recorded (by direct spectrometry of taken coolant samples) 70 days later. Since this moment, the ratio of ^{131}I to ^{134}I normalized release rates confirmed the fuel failure.

Four leaking FAs were found during the outage after cycle E-4. Two FAs operated 2 years, another two FAs – 3 years.

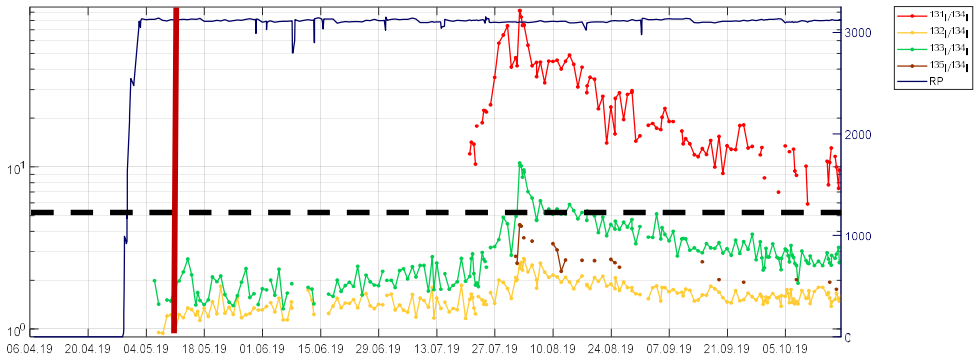

FIG. 11. Ratio of iodine normalized release rates for cycle E-4. The red vertical line shows the moment of the fuel failure.

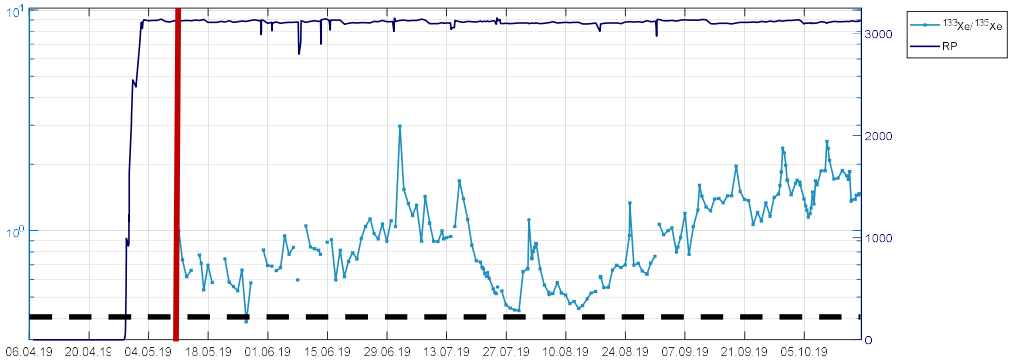

FIG. 12. Ratio of xenon activities during cycle E-4. The red vertical line shows the moment of the fuel failure. The black dotted line is the threshold ratio of ^{133}Xe to ^{135}Xe activity.

3.6 Example 6. Cycle F-5

Cycle F-5 started with low coolant activity. Activity of ^{131}I was below the minimum detectable level for the first 113 days of the cycle. During this period ^{131}I activity was measured by the chemical extraction method. The ratio of ^{131}I to ^{134}I normalized release rates was in the range of 2-3 (Fig 13). Monitoring of the coolant degassing rate evidenced that the threshold ratio of ^{133}Xe to ^{135}Xe activity was 0.4. Activity of ^{133}Xe was first recorded 96 days after the beginning of cycle giving the ratio of ^{133}Xe and ^{135}Xe activities above the threshold value (Fig 14). Iodine activity confirmed the fuel failure only 17 days later.

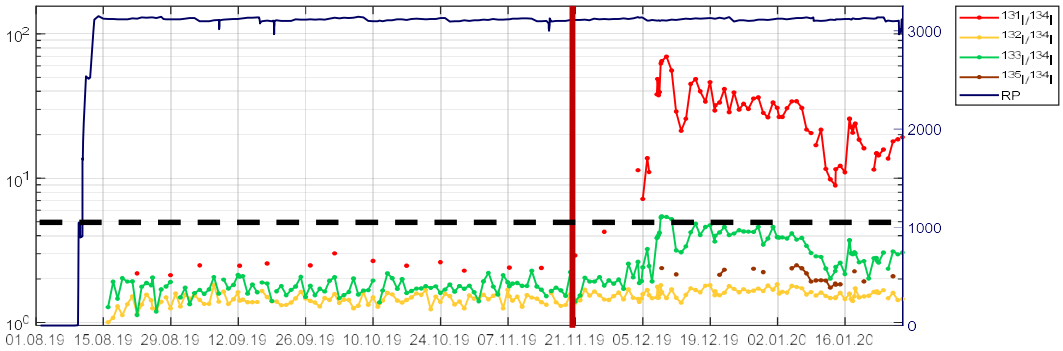

FIG. 13. Ratio of iodine normalized release rates during cycle F-5. The red vertical line shows the moment of the fuel failure. The black dotted line is the threshold for $^{131}I/^{134}I$.

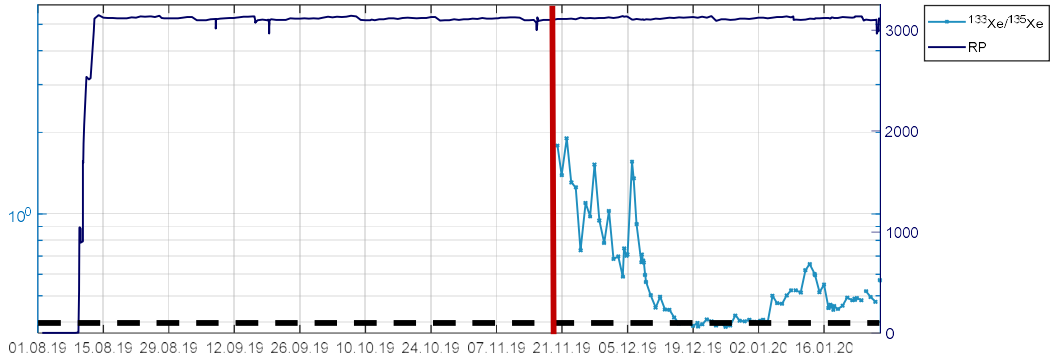

FIG. 14. Ratio of xenon activities during cycle F-5. The red vertical line shows the moment of the fuel failure. The black dotted line is the threshold ratio of ^{133}Xe to ^{135}Xe activity.

3.7 Summary of available experience

Fig. 15 is a summary for analysis of several fuel cycles over the past few years. It relates the actual ratio of ^{133}Xe to ^{135}Xe activity (α) to the threshold value (α_{cr}).

For cycles with clean core, the activity ratio was significantly below the threshold. For all cycles with fuel failures, the threshold was exceeded. The coolant degassing rate was not controlled in some cases (indicated with red circles). For these cycles, the conservative threshold value of 2.48 was used in analysis. So, the ratio of α/α_{cr} is underestimated for these cases.

On the whole, analysis of WWER-1000 cycles for recent years shows that ^{133}Xe and ^{135}Xe activity ratio is a more reliable indicator of a fuel failure than iodine activities.

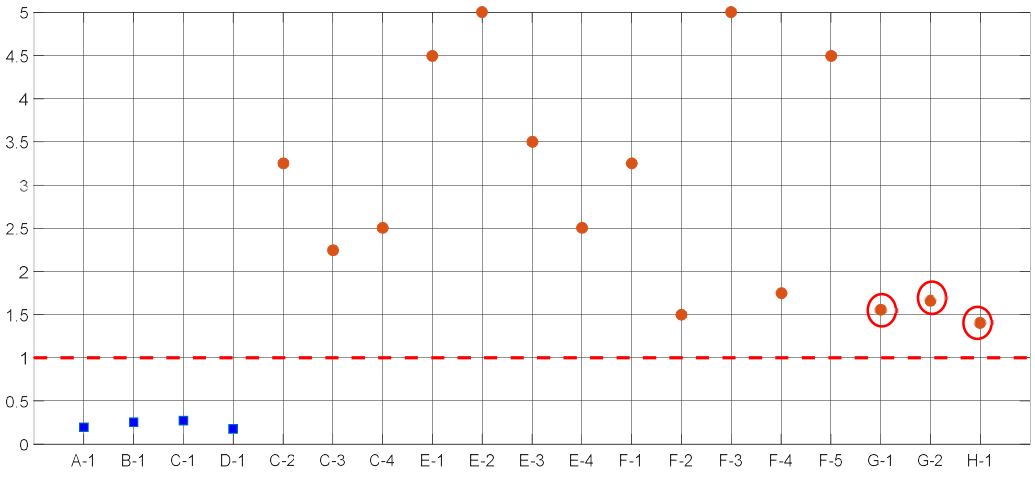

FIG. 15. Relation between the actual (α) and threshold (α_{cr}) ratio of ^{133}Xe to ^{135}Xe activity for several fuel cycles: ■ – cycles with clean core, ● – cycles with leaking fuel (average value for 3 days immediately after fuel failure is shown). Area above the red dotted line corresponds to fuel failures.

4. SOME LIMITATIONS

The ratio of ^{133}Xe to ^{135}Xe activity is a non-monotonic function of the escape rate coefficient μ. For small failures this ratio gradually grows if μ increases. The growth continues due to increasing rate of ^{133}Xe release from the leaking fuel rod until ^{135}Xe activity is governed by fissions in fuel deposits. In case of further fuel degradation (higher μ) the time of 'delay' of fission products inside the leaking fuel rod diminishes. If the rate of ^{135}Xe release becomes noticeable compared to the background level, the ratio of ^{133}Xe to ^{135}Xe activity starts to diminish.

In case of severe secondary degradation, the time of 'delay' may become smaller than the lifetime of ^{135}Xe. In the extreme case, the release of ^{133}Xe and ^{135}Xe would occur as if there was no cladding and fuel pellets were open to coolant. If so, contribution of a leaking fuel rod with low heat rate to coolant activity would be indistinguishable from release of fission products from massive fuel deposits. For high heat rates diffusion is a major contributor to the fission product release from fuel pellets. In this situation the ratio of ^{133}Xe to ^{135}Xe activity in the coolant may also fall within the "uncertainty zone" shown in Fig. 1 (between the solid and the dashed lines). Then, using only the ratio of ^{133}Xe and ^{135}Xe activities it would be not possible to detect the leaker and other fuel failure indicators are needed.

However, in cases of severe fuel degradation the absolute activity of reference radionuclides increases significantly. So, there are no problems to detect the failure. In general, it is believed that the proposed technique complements the traditional way of failure detection in WWERs by iodine activity. The more techniques based on different data is available, the better results of fuel integrity monitoring may be anticipated for the wide range of operational parameters.

5. CONCLUSIONS

The paper briefly describes a method for fuel failure detection by noble gas activity in the primary coolant of a WWER-1000 power unit. A summary of experience with this technique applied to several cycles at different NPPs is given. It is demonstrated that the proposed technique is capable to reveal fuel failures during steady-state reactor operation even if it is not possible by iodine activities. Analysis of Xe activities also provides a proper identification of the moment of fuel failure.

Prompt detection of fuel failure is important for correct analysis of fuel failure mechanisms and root causes. If the moment of the failure correlates with some changes in operational parameters, then these changes may affect fuel failure. If failure is detected with a significant delay, the data may be misinterpreted and incorrect conclusions about the failure mechanism may be drawn.

It should be also noted that mitigating of fuel failures by short-term drops of reactor power is currently discussed [14, 15]. The effect of this corrective effort depends significantly on how quickly the failure was identified. With this challenge, the methods for reliable and prompt detection of fuel failures become urgent for NPPs.

REFERENCES

[1] SHUMKOVA, N. Yu., BYKOV, O.V., BELOUSOVA, L.P., Ukrainian WWER-type NPP units. Results of cladding tightness inspection, in "Fuel failure in water reactors: Causes and mitigation", IAEA-TECDOC-CD-1345, IAEA, Vienna (2003) 77–86.

[2] BURMAN, D.L., et al., Development of a coolant activity evaluation model & related application experience, LWR Fuel Performance (Proc. Int. Top. Mtg Avignon, 1991), Vol. 1, Société française de l'énergie nucléaire, Paris (1991) 363.

[3] BEYER, C.E., An analytical model for estimating the number and size of defected fuel rods in an operating reactor, LWR Fuel Performance (Proc. Int. Top. Mtg Avignon, 1991), Vol. 2, Société française de l'énergie nucléaire, Paris (1991) 437.

[4] PARRAT, D., GENIN G.B., MUSANTE Y, PETIT C, HARRER, M., Failed rod diagnosis and primary circuit contamination level determination, thanks to the DIADEME code, in "Fuel failure in water reactors: Causes and mitigation", IAEA-TECDOC-1345 (2003) 265–276.

[5] EL-JABY, A., LEWIS, B.J., THOMPSON, W.T., IGLESIAS, F., AND IP, M., A General Model for Predicting Coolant Activity Behaviour for Fuel-failure Monitoring Analysis, Journal of Nuclear Materials **399** (2010) 87-100.

[6] LIKHANSKII, V., EVDOKIMOV, I., KHORUZHII, O., SOROKIN, A., NOVIKOV, V., Modelling of Fission Product Release from Defective Fuel under WWER Operation Conditions and in Leakage Tests During Refuelling, Proceedings

of the 2004 International Meeting on LWR Fuel Performance, Paper 083, Pages 798-812, Orlando, Florida, September 2004.

[7] LENA OLIVER, PETER SVENSSON, KENDAL BISHOP, WESTINGHOUSE O.P., Fission product analysis using the FPA code, Westhinghouse Electric Sweden AB (2017).

[8] SLAVYAGIN, P., LUSANOVA, L., MIGLO, V., Fuel failure diagnostics in normal operation of nuclear power plants with WWER-type reactors", in "Fuel failure in water reactors: Causes and mitigation", IAEA-TECDOC-CD-1345 (2003) 303-315.

[9] RD NO[4] 1.1.2.10.0521-2009. Standard Procedure for Monitoring the Cladding Integrity of Fuel Elements. FAs of the WWER-1000 Reactors, Rev. 2. Rosenergoatom, Moscow, Russia (2016)

[10] INTERNATIONAL ATOMIC ENERGY AGENCY, Review of Fuel Failures in Water Cooled Reactors (2006–2015), Nuclear Energy Series No. NF-T-2.5, IAEA, Vienna (2019).

[11] KALINICHEV P.M., EVDOKIMOV I.A., LIKHANSKII V.V., A technique for detection of WWER fuel failures by activity of Xe radionuclides during reactor operation, Nuclear Energy and Technology **4** (2018) 263-270.

[12] WISE, C., The transport of short-lived fission products close to the fuel surface, Journal of nuclear materials **152** (1988) 102-113.

[13] TASAKA, K., KATAKURA, J., IHARA, H., YOSHIDA, T., IIJIMA, S., NAKASHIMA, R., NAKAGAWA, T., TAKANO, H., JNDC nuclear data library of fission products, Second version, 1320, JAERI (1990).

[14] WRIGHT, J., TVERBERG, T., YAGNIK, S., LIMBÄCK, M. and SCHRIRE, D., Summary of test reactor experiments to simulate secondary fuel degradation and its mitigation, 2017 Water Reactor Fuel Performance Meeting (TopFuel-2017), September 10-14, 2017, Ramada Plaza Jeju, Jeju Island, Korea

[15] EVDOKIMOV I.A., KHORUZHII, O.V., SOROKIN, A.A., et al., Short-term drop of the reactor power as a potential remedy against secondary degradation, Proc. Tech. Meet. Fuel Failure in Normal Operation of Water Reactors: Experience, Causes and Mitigation, IAEA Headquarters, Vienna, Austria, 14–17 December 2020.

[4] Regulatory Document of Nuclear Operator.

MONITORING, PREDICTION, AND IDENTIFICATION OF FUEL FAILURES DURING 17TH CAMPAIGN ON EACH UNIT OF TEMELÍN NPP AND OVERVIEW OF ALL FUEL FAILURES SINCE 2010

J. RAINDL
ČEZ, a. s. - NPP Temelín,
Temelín, Czech Republic

Abstract

The paper provides basic description of fuel failures. It shows monitoring, prediction, and identification of fuel failures during 17th campaign on each unit of Temelín NPP. This is shown from radiochemical perspective of fuel failures and their impacts on activity (Bq/kg) of reference radionuclides in the primary coolant. The paper compares predicted number of fuel failures with those found and it shows success of predictions. The paper puts this into a context of all fuel failures found among fuel assemblies supplied by fuel vendor of Temelín NPP, TVEL Fuel Company. It shows critical operating year for TVEL fuel assemblies. TVEL Fuel Company has been fuel supplier of Temelín NPP since 2010.

1. INTRODUCTION

Fuel cladding is an important barrier to hold fission products and to prevent them to spread in the primary coolant. Fuel failure may lead to release of fission products, which cause higher radiation fields close to the primary circuit, higher dose rates to workers during an outage and an increase of radwaste amount. That is the reason, why the integrity of this barrier is very important, and it should remain intact during the whole lifetime of fuel assembly.

Nevertheless, fuel failures can occur at any time during an operation of a nuclear power plant. Fuel failures can be divided according to several different criteria. For example, according to failure mechanism such as hydriding, oxidation, welding defects, grid to rod fretting, debris fretting, etc. or according to the type of fission products released during the operation such as fission products typical to open defects in cladding (caused by direct contact between fuel pellets and primary coolant) and gaseous ones (without direct contact between fuel pellets and primary coolant) [1].

For the monitoring of fuel cladding integrity, it is not important, what caused the fuel failure. It is the type of the defect that is important. Open type of fuel failures allows a direct contact between fuel pellets and the primary coolant. It causes a release of all types of fission products like noble gases, several isotopes of iodine, non-volatile fission products and even a fuel washout is possible. On the other hand, gaseous type of fuel failures is very small and tight. It means that there is no direct contact between fuel pellets and the primary coolant. Temperature on fuel pellets surface is too high and the amount of the primary coolant penetrating fuel cladding is so small, that the primary coolant cannot remain in a liquid state and vaporizes immediately. It creates a mixture of steam and hydrogen between fuel pellets and the cladding. It increases the temperature of fuel pellets even more because of the low rate of heat transfer. This type of a fuel failure causes the release only of noble gases and some isotopes of iodine [2].

Direct monitoring of the fuel cladding integrity is impossible because there is no measurable physical parameter, which indicates a fuel failure during operation, like pressure in fuel rods or changes on in-core detectors. It is possible to monitor it indirectly by measuring radiochemical parameters like activity (Bq/kg) of reference radionuclides in the primary coolant. Then it is possible to identify a fuel failure based on changes of the activity (Bq/kg) of these reference radionuclides or changes of the ratio between them. From the monitoring and identification perspective, it is much more difficult to monitor a gaseous type of fuel failure than an open type because of small changes of radiochemical parameters of the primary coolant.

Calculation or prediction of a burnup of leaking fuel rod can be based on two radiochemical parameters, a ratio of $^{134}Cs/^{137}Cs$ [3] or a ratio of $^{85m}Kr/^{135}Xe$ [1]. It is very difficult to predict a burnup of leaking fuel rod with gaseous type of a fuel failure because of low release or no release at all of cesium isotopes. Prediction based on the ratio of $^{85m}Kr/^{135}Xe$ is very inaccurate because of difficulties with sampling and the resulting measurement inaccuracy of noble gases dissolved in the primary coolant. It means that it is complicated to predict a burnup of leaking fuel rods with a gaseous type of fuel failure.

2. MONITORING, PREDICTION, AND IDENTIFICATION OF FUEL FAILURES ON TEMELÍN NPP DURING LAST FINISHED CAMPAIGNS

2.1 Unit 1, cycle 17

2.1.1 Monitoring and prediction of fuel failures

Cycle 17 in unit 1 [U1C17] was from 28th April 2019 to 13th March 2020 with a short shutdown at the end of December 2019. It achieved 305 effective full power days [EFPD], see Fig. 1.

As can be seen in Fig. 2, it was possible to see first indications of a fuel failure at the end of the first week of full power operation (EFPD = 11.3) on 11th May 2019. It could be seen on changes of ^{133}Xe activity. Activity of ^{133}Xe was under the minimal significant activity (< 1 kBq/kg) before that and between 8 – 10 kBq/kg after that. Activity of ^{135}Xe was a copied progression of the activity of ^{133}Xe and the ratio of ^{133}Xe/^{135}Xe was around ~1.

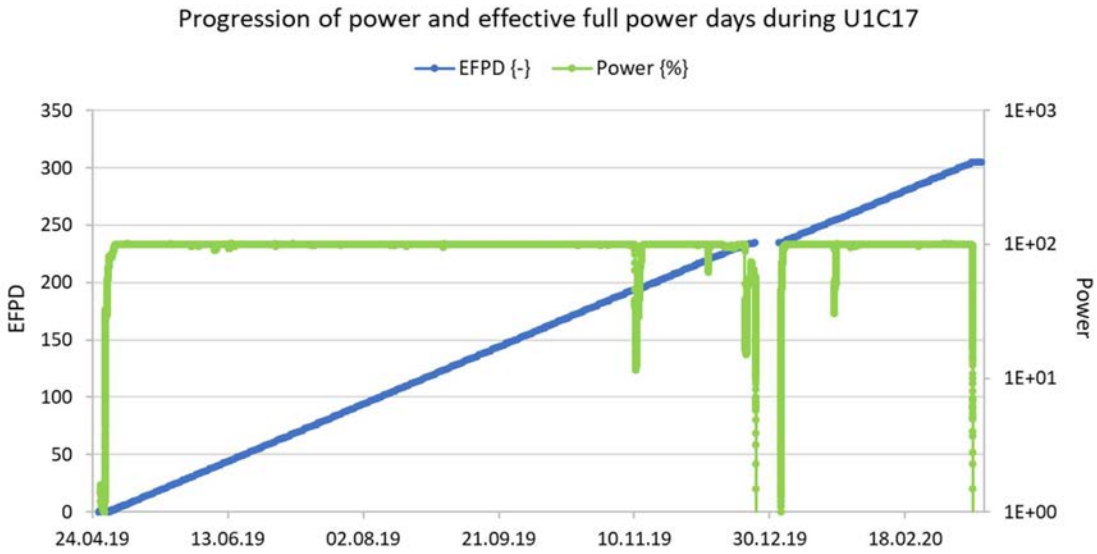

FIG. 1. Reactor power and progression of number of EFPD during U1C17.

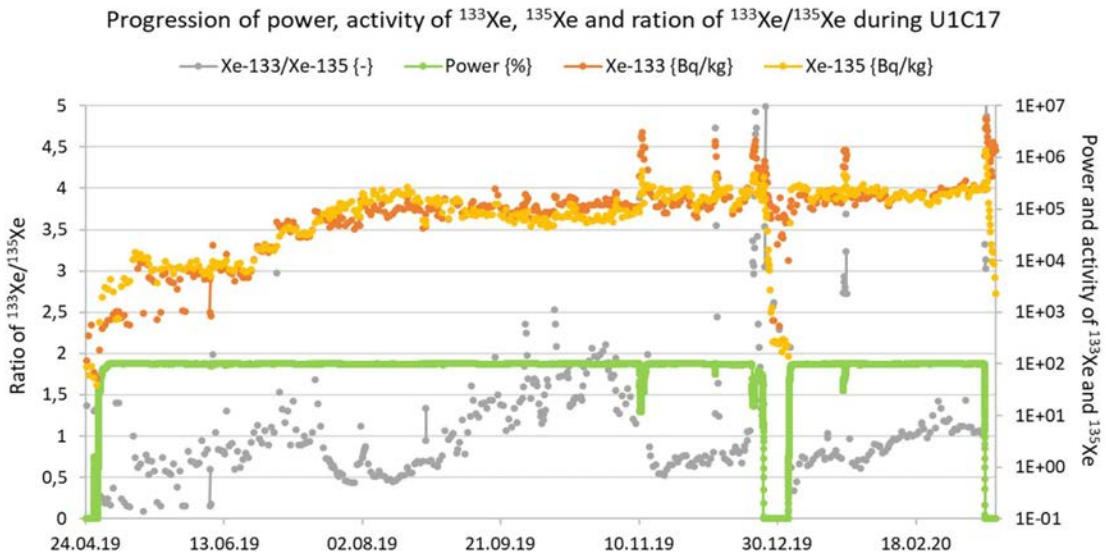

FIG. 2. Progression of activity (Bq/kg) of ^{133}Xe, ^{135}Xe and ratio of ^{133}Xe/^{135}Xe during U1C17.

Activities of ^{131}I, ^{134}Cs and ^{137}Cs were not changed at that time, as you can see in Fig. 3. It was a sign of the gaseous type of a fuel failure. It was not possible to predict a burnup of leaking fuel rod from the ratio of ^{134}Cs/^{137}Cs because of the high initial activities of ^{134}Cs and ^{137}Cs, as you can see in Fig. 3. These activities were residues of fuel failures from previous cycles.

The prediction of a burnup was based on the ratio of ^{85m}Kr/^{135}Xe. As you can see in Fig. 4, the ratio of ^{85m}Kr/^{135}Xe was ~ 0.225 and it corresponded to the burnup of ~ 31 MWd/kgU. This first indication was resolved to the prediction of one leaking fuel rod in the core and it was a fuel rod operating for the third cycle.

As you can see in Figs. 2 and 3, there were no changes in activities for the next 6 weeks until 25th June. Two changes occurred in activities of ^{133}Xe and ^{135}Xe (25th June and 2nd July). The first change was an increase of activities of ^{133}Xe and ^{135}Xe to ~ 19 kBq/kg and the second change was an increase in activity of the same radionuclides to 50 - 60 kBq/kg. Still with no respond of activities of ^{131}I, ^{134}Cs and ^{137}Cs. Activity of ^{131}I was under the minimum significant activity and activities of ^{134}Cs and ^{137}Cs were on the same levels without changes. So, prediction of a burnup based on the ratio of ^{134}Cs/^{137}Cs remained impossible. Activity of ^{131}I increased to ~ 15 kBq/kg for the first time on 21st July. This increase resolved into a fast decrease of the ratio of ^{133}Xe/^{135}Xe from ~ 1.1 to ~ 0.45 and the ratio of ^{85m}Kr/^{135}Xe from ~ 0.225 to ~ 0.18. This could be explained as changes on an existing leaking fuel rod or as a new (second) fuel failure. It resolved into the change of prediction from one to one or two leaking fuel rods in the core. In that moment, prediction of the burnup based on ^{85m}Kr/^{135}Xe was not possible or did not make sense because this ratio corresponded to the burnup ~ 65 MWd/kgU. There was no fuel rod in the core with so high burnup.

One significant peak was on the activity of ^{131}I on 1st August. After that activity of ^{131}I started to decrease slowly to ~ 5 kBq/kg until 10th November 2019. Activities of ^{133}Xe and ^{135}Xe changed slowly, the ratio of ^{133}Xe/^{135}Xe increased from ~ 0.5 up to ~ 2 and the ratio of ^{85m}Kr/^{135}Xe increased from ~ 0.18 to ~ 0.31. This resolved to the change of prediction to two leaking fuel rods in the core. Prediction of the burnup was still not possible, because activities of ^{134}Cs and ^{137}Cs were intact. That meant the ratio of ^{134}Cs/^{137}Cs remained useless for the burnup prediction. Ratio of ^{85m}Kr/^{135}Xe moved to the opposite extreme because the value of 0.31 was not defined as possible. The highest possible value of this ratio was 0.26 for burnup ~1 MWd/kgU.

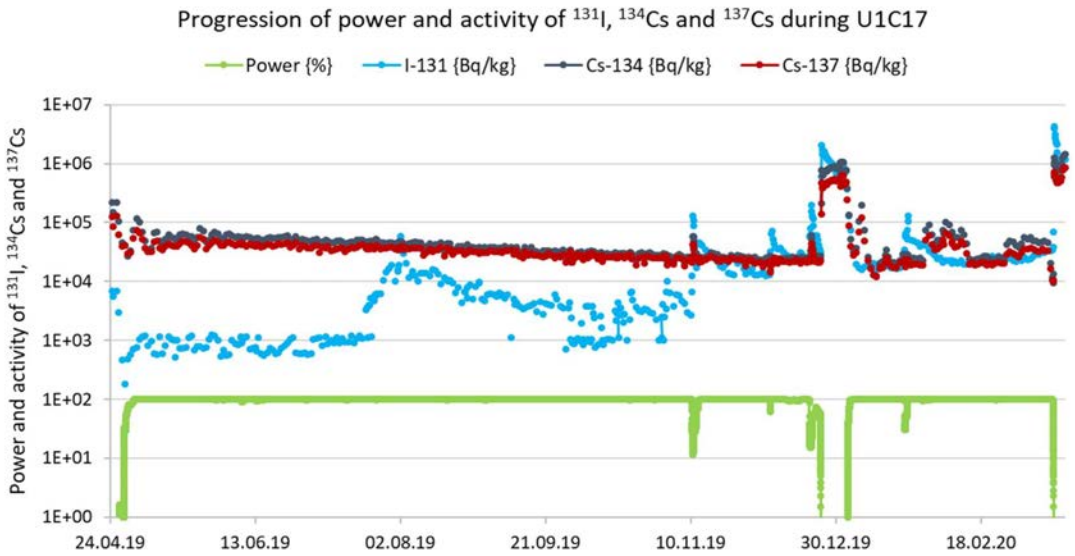

FIG. 3. Progression of activity (Bq/kg) of ^{131}I, ^{134}Cs and ^{137}Cs during U1C17.

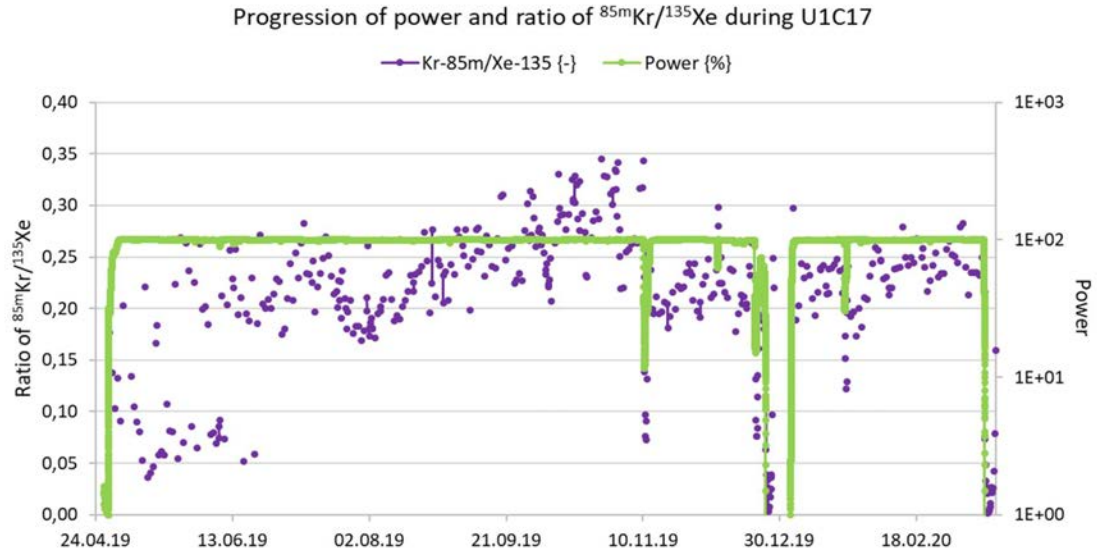

FIG. 4. The ratio of $^{85m}Kr/^{135}Xe$ during U1C17.

On 10th November, there was a spike effect after the power drop. Activity of ^{135}Xe increased by three times from ~ 80 to ~ 220 kBq/kg and the activity of ^{133}Xe was unchanged. This changed the ratio of $^{133}Xe/^{135}Xe$ from ~ 2 to ~ 0.75. This state remained unchanged until 7th December 2019. Activity of ^{131}I increased to ~ 45 kBq/kgU and it started to slowly decrease to ~ 13 kBq/kg. The ratio of $^{85m}Kr/^{135}Xe$ decreased back to possible values ~ 0.215, which corresponds to the burnup of ~ 40 MWd/kgU. This behavior of radiochemical parameters corresponded to changes on an existing leaking fuel, but activities of ^{133}Xe and ^{135}Xe corresponded to more than two leaking fuel rods. So, the prediction was changed to two or three leaking fuel rods, probably operating for third cycle.

This prediction was not changed because of the power drop on 7th December 2019. Changes were not significant enough and they were in the line with the prediction of two or three leaking fuel rods.

There was a short power shutdown between 20th December 2019 and 3rd January. There were no changes on radiochemical parameters after a power up and stabilization of all parameters. So, predictions were not changed.

Another short power drop was on 22nd January. This caused a short increase of ^{131}I activity to ~ 50 kBq/kg and the ratio of $^{133}Xe/^{135}Xe$ started to increase from ~ 0.75 to ~ 1.2. This was explained as a sign of the fourth leaking fuel rod. Ratio of $^{85m}Kr/^{135}Xe$ moved to ~ 0.24 and it corresponded to the burnup ~ 18 MWd/kgU. It meant, these four leaking fuel rods could be a combination of rods operating for second and third cycle.

Prediction was not changed until the shutdown for an outage on 13th March. It was assumed there was only one leaking fuel rod in a single fuel assembly, so the prediction was to find four leaking fuel assemblies.

2.1.2 Identification of leakers

In Temelín NPP, there is an on-line sipping system to test fuel assemblies during an unloading of the core during an outage. All 163 fuel assemblies were measured because of indications of fuel failures and prediction of four leaking fuel rods. The test was performed by measuring of the single energy line of 81 keV in gas passing through the fuel assembly during moving the fuel assembly from the core to the spent fuel pool. This energy line fitted for ^{133}Xe, which was released from the leaking fuel rod because of the drop of hydrostatic pressure during lifting of the fuel assembly from the core to the fuel handling machine.

In-cell sipping system, which is used very rarely in Temelín NPP and only seven TVEL fuel assemblies was measured by this system, is based on thermal stress of tested fuel assembly. In-cell sipping test can be performed as qualitative or quantitative. Quantitative type of test is not used in Temelín NPP. During qualitative test, fuel assembly is loaded to cell, where is heat up by 40 °C (temperature of coolant of spent fuel pool + 40 °C). It causes release of fission products, and it is evidence of leaking fuel rod in tested fuel assembly.

On-line sipping test is an easy and fast method with a very high level of success in finding leaking fuel assemblies. That was the reason, why the in-cell sipping system wasn't used to confirm the found leaking fuel assemblies.

As can be seen in Fig. 5, predictions were correct, because four leaking fuel assemblies were found (CY-19, GD-06, CY-22 and FA-10). Two fuel assemblies were after 2 years of operating and two after 3 years of operating.

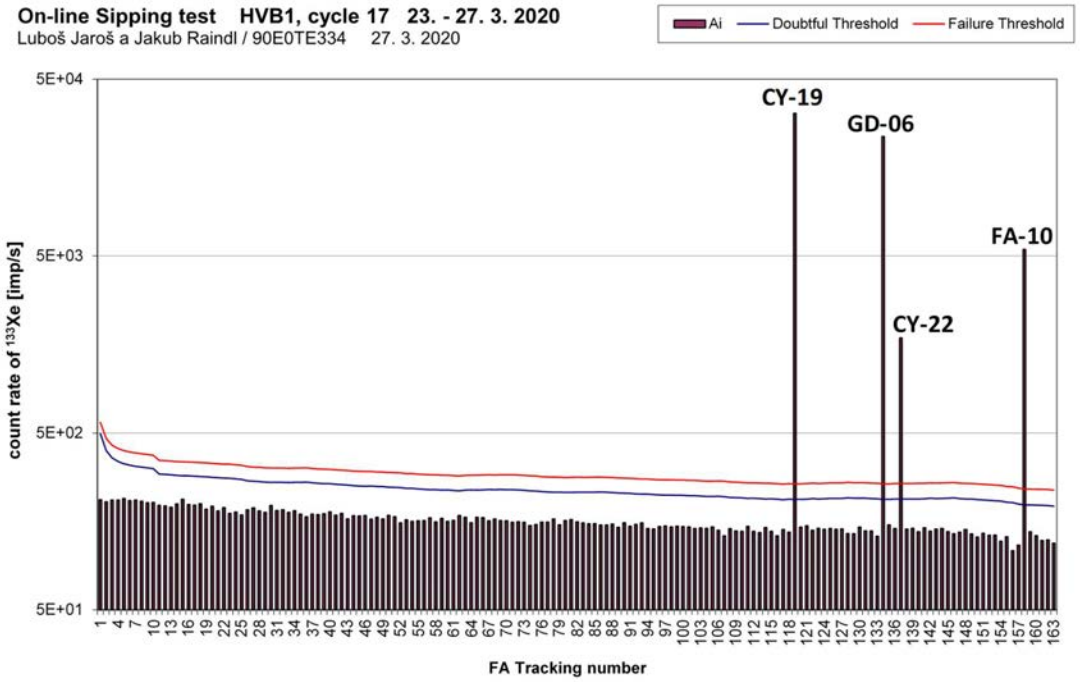

FIG. 5. Results of on-line sipping test after U1C17.

2.2 Unit 2, cycle 17

2.2.1 Monitoring and prediction of fuel failures

Cycle 17 on unit 2 [U2C17] was from 9th August 2019 to 13th June 2020 with a short shutdown at the end of December 2019. It achieved 306 EFPD, as you can see in Fig. 6.

As you can see in Fig. 7, it was possible to see first indications of a fuel failure after three and a half months of the full power operation (EFPD = 100.2) on 20th November 2019. It could be seen on changes of ^{133}Xe activity. Activity of ^{133}Xe was under minimal significant activity (< 1 kBq/kg) before that and ~ 20 kBq/kg after that. Activity of ^{135}Xe did not increase so much as activity of ^{133}Xe and ratio of ^{133}Xe/^{135}Xe increased rapidly to ~ 1.8.

Activities of ^{131}I, ^{134}Cs and ^{137}Cs were not changed at that time, as you can see in Fig. 8. It was the sign of a gaseous type of fuel failure, just like in the case of U1C17. It was not possible to predict a burnup of the leaking fuel rod from the ratio of ^{134}Cs/^{137}Cs and the ratio of ^{85m}Kr/^{135}Xe. The ratio of ^{134}Cs/^{137}Cs could not be used because of the high initial activities of ^{134}Cs and ^{137}Cs, as you can see in Fig. 8. These activities were the residues of fuel failures from previous cycles. The ratio of ^{85m}Kr/^{135}Xe could not be used, too, because the value of this ratio was ~0.17, as you can see in Fig. 9. This value was extremely low, and it corresponded to the burnup of higher than 65 MWd/kgU. This burnup was much higher than the highest burnup fuel rod occurring in the core. This first indication was resolved to prediction of one leaking fuel rod in the core without any prediction of a burnup.

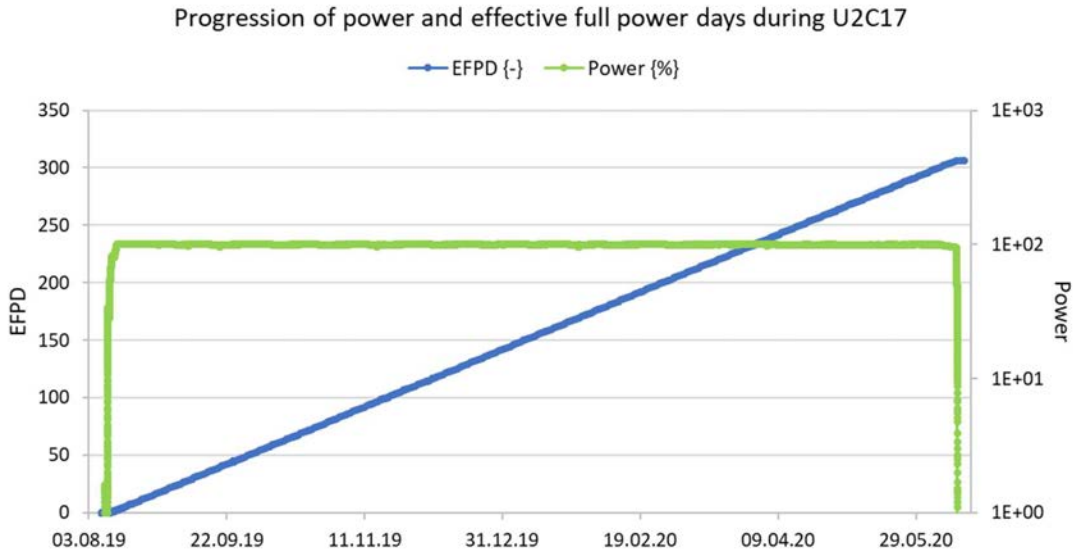

FIG. 6. Reactor power and progression of number of EFPD during U2C17.

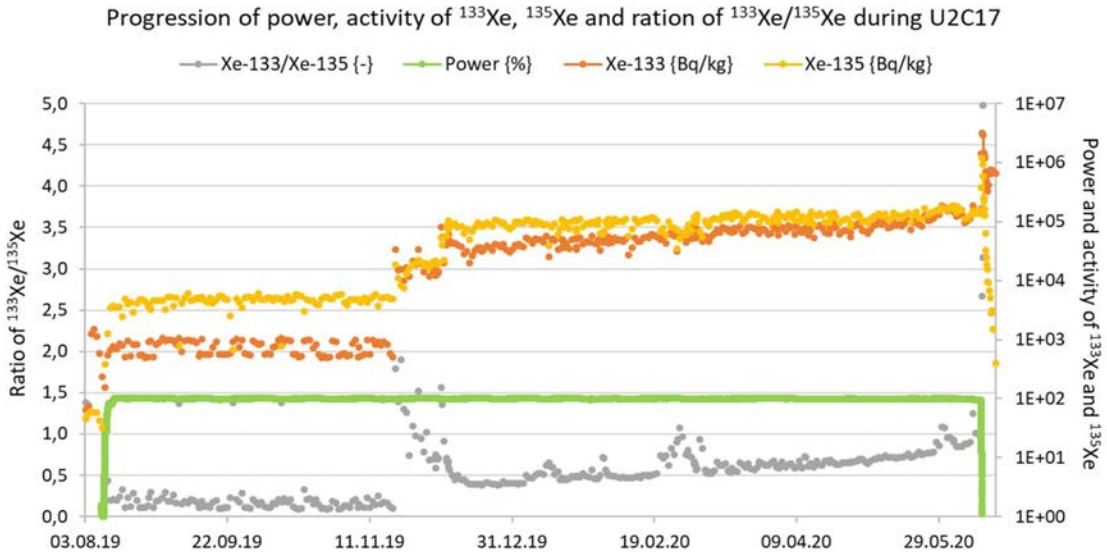

FIG. 7. Progression of activity (Bq/kg) of 133Xe, 135Xe and ratio of 133Xe/135Xe during U2C17.

Activity of ^{133}Xe was relatively stable ~20 kBq/kg after this first increase. On the other hand, the activity of ^{135}Xe slowly increased from ~14 kBq/kg to ~54 kBq/kg. It caused a decrease of the ratio of ^{133}Xe/^{135}Xe from ~1.8 to ~0.4. This decrease was followed by the first significant change of the activity of ^{131}I on 8th December 2019, when the activity increased from less than the minimum significant activity (< 1 kBq/kg) to ~12 kBq/kg. This increase was linked with the second increase of activities of ^{133}Xe and ^{135}Xe. These changes were explained as a sign of the second leaking fuel rod.

As you can see in Figs. 8 and 9, there were no changes in the ratios of ^{134}Cs/^{137}Cs and ^{85m}Kr/^{135}Xe. It meant that prediction of the leaking fuel rods burnup remained impossible.

For the rest of the campaign, there were no significant changes in radiochemical parameters. Activity (Bq/kg) of ^{133}Xe increased slowly as well as the ratio of ^{133}Xe/^{135}Xe, but without any indication of the rapid change, which could be used as an indication of another leaking fuel rod. As you can see in Fig. 8, activity (Bq/kg) of ^{131}I changed rapidly at the end of May 2020, but it was caused by the bypass of ion exchanger lines, so the primary coolant wasn't cleaned-up for a week.

Just like in the case of U1C17, it was assumed that there was only one leaking fuel rod in one fuel assembly, so the prediction was to find two leaking fuel assemblies during the outage.

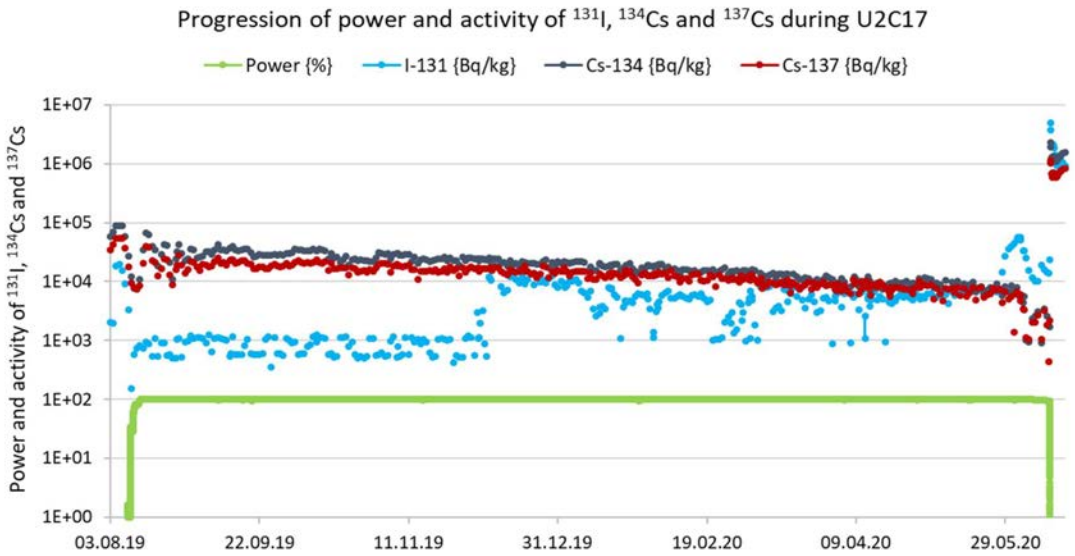

FIG. 8. Progression of activity (Bq/kg) of 131I, 134Cs and 137Cs during U2C17.

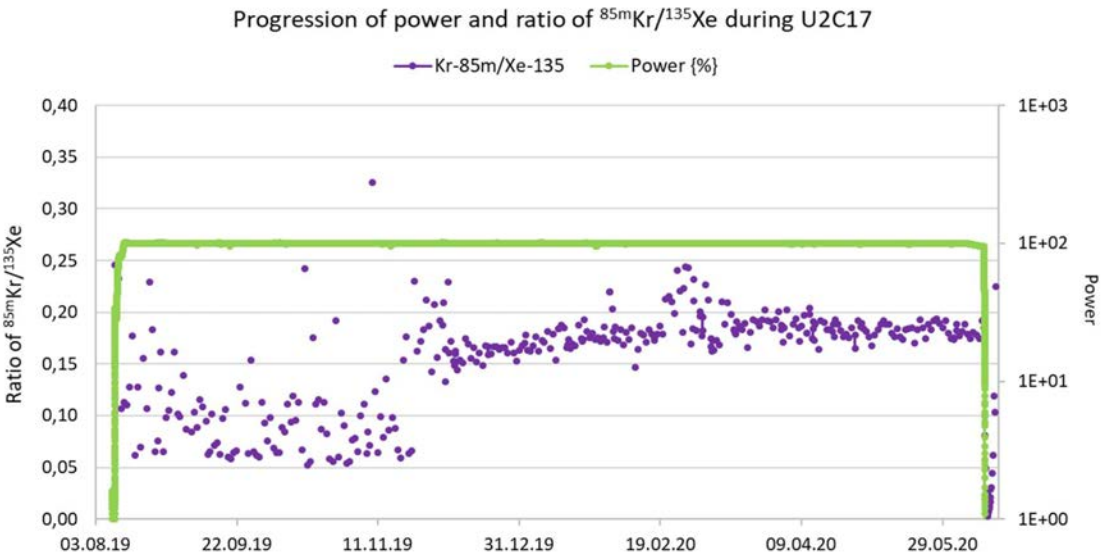

FIG. 9. The ratio of $^{85m}Kr/^{135}Xe$ during U2C17.

2.2.2 Identification of leakers

As in the case of unit 1 after 17th cycle, all 163 fuel assemblies were measured because of indications of fuel failures and the prediction of two leaking fuel rods. The test was performed by measuring single energy line of 81 keV in gas passing through fuel assembly during moving fuel assembly from core to spent fuel pool. This energy line fitted for ^{133}Xe.

As can be seen in Fig. 10, predictions were correct, because two leaking fuel assemblies were found (GB-12 and GB-16). Both fuel assemblies were after 3 years of operating.

As can be seen in Fig. 10, there were four fuel assemblies which were measured twice. One of them was caused by a human error during the calibration check. Another three were caused by problems with the air flow throw the on-line sipping system.

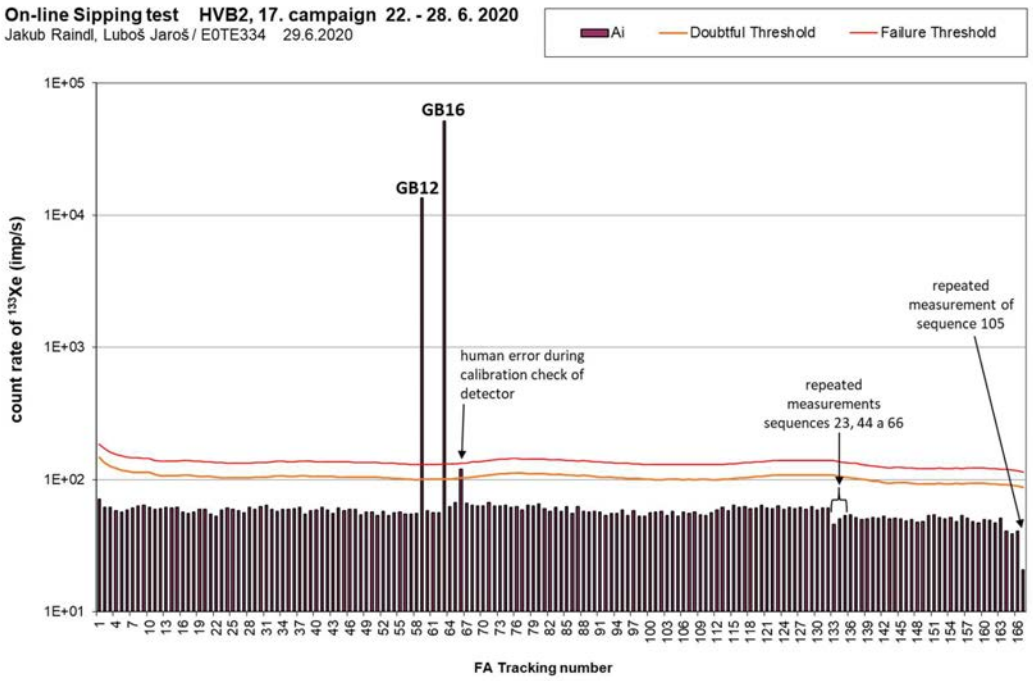

FIG. 10. Chart showing results of on-line sipping test after U2C17.

3. OVERVIEW OF ALL FUEL FAILURES FOUND ON FUEL ASSEMBLIES SUPPLIED BY TVEL FUEL COMPANY IN TEMELÍN NPP

As mentioned in chapter 2, 6 leaking fuel assemblies were found during 2020. Total number of found leaking fuel assemblies of TVEL fuel were 25 in unit 1 and 24 in unit 2, as you can see in Table 1. All found leaking fuel assemblies in Table 1 are divided by units and by years of operation in the core. One can see our predictions of number of leaking fuel assemblies. For better explanation, one can see comparison of predicted number and number of found leaking fuel assemblies for unit 1 in Fig. 11 and the same thing for unit 2 in Fig. 12.

As one can see in Figs. 11 and 12, there were no cycle when leaking fuel assembly occurred in the cores and these cycles were predicted as with no leaking fuel assembly.

Prediction of number of leaking fuel assemblies were correct in 53.8 % of cases. Prediction was wrong by more than one only in 2 cases. That means that predictions did not differ by more than one in 84.6 % of cases. It's high success of predictions by chemistry department of Temelín NPP.

TABLE 1. NUMBER OF PREDICTED VS. DETECTED LEAKING FUEL ASSEMBLIES IN EACH CYCLE ON BOTH UNITS ACCORDING TO YEARS OF OPERATION IN THE CORE

	Unit 1						Unit 2					
	Pred	All	1y	2y	3y	4y	Pred	All	1y	2y	3y	4y
Total	-	25	3	5	16	1	-	24	1	6	11	6
C9	3	3	3	-	-	-	0	0	-	-	-	-
C10	0	0	-	-	-	-	0	0	-	-	-	-
C11	0	0	-	-	-	-	0	0	-	-	-	-
C12	2	2	-	1	-	1	3	7	-	4	2	1
C13	3	7	-	-	7	-	3	4	-	-	3	1
C14	2	2	-	-	2	-	2	3	-	1	1	1
C15	3	3	-	2	1	-	4	5	1	-	3	1
C16	3	4	-	-	4	-	3	3	-	1	-	2
C17	4	4	-	2	2	-	2	2	-	-	2	-

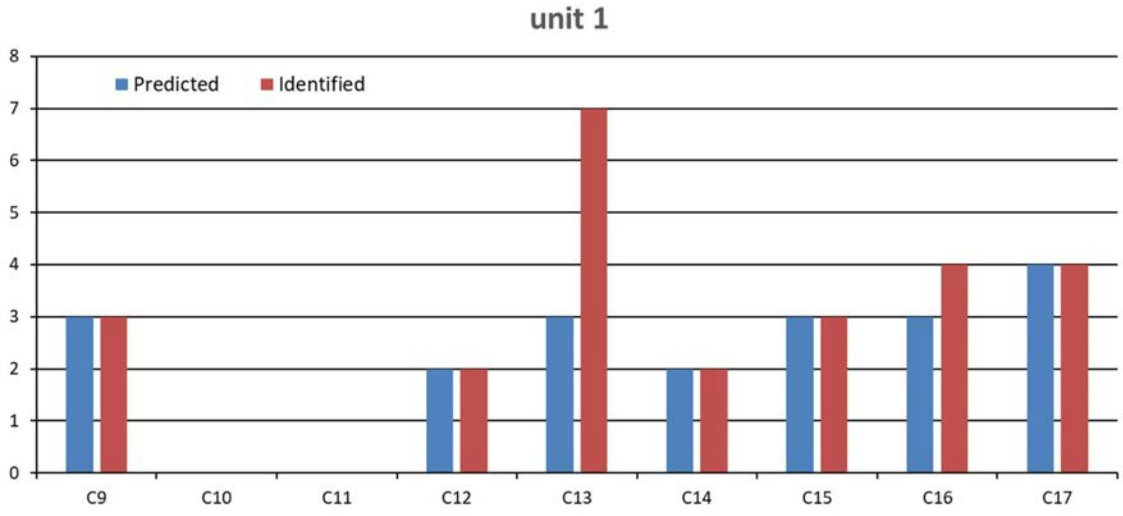

FIG. 11. Comparison between predicted and found number of leaking fuel assemblies in unit 1.

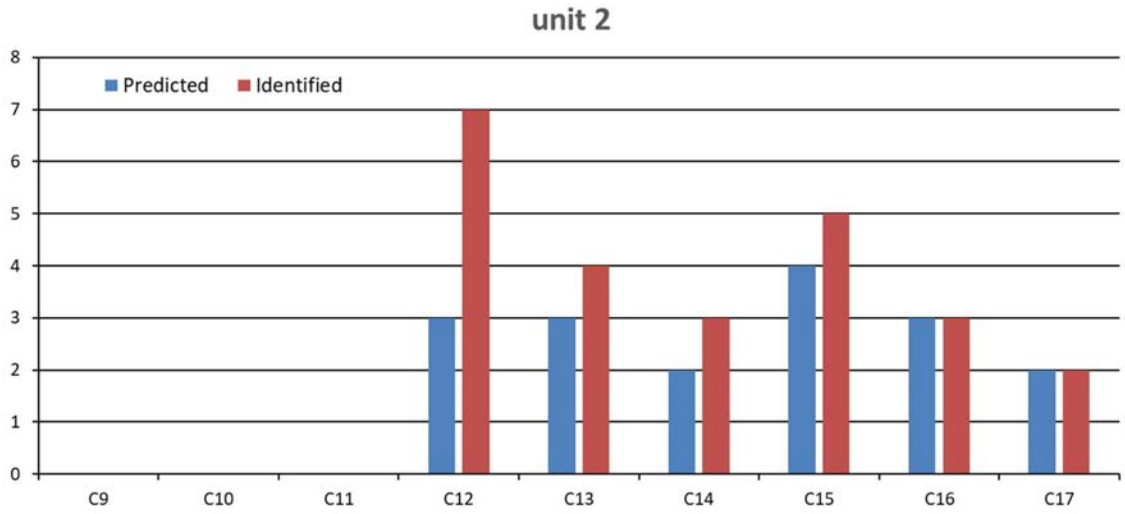

FIG. 12. Comparison between predicted and found number of leaking fuel assemblies in unit 2

One can see the data on found leaking fuel assemblies divided according to lifetime before discharge from Table 1 in Fig. 13 for unit 1 and Fig. 14 for unit 2.

As one can see in Table 1 and Figs. 13 and 14, the first experience with TVEL fuel was good, just three leaking fuel assemblies found after U1C9 were inconvenient, but they were identified as a manufacturer error. There was no leaking fuel rod during another two years. After that, there were two or more leaking fuel assemblies in every cycle on both units. The highest number of leaking fuel assemblies was found in U1C13 and U2C12. There were 14 leakers, 11 of them were from the same production batch. Failure for the same cause had not been proven.

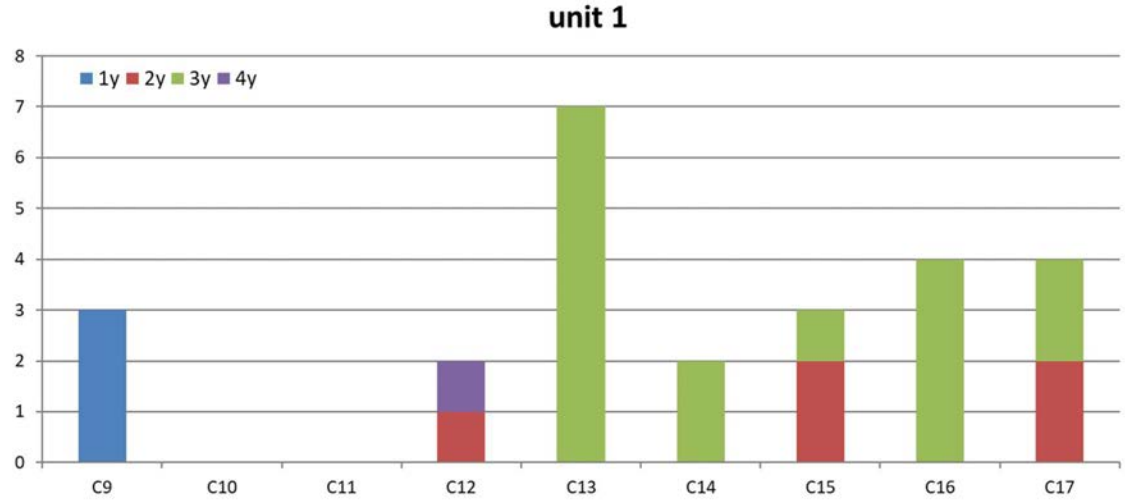

FIG. 13. Leaking fuel assemblies found in unit 1 and divided according to lifetime before discharge.

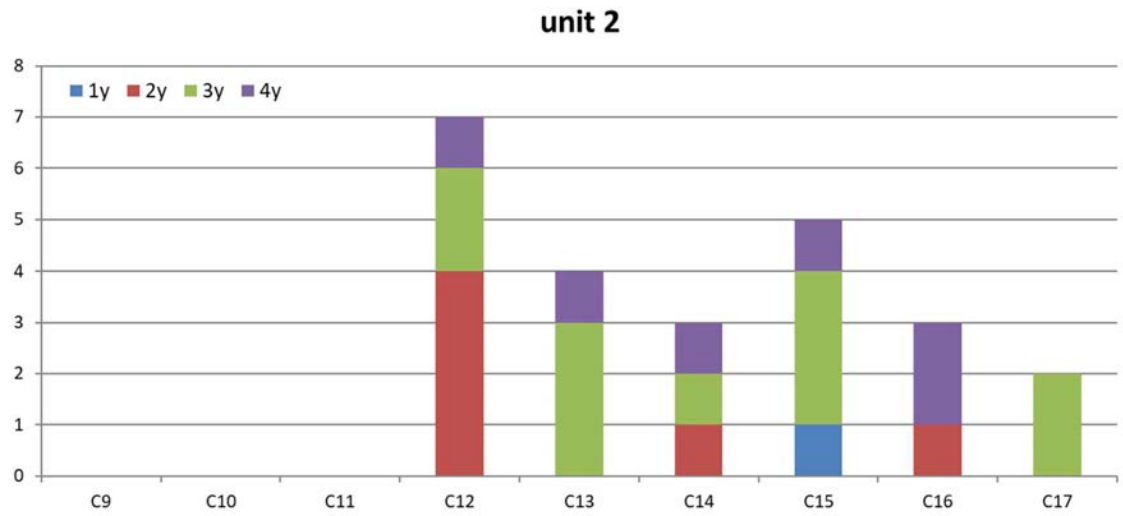

FIG. 14. Leaking fuel assemblies found in unit 2 and divided according to lifetime before discharge.

An average number during last 6 cycles is 3.83 leakers per cycle. It is a high and unacceptable failure rate, but it must be said, all leakers were of gaseous type. So, there were no alfa-radionuclides in the primary coolant. All results of alpha radionuclides were under the minimum detectable activity (< 80 mBq/kg) during the last 12 years. Nevertheless, all released radioactive noble gases, iodine and Cs isotopes had to be filtered by clean-up systems and they were concentrated there. It meant that these clean-up systems had a very high dose rate. It caused problems during regenerations of these filters and problems with the amount of created radwaste.

As one can see in Table 2, only 4 of total 49 leaking fuel assemblies were after the first year of operation. As you can see in Table 2, it´s only 8.2 % of all. The highest number is on leaking fuel assemblies found after 3 years of operating. They represent 27 of total 49, it is more than 55% of all leakers. It could show a failure for the same cause, but this cause was not found or proved. For the better perspective, the data from Table 2 is shown in Fig. 15. Leakers after 2 years of operating represent 11 of total 49, it is more than 22% of all leakers and leakers after 4 years of operating represent 7 of total 49, it is only 14.3 %.

This could be surprising because this fuel assemblies after 4 years of operating represent the highest burnup. Degradation of fuel properties should be highest with highest burnup. That means that fuel failures may be not caused by general degradation of fuel properties, but by some different unfortunately unknown cause.

TABLE 2. TOTAL NUMBER OF FOUND LEAKING FUEL ASSEMBLIES ON BOTH UNITS ACCORDING TO YEARS OF OPERATION IN THE CORE

	Both Units	Percentage
Total	49	
After 1y	4	8,2%
After 2y	11	22,4%
After 3y	27	55,1%
After 4y	7	14,3%

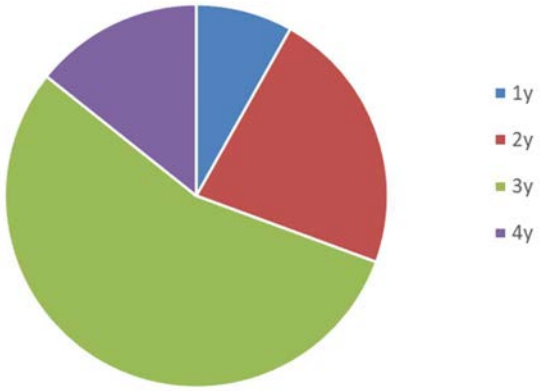

FIG. 15. Representation of individual operation years of leaking fuel assemblies.

4. CONCLUSIONS

Leaking fuel assembly could occur in every time of operating. It is very important to monitor integrity of fuel cladding and find all fuel failures during outage.

Temelín NPP has a problem with the gaseous type of fuel failures. This type of fuel failures is difficult to monitor because of small changes in the activity of reference radionuclides. It is also difficult to predict their number in the core in case of occurring more than one leaking fuel assembly.

Chemistry department of Temelín NPP has a successful experience in prediction and identification of leaking fuel assemblies both during reactor operation and outage.

REFERENCES

[1] INTERNATIONAL ATOMIC ENERGY AGENCY, Review of Fuel Failures in Water Cooled Reactors, Vienna, Austria, 2010

[2] CHENG, B., Fuel Reliability Monitoring and Failure Evaluation Handbook, Revision 2, EPRI, Palo Alto, USA, 2010

[3] BÁRTA, O., Stanovení a vyhodnocení nehermetického palivového proutku v podmínkách provozu ETE (Determination and evaluation of leaking fuel rod in conditions of Temelín NPP), CHEMCOMEX Praha, a.s., Prague, Czech Republic, 2003.

APPLICATION OF AN IMPROVED TECHNIQUE FOR BURNUP EVALUATION OF WWER LEAKING FUEL BASED ON THE DATA ON SPIKING EVENTS

O.V. VILKHIVSKAYA, E.Yu. AFANASIEVA, I.A. EVDOKIMOV
SRC RF TRINITI,
Troitsk, Russian Federation

V.V. LIKHANSKII
NRC Kurchatov Institute,
P.N. Lebedev Physical Institute, RAS,
Moscow, Russian Federation

Abstract

A conventional approach to evaluating burnup of the leaking fuel assemblies (LFA) at operating WWER power units is to use a burnup correlation of $^{134}Cs/^{137}Cs$ activity ratio in the primary coolant during spiking events. This technique was revised in an updated regulatory document, considering the differences in evolution of cesium (Cs) content in fuel pellets and in voids inside a fuel rod. However, from 2000^{s}, analysis of spiking events and data of post-irradiation examinations (PIEs) show this technique to be rather inaccurate in some cases. Recent NPP data on activity spiking events at WWER-1000 power units and LFAs examination results have filled the data gap in the burnup range of 40-50 MWd/kgU for Cs inventory in fuel rods with initial enrichment of 4.95 wt%. This new data enables a thorough comparative analysis of systematic factors causing deviation of experimental estimates compared to the results of the conventional technique for various fuel enrichments including fuel with solid fuel pellets. The paper briefly describes an improved technique introduced previously for express calculation of build-up of Cs isotopes in fuel pellets for every fuel rod in the core. This approach employs the NPPs results of routine neutronic calculations of actual pin-wise linear heat generation rate (LHGR) for each fuel cycle with a particular core loading pattern. The activity ratios $A(^{134}Cs)/A(^{137}Cs)$ in fuel calculated in the frame of this technique show good agreement with the available NPP data for LFAs with solid fuel pellets and are also compared to the new RIAR PIE data. It is suggested that an increased reliability in evaluation of leaking fuel burnup at operating WWERs and subsequent LFAs identification could be achieved if the key factors affecting evolution of $^{134}Cs/^{137}Cs$ activity ratio for each FA in the core are considered simultaneously with distinctive features of mass transfer in leaking fuel rods of different design.

1. INTRODUCTION

Accurate preliminary prediction of burnup, for leaking fuel, during reactor operation remains a challenging issue at nuclear power plants (NPPs), [1-7]. Solving this issue would help expedite identification of the LFA while in the core, for example during the maintenance outages, and facilitate the search for a proper substitute in spent fuel pool. Currently, reliable identification of leaking FAs of advanced design requires considering evolving operational features of contemporary fuel cycles at WWER-1000 and WWER-1200 power units [8, 9].

In the event of fuel failures and release of radionuclides into the primary coolant, one of the most sensitive indicators of burnup for leaking fuel in WWER and PWR power units is the ratio of ^{134}Cs to ^{137}Cs activity during a spiking event due to power transients or reactor shutdown, [1, 10, 11]. This technique has been discussed in various works starting the early 1960^{s} [12], as well as in the most recent studies [3, 13, 14]. However, in recent years, the traditional way of applying this technique in practice has led to an increasing number of cases where fuel burnup was predicted inaccurately. In this regard, development of improved techniques for better evaluation of burnup for leaking fuel is of high importance to the NPPs. Improvement is possible by better estimating cesium (Cs) inventories as they evolve in each fuel rod, for a particular fuel loading pattern in the core, during the fuel cycle.

Currently, a standard pin-wise neutronic calculation for the evolution of linear heat generation rates (LHGRs) and fuel burnup is required before every fuel cycle at WWER power units. However, these calculations do not provide data on Cs inventory in the fuel pellets. Thus, additional methods should be utilised to account for Cs build-up rates in different fuel rods/FAs in each fuel cycle.

It might not be necessary to involve high-precision depletion calculations of Cs inventory in fuel for the analysis of activity spike-events during reactor operation based on the margin available in activity measurements

of water samples taken from the primary coolant, [1, 3, 5]. In simulating the fission product inventories of fuel rods, uncertainties inherent to the non-uniform axial burnup profile have been identified as follows:

— Type of defect (i.e., primary/secondary) and its axial location.
— Size of defect and release rate of fission products into the coolant (with fuel washout requiring consideration for severe cases).
— Non-uniform fuel temperature distribution (where the hottest regions of the fuel column contribute more to Cs inventories released from fuel pellets).

These uncertainties were partially addressed in papers [1, 3-8] by analysis of fuel operating conditions in contemporary fuel cycles at WWER-1000 power units, allowing for an improvement of the existing burnup evaluation technique during reactor operation proposed in [1, 5] and briefly described in Section 2.

The basis for improvement was the models developed for a fast evaluation of the $^{134}Cs/^{137}Cs$ activity ratio versus fuel burnup. The rate of Cs isotopes production in fuel was modelled depending on the FA irradiation history and the neutron spectrum parameters in each fuel cycle. These factors include pin-wise LHGRs, duration of reactor outages, and fuel parameters that contribute to mutual resonance shielding for $^{238}U/^{235}U/^{133}Cs$ and spectrum effects to varying degrees (fuel pellet design, enrichment, temperature profile, number, and content of Gd in U-Gd rods in a FA, [5]). Previous validation [1, 3-8] has shown that the calculated results for Cs inventories in leaking FAs are within the error margin of activity measurements in the primary coolant. Furthermore, ongoing collection and analysis of NPPs operational data and new PIE results, obtained by the Russian Institute for Atomic Reactors (RIAR), provides opportunities for extending application of this technique to burnup evaluation of leaking FAs, as well as continuous validation of the models.

2. CONVENTIONAL APPROACH FOR FUEL BURNUP EVALUATION USING $^{134}CS/^{137}CS$ ACTIVITY RATIO

A common approach to the evaluation of burnup for leaking WWER fuel at NPPs was to use a correlation, from the regulatory guidelines shown in Fig.1 (right), which presents the $^{134}Cs/^{137}Cs$ activity ratio in fuel as a function of fuel burnup.

This correlation was based on averaging of neutronic calculations (NPCs) for typical WWER fuel cycles and was applied in the early 2000s. However, the analysis [1, 3] is not comprehensive and spike events for WWER fuel with hollow (annular) fuel pellets have shown some noticeable discrepancies with this technique when considering contemporary fuel cycles with their higher fuel enrichment and wider application of Gd burnable absorber. These factors result in 'hardening' of the neutron spectrum which influences the effective neutron capture cross-section ^{133}Cs (n, γ) ^{134}Cs in the resonance energy region. At the same time, accumulation of ^{137}Cs and ^{133}Cs in fuel is practically linear with fuel burnup, [1]. This may result in considerably higher ratios of ^{134}Cs and ^{137}Cs concentrations in the fuel at the same burnup level, as repeatedly observed [1, 5, 6].

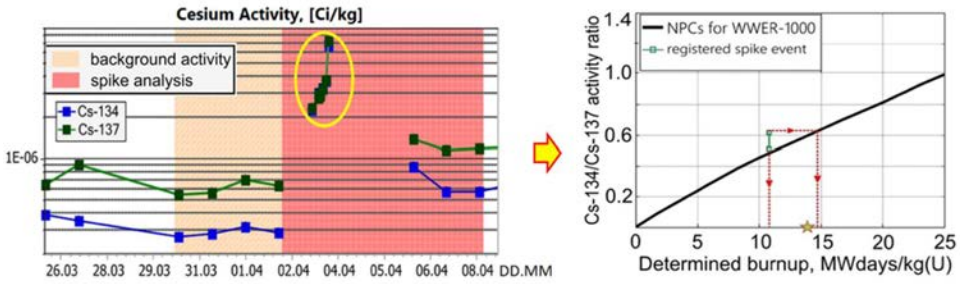

FIG. 1. An example of applying a conventional WWER technique for fuel burnup evaluation based on ^{134}Cs and ^{137}Cs spike-event during a power transient, [1].

This technique was updated in Reference [2] considering the differences in evolution of Cs content in fuel pellets and in voids within a fuel rod. However, application of this updated technique still resulted in noticeable

discrepancies in the burnup evaluation for several recent cases involving leaking FAs with solid fuel pellet, [3, 4]. As an example, Fig. 2 shows the result of applying the updated correlations [2] for evaluating burnup of leaking fuel with solid pellets, using the $^{134}Cs/^{137}Cs$ activity ratio obtained during the end of cycle (EOC) spike-events, as recently discussed in [3]. The regulatory guidelines [2] provide two correlations for the $^{134}Cs/^{137}Cs$ activity ratios: for "voids inside a fuel rod" and for "fuel pellets". They yield the bottom and the upper estimate for the fuel burnup, respectively. The first correlation applied to the spike-event data in case #2 (see Fig. 2) yields a minimal burnup of the leaking FA of 36 MWd/kgU. It is higher than the actual average burnup 30.54 MWd/kgU in the leaking FA found during the outage by the failed fuel detection system (FFDS) testing. Fuel burnup in the leaking fuel rod was 31.65 MWd/kgU, [3]. These discrepancies may be reduced (or avoided in some cases) by applying the proposed models [1, 3-8].

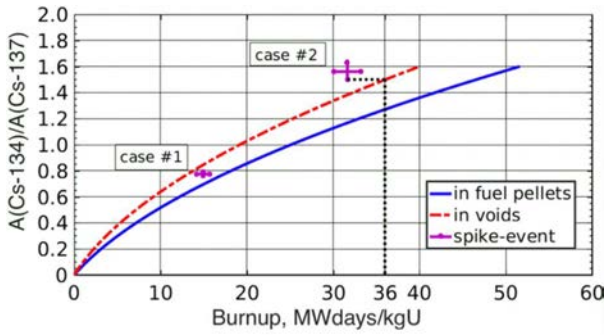

FIG. 2. An example of applying the updated correlations [2] for evaluation of fuel burnup by 134Cs and 137Cs activity spiking at EOC (WWER fuel with solid pellets, see [3] for a detailed case study).

To perform a more detailed assessment of the factors that could contribute to the observed discrepancies, when applying the correlations [2] as shown in Fig. 2, more experimental data was needed for spike-event cases involving a higher fuel burnup range and enrichment. Recent NPP data on activity spiking at WWER-1000 power units and subsequent PIE results of leaking fuel have filled the data gap in the burnup range of 40-50 MWd/kgU for Cs inventory in fuel rods with solid fuel pellets and initial enrichment of 4.95 wt%. This new data enables a detailed comparative analysis of systematic factors causing deviation of experimental estimates compared to the results of the conventional technique for various fuel enrichments including WWER fuel with solid fuel pellet. New cases of spiking and PIE data are discussed in Sections 4.1-4.3. Section 4.4 gives a summary of recent experience when applying the improved technique for burnup evaluations of leaking fuel.

3. BASIC CONCEPTS OF IMPROVEMENTS TO THE CONVENTIONAL APPROACH FOR FUEL BURNUP EVALUATION USING $^{134}CS/^{137}CS$ ACTIVITY RATIO

A detailed description of the model assumptions used for the fuel burnup and Cs inventory calculations for UO_2 and (U, Gd) O_2 rods are provided in open access conference proceedings [3, 5]. Thus, Section 3 only outlines the basic concepts of these models, and closer attention is given to data analysis using these models in Section 4. Isotopic inventory calculations, with the previously developed code [1, 4, 5], are limited to the quick simulation of the build-up of Cs isotopes and estimation of the $^{134}Cs/^{137}Cs$ activity ratio in fuel pellets.

The proposed simplified models enable fast and reliable evaluation of Cs inventory in fuel explicitly accounting for the irradiation history of each FA in the WWER core, [1, 4, 5]. These models utilise the actual LHGR evolution of a Gd-doped fuel rod and the LHGRs of adjacent fuel rods in the FA (obtained by routine neutronic calculations at NPPs). A two-group approximation is adopted for the neutron flux distribution (one for thermal energy neutrons and another for epithermal energy neutrons). A convention for the effective reaction cross-sections in thermal neutron reactors proposed by Westcott et al., [1], was used as well. The parameter γ defines the ratio of epithermal-to-thermal energy neutron interactions with fissile nuclides (i.e., the so-called 'hardness' of the neutron spectrum). A changing contribution of epithermal and thermal energy neutrons into the total LHGR

of a FA during the cycle results in differences of $^{134}Cs/^{137}Cs$ activity ratio in fuel of UO_2 and (U, Gd) O_2 rods in the same FA, [5].

The calculations for Cs production in the fuel accounts for the initial hardness of the neutron spectrum (γ_0) at the beginning of an FA's operation and during its evolution in each core cycle – $\gamma(t)$. The models assume that the total LHGR of a fuel rod (LP^{fr} – of an UO_2-fuel rod, LP^{gr} – of a Gd-doped fuel rod) with fuel enrichment in ^{235}U (enr_{fr} and enr_{gr}) is comprised of the following contributions, see relation (1a): the interaction of fast neutrons with ^{238}U, and interaction of the epithermal (LP_{ET}) and thermal (LP_T) neutrons with ^{235}U in the fuel, [4, 5]. Fast neutron fission rate for ^{238}U is assumed to be proportional to the total fission rate in the FA, the contribution of ^{238}U fissions into the total LHGR of a fuel rod and is calculated by the relation (1b). The proportionality factor $k_{^{238}U(n,f)}$ is characteristic to the reactor type and the fuel burnup level [1].

The models implicitly allow layered burn-out of gadolinium isotopes in a "fresh" Gd-doped fuel rod, which results in an increase of its total LHGR during the first fuel cycle, predominantly attributable to ^{235}U fissions in the thermal energy region, [4]. The relative initial contribution to the total LHGR of a Gd-doped rod $LP_{T,gr}^{t=0}$ from interactions of thermal neutrons with ^{235}U is calculated using the relation (1c), where the parameter k_T^{gr} is a function of initial enrichment in Gd_2O_3 [4]:

$$LP(t) = LP_{^{238}U(n,f)}(t) + LP_{ET}(t) + LP_T(t) \tag{1a}$$

$$LP_{^{238}U(n,f)}(t) = k_{^{238}U(n,f)} \cdot LPt) \tag{1b}$$

$$LP_{T,gr}^{t=0} = k_T^{gr}(LP_{gr}^{t=0} - k_{^{238}U(n,f)} \cdot LP_{fr}^{t=0}) \tag{1c}$$

At the beginning of the fuel cycle, ^{10}B and $^{155,157}Gd$ isotopes (in Gd-doped rods of the feed FAs) contribute significantly to the capture of thermal neutrons, so the contribution of thermal neutron flux into the total power of a FA changes with time. Resonance neutron absorption by ^{235}U is less affected, thus the flux of the resonance neutrons $\Phi_{ET}(t)$ changes weakly with time, considering possible gradual evolution of fuel LHGR (see Eq. 3). Using this assumption, the initial hardness of the neutron spectrum γ_0 and its evolution during the core cycle $\gamma(t)$ can be calculated from the relation:

$$\gamma_0 = \frac{\sigma_T^{235}}{I_{res}^{235}} \frac{LP_{ET,fr}^{t=0}}{LP_{T,fr}^{t=0}} = \frac{\sigma_T^{235}}{I_{res}^{235}} \frac{\left(LP_{gr}^{t=0} - k_{^{238}U(n,f)} \cdot LP_{fr} - LP_{T,gr}^{t=0}\right)}{LP_{T,t=0}^{fr}} \cdot \frac{enr_{fr}}{enr_{gr}}, \ \gamma(t) \propto \frac{\Phi_{ET}(t)}{\Phi_T(t)} \tag{2}$$

where σ_T^{235} is the thermal fission cross-section of ^{235}U, I_{res}^{235} is the resonance integral for ^{235}U fissions, $\Phi_T(t)$ and $\Phi_{ET}(t)$ are the thermal/epithermal neutron flux values, respectively, [$m^{-2}s^{-1}$]. Assuming that the relation between FA's LHGR and epithermal neutron flux $\Phi_{ET}(t)$ varies weakly during the cycle, and considering the calculated initial (t = 0) thermal neutron flux Φ_{T_0} and γ_0, the values of $\gamma(t)$, $\Phi_T(t)$ and $\Phi_{ET}(t)$ are estimated at each time step (j) over the cycle using the fixed-point iteration method:

$$\frac{\gamma_0 \Phi_{T_0}}{LP_{fr}^{t=0}} = \frac{\gamma_j \Phi_{T_j}}{LP_{fr}^{j}} \tag{3}$$

Therefore, the following set of equations is incorporated into the models [1, 5] to describe the rate of build-up of cesium isotopes ($^{133,134,137}Cs$) in the fuel pellet:

$$\begin{aligned} \dot{n}_{133}(t) &= y_{133}^{eff}(t)\dot{F}(t) - \sigma_{133}(t)\Phi_T(t)n_{133}(t) \\ \dot{n}_{134}(t) &= \sigma_{133}(t)\Phi_T(t)n_{133}(t) - \sigma_{134}(t)\Phi_T(t)n_{134}(t) - \lambda_{134}n_{134}(t) \\ \dot{n}_{137}(t) &= y_{137}^{eff}(t)\dot{F}(t) - \lambda_{137}n_{137}(t) \end{aligned} \tag{4}$$

where $\dot{n}_{133,134,137}(t)$ is the atomic density of a Cs nuclide [m^{-3}], $\lambda_{133,134,137}$ is the decay constant of the radionuclide [s^{-1}], $\sigma_{133,134,137}(t)$ is the full neutron absorption cross-section [10^{-28} m] of the corresponding Cs nuclides: $\sigma_i(t) = \sigma_i^m + I_i^{res} \cdot \gamma(t)$, $i = 133, 134, 137$, $\Phi_T(t)$ is the averaged thermal neutron flux [$m^{-2}s^{-1}$] calculated with the relation (3), $\dot{F}(t)$ is the total fission rate of the primary fissile nuclides (^{235}U, $^{239,241}Pu$) in the fuel volume [$m^{-3}s^{-1}$]. The effective fission yield $y_i^{eff}(t)$ for $^{133,134,137}Cs$ isotopes (i =133, 134,137) per fission of heavy atoms is described by the following relation with respect to the evolution of their concentrations:

$$y_i^{eff}(t) = \frac{y_i^{235} n_{235}(t)\sigma_f^{235} + y_i^{239} n_{239}(t)\sigma_f^{239} + y_i^{241} n_{239}(t)\sigma_f^{241}}{n_{235}(t)\sigma_f^{235} + n_{239}(t)\sigma_f^{239} + n_{241}(t)\sigma_f^{241}} \tag{5}$$

Therefore, the presented model enables calculation of the $^{134}Cs/^{137}Cs$ activity ratio in UO_2-fuel accounting for the features of FAs operation in each fuel cycle with its specific core loading pattern. These model calculations utilize the JEFF-3.3 nuclear data library that allows describing the overlapping of ^{238}U and ^{133}Cs first resonances: $E_r^{U-238} = 6.67\,eV / E_r^{Cs-133} = 5.59\,eV$ [4, 5].

Model validation for the fast evaluation of fuel burnup in leaking FAs in papers [1, 3-7] relied on the data provided by the NPPs with WWER-1000 power units (type V-320, [1]). The data included the reactor core power history, parameters of the coolant clean-up system, activities of the reference radionuclides in the primary coolant, and average LHGRs of the FAs (suspect/leaking fuel rods, where known) obtained with neutronic calculations at the NPPs. Calculated results were compared to the recorded $^{134}Cs/^{137}Cs$ activity ratio at spike-events and to the FFDS testing results for each FA (correlated to the NPP data on the calculated fuel burnup in a suspect/identified leaking fuel rod). These comparison results have shown that the model predictions for Cs inventories in leaking FAs are within the error margin of activity measurements at NPPs.

4. APPLYING THE IMPROVED TECHNIQUE FOR BURNUP EVALUATION ON RECENTLY ACQUIRED DATA

The two recent cases of activity spike-events provide an exceptional opportunity for application of the model and analysis of FAs with annular fuel pellets. Case #1 denotes three subsequent fuel cycles at the same power unit, where the leaking FAs under study were identified after the third cycle. In case #2, the FFDS results for the suspect FAs confirmed that TVSA-PLUS #4 was the only leaking fuel assembly in the core. Results of the PIE of TVSA-ALFA #5 (case #3), examined in hot cells at RIAR, suggested that this FA was intact, therefore it was considered as a reference FA in the study (with solid fuel pellets).

At the end of each fuel cycle that was considered, sipping leakage tests were performed for all the FAs from the core of the WWER-1000 power units while they were in the mast of the refuelling machine. Leaking fuel testing in the FFDS casks was performed for the suspect FAs in the core applying a pressure cycling technique [15, 16] after the reactor shutdown. Subsequently, the activities of the reference radionuclides in the water samples from the cask circuit were measured (hereinafter, FFDS results), the leaking assemblies were identified, and their fuel burnup was reliably determined, see Table 1.

TABLE 1. PARAMETERS OF THE LEAKING FUEL ASSEMBLIES IN THE CASES ANALYSED

Case No.	FA type and No.	Number of UO_2 / (U, Gd) O_2 fuel rods	Fuel enrichment in ^{235}U, wt%: UO_2 / (U, Gd) O_2 rods [Gd_2O_3, wt%]	Irradiation period, number of fuel cycles (EFPD)	Calculated FA average fuel burnup, MWd/kgU	Fuel inspections
	TVSA-PLUS #1	306 / 6	4.95 / 3.6 [5.0]	3 (1425.75) *	49.97	FFDS
1	TVSA-PLUS #2	288 / 24	4.95 / 3.6 [8.0]	2 (988.71) *	46.44	*Same power unit, consecutive cycles
	TVSA-PLUS #3	306 / 6	4.95 / 3.6 [5.0]		44.4	
2	TVSA-PLUS #4	306 / 6	4.4 / 3.6 [5.0]	2 (706.63)	30.29	FFDS the only leaking in the core
3	TVSA-ALFA #5 (intact, reference)	306 / 6	4.4 / 3.6 [5.0]	2 (671.9)	32.87	FFDS; RIAR hot cells (2018) [17-19]

Data on the reactor operating parameters in these cycles, as provided by the NPPs, included: values of the specific activities of iodine radionuclides, noble gases, and Cs in the primary coolant (measured at the power units with an error margin of ~ 10%).

The NPPs data for cases #1 and #2 is shown in Fig. 3 and 4: the upper graph shows the time evolution of the reactor thermal power along with the flow rate to ion-exchange filters (Q_{IEF}) to highlight the moment when the activity spike-event occurs; the bottom graph shows the specific activities of ^{134}Cs and ^{137}Cs in the primary coolant for the evaluation of the activity spiking amplitude. When a spike-event occurs, activities of Cs isotopes are evaluated subtracting the background activity level (highlighted in orange), and then the values of $^{134}Cs/^{137}Cs$ spiking activity ratios are processed during that time (typically, for 1-2 days, highlighted in red). Therefore, $^{134}Cs/^{137}Cs$ activity ratio "intervals" in the figures that provide the comparison between the model calculation results and the NPPs data represent the minimum and maximum values of the recorded spiking activity ratio.

4.1 Operational parameters of TVSA-PLUS ##1-3 and analysis of the spike-event in case #1

In case #1, spiking of Cs activities in the primary coolant was recorded after the reactor shutdown. The relevant NPP data is presented in Fig. 3. The recorded spiking $^{134}Cs/^{137}Cs$ activity ratio values in the primary coolant were in the range of 1.82 to 2.00, represented with a purple dashed interval in Fig. 4 (right).

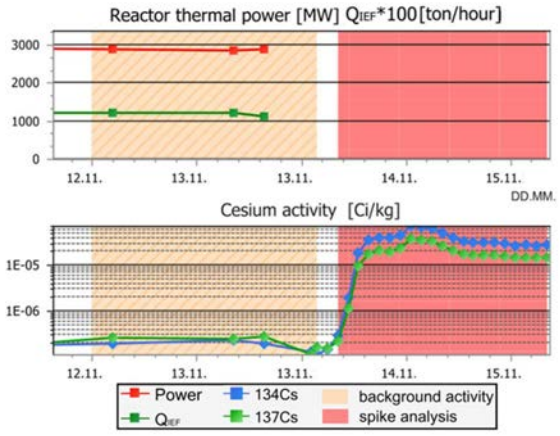

FIG. 3. NPP data for Cs activity spike-event after the reactor shutdown in case #1 (Q_{IEF} is the rate of coolant flow to the clean-up system).

Following the sipping leakage tests after the last fuel cycle, the suspect TVSA-PLUS ##1-3 were additionally tested in the FFDS casks, which confirmed a fuel failure. Fig. 4 (right) shows a comparison of the ratios of measured ^{134}Cs and ^{137}Cs activities at the spike-event and in the water samples from the FFDS cask circuit for TVSA-PLUS ##1-3, correlated to their calculated average FA fuel burnup, see Table 1. Applying the correlation "content of Cs in voids inside a fuel rod" [2] to the spike-event data in this case yields a minimal burnup of 53.4 MWd/kgU in a leaking fuel element(s), marked in Fig. 4 (right).

The location of the failed/suspect fuel rods in TVSA-PLUS ##1-3 was not identified at the NPP. Thus, to gain an estimate of Cs inventory in fuel rods of these FAs, the NPP calculated results for the actual average LHGR of these FAs (shown in Fig. 4, left) were utilised in the model simulations for a UO_2-fuel rod. Note that TVSA-PLUS #1 operated for three fuel cycles before it was identified as leaking, compared to TVSA-PLUS #1 and #2, which operated for two subsequent fuel cycles at the same power unit. Therefore, the irradiation history for these three FAs and scheduled maintenance outages are combined in Fig. 4 (left) for convenience.

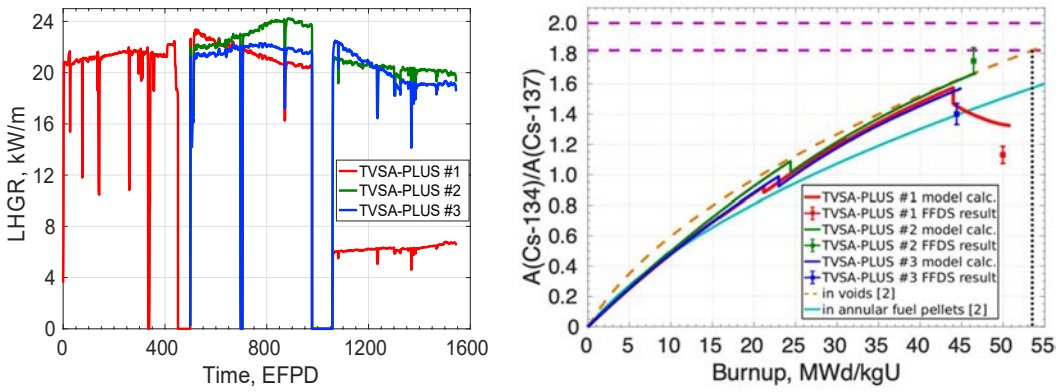

FIG. 4. NPP data and simulation results for TVSA-PLUS ##1-3: average LHGR (left) and comparison of the model calculation results for $^{134}Cs/^{137}Cs$ activity ratios (right) along with spike-event data (represented with a purple dashed interval) and FFDS testing results in case #1.

It can be inferred from comparison of the predicted $^{134}Cs/^{137}Cs$ activity ratio in fuel pellets of the three FAs and their FFDS results that considering actual FAs irradiation histories is the primary step when applying this technique for burnup evaluation. The results suggest that the release of fission products from fuel of TVSA-PLUS #2 might have had the greatest effect on the observed activity spike-event, compared to that of TVSA-PLUS #1 with the highest predicted average fuel burnup. These conclusions could be supported by the simulations of Cs inventories based on the pin-wise LHGRs for these FAs. The effect of a highly non-uniform distribution of fuel burnup across the FAs in UO_2 and (U, Gd) O_2 rods after several fuel cycles has been shown to be non-negligible in evaluations for Cs inventories in function of fuel burnup. The importance and extent of this effect was also shown in a case involving a leaking FA TVSA-U [7] that was examined in the RIAR hot cells. The analysis included a comparison of the simulation results for two intact witness FAs.

4.2 Operational parameters of TVSA-PLUS #4 and analysis of the spike-event

In case #2, spiking of Cs activities in the primary coolant was recorded after the reactor shutdown. The relevant NPP data is presented in Fig. 5.

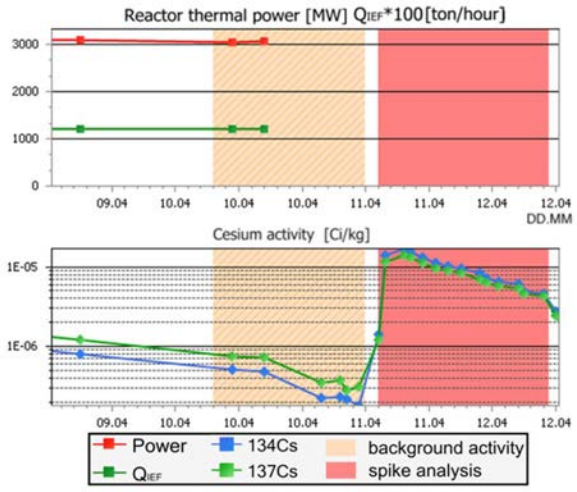

FIG. 5. NPP data for Cs activity spike-event after the reactor shutdown in case #2.

The recorded $^{134}Cs/^{137}Cs$ activity ratio in the primary coolant was in the range of 1.18 to 1.24, see Fig. 6 (right), which correlated with the calculated average TVSA-PLUS #4 fuel burnup since it was identified as the only leaking assembly in the core during the FFDS testing. However, the location of the leaking/suspect fuel rod was not established. A slight discrepancy observed in Fig. 6 (right) between the measured $^{134}Cs/^{137}Cs$ activity ratios in this case could be attributed to the differences in the fission products release dynamics during reactor operation and during the FFDS testing procedure in a cask.

Applying the correlation "content of Cs in voids inside a fuel rod" [2] to the spike-event data yields a minimal burnup of 25.5 MWd/kgU in a leaking fuel element. It is marked with vertical/horizontal dotted line in Fig. 6 (right). The model simulations for Cs inventories in a UO_2-fuel rod utilised the actual average LHGR of TVSA-PLUS #4 (shown in Fig. 6, left). It can be seen in Fig. 6 (right) that the model calculation results of Cs activity ratio overestimate the provided NPP data, which suggests that the leaking fuel rod might have operated at a lower LHGR compared to that of the FA average.

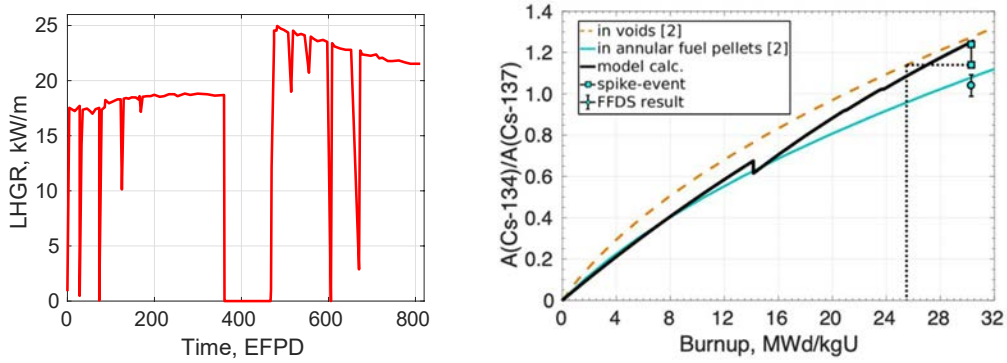

FIG. 6. NPP data and simulation results for TVSA-PLUS #4: average LHGR (left) and comparison of the model calculation results for $^{134}Cs/^{137}Cs$ activity ratios (right) along with spike-event data and FFDS testing result case #2.

4.3 Operational parameters of reference TVSA-ALFA #5 and analysis of PIE data

The primary FFDS testing results for TVSA-ALFA #5 (with solid fuel pellets) indicated a fuel failure; however, it was noted that the ^{131}I activity failure criterion was not reached during the additional test in this case, [17]. The results of the initial examinations performed at RIAR (visual inspection, eddy-current and ultrasonic testing) suggested that the leaking fuel elements were absent in this FA, [18]. To eliminate these inconsistencies, additional examinations were performed at RIAR including gamma-spectrometry for ^{85}Kr inventory measurements in the gas plenum region, [18, 19]. The examinations identified only two rods with debris-induced marks on cladding. However, these marks were characterised as shallow surface defects based on the analysis results of the fission gas inventories from the plenum after puncturing of the fuel cladding, [17]. Therefore, a conclusion was made that this FA could be classified as "intact".

According to the NPP calculated results, average LHGR of TVSA-ALFA #5 ranged from 20.8 to 22.1 kW/m during its first cycle of operation, and gradually decreased from 21.7 to 20.0 kW/m during the second cycle. Average fuel burnup was in the range of 28.21 to 35.21 MWd/kgU in UO_2-fuel rods, and 28.90 to 30.79 MWd/kgU in (U, Gd) O_2-fuel rods.

Available gamma-scanning results, for ^{134}Cs and ^{137}Cs inventories in five UO_2-fuel rods, were utilised for validating the model predictions. Previous work [5] describes the details of the gamma-scanning procedure and the results of the collaboration with RIAR on data analysis and processing. An example of this procedure for the rod with the lowest fuel burnup in this group is shown in Fig. 7. Model calculation results for the $^{134}Cs/^{137}Cs$ activity ratio in this fuel rod are compared with the gamma-scanning results, where the activity ratio at the FA final discharge from the reactor core (EOL) is estimated accounting for the elapsed time/radioactive decay between the EOL and eventual examination in hot cells ('PIE gamma-scan'), see Fig. 7 (left). It can be seen in Fig. 7 (right) that the model calculation of Cs activity ratio for this fuel rod are in good agreement with the experimental data. It can be noted that applying the conventional correlation "in fuel pellets" [2] implies correlating a notably higher fuel burnup with the Cs activity ratio estimated at the EOL (the correlation "content of Cs in voids inside a fuel rod" [2] is shown for a reference).

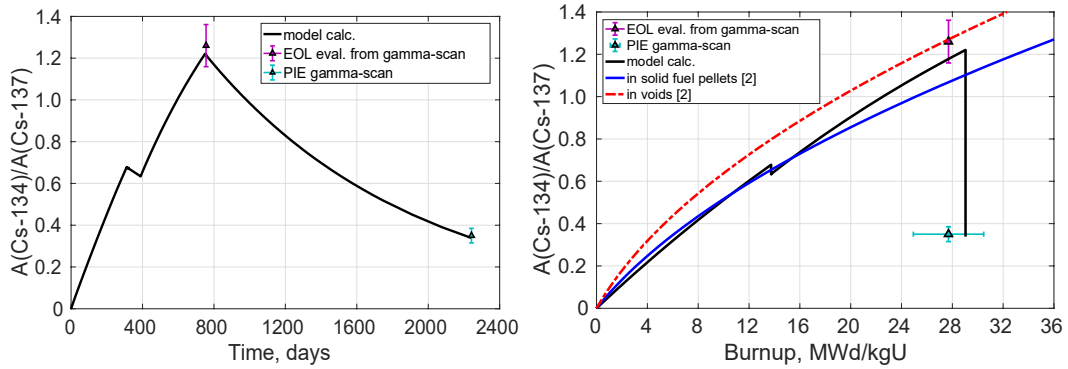

FIG. 7. Comparison of the model calculation results and PIE data for $^{134}Cs/^{137}Cs$ activity ratios in fuel of a UO_2-fuel rod from TVSA-ALFA #5: as function of the FA operation time to the EOL and subsequent cooling period to the moment of PIE (left); as function of fuel burnup (right) along with gamma-scanning results and evaluation of maximal fuel burnup by ^{137}Cs in RIAR.

4.4 A comparative analysis of the NPP data for fuel with different initial enrichment and gadolinium content

Previous works [3, 4, 5, 7, 8] provide validation results for the improved technique for fuel burnup evaluation based on $^{134}Cs/^{137}Cs$ activity ratio, for cases including leaking FAs, with solid fuel pellets (TVSA-12 and TVSA-ALFA types). The experimental data for these benchmarking exercises included NPP data on spike-events and FFDS testing of leaking FAs (time of 2012-2018), and PIE results obtained at the RIAR hot cells [3, 5, 7, 8] shown in Fig. 8: (a) FAs with annular fuel pellets and (b) FAs with solid fuel pellets. The spike-event cases discussed in [3, 4, 5] involved FAs that were confirmed to be the only leakers in the core in each corresponding cycle. Notably, the $^{134}Cs/^{137}Cs$ activity ratio results obtained during FFDS testing of leaking TVSA-PLUS #2 [4] and TVSA-12 #3 [3], which were practically equal to the minimal ratios recorded at the corresponding spike-events.

The FAs considered in the abovementioned papers differed in the initial enrichment in ^{235}U (enr) of UO_2-fuel rods ranging 4.0 to 4.7wt% (only TVSA-12PLUS #4 [4]: enr = 4.95 wt%), and the number of (U, Gd) O_2 rods with enr = 3.6 wt% and initial content of Gd_2O_3 (5.0 wt% or 8.0 wt%). The actual average LHGR of these FAs was utilised in the model calculations of Cs inventories when the location of the leaking fuel rod could not be established [4]; and pin-wise LHGRs were utilised in works where the leaking fuel rod was clearly identified and detailed PIE data provided [3, 5, 7, 8]. For convenience, the experimental results for these FAs are shown in Fig. 8 along with the new data for the FAs in case #1 (enr = 4.95 wt%) and the data for cases #2-3 (enr = 4.4 wt%) that are discussed in Sections 4.1-4.3.

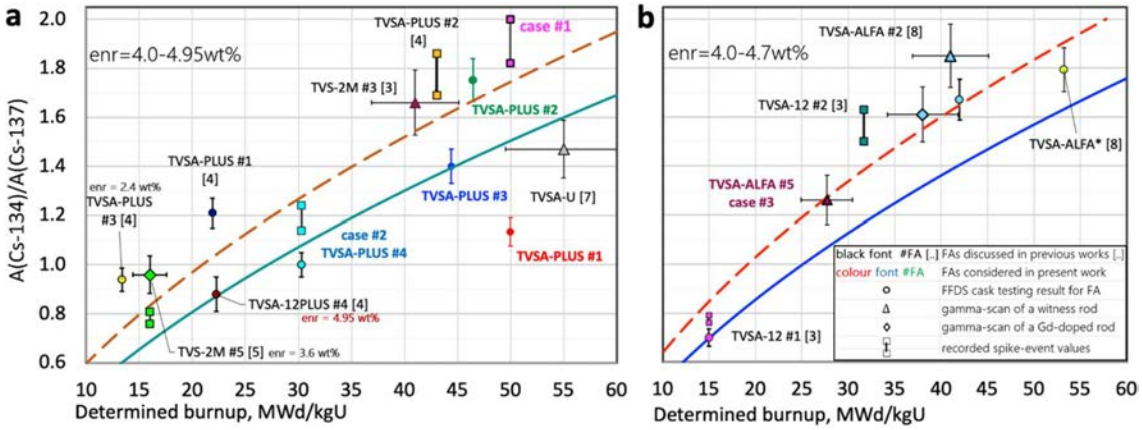

FIG. 8. Summary of the analysed NPP data for $^{134}Cs/^{137}Cs$ activity ratio including leaking FAs with annular (a) and solid (b) fuel pellets: at observed spike-events after the reactor shutdown (shown as intervals); FFDS testing results from the previous works [3-5, 7, 8] and in present case #1 (colored TVSA-PLUS ##1-3) and case #2 (colored TVSA-PLUS #4); results of PIE gamma-scanning spectrometry for fuel rods discussed in [3, 5, 7, 8] and for present case #3 (colored TVSA-ALFA #5, intact), along with the correlations from the regulatory guidelines [2] for fuel burnup evaluation: dashed lines – in voids, solid lines – in fuel pellets.

4.4.1 Fuel of low burnup

In the lower burnup range (< 25 MWd/kgU, typically after 1 fuel cycle), TVSA-PLUS #3 [4] is the only considered FA with no Gd-doped fuel rods and enrichment 2.4 wt.% in ^{235}U. This FA operated for a 12-month fuel cycle with average LHGR ranging between 18 to 22 kW/m. A good agreement of the model calculation results for the Cs activity ratio in fuel, with a notably high FFDS result for this FA, was shown in [4]. The FA average fuel burnup of ~ 13.4 MWd/kgU was determined, see Fig. 8a. In this case, a considerably higher fuel burnup would have been inferred if the correlation "content of Cs in voids inside a fuel rod" [2] was applied to this FFDS result. Notably, an even worse discrepancy would be observed using the "Cs in fuel pellets" correlation.

However, applying the correlation "content of Cs in voids inside a fuel rod" [2] in a different case involving TVSA-12 #1 [3], see Fig. 8b, yielded a better estimate for the leaking average fuel burnup of ~ 15.0 MWd/kgU in a fuel rod (enrichment 4.0 wt%, LHGR 20-22 kW/m). Comparison of the FFDS results for TVSA-PLUS #3 [4] and TVSA-12 #2 [3] that operated at similar LHGR might illustrate the effect of a reduction in neutron capture in ^{133}Cs when fuel enrichment is increased from 2.4 wt% to 4.0 wt% in fresh fuel, considering overlapping of ^{235}U resonances at 4-7 eV with ^{133}Cs first resonance at 5.59 eV.

Further PIE studies related to the effects of mutual resonance shielding of ^{235}U, ^{133}Cs and $^{155,157}Gd$ in fuel would be beneficial. Some of the simulation and experimental results for (U, Gd) O_2-fuel are discussed in [5, 6, 20]. To date, availability of the PIE results obtained at the RIAR hot cells for spike-events involving a leaking (U, Gd) O_2-fuel rod at WWER-1000 is limited to one case: TVS-2M #5 [5] with annular pellets discussed in [3, 5]. The average fuel burnup in this leaking (U, Gd) O_2-fuel rod was estimated to be ~ 16 MWd/kgU by RIAR, and the gamma-scanning results were provided for Cs activity ratio in fuel (◊-marked, enr = 3.6 wt%), see Fig. 8a. The average FA fuel burnup was estimated at 24.4 MWd/kgU. This FA was identified as the only leaker in the core at the FFDS testing. The recorded $^{134}Cs/^{137}Cs$ activity ratio at the EOC is also shown in Fig. 8a for reference: notably, this ratio interval is lower than the gamma-scanning results of the failed (U, Gd) O_2-fuel rod, which might be associated with the features of mass transfer in this fuel type, [20].

4.4.2 Moderate fuel burnup

In the intermediate burnup range (~25-40 MWd/kgU) an onset of pellet-to-cladding interaction and non-uniformity of fuel burnup in rods across the FA are expected to have a greater impact on the evaluation of leaking fuel which rely on the activity spiking data. The discrepancies in burnup evaluation resulting from applying the correlation "content of Cs in voids inside a fuel rod" [2] to the NPP data would be observed for both fuel types

(solid and annular), see Fig. 8a: TVS-2M #3 [3], TVSA-PLUS #1 [4], TVSA-PLUS #4 discussed in Section 4.2, and TVSA-12 #2 [3] shown in Fig 8b.

Model simulation results in these cases [3, 4] and PIE results discussed for TVSA-ALFA #5 in Section 4.3 support the suggestion that it is necessary to consider actual irradiation history and non-uniform fuel burnup for the FAs with the same initial fuel enrichment in order to increase accuracy of Cs inventory predictions. Notably, the FFDS result for TVSA-12PLUS #4 [4] with enr = 4.95 wt% was relatively low (see Fig. 8a, LHGR 20-22 kW/m, operated one 18-month fuel cycle), which supports the assumption of reduced neutron capture in ^{133}Cs in highly enriched fuel of fresh FAs due to ^{235}U/^{133}Cs resonance overlapping.

4.4.3 Higher fuel burnup

The cases of higher fuel burnup (> 40 MWd/kgU) include TVSA-ALFA #2 [8] and TVSA-ALFA* [8] which operated in the same power unit for three and four fuel cycles, respectively, before their final discharge at which point both were identified as leaking. TVSA-ALFA #2 [8] was examined in the RIAR hot cells and the results of gamma-scanning spectrometry for an axial distribution of ^{137}Cs and ^{134}Cs in fuel were obtained for the leaking fuel rod and several reference intact fuel rods. Fig. 8b shows the FFDS result for TVSA-ALFA #2 [8] correlated to the average burnup in the identified leaking fuel rod; the results of gamma-scanning spectrometry for two reference intact fuel rods: UO_2 (Δ-marked, 4.7 wt%) and (U, Gd) O_2 (◊-marked 3.6 wt%) are shown with quoted uncertainties in evaluation of average fuel burnup based on ^{137}Cs by RIAR, [5].

Model calculation results for these rods from TVSA-ALFA #2 [8] have previously been shown to agree with the measured ^{134}Cs/^{137}Cs activity ratio within the experimental uncertainty, suggesting that the improved technique can capture the difference in the build-up rates of Cs inventories in UO_2 and (U, Gd) O_2 fuel at higher burnups. It should be noted that both the experimental and predicted Cs activity ratios in fuel rods from TVSA-ALFA #2 [8] exceed those predicted by the correlation “in fuel pellets” from [2], which was also observed for the rod in TVSA-ALFA #5 in the present case #3.

In addition, comparison of the experimental data shown in Fig. 8 for TVSA-ALFA #2 [8], TVSA-ALFA* [8], TVSA-PLUS #2 [4] and the present spike-event case #1 that involved multiple fuel failures discussed in Section 4.1 (TVSA-PLUS ##1-3) highlights the importance of considering the actual irradiation history of each of these FAs. If available, FAs detailed irradiation history for evaluation of Cs inventories in fuel should include pin-wise LHGR, actual reactor operation periods (EFPD) and duration of reactor outages between them. Notably, the spike-event data and FFDS result for TVSA-PLUS #2 [4] and TVSA-ALFA #2 [8] could be well-described by the correlation “content of Cs in voids inside a fuel rod” [2], whereas the evaluated burnup for TVSA-ALFA* [8] or TVSA-U [7] could be considerably underestimated.

5. CONCLUSIONS

It is suggested that an increased confidence in burnup evaluations of leaking FAs at operating WWER-1000 units and their subsequent identification could be achieved when the main factors affecting ^{134}Cs/^{137}Cs evolution, for each FA in the core, are considered simultaneously with mass transfer of fission products form a leaking fuel rod. A set of models have been elaborated for fast calculation of Cs inventory in UO_2 and (U, Gd) O_2 fuel rods for core loading pattern at NPPs. The input data for these models is based on the routine neutronic calculations performed at NPPs, which serve to characterise evolution of linear heat generation rate and burnup in fuel rods during the fuel cycle with a particular core loading pattern. However, these routine neutronic calculations do not provide data on Cs build-up in fuel.

The model predictions of Cs inventories were compared to the NPPs coolant activity data, testing results in the FFDS casks, and results of hot cell examinations of leaking fuel in RIAR for the previously considered and new cases. It was shown that there is reasonable agreement between the calculations and the experimental data on ^{134}Cs/^{137}Cs activity ratios as a function of fuel burnup in FAs of advanced designs which are being operated in contemporary fuel cycles. The proposed technique for cesium inventory calculations provides quick and reliable evaluation of leaking fuel burnup in the frame of analysis of primary coolant activity during operation of WWER-1000 power units.

Additional studies would be performed on the mass transfer in leaking fuel rods with solid fuel pellets with the RTOP-CA code [21, 22]. Some specific features of mass transfer inside leaking fuel rods with solid pellets will be studied for situations when pellet-to-cladding interaction becomes the primary factor affecting the accuracy of the predictions of fuel burnup.

REFERENCES

[1] LIKHANSKII, V.V., VILKHIVSKAYA, O.V., TOKAREV, S.A., Modeling of burnup express-estimation for UO_2-fuel, Nucl. Eng. Des. **313** (2017) 141–147.

[2] RD NO 1.1.2.10.0521-2009. Standard Procedure for Monitoring the Cladding Integrity of Fuel Elements. FAs of the VVER-1000 Reactors, Rev. 2. Rosenergoatom, Moscow, Russia (2016)..

[3] VILKHIVSKAYA, O.V., EVDOKIMOV, I.A., AFANASIEVA, E.Yu., LIKHANSKII, V.V., Recent validation study of the technique for express evaluation of burnup in leaking fuel assemblies of WWER power units, PHYSOR2020 (Proc. Int. Conf. Cambridge, UK, 2020). ISBN: 978-1-5272-6447-2. Version 1.0, 2020.

[4] VILKHIVSKAYA, O.V., LIKHANSKII, V.V., EVDOKIMOV, I.A., AFANASIEVA, E.Yu., SOROKIN, A.A., Extended validation of engineering models for express-method of burnup evaluation of WWER-1000 fuel elements", TOPFUEL-2018 (Proc. Int. Conf. Prague, Czech Republic, 2018), ENS. Available at: https://www.euronuclear.org/archiv/topfuel2018/proceedings.htm

[5] LIKHANSKII, V.V., VILKHIVSKAYA, O.V., et al, Engineering model for ^{134}Cs and ^{137}Cs production in Gd-doped fuel rods, WRFPM 2017 (Proc. Int. Conf. Jeju Island, Korea, 2017), USB Flash Drive (2017).

[6] LIKHANSKII, V.V. et al, Modified versions of the fuel performance codes RTOP and RTOP-CA, TOPFUEL-2016 (Proc. Int. Conf. Boise, USA, 2016), ANS, USB Flash Drive (2016).

[7] VILKHIVSKAYA, O.V., et al, Extended validation of the CIM procedure modernization at an operating reactor for express evaluation of burnup in leaking fuel assemblies, MNTK-2018 "Safety, Efficiency and Economics of Nuclear Power Industry", Proc. Int. Conf. Moscow, Russian Federation, 2018, Available at: http://mntk.rosenergoatom.ru/materials-of-the-conference (in Russian).

[8] VILKHIVSKAYA, O.V., et al, Engineering models for express method of burnup evaluation of WWER 1000 fuel elements, Proc. 12th Int. Conf. on WWER Fuel Performance, Modelling and Experimental Support, Nessebar, Bulgaria, 2017, Available at: https://inis.iaea.org/collection/NCLCollectionStore/_Public/50/006/50006686.pdf

[9] INTERNATIONAL ATOMIC ENERGY AGENCY, Operation and Licensing of Mixed Cores in Water Cooled Reactors, IAEA-TECDOC-1720, IAEA, Vienna (2014).

[10] INTERNATIONAL ATOMIC ENERGY AGENCY, Coolant Technology of Water-Cooled Reactors, Volume 1: Chemistry of Primary Coolant in Water Cooled Reactors, IAEA-TECDOC-667, IAEA, Vienna (1992).

[11] Radiation Protection Aspects of Primary Water Chemistry and Source-term Management. Report NEA/CRPPH/R (2014)2, Paris: Nuclear Energy Agency, OECD, 2014.

[12] RIDER, B.F., RUSSEL JR, J.L, HARRIS, D.W., PETERSON, J.P., The determination of uranium burnup in MWd/ton. Technical report GEAP-3373, Vallecitos Atomic Laboratory, Atomic Power Equipment Department, General Electric Company, Pleasanton, California, United States Atomic Energy Commission, March 17, 1960.

[13] JUNG, S.K, JEON, Y.S., PARK, S.D., HA, Y.K., SONG, K., Analysis of high burnup pressurized water reactor fuel using uranium, plutonium, neodymium, and cesium isotope correlations with burnup, Nucl. Eng. Tech. **47** (7) (2015) 924–933.

[14] BAGHERI, S., FAGHILI, H., KHALAFI, H., An efficient method for detecting damaged FAs; burnup and PPF estimations by gamma spectroscopy, Applied Radiation and Isotopes **140** (2018) 185–192.

[15] ZBOROVSKII, V.G et al. Modeling of radionuclides release during cask leakage tests of failed fuel rods, Matem. Mod. **23** (2014), 145–160 (2011, in Russian).

[16] POVAROV, V.P. et al. Developing and applying modern methods of leakage monitoring and state estimation of fuel at the Novovoronezh nuclear power plant, Therm. Eng. **61** (2) (2014), 123–132.

[17] SAGALOV, S.S. et al. Post-irradiation examination results for TVSA-ALFA after two fuel cycles at power unit No.1 of Kalinin NPP, JSC SSC RIAR Annual Research Report for 2018, Dimitrovgrad, 86–87 (in Russian).

[18] SAGALOV, S.S. et al., Gamma spectrometry to test the TVS-ALPHA fuel assembly integrity, J. Proceedings of JSC SSC RIAR 3 (2019) 24–31. Available at: https://www.elibrary.ru/contents.asp?id=41810392

[19] SAGALOV, S.S. et al. Integrity testing of the TVSA-ALFA fuel elements by gamma-spectrometry of the gas plenum, 11th Conference on Reactor Materials Science dedicated to the 55th Anniversary of the RIAR's Reactor Materials Testing Complex (Proc. Int. Conf. Dimitrovgrad, Russia, 2019), RIAR. Available at: http://www.niiar.ru/eng/rm11.

[20] SOROKIN, A.A. et al, Modeling in support of experiments in the MIR reactor for justification of fission products release from failed fuel of advanced design and from (U, Gd) O_2 fuel, Proc. 12th Int. Conf. on WWER Fuel Performance, Modelling and Experimental Support, Nessebar, Bulgaria, 2017. Available at: https://inis.iaea.org/collection/NCLCollectionStore/_Public/50/006/50006676.pdf

[21] INTERNATIONAL ATOMIC ENERGY AGENCY, Review of Fuel Failures in Water Cooled Reactors (2006–2015), Nuclear Energy Series No. NF-T-2.5, IAEA, Vienna (2019).

[22] SOROKIN, A., LIKHANSKII, V., EVDOKIMOV, I., *et al.*, Capabilities of the RTOP-CA code to simulate leaking fuel behavior and release of radioactive fission products into primary coolant of light-water reactors, Proc. Tech. Meet. Fuel Failure in Normal Operation of Water Reactors: Experience, Causes and Mitigation, IAEA Headquarters, Vienna, Austria, 14–17 December 2020.

STUDYING THE EFFECT OF OPERATING PARAMETERS ON RESPONSE OF THE FUEL-CLADDING FAILURE MONITORING SYSTEM IN MTRs

A.H. ELHEFNAWY, M. A. GAHEEN
Egyptian Atomic Energy Authority,
Cairo, Egypt

Abstract

Most monitoring and detection systems for nuclear fuel failure during reactor normal or accidental conditions depend on measuring the gamma activity released from radioactive fission products that diffused from the fuel element using gamma spectrometry. In contrast, this system in the Typical MTR research reactor depends on measuring the activity of delayed neutrons released from the delayed neutron precursors escaping from the reactor core in an intense gamma field using a BF_3 detector. Because of the relatively big difference in half-lives for the six groups of these delayed neutrons precursors, the measured delayed neutrons count-rate depends mainly on the time that water takes to transfer from the reactor core to the neutron detector of the monitoring system. The calibration process of this monitoring system was based on a constant flow rate of water in this cycle (≈ 7 Liter/min) that limits the detection probability to the first two groups of delayed neutrons precursors particularly (^{87}Br and ^{137}I). During reactor operation, two operating parameters are noticed to affect the readings of the detector which was not considered in the calibration process before. The first parameter is the disturbance of water flow rate from the reactor core to the detector by the effect of the reactor's main cooling system. It decreases the probability of the other four groups of delayed neutron precursors to be included in the measuring process. The second parameter is the dependence of diffusion of delayed neutron precursors on the burnup rate of the fuel elements. Because of discarding these effects, high fluctuations in the response of the detector are occurred causing a false alarm to be recorded. Therefore, it became necessary to redesign the calibration process of the fuel-cladding failure monitoring system calculating a new calibration constant that compensates the effect of these operating parameters.

1. INTRODUCTION

Multiple monitoring techniques were developed to detect the nuclear fuel failure at normal operation of the nuclear reactor, monitoring the release of fission products from the reactor core effectively, analyzing trends in the released quantities of fission products, and using practical models based on different physical principles. All approaches are based on the same fundamentals but differ in the mechanism of application [1]. CANDU reactors have different types of fuel failure monitoring systems. Some of these reactors use systems that monitor delayed neutrons precursors to locate fuel defects in the reactor core that are called the delayed neutron (DN) systems. BF_3 detectors monitor the build-up of delayed neutron-emitting precursors (^{137}I and ^{87}Br) in multiple sampling lines, so if the neutron activity is higher than normal in each sampling line, the corresponding fuel channel is suspected of containing a failed fuel element. Although the delayed neutrons system was designed with enough sensitivity to detect fuel defects with very small holes, the sensitivity has decreased with time due to tramp uranium contamination because of fuel release from previous defects [2].

The main difference between DN system of CANDU reactors and the detection system of the MTR research reactor is the analysis of failed fuel element location based on an assessment of the release behavior of delayed neutrons precursors. With the lack of a failed-fuel delayed-neutron (DN) location system, it may be difficult to locate and remove defective fuel from the core [2]. Other fuel failure detection approaches use analytical models that theoretically describe the activity of radionuclides released from failed fuel elements. Release of fission products is divided into two stages: release from fuel meat and release from fuel element to coolant. The coefficients of the models are then determined either using theoretical calculations or empirically from a large set of coolant activity data for which the number of leaking fuel elements in each of the operating cycles is well defined. In these models, release of fission products is generally characterized by the release to birth ratio R/B, where R is the instantaneous rate of fission product release (atom/s) into the reactor core coolant from all defective fuel elements and B is the birth rate (atom/s) of any radioisotope in a fuel element due to its burnup at average reactor power [1].

2. MTR REACTOR CORE SPECIFICATIONS AND FUEL FAILURE MONITORING

MTR is a Multi-Purpose Thermal Research Nuclear Reactor of plate-type fuel elements generating 22 MW as thermal energy. The dimensions of the MTR reactor core zone are (120 x 97 x 80) cm^3 where (80 cm) is the

active length of the fuel element. The reactor core contains 27 fuel elements, 6 control plates, and an in-core irradiation box. The design of the fuel element assembly is based on the U_3O_8-Al fuel, which is a low enriched uranium (LEU) fuel element. The main fuel element parameters are given in Table 1. Fig. 1 shows schematic diagrams of the fuel element with 19 flat plates inserted in two grooved lateral walls which lead to an external section of 8.0 x 8.0 cm^2 [3].

TABLE 1. MAIN DATA OF FUEL ELEMENT [3]

Number of fuel plates:	19
Enrichment:	19.7%
Active length	80.000 cm
External section of fuel element	8.0 x 8.0 cm^2
Plate thickness	0.150 cm
Fuel meat thickness	0.070 cm
Fuel meat width	6.400 cm

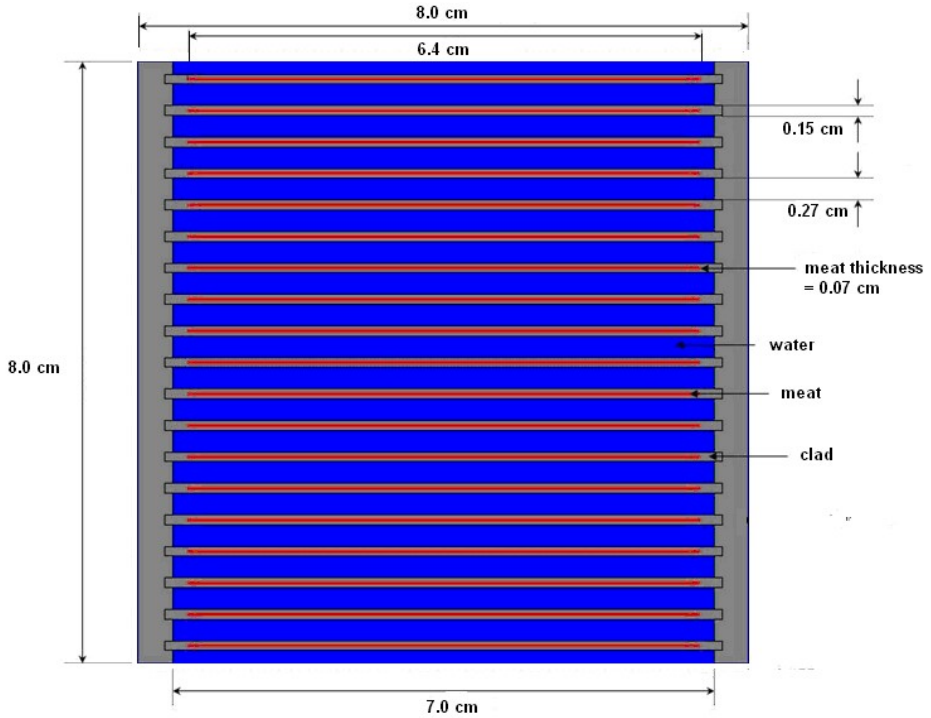

FIG. 10. Assembly of fuel element [3].

The fuel meat contains U_3O_8 in a pure aluminum matrix with no gap between the fuel meat and the Al cladding. The main material composition data of fuel meat for the fuel elements are given in Table 2. The monitoring of the possible failures of fuel elements is done using a BF_3 detector to measure the activity of delayed neutrons emitted from the delayed neutron precursors released from the reactor core. The technique of failure detection used at MTR is that the BF3 neutrons detector measures the count/sec of neutrons in water initially during around 6 minutes recording multiple readings and then gives their average as the background activity of neutrons in water.

Then the detector measures the new activity in count/sec of neutrons and converts it into the area of the defect in the fuel element through equation (1) using the detector calibration constant defined in the setting of the

system in cps/cm^2. So, the system depends mainly on the delayed neutrons activity that depends on the buildup rate of their precursors. The detection system doesn't take the total concentration of radioactive precursors into account because of their fast decay into stable isotopes. So, the suggested method of measuring the accumulation of these stable daughters of delayed neutrons precursors in the coolant and water treatment system will give us the ability to monitor the total concentration of precursors.

$$Fuel\ element\ defect\ area = \frac{A_{new-}\ A_{Background}}{Calibration\ constant} \quad (1)$$

where A is the neutron activity in water (cps).

TABLE 2. FUEL MEAT COMPOSITION [3]

Parameter	Value	Parameter	Value
Enrichment	19.7 %	Weight fraction – U-235	12.377 %
Al density	2.7 g/cm^3	Weight fraction – U-238	50.450 %
U_3O_8 density	8.1 g/cm^3	Weight fraction – O	11.263 %
Void fraction in fuel meat	10.0 %	Weight fraction – Al	25.910 %
Mass of U-235 in each plate	21.3 g	Uranium density in fuel	3.017 g/cm^3
Fuel meat density	4.802cm^3		

3. PROBLEM DEFINITION

Delayed neutrons precursors were divided into six groups as indicated in table 3 according to their half-life of decay with delayed neutrons indicating the contribution of each group in delayed neutrons fraction. Their release in the coolant was monitored continuously with an on-line neutron detector to detect the possible failure of fuel elements at the MTR reactor core. The release of these precursors has multiple mechanisms depending on reactor core operating parameters. So, the response of the detector of the monitoring system depends also on the operating parameters of the reactor that changes strongly in the start-up state of the reactor.

TABLE 3. DELAYED NEUTRONS PRECURSORS GROUPS GENERATED FROM U235 FISSION [4]

	Possible precursor nuclei	Average half-life of the group (s)	Delayed neutron fraction (%)
1	Br^{87}, Cs^{142}	55.72	0.021
2	I^{137}, Br^{88}	22.72	0.140
3	I^{138}, Br^{89}, Rb^{93}, Rb^{94}	6.22	0.126
4	I^{139}, Kr^{93}, Kr^{94}, Xe^{143}, Br^{90}, Br^{92}	2.3	0.252
5	I^{140}, Cs^{145}	0.61	0.074
6	Br^{93}, Rb^{95}, As^{87} etc.	0.23	0.027

4. METHODOLOGY OF STUDY

A cell of fresh fuel plate is modeled as an input of WIMS5B cell calculational code that is used for neutronic calculations of core inventory as a function of reactor core burnup. WIMS5B code uses the collision probabilities option in one-dimensional geometry (slab) for cell calculations for neutrons transport equation. The code has its nuclear multi-group neutrons microscopic cross-sections library [5].

4.1 Effect of start-up state on the performance of fuel-cladding failure monitoring system

Two proposed scenarios of power change during the start-up state of the reactor is used in the study. The first scenario (S1) is increasing the reactor power from zero to 22 MW (Full power) with a constant rate of 1 MW every 3 minutes.

The effect of reactor power change on the buildup rate of delayed neutron precursors in fresh fuel plate was studied as indicated in Fig. 2. The figure shows that at a low power region the buildup rate of these precursors depends strongly on reactor power, the fission rate, or burnup rate of the fuel element. But, in the high-power region, the buildup rate of precursors starts to reach an equilibrium value. So, if the setting of the monitoring system is adjusted to have a constant calibration factor during the start-up state, it will give a false alarm of fuel failure, especially in the low power region.

The second proposed scenario (S2) is the increase of the reactor power from zero to 22 MW (Full power) with a constant rate of 1 MW every 10 minutes. Fig. 3 indicates the comparison between the two scenarios for the first and fifth groups of precursors where the variation of power increasing rate affects the buildup rate of the precursors. As the power rate is increased the buildup rate of delayed neutron precursors is increased. So, optimization of the calibration process of the fuel failure monitoring system needs to take the variation of buildup rate with reactor core power and start-up scenario into account.

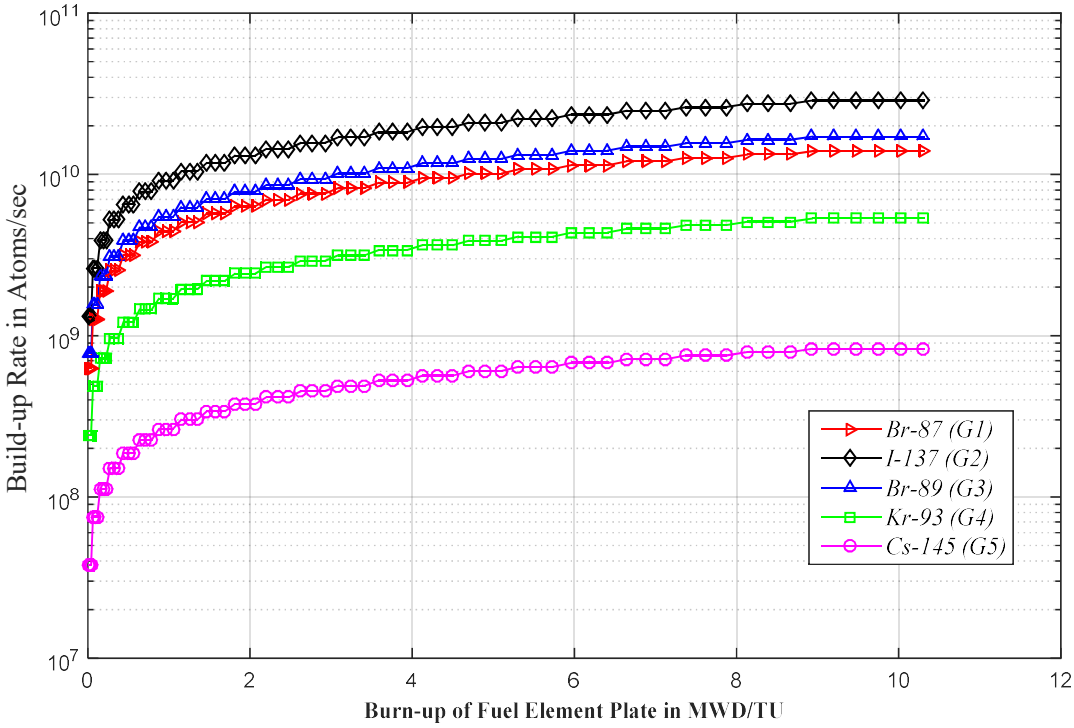

FIG. 2. Change of buildup rate of delayed neutron precursors at reactor start-up state (G1, G2, ... are the groups in Table 3).

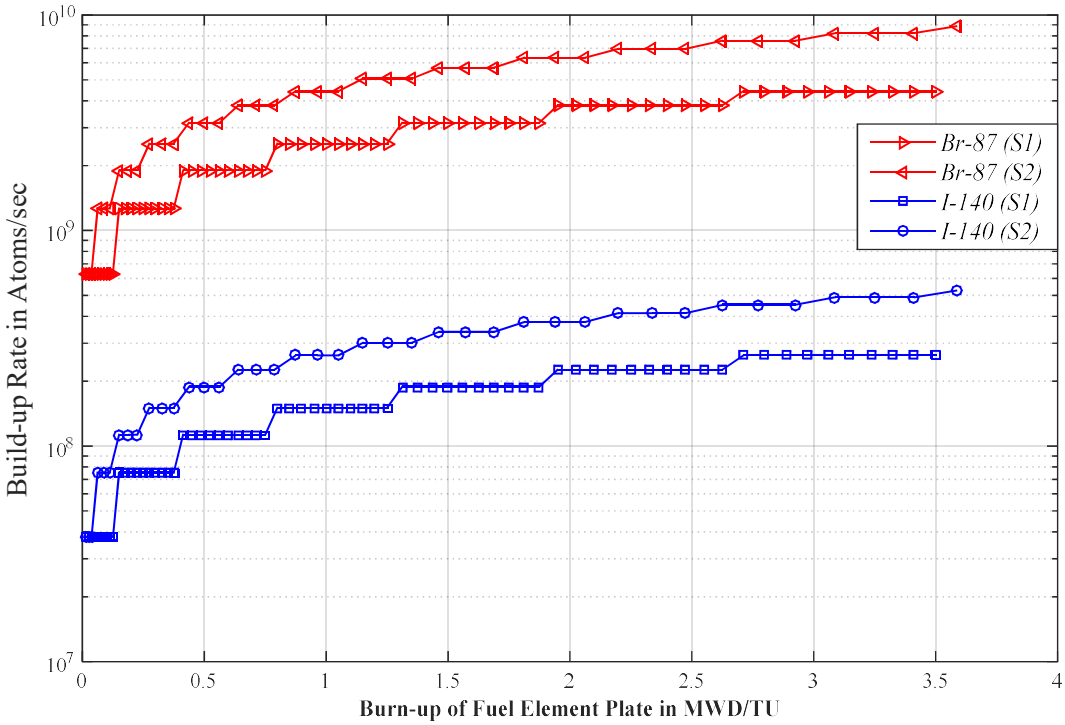

FIG. 3. Buildup rate of delayed neutron precursors dependency on scenarios of power change at start-up state (S1, S2 are the start-up scenarios).

4.2 Accumulation of daughters of delayed neutron precursors as a monitoring technique

Another method was proposed to monitor the release of precursors producing delayed neutrons into the reactor coolant assuring an earlier detection of any initiation of fuel elements failure. This method is to take a sample of water passing through the detector pump within equal periods and to perform a qualitative and quantitative analysis of this sample using a hyper-pure germanium detector. Because of the very short half-life of these precursors, this method wasn't practically applicable. But, knowing that most of the daughters of the precursors' decay are stable isotopes as indicated in Table 4, the release of these daughters into reactor coolant can be an indicator of the release of the precursors itself especially in case of very small fuel failures.

The most important result of the stability of these daughters is their accumulation in the reactor cooling system and water treatment system. So, if a sample of the reactor water treatment system can be analyzed using X-ray fluorescence spectrometry or any other chemical analysis techniques, these results can be compared with the response of the detector of the fuel-cladding monitoring system and to be used in its calibration process. Monitoring the accumulation rate of stable daughters of precursors in the coolant will give a method to verify the calibration of the fuel failure monitoring system. This method wasn't applied in practice or verified. It is just a possible way recommended to be used to verify the performance of the detection system. So, its practical application is still questionable.

The daughter isotopes indicated in Table 4 were selected because they were included in WIMS output as lumped pseudo-fission products [6] so their total buildup per fuel element was calculated using equation (2) where the fuel element contains 19 fuel plate.

$$Bd_{ij} = B_{ij} - Y_i F V \times 19 \quad (2)$$

where Bd_{ij} is buildup rate of istope (i) from the decay of delayed neutron precursor of group (j), B_i is total Buildup rate of istope (i), Y_i is fission yield of istope (i), F is sission rate (s^{-1}), V is volume of fuel plate.

TABLE 4. POSSIBLE DAUGHTERS OF DELAYED-NEUTRONS PRECURSORS AT DIFFERENT GROUPS

Group	Delayed Neutrons Precursor	Daughter	State of daughter	Mode of decay
1	Br87	Kr86	Stable	β & n *
	Cs^{142}	Pr^{141}	Stable	β & n
2	I^{137}	Xe^{136}	$T_{1/2}$>2.36E21 y	β & n
3	Br^{89}	Sr^{88}	Stable	β & n
	I^{138}	Ba^{137}	Stable	β & n
	Rb^{93}	Zr^{92}	Stable	β & n
4	Br^{90}	Y^{89}	Stable	β & n
	I^{139}	Ba^{138}	Stable	β & n
	Br^{92}	Zr^{91}	Stable	β & n
5	Cs^{145}	Ce^{140}	Stable	β & n

(β) represents the decay of beta particle, and (n) the decay of neutron particle.

A proposed scenario of reactor operation was used to study the accumulation of the daughters of delayed precursors as a function of reactor power. This scenario included five days of operation under 5.5 MW (1/4 Full power) then five days of operation under 11 MW (1/2 Full power) then ten days of operation under 22 MW (Full power). Fig. 4 indicates that the buildup of the daughters due to delayed neutrons precursors decay is almost constant as the reactor power changes. So, any rapid increase in the buildup of these daughter means a high probability of fuel element failure. However, the daughter's buildup due precursors decay started to be detectable according to reactor power, where Xe^{136}, Kr^{86}, and Pr^{141} appeared during operation under the power of 5.5 MW, and the rest of the daughters appeared during the operation under the power of 11 MW.

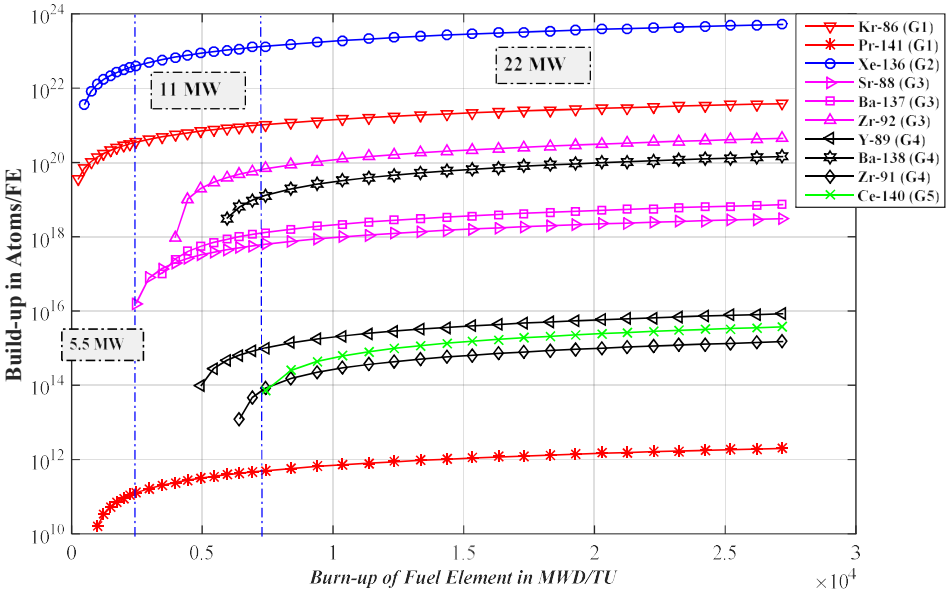

FIG. 4. Accumulation of Delayed Neutrons Precursors Daughters in fuel element.

5. RELEASE OF DELAYED NEUTRON PRECURSORS FROM REACTOR CORE TO COOLANT

The MTR core regions temperatures at full power shown in Table 5 are dependent on the core state where the fuel temperature is almost 353 ºC at reactor full power. At such low fuel temperatures (< 800 ºC), the release of fission products from the fuel plate is diffusional, generally independent of temperature, and thought to be irradiation-enhanced where diffusion coefficient (D) is proportional to the fission rate [7]. For the shorter-lived fission products as delayed neutrons precursors, the release due to the diffusion process was neglected at such very low temperatures and fission rates [8].

TABLE 5. CORE OPERATING PARAMETERS AT FULL POWER [3]

	Temperature (°C)		
Region	Fuel	Al	H_2O
Full Power	353	343	318

Release of delayed neutrons precursors from the fuel meat can also occur by a temperature-independent process of release that is knockout, when either a primary fragment or energetic particle created in a collision cascade, interacts elastically with a fission-product atom. The knockout release rate to birth rate (*R/B*) of any fission product was calculated using equations (3) and (4) [7]. *R/B* calculations are used to build a calculational path used as analytical tool to predict the release rate of delayed neutrons precursors into the coolant in cases of a very small defect area and large defect area. Then, this release rate may be used to calculate its measured ratio in the detection system at different flow rates of the detector pump. So, using this calculational path it will be possible to predict the response of the detection system detector under variable pump flowrate during reactor operation.

$$\frac{R_{knockout}}{B} = I(H)\ \frac{S_t}{V}\ \mu^{ko} \tag{3}$$

where $R_{knockout}$ is the release rate of delayed neutron precursors from fuel meat due to knockout, B is the total buildup rate of delayed neutrons precursors in fuel plate, $I(H)$ is the knockout integral, μ^{ko} is the range of higher order knock out of uranium atoms, S_t/V is the ratio of total surface area of fuel plate to its volume.

The relation of knockout integral as a function of H was described in Ref. 7.

$$H = \frac{2\gamma\ \alpha_U F^{\cdot}}{\lambda N_U} \tag{4}$$

where H is the ratio of the rate of removal by knockout compared with that by radioactive decay, γ is the ratio of the range of fission fragements to that of knockout, α_U is the number of uranium atoms emitted per escaping fission fragement, $F^{\cdot}$ is the fission rate (fissions/(m^3sec)), λ is decay constant of delayed neutron precursor, N_U is atomic density of Uranium (atoms/m^3).

In case of very small defect area, the release rate of precursors due to knockout effect will be considered only. Fig. 5 represents the release to birth rate ratio of delayed neutron precursors due to knockout when a fission event occurs near the fuel plate surface.

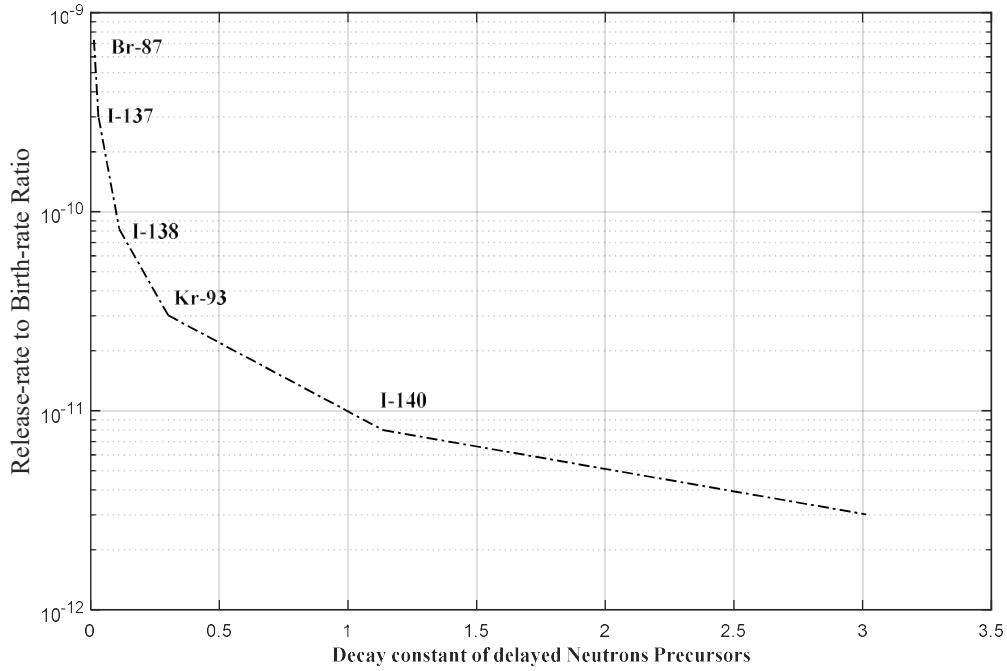

FIG. 5. Release rate of delayed neutron precursors to birth rate for each group.

The recoil of delayed neutrons precursors at the instant of fission event is another mechanism of release from fuel meat. The release of fission products due to recoil effect was calculated using equation (5) [8].

$$\frac{R_{rec}}{B} = \frac{1}{4}\,\mu_f\,\frac{S}{V}\,\frac{S_{def}}{S_f} \tag{5}$$

where S_{def} is exposed defect area (cm^2), μ_f is average range of fission fragment in uranium oxides (cm), S/V is FE geometric surface area to volume ratio (cm^{-1}).

According to equation (5), the recoil release depends on the surface area of the defect so it can be neglected in case of very small defects or no defects in the fuel-cladding matrix. Also, to consider the recoil release, the fission event must occur inside the fuel meat or at its surface where the fission product has a very short half-life. So, it's neglected in case of initiation of a very small defect in the fuel-cladding matrix [8].

But in case of the large surface area of failed fuel element defect, the recoil effect of very short-lived delayed neutrons precursors will be valuable and has high contribution in the release rate of these precursors [8]. If a large defect occurs in a fuel plate with almost 1 cm^2 surface area, the release to birth rate ratios due to the knockout and recoil effects are compared in Fig. 6.

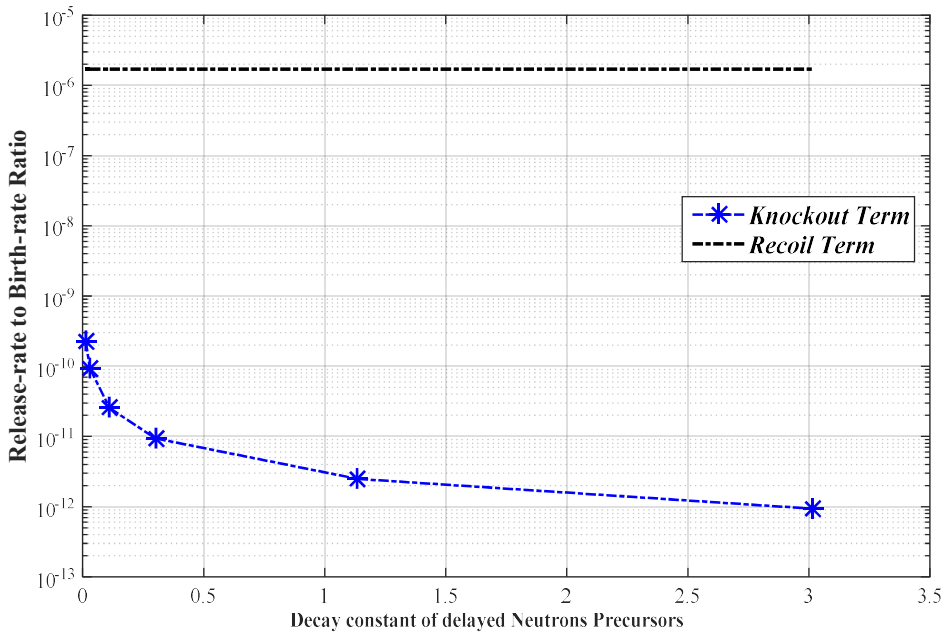

FIG. 6. Release to birth rate of delayed neutron precursors groups due to recoil and knockout effects at 1 cm2 defect surface area.

From the figure, it's clear that direct recoil of the very-short-lived delayed neutrons precursors dominates as the major release mechanism, especially with a large defect surface area, because of these precursors decay as they transport from the fuel surface [8].

5.1 Release of delayed neutron precursors to reactor coolant

The release rate of delayed neutron precursors from the defected fuel element to the coolant can be calculated using equation (6), where the escape rate coefficient of each isotope can be calculated from equation (7) where n = 1 for a mid-plate defect or ½ for an endplate defect [8]. Fig. 7 indicates the release rate of each delayed neutron group as a function of defect position for a very small defect calculated at full power of the reactor.

$$R_i = \frac{\nu_i}{(\nu_i+\lambda_i)}\ RB_i \times B_i \tag{6}$$

where RB_i is the release rate of delayed neutron precursors from fuel plate meat to birth rate ratio, $B_i = Y_i\, F{\cdot}V$ is buildup rate of isotope inside fuel plate matrix, ν is escape rate coefficient of isotope (i), λ is decay constant of delayed neutron precursor (i),

$$\nu = \frac{2n}{l} \tag{7}$$

where α is the surface exchange coefficient to the coolant, α is escape rate coefficient of isotope (i), n is factor for defect position, l is plate active length.

Fig. 8 indicates the release of delayed neutrons precursors into the coolant in case of a large defect area due to combined actions of recoil and knockout effects.

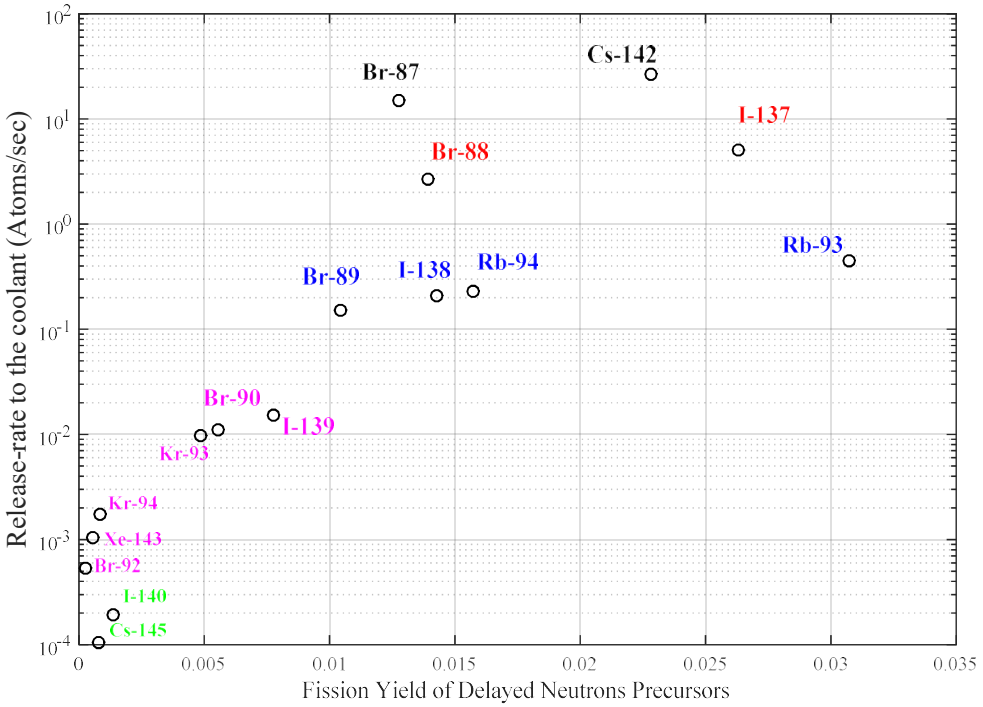

FIG. 7. Release rate of delayed neutron precursors in case of very small defect (each color represents one group).

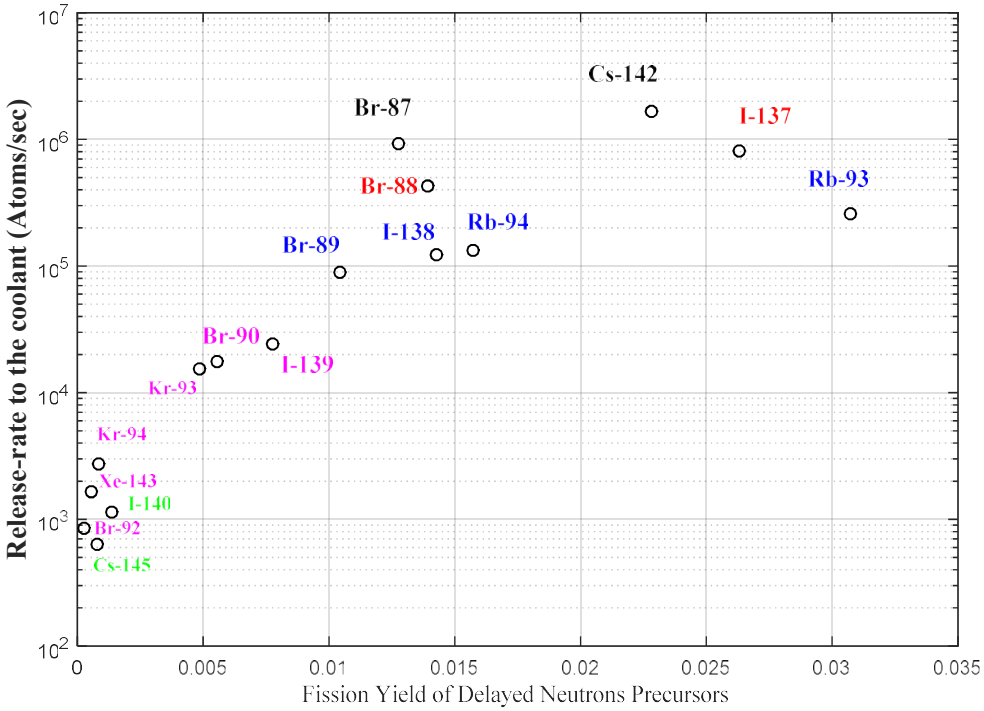

FIG. 8. Release rate of delayed neutron precursors in case of large defect of 1 cm2 (Each color represents one group).

5.2 Performance of fuel-cladding monitoring system under variable detector pump flowrate

During reactor operation. The reactor core cooling system flowrate disturbs the monitoring system pump flowrate, so it may change from its designed value. In addition to the probabilities of loss of pump flowrate due to any abnormal conditions where the main valve of the detector pipeline may be partially open. These changes in the pump flowrate have a noticeable impact on the reading of the monitoring system. Calculating the ratio of the neutron count-rate measured in the detector at a certain flowrate of detector pump to the total neutron count rate in the water using the contribution of each delayed neutron precursors group in the total count-rate using equation (8) indicated the effect of flowrate disturbance on the response of the monitoring system as shown in Fig. 9.

$$Count - rate = \Sigma_i^6 \frac{Y_i}{Y_T} \left(\frac{1}{2}\right)^{\frac{V_L}{Q_V T_{1/2}^i}} \quad (8)$$

where Y_i/Y_T is contribution of group (i) in neutron count rate measured in the detector, V_L is volume of water in measuring loop, Q_V is detector pump flow rate, $T_{1/2}^i$ is half-life of each delayed neutron precursors group.

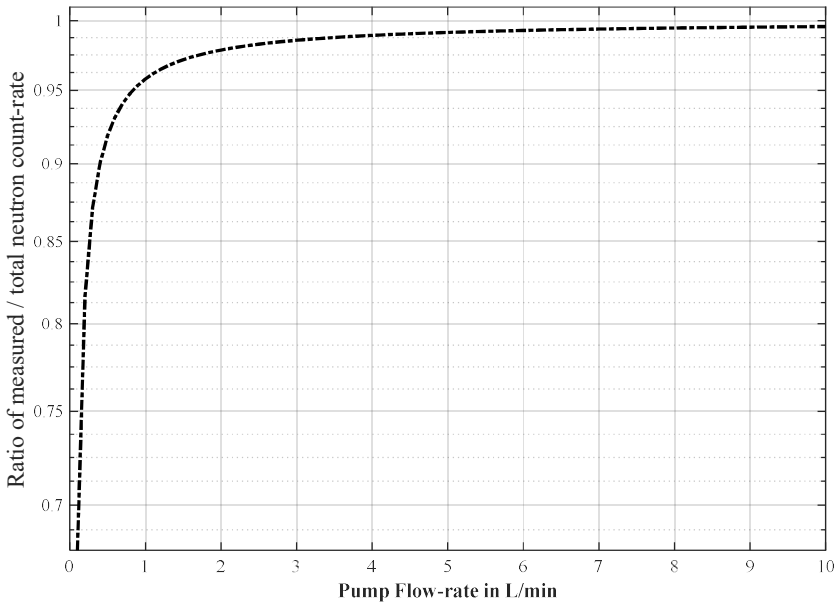

FIG. 9. Fuel-cladding monitoring system performance under disturbance of pump flowrate.

As shown in Fig. 9, it became clear that the measured neutron count-rate in the monitoring system detector depends strongly on the pump flowrate. Less than 4 L/min, a very small change in the pump flow rate leads to high fluctuations in detector reading. So, the designed flow rate of 7 Lit/min was shown to be the best choice where the small changes in pump flowrate don't affect the detector measured count-rate.

Similar sensitivity problems occur in the fuel failure monitoring systems of NPPs. The DN system of CANDU reactor responds to a measurement of neutrons produced from the short-lived delayed-neutron precursors ^{137}I and ^{87}Br. However, a decrease in sensitivity of the delayed neutrons monitors has been noticed with possible reasons of:

— Increased transport time to the DN water boxes from the design value due to fouling of the sampling tubes.
— Contamination of the core by tramp uranium [2].

6. CONCLUSION

The operating parameters of the reactor have an impact on the performance of the fuel-cladding failure monitoring and detection system of the reactor. An increase of reactor power during a start-up state within a short period or operating reactor core cooling system may lead to a false alarm from the neutron detector of the monitoring system. So, the calibration process of the monitoring system has to include the feedback of these effects

adjusting the setting of the calibration constant. The results of this study were used to adjust the calibration constant value of the failure detection system to compensate for the effect of reactor power change during reactor start-up on the build-up rate of delayed neutrons precursors and the effect of altering the pump flowrate of the detection system on the ratio of measured neutrons activity in the detector to the released activity in the coolant. So, the problem was noticed to be solved where the false alarm of the fuel failure monitoring system stopped to appear during the reactor operation.

The method of adjusting the calibration constant of the detection system or monitoring the fuel failure defect using measured accumulation rates of stable daughters of delayed neutrons precursors in the coolant and water treatment system that mentioned in section 4.2 in the paper, must be practically tested to prove its efficiency in fuel failure detection. In this case, it can be recommended to be applied in NPPs.

REFERENCES

[1] INTERNATIONAL ATOMIC ENERGY AGENCY, Review of Fuel Failures in Water Cooled Reactors, Nuclear Energy Series No. NF-T-2.1, IAEA, Vienna (2010).

[2] FITCHETT, A., LEWIS, B.J., IGLESIAS, F.C., AND SHAHEEN, K., Assessing the Impact of Increased Transport Time between Failed Fuel and Delayed Neutron Detectors, 11th International Conference on CANDU Fuel, Niagara Falls, Ontario, Canada, October 17-20, 2010.

[3] INTERNATIONAL ATOMIC ENERGY AGENCY, Research Reactor Benchmarking Database: Facility Specification and Experimental Data, Technical Reports Series No. 480, IAEA, Vienna (2015).

[4] Precursors of Delayed Neutrons, https://www.nuclear-power.net/nuclear-power/fission/delayed-neutrons/precursors-of-delayed-neutrons/

[5] ASKEW, J. R., FAYERS, F. J., KEMSHELL, P. B., General description of the lattice code WIMS, Atomic Energy Establishment, Winfrith, Eng. (1966).

[6] IAEA Nuclear Data Section, WIMS Library Update Project, https://www-nds.iaea.org/wimsd/pseudofp.htm.

[7] LEWIS, B.J., Fundamental aspects of defective nuclear fuel behaviour and fission product release, Journal of Nuclear Materials **160** (1988) 201-217.

[8] LEWIS, B.J., CHAN, P.K., EL-JABY, A., IGLESIAS, F. C., FITCHETT, A., Fission product release modelling for application of fuel-failure monitoring and detection - An overview, Journal of Nuclear Materials **489** (2017) 64-83.

WANO FUEL RELIABILITY INDICATOR FOR CANDU FUEL

R.E. LEWIS
Bruce Power, Fuel Design and Assessment,
123 Front St. W. ON M5J 2M2

B.J. LEWIS, K. FARAHANI
Royal Military College of Canada, Department of Chemistry and Chemical Engineering,
PO Box 17000, Kingston, ON K7K 7B4

Abstract

The standardization of a Fuel Reliability Indicator for defective fuel in CANDU reactors has been developed as an extension of that proposed by the World Association of Nuclear Operators. This methodology provides a means to distinguish the release of fission products from fuel defect(s) and from tramp uranium in the primary heat transport system using the isotopes of I-131 and I-134. The treatment includes the development of a common power-scaling correlation for the higher-powered CANDU fuel for both 28-element (Pickering reactor) and 37-element fuel bundles (CANDU-6, Darlington, and Bruce reactors). A methodology is outlined for correcting coolant activities for the effects of coolant purification and identifies requirements for normalization of the fuel reliability indicator to a reference purification rate constant and average fuel rating. This analysis is further extended with the possible use of the isotope, Xe-133, for common analysis among various CANDU reactor types since this isotope is not affected by ion-exchange purification effects, coolant chemistry or fuel defect size. This latter isotope can be used to predict the number of fuel defects and the average linear power of the defective elements that are in-core. The isotope, I-134, can also be used to estimate the amount of in-core tramp uranium. The complete model provides a CANDU-specific fuel reliability indicator as a suggested means of standardization for defective fuel analysis for comparison across the nuclear industry.

1. INTRODUCTION

A fuel reliability indicator (FRI) has been proposed by the World Association of Nuclear Operators (WANO) [1, 2] to monitor industry progress in achieving and maintaining high fuel integrity. With defective fuel, there is a release of fission products into the primary heat transport system (PHTS) as well as possible fuel debris. Element performance is affected with a reduced fuel thermal conductivity and enhanced fission-product diffusivity in defective fuel. Restrictions exist on the amount of I-131 in the PHTS that could potentially force a reactor to prematurely shut down. Hence, the presence of failed fuel can have a detrimental effect on the operating cost and performance of the reactor, with an increased radiological hazard to plant workers. Consequently, WANO has defined an indicator to assess fuel integrity based on a steady-state measurement of the coolant activity of I-131. This indicator is corrected for the tramp uranium contribution using I-134 and normalized to a common purification rate and element power level.

This paper examines the underlying theory for the performance indicator and presents a methodology for the application of the WANO model to CANDU fuel operation and integrity assessment.

A. FISSION PRODUCT RELEASE THEORY FOR DEFECTIVE CANDU FUEL

Above about 1000°C, fission products migrate primarily by thermally induced diffusion in the bulk UO_2 [3-10]:

$$\frac{R_{dif}}{B} = 3\sqrt{\frac{D\prime}{\lambda}} \tag{1}$$

Here R is the release rate and B the birth rate where $B = FY$ [F is the fission rate (fissions s^{-1}) and Y is the cumulative fission product yield (atom fission^{-1})], D' is the empirical diffusion coefficient in the UO_2 fuel [$= D/a^2$ where D is the diffusion coefficient and a is the grain radius] (s^{-1}) and λ is the radioactive decay constant (s^{-1}). Below 1000°C, the fission product release is generally independent of temperature but is activated because of the fission event. Fission gas can be released by athermal diffusion in accordance with Eq. (1), which dominates any release by the mechanisms of recoil and knockout since fuel oxidation can affect the vacancy-enhanced diffusion rate of fission products in the fuel matrix of defective elements [3, 11].

Release of fission products from the gap of the defective rod into the coolant can occur by a first-order rate process, where the coolant release rate (R_c) is proportional to the available inventory in the gap, N_g:

$$R_c = \nu N_g \tag{2}$$

and ν is the gap escape-rate constant (s^{-1}). The subsequent mass balance in the gap at steady state is:

$$\frac{dN_g}{dt} = R_{dif} - \lambda N_g - \nu N_g = 0 \tag{3}$$

Thus, with diffusion as the dominant release mechanism from the fuel, the observed release fraction into the coolant is:

$$\left(\frac{R_c}{B}\right) = \left\{\frac{\nu}{\lambda+\nu}\right\} 3\sqrt{\frac{D\prime}{\lambda}} \tag{4}$$

The term in curly brackets describes the holdup of fission products in the gap during their transport to the defect opening.

Traces of uranium compounds may be found on the surfaces of the heat-transport system primarily from a previous loss from defective fuel elements. The debris is in the form of very fine particles, where fuel is lost after individual grains of fuel are loosened by oxidation along their boundaries (see Fig. 1).

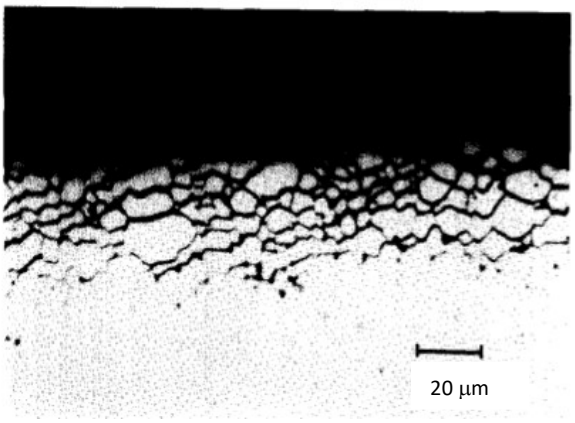

FIG. 1. Oxidation of UO_2 under a defect hole in the Zircaloy sheath. Oxidation is progressing along the grain boundaries causing the grains to separate from the bulk of the pellet.

For small particles of fuel at low temperature, since the range of the fission fragment ($\mu_f \sim 10$ µm) is comparable to the size of the UO_2 fuel particle itself, each fragment will leave the individual particle of the fissioning U-atom. For instance, experimental ratios of release rates of ^{88}Kr to ^{138}Xe were between 0.4 and 0.7 in a pressurized-water loop containing fuel debris on the piping surface [3]. The release expression for a small particle of fuel of diameter d, deposited onto a solid surface is [12]:

$$\left(\frac{R}{B}\right)_{tramp} = \frac{1}{2}\left\{\frac{1}{\alpha^3} + \frac{3\mu_f}{2d}\left(1 - \frac{1}{\alpha^2}\right)\right\} \tag{5}$$

where $\alpha = 1$ or d/μ_f, whichever is greater. Since B is proportional to the fission yield Y, and the right-hand side of Eq. (5) is a constant, a release ratio of $R_{88}/R_{138} = Y_{88}/Y_{138} = 0.55$ is calculated in excellent agreement with the measured range. In this calculation, the cumulative yield has been used to account for the decay of the precursor products also emitted into the recirculating coolant. Since $3\mu_f > d$, $\alpha = 1$ and Eq. (5) simply reduces to:

$$\left(\frac{R}{B}\right)_{tramp} = \frac{1}{2} \tag{6}$$

3. APPLICATION OF WANO METHODOLOGY

The WANO methodology converts a measured coolant activity A_m (Bq) into a release rate R (atom s^{-1}) for defective fuel. As shown in Fig. 2, one can distinguish releases from defective fuel [Eq. (4)] and tramp uranium [Eq. (6)] by examining the release rate R (atom s^{-1}) when normalized by the isotopic yield Y (atom $fission^{-1}$) in which a composite curve result:

$$\left(\frac{R}{Y}\right) = a\lambda^b + c \tag{7}$$

Here b ranges from –1/2 to – 3/2 from the fission product release theory in Section 2. The amount of fuel debris in the core can be estimated directly from the fitted parameter $c = ½ F_t$ (~ $1.1 \cdot 10^{12}$ fissions/s) [3]. The normalized release rate from defective fuel depends on the radioactive decay constant λ, with a typical exponential dependence ranging from $\lambda^{-1/2}$ for a large defect (indicating only diffusion in the fuel) to $\lambda^{-3/2}$ for a small defect (due to diffusion in the fuel with significant holdup in the fuel-to-sheath gap). On a log-log plot, this dependence is simply the slope of the straight line shown in Fig. 2. For tramp uranium fuel, as discussed in Section 2, the fuel temperature is too low for diffusion to be important so that only fission product recoil occurs (i.e., the flat line shown in Fig. 2). For instance, off-gas data from the HATCH-1 Boiling Water Reactor plant, a flat recoil release was observed for the radioactive noble gas species (including the longer-lived Xe-133 isotope) when no failures were present [3]. The isotope I-131 has a long half-life and is therefore the predominant isotope with a large diffusional release. On the other hand, the short-lived I-134 isotope will decay before it is released from a defective fuel element so that its contribution is mainly due to a recoil release from tramp debris. Consequently, these two isotopes can be used to distinguish defective fuel from tramp fuel contributions.

There is a very small diffusional release for the short-lived isotopes as compared to a recoil process from the fuel element as seen, for example, in the FFO-102-3 loop experiment [3]. This result is especially true for the iodine species because of holdup in the gap, where the transport is hindered by chemical effects during transport along the gap. Recoil release around the defect site would be limited to only the solid angle seen by the fuel exposed to the coolant. Moreover, for the very short-lived I-134, any diffusional release must be very localized around the defect site due to its short diffusion length in the gap (especially compared to that of I-131). In contrast, recoil release from tramp uranium is instantaneously released from the piping surfaces with no chemical hold up. Hence, diffusion would predominate for the longer-lived I-131 and a recoil release would be important for the tramp uranium release.

The mass balance for the fission product inventory N_i (atom) released into the coolant for isotope i is [8-10]:

$$\frac{dN_i}{dt} = R_i - (l_i + B_a)N_i \tag{8}$$

The parameter B_a is the actual purification rate constant (s^{-1}). Thus, the release rate contribution R_i from both defective and tramp fuel is:

$$R_i = \underbrace{\underbrace{\left(\frac{\nu}{\lambda+\nu}\right)}_{\text{gap transport}} \underbrace{3\sqrt{\frac{D'}{\lambda}}F_f Y}_{\text{transport in fuel matrix}}}_{\text{defective fuel contribution}} + \underbrace{\tfrac{1}{2}F_t Y}_{\text{tramp fuel contribution}} \tag{9}$$

Here F_f is the fission rate for the defective element (fission s^{-1}) and F_t is the fission rate in the tramp fuel (fission s^{-1}). Equation (9) gives rise to the observed release rate behaviour in Fig. 2 when normalized by the fission product yield Y.

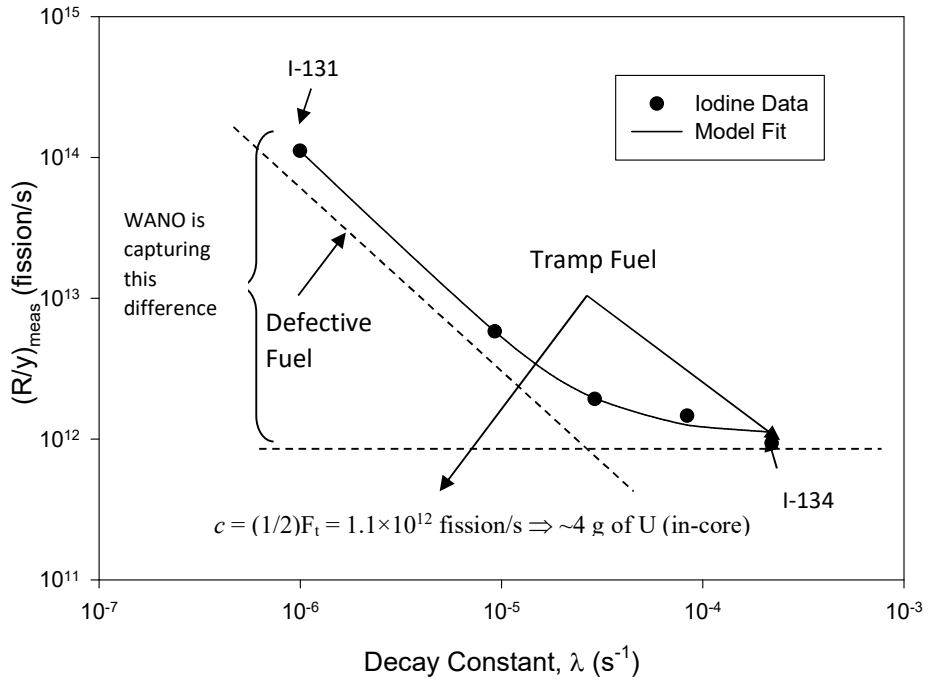

FIG. 2. Schematic showing fission product release from defective fuel (sloped line) and recoil release from tramp fuel (flat line independent of the decay constant) with the model fit to data derived from measured coolant activities.

For high mass chain products, the yield Y will not change considerably with fuel burnup because of similar yields for the fissile species of U-235 and Pu-239. For instance, to account for the burnup of the fissile U-235 with a production of Pu-239 in the fuel, an effective yield Y_{eff} as a function of burnup B (in MWh/kgU) can be considered with the weighted function [12]:

$$Y_{eff} = \frac{(Y_o w\sigma_f g_f/A)_{U-235}+(Y_o w\sigma_f g_f/A)_{Pu-2}}{(w\sigma_f g_f/A)_{U-235}+(w\sigma_f g_f/A)_{Pu-2}} \tag{10}$$

For example, the fission product yield Y_o for I-131 is 2.88% atom fission^{-1} (U-235) and 3.85% atom fission^{-1} (Pu-239) (this isotope has the largest difference in yield amongst the shorter-lived iodine isotopes). The specific fissile content w (in g/kgU) can be evaluated from correlations in Ref. [8]. The other parameters include the microscopic fission cross sections σ_f = 580 b (U-235) and 742 b (Pu-239), the non-1/v fission factor g_f = 0.9389 (U-235) and 1.3314 (Pu-239) and the atomic mass A= 235 g/mole (U-235) and 239 g/mole (Pu-239). At a nominal fuel burnup for CANDU fuel of 100 MWh/kgU, the effective yield is 3.37% atom fission^{-1}, yielding a small percentage error of 17% compared to 2.88% atom fission^{-1} by just assuming fresh fuel. Doubling this burnup to 200 MWh/kgU, yields a slightly larger discrepancy of 24%. For I-134, the percent difference error is less than 3%. Hence, no correction is needed for either the iodine or xenon isotopes with fuel burnup, where the U-235 yield can be directly used with minimal error. This insensitivity is a useful property because one does not know *a priori* the respective burnup of the defective fuel rods versus how long fuel debris has resided on in-core surfaces from past defect occurrences.

3.1 FRI Derivation

The R/Y value for I-131 is corrected by subtracting the tramp uranium contribution (as estimated by the R/Y value for I-134). At steady-state, Eq. (8) becomes:

$$\frac{dN_i}{dt} = R_i - (\lambda_i + B_a)N_i = 0 \Rightarrow A_i \equiv (\lambda N)_i = \left(\frac{\lambda_i}{\lambda_i + B_a}\right)R_i \tag{11}$$

The release rate R_i (in atom s^{-1}) is simply proportional to the coolant activity A_i (in Bq). One can normalize the measured coolant activity by the coolant mass which will shift the I-131 and I-134 data points by the same amount but respect their difference in Fig. 2. Thus, the FRI as used by WANO follows from the basic concept:

$$(R/Y)_{def} = (R/Y)_{I-13} - (R/Y)_{I-13} \tag{12}$$

Solving for R in Eq. (11), substituting this result into Eq. (12), and normalizing by the mass of the reactor coolant system (m_c in grams) yields:

$$\left(\frac{R/Y_{def}}{m_c}\right) = A_{M,I-131}\left(\frac{\lambda+B_a}{Y\lambda}\right)_{I-131} - A_{M,I-134}\left(\frac{\lambda+B_a}{Y\lambda}\right)_{I-134} \tag{13}$$

where A_M is the measured coolant activity concentration in Bq/g. To normalize to a reference rate constant (B_n), Eq. (13) can be rewritten as:

$$\left(\frac{R/Y_{def}}{m_c}\right) = \left\{A_{M,I-131}\left(\frac{\lambda_{131}+B_a}{\lambda_{131}+B_n}\right)\right\}\left(\frac{\lambda_{131}+B_n}{Y_{131}\cdot\lambda_{131}}\right) - \left\{A_{M,I-134}\left(\frac{\lambda_{134}+B_a}{\lambda_{134}+B_n}\right)\right\}\left(\frac{\lambda_{134}+B_n}{Y_{134}\cdot\lambda_{134}}\right) \tag{14}$$

The term is curly brackets is the respective coolant activity normalized to B_n (s^{-1}) where:

$$\left(\frac{R/Y_{def}}{m_c}\right) = A_{N,I-131}\left(\frac{\lambda_{I-131}+B_n}{Y_{I-131}\cdot\lambda_{I-131}}\right) - A_{N,I-134}\left(\frac{\lambda_{I-134}+B_n}{Y_{I-134}\cdot\lambda_{I-134}}\right) \tag{15}$$

and (with i = I-131 and I-134):

$$A_{N,i} = \left\{A_{M,i}\left(\frac{\lambda_i+B_a}{\lambda_i+B_n}\right)\right\} \tag{16}$$

WANO specifically normalizes to a "reference" purification rate constant of $B_n = 2\times10^{-5}$ s^{-1}. However, for CANDU operation a more representative value is $B_n \sim 5\times10^{-5}$ s^{-1}. Finally, multiplying Eq. (15) through by the factor $(Y_{I\text{-}131}\lambda_{I\text{-}131})/(\lambda_{I\text{-}131} + B_n)$ yields:

$$A_{D,C}(Bq/g) \equiv \left(\frac{Y_{I-131}\cdot\lambda_{I-131}}{\lambda_{I-131}+B_n}\right)\left(\frac{R/Y_{def}}{m_c}\right) = A_{N,I-131} - A_{N,I-134}\left(\frac{Y_{I-131}\cdot\lambda_{I-131}}{\lambda_{I-131}+B_n}\right)\left(\frac{\lambda_{134}+B_n}{Y_{134}\cdot\lambda_{134}}\right) \tag{17}$$

or

$$A_{D,C}(Bq/g) = A_{N,I-131} - k_C A_{N,I-134} \tag{18}$$

$$k_C = \frac{[Y\lambda/(\lambda+B_n)]_{I-131}}{[Y\lambda/(\lambda+B_n)]_{I-134}} \tag{19}$$

Equations (18) and (19) are identical to the WANO methodology except for a slight discrepancy for their proposed k factor:

$$k_C = k\left(\frac{\lambda_{I-131}}{\lambda_{I-134}}\right)^{0.045} \tag{20}$$

This slight difference occurs where WANO assumed a small dependence of the decay constant for the tramp uranium contribution based on empirical observation. As detailed in Section 2, this empirical dependence is not consistent with recoil theory, where the use of a flat line for the tramp contribution allows for a good fit of the model to the data in Fig. 2. The value of the ratio of the k factors in Eq. (20) for the CANDU versus WANO model is $k_c/k \sim 0.8$, which, nevertheless, is close to unity. This difference makes little impact on the calculated FRI value especially given the measurement uncertainty in the coolant activity data.

3.1.1 Power Correction and Normalization

Reactor power will impact the I-131 activity concentration. As such, WANO normalizes A_D to a reference heat generation rate of 18 kW·m^{-1} assuming a dependence on the linear heat generation rate of $LHGR^{1.5}$. This correction is appropriate for athermal diffusion for the lower-powered PWR fuel. For instance, the diffusion coefficient D for fission gases for oxidized fuel consists of three components over temperature: (i) intrinsic diffusion at high-temperature (which is an Arrhenius function of temperature T), (ii) irradiation-enhanced vacancy production at intermediate temperatures (where the uranium vacancy concentration is also a function of the deviation from stoichiometry x in UO_{2+x}), and (iii) irradiation-enhanced (athermal) diffusion at low temperature (which depends on the fission rate density F_v) [13]:

$$D(x,T) = D(T) + D(x,T) + a \cdot F_v \tag{21}$$

LWR's operate at much lower linear ratings and to higher burnups as compared to CANDU fuel. A dependence of $LHGR^{1.5}$ for the release rate strictly implies athermal diffusion for the lower-powered fuel as follows from Eqs. (4) and (21) for Booth diffusion given the square-root dependence on D' and the fact that the birth rate B is also proportional to the linear heat rating [14]. Since defective fuel in CANDU reactors operate at much higher ratings, diffusion occurs as an Arrhenius function of temperature and depends on the stoichiometry deviation.

Although WANO used a linear power normalization of L_n = 18 kW·m^{-1}, a more appropriate reference value for CANDU fuel is: L_n = 38 kW·m^{-1} as shown in Table 1 based on median bundle powers for various reactors (i.e., assuming 28 elements/bundle for Pickering and 37 elements/bundle for the others with a fuel stack length of 0.48 m) [15]. An extrapolation from the low linear power in the PWR to typical CANDU values would result in a significant source of error.

As shown in NRX reactor loop tests, the empirical diffusion coefficients for iodine and noble gas are equal [3, 4, 6, 16, 17]. To evaluate the power dependence of the empirical diffusion coefficient D' in Eq. (9), one can use the steady-state release rate of ^{133}Xe from commercial reactor experience. Due to the relatively long half-life ($t_{1/2}$ = 5 days), and chemically inert nature, ^{133}Xe is the least affected by defect size because its diffusion length in the gap is comparable to the fuel-element length. This approximation is illustrated in Fig. 3(a) which shows ^{133}Xe release rates versus linear power $LHGR$ (in kW m^{-1}) for defects of various sizes and burnups for different reactors [18].

TABLE 1. MEDIAN BUNDLE POWERS AND BURNUP AND AVERAGE ELEMENT RATING FOR CANDU REACTORS FROM 1970-2010

Reactor	Median Burnup (MWh/kgU)	Median Bundle Power Rating (kW)	Average Element Rating (kW·m^{-1}) ($LHGR$)
Bruce A	195	658	37.0
Bruce B	188	638	35.9
Pickering A	202	547	40.7
Pickering B	191	550	40.9
Darlington	201	690	38.9
Gentilly-2	174	653	36.8
Point Lepreau	170	653	36.8
Aggregated	192	624	38.1 (= L_n)

For a steady-state diffusional release, the release-to-birth ratio (R/B) of ^{133}Xe is obtained from Eq. (4), where $\lambda \ll \nu$ for the long-lived ^{133}Xe isotope so that

$$\frac{R}{B} = \frac{10^{a+b\,LHGR}}{f_f Y \cdot LHGR} = \sqrt[3]{\frac{D\prime}{\lambda}} \tag{22}$$

Here f_f = 1.489×10^{13} [fission.m. kW^{-1}] (i.e., $F = f_f \cdot LHGR$) , Y = 0.066991 [atom.fission^{-1}] is the ^{133}Xe cumulative yield, and λ = 1.53×10^{-6} [s^{-1}] is the ^{133}Xe decay constant. This dependence of the Xe-133 release rate versus the linear element power is shown in Fig. 3(a).

Using Eq. (22), the empirical diffusion coefficient D'(in s^{-1}) is given by:

$$D' = 8.6\,´\,10^{-1}\ \left[\frac{\mathbf{10^{(0.114 \cdot LHGR)}}}{\mathbf{LHGR^2}}\right] \tag{23}$$

Equation (23) is based on the data in Fig. 3(a) for CANDU operational experience in the power range of 30 to 50 kW·m^{-1}. In comparison, for PWR rods that operate typically below ~22 kW·m^{-1}, D' is directly proportional to the linear power rating $LHGR$ [1, 2, 14]. The power-law correlation $R = 10^{9.86+\ .057 \cdot LHGR}$ from Ref. [18],

shown in Figs 3(a) and 3(b), can be reasonably extrapolated to a higher rating of 60 kW m^{-1} as well as to a lower limit of 22 kW·m^{-1}. The lower rating is demonstrated where linear powers predicted using Eq. (22), based on observed ^{133}Xe release rates for an element power-cycled between ~23 to 39 kW·m^{-1} in a X-2 loop experiment, were in excellent agreement with the actual power ratings. Thus, the PWR scaling law of $R = a_1 \cdot LHGR^{1.5}$ can be applied with continuity at 22 kW·m^{-1} in Fig. 3(b). Thus, the following empirical diffusion coefficient can be directly applied over the full linear power range:

$$D' = \begin{cases} 2.71 \times 10^{-13} \cdot LHGR, & LHGR < 22\ kW/m \\ 8.6 \times 10^{-12} \left[\frac{10^{(0.114 \cdot LHGR)}}{LHGR^2}\right], & LHGR \geq 22\ kW/m \end{cases} \quad (24)$$

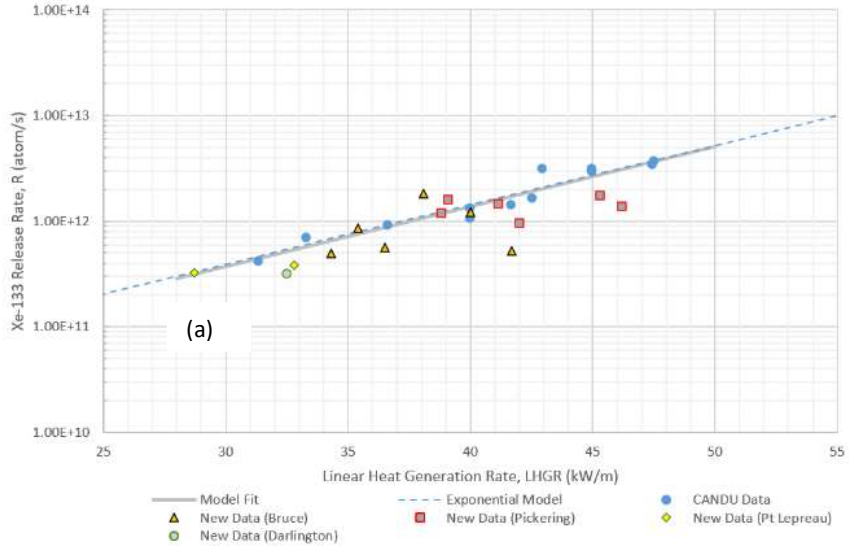

FIG. 3. (a) ^{133}Xe release rate [atom·s^{-1}] as a function of defective element linear power [kW·m^{-1}] (Adapted from Ref. [18]).

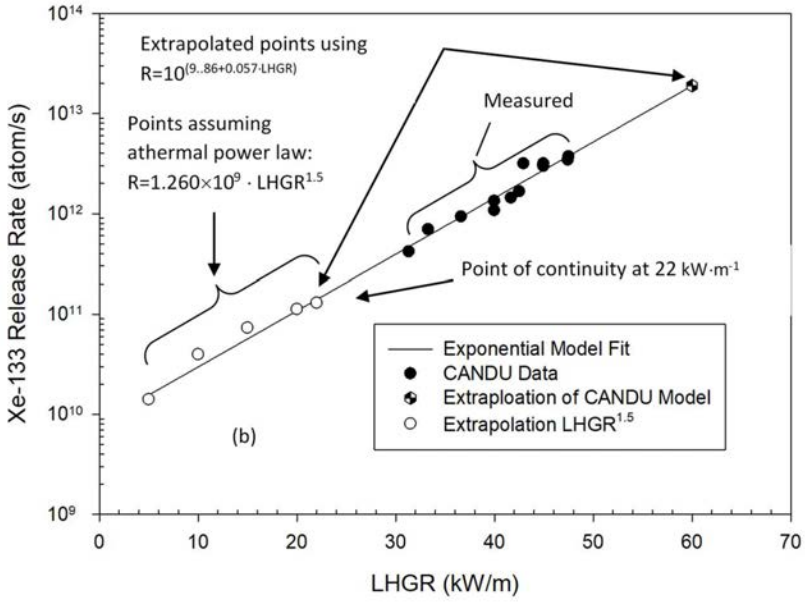

FIG. 3. (b) Exponential scaling model for extrapolated reactor power analysis.

4.FRI ANALYSIS

Using Eqs. (18) and (19), with the power scaling correlation developed in Fig. 3, the FRI model as derived in this work specific for CANDU fuel is given by:

$$FRI = A_{D,C}\,' \, 10^{0.057\times\left[L_n - LHGR\left(\frac{P_0}{100}\right)\right]} = \left[(A_{131})_N - k_C(A_{131})_N\right]' \, 10^{0.057\times\left[L_n - LHGR\left(\frac{P_0}{100}\right)\right]} \quad (25)$$

$$A_N = A_M \left[\frac{\lambda + B_a}{\lambda + B_n}\right] \quad (26)$$

$$k_C = \frac{[Y\lambda/(\lambda+B_n)]_{I-131}}{[Y\lambda/(\lambda+B_n)]_{I-134}} = 0.00900 \quad (27)$$

with reference values: $L_n = 38$ kW·m^{-1} and $B_n = 5\times10^{-5}$ s^{-1}. The FRI is reported in units of Bq/g when the measured coolant activity A_M is expressed in this unit. All sampled data are at equilibrium conditions. Values for the linear heat generation rate (*LHGR*) at 100% power can be obtained from Table 1 for the respective CANDU station. The values in Table 1 are scaled accordingly depending on the percent of reactor power P_o.

An example FRI analysis for Bruce Power is shown in Table 2. Data from various CANDU reactors are summarized in Fig. 4, showing the FRI values along with the proposed threshold that delineates defects from tramp uranium in the core.

This analysis supports a single choice of model parameters for the "normalized" purification rate constant and "normalized" linear element power. The assumed value for the normalized purification rate constant B_n is representative of typical purification rate constants experienced in these reactors (i.e., ~5×10^{-5} s^{-1}). This quantity is obtained by dividing the purification flow rates in the single- and double-loop systems by the PHTS mass, accordingly. Moreover, the normalized element linear power L_n taken from Table 1 is consistent with most defective element powers contained in the dataset of defect occurrences. One needs to consider the average linear power rating *LHGR* in the reactor because the specific linear power of the defective element is not known *a priori* when considering a FRI analysis in the commercial power station.

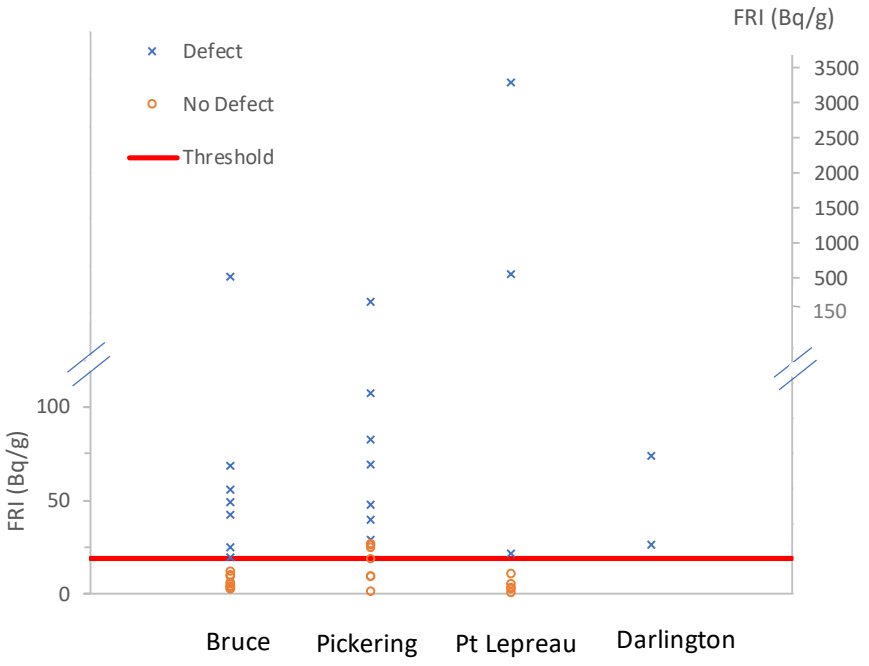

FIG. 4. FRI values for the power reactor database showing the threshold that depicts defects from tramp uranium in the core. The average FRI values are used for Pickering.

A threshold value of 19 Bq g^{-1} can be used to distinguish between fuel defect(s) and tramp uranium. The FRI model was successful in identifying most occurrences of defective fuel in all reactors at this given threshold value. However, in the Pickering reactor that uses a "common sampling point" arrangement, several cases indicated a slightly higher FRI threshold value (i.e., with a calculated value of ~26 Bq g^{-1}) with no defects present when averaging the purification flow rate for the two independent loops. Interestingly, the FRI value dropped below 19 Bq g^{-1} (as seen in all other cases), when the lower of the two single-loop purification flow rates were considered. This situation is unique to the Pickering arrangement because of a common sampling point for the two-loop system. All measured Xe-133 release rates were relatively consistent, and in general agreement, with the proposed power-scaling law in Fig. 3(a).

4.1 Xe-133 Analysis

The additional use of Xe-133 as an indicator may help improve model predictions since it offers several advantages including:

(i) No effect of ion-exchange purification on the calculation due to the inherent chemical inertness of the noble gases (hence, there is no impact of different flow rates being used at various CANDU stations when trying to normalize to a common purification flow rate).

(ii) Since Xe-133 is not affected by ion-exchange operations, the model would not be dependent on the different loop configurations (e.g., single versus a double loop arrangement). The total PHTS mass would therefore be used for a xenon analysis in all reactors.

(iii) Because of the long half-life and chemical inertness of Xe-133, it is not affected by the defect size of the defective element and thus its release rate is more prominent (i.e., as compared to that of I-131). As demonstrated in Fig. 3(a), the release rate is reasonably correlated to the defective element linear power for all reactor types. Hence, using Eq. (25) and replacing the coolant activity concentration $A_{D,C}$ by the release rate R (in atom s^{-1}), or equivalently by the coolant activity (in Bq), one obtains the following expression for a Xe-133 scaling:

$$FRI_{Xe-1} = R_{Xe-1} \times 10^{0.057\times\left[L_n - LHGR\left(\frac{P_0}{100}\right)\right]} \tag{28}$$

As demonstrated in Fig. 3(a), the release rate correlates well with the linear power for all Pressurized Heavy Water Reactor (PHWR)-types. In fact, as shown in Eq. (22), the release rate is directly related to the empirical diffusion coefficient in the fuel matrix for the long-lived Xe-133 isotope.

The main disadvantage of using Xe-133 as a "common" FRI is that some gas loss may occur if a measurement is made off-line without the use of a pressurized sample bomb.

Thus, a "normalized" value for the release rate for the defective-fuel assessment can be evaluated which delineates defective fuel from cases where there are no defects. A scaling is considered from the average element rating (*LHGR*) for each unit/station (listed in Table 1) to the aggregate linear power value of 38 kW m^{-1} since the specific linear power of the defective element is not known *a priori*. This scaled quantity can be used as a "common" FRI for reporting purposes, where a steady-state threshold value of ~4 x 10^{11} atom s^{-1} (or ~4 x 10^{11} Bq) in Fig. 5 indicates the presence of a defect.

TABLE 2. FRI ANALYSIS FOR BRUCE A AND B NUCLEAR GENERATING STATION

Unit*/ (Case)	Date and Time		I-131 (Bq g^{-1})	I-134 (Bq g^{-1})	Xe-133 (Bq g^{-1})	Purification Flow Rate (kg s^{-1})	B_a (s^{-1})	Bundle Power (kW)	Reactor Power (%)	Element Linear Power ** (kW m^{-1})	FRI (Bq g^{-1})	Remarks	Xe-133 Release Rate (atom s^{-1})
	No Defects in Core												
5 (Case 1)	2018-08-06 9:40		3.33	298.6	84.7	13.7	6.58E-05	N/A	92.9	N/A	2.8	No defect predicted	1.76E10
3 (Case 2)	2018-05-24 8:25		23.7	1151	368.9	8.12	3.37E-05	N/A	89.6	N/A	12.1	No defect predicted	8.88E10
7 (Case 3)	2018-03-20 11:00		4.07	281.6	103.6	12.2	5.85E-05	N/A	93.0	N/A	3.9	No defect predicted	2.15E10
8 (Case 4)	2017-03-28 11:45		2.59	107.6	57.4	13.3	6.39E-05	N/A	92.9	N/A	4.2	No defect predicted	1.19E10
7 (Case 5)	2016-04-26 10:25		4.07	196.1	85.1	13.7	6.57E-05	N/A	93.0	N/A	6.3	No defect predicted	1.77E10
	Defects in Core* **												
3 (Case 6)	2018-02-22 9:50		17.02	762.2	2179	12.1	5.00E-05	744.7	89.2	41.7	19.6	Defect predicted (> 19 Bq g^{-1}).	5.25E11
8 (Case 7)	2015-11-17 9:50		24.79	172.8	2401	12.0	5.78E-05	600.8	93.0	34.3	49.3	Defect predicted (> 19 Bq g^{-1}).	4.99E11
8 (Case 8)	2014-06-17 10:31		11.8424.42	88.8	2697	12.7	6.13E-05	652.7	92.9	36.5	25.1	Defect predicted (> 19 Bq g^{-1}).	5.61E11
3 (Case 9)	2016-01-14 21:35		56.24	1200	5069	8.32	3.45E-05	700.4	89.4	40.0	55.5	Defect predicted (> 19 Bq g^{-1}).	1.22E12
6 (Case 10)	2018-03-05 9:30		207.2	275.3	8806	14.34	6.90E-05	666.4	92.8	38.1	522	Defect predicted (> 19 Bq g^{-1}).	1.83E12

*Bruce A (Units 1 to 4: Loop mass = 2.70E5 L; *LHGR*=37 kW m^{-1}) and Bruce B (Units 5 to 8: Loop mass = 2.33E5 L; *LHGR*=35.9 kW m^{-1})

** Linear power (in kW m^{-1}) for: (i) an intermediate-ring element is bundle power (kW)/ (37 elements/0.48 m) × (0.98/0.9857) and (ii) an outer-ring element bundle power is: bundle power (kW)/(37 elements/0.48 m) × (1/0.9857).

***Defect Description:

Case 6: Separated downstream endcap on intermediate element 20. Fission product flow stains visible.

Case 7: Hydride/deuteride blisters and axial crack-like feature near center bearing pad of outer element 14. Fission product flow stains visible.

Case 8: Ruptured hydride/deuteride blister and fission product flow stains downstream of spacer pads on intermediate element 24.

Case 9: Axial cracks adjacent to both sides of the upstream outer board bearing pad braze of outer element 6. Blown hydride/deuteride blister with cracks adjacent to the upstream OBBP. Fission product flow stains.

Case 10: Debris fretting adjacent to spacer pad on outer element 4. Secondary deuteriding resulting in a separated downstream end cap. Fission product flow stains visible.

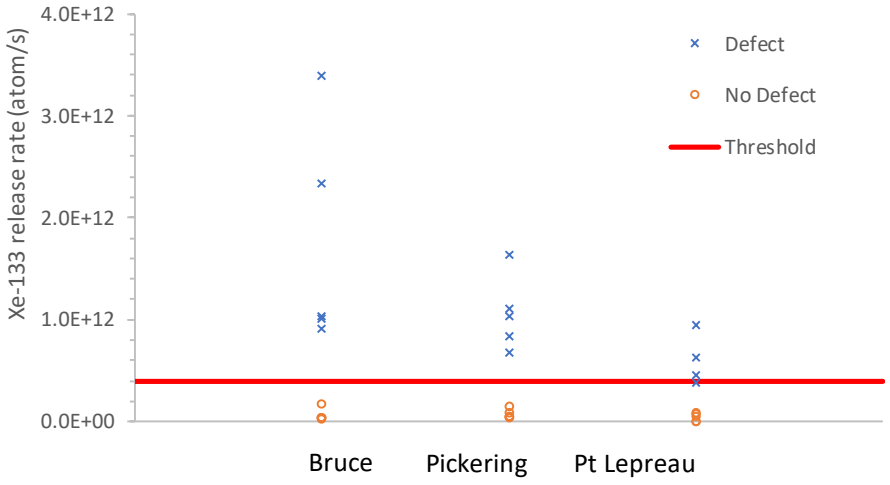

FIG. 5. Threshold plot of the normalized Xe-133 release rate data from all power stations (except Darlington Nuclear Generating Station).

AFRI analysis is hampered by the fact of having to wait for ~30 days at steady reactor operation for equilibrium to establish to determine a release rate from the equilibrium coolant activity. On the other hand, one can back out a release rate from measured (time-dependent) coolant activity data using a Savitzky-Golay (S-G) data filter [19-21]. The release rate can be evaluated assuming a quadratic fit (i.e., $n = 2$) to a 7-point data interval (where i ranges from -3 to +3) for the points y_i in the interval. The fitting coefficients are evaluated with a simple arithmetic operation for the smoothed value and its derivative, respectively:

$$b_{20} = \frac{1}{21}[-2y_{-3} + 3y_{-2} + 6y_{-1} + 7y_0 + 6y_1 + 3y_2 - 2y_3] \tag{29}$$

and

$$b_{21} = \frac{1}{28}[-3y_{-3} - 2y_{-2} - 1y_{-1} + 0y_0 + 1y_1 + 2y_2 + 3y_3] \tag{30}$$

Using a moving calculation with a standard spreadsheet analysis, one simply shifts the centre of the interval from the point i to the point i+1 to evaluate the next point with Eqs. (29) and (30). Thus, the formula is applied for the ith data point after which it is extended over the remaining data entries, where the value and derivative of the second-order polynomial are found at each subsequent point. Hence, solving for the time-dependent release rate in Eq. (8) with $B_a = 0$ for the noble gas isotopes, the release rate R (in atom s^{-1}) can be directly calculated from the coolant activity concentration data (in Bq g^{-1}) for a given PHTS mass m_c (in g) according to:

$$R = m_c \left[\frac{1}{\lambda}\frac{(b_{21})}{\Delta t} + (b_{20})\right] \tag{31}$$

A demonstration of the technique is shown in Fig. 6. Consider a time-dependent analytic solution for Xe-133 of the mass balance equation in Eq. (11), for a constant release rate $R_i = 1$ (normalized) with $B = 0$ such that $A_i(t) = \lambda_i N_i(t) = R_i\left(1 - e^{-\lambda_i t}\right)$. As shown in Fig. 6 even with random noise added to the activity curve for Ai, the S-G technique can recover the release rate Ri. Hence, this plot reveals a relatively flat Ri over the whole-time span even as the activity Ai builds in towards an equilibrium value at a much later time. This result indicates that one can perform a coolant activity analysis using an S-G analysis in order to determine Ri without having to wait ~30 days for the Xe-133 activity to reach a steady-state value where $A_i \to R_i$ as $t \to \infty$.

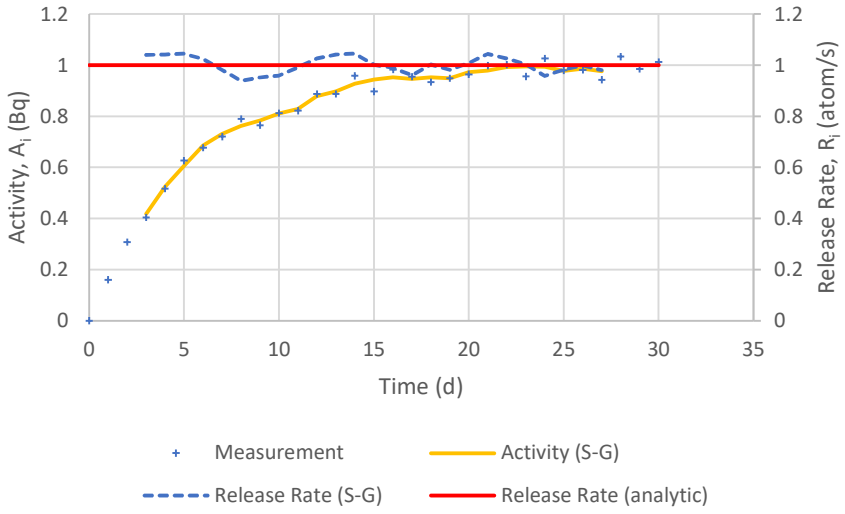

FIG. 6. S-G analysis for smoothing of the coolant activity and release rate versus time for an analytic solution with random noise added to the activity (taken from Ref. [21]).

The data must be sampled (or interpolated as required) at regular time steps (Δt). With the smoothing algorithm, one loses values for the first and last three-time entries, although one can smooth though in a piecewise fashion for sparse data as required.

4.2 FUEL DEFECT AND TRAMP URANIUM CHARACTERIZATION

The FRI model using Xe-133 can be developed further to estimate the number of defective fuel elements as well as the average linear power rating of these element(s) [22]. If the FRI analysis indicates no defect, the amount of tramp uranium, due to a previous release of fuel debris from defective fuel elements, can also be assessed accordingly [22].

4.2.1 Number of Defective Fuel Elements

Since the curve in Fig. 3(a) is for a single defective element, it can be used to estimate the number of defects once one knows the (average) linear power rating for the defective fuel element(s) by simply normalizing the measured coolant activity $A_{\text{Xe-133}}$ (in Bq) by this single-element value $R_{\text{Xe-133}}$ (in atom s^{-1}). This calculation follows from Eq. (11) with no degassing operations. For instance, the average linear heat rating *LHGR* for a given reactor of interest in Table 1 can be used to estimate the number of defects x from the steady-state activity coolant A_i (or from the S-G derived release rate R_i in Section 4.1):

$$x = \frac{(A_{Xe-1}\ \ )_{multiple\ defects}}{(R_{Xe-1}\ \ )_{single}} \tag{32}$$

4.2.2 Average Linear Power Rating of Defective Elements

For an assessment of the number of in-core defects in Section 4.2.1, one needs an estimate of the average defective element linear power rating. As mentioned, one can use the average element rating for the reactor in Table 1. However, an improved estimate can be obtained by sampling the *steady-state* coolant activities (or S-G derived release rates R) of Xe-133 after equilibrium has been reached at two different reactor power levels. The defective element linear power can be assessed by measuring the coolant activity concentration $A_{M,Xe\text{-}133}$ at two different power reactor levels P_1 and P_2 (that are relative to full power). The measured release rate R_{meas} (atom/s) ratio from Eq. (11) follows:

$$\frac{R_{meas,1}}{R_{meas,2}} = \frac{A_{M,1}}{A_{M,2}} \tag{33}$$

where the subscripts 1 and 2 refer to measurements at the relative power levels P_1 and P_2.

An exponential fitting of all data in Fig. 3(b) over the linear power range from ~5 to 60 kW·m^{-1} alternatively yields the equivalent scaling law:

$$R = a_2 \cdot e^{b_2 \cdot LHGR} \tag{34}$$

Here, the fitted coefficients based on a Marquardt-Levenberg non-linear regression analysis are: a_2 = 8.195×109 ± 4.82×108 and b_2 = 0.1291 ± 0.0041. The use of this fitting makes little difference (typically less than ~1%) from the calculated values with the correlation depicted in Fig. 3(b) over this power range. Thus, from this exponential fitting, one can back out a simple functional form for the calculation of the *LHGR*:

$$\frac{R_1}{R_2} = \frac{8.195\times10^9 e^{0.1291\cdot P_1 \cdot LHGR}}{8.195\times10^9 e^{0.1291\cdot P_2 \cdot LHGR}} = e^{0.1291\cdot(P_1-P_2)\cdot LHGR} = e^{0.1291\cdot P_1(1-\xi)\cdot LHGR} \tag{35}$$

where $\xi = P_2/P_1$ (i.e., with $P_2 < P_1$) and *LHGR* is the defective element linear heat generation rate at full reactor power. Thus, on equating the release rate ratios in Eqs. (33) and (35):

$$e^{0.1291\cdot P_1(1-\xi)\cdot LHGR} = \frac{A_{M,1}}{A_{M,2}} \Rightarrow LHGR_{est} = LHGR \cdot P_1 = \frac{q}{0.129(1-\xi)} \tag{36}$$

Here q = ln [$A_{M,1}/A_{M,2}$] and $LHGR_{est}$ is the estimated fuel element linear heat generation rate at reactor power level P_1. The evaluated linear power rating can be subsequently used in Eq. (32) to better estimate the number of failed elements with a normalization of the measured coolant activity $A_{M,Xe\text{-}133}$ with the single element release rate value.

4.2.3 Amount of Tramp Uranium

If no fuel defects are determined from a FRI analysis with either the I-131 or Xe-133, or as predicted from Eq. (32), one can estimate the amount of tramp uranium deposited on in-core reactor surfaces [3]. From Fig. 2, the recoil contribution is represented by the I-134 coolant activity measurement $(R/Y)_{I\text{-}134}$. The quantity R/Y can be evaluated from Eq. (11), which accounts for coolant purification effects using the measured I-134 coolant activity $A_{I\text{-}134}$ (in Bq). Hence, from Eq. (6):

$$\left(\frac{R}{Y}\right)_{I-134} = \tfrac{1}{2}F_t = \tfrac{1}{2}N_f\bar{\sigma}_f\langle\phi_T\rangle \qquad \bar{\sigma}_f = \frac{\sqrt{\pi}}{2}g_f(T)\left(\frac{T_o}{T}\right)^{1/2}\sigma_f(E_o) \tag{37}$$

The fission rate F_t in the tramp uranium (fission s^{-1}) depends on the number of atoms of fissionable material N_f (= $m_f N_o/A$) and the volumetrically averaged thermal neutron flux (<ϕ_T> (~ 8 × 10^{13} n cm^{-2} s^{-1}). Here m_f is the mass of fissionable material (g), N_o is Avogadro's number = 6.022×10^{23} atom mol^{-1}, and A is the atomic mass of fissionable isotope (= 235 g mol^{-1} for U-235 and 239 g mol^{-1} for Pu-239). The average thermal fission cross section is given by:

$$\bar{\sigma}_f = \frac{\sqrt{\pi}}{2}g_f(T)\left(\frac{T_o}{T}\right)^{1/2}\sigma_f(E_o) \tag{38}$$

where $g_f(T)$ is the non-1/v fission factor (=0.9374 for U-235 and 1.3316 for Pu-239) at a neutron temperature T (= 509 K e.g., for a 600 MW CANDU reactor), T_o (= 293.6 K), and $\sigma_f(E_o)$= 580 b for U-235 and 742 b for Pu-239 at an energy of E_o = 0.0253 eV). Hence, substituting these expressions into Eq. (37) and solving for the tramp uranium mass yields:

$$m_U = \frac{(R/Y)_{I-134}}{N_o\langle\phi_T\rangle\psi} \tag{39}$$

The quantity ψ reflects reactor physics considerations:

$$\psi = \frac{\sqrt{\pi}}{4}\left(\frac{T_o}{T}\right)^{1/2}\sum_{i=U^{235},Pu^{239}}\left[\frac{w}{A}g_f(T)\sigma_f(E_o)\right]_i \tag{40}$$

The specific fissile content w (in g per kg of U) is the weight fraction of fissile material of U-235 and Pu-239 that can be evaluated as a function of burnup from Ref. [8]. Equation (39) can in fact be simplified further given that the burnup of the tramp uranium is not known *a priori*. For example, for fresh fuel that is naturally enriched, w = 7.2 g/kg of U = 0.0072 g/g of U (or 0.72 weight percent enrichment of U-235 in U). At a typical

fuel burnup for a defective element of ~100 MW. h/kg U, w = 3.75 g/kg natural U for U-235 and 2.13 g/kg natural U for Pu-239. Thus, ψ is relatively insensitive to the burnup, changing by only ~4% over this burnup range. Hence, given the uncertainty in the tramp uranium burnup, Eq. (39) can be reasonably approximated using only the U-235 values:

$$\psi = \frac{\sqrt{\pi}}{4}\left(\frac{T_o}{T}\right)^{1/2}\left[\frac{w}{A} g_f(T)\sigma_f(E_o)\right]_{U^{235}} \sim 5.6 \times 10^{-27}\ mol \cdot cm^2 \cdot (gU)^{-1} \quad (41)$$

For example, consider the measured $(R/Y)_{meas}$ value of ~1×10^{12} fission s^{-1} for I-134 in Fig. 2. Using Eqs. (39) and (40) in Eq. (38), with the given parametric values, the amount of in-core tramp uranium is estimated as $m_U \sim 4$ g (i.e., 3.5 and 3.7 gU, respectively). Typically, one would estimate about one to several hundred grams of in-core uranium, depending on the number of past defect occurrences and the reactor age.

5. CONCLUSIONS

Using a calculation of the release rate from measured coolant activity data, and normalizing this quantity by the fission yield, one can distinguish between defective fuel and a tramp fuel contribution. This approach has been employed by WANO in the development of a fuel reliability indicator (FRI). This analysis specifically accounts for different mechanisms of fission product release based on a Booth diffusion model and recoil theory. In this treatment, the coolant activity concentration of I-131 provides for an assessment of defective fuel in the reactor. This quantity is corrected for tramp uranium effects using a measured coolant activity concentration of I-134.

In the WANO methodology for development of a common fuel reliability indicator for PWR's, the coolant activity is corrected for coolant purification effects and normalized to a reference purification rate constant (i.e., B_n = 2 x 10^{-5} s^{-1}). This latter correlation also depends on the average linear heat output for a given reactor unit at 100% full power, which is further adjusted by the percentage of reactor power at the time of measurement. However, because of the higher linear powers experienced in the CANDU reactor, the power scaling relation for CANDU fuel must consider intrinsic and vacancy-enhanced diffusion in the oxidized fuel. This law replaces the PWR one that implicitly assumes athermal diffusion. This correlation can be developed from operational defect experience in CANDU reactors for 28- and 37-element bundle designs. Different reference values from CANDU experience are further employed for the model normalization (B_n= 5×10^{-5} s^{-1} and L_n = 38 kW·m^{-1}). This study therefore yields an FRI for defective fuel assessment in CANDU reactors, where a threshold value of 19 Bq/g indicates the presence of fuel defect(s).

Xe-133 can also be used for an FRI analysis since this isotope avoids complications of ion-exchange purification and different loop configurations. It is also not sensitive to the defect size. The release rate of Xe-133 correlates to the linear power of the defective fuel element, which can be scaled to a common linear power rating at full reactor power for the reporting of a common FRI value. A steady-state FRI threshold value of ~4×10^{11} atom s^{-1} (or a coolant activity of 4×10^{11} Bq) indicates the presence of a defect at a reference linear power of 38 kW m^{-1}. The power scaling curve can be further employed to provide an estimate of the average linear power rating of the defective element(s) with a sampling of the Xe-133 coolant activity at two different reactor power levels. A smoothing of the concentration data using a Savitzky-Golay filter can provide a release rate value that approaches steady-state conditions much more quickly than the coolant activity concentration. A methodology is also proposed for the estimation of the number of fuel defects in-core based on a Xe-133 analysis. The amount of in-core tramp uranium can also be estimated from a measurement of the I-134 coolant activity using a recoil model.

ACKNOWLEDGEMENTS

The authors also wish to thank the following personnel for providing utility data, including: K. Vizmuller (Pickering Nuclear Generating Station), E. Middaugh (OPG) and D. Law (Point Lepreau Nuclear Generating Station). Finally, the authors would like to acknowledge recent support for the project from Dr. W. Shen from CANDU Owners Group (COG) for administrative assistance, and continual support from utility members of the Fuel Normal Operating Committee Working Group and Fuel Integrity Task Team, including: D. Law (NBPN), T. Whynot (NBPN), E. Middaugh (OPG), M. Dobrean (OPG) and M. Foster (OPG).

REFERENCES

[1] Chapter 5: Fuel Reliability, Report from the World Association of Nuclear Operators (WANO), October 2001, pages 223-239.

[2] CHIARELLI, R., WANO Performance Indicator Programme Reference Manual, WANO MN 2014-2, May 2014.

[3] LEWIS, B.J., J. Nucl. Mater. **160** (1988) 201.

[4] LEWIS, B.J., MACDONALD, R.D., IVANOFF, N.V., IGLESIAS, F.C., Nucl. Technol. **103** (1993) 220.

[5] BOOTH, A.H., A Suggested Method for Calculating the Diffusion of Radioactive Rare Gas Fission Products from UO2 Fuel Elements and a Discussion of Proposed In-Reactor Experiments that may be used to Test its Validity, AECL-700, Atomic Energy of Canada Limited (1957).

[6] HASTINGS, I.J., HUNT, C.E.L., LIPSETT, J.J., J. Nucl. Mater. **130** (1985) 407.

[7] APPELHANS A.D., TURNBULL, J.A., Measured release of radioactive xenon, krypton and iodine from UO2 during nuclear operation and a comparison with release models, in: Proc. 8th Water Reactor Safety Research Information Meeting, Gaithersburg, Maryland, Oct. 27-31, 1980.

[8] LEWIS, B.J., GREEN, R.J., CHE, W.T., Nucl. Technol. **98** (1991) 307.

[9] LEWIS, B.J., EL-JABY, A., HIGGS, J., THOMPSON, W.T., IGLESIAS, F.C., LAIDLER, R., ARMSTRONG, J., STONE, R., ODUNTON, R., J. Nucl. Mater. **366** (2007) 37.

[10] EL-JABY, A., LEWIS, B.J., THOMPSON, W.T., F. IGLESIAS, IP, M., J. Nucl. Mater. **399** (2010) 87.

[11] TURNBULL, J.A., FRISKNEY, J.R., FINDLAY, F.A., JOHNSON, F.A., WALTER, A.J., J. Nucl. Mater. **107** (1982) 168.

[12] LEWIS, B.J., J. Nucl. Mater. **148** (1987) 28.

[13] KILLEEN, J.C., TURNBULL, J.A., An experimental and theoretical treatment of the release of 85Kr from hyper-stoichiometric uranium dioxide, in: Proc. Workshop on Chemical Reactivity of Oxide Fuel and Fission Product Release, Berkeley, Gloucestershire, England, April 7-9, 1987.

[14] BEYER, C.E., Methodology Estimating Number of Failed Fuel Rods and Defect Size, Electric Power Research Institute, EPRI NP-6554, September 1989.

[15] WILK, L., CANDU Fuel Burnup and Power Rating 2012 Update, NWMO TR-2013-02, February 2013.

[16] LEWIS, B.J., PHILLIPS, C.R., NOTLEY, M.J.F., Nucl. Technol. **73** (1986) 72.

[17] LEWIS, B.J., HUNT, C.E.L., IGLESIAS, F.C., J. Nucl. Mater. **172** (1990) 197.

[18] LIVINGSTONE, S., LEWIS, B.J., IP, M., IGLESIAS, F.C., FITCHETT, A., Progress in developing an on-line fuel-failure monitoring tool for Candu reactors, 11th International Conference on CANDU Fuel, Niagara Falls, Ontario, Canada, October 17-20, 2010.

[19] HARNDEN-GILLIS, A.C., BENNETT, L.G.I., LEWIS, B.J., Experiments and Analysis of Fission Product Release in HEU-Fuelled SLOWPOKE-2 Reactors, Nuclear Instruments and Methods in Physics Research A, **345** (1994) 520-527.

[20] SAVITZKY, A., GOLAY, M.J.E., Smoothing and Differentiation of Data by Simplified Least Squares Procedures, Analytical Chemistry 36 (1964) 1627-1639.

[21] LEWIS, B.J., ONDER, E.N., PRUDIL, A., Advanced Mathematics for Engineering Students: The Essential Toolbox, Elsevier, in press

[22] LEWIS, B.J., CHAN, P.K., EL-JABY, A., IGLESIAS, F.C., FITCHETT, A., Fission product release modelling for application of fuel-failure monitoring and detection - An overview, J. Nucl. Mater. **489** (2017) 64-83.

EXPERIENCE IN DETECTION OF FUEL WASHOUT FROM LEAKING FUEL RODS DURING OPERATION OF WWER POWER UNITS

I.A. EVDOKIMOV, A.G. KHROMOV, P.M. KALINICHEV
SRC RF TRINITI,
Troitsk, Russian Federation

V.V. LIKHANSKII, A.A. KOVALISHIN, M.N. LALETIN, M.I. GUREVICH
NRC "Kurchatov Institute",
P.N. Lebedev Physical Institute,
Moscow, Russian Federation

Abstract

Fuel failures still occur during operation of nuclear power plants (NPPs). One of the possible and most severe consequences of a fuel failure is that fragments of fuel pellets or fuel grains may be washed out from the leaking fuel rod into the coolant. Reliable detection of fuel washout is important for further handling of leaking fuel assemblies. An indication of fuel washout is achievable in the frame of coolant activity evaluations during reactor operation. For this purpose, ^{134}I activity is historically utilized in WWER power units. However, observed ^{134}I activity may increase during operation even in cases when leaking fuel in the core is absent, and fuel deposits are the only source of the fission products release. The paper discusses experience in application of a recent technique for detection of fuel washout during operation of WWER power units. The proposed technique is capable of distinguishing whether the increase in activity of short-lived radionuclides is due to fission products released from the existing fuel deposits in the core or it is due to washout of fuel particles from leaking fuel.

1. INTRODUCTION

Fuel failures still occur during operation of nuclear power plants (NPPs). A failure may lead to increased primary coolant activity, higher dose rates for personnel, increase in the amount of liquid radioactive waste being generated, and the need for additional operations to search for and replace leaking fuel assemblies. These negative factors may entail significant financial losses.

One of the possible and most severe consequences of a fuel failure is that fragments of fuel pellets or fuel grains may be washed out from the leaking fuel rod into the coolant. Radiological consequences of fuel washout may persist for a long period of time up to 10 years – in the form of high background activity for on-power units [1]. Reliable detection of fuel washout is important for handling of leaking fuel assemblies after discharge.

Detection of fuel washout is possible in the course of evaluation of primary coolant activity during reactor operation, [6-10]. The amount of fuel deposits on surfaces of the in-core structures is evaluated using activities of the most short-lived radionuclides that can be detected in the primary coolant [11]. In WWER power units, activity of ^{134}I (decay constant $2.2\cdot10^{-4}$ s^{-1}) is traditionally used for this purpose [10]. In PWRs, ^{89}Rb (decay constant $7.5\cdot10^{-4}$ s^{-1}) may be used in addition to ^{134}I [1].

However, coolant activity (including activity of the short-lived radionuclides) may gradually increase during operation even if there are no fuel failures and fuel deposits are the only source of the fission products release. This gradual activity increase is attributed to the following. Nuclide inventory in fuel evolves during irradiation. In fuel deposits, plutonium builds up faster and up to higher concentrations compared to its average concentration in fuel pellets. This behavior is due to lower self-shielding effect for the ^{238}U neutron capture cross section in fuel deposits on the outer cladding surface (the self-shielding effect in fuel pellets is discussed, for instance, in [12]). Intensive plutonium buildup leads to increase in the fission rate in fuel deposits (if the heat generation rate in the fuel assembly (FA) is kept constant). This may lead to gradual increase in the rate of fission product release from fuel deposits into primary coolant during reactor operation. Recently, a criterion was proposed to distinguish between cases when the increase in activity of short-lived radionuclides is due to fission products release from the existing fuel deposits in the core or it is due to washout of fuel particles from leaking fuel [17].

The paper briefly outlines the method [17] for detection of fuel washout during operation of WWER power units. The focus is made on experience of practical applications.

2. OUTLINES OF THE TECHNIQUE

It is possible to calculate the maximum potential increment of the background activity during the fuel cycle for any pattern of fuel loading into the core if the amount of fuel deposits is thought to remain unchanged. Then in practice, if a fuel failure occurs and the increase in ^{134}I activity observed during reactor operation exceeds the threshold value, it may be concluded that there is a source of fuel particles in the core. The criterion of fuel washout from a leaking fuel rod is described below on this basis.

According to [17], activity due to fission products release from fuel deposits can be evaluated as

$$A \propto LPf(Bu) \tag{3}$$

where *LP* is the linear heat rate of a fuel rod with fuel deposits on the outer cladding surface. The function *f* describes relative activity increase with burnup in a fuel rod of given enrichment, provided by fission product release from fuel deposits on the cladding.

Examples for the *f* function calculated with the SVL code[5] for two different fuel enrichments are shown in Fig. 1.

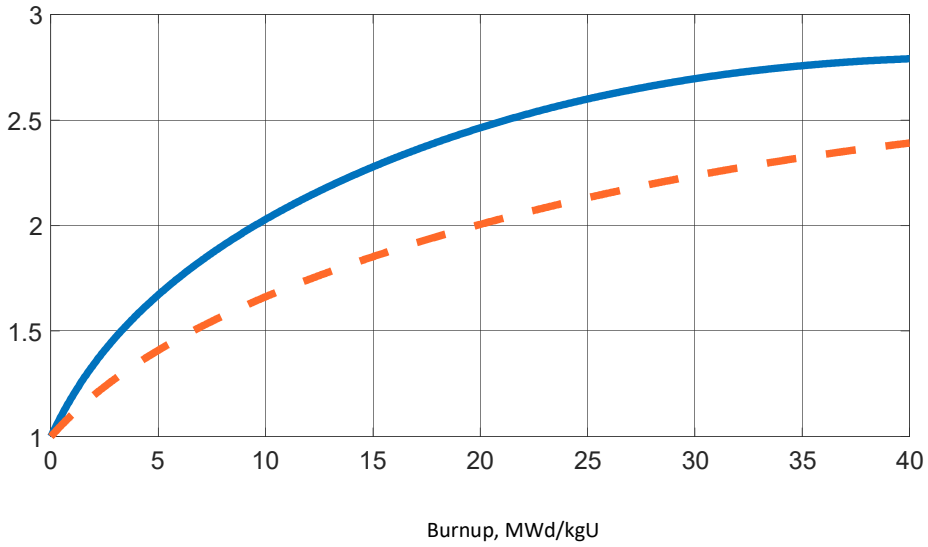

FIG. 1. Relative increase in ^{134}I activity as a function of burnup for fuel enrichment of 2.4% (——) and 4% (— —).

In general, fuel deposits in the core will likely reside on fuel rods with different burnups. Taking into account the contribution of every i^{th} rod, according to Eq. (3), evolution of activity during the fuel cycle can be described as

$$A(t) \propto \sum_i m_i K q_i(t) f_i(Bu_i(t_0) + \Delta Bu_i(t)) \tag{4}$$

Here m_i is the 'effective' mass of fuel deposits on the ith rod (the mass of fuel deposits in the form of a 'monolayer' that is capable of providing the same release rate for ^{134}I), $Kq_i(t)$ is the relative heat generation rate, Bui(t0) is the fuel burnup at time t_0, and $\Delta Bu_i(t)$ is the increment of fuel burnup in the time interval $[t_0, t,]$.

For a fixed amount of fuel deposits, Eq. (4) can be expressed in the form

$$A(t) \leq A(t_0) k\varphi \tag{5}$$

[5] It should be noted that plutonium buildup in fuel pellets depends on the neutron spectrum. The spectrum is affected, in particular, by the evolution of boric acid concentration, temperature and density of primary coolant. Effect from variation of these parameters was studied using the licensed neutronic code SVL (the multigroup code for WWER fuel cells and FAs). Calculations showed that variations of the mentioned parameters do not noticeably affect the form of the f function. Therefore, it can be assumed that for a given fuel type with a specified enrichment, the function f depends only on fuel burnup Bu.

The multiplication factor $k\varphi$ describes the maximal relative activity increase in the interval $[t_0, t]$ with

$$\varphi = max\left(\frac{fi_{0_{ii}}}{f_i(Bu_i(t_0))}\right) \quad (6)$$

$$k = max\left(\frac{Kq_i(t)}{Kq_i(t_0)}\right) \quad (7)$$

Inequality (5) should be valid in all time intervals $[t_0, t]$ without fuel washout.

Analysis of WWER fuel cycles shows that coolant activity associated with fission products release from fuel deposits under steady-state operation conditions may be reasonably fitted by the linear approximation:

$$A(t) \approx \alpha(t - t_0) + A(t_0) \quad (8)$$

Here α is the linear approximation coefficient that represents the rate of activity increase.

Assume that activity increase follows approximately a linear trend according to Eq. (8) at time interval $t_0 \le t \le t_1$. Then it can be derived from Eqs. (5) and (8) that:

$$\alpha \le \alpha_{cr} = \frac{(k\varphi - 1)A(t_0)}{(t_1 - t_0)} \quad (9)$$

Thus, the linear trend for measured activity should be compared with the obtained threshold value. Inequality (9) should be valid in all cases when coolant activity is governed by fission product release from the unchanged amount of fuel deposits in the core. If there is a fuel failure and inequality (9) is violated it may be concluded that fuel is washed out from the leaking fuel rod.

The value of φ can be obtained from the neutronic calculations for the fuel cycle under consideration. The common practice for Russian WWERs is that fuel loading pattern is not noticeably varied from cycle to cycle. In such cases, the value of φ may be determined on the basis of typical fuel irradiation histories. If so, there is no need to calculate it for every fuel cycle.

In practice a simplified version of the criterion may be also used with a conservative upper estimate for the rate of ^{134}I activity increase. The conservative estimate is achieved if the value of $Bu(t_0)$ in Eq. (6) is taken to be equal to zero for every fuel rod as if it was fresh. For example, taking average $\Delta Bu \sim 15$ MWd/kgU per year of irradiation, the value of φ may be estimated from Fig. 1 as ~ 1.8 for enrichment of 4%. The typical value for k may be taken as 1.2.

The above criterion of fuel washout should be applied in practice in the following way:

— Time intervals of steady-state reactor operation are selected within the fuel cycle.
— The data on ^{134}I activity are fitted by the linear trend according to Eq. (8) in these time intervals. The coefficient α is determined by the least squares method.
— The obtained value of α (the rate of activity increase) is then compared to the threshold value of α_{cr} given by the right hand member of inequality (9). If $\alpha / \alpha_{cr} > 1$, it is concluded that fuel washout has occurred.

3. EXAMPLES OF APPLICATION FOR WWER-1000 POWER UNITS

This technique was applied as part of coolant activity evaluations for different WWER-1000 power units. Some examples are listed below (the coolant clean-up rate for all the cases below was close to the nominal value ~ $3 \cdot 10^{-5}$ s^{-1}).

3.1 Example 1. Cycle B2 without fuel failures

An example of iodine activity in primary coolant with no leaking fuel in the core is shown in Fig. 2 (cycle B2).

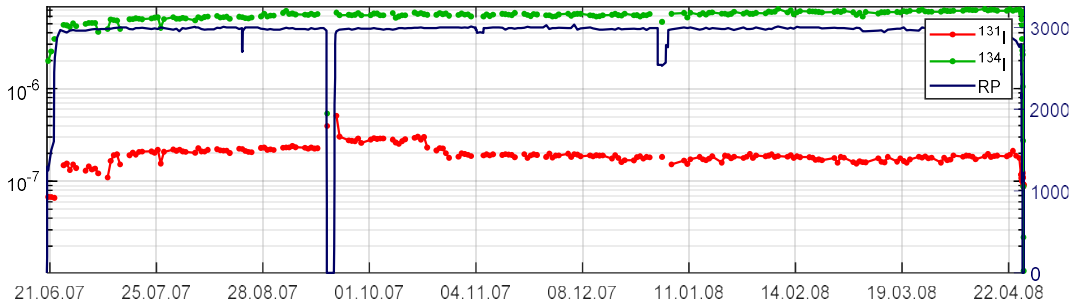

FIG. 2. Activity of ^{131}I and ^{134}I (Ci/kg, the left vertical axis) and reactor thermal power RP (MW, the right vertical axis) during cycle B2.

Fig. 3 illustrates analysis of 134I activity. The red line in Fig. 3 corresponds to the threshold rate of activity increase (α_{cr}) for this particular cycle. According to Fig. 3, 134I activity grew gradually during the cycle despite the absence of leaking fuel. However, the rate of 134I activity increase was below the threshold. This is as it should be with no source of fuel particles in the core from leaking fuel rods.

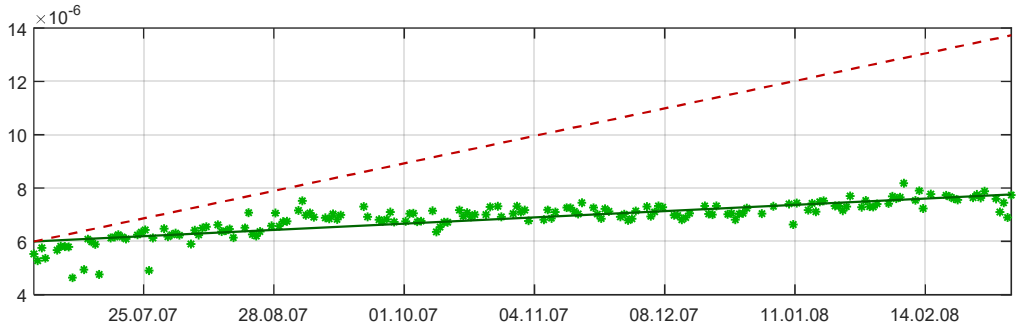

FIG. 3. Increase in ^{134}I activity during cycle B2. The red dotted line corresponds to the threshold activity increase rate α_{cr}.

3.2 Example 2. Cycle A5 without fuel failures

Figs 4-5 show the data for cycle A5. There were no fuel failures in the core. Despite this fact, there was about a two-fold increase of ^{134}I activity during this cycle. This growth is attributed to evolution of nuclide inventory in fuel deposits as mentioned above. However, the rate of ^{134}I activity increase was below the threshold.

Cycles B2 and A5 provide examples and confidence that the proposed criterion does not give a false alarm of fuel washout. Application of this criterion to all available failure-free cycles provided the same result.

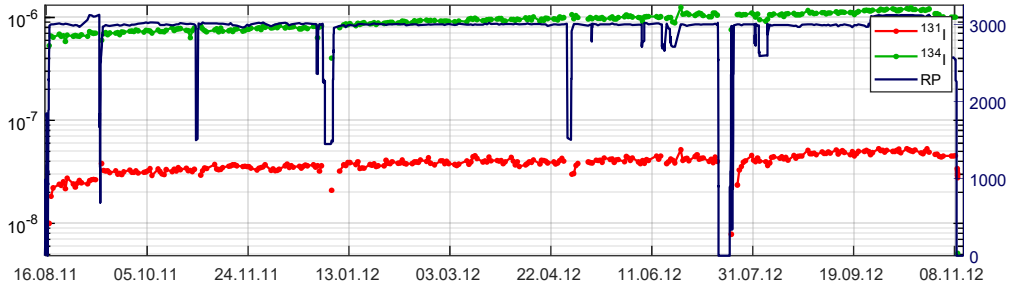

FIG. 4. Activity of ^{131}I and ^{134}I (Ci/kg, the left vertical axis) and reactor thermal power RP (MW, the right vertical axis) during cycle A5.

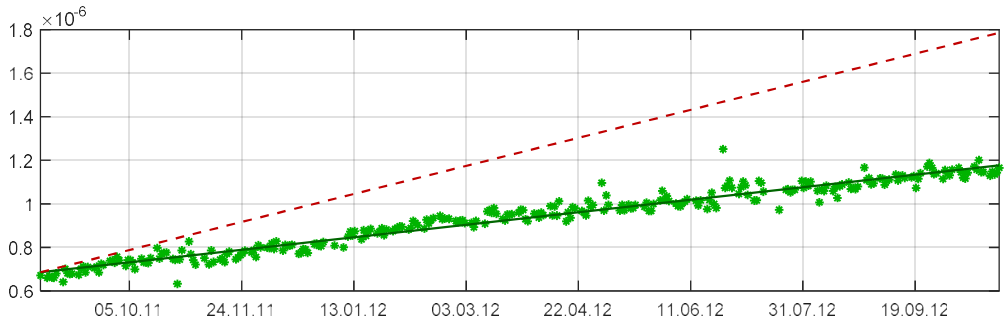

FIG. 5. Increase in ^{134}I activity during cycle A5. The red dotted line corresponds to the threshold activity increase rate.

3.3 Example 3. Cycle C2

Figs 6-7 show iodine activity for cycle C2. Occurrence of a fuel failure is evident by sharp increase in ^{131}I activity in August 2013. According to Fig. 7, ^{134}I activity demonstrated a considerable growth after the failure. It was much above the threshold rate. Based on the proposed technique, results indicate that fuel washout occurred during this cycle.

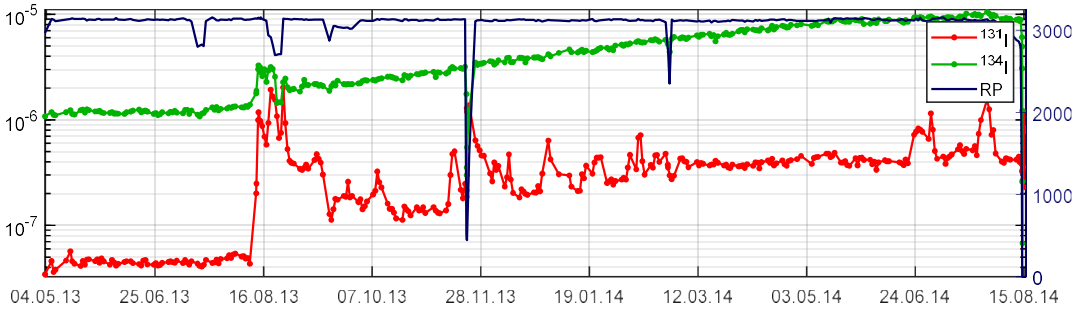

FIG. 6. Activity of ^{131}I and ^{134}I (Ci/kg, the left vertical axis) and reactor thermal power RP (MW, the right vertical axis) during cycle C2.

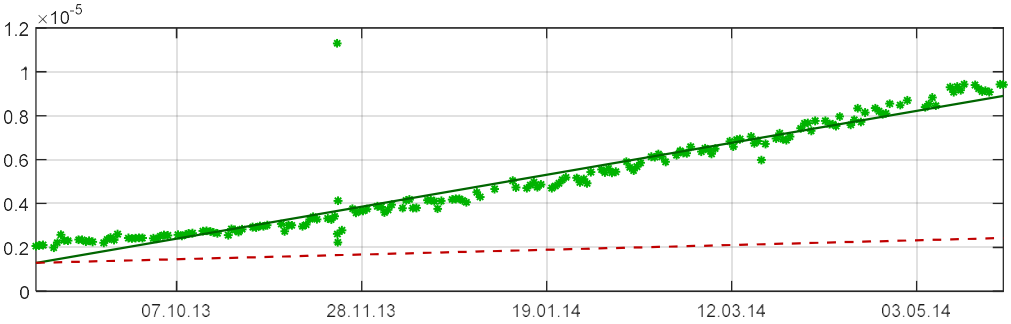

FIG. 7. Increase in 134I activity during cycle C2. The red dotted line corresponds to the threshold activity increase rate.

One failed fuel assembly was identified after reactor shutdown. This fuel assembly was examined in hot cells of RIAR (Dimitrovgrad). Examinations revealed one leaking U-Gd fuel rod with a coarse open defect in the cladding. Fuel pellet fragments near the defect were extensively oxidized over the grain boundaries. Cracking along grain boundaries was observed. A substantial fragment of the fuel pellet was also missing thus giving confirmatory evidence of fuel washout.

3.4 Example 4. Cycle B3

Another case of confirmed fuel washout is shown in Figs 8-9 for cycle B3. Spiking in ^{131}I activity indicated a fuel failure at the beginning of the cycle. The rate of ^{134}I activity increase was above the threshold (Fig. 9). Therefore, fuel washout was predicted by the proposed technique.

Several leaking FAs were subsequently identified during the reactor outage. They were visually inspected at the NPP. For one of these fuel assemblies, observations revealed a missing cladding fragment for one of the peripheral fuel rods. The breach in cladding was quite severe. This fuel assembly was examined in RIAR hot cells later. Non-destructive examinations were only performed. When extracted from the fuel assembly, the leaking fuel rod broke at the level of the visible defect. Further inspection showed that it was a secondary defect in cladding. Near it, fuel pellets were substantially eroded. Besides this fact, there was an additional evidence of fuel washout. The next fuel cycle on this power unit was failure free. But initial activity of ^{134}I was high. It exceeded ^{134}I activity at the beginning of cycle B3 by a factor of ~ 2.5. Consequently, the amount of fuel deposits in the core after cycle B3 became noticeably bigger.

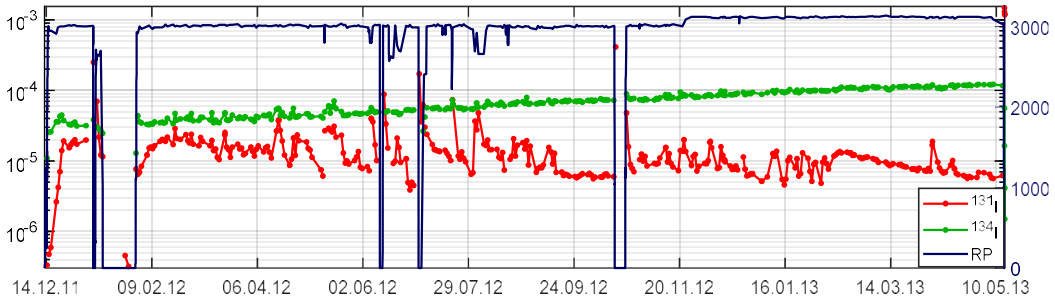

FIG. 8. Activity of ^{131}I and ^{134}I (Ci/kg, the left vertical axis) and reactor thermal power RP (MW, the right vertical axis) during cycle B3.

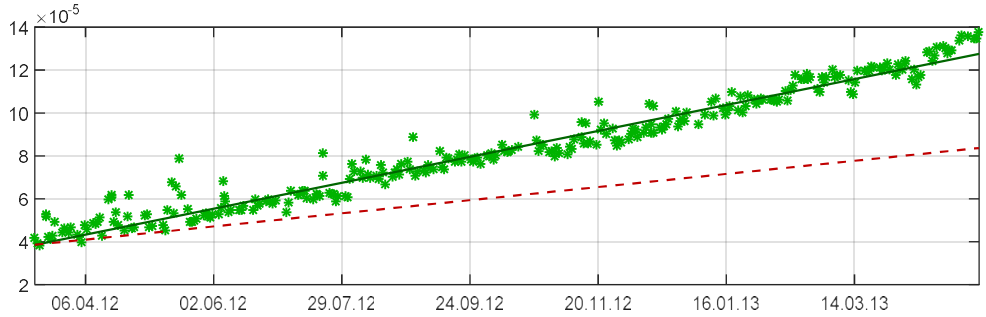

FIG. 9. Increase in ^{134}I activity during cycle B3. The red dotted line corresponds to the threshold activity increase rate.

3.5 Example 5. Cycle D2

Figs 10-11 show the data for cycle D2. Fuel failure occurred at the beginning of the cycle. A prominent increase in ^{134}I activity (Fig. 11) was a basis to predict fuel washout.

One failed fuel assembly was identified after the reactor shutdown. Visual inspection at the NPP supposed deviation from normal geometry for one of the fuel rods. It was a fuel rod in the second row from the FA periphery and its observation was limited. Post-irradiation examinations in hot cells were not performed for this leaking fuel assembly. However, the next fuel cycle at this power unit was failure-free but the initial ^{134}I activity was about 20 times higher than that at the beginning of cycle D2. Consequently, the amount of fuel deposits in the core after cycle D2 became significantly larger. It gives an indirect confirmation for the predicted fuel washout.

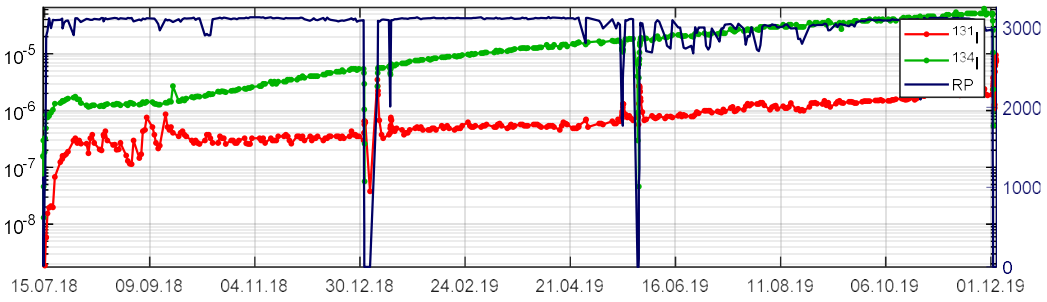

FIG. 10. Activity of ^{131}I and ^{134}I (Ci/kg, the left vertical axis) and reactor thermal power RP (MW, the right vertical axis) during cycle D2.

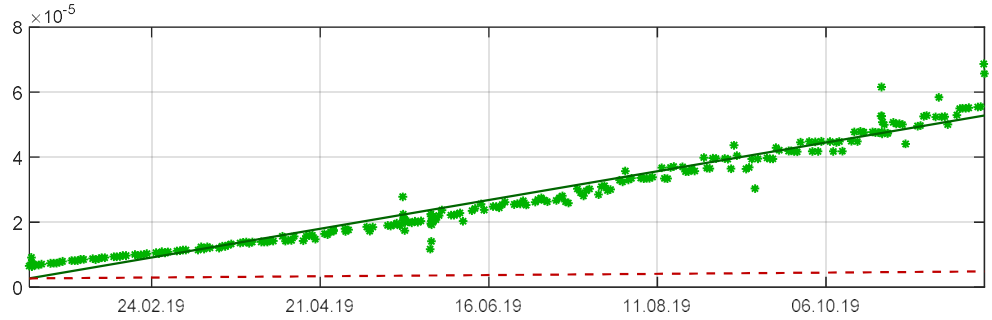

FIG. 11. Increase in 134I activity during cycle D2. The red dotted line corresponds to the threshold rate of activity increase.

3.6 Summary of available experience

Fig. 12 shows a summary of fuel washout predictions for several fuel cycles at WWER-1000 power units. Fuel cycles both with and without fuel failures were considered. The actual rates of ^{134}I activity increase α were compared to the threshold value α_{cr}. The ratio of α to α_{cr} is shown in Fig. 12.

It can be seen in Fig. 12 that inequality $\alpha/\alpha_{cr} < 1$ holds true for all fuel cycles with no fuel failures. This is how it should be with the unchanged amount of fuel deposits.

The ratio of α to α_{cr} did not exceed 1 also for several fuel cycles with leaking fuel in the core. This fact is consistent with an idea that not every fuel failure is followed by fuel washout into primary coolant. In general, this idea is supported by a big set of post-irradiation examinations of leaking fuel. As for Fig. 12, there is some additional information for cycle D1. One leaking fuel assembly was found after this cycle. The leaking FA was examined in hot cells. Examinations confirmed definitively that there was no fuel washout from the leaking fuel rod, as expected from predictions. Leaking fuel after other cycles in Fig. 12 with $\alpha/\alpha_{cr} < 1$ was not examined in hot cells.

Fuel washout was predicted by the proposed technique for several fuel cycles with fuel failures. These fuel cycles are represented by the square markers in Fig. 12. The data points for three of these cycles are enclosed in a circle. In these three cases the occurrence of fuel washout was later confirmed experimentally (see Sections 3.3 – 3.5).

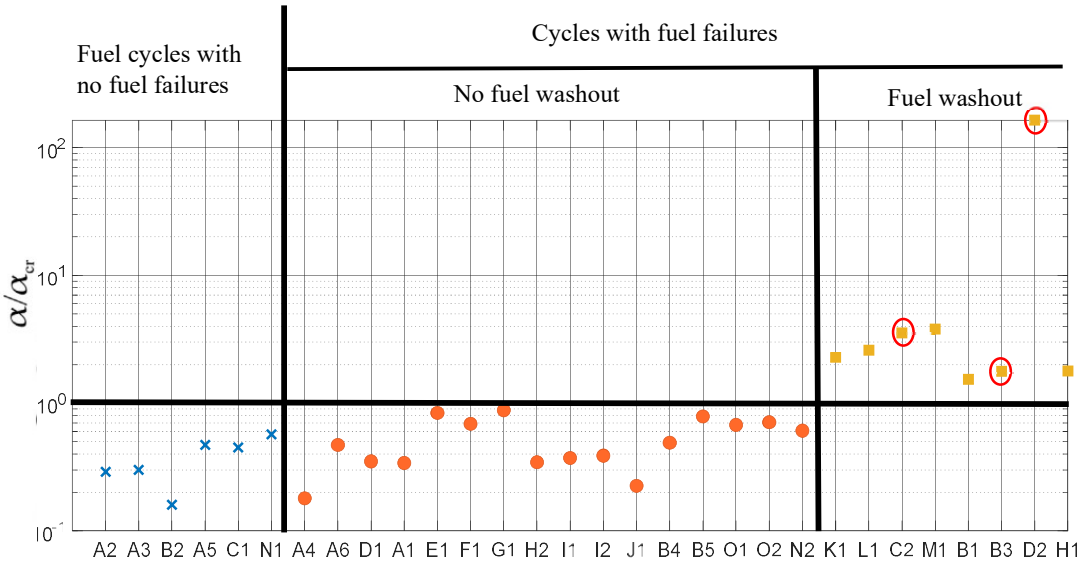

FIG. 12. Applications to WWER-1000 fuel cycles: comparison between the actual rate of gradual increase in 134I activity α and the threshold value α_{cr}.

4. SOME LIMITATIONS

The above criterion assumes that the activity of relatively short-lived ^{134}I is governed by the amount of fuel deposits in the core. However, in some cases leaking fuel may contribute noticeably to the total ^{134}I activity. It is possible, e.g., in case of a secondary failure in the uprated fuel rod.

Observations show that in most cases in WWERs the rise of ^{134}I activity above the background level is rather limited in time. The reason is that fuel pellets in the uprated leakers are subjected to extensive oxidation and subsequent swelling. This leads to collapse of the pellet-to-cladding gap and decrease of the rate of mass transfer between the leaking fuel rod and primary coolant. The major effect is produced for the short-lived radionuclides. Their activity may return to the background level in a relatively short period of time. Better results with the above criterion may be achieved if the time intervals with the temporary elevated ^{134}I activity are excluded from the analysis. It is better also to perform analysis for longer periods of time (a month or more). It may help to derive a consistent trend in gradual increase of ^{134}I activity.

Activity of the more short-lived ^{89}Rb may be used for more reliable detection of fuel washout as it was proposed in [1]. The present research included calculations of *f* functions for ^{89}Rb as well (like that in Fig. 1). These results were tested against the data of Kalinin NPP. It was shown that in most cases, similar analysis using ^{89}Rb activity confirmed conclusions drawn from ^{134}I activity. However, monitoring of ^{89}Rb activity is currently not mandatory according to the WWER operating regulations. Typically, data on ^{89}Rb activity is not available for most of the WWER fuel cycles and ^{134}I appears to be the only available indicator for detecting fuel washout.

On the other hand, the above criterion may be interpreted more generally as an indicator of severe degradation of fuel cladding in the leaking fuel rod. Assume, we have a time interval with elevated ^{134}I activity due to its release from the leaking fuel rod. Then, even in these infrequent cases, the proposed criterion will achieve its objective. In this formulation it still provides opportunities for making decisions about further handling of leaking fuel assemblies.

It is worth noting that nuclear operators in different countries apply various methods for assessment of cladding degradation in leaking fuel. For instance, activity ratios of ^{131}I/^{133}I [18] and ^{131}I/^{134}I [12] are used for this purpose. These ratios are high for small defects in cladding and lower for coarse defects. Criteria presented in [12] and [18] remain reasonable, if the main contribution to activity of these radionuclides is due to release from leaking fuel rods. Meanwhile, it was repeatedly observed that activity of relatively short-lived radionuclides was governed by fuel deposits, but the activity of the longer-lived ^{131}I was not. As a result, the activity ratios ^{131}I/^{133}I and ^{131}I/^{134}I took low values corresponding to a large defect in cladding. At the same time, the observed low values of absolute activity clearly indicated a low degree of fuel degradation.

The present technique (if it is considered as an indicator of severity of cladding failure) has no such limitations. In any case, it may be anticipated that the more diversified the methods are that are applied for coolant activity evaluation, the better results the NPP will have.

5. CONCLUSION

The paper briefly describes a method for detection of fuel washout by ^{134}I activity during operation of WWER power units. The experience in application of this technique to several cycles at different NPPs is considered.

It has been shown that the rate of ^{134}I activity increase was always below the threshold value for fuel cycles with no fuel failures. On the contrary, the threshold value was exceeded for fuel cycles which had confirmed fuel washout during reactor operation.

Reliable detection of fuel washout allows for input into decisions on handling of leaking fuel after discharge. For example, fuel washout may impose some constraints on conditions of interim storage of fuel assemblies in spent fuel pool at a NPP. In case of fuel washout, leaking fuel assembly should be stored in a sealed cask in the spent fuel pool. Supplementary constraints for transportation of these fuel assemblies from the NPP for reprocessing or long-term storage may be applicable.

Some nuclear operators apply the repair and reconstitution techniques at NPPs. In the repair process a leaking fuel rod in a fuel assembly is replaced by a dummy rod. Currently, this technique is under development for WWER-1000/1200 power units in Russia. Understanding the magnitude of fuel washout provides insight into the severity of potential cladding degradation. This can help inform the NPP as to the risk of damaging or destroying portions of the leaking fuel rod when it is extracted from the fuel assembly. Evaluation of fuel washout during reactor operation may therefore be used to assess the repair feasibility of a leaking FA.

REFERENCES

[1] INGEMANSSON, T., RUDLING, P., LUNDGREN, K., Assessment of Fuel Washout in LWRs – New Methodologies, Proc. Int. Meet. on LWR Fuel Performance, Orlando, Florida, September 19-22, 2004, paper 1002.

[2] RD NO[6] 1.1.2.10.0521-2009. Standard Procedure for Monitoring the Cladding Integrity of Fuel Elements. FAs of the VVER-1000 Reactors, Rev. 2. Rosenergoatom, Moscow, Russia (2016).

[3] SHESTAKOV, YU., M., SEMENOVYKH, A., S., Problems and perspectives of moving toward zero fuel failures and mitigation of fuel failure consequences at NPPs with WWER reactors in Russia, 11th Int. conf. «WWER fuel performance, modelling and experimental support» Bulgaria, Varna, September 26-October 03, 2015.

[4] POVAROV, V. P., TERESHCHENKO, A. B., KRAVCHENKO, YU. N., POZYCHANYUK, I. V., GOROBTSOV, L. I., GOLUBEV, V. I., BYKOV, V. I., LIKHANSKII, V. V., EVDOKIMOV, I. A., ZBOROVSKII, V. G., SOROKIN, A. A., Development and application of state-of-the-art techniques for fuel integrity monitoring and fuel assessment at Novovoronezh NP, Teploenergetika **2** (2014) 54–64 (in Russian).

[5] INTERNATIONAL ATOMIC ENERGY AGENCY, Review of Fuel Failures in Water Cooled Reactors, Nuclear Energy Series No. NF-T-2.1, IAEA, Vienna (2010).

[6] PARRAT, D., GENIN, G., B., MUSANTE, Y, PETIT, C, HARRER, Failed rod diagnosis and primary circuit contamination level determination, thanks to the DIADEME code, IAEA-TECDOC-CD-1345, 2003, pp. 265–276.

[7] EL-JABY, A., LEWIS, B. J., et al. A General Model for Predicting Coolant Activity Behaviour for Fuel-failure Monitoring Analysis. J. Nucl. Mater. **399** (2010) 87-100.

[8] LIKHANSKII, V. V., EVDOKIMOV, I. A., *et al.* Modelling of Fission Product Release from Defective Fuel under WWER Operation Conditions and in Leakage Tests During Refuelling, Proc. Int. Top. Mtg LWR Fuel Performance, Florida, 2004, pp. 798-812.

[9] OLIVER, L., SVENSSON, P., et al. Fission product analysis using the FPA code, Proc. Int. Westhinghouse Electric Sweden AB, 2017, pp. 2-3.

[10] SLAVYAGIN, P., LUSANOVA, L., MIGLO V., Fuel failure diagnostics in normal operation of nuclear power plants with WWER-type reactors, IAEA-TECDOC-CD-1345, 2003, pp. 303-315.

[6] Regulatory Document of Nuclear Operator.

[11] LEWIS, B. J., CHAN, P. K., EL-JABY, A., IGLESIAS, F. C., FITCHETT, A., Fission product release modelling for application of fuel-failure monitoring and detection – An overview, J. Nucl. Mater. **489** (2017) 64-83.
[12] GALANIN, A., D., Introduction Into the Theory of Thermal Neutron Nuclear Reactor. Rev.2, Energoatomizdat, Moscow, Russia 1989, pp. 209-217.
[13] SLAVYAGIN, P., LUSANOVA, L., MIGLO, V., Regulation of the fission product activity in the primary coolant and assessment of defective fuel rod characteristics in steady state WWER-type reactor operation, IAEA-TECDOC-CD-1345, 2003, pp. 326-337.
[14] KALINICHEV, P. M., EVDOKIMOV, I. A., LIKHANSKII, V. V., A technique for detection of a fuel failure relying on activity of Xe radionuclides during operation of WWER power units, Izvestiya Vuzov, Yadernaya Energetika **2** (2018) 110-113.
[15] NIKITIN, O. N., Microstructural changes and xenon distribution in UO_2 at high fuel burnup in WWER operational conditions. Doctoral thesis, JSC SRC RIAR, Dimitrovgrad, 2010.
[16] KRYUKOV, F. N., Electron Probe Microanalysis of nuclear fuel composition and fuel rod claddings, Doctoral thesis, JSC SRC RIAR, Dimitrovgrad, 2010.
[17] EVDOKIMOV, I. A., KHROMOV, A. G., KALINICHEV, P. M., LIKHANSKII, V. V., KOVALISHIN, A. A., LALETIN, M. N., GUREVICH, M. I., ZBOROVSKII, V. G., Detection of fuel washout from leaking fuel rods during operation of WWER power units, J. Nucl. Mater. **538** (2020) 152205.
[18] LIN, C., Radiochemistry in Nuclear Power Reactors, Nuclear Science Series, National Academy Press Washington, D.C, 1996, pp. 3-21.

IMPACT OF PLANT OPERATION ON FAILURES/DEGRADATION AND POSSIBLE MITIGATION ACTIONS BY PLANT OPERATION

(Session 3)

Chairperson

I. ARIMESCU
USA

FUEL FAILURE IN NORMAL OPERATION OF ANGRA 2 BRAZILIAN NUCLEAR POWER PLANT

LAPA, NELBIA
National Nuclear Energy Comission,
Rio de Janeiro, Brazil

MADEIRA, ALZIRA
National Nuclear Energy Comission,
Rio de Janeiro, Brazil

NERY, RENATA W. R.
Eletronuclear,
Rio de Janeiro, Brazil

Abstract

Angra 2 is a PWR German design plant, operating in Rio de Janeiro since 31 January 2001, with a net capacity of 1,350 Mw(e). At the beginning of the 16th operational cycle, during the chemical sampling of the Reactor Cooling System (RCS), an increase in the concentration of Iodine (I-131) and Xenon (Xe-133) was observed, indicating a Fuel Assembly (FA) failure. All chemical control and diagnosis parameters of the primary system have always been within specifications, and during the cycle there were no shutdowns at the unit. Due to the indication of FA failure, a sipping test and visual inspections were performed to verify the integrity of the FAs discharged during the core-unloading task. The sipping test showed that only one fuel assembly indicated failure. Visual analysis showed that small shiny particles were released during the FAs removal from the reactor core to the refill machine. While unloading, these particle releases increased. Visual inspection of all FAs discharged into the spent fuel pool demonstrated that the particles came from the cladding. A chemical analysis of these particles showed that the main chemical elements were zirconium (Zr) and niobium (Nb), as the same from the cladding alloy. Visual inspections performed showed that all 52 FAs of R series (first cycle in core) had presented enhanced corrosion with some flaking in the uppermost span between the 8th and 9th spacer grids, located at the top of the FA, at the transition of the end of the active column to the upper plenum. This corrosion event is not related to the failed fuel observed. The root cause is under analysis and the possible hypotheses for this corrosion event are cladding material composition and structure, the manufacturing process, the thermal hydraulic operating conditions as the linear heating rate, water flow, and the primary water chemistry composition. Angra 2 operated 16th Cycle with operating parameters within the specifications, as in all previous cycles.

1. INTRODUCTION

The Pressurized Water Reactor (PWR) is the most widely commercialized nuclear power plant type. The defense-in-depth approach used in its design ensures that any release of hazardous amounts of radioactive materials to the environment will be extremely unlikely. This approach uses barriers to prevent the release of fission products from the reactor core to the environment and one of them is the fuel cladding. The reliability of nuclear fuel is grounded in a strong nuclear safety culture and the fuel cladding is the key safety barrier for fission products release. The cladding is exposed to very specific and demanding conditions, and, sometimes, a failure may occur. Several mechanisms are known to adversely affect the fuel cladding integrity and may subsequently cause fuel rod failure.

The paper presents a fuel cladding damage event that occurred during the 16th Cycle of the Angra 2 Brazilian Nuclear Power Plant (NPP) and a summary of the ongoing evaluations to determine the potential root cause.

2. AN OVERVIEW OF FUEL REPORTABLE EVENTS

2.1 German operational experience

Angra 2 is a PWR German design, having the Pre Konvoi PWR as reference plant. The major purpose of this section is to provide a short overview of German PWRs recent fuel failures, so that any failure can be compared to the Brazilian PWR plant.

This review is based in the Reactor Safety Commission (RSK) recommendation [1] presented in the 514th meeting on 12 February 2020, on the subject "increased oxide layer thicknesses in the upper part of FAs with M5 cladding tubes". It also briefly shows the fuel event introduced during the 8th Meeting of the KWU Regulators Group by Mildenberger [2].

In February 2017, during the core unloading of the German NPP Brokdorf, many white particles was observed on the FAs and other structures. Visual inspection showed a white oxide layer on fuel rods at the upper area of the fuel assembly (FA) due to an enhanced corrosion process. This process happened in the area that includes the end of the active fuel length and the gas plenum inside the fuel rod, between the 8th and 9th spacer grids. This fuel rod cladding material is the M5, an AREVA/Framatome zirconium alloy.

Although oxide layers greater than 100 μm circumferentially average and 130 μm locally were measured, i.e., greater than the general core specification, no cladding defect has been detected. In other words, no fuel rod leak was observed due to this event.

Since 2005, oxide thicknesses greater than 70 μm, in the upper area of M5 fuel rodqs, were already known in German NPP plants, as shown in Table 1. Many investigations have been carried out, but a precise root cause has not been determined. The RSK recommended to extend the visual inspection to all M5 FAs planned to be reloaded in all plants.

TABLE 1. GERMAN OPERATIONAL EXPERIENCE

NPP	Year
Pre-Konvoi PWR Philippsburg	2005
Pre-Konvoi PWR Philippsburg	2012
Pre-Konvoi PWR Brokdorf	2012
Pre-Konvoi PWR Grohnde	2012
Konvoi PWR Isar 2	2012
Pre-Konvoi PWR Brokdorf	2013
Pre-Konvoi PWR Grohnde	2013
Pre-Konvoi PWR Brokdorf	2017
Pre-Konvoi PWR Philippsburg	2019

2.2 Angra 2 operational experience

Angra 2 NPP has been operated since early 2002 near Angra dos Reis city, in Rio de Janeiro, Brazil. It operates with a gross electric capacity of 1,350MW and a thermal capacity of 3,764MW. Table 2 presents a summary of Angra 2 fuel performance with indications of fuel failure.

TABLE 2. ANGRA 2 FA FAILURE OPERATIONAL EXPERIENCE

		Root Cause			
Year	Cycle	Debris	Unknown	Total	Comment
2002	1	1	0	1	106 (repaired)
2003	2	1	0	1	144 (repaired)
2004	3	0	0	0	
2005	4	1	0	1	C033 (repaired)
2007	5	0	0	0	
2008	6	0	0	0	
2009	7	0	0	0	
2010	8	0	0	0	
2012	9	0	0	0	
2013	10	0	0	0	
2014	11	0	1	1	H036
2015	12	0	0	0	
2016	13	0	0	0	
2018	14	0	0	0	
2019	15	0	0	0	
2020	16	0	1	1	R013
Total		**3**	**2**	**5**	

3. 16th CYCLE OF ANGRA 2 NPP EVENTS REPORTED

3.1 Angra 2 fuel damage

On May 21, 2019, at the beginning of the 16th Cycle of Angra 2, a drastic increase in the concentration of I-131 and Xe-133 was detected in the primary system, indicating a fuel failure event, Fig. 1. The gradual reduction in the I-131 activity levels in combination with elevated, however constant Xe-133 concentration, indicated a first cycle failure that occurred early in the cycle. In addition, the large increase in Xe-133 and I-131 activity, by 1000-10000 times, was an indication of a high-power rod failure. The Xe-133 concentration remained constant throughout the cycle, increasing again during the plant coastdown.

It is noteworthy that although the activities of Xe-133 and I-131 have increased, the concentrations of these isotopes remained well below the Technical Specifications limits.

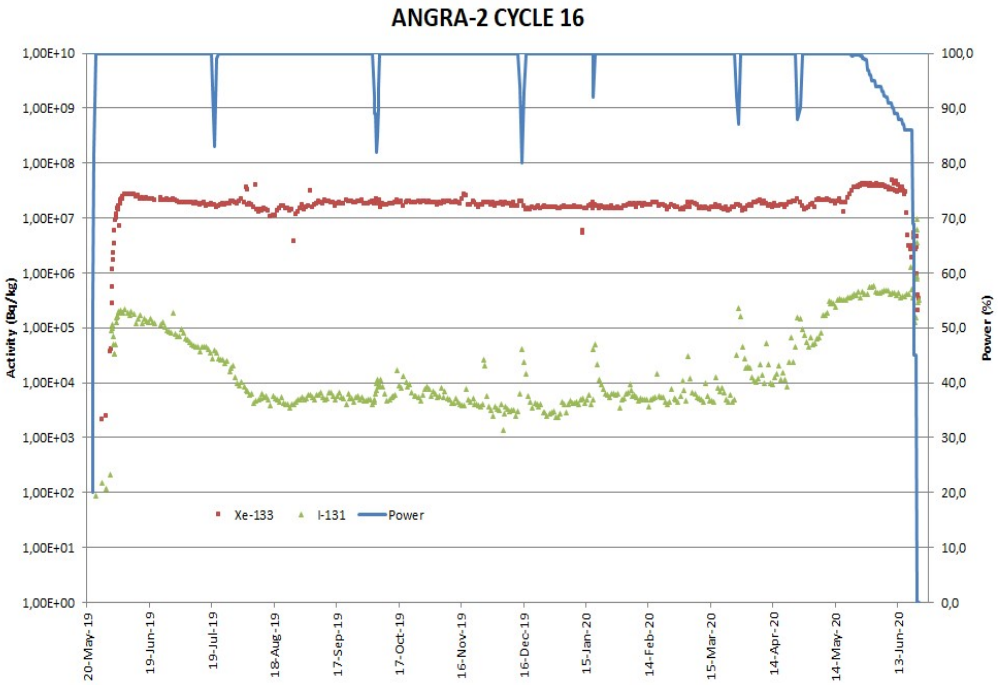

FIG. 1. Angra 2 16th Cycle: dose equivalent I-131 and Xe-133.

In order to mitigate increases in FA failures due to load variations, a limitation on the power ramp rate was applied to planned power changes during the 16th Cycle, according to the specific operating procedures of the plant shown in Table 3. The maximum power ramp for a planned load change during the 16th Cycle was 10 MW/h.

TABLE 3. SPECIFICATION FOR THE RATE OF VARIATION OF POWER

Power range		Up/Down rate		Justification
%Regular Power	Mwe	Electric Generator	Reactor	
0-15	0	-	1%/min	High vibration in the secondary system, near the pumps LAC10, 20 AND 330AP001
15-30	0	-	2%/min	Risk minimization in the condenser – MAG 10,20 and 30
30-45	370-600	10 MWe/h	~0.8%/min	Up and down power rate in case of FA damage
45-60	600-880	20 MWe/h	~1.5%/min	High vibration in all secondary system
65-100	880-1350	10 MWe/h	~0.8%/min	Up and down power rate in case of FA damage

Due to the indication of fuel failure in the 16th Cycle, an In-Mast Sipping test was performed to identify the fuel that was leaking as the core was being unloaded to the spent fuel pool. The reduction in hydrostatic pressure as the assembly is raised during fuel movement in the reactor cavity releases fission products from the defects in fuel rods. A liquid sample is taken, and the stripped fission gases pass through a gaseous activity counting system. A liquid sample can also be taken and analyzed using gamma spectroscopy. In-Mast Sipping fuel inspection identified one failed fuel assembly (R013 FA), Fig. 2.

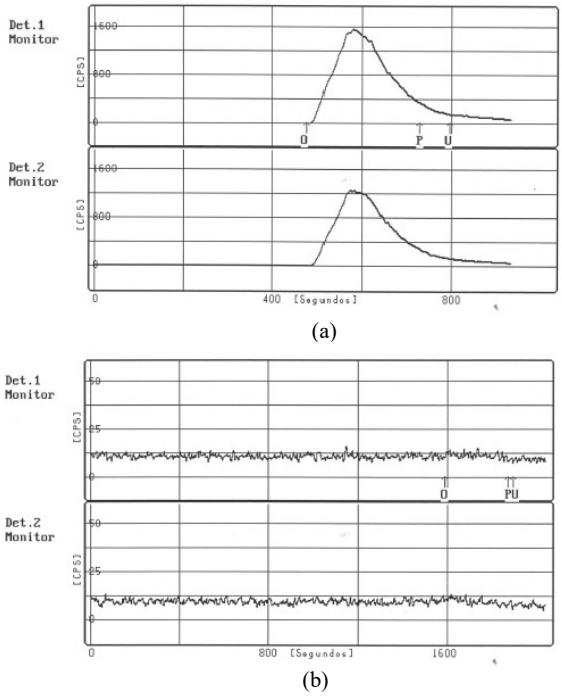

FIG. 2. In-Mast Sipping results: (a) No Failure (b) R013 Fuel Assembly

The main fuel failure mechanisms observed in the beginning of an operational cycle may have manufacturing, handling damage or debris as its root cause. Since debris fretting has been the major cause of fuel failures in Angra-2, the operator decided to visually inspect all FAs that were scheduled for irradiation in the 17th Cycle to check for the presence of foreign objects, as well as checking the mechanical and structural integrity of the fuel and oxidation phenomena on the surface of fuel rods.

The visual inspection of the fuel assembly R013 did not show any defect in the peripheral fuel rods or the presence of debris. However, an abnormal oxidation was observed in the uppermost grid, an unexpected event that is shown in Fig. 3.

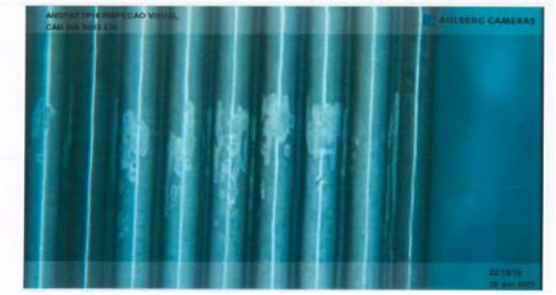

FIG. 3. Visual Inspection R013.

3.2 Angra 2 fuel cladding oxidation

During the core unloading of 16th Angra 2´s cycle, some white particles were observed to have been released from the FAs, as can be seen in Fig. 4.

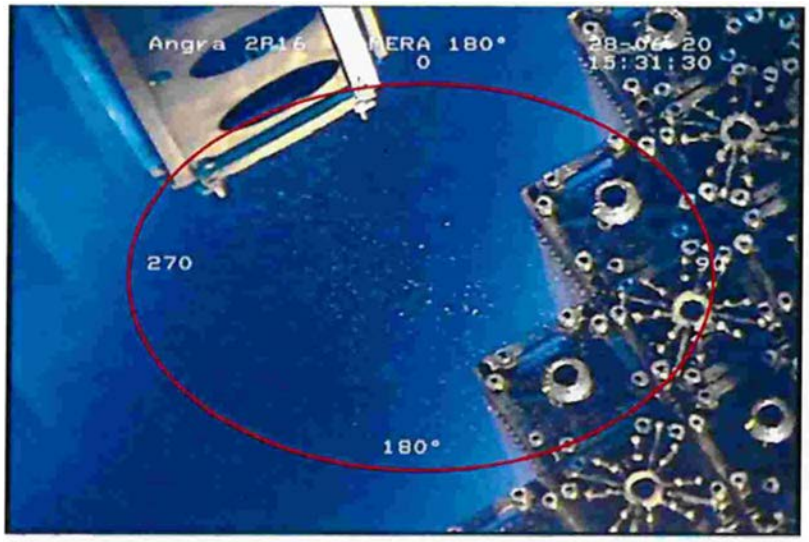

FIG. 4. White Particles unleashed from FAs.

Inspection of the inside of the Reactor Pressure Vessel (RPV) identified identical particles deposited on its internal parts and bottom, as shown in Fig. 5.

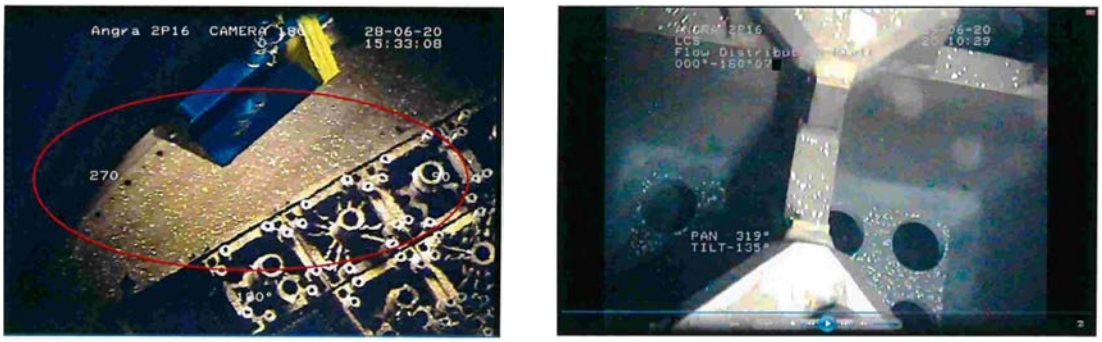

FIG. 5. White Particles deposited in the RPV's internal (left) and RPV's bottom (right).

Chemical analysis of the white particles revealed that their composition was mostly Zirconium (Zr-95) and small quantities of Nb and other substances, as shown in Fig. 6. This indicated that the material likely came from the cladding of fuel like Zircaloy-M5, whose composition is 98.93% Zr, 1% Nb and 0.07 % other materials. The Zircaloy-M5 was loaded for the first time in Angra 2 NPP in the 8th Cycle and no issues were identified until the 16th Cycle.

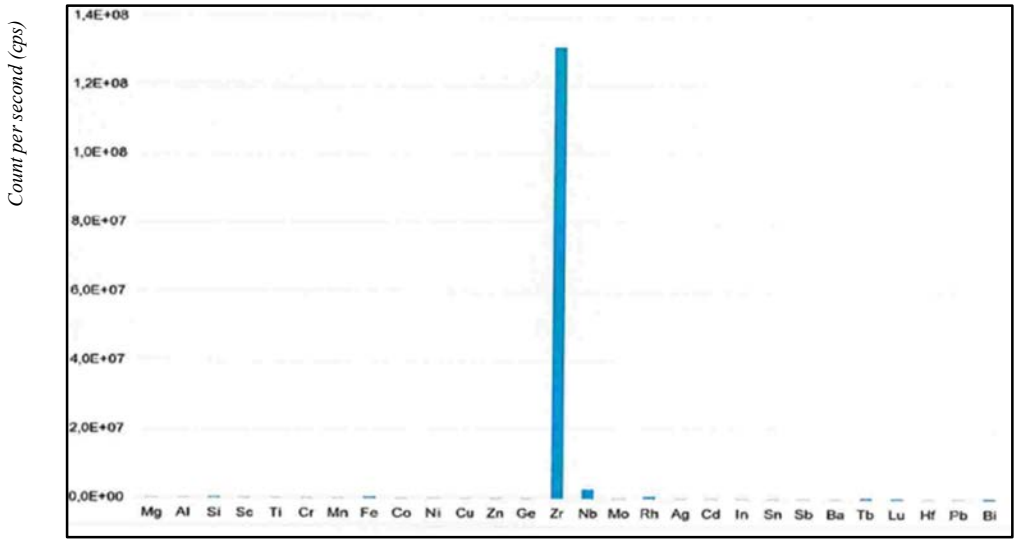

FIG. 6. White particles chemical analysis results.

Visual inspections performed during the plant outage showed that all 52 FAs of R series had enhanced corrosion with some flaking in the uppermost span between the 8th and 9th spacer grids, located at the top of the FA, at the transition of the end of the active column to the upper plenum, Fig. 7 and Fig. 8. The corrosion ranged from only light indications of a brighter gray aspect without flaking to extended oxide spallation and both peripheral and internal fuel rods were affected.

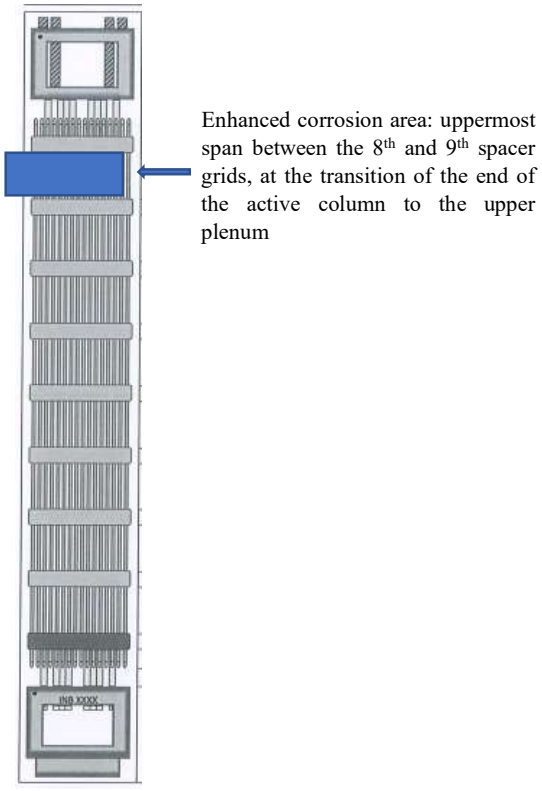

FIG. 7. Sketch of the fuel assembly demonstrating location of enhanced corrosion.

Axial position	0^0 Face	90^0 Face	180^0 Face	270^0 Face
Above Grid 9				
8 - 9 Grids				
7 - 8 Grids				
6 - 7 Grids				
5 - 6 Grids				
4 - 5 Grids				
3 - 4 Grids				
2 -3 Grids				
1 -2 Grids				
Below Grid 1				

FIG. 8. Visual inspection in the four faces of a FA (red cicles: increased oxide location).

Visual inspections of these 52 FAs and other FA series that were irradiated during 16th Cycle were evaluated. The FAs exhibit three levels of enhanced corrosion:

— Level 1: only light indications of a brighter grey aspect without flaking.
— Level 2: white aspect, adherent oxide layer without flaking.
— Level 3: white aspect with spallation, Fig. 9.

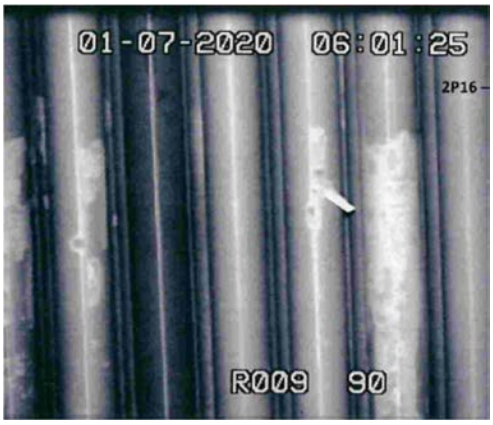

FIG. 9. Oxide spallation at the end of the active zone and in the region of the upper plenum.

The FAs of the P series (second cycle FA) exhibited a white appearance in the same area (at the end of the active column in the transition to the upper plenum), indicating they also experienced some enhanced, but less pronounced corrosion and with no oxide flaking (level 2). Comparing the results from the visual inspection carried out after 16th Cycle with the inspection carried out in the previous cycle, it was possible to verify that the FAs of this series already exhibited corrosion level 2 after their first cycle, and that there was minimal degradation of this condition during the second irradiation period.

All other FAs showed a behavior ranging from normal to a light indication of a brighter grey aspect, comparable with past experience for this reactor type.

Fig. 10 shows the core positions of the FAs of the R series in the 16th Cycle and the faces of these assemblies that exhibited enhanced corrosion.

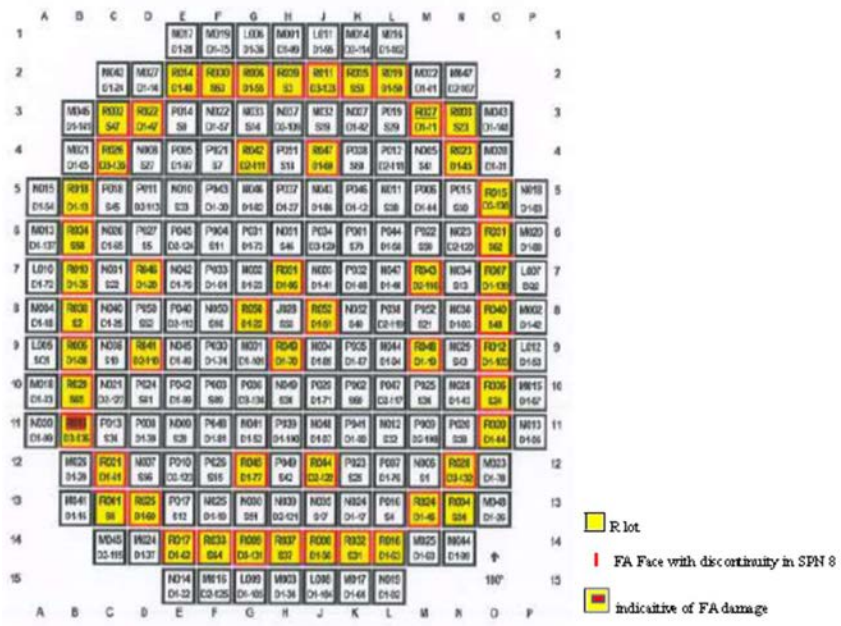

FIG. 10. Angra 2 Cycle 16th: failures and oxidation FA location.

4. 16th CYCLE FUEL CLADDING OXIDATION ANALYSIS

4.1 Root cause evaluation

The growth of enhanced oxide layers on Zr-alloy fuel rod claddings has been extensively investigated and the most important parameters impacting PWR corrosion rate are, as determined by Garzarolli [3]: temperature, exposure time, water chemistry, neutron flux, Zr-alloy composition, and increase of corrosion or decrease of oxide thermal conductivity at high burnups.

To identify what occurred and the possible causes, an initial investigation plan was developed.

First, a visual inspection was carried out on all FAs discharged from the core. During this phase, underwater cameras were used to inspect the surface of the FAs. Some of the images from this inspection are shown in Section 3.2 of this article.

After the visual inspection, the Foreign Object Search and Retrieval (FOSAR) equipment was used in order to collect a particle sample from the reactor cooling system. As discussed previously and shown in Fig. 7, the results indicated that the material came from the cladding of fuel like Zircaloy- M5. However, it is important to observe that only M5 cladding material, but not all M5, has been affected by increased corrosion at the upper end of the fuel rods.

An inspection and independent verification of possible operational equipment faults was also performed in parallel with the above steps, but nothing anomalous was found.

Based on the preliminary results, international literature was consulted in order to identify similar events. As described in Section 2.1, the visual inspection of M5 FAs in some German NPP revealed an unusual surface appearance in the same area this was identified in Angra 2 FAs.

Given these occurrences, the following factors were taken into account in the root cause analysis [2]:

— Composition and structure of the material.
— Manufacturing (including agents used to clean the cladding tubes after welding on the end plug).
— Thermohydraulic operating conditions (void content at the FAs outlet).
— Linear heat rate.
— Water chemistry.
— Thermomechanical conditions, considering temperature fluctuation caused by flow variation.

The extensive reviews by an international expert group of the International Atomic Energy Agency (IAEA) and published as IAEA-TECDOC 996 [4] clarified that the required performance of zirconium alloys in reactors depends on a complex interaction of many parameters. From reference [5], a multi-matrix illustrated in Fig. 11, was developed in reference [4] to show these complex relationships for Zircloy-4 used in PWR fuel. However, in principle these relationships are the same for any Zr-material in any LWR or HWR fuel.

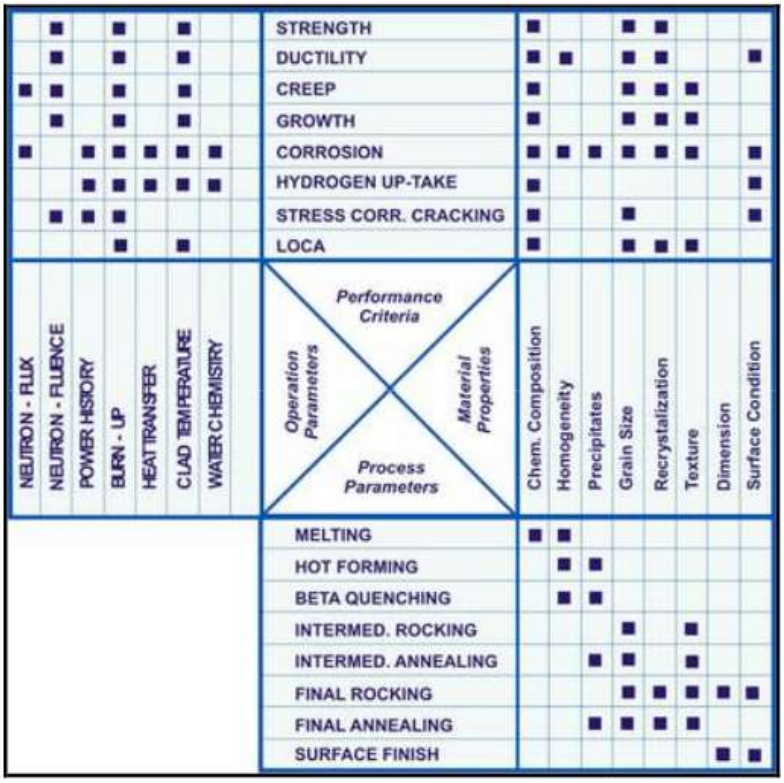

FIG. 11. Interaction of operating parameters, performance criteria, lubrication process parameter and material properties of Zircaloy cladding.

Concerning the composition and structure of the material, as recommended by [6], the cladding material shall be fabricated from reactor grade zirconium alloy, cold rolled, and vacuum annealed to full recrystallization in conformance to the specification and supporting documents. The material´s composition shall be in conformance with the alloying chemical elements and impurity levels in the range shown in Tables 4 and 5, respectively, for the M5 (Zr-1 alloy).

TABLE 4. ALLOYING ELEMENTS CHEMICAL COMPOSITION RANGE FOR M5 (ZR-1 NB ALLOY)

Element	Composition Range, Weight (%)	
Zirconium, Zr	Balance Weight % Zr	
Niobium, Nb	≥ 0.8	≤ 1.2
Oxygen, O	≥ 0.12	≤ 0.14
Sulfur, S	≥ 0.0010	≤ 0.0035

TABLE 5. MAXIMUM IMPURITY CONCENTRATION IN M5 (ZR-1 NB ALLOY)

Impurity Element	Maximum Allowable Content (ppm)	Impurity Element	Maximum Allowable Content (ppm)	Impurity Element	Maximum Allowable Content (ppm)
Aluminium, Al	≤ 75	Copper, Cu	≤ 50	Nickel, Ni	≤ 70
Nitrogen, N	≤ 80	Tin, Sn	≤ 100	Lead, Pb	≤ 30
Boron, B	≤ 0.5	Iron, Fe	≤ 500	Silicon, Si	≤ 120
Cadmium, Cd	≤ 0.5	Hafnium, Hf	≤ 100	Tantalum, Ta	≤ 100
Calcium, Ca	≤ 30	Hydrogen, H	≤ 25	Titanium, Ti	≤ 50
Carbon, C	≤ 100	Magnesium, Mg	≤ 20	Tungsten, W	≤ 100
Chromium, Cr	≤ 150	Manganese, Mn	≤ 50	Uranium, U	≤ 3.5
Cobalt, Co	≤ 10	Molybdenum, Mo	≤ 50	Vanadium, V	≤ 50

An overview on the historic development of Zr-based cladding presented in [7] discussed the impacts of alloying elements on the material properties. In this review, it was observed that the additives Fe, Cr, and Ni are important for the corrosion behaviour of Zr-based alloys. These impurities are beneficial to the corrosion resistance at high temperature. According to the literature, these factors should be investigated during the study to identify the possible root case. This behaviour can be seen in the Fig. 12, from [4].

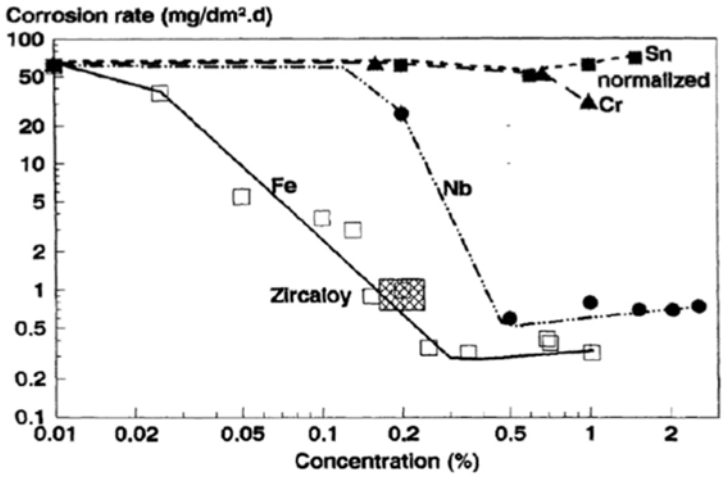

FIG. 12. Effect of various alloy constituents on corrosion in 400 ^{0}C, 105 bar steam [4].

According to the research discussed in [8] about the development of zirconium alloys and the study of hydride formation, the Zr-alloy element effects can be explained by Table 6.

TABLE 6. ELEMENTS EFFECTS IN THE ZR-ALLOY

Element	Corrosion resistance	Mechanical proprieties
Sn	↓	↑
Nb	↑	↑
Fe	↑	↑
O	↓	↑ *
Cr	↑	--
Mo	↑	↑

* in low concentration

Based on the review discussed above, it is essential to review the FAs technical specification and the manufacturing record, as well as to identify any anomalies with previous FAs operated successfully in Angra 2.

It is known that the effect of reactor chemistry and operating parameters are important factors on the Zircaloy cladding corrosion process. The maximum radial power peaking factor (RPF) is an index of fuel thermal duty on heat flux that has a significant effect on the cladding corrosion rate because it affects the fuel rod cladding surface temperature. As explained in [9] an increase in the Zircaloy cladding corrosion rate can occur under subcooled boiling conditions. A possible explanation, as described in [4], is that when the bubbles depart from the cladding surface, an oxygenated mixture of water and steam could be created and, consequently, an increase in either steam or oxygen concentration occurs. This results in a larger oxide film thickness, and nodular corrosion of the alloy may occur.

Other important operational parameters are the core inlet and outlet temperatures. These can increase the cladding wall temperature and can expose the M5 fuel rods to oxidative conditions.

The root cause investigation of the 16th Cycle Angra 2 oxidation must consider the potential contributions discussed above. The operating parameters during this cycle must be determined. It may be possible to characterize all operational parameters that could have an influence on the corrosion process. Measured parameter data of the operational cycle are also important to check for trends or anomalies. A comparison with previous cycles must be made to identify possible changes in the operational profile. In addition, the chemical control of the primary system water must be investigated to determine if a variation of some component could have induced the corrosion process.

The aim of this review is to correlate the phenomena and parameters from the 16th Angra 2 cycle to several examples available in the literature on Zr-alloy behaviour.

4.2 Preliminary results

Presently, there are no conclusive answers about the root cause. Some possible hypotheses to be investigated could be proposed.

One of these is concerning the Zr-M5 composition. Specifically, the Zr-M5 oxidised cladding from the 16th Cycle could be compared with the composition of the fuel cladding from the previous cycles.

Regarding of the manufacturing process, it will be important to investigate all phases, including the storage and transportation conditions that the fuel is exposed to.

It may also be beneficial to compare the operational history between cycles to understand whether there was some condition that could have induced void fraction formation in the affected region, e.g., increasing temperature in the position between the 8th and 9th grid spacer.

Another important source of data would be the history of the linear heat rate during the entire 16th Cycle as this would show whether there was a sufficient temperature increase to favor the oxidation process.

It is also important to verify the historical water chemistry data to know whether compositional variance may have inadvertently resulted in adverse and more aggressive water effects, than normally observed, and which may have enhanced the corrosion process.

As important as the previous observations, it is to verify the FAs arrangements to investigate some flow variation that could have caused a wrong flux distribution and, consequently, promote a temperature variation in the core.

It is important to note that presently, none of these factors have been identified as the root cause of the unusual corrosion.

In addition, national experts are evaluating this event.

As part of this planning, a service has been contracted to measure the oxide thickness and the residual wall thickness of the cladding tube, but no results have been obtained yet. These measures are important to assess the possibility of reloading some of these FAs in next cores.

It is important to note that in the 16th Cycle there were two kinds of events. The first event involved fuel damage which occurred at the beginning of the cycle, for which a root cause has not yet been determined. Although releases of I-131 and Xe-133 to the reactor cooling system were recorded, the concentration of these releases remained within the applicable safety limits criteria. The second event involved fuel cladding oxidation which happened during the first cycle batch. Nevertheless, these events of early fuel failure and excessive oxidation are not correlated to each other. As pointed out in Section 3.1 above, R013 most likely failed due to debris. However, the visual inspection did not show any defects in the peripheral fuel rods or confirm the presence of trapped debris. As can be seen in Fig. 1, the I-131 and Xe-133 activities increased at the beginning of the cycle. Therefore, both events are considered independent, and each one is expected to have its own unique root cause.

5. CONCLUSIONS

According to the current operational experience of other plants, it can be assumed that the enhanced corrosion in the uppermost span at the end of the active column transition to the upper plenum of the 52 first cycle FAs in 16th Cycle of Angra-2 is a result of several contributing factors.

The composition of the cladding material, manufacturing of the cladding tube, handling, storage, and operating conditions (power distribution, water chemistry, neutronic and thermal-hydraulic parameters) are some of the potential contributing factors which are being investigated to identify the root cause of the event.

While the root cause is still under investigation, all safety protocols will be followed. To comply with the design limits and ensure adequate margin exists, the operator has decided not to use any of the enhanced corrosion FAs, in the subsequent cycle of Angra-2, until data on fuel cladding and oxide thickness measurements become available for consideration.

Additionally, to mitigate the potential risk of enhanced corrosion re-occurring during the 17th Cycle, reactor power was reduced by an appropriate amount (~5%). The Brazilian regulatory body, National Nuclear Energy Commission (CNEN) is closely following the investigations presented herein, as part of the associated follow-up to licensing activities.

ACKNOWLEDGEMENTS

We would like to acknowledge Dr. José Augusto Perrotta, from IPEN/CNEN, São Paulo, Brazil, for his cooperation in clarifying fuel behaviour at the present time, and for his support on these studies and article.

REFERENCES

[1] RSK/ESK-Geschäftsstellebeim - Increased oxide layer thicknesses in the upper part of fuel assemblies with M5 cladding tubes, 514th meeting of the Reactor Safety Commission, RSK, 12 February 2020.

[2] MILDENBERGER, O., Recent Operating Experience of German PWRs, GRS, 8th Meeting of the KWU Regulators Group, Video Conference, 1-2 July2020.

[3] GARZAROLLI, F., GARZAROLLI, M., PWR Zr Alloy Cladding Water Side Corrosion, Advanced Nuclear Technology International, Mölnlycke, February 2012.

[4] INTERNATIONAL ATOMIC ENERGY AGENCY, Waterside Corrosion of Zirconium Alloys in Nuclear Power Plants, IAEA-TECDOC-996, IAEA, Vienna (1998).

[5] WEIDINGER, H.G., Zr-Alloys, the Nuclear Material for Water Reactor Fuel. Survey and Update with Focus on Fuel for Pressurized Water Reactor System 7th International Conference on WWER Fuel Performance, Modelling and Experimental Support, Albena, Bulgaria, 17 – 21 September 2007.

[6] PARGA, J. C., M5 Alloy Specification for TREAT Conceptual Fuel Cladding Selection, Idaho National Laboratory, Idaho Falls, Idaho, March 2018.

[7] DUAN, Z. et al., Current status of materials development of nuclear fuel cladding tubes for light water reactors, Nuclear Engineering and Design **316** (2017) 131–150.
[8] MARTINS, C. D., Development of zirconium alloys and the study of hydride formation (Desenvolvimento de ligas de zircônio e o estudo da formação de hidretos), Dissertação de Mestrado, UFRJ/COPPE/EMM, Rio de Janeiro, September 2013.
[9] PARK, M. G. and LEE, S. H., Effect of Reactor Chemistry and Operating Variables on Fuel Cladding Corrosion in PWRs, The 2nd Seminar on the New Fuel Technology Toward the 21st Century, KAERI, Taejon, Korea, 25 – 26 November 1997.

FUEL FAILURE IN KRŠKO NUCLEAR POWER PLANT – CAUSES AND CORRECTIVE MEASURES

T. NEMEC
Slovenian Nuclear Safety Administration,
Ljubljana, Slovenia

Abstract

In October 2013, during core unloading in the Krško NPP refuelling outage damaged fuel assemblies with open cladding defects were found. Visual inspection of all fuel assemblies unloaded from reactor core showed open defects in 8 fuel rods' cladding of 3 fuel assemblies. The primary cause of fuel rods damage was determined to be baffle jetting that can occur at these fuel assemblies' locations at the core baffle plate. During fuel inspection other 3 leaking fuel assemblies with tight defects were found. Extensive inspection of fuel assemblies and the core baffle plate was carried out to determine the cause of fuel defects and to assure the integrity of the fuel assemblies to be reloaded into the new reactor core. A Root Cause Analysis was prepared by the fuel provider and determined the causes of fuel leakage and possible corrective actions to prevent recurrence of the event. The open fuel defects occurred again in the next fuel cycle on locations predicted by the Root Cause Analysis as those subjected to the baffle jetting. The Krško NPP implemented corrective actions in the years 2015 and 2016. These actions included the upflow conversion modification to eliminate baffle jetting and improvements to the fuel assembly design to increase robustness of the fuel to vibrations and to debris present in the primary coolant. The operation of the Krško NPP from 2016 onwards showed that these actions were successful in eliminating the causes of fuel damage and the fuel integrity is again assured in normal operation of the plant.

1. INTRODUCTION

The fuel integrity is important in prevention of fission product release from irradiated fuel assemblies. The fuel cladding is the first barrier, and its integrity shall be maintained throughout the life cycle of the fuel. In case of fuel leakage, this will impact the operation of the plant, the design of next reactor cores, the radiological conditions for the workers during the outage activities, the radiological releases to the environment and the handling of the spent fuel. In the event with open fuel defects the consequences are more severe due to dispersion of fuel pellets into the primary coolant system where radiological hot spots can occur in primary components and the damaged fuel assembly requires handling with special tools. Such damaged fuel assembly will need also specific storage in the spent fuel pool and later when transferred to a dry spent fuel storage. The dispersed fissionable material (the debris of fuel pellets) provides additional source of activity, named tramp uranium, that increases the activity of radiation in primary coolant during next outages and requires additional shielding for workers.

During its operational history the Krško NPP experienced some degradation of fuel cladding integrity [1]. The number of leaking fuel assemblies increased in the mid 1990s (cycles 10-13 in Figure 1), mostly due to debris present in the core, which was a consequence of maintenance to the leaking steam generators. To resolve this problem and to ensure the safe and reliable operation of nuclear fuel, the Krško NPP established Fuel Integrity Program in November 1995 (as described in the reference [1]). All areas affecting fuel integrity were addressed and proper course of actions to reach zero fuel defect goal were clearly defined. This approach was effective for the period when the plant operated in 12 months long cycles, as can be seen in Figure 1 (cycles 14-19). However, when the Krško NPP performed the modernization with power uprate in 2000 and cycle extension to 18 months in 2004, fuel failures re-occurred (see Figure 1, cycle 20 onwards). These were tight fuel defects caused by grid-to-rod fretting in locations close to the baffle plate.

The Krško NPP is a Westinghouse PWR of 2000 MWt. The plant commercial operation started in 1983 and the modernization was performed in 2000. The reactor core is composed of 121 fuel assemblies with 16×16 fuel rods. The current operating cycles are 18 months long with refuelling outages of 28-30 days. The design fuel burnup limit is 60 GWD/MTU, however the maximum actual burnup reaches up to 55 GWD/MTU. The spent fuel is currently stored in the spent fuel pool. A project for a spent fuel dry storage at the Krško NPP site is currently in the licensing process and will be completed in a few years.

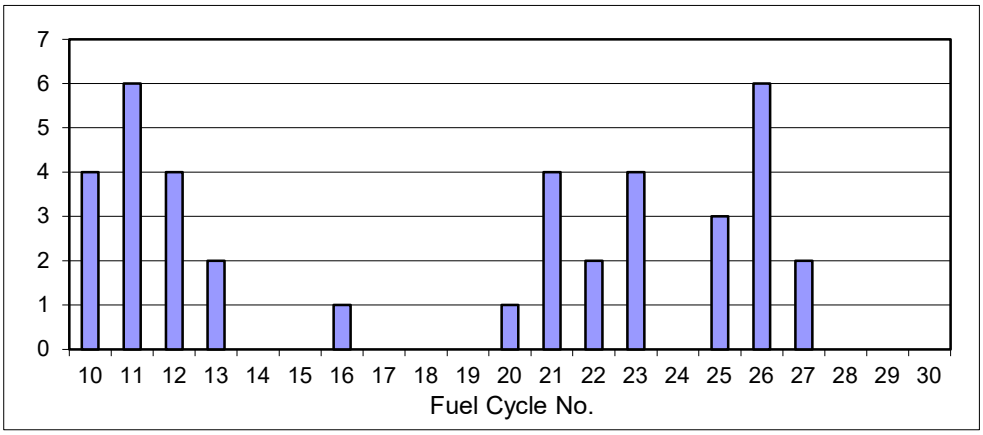

FIG. 11. Number of leaking fuel assemblies in fuel cycles No. 10 to 30 at Krško NPP (1993-2019).

2. OPEN FUEL DEFECTS IN 2013 REFUELING OUTAGE

2.1 Event description

The event occurred in October 2013 when the refuelling outage started in the Krško NPP. At core unload all fuel assemblies were checked for integrity of fuel rods by the In-Mast Sipping (IMS) method. Six fuel assemblies were found to be leaking which was expected based on coolant activity during the operation. During transfer of fuel assemblies from the reactor to the spent fuel pool a 50 cm long unknown object was found at the bottom of fuel transfer channel (Figure 2). When the object was retrieved, it was determined that this is a segment of a fuel rod from fuel assembly AD11. Visual inspection of all fuel assemblies unloaded from the reactor core showed open cladding defects in 8 fuel rods from three fuel assemblies. All these fuel rods were broken with some parts of cladding missing and some fuel pellets were dispersed.

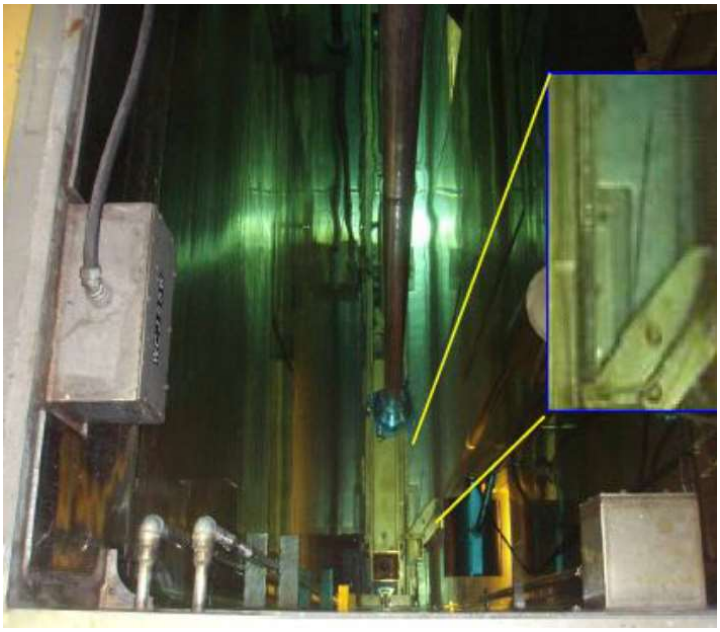

FIG. 12. The broken fuel rod of fuel assembly found in the fuel transfer channel.

The primary cause of the fuel rods damage was determined to be baffle jetting that can occur at these fuel assemblies' locations at the core baffle plate. This was not expected based on previous operating history and the foreign operational experience. But further investigation confirmed this failure cause.

2.2 Other leaking fuel assemblies

In the reactor core there were three other leaking fuel assemblies with cladding defects at one fuel rod per fuel assembly. One of these rods was broken and other two had only tight fuel cladding defects. The apparent cause was flow-induced vibration that is attributed to the grid-to-rod fretting (GTRF) or debris fretting. This cause was present since the fuel cycle extension from 12 months to 18 months in 2004 and such fuel leakage was already observed in previous 6 fuel cycles. The location of leaking fuel assemblies in the core is shown in Figure 3.

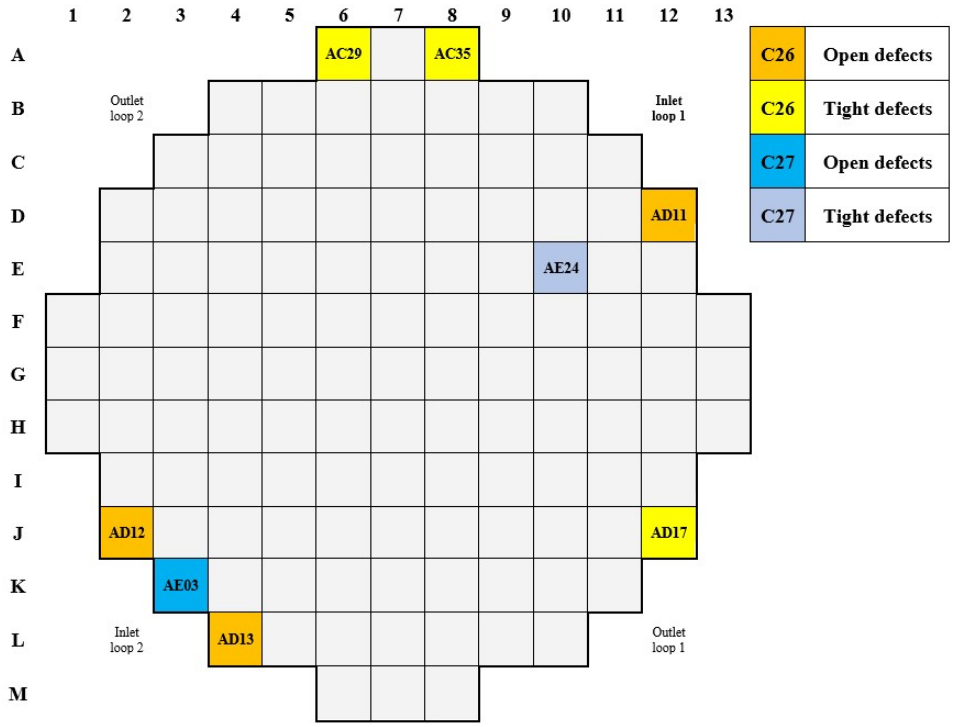

FIG. 13. Core locations of leaking fuel assemblies in fuel cycles 26 and 27 of the Krško NPP.

The primary coolant activity is measured regularly to determine fuel cladding integrity during operation. The coolant activity data showed a leaker-free core at the beginning of cycle 26. The xenon and iodine activity levels increased at about 53 days from the beginning of the cycle, indicating the presence of leaking fuel in the core. The simultaneous increase of iodine and xenon isotopes indicated the leaker had an open defect. One month before the planned outage in October 2013 alpha emitters were detected in the reactor coolant. During Cycle 26 two unplanned reactor shutdowns occurred which might have had an impact on further degradation of leaking fuel rods.

3. DETERMINATION OF ROOT CAUSE

To determine the root cause of the fuel damage several analyses were performed by the fuel designer Westinghouse, the operator, a team composed of four different authorized independent expert organizations (Technical Support Organisations, TSOs) and the regulatory body. The regulatory body reported on the event via the SNSA website as well as to the INES NEWS [2] and to the IRS [3] databases. The event was followed by media and public in Slovenia and in neighbouring countries.

3.1 Inspection results with the NDT methods

To determine the cause of fuel defects the operator together with contractors performed extensive inspections of fuel assemblies. The operator prepared extensive reports on the In-Mast Sipping, ultrasonic and visual inspections performed on the fuel assemblies from the reactor core of Cycle 26. Other inspections were performed in connection with attributed causes for the fuel damage (the baffle jetting). Core baffle was visually inspected to estimate the size of gaps between core baffle plates, especially at the locations and elevations of damaged fuel rods. The integrity of baffle to former bolts was checked by UT inspection and confirmed that no bolts were broken. Thorough FOSAR (Foreign Object Search and Retrieval) inspections of reactor pressure vessel, reactor vessel internals, reactor cavity and fuel transfer channel were performed with the aim of the identification and collection of debris, including dispersed fuel pellets material. Debris were found also in nozzles and grids of other fuel assemblies and were removed. The integrity of all fuel assemblies designed for the reload core of the new Cycle 27 was also checked by ultrasonic and visual inspections. All these unplanned outage activities required an extension of the outage time by additional 2 weeks.

3.2 Causes and corrective actions

The causes of fuel leakage and proposal of corrective actions to prevent recurrence of the event were prepared by the fuel designer [4] and an independent expert opinion of the TSO [5] confirmed the correctness of the analysis and the proposed corrective actions. The SNSA decided to publish both documents on the SNSA web site as information for the public. The regulator also reviewed the international operational experience databases (e.g., IAEA IRS) and reports on fuel failure [6,7,8] and exchanged the experience with foreign regulators. The apparent cause for fuel damage was determined as baffle jetting based on the fuel designer root cause analysis and results of fuel inspections. For the leaking fuel with tight defects the apparent cause was determined as the flow-induced vibration which led to the grid-to-rod fretting (GTRF) or debris fretting.

The following corrective actions that provide design improvements for the Krško NPP were proposed:

— Implementation of the reactor vessel upflow conversion to eliminate pressure gradients that cause baffle jetting (UFC);
— Fuel assemblies design changes to enhance the GTRF and debris margins.
— Sharing the experience of this event with other operators.

The immediate corrective actions were aimed at constructing a new core for the next fuel cycle. Fuel reconstitution campaign was carried out to replace several fuel rods at exposed locations close to the core baffle plate with stainless steel dummy rods that can resist baffle jetting. In four (undamaged) fuel assemblies seven fuel rods were replaced with stainless steel dummy rods. The broken part of the fuel rod from fuel assembly AD11 was retrieved from the bottom of the fuel transfer channel and was temporarily stored inside a strainer basket in the spent fuel pool. The Krško NPP prepared a specification for the fuel rod segment encapsulation project to provide a permanent storage solution for the broken rod.

The regulator insisted that prior to the start of operation the Krško NPP has to prepare an extended Failed Fuel Action Plan describing appropriate actions in case of a fuel leakage with open defects during the next fuel cycle. Because of core redesign and use of reconstituted fuel in the core a revised Reload Safety Evaluation was issued for the core of cycle 27 with consideration of the effect of stainless-steel rods in reconstituted fuel.

3.3 Lessons learned from the event

The lessons learned from the reviewed foreign operating experience [9] are that the fuel damage caused by baffle-jetting can occur suddenly and without prior signs of reactor internals degradation. Solutions required to prevent recurrence of the event are modifications of the reactor vessel internals (implementation of the Upflow Conversion modification) and of the fuel assemblies (development of improved fuel assemblies' mechanical design). The operator learned that indication of open fuel cladding defects can deteriorate with continued power operation and accordingly a strict failed fuel action plan was prepared that requires plant shutdown or an anticipation of an outage before the end of the fuel cycle in case that fuel conditions would deteriorate.

This event caught wide attention of the public in Slovenia as well as of the foreign regulatory bodies. The SNSA and the Krško NPP aimed to provide open communication with the Slovenian and foreign media and the public and this included open reporting of all available information on the SNSA web site. This open communication resulted in regained public confidence in the safety of NPP operation and in the appropriateness of the SNSA supervision of the Krško NPP operation.

4. PLANT OPERATION IN NEXT CYCLE AND MODIFICATIONS TO PREVENT FUEL DAMAGE

The plant operated in fuel cycle 27 that lasted 18 months. The operation was without detected fuel leakage for first 15 months and after that increased activities of xenon and iodine isotopes in the coolant were detected, indicating open cladding defect of several leaking fuel rods. The Failed Fuel Action Plan was deployed, and the plant reached the action level 3 before the outage. Two leaking fuel assemblies were found by fuel inspections, one on the baffle with open cladding damage and another one with tight leakage that was not on the baffle (as shown in Figure 3). A 10 cm long piece of fuel rod of the fuel assembly AE03 was broken and fell off to the bottom of the core. Dispersed fissionable material and debris resulting from damaged fuel assembly were collected by FOSAR inspection from the bottom of the reactor pressure vessel as well as some nearby fuel assemblies. The cause of open fuel defects was baffle jetting.

The plant modification Upflow Conversion reversed the flow of the primary coolant behind the baffle plates and thus mitigated or prevented vibrations caused by baffle jetting. The modification was implemented during the 2015 refuelling outage. The fuel assemblies were additionally protected with oxide coating that shields the bottom six inches of each fuel rod, thus increasing wear resistance over uncoated cladding. This fuel was loaded into the core during the 2015 outage. This provides improved resistance of the fuel rods against the debris and grid-to-rod fretting. In 2015, the Krško NPP started a project to develop an improved mechanical design of the Krško NPP 16x16 fuel assemblies that have a modified mid grid design and improved design of the bottom nozzle. These fuel assemblies were included in the core during the 2016 outage. Three fuel assemblies planned for reactor core of the cycle 28 had to be replaced and thus redesign of the core was prepared.

5. CONCLUSIONS

The operator reported on the event to the industry and regulator reported on the event to the IRS database to inform the international community on the findings, causes of fuel damage and the corrective actions that successfully eliminated the causes for cladding damage. The regulator also published an INES report to inform Slovenian and international public on the consequences of the event. The event was rated as Level 0 on the INES scale.

Following the implementation of corrective measures to prevent open defects of fuel assemblies, where the major effect was due to the change of the reactor core bypass flow in modification Upflow Conversion, there have been no leaking fuel rods since fuel cycle 28 (Figure 1). Both operator and the regulator closely follow the fuel performance during every fuel cycle through performance indicators.

REFERENCES

[1] ANTOLOVIČ, A., KURINČIČ, B., Nuclear Fuel Reliability in NPP Krško, Nuclear Energy in Central Europe 2001, Proc. Int. Conf. Portorož, Slovenia, 2001, Nuclear Society of Slovenia, Ljubljana (2001).

[2] Discovery of Damaged Fuel Rods During Core Unloading and Fuel Inspections, INES Level 0 Event, INES Report (Final), SNSA, 5 November 2013, published on NEWS, https://www-news.iaea.org/

[3] Discovery of Damaged Fuel Assemblies During Core Unloading and Fuel Inspections, IRS Report No. 8376 (Main), IAEA IRS, Vienna (2015).

[4] Root Cause Analysis Summary, Krško Cycle 26 Leaking Fuel Assemblies, Westinghouse, February 3, 2014.

[5] FIER: Independent Evaluation of Root Cause Analysis for Six Leaking Fuel Assemblies in Krško Cycle 26, June 2014.

[6] INTERNATIONAL ATOMIC ENERGY AGENCY, Fuel Failure in Water Reactors: Causes and Mitigation, IAEA-TECDOC-CD-1345, IAEA, Vienna (2003).

[7] INTERNATIONAL ATOMIC ENERGY AGENCY, Review of Fuel Failures in Water Cooled Reactors, Nuclear Energy Series No. NF-T-2.1, IAEA, Vienna (2010).

[8] European Clearinghouse: Analysis of Fuel Related Events, Technical Report, NPP Clearinghouse SPNR/CLEAR/09 11 006 Rev.00 (Restricted Distribution), EU, Petten (2009).

[9] Baffle Jetting Results in Fuel Element Damage, IRS Report No. 8449 (Main), IAEA IRS, Vienna (2014).

INSPECTION AND REPAIR OF DAMAGED FUEL ASSEMBLIES

AN NA
Hainan Nuclear Power Co., Ltd.,
Changjiang County, Hainan Province, China

SHI ZHIBIN
Hainan Nuclear Power Co., Ltd.,
Changjiang County, Hainan Province, China

Abstract

The unit 2 of Hainan Changjiang nuclear power plant was started for the first time in June 2016. When the power was increased to 30% FP for the first time, it was found that the activity of Xe-133 in the primary loop was 5-10 times higher than in unit 1. After that, it was found that the activity still increased in the process of power increase to 100% FP, with the maximum value reaching 9795.8bq/g. It was preliminarily judged that one fuel assembly was damaged. After that, the unit power was reduced to 75% FP and remained at that level for a while resulting in I-131 and Xe-133 activities gradually leveling off and remained stable. According to the regulation of *Instantaneous Activity Limit of Primary Loop in Power Operation State*, the unit can still maintain power operation. Because the off-line sipping device was canceled in the design stage, the unit only has the ability of online sipping inspection and underwater video inspection of fuel assembly. According to the experience of peers using online sipping device, assemblies with small break can not be detected. Therefore, it is necessary to prepare feasible inspection methods. The paper introduces the relevant experience of the power plant to develop the inspection and repair device for damaged fuel assemblies, and how to successfully find two failed fuel assemblies. One of the fuel assemblies was repaired and put back into the next cycle. After that, monitoring showed that it was in good performance. Up to now, this plant is the first one in CNNC to inspect and repair damaged fuel assemblies. It has a lot of experience and has formed a set of mature management system related to it.

1. INTRODUCTION

The nuclear fuel assembly in the PWR may be damaged during the power operation of the reactor due, among other causes, to foreign materials in the core causing debris fretting wear on the cladding and defects in the cladding weld, resulting in the release of radioactive fission products into the primary circuit and challenging the operation of the unit. Nuclear power plants should therefore be able to detect damaged fuel assemblies.

In the fist phase of Hainan Nuclear Power Plant, two CNP650 units were designed without offline sipping detection devices for fuel assemblies, which can only be used for online sipping detection and underwater video inspection.

During the first start-up of unit 2 of the power plant, abnormal radiochemical data were found, and fuel failure was suspected. According to the experience feedback of domestic peers, the inspection results of online sipping device on small break failures is not reliable, becase it is unable to locate the damaged fuel assembly with small break. Therefore, it is necessary to find new off-line detection technology to find out the damaged fuel assembly during the first outage of unit 2.

In addition, the power plant also considers repairing the damaged fuel assemblies that did not reach the discharge burnup, by replacing the damaged fuel rods, and loading the so repaired assemblies for further operation, in order to improve the utilization rate of nuclear fuel and the economic benefits of the power plant.

2. CASE DESCRIPTION

2.1 Radiochemical data tracking during unit startup

On June 29, 2016, during the first cycle of Hainan nuclear power unit 2, when the power of the unit was increased to 30% FP for the first time, it was found that the activity of Xe-133 in the primary circuit was increased to 55.19 Bq / g, which was significantly higher than in unit 1, namely about 10 times that of unit 1.

On July 7, after the unit completed the 50% FP platform test, the power was increased to 75% FP, and the activity of Xe-133 in the primary circuit showed an upward trend with the increase of power and reached 353.96bq/g.

On July 20, the power was further increased to 85% FP, and the activity of Xe-133 further increased to about 1000 Bq / g and remained at that level until the July 25.

On July 25, the power was increased to 100%FP, on the same night the power decreased from 100% FP to 50% FP, the activity of Xe-133 increased to 4344.9bq/g the next day, and also, I-131 activity spiked to 688.1bq/g.

The load rejection test was carried out on July 28, and the unit was shut down. After shutdown on July 29, the iodine activity also showed an obvious spike maximum value of I-131 activity reaching 896.68bq/g.

The Xe-133 activity continued to increase after reaching full power on August 4 and reached the maximum value of 9795.8bq/g on August 13.

On August 10, 2016, the unit decreased to 75% FP, and then kept steady operation. The activities of I-131 and Xe-133 gradually stabilized, Xe-133 at about 2000 Bq / g, and I-131 at about 2-5 Bq/g.

The data trends of the two isotopes are shown in Figure 1 and Figure 2.

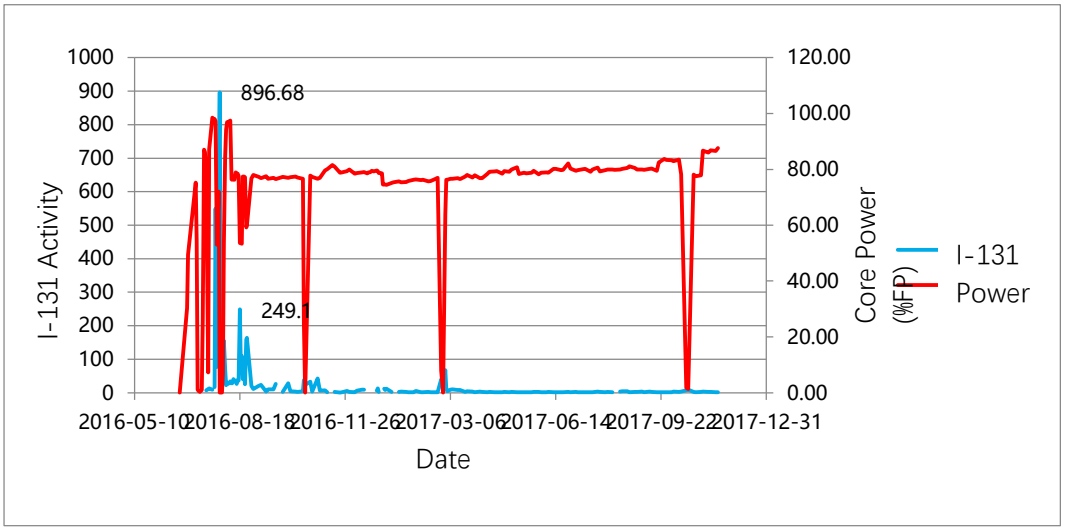

FIG. 1. I-131 Trends with power.

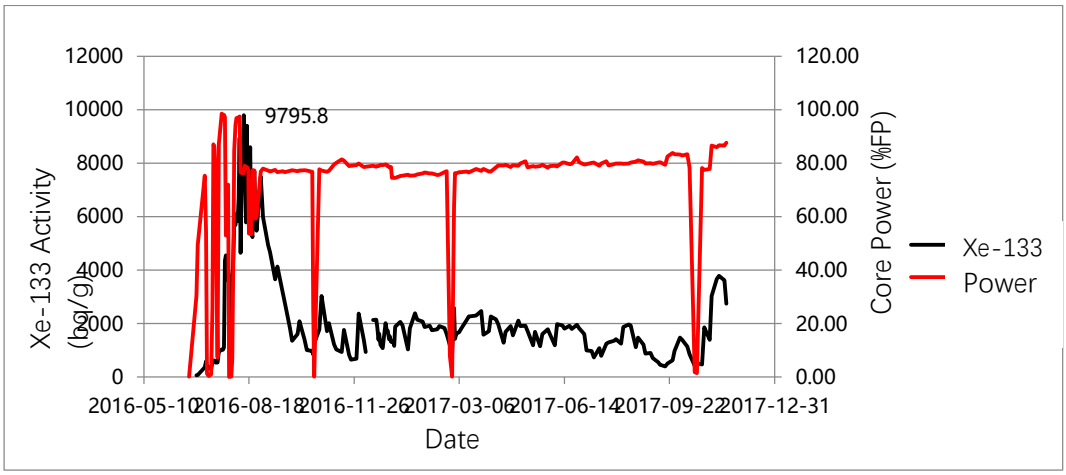

FIG. 2. Xe-133 Trends with power.

2.2 Radiochemical data tracking during operation

During the operation of unit 2, the radiochemical data were continuously monitored. When the power changed, the radiochemical data fluctuated slightly. The overall data I_{eq}-131 (instantaneous specific activity of equivalent of iodine-131) was less than 10 MBq/t and ∑gas (total instantaneous specific activity of inert gas including ^{85m}Kr, ^{87}Kr, ^{88}Kr, ^{133}Xe, ^{135}Xe, ^{138}Xe) was less than 2000 MBq/t. According to the provisions of "instantaneous radioactivity limit value of primary circuit in power operation state", as shown in the Figure 3, the current unit is in the power operation area (the limit value of this area is Ieq-131 < 4440) MBq/t, ∑gas＜370000 MBq/t）.

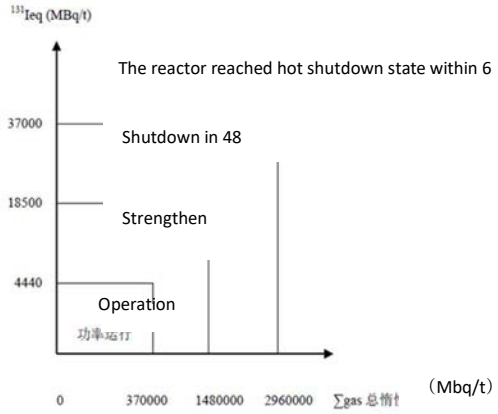

FIG. 3. Instantaneous activity limit of primary circuit in power operation state.

In view of this situation, the power plant staff took the following measures according to the requirements of regulations and procedures:

— The frequency of radiochemical data sampling and analysis in the primary circuit is adjusted from twice a week to once a day.
— Continuously analyze the trend of primary circuit radiochemical data.
— The unit power up and down rate was limited to 0.5mw/min.

2.3 Radiochemical data tracking during shutdown

When the unit was shut down for a refuelling outage after the end of cycle life, it was found out that the activity of I-131 increased suddenly and then decreased, with a peak value of about 152bq / g, as shown in Fig. 4.

The monitoring results of radiochemical data under different operating conditions of the whole cycle showed that there was some fuel assembly damage(failure). When abnormal radiochemical data were found during the commissioning and power up period, the company established a "special working group on disposal of damaged fuel assemblies" to promote the work and find the best solution.

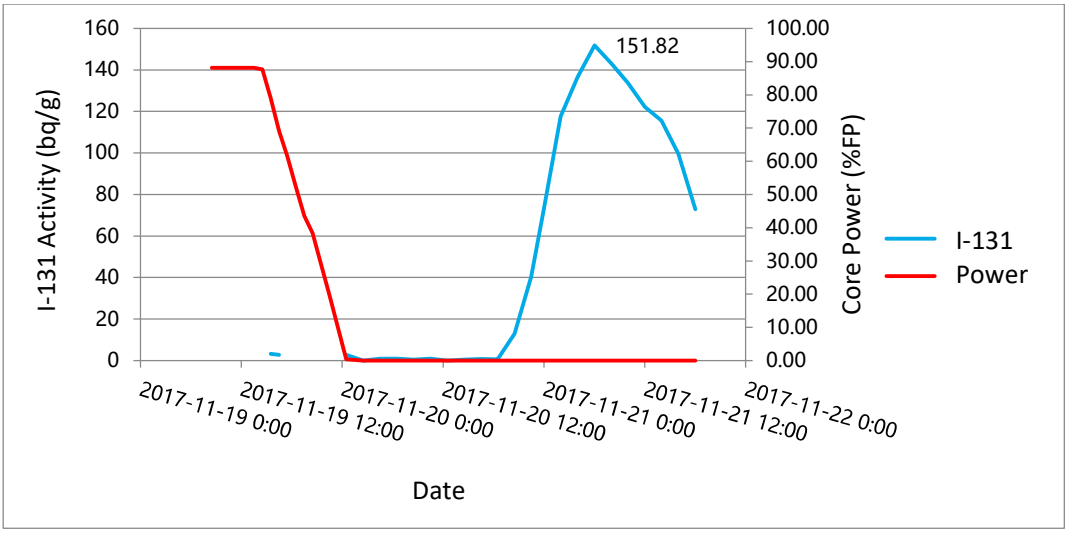

FIG. 4. Trend of I-131 activity during shutdown

3. PROJECT MANAGEMENT

3.1 Investigation and research

A special working group then carried out the investigation on the off-line inspection technology of fuel assembly for domestic nuclear power plants, research institutions and suppliers.

From 2010 to 2016, 34 domestic units experienced 102 fuel cycles (including 23 in the first cycle), and fuel assembly failures occurred in 24 cycles (including the first cycle of 15 units).

Most nuclear power plants in China are not equipped with ultrasonic inspection and repair equipment, that is, they do not have the equipment and ability to repair damaged fuel assemblies. In case of fuel assembly failure, the damaged fuel assembly is usually found out by online sipping inspection and stored in the special storage chamber for damaged fuel. Then, the core loading scheme of the next cycle is redesigned by adopting the emergency refuelling design method. The damaged fuel assembly is basically not repaired and no longer used in the reactor. There is no ready-made off-line inspection equipment for procurement in China. The purchase cost of foreign equipment is high, and the procurement time is long. In addition, the equipment usage and maintenance costs are also high.

3.2 Technical solutions

To effectively avoid the washout (dispersal into the coolant) of nuclear fuel caused by fuel assembly damage during unit operation, it is necessary to find the damaged fuel assembly during shutdown maintenance and repair the fuel assembly that needs to be returned to the reactor in the next cycle.

Mobile ultrasonic inspection equipment and mobile off-line sipping inspection equipment are the mainstream inspection equipment for damaged fuel assemblies at home and abroad. Based on the previous investigation and comparison from the aspects of supply, operational experience, equipment characteristics, procurement costs, etc., it was finally decided to introduce ultrasonic inspection equipment in the form of cooperative research and development with China Nuclear Power Operation Technology Corporation， LTD., and simultaneously introduce single rod replacement and repair equipment.

3.3 Equipment development

Hainan Nuclear Power Co., Ltd. and CNPO jointly established a special working group. In 2016, the first self-developed ultrasonic inspection device in China was manufactured. In February 2017, the first independently developed single rod replacement and repair device in China was completed. In April and June 2017, the ultrasonic inspection device and single rod replacement and repair device completed the field verification test in Hainan Changjiang nuclear power plant unit 2. In June of the same year, the equipment qualification was completed.

3.4 Procedure's development

Since the plant first encountered a fuel assembly failure event, there was no experience in this work.

The power plant communicated with the design unit, equipment R & D unit and peer experts for many times, combined with the experience feedback of field simulation test, from the aspects of risk identification and prevention and on-site operation implementation, a series of procedures and documents were prepared to support the implementation of field work, effectively avoiding the occurrence of various accidents. The relevant procedures are as follows:

— Site operation procedures for ultrasonic inspection of damaged fuel assemblies.
— Risk analysis and plan for ultrasonic inspection of damaged fuel assembly.
— Ultrasonic inspection procedure for damaged fuel assembly.
— Operation manual of single rod replacement equipment.
— Single rod replacement technology research site implementation quality plan.
— Risk control and emergency response plan of single rod replacement.
— Implementation plan for ultrasonic inspection and repair of damaged fuel assemblies in Hainan Changjiang nuclear power plant.

After the personnel, equipment, documents, and a series of work are ready, unit 2 carried out on-site implementation work.

4. ON SITE IMPLEMENTATION

4.1 Fuel assembly inspection

4.1.1 Online sipping detection during unloading stage

During the unloading period of 201 outage in 2017, the online sipping was carried out on all 121 groups of unloaded nuclear fuel assemblies. According to the inspection results, no damaged or suspected to have been damaged fuel assemblies were found. The detection data is shown in the Figure 5, and the judgment basis is as follows:

— Sipping factor ≤ 1.3, no damage.
— $1.3 <$ sipping factor ≤ 3, is suspected damage.
— Sipping factor > 3 means cladding break.

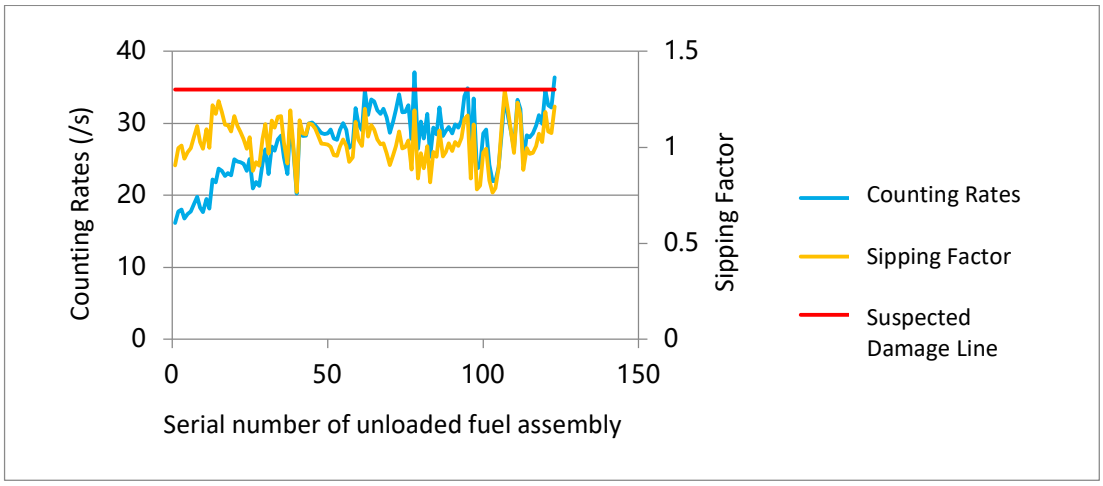

FIG. 5. Results of online sipping inspection of 121 groups of unloaded fuel assemblies.

4.1.2 Ultrasonic examination after unloading

The main working principle of ultrasonic inspection of damaged fuel assembly is to put the ultrasonic probe (including transmitter and receiver) close to the end of fuel rod from axial direction or insert it into the gap between fuel rods on each line of fuel assembly and send ultrasonic wave to fuel rod. The amplitude of reflected wave (or echo) will be affected by cladding defect or water in fuel rod. It can be used to determine whether the fuel rod is damaged. If the fuel rod is damaged and leaking, and the fuel rod is filled with water, in which case the reflected ultrasonic signal will be greatly weakened; if the fuel rod cladding is intact, the ultrasonic receiver will measure a strong ultrasonic signal.

For the simulated fuel assembly, the wet sand provides energy leakage path for plate wave propagation, so the amplitude of plate wave echo received by wet sand loaded fuel rod (wet sand is attached to the inner wall of the fuel rod cladding) is lower than that of normal fuel rod; meanwhile, the diameter of guide tube is 12.45mm, which is larger than that of fuel rod (9.45), so the plate wave propagation distance is far in the guide tube, and the guide tube signal can be clearly distinguished by B-scan signal. The wet sand loaded fuel rod, normal fuel rod and guide tube can be clearly distinguished by observing the plate wave echo signal in the B-scan image of each probe [1].

During the assembly inspection, the ultrasonic probe is inserted into the fuel rod gap of the fuel assembly from 0 ° direction, as shown in Fig. 6. Then ultrasonic measurement was carried out, and the feedback signal was formed into the ultrasonic inspection effect diagram, as shown in Fig. 7 and Fig. 8. The abnormal ultrasonic image was obviously visible at the Red Square mark in Figures 7 and 8, which was interpreted to be due to the fuel rod breach and subsequent the primary coolant ingress into the fuel rod.

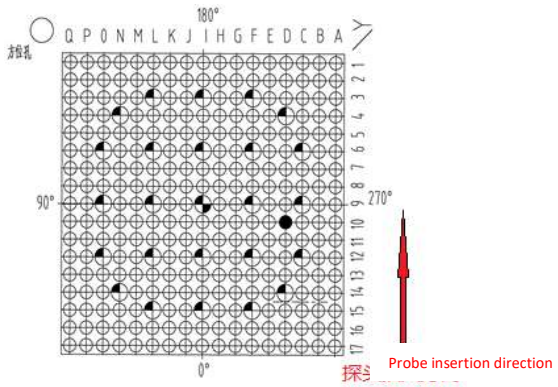

FIG. 6. Schematic diagram of ultrasonic probe insertion from 0 ° direction.

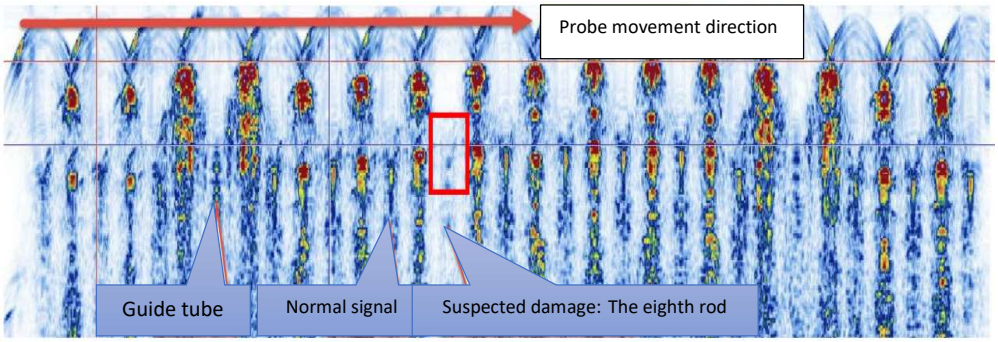

FIG. 7. B-scan signal diagram of fuel assembly YQT 04r fuel rod (inserted at 0 ° direction, 30mm above the first layer grid).

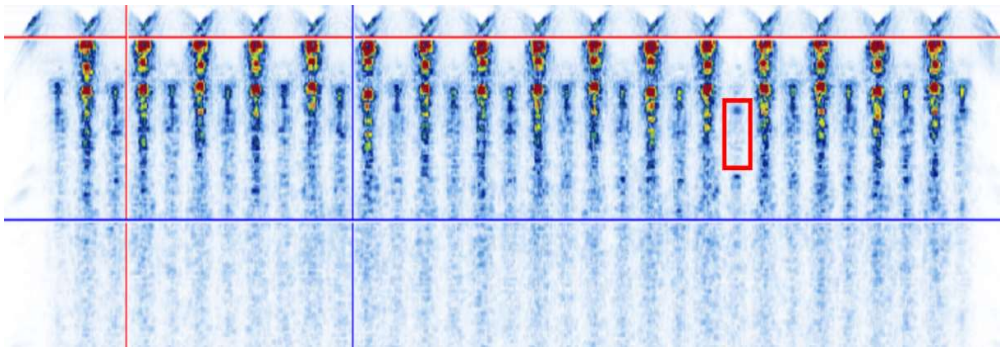

FIG. 8. B-scan signal diagram of fuel assembly YQT 01d fuel rod (inserted in 0 ° direction, 30mm above the first layer grid).

According to the results of ultrasonic inspection, it is determined that there are two fuel assemblies damaged. The relevant information is shown in the table 1, and the assembly location is shown in Figure 9, with thick red edge around the respective cells.

TABLE 1. DAMAGED FUEL ASSEMBLY INFORMATION

Serial number	Assembly number	Enrichment	Core location	Spent pool location	Damaged rod location	Remarks
1	YQT04R	2.6%	K09	I18	D10	Need to be returned to the reactor
2	YQT01D	1.9%	E05	O4	Q05	No need to return to the reactor

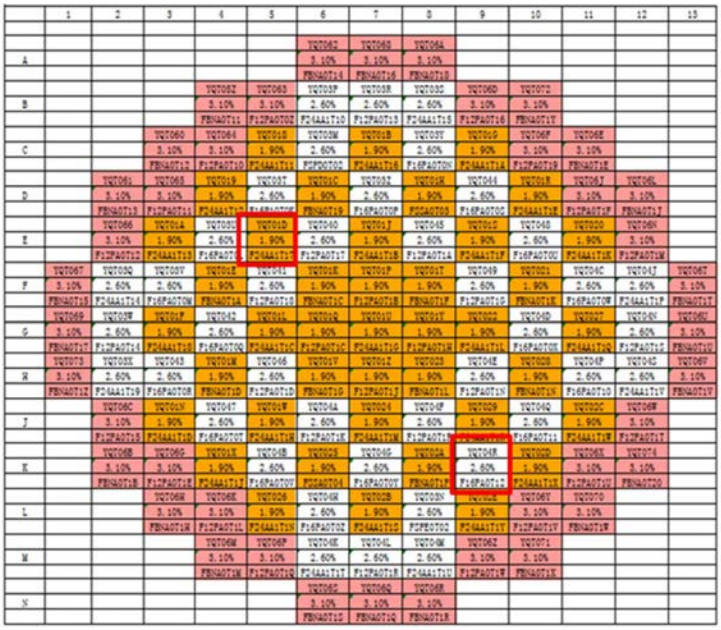

FIG. 9. Location of damaged fuel assembly core.

4.2 Repair of damaged fuel assembly

When the damaged assembly was successfully located, it was less than 20 days before the planned start-up of the reactor. The four on-site standby assemblies contained fuel with enrichment of 3.1%. Compared with YQT04R, which was planned to be used in the second cycle, the enrichment was higher. At that time, the start-up emergency refueling design could not meet the outage duration requirements. After communication with R & D department, industry experts and regulators, the company finally decided to replace and repair the single failed rod. Representatives from the design company and the fuel manufacturer witnessed the repair process on site. In addition, YQT01D, which does not return to the reactor in the subsequent cycle, was stored in the spent fuel pool of unit 2.

Before the repair, the integrity of YQT04R upper socket, sleeve screw, lower socket, positioning grid, mixing grid and peripheral fuel rod of YQT04R was inspected by underwater television, and the inspection results were normal. At the same time, visual analysis and judgment should be carried out carefully for the damaged single rod. In case of the following situations, the fuel assembly repair operation cannot be carried out:

— The single rod has been found to be broken into two pieces.
— The damage of single rod is too large, and there is a great risk of fracture and separation into two or more pieces in the process of pulling out the rod.
— The upper end plug of single rod was damaged or missing.
— The grid was seriously damaged.

4.2.1 Repair process

After confirmed the site conditions, the damage rod was not severely damaged and could be replaced, and there was no situation that the above-mentioned could not be replaced. Therefore, the replacement of the damaged single rod was carried out in the spent fuel pool of the nuclear fuel plant. The main process includes:

— Install the positioning tool (as shown in Figure 10).
— Remove the upper socket.
— Pull out the single rod.
— Steel rod insertion.
— Reassemble the upper socket.
— Sleeve screw bulging.
— Remove the positioning tool.

The whole replacement process was carried out in accordance with the operating procedures and risk plan. Finally, the replacement of fuel rods and the storage of damaged single rods were successfully completed.

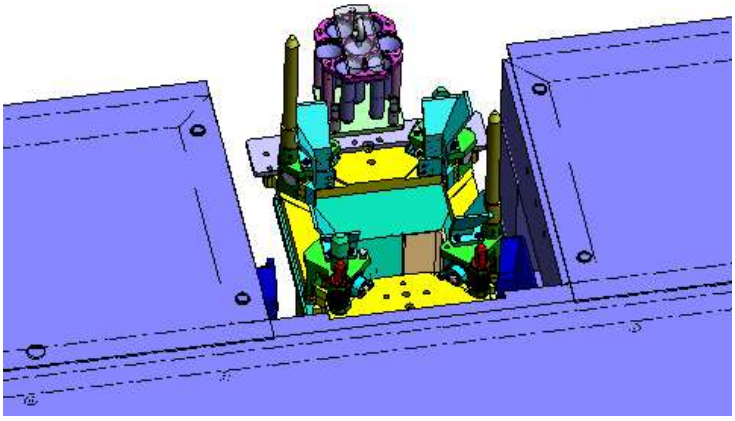

FIG. 10. Installation diagram of positioning tool.

4.2.2 Inspection after repair

After the repair, the fuel assembly was inspected as follows:

— Underwater TV video inspection shows that the structure is complete, and the fuel assembly is normal.
— The pulling and inserting test of control rod shows that the pulling and inserting force is within the limit value, and there is no foreign matter in the guide pipe, which meets the technical requirements.
— Ultrasonic inspection confirms that the damaged single rod has been replaced, and no new damaged rod is generated during the repair of fuel assembly. The comparison of ultrasonic signals before and after repair is shown in Fig. 11.

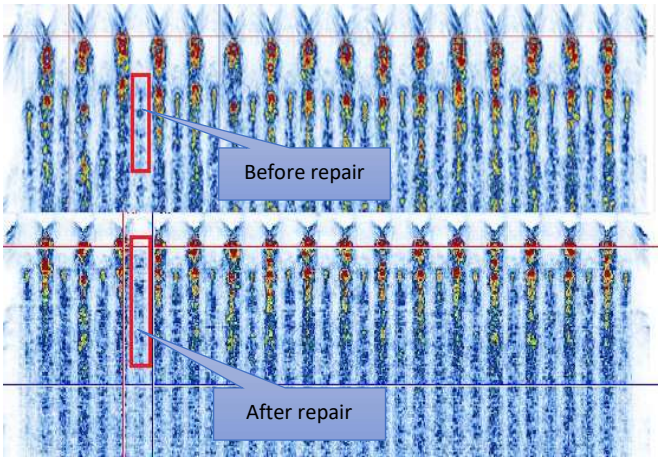

FIG. 11. The comparison of ultrasonic signals before and after repair.

4.2.3 Return the repaired fuel assembly to the reactor

The designer and the fuel manufacturer evaluated the performance of the repaired YQT04R fuel assembly for reprocessing. The opinions are as follows:

— After the fuel assembly is repaired with stainless steel replacement rod, the mechanical properties of the fuel assembly will not be affected, and the structural integrity of the fuel assembly in the reactor will not be affected.
— By comparing the assembly relative power and maximum rod power of YQT04R (the second cycle core position is J09) with the maximum value of the whole core, we can see the YQT04R of the fuel assembly is not located in the thermal assembly of the core, and its assembly power and maximum rod power are far less than the maximum value of the core. The repair of the damaged assembly only involves one D10 fuel rod, which has little impact on the neutronics calculation of the assembly and the core and does not affect the thermal hydraulic analysis results and safety evaluation conclusions.

On February 18, 2018, unit 2 reached criticality after the first shutdown overhaul. The radiochemical data Xe-133 and Ieq-131 of the primary circuit were continuously monitored. No abnormality was found during the whole cycle life. The repaired fuel assembly has good performance.

5. EXPERIENCE AND FEEDBACK

After the practical application of the on-site rod change operation, the following important experiences and feedback are summarized.

5.1 Starting time and duration of rod pulling

The repair time of single fuel assembly is about 5 days, and the pulling out time of single rod is about 10 minutes. During rod pulling, relevant systems in nuclear fuel building shall be available, power supply shall be stable (including crane, lighting, dose monitoring, etc.), and iodine filter circuit shall be started.

5.2 Risk and Countermeasures of rod pulling

The damaged fuel rod should be evaluated before pulling out the rod. Considering the fracture risk of the broken rod, the pulling force is monitored and the limit value is set. At the same time, the radiation risk of personnel should be considered, and the number of people on site should be strictly controlled. In case of abnormal situation, emergency evacuation should be carried out.

5.3 Peak-load regulation

After suspected fuel damage in the core, combined with the operation data of the unit and after discussion among various disciplines of the company, the unit still participates in peak load regulation, but the rate of unit power increase and decrease will be limited to 0.5mw/min.

5.4 Precautions and exception handling during rod replacement

— During the operation, special personnel should be assigned to observe the operation status at each key position. In addition, the observation and operation personnel can stop the operation at any time, and the operators at other positions should stop all the operations immediately.
— According to the above operation steps, the next operation can be started only after the status of each step is confirmed to be normal.
— During the test, always pay attention to the display value of the hook scale under the crane and monitor the equipment status in the video.
— There shall be two or more personnel on site familiar with the operation process, one of whom is the commander in chief. Other personnel supervise the operation process to avoid human error.
— The site should strengthen the control of foreign matters, and all tools should be equipped with anti falling measures.

— During operation, after the tool is hung on the tool rack, the hook on the hanger shall be used to lock the tool lifting ring to ensure there is no risk of loosening, before the tool is taken out, the hook shall be unlocked.

5.5 Procedure and management

In addition, the nuclear material account and control management system and nuclear fuel management system of the plant have been upgraded to make them consistent with the actual situation on site.

Considering all kinds of factors that cause fuel assembly damage, in addition to the assembly production and manufacturing process, the biggest influence factor in the process of power plant operation is foreign matters in the core and spent fuel pool. Therefore, the power plant revised the management procedure of foreign matters prevention and strengthened the management of foreign matters prevention in nuclear fuel building.

6. BENEFITS

6.1 Economic benefits

Hainan Changjiang nuclear power plant unit 1 and 2 canceled the original off-line sipping detection device, reducing the construction cost of about 12 million yuan.

In this project, a group of fuel assemblies that must be returned to the reactor were repaired. Due to the symmetrical layout of the reactor core, the loss of four groups of fuel assemblies that could not be returned to the reactor was recovered, and the loss of nuclear fuel was directly recovered about 16 million yuan. The implementation cost of the management strategy optimization includes equipment research and development, field service, technical support, etc., with a total of about 3.7 million yuan. That is to say, the implementation of this project has produced economic benefits of more than 12 million yuan.

6.2 Social benefits

The successful implementation of the optimization project of failed fuel assembly management strategy has realized the localization of fuel assembly ultrasonic inspection equipment and repair equipment, which has made a positive contribution to the national nuclear power autonomy; the off-line inspection and restoration of damaged components are completed in a single overhaul, which is the first case in China, and provides a new disposal scheme for subsequent domestic damaged fuel assembly management. In the past, once the fuel assembly is damaged, only the emergency refueling core design and safety assessment can be used, so as to increase the way to solve the damage disposal for the power plant; a set of system for the detection, location, repair and return to the reactor of the fuel assembly of nuclear power plant has been established; more than 30 fuel assembly failures have occurred in domestic nuclear power plants, which has strong social benefits.

6.3 Management benefit

In the design review stage of Hainan Changjiang nuclear power plant unit 1 and 2, the relatively backward off-line sipping inspection device was cancelled, which reduced the cost of the power plant. Compared with the original off-line sipping detection device, the imported ultrasonic inspection device has greatly reduced the maintenance and management costs of the equipment.

The damaged assemblies are repaired in one overhaul and returned to the reactor for use, which avoids the risk of long-term shutdown caused by multiple fuel assembly failures in one fuel cycle.

6.4 Prospect of popularization and application

Up to now, more than 30 fuel assembly failures have occurred in China's nuclear power plants. The management strategy optimization project of failed fuel assemblies can be widely used in PWR nuclear power plants and similar nuclear facilities and devices and has a strong application prospect.

7. CONCLUSION

Fuel assembly is the critical component of nuclear power plant reactor. Its main function is to release heat and act as the first barrier of three barriers for nuclear safety. The integrity of fuel assembly and single rod is very important for the safe operation of reactor.

By the end of 2019, there are 47 commercial nuclear power units in China. Based on the actual conditions that millions of fuel rods operate in the reactor every year, although many measures have been taken to reduce the failure rate of fuel assemblies in the design, the fuel assemblies will inevitably be damaged during operation due to the influence of foreign matters in the primary circuit and minor defects during fuel rod manufacturing. Based on the increasing number of nuclear power units in China, the number of damaged components has increased in recent years.

Through the inspection and repair of the damaged fuel assembly during the overhaul of the nuclear power unit, the damaged fuel assembly can be immediately repaired and returned to the reactor for reuse, so as to avoid the delay of the overhaul period caused by the temporary change of the refueling design, and effectively increase the generating time of the unit. At the same time, the burnup loss of three groups of assemblies symmetrical to the damaged assembly is avoided, and the fuel cost of nuclear power plant is greatly reduced. In addition, it can effectively reduce the number of damaged fuel assemblies and reduce the cost of spent fuel reprocessing. Therefore, the damaged fuel assembly maintenance system can effectively improve the fuel assembly utilization rate and reduce the operation cost, but also provide an effective guarantee for the safe operation of nuclear power facilities and has a broad market prospect.

REFERENCES

[1] GAN, W., CAI, J., ZHOU, L., ZHU, X., Ultrasonic Inspection of AFA 3G Failure Fuel Rod, J. Nondestructive Testing, **40** (2018) 29−33.

MEASURES TO IMPROVE FUEL RELIABILITY

V. MEČÍŘ
ČEZ, a.s.,
Prague, Czech Republic

J. KLOUZAL, V. MATOCHA
NRI,
Řež, Czech Republic

Abstract

The paper gives description and status of possible measures investigated in order to improve fuel reliability in general and as applied to Temelín NPP during period of last several cycles of operation. These measures are categorized as Design, Manufacturing and Operational with prime focus on Design and Operation. Effectiveness of measures implemented at Temelín NPP is discussed along with possible future steps to improve fuel reliability. Conclusions are drawn based on activities performed during last years within the international project for VVER 1000 focused on approaching zero level leaking fuel and activities performed by Temelín NPP along with its technical support organization NRI.

1. INTRODUCTION

NPP operation safety and efficiency depend on numerous aspects. Safety aspects are strictly regulated by requirements enforced by national regulations and following international recommendations and in NPP operation they are number one. To operate NPP efficiently, in addition to safety, other aspects need to be properly considered, of highest importance being fuel reliability during normal operation. Fuel reliability can be considered from different points of view by its consequences, or by corresponding phenomena, affecting it at different stages of fuel assembly life cycle.

Although the fuel is designed to not fail even during abnormal operation, tested and manufactured to highest standards, handling and operation is within limits specified by design, some fuel failures during normal operation occur. Fuel reliability nowadays is most frequently degraded by fuel failures like loss of fuel cladding tightness with consequent operational restrictions e.g., limitation of power changes demanded by grid, increase of maintenance costs due to extensive fuel inspection, decontamination, etc.

Except of 3 fuel assemblies leaking at very beginning of the first full core loading at Temelín NPP unit 1 in 2010, failure of which was attributed to manufacturing reason, there were no fuel assemblies identified as leaking after first 3 cycles on both units. Furthermore, in subsequent cycles, no once burned fuel assemblies were identified as leaking. Most of leaking fuel assemblies were identified as three times burned.

To understand root causes of such fuel failures, especially when failed fuel rod removal and inspection as well as detail data from operational transients are not available and it is in principle impossible to determine at which fuel assembly failed cladding at which time of operation, significant effort is needed. This effort is further burdened by lot of uncertainties, since potential causes may act together, promote one another. In addition, they may emerge either from design, manufacturing, or operation stage or all of them together due to cliff edge effects, unexpected margin consumption.

2. POSSIBLE MEASURES

During Temelín NPP fuel design, manufacturing process and operation evaluations, started in 2014 when coolant activity indicated more than one leaker in unit 1 core, no obvious omissions or violations were revealed. Nevertheless, it is worth to keep in mind the following remarks.

2.1 Design evaluation

It is important to consider as part of fuel design stage comprehensive fuel handling, core design and core operation criteria, requirements, and recommendation. At the same time clear distinction between criteria,

requirements and recommendation for operation shall be reflected in the fuel design stage. For successful fuel design, in addition to fuel designer`s knowledge, extensive experimental database and testing facilities, a perfect understanding of operating environment is needed. Operating environment essentially includes plant design data NPP along with its proper interpretation, but not only.

The topic of the fuel rod design criteria is currently complicated by the worldwide decline in the irradiation capabilities in the material test reactors. While the optimization process, especially for the fuel cladding zirconium-based alloys, is ongoing to improve the fuel cycle economy, the potential for mass scale testing of the new products is decreasing. Although there is a drive to replace the quantity of the experimental data generated by “advanced modelling”, it may be dangerously misleading to rely on few data points only. For example, the extent of the pellet–cladding mechanical interaction has been studied on-line in some of the OECD Halden Reactor Project experiments by evaluating the cladding elongation resulting from the mutual interaction with the fuel stack. These results are valuable, but when we look at the elongation of the fuel rods irradiated in the commercial reactor, significant spread of the elongation is observed even for the neighboring rods in one fuel assembly, which were irradiated under nominally similar conditions. Therefore, it was impossible to tune computational models based on single or few experiments only and our fuel-cladding friction model was therefore statistically validated with the Temelín data. While conservative approach is suitable for safety demonstration, it is not enough for detail investigation of the reason for fuel failures during normal operation. For the sake of understanding of the reason for such spread in measured data it is important to understand what the contribution of the measurement technique is and what are the other reasons for such spread of the experimental data to be able properly account for them in Best Estimate (BE) models.

Very important turned out to be good knowledge of operational (including maintenance) practices for at least two reasons, as follows: a new type of fuel will be operated in a mixed core alongside the previous old fuel type and, but operational instructions do not cover all cases of operation, or even for some cases alternative approaches are recommended and one of them may be preferable for some operational reasons. This aspect appears to be even more important in connection with Core Monitoring System (CMS) features and capabilities, e.g., pin power reconstruction is adjusted based on the In-core Rhodium Self Power Detectors (SPD) signals, while the core control strategies are defined via Axial Flux Difference (AFD) control based on ex-core ionization chambers at given positions of control groups in core. As example may serve:

— Core power distribution control and local LHGR change rate. To make sure that fuel rod reliability is justified properly, the above may be addressed in different way, e.g., design restriction on Rod Cluster Control Assembly (RCCA) movement, in reload core design criteria built in additional margin, specific reload core design methodology.
— Reload core design shuffling schemes with or without rotation of fuel assemblies because of different goals, such as fuel economics, optimized reactor pressure vessel fluence, avoidance of radial power distribution anomaly.

Since coolant activity indicated first leaking fuel shortly (10-60 EFPD) after startup, in the fourth cycle and following cycles in both units, it is reasonable to consider not just position of fuel assembly relative to positions of control banks but their positions in previous cycle too to evaluate possible effects of operational transients on fuel failures. Figures 1–3 provide summary on the number and distribution of fuel failures in twice, three times and four times burned assemblies and statistics relative to the control bank position. Among leaking fuel assemblies, 4,5 % of them were operating in current cycle under control banks, 13,6% were not operated under or next to control banks position in current and previous cycle at all, 15,9 % were operated in previous cycle under or next to control banks positions, but not in current cycle, 25% of them were operated in current cycle next to control bank positions but not in previous cycle, 29,5% were operated in current and previous cycle next to bank positions and 11,4% were operated next to, but in previous cycle under, control bank positions.

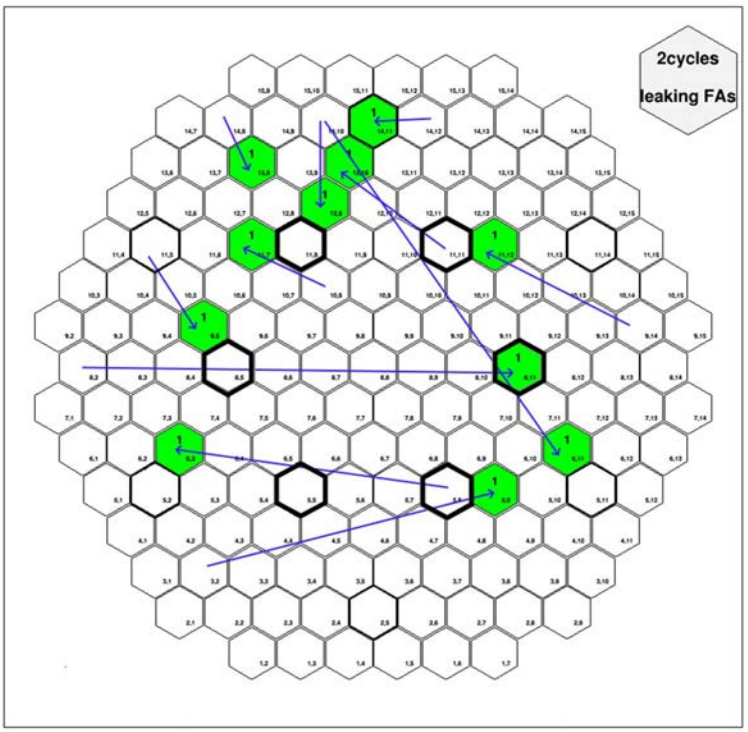

FIG. 1. Failures after 2 cycles of FA operation relative to control banks 10 and 9.

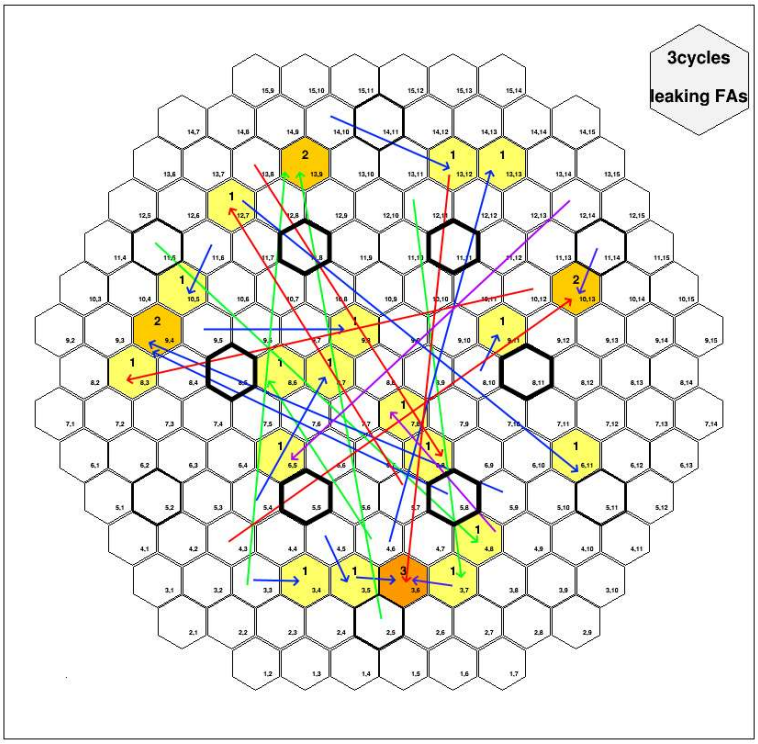

FIG. 2. Failures after 3 cycles of FA operation relative to control banks 10 and 9.

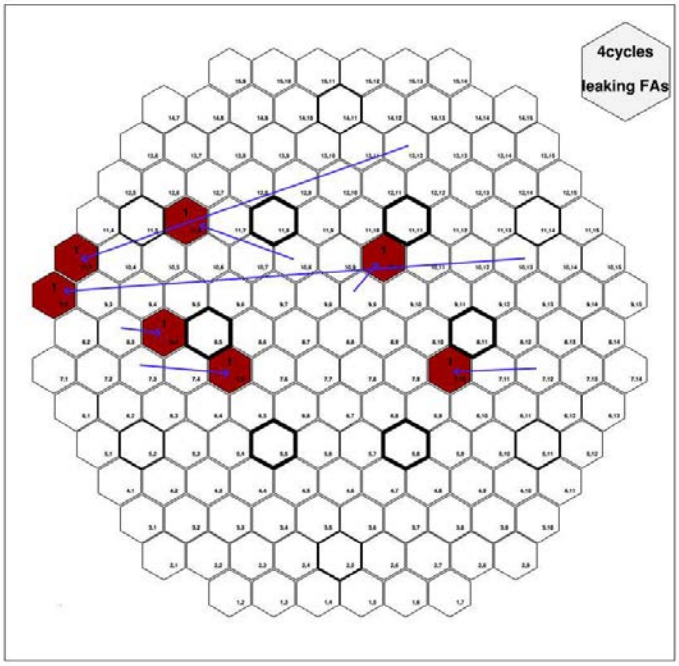

FIG. 3. Failures after 4 cycles of FA operation relative to control banks 10 and 9.

These figures show that most leakers appeared to be in fuel assemblies operated for 1 or 2 cycles close to control banks; however, 13,6% of failed fuel assemblies were not operated in current and previous cycle close to control banks at all. It follows that no conclusion can be drawn unambiguously with respect to debris or core power distribution control during operation as being the most likely the root cause of failures.

A study on relation between of single fuel rod axial offset and axial offset (AO) computed based on in-core SPD and 3-D power reconstruction was performed. From this study follows that there is strong correlation between core AO and highest power fuel rods AO with the following tendency. It was shown that starting from AO of 5 % and more, 95 % of the most of highest power fuel rods exhibit AO less then core average AO, the corresponding difference being higher the higher the AO is. On the other hand, when core average AO is about 0%, the single fuel rod AO can be higher, which needs to be properly accounted for in AO penalty development. Core average AO based on the ex-core detectors, taking in to account its periodical calibration to the AO based on in-core power distribution, is adequate parameter for axial power distribution control.

The difference between local power distribution and AO based on ex-core detectors does not seems to be cause for fuel failures during normal operation. However further studies on comparison of operational transient on units with higher and no fuel failures are ongoing.

The CFD analyses performed at ÚJV have focused on the impact of the fuel assembly deformation on the cladding temperatures and the fraction of steam in the coolant, Figs 4 and 5. The obtained results indicate that although the cladding temperature is not significantly affected by the rod-to-rod or rod-to-angle rail contact (due to azimuthal heat transfer through the cladding), the steam fraction rises rapidly in the affected areas. Such conditions would result in increased corrosion and hydrogen pick up. The fuel reliability is therefore a combined result of both fuel rod and fuel assembly design. Ignoring the global (fuel assembly, core-wide) effects and focusing only on the fuel rod in isolation may result in a systematic occurrence of certain types of fuel failures that stem from global effects (at Temelín this was the case with the VVantage-6 fuel which showed degraded resistance to the grid-to-rod fretting and also with the 1st generation of the TVSA-T fuel for which there seems to be a correlation between the fuel assembly deformations and the occurrence of the fuel failures).

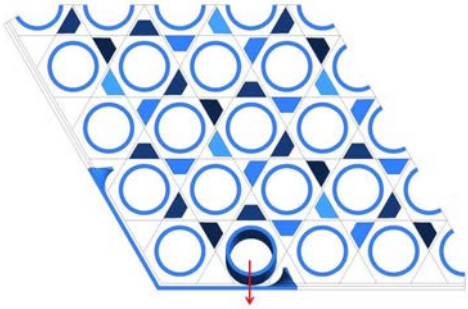

FIG. 4 Calculation domain of the CFD evaluation of the impact of the fuel rod bowing, red arrow indicates the deformation of the fuel rod towards the corner rail of the fuel assembly (L. Vyskočil, V Železný: CFD Simulation of Flow and Heat Transfer on Bent Rods Behind Corner Plate in TVSA-T Fuel Assembly, UJV Řež).

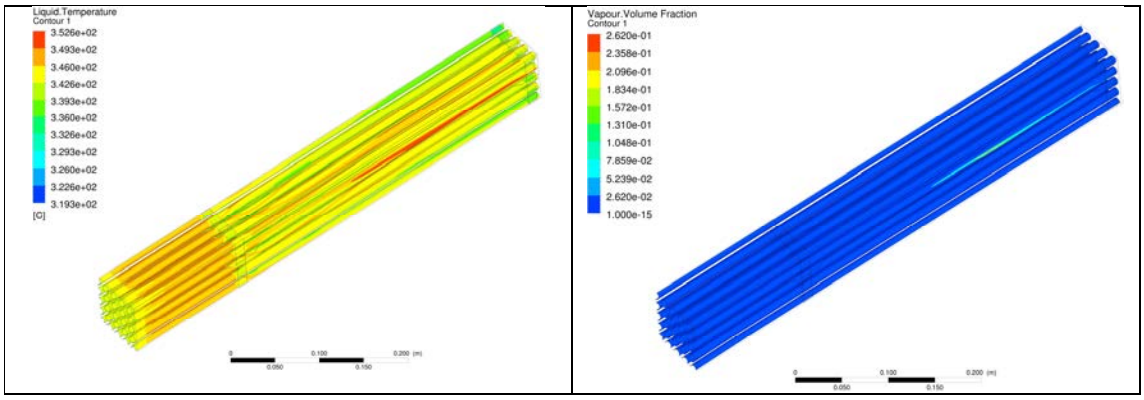

FIG. 5 Calculated impact on the cladding temperature (left) and steam fraction (right) in the deformed assembly (L. Vyskočil, V Železný: CFD Simulation of Flow and Heat Transfer on Bent Rods Behind Corner Plate in TVSA-T Fuel Assembly, UJV Řež)

Another investigation performed at UJV of factors potentially contributing to fuel failures was in connection with increased stresses resulting from fuel rod bow. This included evaluation of the of scratches or potentially unidentified flaws on the cladding inner surface, pellet-cladding misalignment, and azimuthally non uniform heat transfer. These were found to not be significantly contributing to potential fuel failures as a root cause.

To the maintenance area practices which need to be properly addressed during design phase belong the capabilities and accuracy of fuel assembly and upper internals positions in reactor vessel measurement. These parameters along with proper understanding of core coolant minimum and maximum flowrate and distribution including measurement accuracy significantly affect the FA mechanical design and limiting parameters for operation and maintenance. The FA hold down force essentially affects FA structural stability and consequently RCCA drop time, but it may contribute to fuel rod failure too. They were reviewed and no potential for fuel failures was revealed.

In the fuel design phase, the independent design evaluation at all design steps is important for several reasons. It helps better interpretation and understanding of plant practices and better understanding of the design criteria and their justification but not only. As important and useful for understanding and resolution of eventual fuel failures, which may occur during normal operation, showed up alternative approach to design criteria evaluation and justification based on latest experiments. Beyond standard (based on previous designer`s experience), design scope evaluation showed up useful too.

2.2 Manufacturing process evaluation

Different VVER 1000 units operate different fuel assemblies from the same supplier, but of different designs, with different number of spacer grids, which are also different in some details; therefore, there are significant differences in manufacturing process.

It was noticed that process improvements are implemented step by step. At the stage of manufacturing the customer audits are very important along with the independent customer representatives witnessing the manufacturing. This process is well established.

There was a case when, during receipt inspection of a fuel batch in fresh fuel area at Temelín NPP a suspect appearance of fuel rod cladding was identified. Subsequently, in consultation with the fuel supplier it was concluded that the noticed fuel assembly appearance meets all criteria and following its loading into core operation was successful as failure was revealed so far.

2.3 Operation evaluation

Operational results only are the true measure of the fuel reliability, giving under real operating conditions the integrated feedback on design and manufacturing excellence, under the assumption that all the operational conditions prescribed by fuel design are observed. These conditions can be characterized as fuel handling and storage, reload core design and safety evaluation, core operation including operational transients, core monitoring and FA monitoring.

The criteria, conditions and guidelines for fuel handling and storage are strictly observed except of case, when supplier was asked to assess suitability of fuel assembly for operation. After given fuel assembly repair in fresh fuel area, it was successfully operated for their entire scheduled lifetime - no failure was revealed.

The criteria for reload core design and reload safety evaluation are easy to follow and for all fuel assembles loaded into core were met in all cases.

The core operation criteria and its monitoring including peaking factors, AFD, power change rates, number of transients, coolant specification etc. were met in all cases too.

As a part of the root cause investigation retrospective core-wide calculations of the fuel rod behavior, using the reconstructed power histories, were performed after each cycle with fuel rod failures, Fig. 6. No violations of the fuel rod design limits were revealed. Also, it was evident that the rods located in the leaking fuel assemblies were not the limiting ones considering the stresses in the cladding.

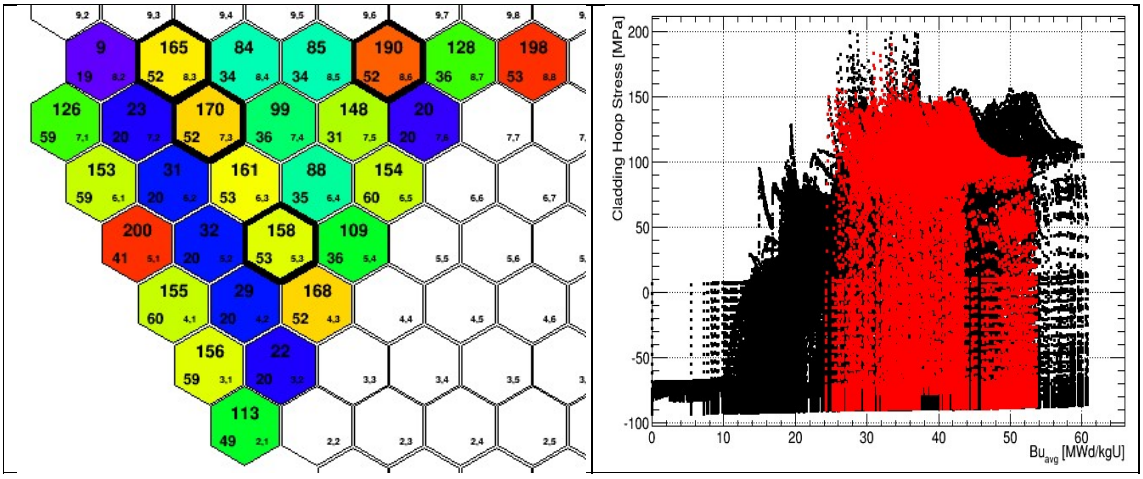

FIG. 6. Example of the analysis of the cycle with leaking fuel assemblies at Temelín NPP – calculated peak cladding hoop stress in leaking (red) and intact (black) fuel assemblies as a function of burnup are shown on right, map of the core with peak hoop stress per assembly on left.

According to NPP design specification coolant is supposed to be free of foreign materials.

Tremendous attention is paid to FME activities, but one can never be 100% sure that some of foreign materials (FM) are not present in coolant during operation. This unfortunate reality is addressed by fuel assembly

design by introduction of Anti Debris Filters (ADF) of different design with different efficiency, but always resulting in increase of necessary fuel assembly hold down forces. These ADF can however protect fuel rod cladding against debris entering the bottom nozzle, but not from those which may enter the bundle through other eventual paths as technology holes in core support plate, those debris, which may reside at core support plate or from the top of the core during outage. For these reason at the operation stage, it is wise to further improve FME approaches. Categorization and possible ways of falling FM into FA was developed to further promote the maintenance staff better understanding of the importance of FME and reporting of FM identified and to support the analysis of the sources of FM identification.

To be able in timely manner identify and remove eventual FM threating the fuel cladding integrity as well as to reveal those FM which unfortunately appeared to be in the primary circuit during operation, the approach of full core offload during outage for refueling is adopted at Temelín NPP. This approach in addition to full core offload includes as much as possible primary circuit pipelines flushing before core loading and scheduled special FM search inspections in the following outage stages:

- S1: Before FA unloading (shortly after upper internals removal) from reactor.
- S2: After FA unloading from reactor.
- S3 Before FA loading into reactor.
- S4 After FA loading into reactor (shortly before upper internals and vessel lid installation.

All FM/debris at each of these stages are reported and removed except of those which are firmly stacked in position, from which it is not impossible to remove it. Such position is then subject to inspection during next stage and next outages. In all cases such FM did not change the position. The FM revealed at S1 and S2 stages then represents FM unidentified under FME guidelines during previous outage maintenance activities and/or appeared because of some of components wear/failure during operation. The FM revealed at S3 and S4 stages represents FM identified under FME guidelines in current outage in the reactor cavity, but typically may be because of lack of identification of FM under FME guidelines in different then reactor cavity nuclear island maintenance activities. Since sequence of maintenance activities on both units in different outages are not identical, it will not be rigorous to judge effectiveness of FM exclusion activities with respect to potential for fuel failure based on changing ration of FM identified. It is however possible to conclude that the trend indicates improvements after introduction of the new position - FME coordinator.

In addition to such evaluation, an investigation was performed on eventual correlation between maintenance activities such as e.g., steam generator tubing plugging and number of cladding failures in following cycles. No correlation was revealed at Temelín NPP.

In such a way, thorough reporting, recording and analysis of FM found at the above indicated stages of outage at the same time allow assess effectiveness and probability debris to be a cause of fuel failure. Based on the analysis of FM revealed during the above outage stages, the FM revealed during first 3 cycles of operation when no fuel failure was revealed in comparison to cycles starting form forth, the current FME approach seems to be effective and probability of debris to be a cause of cladding failure seems to be very low.

As an important part of outage activities are the fuel inspections. The current Mobile Fuel Repair and Inspection Equipment (FRIE) installed for the inspection purposes in GA 402 (B04) fresh and spent fuel containers pit allows in principle to inspect not just Fuel Assembly but Fuel Rod too. Location of FRIE in GA 402 pit however is posting numerous restrictions on its use. In case of unscheduled activities due to problems with fuel rod manipulation e.g., break, top nozzle reinstallation, there are very high risks of outage extension. Due to this fact FRIE is for many outages used for fuel assembly visual and geometry inspection only. Number of assemblies inspected ranges typically from 7 to 20 and includes all fuel assemblies identified as failed and some not failed with different burnup. For the above disadvantages of FRIE, it is scheduled to be replaced by newly design “SIPS” in spent fuel pool B02 in 2021 outages. The new concept (Fig. 7) will allow to increase number of fuel assemblies inspected significantly without any negative impact on outage length and scheduling of other outage activities. Since its location and principal design, it is possible to extend in future its functionality to fuel rod inspection and fuel assembly repair - “SOPS” which should allow to locate, remove and inspect failed fuel rod without any threat to outage length and other outage activities.

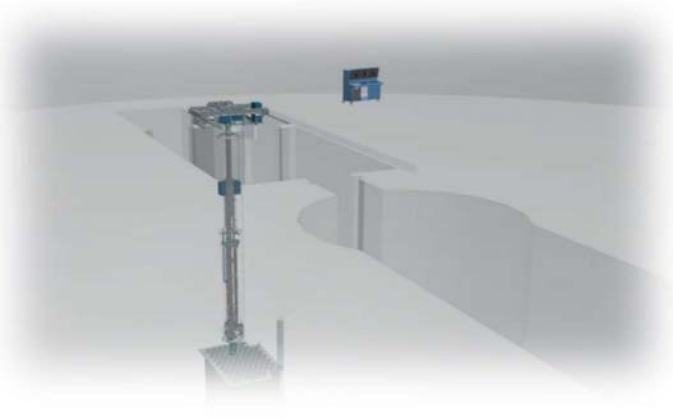

FIG.7. Illustration of new fuel inspection equipment –"SIPS".

Comparing operational result among units in order to reveal possible reason for higher failure rate in some units in comparison to others, one of key points is firm basis for comparison not just form fuel design point of view but from the point of view interpretation of the data provide by plants too. To such parameters in addition to such as upper internals position, coolant reactor and loops flow rates, core inlet and outlet temperatures etc, belong the failure evaluation based on coolant activity during outage and operation. Despite basic principle is the same in all WWER 1000 there are numerous differences in coolant sampling, detectors used, the way how the threshold is established, technology used. It was concluded, after numerous discussions, that known differences may result in different number of leakers detected in given outage, but probably not in total number of leakers detected in two consecutive outages except of those fuel assemblies which are discharged on a scheduled basis without being detected. However further discussion on possible differences in number of leakers detected due to plant specifics are scheduled.

3. CONCLUSION

Investigation of root causes of fuel failures during normal operation is very challenging and assumes that experts from area of design, manufacturing and operation will work together in a very openminded way. Fuel reliability during normal operation is area, which need to be further investigated, to further enhance current models to account for phenomena and fuel assembly components interaction currently typically not explicitly treated in fuel assembly design e.g., influence of number of spacer grids on cladding failure.

To better follow fuel performance during normal operation and help understanding a departure from expected fuel performance the moment when departure starts need to be captured and real operating and manufacturing conditions need to be known in very detail. To register the moment of departure from expected fuel behavior, as a part of the fuel design stage a set of burnup dependent fuel performance criteria is reasonable to be developed. Such fuel performance criteria shall consider plant specific operational and maintenance practices.

A recommendation on set and frequency of core monitoring parameters and its storage may be reasonable to be developed.

ACKNOWLEDGEMENTS

Authors would like to express acknowledgements for numerous discussions to experts participating in international project aimed to achieve fuel failure zero level in VVER-1000 and expert of NRI and Temelín NPP involved in support of the international project.

MITIGATION OF FAILURES BY DESIGN AND MANUFACTURING

(Session 4)

Chairperson

I. ARIMESCU
USA

FAILED FUEL ASSEMBLIES IN EDF PWRS OVER THE LAST 25 YEARS: MAIN CAUSES, MITIGATION AND FAILED FUEL EVACUATION

MARIE MOATTI
EDF, Nuclear Fuel Division,
Saint-Denis, France

THIERRY MEYLOGAN
EDF, Nuclear Generation Division,
Lyons, France

OLIVIER EVESQUE
EDF, Nuclear Fuel Division,
Saint-Denis, France

Abstract

EDF operational experience acquired over the last 25 years in its 58 PWRs in France includes more than 400 failed fuel assemblies. The main failure causes were related to grid-to-rod fretting and exogenous, or fuel-related debris, the latter may have originated in the fuel fabrication processes. The mitigation actions encompass fuel design evolutionary changes, foreign material exclusion measures and manufacturing processes adaptations. A significant decreasing trend on the fuel assembly failure rate has been confirmed over the last 5 years, with an average annual fuel assembly failure rate close to 0.1%. Transport of failed fuel rods to La Hague reprocessing plant is also an important issue for EDF.

1. INTRODUCTION

EDF currently operates 56 PWRs in France; the main features of this fleet with respect to the issue addressed in the paper are summarized in Table 1:

TABLE 1. EDF 56 PWRS

Type of Reactor	Number	Fuel assemblies' length (fissile stack)	Type of fuel
CP0 900 MW	4	12 FT	17X17 UO_2
CPY 900 MW	28	12 FT	17X17 UO_2, 17X17 MOX
P4 1300 MW	8	14 FT	17X17 UO_2
P'4 1300 MW	12	14 FT	17X17 UO_2
N4 1450 MW	4	14 FT	17X17 UO_2

This description considers the fact that two CP0 reactors, namely, Fessenheim 1 and Fessenheim 2, were permanently shut down in February and June 2020, respectively.

2. MAIN CAUSES AND MITIGATION ACTIONS

2.1 Fuel assembly failure rate over the last 25 years for EDF reactors

The evolution of the annual fuel assembly failure rate(*) for the EDF French PWRs is shown below in Fig. 1.

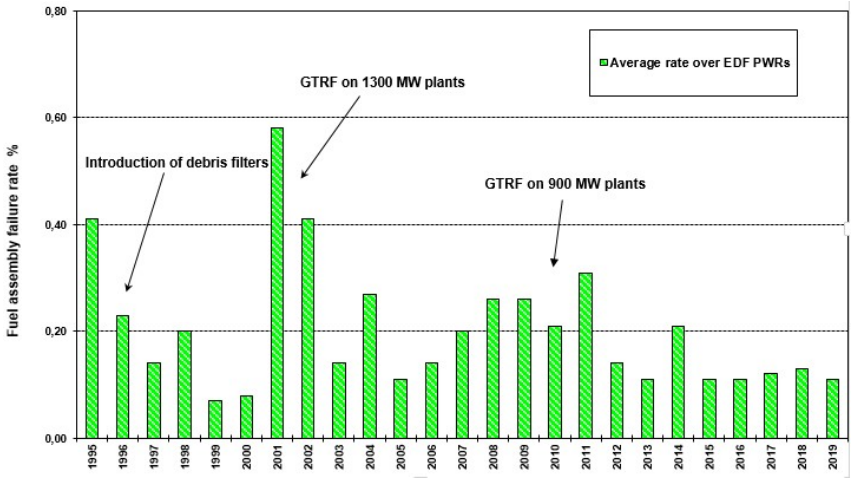

FIG. 1. Fuel assembly annual failure rate for EDF PWRs over the last 25 years.

The main causes linked to more particularly dated period are mentioned in Fig. 1. However, other causes spread in various amounts over the whole period such as debris or fabrication are also involved. The following chapters detail the main causes and the mitigation actions associated to fuel failures at EDF.

2.2 Grid-To-Rod Fretting

Grid-To-Rod-Fretting (GTRF) has been the cause of around 100 fuel assemblies' failures, with roughly 70 failed fuel assemblies in 1300 MWe reactors and 30 failed fuel assemblies in 900 MWe reactors; the most significant events took place in 1300 MWe reactors (Cattenom 3 in 2001 with 28 failed fuel assemblies, containing a total of roughly 90 failed fuel rods, and Nogent 2 in 2002 with 22 failed fuel assemblies). Most leakers were observed during their last irradiation cycle.

2.2.1 GTRF in 1300 MWe reactors

GTRF observed in EDF 1300 MWe reactors occurred at the bottom grid level of fuel rods belonging to fuel assemblies located in the inner periphery of the core, as illustrated in Fig. 2 for Cattenom 3, cycle 8, and Fig. 3 for Nogent 2, cycle 11.

As described in [1], the location of failed fuel assemblies is linked to cross flows at bottom grid level, with high cross flow velocities in the lower part of the fuel assemblies and in the intermediate "ring" of the core; this is consistent with the locations of the leaking fuel assemblies. Mixed cores configurations were shown to be of the second order with respect to flow distribution at bottom grid level, either at core scale or fuel assembly scale.

The grid springs' stress relaxation induced by irradiation creep lowers their holding forces on the fuel rods in the bottom grid, leading to increased fuel rods vibration, which could culminate in fuel rod failure by cladding wear, such as in the case of Cattenom 3 and other 1300 MWe reactors such as Nogent 2. In the case of the 1300

(*) fuel assembly failure rate = number of failed fuel assemblies / total number of unloaded fuel assemblies

MWe reactors, the transition from 12-month cycles to approximately 18-month cycles were a major contributing factor to the failure of many fuel assemblies.

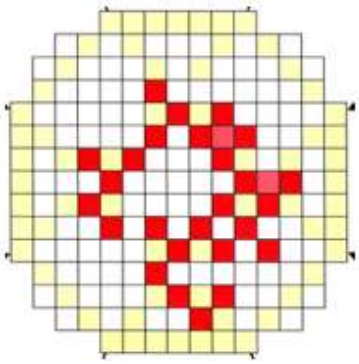

FIG. 2. Failed FAs at CAT308 (red).

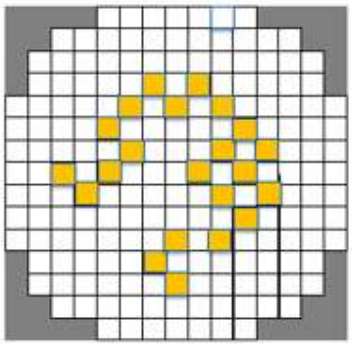

FIG. 3. Failed FAs at NO211 (yellow).

Following the Cattenom 3 GTRF event, several changes were decided, with respect to fuel design and fuel fabrication.

The new fuel assembly design involved an additional grid in the bottom part of the fuel assembly, thus significantly increasing rods' support in this most GRTF sensitive region of the core. Simulations and evaluations performed on this new design [2] convinced EDF about its expected improved performance with respect to GTRF. However, the ultimate demonstration of the adequacy and benefit of the design evolution could only come from operational experience and that needed a minimum of three 18-month irradiation cycles, with on-site rod-wear measurements at the end of each cycle.

The first reload of fuel assemblies with the modified design was loaded in the fall of 2002, and that reload ended its 3rd irradiation cycle at the end of 2006. During the 3rd cycle, some increased coolant primary activity occurred, which led EDF to worry about possible GTRF occurrence, despite the improved fuel design. At the end of the cycle, it was found out that the leaking fuel assembly had been damaged by an operator's glasses! even though foreign material is never welcome, in that case, it was much preferable than having to conclude about the inadequacy of the improved fuel design, 5 years after having selected the design, performed the associated thermo-hydraulic and mechanical tests, and provided the necessary justifications.

Fig. 4 below shows the failed fuel assembly detected at the end of 2006, with arrows pointing to the pieces of the frame of the glasses that caused the leak.

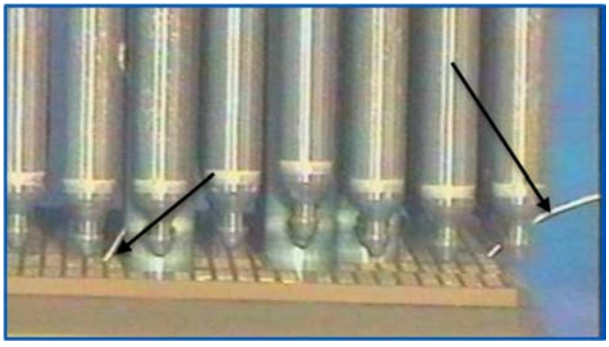

FIG. 4. Failed FA at CAT311.

Pool-side rod wear measurements(**) performed at the end of the 3rd cycle showed a satisfactory behaviour of the improved fuel assembly design, and its deployment in all 1300 MWe and N4 reactors followed that reassuring result. No GTRF has ever been observed since in any EDF reactor on a14-ft fuel assembly.

However, because the new fuel design could not be supplied right away for all 14-ft reactors and given the high stakes in terms of failure rate, a manufacturing improvement was also considered and immediately implemented. For the fuel assembly designs loaded at that time in 1300 MWe reactors, each fuel rod was held in place by two sets of two dimples and one Inconel spring in each cell of the bottom grid. The diminishing evolution of the rod holding force with irradiation is dependent on the initial holding force, which is created by the initial deflection of the spring, as illustrated qualitatively in Fig. 5., in which the lower "tail-end distribution" curve corresponds to the cells with the smaller holding forces (or spring deflections) at BOL.

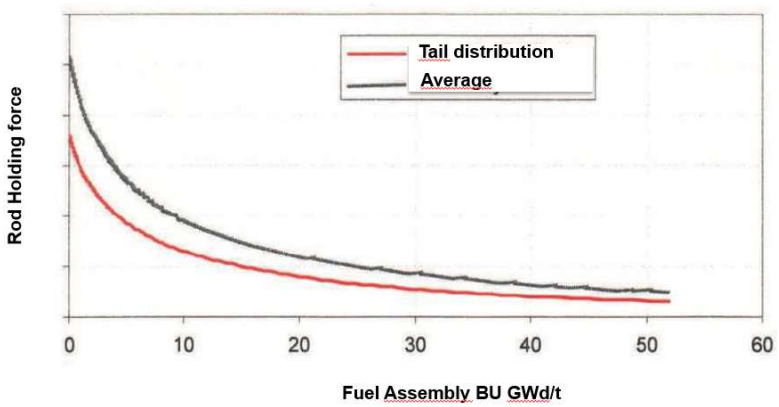

FIG. 5. Evolution of the fuel rods holding forces within a FA with respect to the to the FA burn-up.

The difference between cells at nominal holding force and cells with tail-end holding forces becomes smaller at longer irradiation times. However, tail-end cells are potentially wearing off the fuel rods during a longer time period than cells with nominal spring characteristics.

The fabrication specification was initially expressed in terms of maximum distance between dimples and spring for each dimples-spring couple. The associated criterion was equivalent to a criterion on a minimum spring deflection.

Given the fact that the bottom grid is made of 264 rod cells, increasing even slightly the requirement on manufacturing criteria related to cell characteristics can lead very quickly to unsustainable rejection rates in the manufacturing process. To illustrate that point, a 1% rate of defective cells would lead to more than 90% of defective grids. Thus, relying only on a reduction of the allowed maximum dimple-spring distance appeared prohibitive in manufacturing.

A more complex approach was implemented, considering the coupling effect of some springs between adjacent cells. Springs involved in the holding of the rods are either half hairpin springs (simple bow springs) or full hairpin springs (double bow springs) spanning over the strap between two adjacent cells. An additional criterion was introduced to guarantee a minimum deflection for each bow of full hairpin springs; that criterion took into account the potential asymmetry between the two bows. It was a complex manufacturing evolution that needed a specific adaptation of the grid control equipments. This manufacturing improvement was implemented at the beginning of 2002. It can be emphasized that no GTRF has ever been observed on fuel assemblies with grids controlled with the new approach, which was particularly beneficial during the intermediate transition period preceding the deployment of fuel assemblies equipped with the additional bottom grid.

(**) Wear evaluations rely on wear width measurements performed with a visual exam, and assessing wear depth as a function of wear width depending on the geometry of the involved parts in contact with the cladding (either a spring or a dimple)

2.2.2 GTRF on 900 MWe reactors

GTRF observed on 900 MWe reactors did not appear following a change of core management policy like for 1300 MWe reactors where the transition to longer cycles was one of the involved factors.

In that case, it was triggered by the introduction of a new fuel assembly design, for which high turbulent crossflows excitation at the inlet of the fuel assembly caused high fluid elastic excitation in the bottom part of the rods located at the periphery of the fuel assembly, with some rod's locations clearly more impacted than the others.

Contrarily to what had been observed on 1300 MWe reactors, no correlation was identified with specific locations of the fuel assembly within the core; leakers were observed both in the central part of the core or in the inner boundary of the core periphery. No correlation was identified neither with primary flow levels nor with mixed cores configurations.

All those trends could be confirmed with CFD calculations.

The introduction of an additional grid and the subsequent span adjustment (shorter span from the bottom grid to the first mid-grid) has eliminated the GTRF leakers on the 900 MWe plants.

2.3 Debris fretting

Debris has been significantly mitigated with the introduction of debris filters in all fuel assembly designs in the 90's. However, debris fretting is still a potential cause for fuel assemblies' failure.

Some debris can come from the fuel assembly itself, and in that case the mitigation relies either on a fuel design upgrade, or on changes in the fuel manufacturing process; for instance, as described in [3], Irradiated Assisted Stress Corrosion Cracking (IASCC) of Inconel cell springs led to the rupture of some springs, which then became debris. The use of material significantly less sensitive to IASCC crack initiation has been implemented.

For exogenous debris, foreign material exclusion (FME) is a constant concern and relies on the following actions:

— Actions on FME hazard work area: establishment of boundaries, maintenance of a clean and tidy work area.
— Inspection performed to ensure that no foreign material ingress has occurred.
— Securing tools and personal protection equipment.

Also, the identification of debris at different locations relies on reinforced televisual inspections performed during outages. Retrieving tools are used to eliminate the debris as soon as possible.

2.4 Manufacturing processes adaptation

Even if fabrication is not the root cause of some types of fuel failures, a fuel fabrication improvement might contribute to the mitigation of the identified issue. For instance, modifying the criteria associated to initial rod holding force in the bottom grid was an important step decided in the context of 1300 MWe GTRF mitigation actions, as described in §2.2.1.

In some cases, qualified fuel manufacturing processes need to be adapted in case of a change of material. For example, in the case of EDF operational experience, end plugs welding processes and rod insertion process in the spacer grids have both displayed a significant sensitivity to the involved end plug or cladding material, with fuel failures that have led to adapt the fabrication processes.

3. DISPOSAL OF FAILED FUEL RODS

The casks used by EDF to transport spent fuel assemblies to the Orano-operated reprocessing facility at La Hague are listed in Table 2.

TABLE 2. CASKS USED BY EDF FOR SPENT FUEL TRANSPORT

Cask Design	Type of Plant	Loading (# of FAs)
TN112	CPY	12 MOX
TN12-2	CP0, CPY	12 FAs with a maximum of 4 MOX
TN13-2	P4, P'4, N4	12 FAs

TN12-2 and TN13-2 are MARK II types of casks, and TN112 is a MARK III type of cask.

Up to 2007, EDF used to transport failed fuel assemblies in TN12-2 and TN13-2 casks, provided that no failed rod was located at the periphery of the FA, and that no MOX FA was included in the load for TN12-2 casks. In 2007, concerns about cask internal pressure, with a possible increase due to water vaporization and water radiolysis, led the French Safety Authority to require H_2 measurements, just after the cask loading and conditioning, and one more time after 48 hours: these two measures allowed estimating the allowable transportation time period. It was assumed that hydrogen level was increasing following a linear extrapolation of these two points. The maximum transportation time period was evaluated so that this level would not exceed the lower bound of the H_2 flammability limit.

In 2014, the total number of failed fuel assemblies stored in EDF Spent Fuel Pools (SFPs) amounted to around 300. EDF justified that if H_2 is released, the generated level doesn't exceed the H_2 lower flammability limit for fuel assemblies with a sufficiently low decay heat (less than 1 kW) and a limited number of leaking fuel rods. The Safety Authority allowed to suppress H_2 measurements for those assemblies, provided the transport period is kept to under 30 days. In any case, the number and identification of the leaking fuel rod(s) are required prior to transport, and transport is not allowed if a leaking rod is located in the FA periphery.

In particular, the relaxation on H_2 measurements allowed EDF to evacuate 7 failed FAs stored in CAT3 SFP since 2001, following the fretting event that took place at CAT3. The 7 FAs were loaded in the same cask together, with a total number of 14 leaking fuel rods. The residual decay heat of these FAs was very low (0,85 kW/FA). These evacuations were very helpful to carry out in good conditions the renovation of the SFP of CAT3 rendered necessary by the swelling of the boral material of the racks.

Since July 2018, up to 15 failed fuel rods can be loaded in a TN13-2 cask and 20 failed fuel rods in a TN12-2 cask, provided the casks are equipped with a catalytic device for hydrogen recombination (which is the case for 2 of the TN13 casks and one of the TN12 casks). The maximum number of failed rods is associated to the lower flammability criterion, considering a certain amount of water in the plenum of the failed rod. The limit on the residual power per assembly is inversely proportional to the total number of failed rods in the load to be evacuated.

4. CONCLUSIONS

Eliminating fuel failures is a constant concern for EDF. The operational experience over the last 25 years on 58 PWRs in France covers more than 400 failed fuel assemblies, with fuel failure causes mainly associated to fuel design and debris. A significant decreasing trend has been confirmed over the last 5 years, with an average annual fuel assembly failure rate close to 0.1%.

The total number of failed fuel assemblies stored in EDF SFPs has started to decrease significantly since 2014, following relaxation on H_2 measurements after casks loading and conditioning.

REFERENCES

[1] BAILLON, N., WAECKEL N., Grid to rod fretting wear in EDF PWR: From operating problems to new designs qualification method, TOPFUEL 2005, Kyoto, Japan Oct 2-6, 2005, Paper #1126.

[2] WAECKEL, N., Fuel failure mitigation is a key challenge for the nuclear operator, Technical Meeting on Fuel Failure in Normal Operation on Water Reactors: Experience, Causes and Mitigation, IAEA, December 2020

[3] INTERNATIONAL ATOMIC ENERGY AGENCY, Review of Fuel Failures in Water Cooled Reactors (2006–2015), Nuclear Energy Series No. NF-T-2.5, IAEA, Vienna (2019).

SANMEN NUCLEAR POWER PLANT (AP1000) FUEL MANAGEMENT

HAO TENGFEI
Sanmen Nuclear Power Co., Ltd.,
Taizhou Zhejiang, China

DU CHAO, DING ZHENTING, LIU JING
Sanmen Nuclear Power Co., Ltd.,
Taizhou Zhejiang, China

Abstract

The AP1000 Fuel assembly, benefits from a special fuel design which is intended to protect against fuel failure, use of well-developed mechanical handling tools and mature operating procedures. As a result, there is a low risk of fuel damage due to design defects or mechanical damage. At the same time, Sanmen Nuclear Power Plant (NPP) has constantly reinforced the management of fuel assembly manufacturing supervision, new fuel reception and inspection, foreign material exclusion, primary loop chemistry control, and fuel performance monitoring. These efforts have greatly improved fuel reliability and allow for excellent fuel operating performance for the first cycle of first AP1000 plant (i.e., "Zero Leakers"). This paper introduces the fuel management strategy adopted by Sanmen Nuclear Power Plant related to the aspects above, as a potential reference for other nuclear power plants to improve operating performance.

1. INTRODUCTION

Sanmen Nuclear Power Plant is the world's first AP1000 generation III PWR nuclear power plant, which adopts advanced core fuel management strategy with long cycle, low leakage, and high burnup. The core consists of 157 square fuel assemblies, and the thermal power output of the reactor is 3400MWt.

Sanmen Nuclear Power Plant Unit 1 was brought into commercial operation on June 21, 2018, and the first cycle was successfully completed on December 3, 2019. The design cycle length of the first cycle was 450 EFPD. Actually, the cycle length is extended to 471.4 EFPD by reducing power operation at the end of life, which avoids the time window that is not suitable for shutdown and overhaul, increases 730 million KWh of power generation, and improves the fuel utilization ratio of discharge assembly in the first cycle. During the whole first cycle, the specific activities of I-131, Cs-134, xe-138 and other radionuclides in the primary loop were all lower than the detection limit. There was no iodine spike during the large power change. The monthly fuel reliability index (FRI) of the whole cycle was no more than 0.037 Bq / g. indicating that fuel integrity was maintained.

The good operation performance of Sanmen Nuclear Power Plant Unit 1 is inseparable from the comprehensive fuel management strategy. The following describes the works done by Sanmen Nuclear Power Plant in ensuring fuel reliability from three aspects: fuel assembly manufacturing, foreign material prevention management and reactor operation control.

2. FUEL MANUFACTURING

Qualified fuel manufacturing is one of the bases for ensure fuel reliability. In recent years, with the progress of production technology, the quality of fuel assembly manufacturing has been continuously improved. However, due to the complexity of the fuel assembly manufacturing process and difficulties with technical parameters control, the production rate of qualified intermediate products such as fuel pellet and clad tube is still less than 100%. Therefore, the fuel management engineers of the power plant must strengthen supervision of the fuel manufacturing process, improve the quality of new fuel receiving inspections, and ensure that procedures are in place to only allow qualified fuel assemblies to be used in the reactor.

2.1 Fuel manufacturing supervision

For nuclear fuel manufacturing supervision, Sanmen Nuclear Power Plant has developed a special management procedure entitled “Implementation of On-site Supervision Activities of Nuclear Fuel Plant”. In the process of fuel manufacturing, staff of Sanmen Nuclear Power Plant provide quality supervision of the whole process of fuel assembly manufacturing in strict accordance with the provisions of the management procedures, that is, the re-inspection of raw material and parts, the manufacturing process, and the loading of nuclear fuel into transportation containers and vehicles.

Before the supervision, the Sanmen NPP fuel staff reviews and feeds back the manufacturing quality plan provided by the nuclear fuel manufacture plant, and selects the R point, W point and H point (Quality Control Point) according to the importance of the process.

During the manufacturing of the fuel assembly, the representatives dispatched by Sanmen Nuclear Power Plant supervise the whole process of fuel assembly manufacturing, carry out quality inspection document review, parts and product release, witness points and hold points witness, qualification appraisal and re-qualification witness, milestone witness and manufacturing process supervision according to the quality plan, and regularly counter to Sanmen Nuclear Power Plant through weekly report feedback the production progress and quality of the contract products.

After the completion of fuel assembly manufacturing, Sanmen Nuclear Power Plant dispatched acceptance personnel to carry out factory acceptance of the products according to the fuel assembly contract, check the identification status, assembly integrity, cleanliness, control rod assembly drag force, size, quality, and spot check the quality documents, non-conformance report and other documents.

2.2 New fuel receiving inspection

After the new fuel assembly arrives at the plant, the document review and acceptance shall be carried out first, and the type, number of copies, printing, binding quality, document originality, effectiveness, accuracy, and traceability of the documents submitted by the fuel supplier shall be checked to confirm that they meet the requirements of the contract. At the same time, the transportation container inspection and fuel assembly inspection are carried out.

Sanmen Nuclear Power Plant has compiled new fuel receiving and inspection, fuel assembly receiving, storage, shipping and transfer management and fuel assembly transport container accelerometer tripped processing and other regulations to standardize the whole process of new fuel receiving and conduct desktop deduction according to the specific new fuel receiving inspection scheme before each receiving and simulate the normal receiving and inspection process and abnormal disposal process.

The inspection of the transportation container is divided into internal and external inspection. The external inspection needs to confirm whether the external heat drain plug of the transport container is missing, whether the radioactive identification and sealing welding of the transportation container are complete, and whether the accelerometer outside the container tripped or not. The internal inspection is more critical (relatively speaking), and needs to confirm the accelerometer condition, locking bolt, inner shell grid support block, fuel assembly positioning, polyethylene bag (yellow) integrity and cleanliness, absence foreign material in the bottom nozzle, etc.

Compared with the internal and external inspection of the container, the inspection of the fuel assembly itself can directly reflect the integrity of the assembly, and the requirements are stricter. The following inspection shall be carried out during the transfer of fuel assembly:

1）Check the bottom nozzle. Use a plane mirror to visually inspect all surfaces of the bottom nozzle for abnormal marks, dents, holes, or other defects, and visually check whether all the thimble screws are expanded and whether the bottom part is matched with the flow plate of the bottom nozzle and confirm that all parts of the surface of the bottom nozzle are smooth.

2）Grid inspection. Visually inspect the outer surface of all grids to check whether there are dents, holes, cracks, abnormal marks, or other damages, and check whether there is obvious damage or bending on the grid strip, guide wing, dimple and spring using the light.

3）Fuel rod inspection. The inspector shall perform a visual inspection of the fuel rods on each surface from at least three angles to confirm that the surface of the visible part of the fuel rod is free from dents, holes, scratches,

welding defects, abnormal marks, and other defects. The inspector is also expected to check whether there is foreign material between fuel rods by light source.

4）Check the top nozzle. Check whether the fuel assembly identification number is consistent with the contents in the packing list, and visually inspect the visible parts of the hold down spring for damage (including dents, holes, etc.) and the surface cleanliness of the fuel assembly.

3. FOREIGN MATERIAL PREVENTION MANAGEMENT

Foreign material is the main factor causing the damage of nuclear fuel assemblies. Under the huge impact force of water flow, the foreign material in the primary loop may wear the fuel rod cladding, or even cause perforation of the cladding. During the operation of the power plant, preventing debris from entering the core is the primary means by which to mitigate the failure of fuel assembly.

3.1 Foreign material prevention management in commissioning phase

In the construction and installation phase, the power plant paid attention to the prevention of foreign material, and any RCS (Reactor Coolant System) boundary with openings should be managed to prevent foreign material from leaving or entering the reactor core [1]. Therefore, Sanmen Nuclear Power Plant began to implement the management of foreign material prevention at the commissioning phase, set up a foreign material area, and took strict anti-foreign material measures for the relevant systems and equipment of the primary loop [2, 3].

Before the initial core loading, Sanmen Nuclear Power Plant absorbed advanced fuel management experience, and combined with its own characteristics, carried out a comprehensive foreign material inspection and disposal (FOSAR) process in the primary loop, and carried out a comprehensive foreign material inspection in the core, fuel, system, and equipment connected to the core. See Table 1 for details. At the same time, the corresponding inspection requirements and inspection methods were formulated for each inspection object, and 30 foreign material inspection and disposal tools such as telescope, inspection mirror, endoscope, vacuum cleaner, and high-pressure water washing machine were prepared. After more than 60 days, after the implementation of FOSAR, temporary plugging and other measures were taken immediately to ensure that no new foreign material were introduced into the primary loop.

3.2 Management of foreign material prevention during loading and refueling

Before refueling, Sanmen Nuclear Power Plant uses a special plastic cloth for radiation control area to wrap the fence around the spent fuel pool, the guardrail around the refueling pool, the top floor of the steam generator compartment, the platform railing of the intermediate layer and the stair platform on both sides of the refueling pool to form an effective closed boundary. Set up access control points at the entrance and establish level 1 foreign material exclusion area. During the loading and refueling period, storage of items and, entry and exit registration isolation area shall be set at the entrance and exit of the foreign material exclusion area, and a special person shall be designated as the foreign material prevention supervisor to check the personnel, tools, and material in and out of the foreign material exclusion area, update the material responsibility registration form, and supervise the operation in the foreign material control area. During loading and refueling, the discharge areas of foreign material in the refueling pool and spent fuel pool are shown in Figure 1 and Figure 2 respectively.

3.3 Foreign material prevention management in normal operation

During the operation process, the cleanliness of the system shall be established and maintained in strict accordance with the management procedure entitled “Site Foreign Material Prevention Management”, so as to prevent material, tools, parts and other foreign material from invading into the open system uncontrollably during the work activities, and the specific foreign material prevention scheme shall be specially prepared for the work with great risk of foreign material, such as the fuel receiving work, The foreign material removal plan for receiving, inspecting and transferring fuel and related items and the foreign material removal scheme for plug-in operation

tools and spent fuel assembly operation tools in spent fuel pool has been prepared for the matching and insertion of related components in the spent fuel pool.

TABLE 1. INSPECTION SITE OF FOREIGN MATERIAL BEFORE FIRST LOADING OF SMNPC UNIT 1

Inspection area	No.	Check object	Inspection area	No.	Check object
Reactor System	1	Pressure Vessel	Reactor Coolant System	16	Steam Generator bottom head water chamber
				17	Steam Generator top platform
	2	Lower internals		18	Cool and hot leg of primary loop
	3	Upper internals	Polar Crane	19	Trolley platform and main and secondary hook wire rope
	4	Reactor internals lifting rig		20	Upper surface of trolley track beam and end beam
	5	Integrated head		21	Bridge corridor
Refueling Pool	6	High span/ Low span、floor of pool 、pool wall		22	Main and secondary hook surfaces
	7	Border area	Auxiliary Building	23	Spent fuel pool
	8	Pool reactor internals storage grid		24	Spent fuel container loading wells
Passive Core Cooling System	9	Water collection trough、Water collection tank		25	Spent fuel container washing wells
	10	Refueling water storage tank		26	Fuel transfer cabin
	11	Refueling water storage tank air-vent		27	Fuel transfer channels
	12	Refueling water storage tank manhole area		28	Fuel grab machine
	13	Filter screen		29	Auxiliary Building upender
Fuel Handling and Refueling System	14	Loading and refueling machine		30	New fuel elevator /NFE
	15	Containment building upender		31	Fuel assemblies and related components

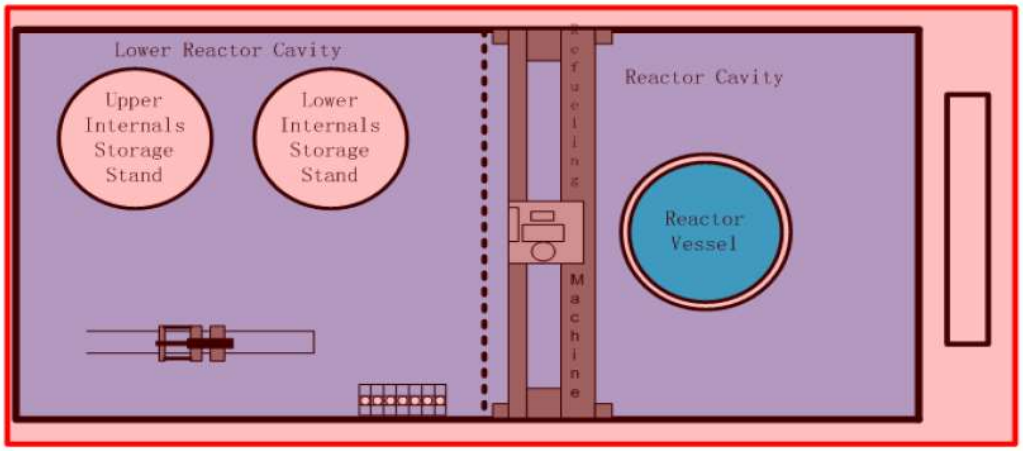

FIG. 1 Refuel fuel pool foreign material exclusion area.

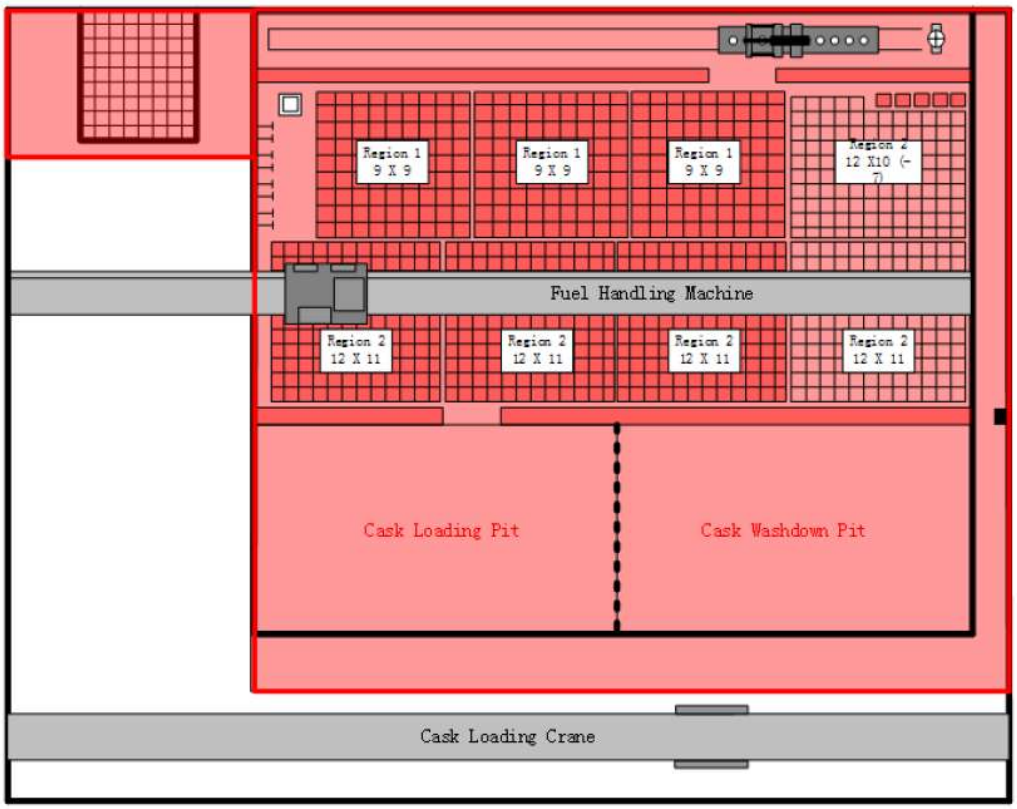

FIG. 2 Spent fuel pool foreign material exclusion area.

4. FUEL OPERATION CONTROL

4.1 Chemistry control

The main purpose of the primary loop chemistry control is to ensure the safety of the fuel cladding. Sanmen nuclear power plant controls the key chemical parameters such as dissolved hydrogen, dissolved oxygen, PH and halogens, thus reducing the potential for corrosion of the fuel cladding.

The dissolved oxygen of the RCS is removed by adding hydrazine during heating and starting of the unit, and the dissolved oxygen in RCS is controlled by high pressure hydrogenation during normal operation to avoid the formation of oxidation environment and reduce the production rate of corrosion products. Sanmen nuclear power plant controls the average concentration of dissolved hydrogen at about 30-40 cc/Kg, effectively inhibits the radiation decomposition of water and controls the concentration of oxygen in primary circuit.

According to the plant conditions, Sanmen nuclear power plant considers the control mode of boron, lithium and pH, optimizing the chemistry control of power plant. The SG heat transfer pipe of the Sanmen nuclear power plant unit uses INCONEL， and the fuel cladding uses ZIRLOTM alloy， both material's corrosion sensitivity is low. The improved PH control method is selected based on the requirements of the designer: after the unit starts, lithium hydroxide is added according to the boron concentration before the critical point. When the boron concentration is > 220 ppm, the target lithium concentration is 4.75 ppm. During the dilution to critical and xenon equilibrium, the primary circuit lithium concentration and boron concentration were diluted along the curve of PH=7.0. Remained constant when the lithium concentration was reduced to 3.3 ppm until the target PH value was 7.3. Follow-up lithium concentration changes with boron concentration to maintain target PH to be 7.3.

Among the halogen elements, fluorine has the most obvious corrosion effect on zirconium alloy, while trace fluorine can significantly increase the initial corrosion rate and hydrogen absorption of zirconium alloy. Chlorine and sulfate ions have corrosion effects on austenitic stainless steel and nickel-based alloys. In the normal operating environment of unit, the chloride ion, fluorine ion and sulfate ion concentration are controlled within the limit value, and the corrosion effect on the material is very little.

By adding zinc acetate solution to maintain the average zinc concentration at 10 ppb, during the whole cycle, no power offset and fuel deposition caused by corrosion fouling has been found in Sanmen Unit 1. However, when adding zinc, it is necessary to strengthen the control of nickel and active silicon concentration. If the silicon concentration is too high, it will production zinc silicate precipitates with zinc. And because of the negative temperature solubility coefficient of zinc silicate precipitates, it will be preferentially deposited on the fuel cladding surface, forming a dense, porous scale, increasing the risk of zirconium alloy corrosion.

4.2 Radionuclide monitoring

Sampling, analysis, and evaluation of primary coolant radionuclides regularly during reactor operation can identify damaged fuel assemblies in time and provide effective support for reasonable treatment measures for nuclear power plants. The determination of fuel breakage, the estimation of fuel consumption of damaged fuel assembly and the estimation of the number of damaged fuel rods all need the activity data of primary circuit radionuclide as the basis, and the more accurate and detailed the data, the more reliable the analysis results are. To continuously tracking the fuel operation performance, the Sanmen Nuclear Power Plant sampled at the following frequency, collated and analyzed the sampling results of radionuclides such as iodine, xenon and cesium, and established a database AP1000 the operation performance of the unit:

To ensure the validity and accuracy of the data, in the process of continuously monitoring the activity of radionuclides in the first loop, once a certain nuclide is found to deviate from the normal trend, Sanmen nuclear power plant fuel management personnel will promptly communicate with the chemical analysts to determine the causes of abnormal fluctuations and eliminate the interference of external factors such as analytical instruments, sampling methods and purification flow.

4.3 Fuel operation restrictions

Because the thermal expansion rate of the core and the cladding is different, the fuel cladding may be damaged by the pellet-cladding interaction-stress corrosion cracking (PCI). Therefore, we must limit the fuel performance operation during the rise power period. During the first return to power operation after the refueling

shutdown or the cold shutdown of the operating fuel assembly, the Sanmen nuclear power plant has the following provisions for the rising power rate:

— Rise power rate limit： The rate of reactor power rise between 50% and 100% RTP (Reactor Thermal Power) should be controlled at less than or equal to 3% RTP/h, and the single step power increase should not exceed 3% RTP as far as possible.
— Axial flux difference (AFD) operation restrictions： When rising reactor power at more than 75% RTP, the AFD should be controlled within the actual operation experience. The recommended operating limits are: within ±3% of the full power target AFD or within ±3% of the target AFD corresponding to the reactor power.
— When the reactor power level of the power plant is equal to or higher than the P power (50%<P<100%) for more than 72 hours in any 7 days, and on conditions below the P power level, the above restrictions will not be forced to observe.

Sanmen nuclear power plants prepare corresponding reactive management plans for reactive change activities, which will combine the power history of the reactor, consider the PCI effect, provide corresponding power rate limits for PCI requirements, and be reflected in the reactive management plan. This can ensure that fuel operation meets the requirements of PCI restrictions and ensure fuel safety.

5. SUMMARY

Sanmen NPP improves fuel reliability through the following aspects of management:

— Dispatching plant representatives to conduct overall supervision of the whole process of fuel assembly manufacturing, inspection of the receiving of new fuel in strict accordance with the procedures for new fuel.
— Formation of a comprehensive foreign material exclusion management system, including all links like construction and installation of commission, reloading and normal operation.
— Continuously optimize the control range of chemistry parameters, analyze and evaluate radionuclide data regularly, and strictly abide by fuel operation restrictions.

Strict fuel supervision and inspection, Comprehensive perfect foreign material exclusion management system, high standards of plant chemical control procedures and execution, appropriate radionuclide monitoring frequency and conservative fuel operation conditions have promoted good fuel operation and performance in the world's first AP1000 unit. Through additional experience, consideration of feedback and focus on continuous optimization, fuel reliability can continue to be ensured and improved.

REFERENCES

[1] BROWN, M., CHENG, B., CLARK, A., et al., Fuel Integrity Monitoring and Failure Evaluation, Handbook Committee [R], EPRI, G-NF-GBP-203, 1998.
[2] Sanmen NPP procedure, Implementation of On-Site Supervision Activities of Nuclear Fuel Plant, 2019.
[3] Site Foreign Material Prevention Management, G-MA-GBP-312, Sanmen NPP procedure, 2020.

OVERVIEW OF STATUS AND EXPERIENCE REGARDING FUEL FAILURES AT NPP TEMELÍN FOR 20 YEARS OF OPERATION

DANIEL ERNST
ČEZ, a. s. – NPP Temelín,
Temelín, Czech Republic

Abstract

NPP Temelín was the first VVER-1000 NPP which was loaded with Westinghouse fuel (in 2000). Since ten 72 (27 were repaired and reused) out of 1008 fuel assemblies were identified as leaking in 8 cycles in both units. The root cause of failure of the leaking fuel assemblies was grid-to-rod fretting. There were no design changes implemented. After ten years of operation ČEZ decided to change the fuel supplier. Russian company TVEL is now fuel supplier for Temelín units. In 2020 TVEL fuel assemblies finished 10th cycle in Unit 1 and 9th cycle in Unit 2. With a total of 49 leakers out of 1096 fuel assemblies. The failure root cause is unknown except for 3 fuel assemblies from the Unit 1 first cycle, for which the root cause of failure was identified to be a manufacturing issue, however, there are some indications pointing towards the root cause being excessive fuel rod bow. The design changes from TVSA-T to TVSA-T, mod.2 show promising improved mechanical behavior of fuel assembly/fuel rods. In 2 cycles TVSA-T, mod.2 design did not show any serious problems or issues. Important fact which helped us to monitor fuel performance is the use of the Fuel Repair and Inspection Equipment. Extensive visual inspections are used for leaking fuel assembly surface inspection. Selected parameters as fuel assembly bow, twist and length as well as fuel rod bow and length are also measured during the outages. During two decades of the Temelín NPP operation, formidable mission of implementing and development program of the new fuel assembly designs has been accomplished. It is believed TVSA-T, mod.2 design is "the solution" to eliminate the leakers from Temelín cores.

1. INTRODUCTION

Despite the low fuel failure rates in current operation of water-cooled nuclear power reactors, there is continued high interest in fuel failures for two reasons. First, problems and inconveniences caused by fuel failures in plant operation can still be significant. Second, the generally accepted goal to move towards zero failure rates as closely as possible requires detailed knowledge of existing failure mechanisms, their root causes and remedies. Nuclear fuel continues to perform well around the world; however, fuel failures still occur in all countries operating nuclear power reactors.

The situation in Czech Republic is such that while the reactor cores in NPP Dukovany (VVER-440) are leaker free in both reactor cores in NPP Temelín (VVER-1000) leaking fuel still appears. Practically from the beginning of operation of both units, leakers appeared in several cycles in a larger or smaller quantity.

2. SYSTEMS USED TO MONITOR, INSPECT AND REPAIR LEAKING FUEL ASSEMBLIES

The standard gamma-spectrometry system is used to monitor Xe and I in the primary coolant loop during operation. In-mast and in-cell sipping systems are used to detect any leaking fuel assembly (FA) during outages. Fuel Repair and Inspection Equipment (FRIE) is used to inspect and repair leaking fuel as well as to inspect non-failed FAs as a part of Post Irradiation Inspection Program. FRIE is described in detail in the following chapter.

2.1 Fuel Repair and Inspection Equipment

The Fuel Repair and Inspection Equipment was designed and supplied by Westinghouse and was used to identify the leaking rod(s) in a leaking FA. FRIE is a mobile equipment, which can be used at both units. This equipment is stored in the fresh fuel storage area during reactor operation, and during outage is transported to the reactor hall where it is assembled. Then it is placed into the special part of the spent fuel poll. The main components of the system are a workstation and a multifunction XYZ inspection stand that is used for many of the inspections (visuals, FA bow and twist measurements, FA overall length measurements, etc.). In addition, the equipment includes tools to perform FA ultrasonic examinations and to handle and transfer leaking rods. The FA rests on a turntable which allows it to be rotated 360 degrees during the inspection process. The leaking rods can be placed into the Failed Fuel Rod Storage Basket (FFRSB). FFRSB is stored in a hermetically sealed container during the operation of Unit and is moved to the workstation during the outage. The FRIE workstation, XYZ inspection stand and FFRSB are shown in Fig. 1.

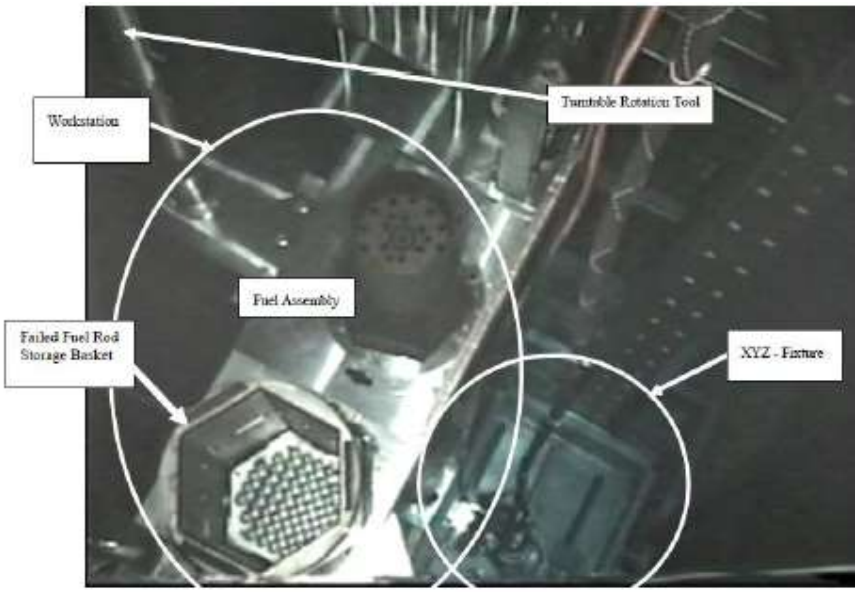

FIG. 1. FRIE in the Universal cell (under the water).

The FRIE is operated and maintained by the Research Institute Řež and ČEZ personnel. The measured data are provided to fuel supplier for further processing and analyses. The results are then supplied to the Regulatory body (SÚJB).

3. EXPERIENCE WITH FUEL FAILURES AT NPP TEMELÍN IN LAST 20 YEARS

First ten years of operation both cores (Unit 1 and Unit 2) were operated with Westinghouse fuel (VVANTAGE-6 design), next ten years were operated with TVEL fuel (TVSA-T design). Totally, 121 leakers out of 2104 FAs were identified.

Note: The number of fuel assemblies/rods supposed to have failed is determined based on safety analyses as detailed in Technical Specifications in the form of Safety Limits & Conditions - at the Temelín NPP the fuel rods are checked for tightness by monitoring the specific activity in the primary circuit – the overall specific activity limit of $\leq 3{,}7 \times 10^9$ Bq/l [1].

3.1 Westinghouse Fuel (2000-2010)

The Unit 1 Cycle 2 data showed the presence of leaking fuel based on high Xe-133 level and high Xe-133/Xe-135 ratio. Iodine spiking during power maneuvers confirmed the presence of leaking fuel. This was later confirmed by the In-mast and In-cell sipping results. Twice-burned FA was identified as a leaker. The same situation was observed in Unit 2 during Cycle 2. Again, the sipping systems confirmed that 3 FAs are leaking. In next cycles, 68 leaking FAs were found in the two cores. The VVANTAGE-6 fuel has a removable top nozzle design and with the top nozzle removed, direct access is provided for leaking fuel rod replacement. The root cause of leaking FAs was found out to be grid-to-rod fretting (typical fretting marks are shown in Fig. 2a). Some of leaking FAs were reconstituted (by replacing the leaking rods with stainless-steel dummy rods) and reloaded in the core. However, in one case there was a leaking fuel rod rupture (separation) during the replacing process. Visual examination of the fracture location indicated the secondary degradation involved heavy local hydriding, which embrittled the cladding and led to fuel circumferential crack while pulling the top of the rod to extract it from the assembly (see Fig. 2b). Visual examinations showed that no fuel pellets were lost during the fracture event [1].

FIG. 2a. Fretting mark on fuel rod.

FIG. 2b. Ruptured fuel rod.

3.2 TVEL Fuel (2010-2020)

First TVEL FAs – TVSA-T design (FA skeleton with 8 grids) - were loaded into the reactor of Unit 1 in July 2010 and into the reactor of Unit 2 in May 2011, respectively (all Westinghouse FAs were discharged from both cores before that). Already during the first cycle in Unit 1 the Gama-spectrometric data showed the presence of leaking fuel. In-mast sipping system identified 3 leaking FAs. FRIE was used to visually examine these FAs. Secondary hydriding was found on one fuel rod (see Figs 3a and 3b). The detailed analysis of manufacturing data established an end plug material manufacturing issue. There were pores in some end plug material without being excluded from the manufacturing process.

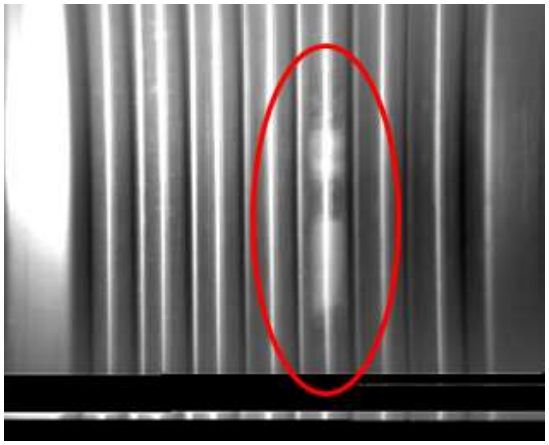

FIG. 3a. Secondary hydriding on FR cladding.

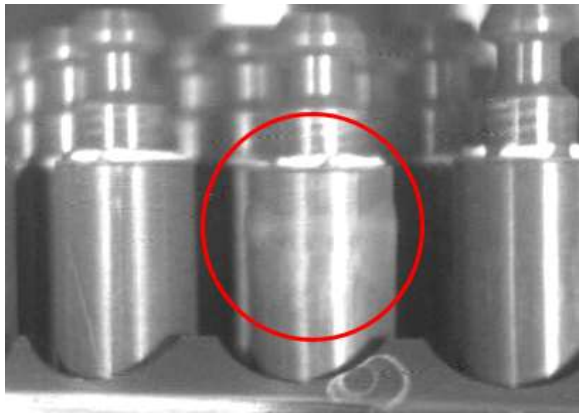

FIG. 3b. Secondary hydriding on FR end plug/cladding weld.

However, during subsequent cycles 46 leaking FAs were found. For example, 14 leaking FAs were found in 2015 (7 FAs in each Unit). During the outages in 2020 six leaking FAs were found in both Units (4 FAs on Unit 1 and 2 FAs on Unit 2). Unfortunately, only one FA was reconstituted, and no clear failure root cause was found. There are some signs which indicate the root cause is excessive fuel rod bow and interaction of bowed fuel rod with the angle piece. These signs include higher radiation growth of fuel rods behind the angle piece. More than 80% of leaking FAs have at least one fuel rod behind the angle piece longer than other fuel rods (see Fig. 4) [2]. An adverse consequence of fuel failures is the need to do quick core redesign.

In 2018 the TVSA-T fuel assembly design was changed and loaded into the reactor core of Unit 2. New design called “TVSA-T, mod.2” has, among other things, 12 grids (instead of 8 in TVSA-T design). More grids mean shorter gap between them and greater resistance to excessive fuel rod bow.

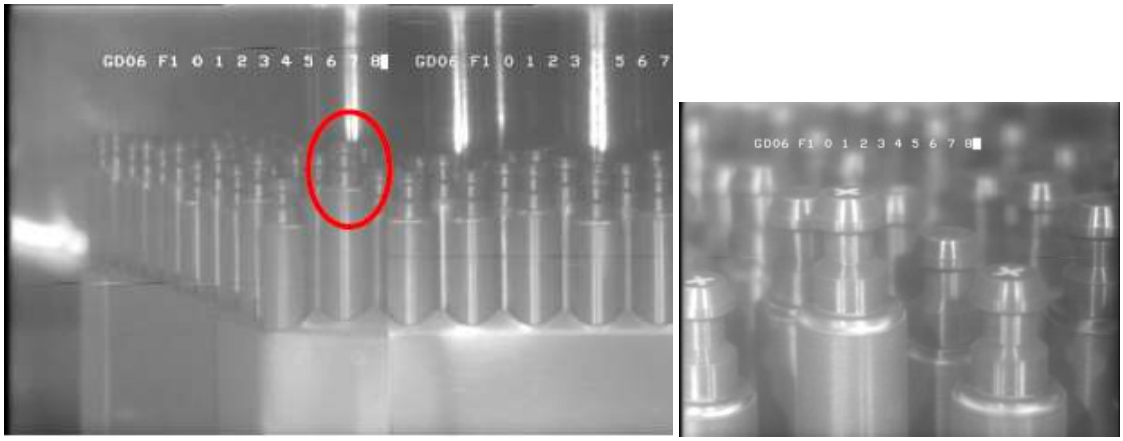

FIG. 4. Longer FR behind the angle piece.

4. CONCLUSION

During the 20 years of NPP Temelín operation there were only few cycles with no leakers. Fuel suppliers change in 2010 did not lead to a reduction in the number of leaking FAs. The FA design has changed in the recent years (from TVSA-T to TVSA-T, mod.2). Such changes show promising improved mechanical behavior of fuel assembly/fuel rods. In two cycles TVSA-T, mod.2 design did not indicate any serious problems or issues and all FAs (84) are leaker free.

REFERENCES

[1] ERNST, D., 10 years of experience with Westinghouse Fuel at NPP Temelín, Paper presented at VVER 2010 seminar, Prague, 2010, Page No. 13.

[2] ERNST, D., MILISDÖRFER L., 5 years of experience with TVEL Fuel at NPP Temelín, Paper presented at 11th International Conference on WWER Fuel Performance, Modelling and Experimental Support, Varna, 2015, Page No. 11.

PIES, EXPERIMENTAL STUDIES AND MODELLING OF LEAKING FUEL BEHAVIOUR

(Session 5)

Chairperson

N. WAECKEL

France

FUEL FAILURE MITIGATION IS A KEY CHALLENGE FOR THE NUCLEAR OPERATOR

NICOLAS WAECKEL
EDF Engineering Division,
Lyon, France

Abstract

Nuclear fuel is a consumable item of the reactor core but, opposite to the early days of the nuclear industry, it can now stay in the reactor as long as 6 years, in a very aggressive environment (longer fuel cycles, higher fuel duty, extensive load following, advanced coolant chemistries, etc..). Since the cladding of the fuel rods is considered as "the first barrier" (by reference to the defense in depth concept), it is crucial to know as accurately as possible how irradiation impacts the fuel behavior under normal, incidental, and accidental conditions to avoid any type of fuel failures. Knowing that more than 2.5 million fuel rods are simultaneously under irradiation in EDF's Nuclear Power Plants fleet, all means leading to minimize/mitigate the risk of fuel failures is welcome. Mitigation actions are mainly based on appropriate fuel design/fuel safety criterion and water chemistry requirements the operator must comply with, always, while operating the nuclear power plant. Nevertheless, fuel failures may occur even within the authorized safety domain (e.g., grid-to-rod fretting wear / cladding shaving wear). In that case, detailed root cause analysis has to be performed by the stakeholders to define and to implement the proper mitigation actions (e.g., modification of the fuel assembly design, improvement of the manufacturing process, etc..). It will be shown that relevant out of pile loop tests together with advanced modeling of the fuel assembly could be very helpful to validate such mitigation actions. Over the last 20 years, fuel reliability has improved significantly. Nevertheless, limited, and unexpected failures can still occur (e.g., foreign material induced cladding wear). As a result, water ingress in the defective fuel rod can induce cladding secondary hydriding and subsequent cladding embrittlement. To account for this phenomenon, the regulator has requested the stakeholders to assess the consequences of the presence of a limited number of failed (weakened) fuel rods on the overall fuel core behavior during an accidental transient. It will be shown, based on the bounding Rod Ejection Accident analysis, that the core safety is not challenged by the presence of a limited number of failed fuel rods.

1. INTRODUCTION

Managing failed fuel rods is potentially a matter of safety and is also considered as being more costly than buying fresh fuel. In that perspective the common interest of the nuclear utilities is to aim at limiting the occurrence of fuel failures during normal or incidental operation conditions.

As a matter of fact, the industry has been rather successful in decreasing the annual in-reactor failure rate over the years.

In the 70's, the annual failure rates for the EDF French NPPs fleet (58 PWR plants in France, including 900MWe plants (34 NPP but two of them have been shut down early 2020), 1300MWe plants (20 NPP), and 1450MWe plants (4 NPPs) were remarkably high (in the order of 80E-05/year against less than 1E0-5/year today). At this time fuel failures were troublesome but not as significantly as today (for instance, it was authorized to reload fuel assemblies with failed fuel rods for an additional cycle). The numerous failures of the 70's was mainly due to inappropriate fuel design (e.g., absence of fuel pellets chamfers and dishes), to manufacturing issues (e.g., presence of tiny fuel fragments in the pellet-cladding gap) or to incomplete proven operational guidelines (e.g., power changes leading to PCI-SCC (Pellet Cladding mechanical Interaction Stress Corrosion Cracking) -failures). All these concerns have been addressed during the 70's.

The root cause analysis from the 80's to nowadays show that slight changes in the fuel management (e.g., longer cycles or higher discharge burnups) requesting design modifications (claddings exhibiting higher corrosion resistance) led to various new types of fuel activityfailures (Fig 1).

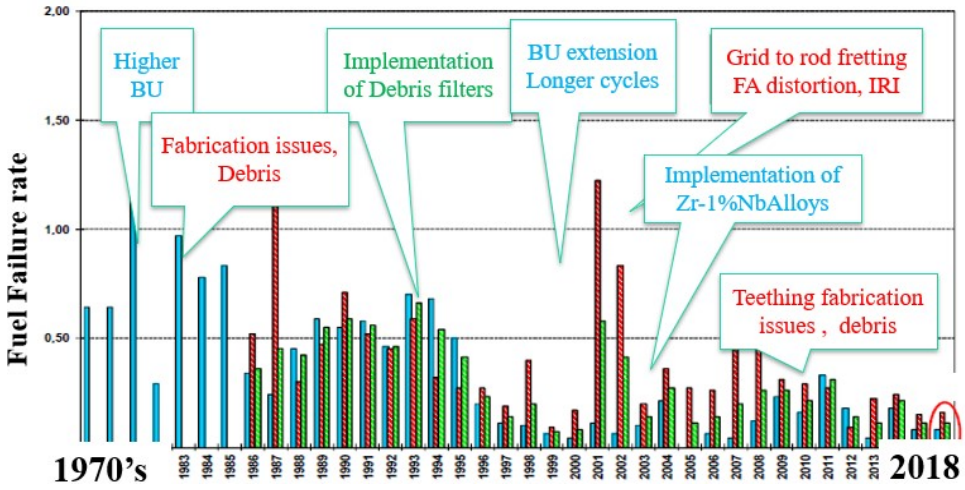

FIG. 1. Fuel failure rate (%) history in the French NPPs fleet show that changes in the fuel management led to design modification which in turn led to new types of fuel degradation.

Nevertheless, even at a historically low level, fuel failures have not been totally eradicated. To address the remaining issues the industry needs to continuously analyze the root causes, to investigate / simulate the fuel behavior in all conditions and to innovate with the aim of restoring fuel safety and operational margins (and as such, improving fuel reliability)

2. INNOVATION TO IMPROVE IN-CORE FUEL RELIABILITY

Areas of innovation to enhance safety/reliability or to restore licensing or design margins include:

— Advanced modeling and simulation to generate margins (e.g., safety, design, and operational margins);
— Advanced techniques to better analyze data (e.g., big data algorithms to value in-reactor and in-pile tests massive data).
— New concepts of fuel to simplify fuel core safety analysis while maintaining a high level of operational reliability (e.g., ATF Advanced Technology Fuel).

Of course, these areas are strongly interdependent: new types of fuels cannot be developed without appropriate calculation and simulation tools, and those tools cannot be validated without using new ways of collecting and analyzing data.

2.1 Advanced modelling and simulation tools to generate margins

Advanced multiscale modeling may help reduce the need for costly tests but only on the long term, after all physical mechanisms / phenomena have been well identified and characterized. To achieve this goal, experimental validation of the calculation tools (V&V UQ) is inescapable and might be a serious issue, depending on the level of sophistication of the models. For instance, multi-scale, multi-physics calculations tools will necessitate development of new ways to ensure proper validation. This may include developing dedicated, advanced R&D tests and instrumentations which may prove to be a real challenge.

On the other hand, multi-scales modeling tools are well suited to define mechanistic scenarios and help analyze complex in-pile tests such as power transient tests which are performed to assess the resistance of the fuel to one type of fuel failure (e.g., PCI-SCC (Pellet Cladding Interaction assisted by Stress Corrosion Cracking) fuel failure).

As an example, multi-scale mechanistic approaches which have been developed recently at CEA and EDF [Ref. 1] to simulate the thermo-chemical behavior of the fuel pellets during a power ramp are well suited to identify and characterize the key physical phenomena which occur in the fuel in case of strong PCI-SCC.

It must be noted that such a mechanistic approach is too sophisticated to assess core wide PCI-SCC available margins (a reactor core contains more than 60 000 fuel rods, or about 19 million pellets, each of them having its own power history). That is why only simplified approaches are used to assess core wide PCI-SCC margins. Nevertheless, a mechanistic approach is relevant to improve, confirm or validate the simplified models implemented in commercial fuel performance codes requested by standard PCI-SCC design methods.

In addition, a good understanding of the physical mechanisms which occur during a power ramp will help to develop and justify innovative PCI-SCC resistant fuels.

Advanced modeling may help gaining design margins (to be released to the designer, to the Regulators or to the Nuclear Plants Operators). However, using advanced modeling (e.g., multi-scale, multi-physics coupled approaches) is not always adapted because current standards have been defined based on the former decoupled 1D static method.

More practically, beyond the design/safety margins enhancement, the goal is also to demonstrate that these advanced tools could help the fuel manufacturers to improve the reliability of their fuel products by simulating in detail the various irradiation conditions the fuel rods and the fuel assembly components are going to face during their lifetime (e.g., corrosion, creep and growth, distortion, SCC, etc..).

2.2 Advanced techniques to better analyse data

Innovation in Nuclear Power Energy may also concern massive data analysis which could be significantly improved by using advanced techniques. Like in other scientific fields, “Big Data” approaches and algorithms might be used to cross-analyze a bigger number of data and experiments. These digital analyses might be greatly beneficial to diversify the identification strategy of key parameters, to detect “weak signals” and phenomenological trends, to suggest new scenarios, hypothesis, or correlations. A similar approach could be used to analyze thoroughly all the information recorded on-line in any commercial power plants. Such analysis could help characterize the specific behavior of the plant (as compared to others), anticipate any abnormal behavior or events (e.g., Fuel Assembly distortion, cruds deposition, etc..) and, as a result, reduce the risk for fuel failure.

Of course, there is room for valuable synergies between multi-scales simulations, massive in-reactor data, and experimental data, and “Big Data” analysis. It is noted however that “big data” approaches do not prevent the licensees to develop relevant experiments to verify the hypotheses derived from such approaches.

2.3 Innovative fuel concepts to simplify design while maintaining a high level of operational reliability

The current UO_2-zirconium alloy fuel system is a mature technology and meets all performance and safety requirements. Alternative fuel system technologies are under development (ATF), mainly to restore the fuel design/safety margins in accidental conditions, that could improve fuel reliability as well.

By definition, a nuclear operator is conservative and is usually reluctant to implement new types of fuel that may generate (bad) surprises during normal operation. As a matter of fact, nuclear utilities prefer proven fuel systems with good safety and operational record, rather than testing unknown fuel concepts with no or little in-reactor experience. As a result, the incentives to switch from a proven fuel system to an innovative fuel system should be well founded. Usually, utility’s motivation for a new fuel is focused on safety margins restoration and fuel cycle costs reductions (through enhanced fuel reliability), both aspects being intricately linked.

Cr coated cladding concepts are good examples of ATF that could be more resistant to debris and grid-to-rod fretting wear, one of the most prevalent cause of fuel failure today.

3. GRID-TO-ROD FRETTING WEAR IN EDF NPPS: FROM THE OPERATING ISSUE TO THE MITIGATION SOLUTION

In early 2000, EDF experienced 92 fuel rod failures distributed in 28 FAs, in one of its 1300MWe PWRs. Many leakers were observed in some other 1300MWe plants but to a lesser extent. The cause for this unexpected event has been rapidly identified: grid-to-rod fretting (GTRF) wear at the first grid level of a series of Fuel Assemblies (FAs) located in specific areas within the reactor core.

It was obvious that the Fuel Assembly had to be modified. But how to be sure that the new design is going to address the GTRF issue? That it is not going to generate new problems (e.g., above the first grid)?

EDF and its industrials partners developed a dedicated engineering approach to address this specific issue that might affect thousands of fuel assemblies within the NPP fleet. The idea was to develop an approach

combining analytic tools and experimental tests to select and qualify the new FA designs proposed by the fuel vendors.

3.1 EDF's engineering approach to address the GTRF issue and to qualify the mitigation options

EDF qualification method is based on the following steps:

— Operating feedback analysis: diagnosis, identification of the boundary conditions leading to GTRF.
— Full size FA vibration and endurance tests enabling proper discrimination between FA designs that are sensitive to GTRF or not.
— Advanced simulations of the FA behaviour to define the qualification criteria aiming at selecting the best mitigation design option (i.e., no FA flow induced resonance and no risk of GTRF wear).

3.2 In-reactor experience analysis

The numerous fuel failure observed in the EDF 1300MWe PWR in the early 2000 has been thoroughly analyzed. Computer Fluids Dynamics (CFD) calculations [2] showed that specific areas of the core were affected with enhanced cross flows (Fig. 2a). It turns out that the leaking fuel rods were in these specific cross flow areas (Fig. 2b), inducing that the cross flows, associated with poor grid-to-rod supports in some of the FAs, was the cause of the multiple failures.

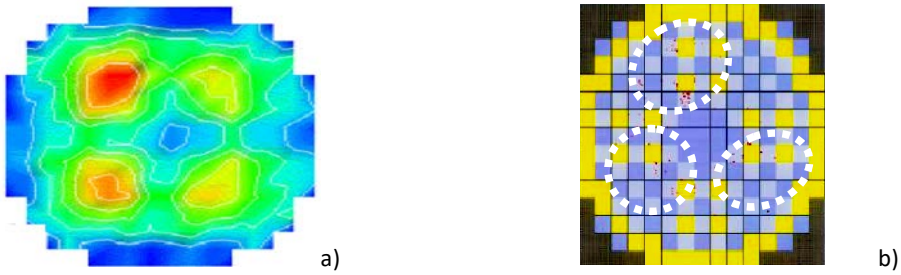

FIG. 2. CFD calculations show strong cross flow areas in the bottom part of the reactor core (at the first grid level). Leakers (red points) are concentrated in the same areas.

However, the FA design which experienced these GTRF failures was known as a proven and robust design, with excellent in-reactor feedback experience. The investigators did not identify any manufacturing or off-normal operational event. The only noticeable modification was related to a switch from 12-month to an 18-month fuel cycle management scheme, a few years earlier.

As a result, the time of residence was identified as an indirect initiator. Interestingly, other nuclear utilities, extending burnup and cycle lengths to reduce operation costs at the same time, observed GTRF fuel failures as well, in many other PWRs around the world.

3.3 Simulation tools

Fretting wear results from the sliding motion of two surfaces in contact. In the reactor core, GTRF occurs when the relative motion of the rods with respect to its grid cell supports (spring and dimples) is sufficient to generate sliding and impacts.

These relative motions are induced either by the vibration of the FA or the vibration of the fuel rods.

The vibration of the FA is typically quite low. Nevertheless, in case the FA is excited at one of its eigen frequency value, the vibration may be high enough to generate significant relative motion between the fuel rods and the grid cell. This phenomenon used to happen with old grid designs.

The fuel rod vibration typically results from three sources of excitation: (i) vortex shedding, at a frequency close to one of the fuel rod frequencies, (ii) fluid elastic instability since the fuel rod is unable to fully dissipate

the energy transmitted by the flow and (iii) turbulence excitation. The first two sources can be simulated to demonstrate they are minor. The third one is more difficult to assess and requires experimental validation.

The vibration of the fuel rods within the grid cells is obviously enhanced by the evolution of the grid cell supports under irradiation. At the beginning of life (BOL) the initial loading generated by the supports (grid springs and dimples) is sufficient to prevent rod vibration.

During irradiation, the spring force decreases and a gap between the rod and the spring may occur. This phenomenon is due to (i) stress relaxation in the spring and in the dimples, (ii) grid growth and (iii) reduction of the rod diameter.

Two models have been developed [1] to predict the behaviour of the rod within the cell. The first model (Fig. 3) is dedicated to the evaluation of the spring force relaxation during irradiation. The second one enables to assess the rotation characteristics of the fuel rod in the cell, as a function of the spring force. The main input parameters are (i) the creep laws of the grid materials, (ii) the growth law of the grid, (iii) the evolution of the rod diameter and (iv) the design/geometry of the fuel rod supports.

The calculation results show that at End-Of-Life (EOL):

— The Rod-to-grid cell Gap increases with irradiation (up to 10µm in mid-grids).
— The Spring Forces are 90% relaxed in the bottom grid (where GTRF is occurring) and 50 % in the upper grids.

The model can be used to calculate the corresponding insertion/extraction forces of the fuel rod in an irradiated grid. The results fit well the measurements (Fig. 4.) When this model is applied to a 12-month fuel cycle, none of the grid-to-rod gaps re-open. On the opposite, when it is applied to an 18-month fuel cycle, some of the fuel grid cells, belonging to the initial spring force distribution tail, may operate with an open gap.

The second mechanical model (Fig. 5) is used to assess the rotation and sliding thresholds of the fuel rod in contact with the dimples and the springs within the grid cell.

This model has been used to assess the risk of vibration of the fuel rod when it is subjected to a cross flow like the one calculated above, in the real core cavity of the affected plants. To address the problem, the calculations have been done on the FA design (“old design A”) which led to GTRF on the first grid and on the new FA design (“new design B”) proposed by the fuel vendor to mitigate the risk of GTRF. In Fig. 6 one can see that the “old design A” exhibits a clear risk of GTRF on the bottom grid while the “new design B” shows no risk at the bottom grid and no detrimental behavior on the upper grids. The latter observation is important because many investigators were concerned that the vibration problem observed in the bottom grid would be transferred to the upper grids after the grid-to-rods support of the first grid are reinforced.

Since everything cannot be calculated in detail, EDF has complemented the calculation approach with an experimental protocol to qualify the new FA designs.

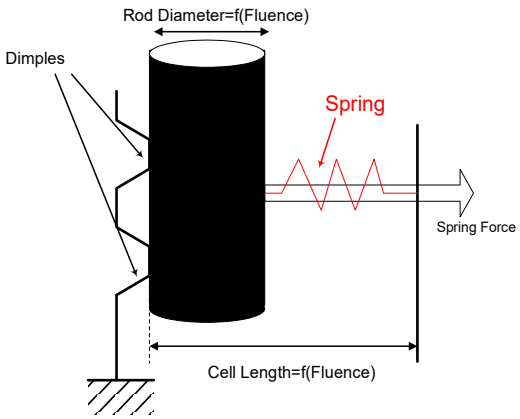

FIG. 3. Fuel rod support model.

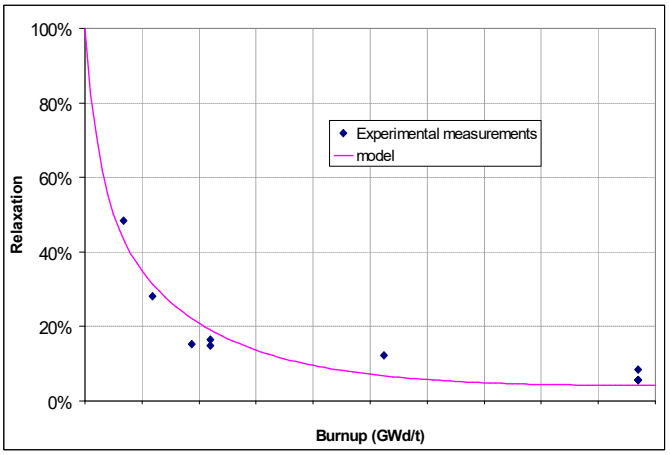

FIG. 4. Comparison between model and experimental measurements of the fuel rod insertion forces in an irradiated grid.

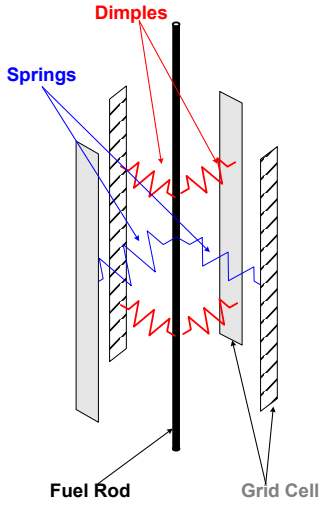

FIG. 5. Fuel rod support rotation characteristic.

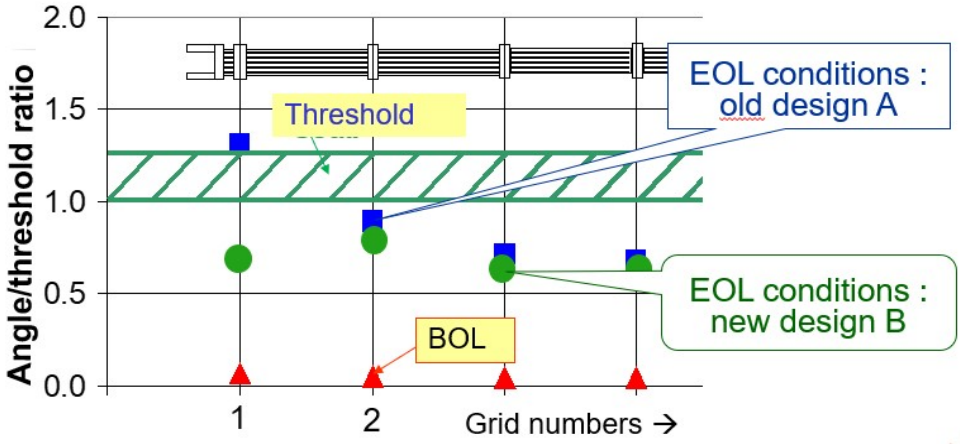

FIG. 6. Comparison of two FA designs with respect to the calculated risk of GTRF at the first grid level.

3.4 Out-of-pile full scale fuel assembly test protocol

This experimental approach [2] is based on full scale out-of-pile hydraulic loop tests and on associated separate effect tests to validate various test parameters. The goal is to confirm the relevance of the analytical approach and to demonstrate that the test protocol can reproduce the in-reactor GTRF phenomena on the "old design A" such that the "new design B" can be qualified with a good level of confidence.

An 1000h endurance test protocol, including, as testing parameters, various grid-to-rod residual holding forces and cross flows levels, has been successfully defined. The full-scale test assembly is a commercial assembly structure with dummy pellets in the fuel rods (depleted Uranium). By straining in the plastic domain, the grid cells springs or dimples, the experimenter generated a series of grid-to-rod gap sizes, simulating the effect of irradiation, and covering classes of gap sizes prototypical of the standard operation time and beyond (Fig. 7).

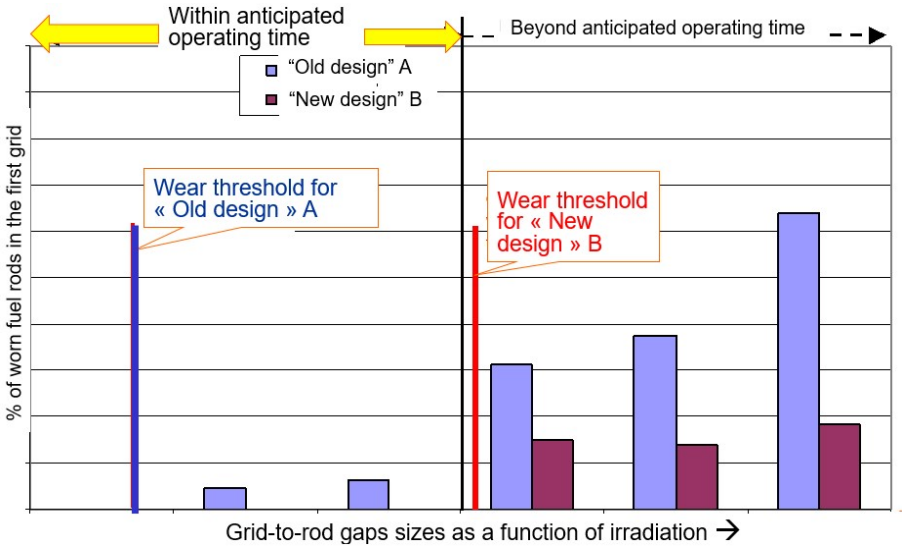

FIG. 7. An out-of-pile loop 1000h endurance test on full-scale fuel assemblies, with various grid cells sizes simulating increasing gap sizes with irradiation, show that the fuel rods in the first grid of the "old design A" start to wear during the standard operating period (as seen in the real life) while the "new design B" doesn't exhibit any wear during the same fuel cycle period.

In conclusion, the out-of-pile tests, including various levels of cross flows, is a particularly useful tool to qualify a new FA design. The calculations described in Section 3.3 with the experimental protocol described in this section, constitute an analytical/experimental qualification process of the new FA designs proposed by the fuel vendors. This approach has been reviewed thoroughly by the French Regulators and accepted.

In-reactor GTRF experience of the "new design B" has been exceptionally good up to now.

It took less than 3 years after the massive leakers event occurred, to analyse the root cause, to propose a new FA design, to develop the models and to establish the test protocol enabling to confirm the hypothetical scenario and to qualify the new designs.

4. ENGINEERING CONSIDERATION REGARDING LEAKING FUEL RODS IN POSTULATED ACCIDENTS

Over the last 20 years, fuel reliability has improved significantly. Nevertheless, limited, and unexpected failures still occur (e.g., foreign material induced cladding wear) in normal operation.

During normal operation heavy secondary hydriding of the inner side of the cladding can take place due to water penetration through the primary leak into the free volume of the leaking rod. The secondary hydriding occurs typically 2-3 m below or above the primary leak, in a very localized area. This local cladding embrittlement can be severe and can cause a (guillotine type of) rupture of the fuel rod, even during normal operation.

4.1 Impact of leakers on loss of cooling accidents evaluation

In most of the countries, fission products release due to leaking fuel and iodine spike are considered for radiological consequences evaluation in case of Design Basis Accidents (DBA) analysis [3].

Most common accidents (adopted for radiological consequences evaluation) are Steam Generator Tube Rupture and Main Steam Line Break (in PWR) because in those accidents, containment bypass potentially occurs (although it depends very much on postulated event and related boundary conditions).

There are countries in which fission products releases coming from the pre-transient leaking fuel rods are not considered [3]. In the safety analyses they normally consider a given number of leaking fuel rods, even if no fuel failure takes place during the accident. Typically, the gap inventory of 1% to 2% of all fuel rods is considered in many types of analyses (it could be replaced, instead of several leakers, by the maximum coolant activity authorized by the radiochemistry technical specifications).

Regarding fission products releases in case of LOCA transients, the effect of leaking fuel rods is small compared to activities coming from the fuel rods that fail during the accident. Typically, depending on the country nuclear regulation, up to 100% failed fuel rods caused by a LBLOCA in PWR can be considered for the radiological consequences assessment. As such, the spiking effect of a few pre-transient leakers can be neglected.

For a thermomechanical point of view, water ingress in the defective fuel rod can induce cladding secondary hydriding and subsequent cladding embrittlement. However, the pre-leaking fuel rods are not going to balloon and burst during the transient and transient secondary hydriding phenomenon is not expected in those leakers. For long oxidation times a fuel rod that experienced ballooning and burst is expected to be even more brittle upon quench than a pre-transient leaker.

In conclusion, the same safety criteria are applied for intact fuel rods and for leakers present in the reactor core prior to a typical loss of coolant accidental transient.

4.2 Impact of pre-transient leakers on Reactivity Initiated Accident (RIA) evaluation

Opposite to loss of coolant transients, Reactivity Initiated Accident (RIA), such as Rod Ejection Accident (REA) transients in PWR, when they apply to defective fuel rods, may lead to premature failure with specific phenomena that could impact the adjacent fuel rods and even the reactor core vessel.

If the flawed fuel rods fail during an RIA transient (with a high probability of fuel fragments dispersal and fuel coolant interaction), a significant pressure pulse is generated in the coolant. Since the transient is not terminated when the fuel fragments are dispersed in the coolant, the deposition of the remaining energy in the dispersed fuel fragments will enhance this pressure pulse (Fig. 8.).

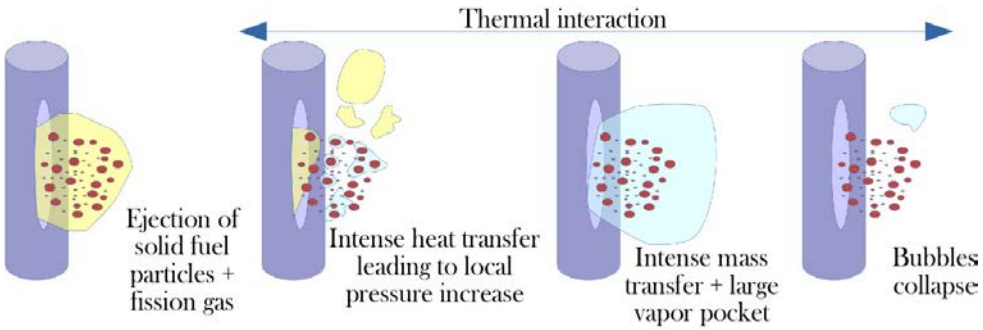

FIG. 8. Phenomena occurring in the coolant near a flawed fuel rod failing prematurely during the first tenths of milliseconds of an RIA transient [3].

To account for these phenomena, the regulator has requested the industry to assess the consequences of the presence in the reactor core of a limited number of failed (weakened) fuel rods on the overall fuel core behavior during an accidental RIA transient (is there a “domino effect” on the neighbor rods? Is there an impact on the reactor pressure vessel itself?).

To address the issue [2], EDF has identified in Table 1 the REA bounding cases for all the fuel management schemes of its NPP fleet. The worst case is found in the MOX fuel management.

TABLE 1. BOUNDING REA CONDITIONS

Initial condition	Initial enthalpy (cal/g)	Enthalpy rise (cal/g)	Available enthalpy (cal/g)
Hot Zero Power (HZP)	17	106	106
Hot Full Power (HFP)	77	77	137

The available energy is the difference between the fuel maximum local enthalpy and the fuel enthalpy at the coolant temperature (~ 300°C):

— Acoustic pressure wave due to the burst of an over-pressurized cladding.
— Second pressure wave due to fuel ejection and FCI (Fuel Coolant Interaction).

First the acoustic pressure wave due to the cladding burst of an over-pressurized cladding is conservatively calculated, assuming an instantaneous disintegration of the cladding (it “disappears”), an instantaneous ejection of all the fuel particles available, the smallest fuel particle sizes corresponding to the grain size (0,2 µm in the restructured zone (the Pu clusters in the outer half of the pellet radius) and 10µm elsewhere), and the available energy corresponding to the worst cases (HZP or HFP).

Then, pressure wave generation and propagation, both acoustic and the one due to FCI, are simulated with the EUROPLEXUS, code dedicated to fast transient dynamics (the code is co-owned by CEA and EC/JRC), to calculate the loading on the neighbor rods and on the reactor pressure vessel.

Calculation hypotheses include explicit time resolution, finite volume formulation in fluid elements, finite element formulation in solid structures, two-phase homogeneous and balanced fluid model (Euler’s equations).

A 2D-plane EUROPLEXUS scheme is used to evaluate the generation and the propagation of the pressure wave through a fuel assembly and the maximum forces applied to the adjacent fuel rods. Various mesh sizes have been used to confirm that the linear forces applied to the two closest adjacent fuel rods do not depend on the number of rows considered in the model (Fig. 9).

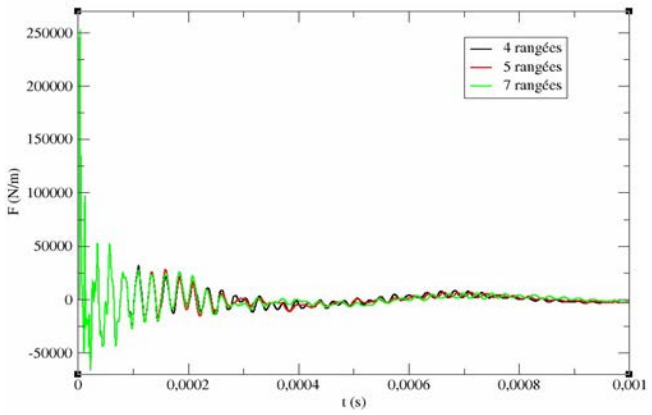

FIG. 9. Time-history of the linear force applied to an adjacent fuel rod considering 3 different meshes (4, 5 and 7 rows).

Then the strain energy is obtained by coupling the results with the EUROPLEXUS mechanical calculations. For the bounding case, the maximum bending strain energy on the adjacent fuel rods is 0,24 J/m which is much

lower than the strain energy density at failure measured on 3-point bending tests performed on irradiated fueled rodlets: ~ 32,5 J/m.

It can be concluded that the premature failure of flawed rods during a bounding REA transient has no detrimental impact on the adjacent rods (i.e., no "domino effect" to fear).

These 2D-plane calculations are complemented with 2D-axisymmetric calculations to evaluate the impact of the pressure wave on the reactor pressure vessel wall, assuming a conservative free propagation.

To run these 2-D axisymmetric EUROPLEXUS calculations, we must determine the number of leakers which may be present in the reactor core, prior to the transient. EDF in-reactor experience feedback over the last 15 years shows that the maximum number of leakers is less than 5 in a reactor core and less than 2 in a single Fuel Assembly.

Among the other conservative assumptions, we have considered a reduction in 1/x0,5 (x = distance from the failed rod) of the pressure wave propagation, 2 rods located at the very periphery of the core to enhance the dynamic loading on the RPV wall, and a dynamic loading multiplied by 2 to take into account incident and reflected pressure waves.

Based on the calculations results presented in Fig. 10, it can be concluded that the dynamic pressure wave generated by the premature failures of a few pre-transient leakers has no detrimental impact on the reactor pressure vessel wall integrity.

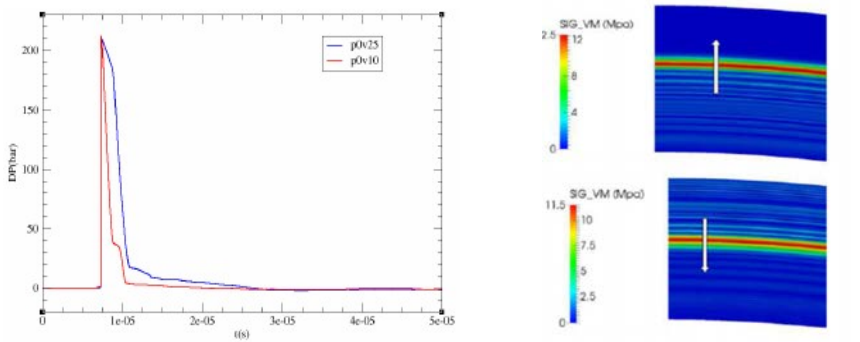

FIG. 10. Dynamic loading on the reactor pressure vessel wall (the pulse is very sharp; <50µs). The max dynamic Von Mises stress propagating through the wall is less than 15 MPa.

It should be noted that in Japan, different threshold for rod rupture is to be applied to leaking fuel. The threshold and consequences of rod rupture are direct outcomes of RIA experiments with waterlogged fresh fuel rods in NSRR test reactor [5]. Namely, the rod rupture limit is reduced, and fuel rods beyond the limit are treated as ruptured. A certain existing ratio of leaking rods is to be assumed (Japanese guidelines suggests 1% of all the fuel rods in the core).

5. CONCLUSIONS

The presence of a few leakers in a core reactor could be costly for the nuclear utility. As such the incentive to minimize the risk for fuel failures during normal operation is high.

The fuel behavior under irradiation is extremely complex and the slightest modification in the operation conditions (chemistry changes, duty, longer cycle, higher burnups, mixed cores, FA design evolutions, etc..) may have a detrimental impact. That is why the paper focused on the role played by R&D and modeling to better assess the potential effects of these changes on the overall fuel reliability.

An engineering approach has been described to qualify FA design changes proposed by the fuel manufacturers to solve a problem (to demonstrate that the proposed design change is a true solution and is not going to generate another issue). Similar engineering approaches can be used for various design changes (grid design modifications, hold down spring system design modification, etc.)

Advanced modeling (multi-scales / multi-physics calculation tools) and techniques (big data analysis) are also useful to diagnose specific in-reactor events and to help the industry to propose relevant solutions to address chemistry changes, PCI-SCC risks, fuel rod vibration, etc. These solutions include the development of Advanced Technology Fuel (ATF), such as Cr coated claddings, that will exhibit better resistance to debris fretting (debris fretting remains the major cause of fuel failure in normal operation).

Regarding the impact of leaking fuel on the DBA safety margins and criteria, it has been shown that both are not affected by the presence of a few leakers in the reactor core although it is recognized that leaking fuel has lower capability in withstanding a RIA and consequently a higher probability to cause fuel coolant interaction. Specific calculations have been performed to confirm that the premature failure of the leakers, and the subsequent fuel coolant interaction, has no detrimental consequences on the adjacent fuel rods (no "domino effect" to be concerned about) or on the reactor pressure vessel wall.

REFERENCES

[1] BILLEREY, A., WAECKEL, N., Evolution of the fuel rod support under irradiation: impact on the mechanical behaviour of the fuel assemblies, TOPFUEL 2005, Tokyo, Japan, Oct 2-6, 2005, Paper # 1125.

[2] BAILLON, N., WAECKEL, N., Grid to Rod Fretting Wear in EDF PWR: From Operating Problems to New Designs Qualification Method, TOPFUEL 2005, Kyoto, Japan Oct 2-6, 2005, Paper #1126.

[3] NEA/CSNI/R (2014)10 Report, Leaking Fuel Impacts and Practices, July 18, 2014.

[4] BERNAUDAT, C., WAECKEL, N., Consequences of Leaking Fuel Rod Failure During Ria Transients, TOPFUEL 2018, Prague Czech Republic, Sept 30-Oct 4, 2018, Paper #A0208.

[5] RUYER, P., et al., Evaluation of The Consequences of Fuel Dispersion and Interaction with Coolant Following a Cladding Failure Induced by a RIA, TOPFUEL 2018, Prague, Czech Republic, Sept 30-Oct 4, 2018, Paper # A0081.

SHORT-TERM DROP OF THE REACTOR POWER AS A POTENTIAL REMEDY AGAINST SECONDARY DEGRADATION OF LEAKING FUEL

I.A. EVDOKIMOV, A.A. SOROKIN, K.E. ULIBYSHEV, E.Yu. AFANASIEVA, V.D. KANUKOVA
SRC RF TRINITI,
Troitsk, Russian Federation

O.V. KHORUZHII, V.V. LIKHANSKII, V.G. ZBOROVSKII, A.A. KOVALISHIN, M.N. LALETIN
NRC "Kurchatov Institute",
P.N. Lebedev Physical Institute,
Moscow, Russian Federation

Abstract

The major radiological risks associated with fuel failures are related to severe secondary degradation of fuel cladding. It happens due to local severe hydriding and embrittlement of fuel cladding material. Severe secondary degradation may cause escalation of primary coolant activity by orders of magnitude. Economic losses due to fuel failure rise up markedly if radiation safety limits for reactor operation are exceeded. In this case power unit is to be shut down out of schedule with ensuing reduced generation of electricity. Currently, the most promising way to mitigating severe secondary degradation seems to be a short-term reduction of reactor power after detection of a failure. However, if the reactor power is restored rapidly, mechanical stress in cladding may increase. Cladding in a leaking fuel rod becomes more brittle not only due to possible formation of local hydride blisters but also due to enhanced hydrogen uptake. So, power transients may lead to cladding rupture. To avoid these adverse processes somewhat slower rates of power changes may be needed compared to the current regulations. The paper provides some results of numerical simulations of leaking fuel behavior during power transients shortly after a failure. Changes in hydrogen inventory inside a leaking fuel rod are studied. Potential mechanisms able to prevent severe secondary degradation by short-term power reductions are also discussed. Simulations were carried out with the RTOP-CA fuel performance code.

1. INTRODUCTION

Fuel failures may occur during operation of nuclear power plants (NPPs). This may lead to escalation of primary coolant activity, higher dose rates for personnel, increase in the amount of liquid radioactive waste, and the need for additional operations to search for and replace fuel assemblies with leaking fuel rods.

In recent years, several projects aimed at elimination of fuel failures in NPPs were initiated by different countries, [1-3] These projects led to better operational reliability of PWR, BWR and WWER fuel. The best industry records are thought to be as follows:

— The fraction of power units operating defect free fuel cycles about 95%.
— The fuel failure rate about $(1–3) \times 10^{-6}$ (related to the total number of fuel rods).

Nevertheless, in recent years no improvement has been observed for these best recorded performance indicators despite the taken efforts. It can be inferred that it is hardly possible to avoid fuel failures completely by reasonable costs [4]. Thus, fuel failures will still occur, and the mitigation of their adverse consequences remains a relevant issue.

Secondary degradation of leaking fuel rods during reactor operation represents potential radiological risks. It happens due to local severe hydriding and embrittlement of fuel cladding, [5-10]. Severe secondary degradation may cause escalation of primary coolant activity by orders of magnitude. One or two leaking fuel rods at high power with severe secondary degradation may be sufficient for primary coolant activity to exceed the radiation safety limits for reactor operation. In this case economic losses due to fuel failure rise up markedly since power unit should be shut down out of schedule with ensuing reduced generation of electricity. Fuel may be washed out into the primary coolant from the leaking rods with coarse defects in cladding. Radiological consequences of fuel washout may persist at power unit in a form of high background activity for a long period of time.

Currently, the most promising way to mitigating severe secondary degradation seems to be a rapid power reduction after detection of a failure for some period [11]. However, in cases when the reactor power is restored

rapidly, mechanical stress in cladding may increase. Current regulations for power maneuvers in WWERs assure integrity of intact fuel rods. But in case of a failure, cladding in a leaking fuel rod may become more brittle due to hydrogen uptake and power transients may lead to cladding rupture. To avoid these adverse processes somewhat slower rates of power changes may be needed compared to the current regulations.

The paper provides some results of simulations with the RTOP-CA[7] [12, 13] fuel performance code. The influence of power transient parameters on behavior of leaking fuel during short-term power reductions is discussed. Analysis covers the following issues.

- How does the amplitude of power reduction affect the condition of leaking fuel rods?
- How does the time between the moment of a primary failure and the beginning of power reduction influence the level of cladding hydriding and the peak stress-strain in fuel cladding?
- What is the effect of axial position of the defect in cladding?

The paper also suggests preliminary recommendations on scenarios of power regulation after detection of a failure during operation of WWER power units. All simulations with the RTOP-CA code in the present study were confined to WWER fuel with hollow fuel pellets in the fuel rods.

2. AVAILABLE DATA INDICATING A POSITIVE EFFECT OF POWER REDUCTIONS AFTER A PRIMARY FUEL FAILURE

2.1 Halden tests with simulated primary failure

Positive effect of power reduction for suppression of severe degradation of leaking fuel has been experimentally demonstrated at the Halden research reactor (Norway) [11]. A primary failure during reactor operation was simulated in a series of Halden tests with variation of different parameters:

— Pellet-to-cladding gap.
— Alloy composition/heat treatment of cladding.
— Alloying additives in zr-liner at inner surface of cladding, pre-oxidation level of zr-liner (for bwr fuel rods).
— Addition of co fill gas inside fuel rods to inhibit hydrogen pickup.
— Fuel heat generation rate, time of operation after the failure.

In all the tests, the enriched fuel length was 1.2 m.

In the IFA-684 test, several fuel rods were subjected to the simulated primary failure during irradiation (peak local power was 28 kW/m). In one of the fuel rods, 1 hour after the “failure” the power was reduced deliberately to zero for ~ 2 days. During these 2 days, the fuel stack in the rod was expected to be completely covered with water. Then the power was restored, and this fuel rod was irradiated with the others for ~ 30 days under the same conditions. After irradiation all fuel rods were examined. The fuel rod which experienced a short-term power drop was the only one that did not have any marks of severe cladding hydriding. In contrast, secondary degradation did occur in all the remaining fuel rods that operated without any power reductions.

In the subsequent IFA-742 test the rate of secondary degradation was studied [11]. Several fuel rods were irradiated during relatively short period of time after the simulated failure. Fuel rod 2 was irradiated for 3 days after the ‘primary failure’ occurred and there was no secondary hydriding in its cladding. But fuel rod 6 irradiated at the same level of heat rate exhibited secondary failure already 12 hours after the ‘primary failure’ was simulated. On the basis of these data it was supposed, [11], that initiation of secondary hydriding may bear some stochastic nature (at least in a certain range of operation conditions).

Halden tests showed that secondary degradation could develop in a short period of time (about several hours) if high linear heat generation rate (LHGR) of the leaking fuel rod is sustained after the primary failure. This means that the plant personnel should quickly respond to fuel failures. Considering reduction of reactor power as a tool for mitigation of severe cladding hydriding implies that the reactor power has to be reduced in several hours, possibly a few days, after the primary failure. The higher the LHGR of the leaking fuel rod is, the faster the rate of its secondary degradation would be as well, [5, 6], and the less time is left for deciding on the remedial actions. Under this challenge at NPPs, it is relevant to implement the on-line systems for monitoring and evaluation of

[7] RTOP-CA (**R**eac**T**or **OP**eration – **C**oolant **A**ctivity) is the code of TVEL Fuel Company designed for modeling of leaking fuel behavior.

primary coolant activity. More sensitive analytical methods for prompt detection of fuel failures become urgent as well [14, 15].

Evaluation of leaking fuel parameters may take some time in NPPs. For instance, fuel burnup may be unknown until the nearest power transient with subsequent spiking of ^{134}Cs and ^{137}Cs activity. So, in the ideal case, parameters of urgent mitigating actions such as the amplitude and duration of short-term power drop should be chosen in advance regardless leaking fuel burnup, its heat rate, size and axial position of the breach in cladding.

2.2 Experiments with artificial defects in fuel cladding

It is mentioned in reviews [6, 16] that secondary hydriding did not take place in test fuel rods with artificial defects in cladding (artificial defects were made prior to the start of the in-reactor experiments).

Another series of experimental studies with artificial defects in cladding of the test fuel rods was recently carried out in the MIR research reactor (see, e.g.,[13]). In these studies, the test fuel rods with fuel length of 1 m were fabricated from the full-length fuel rods irradiated in commercial WWER-1000 power units. Artificial defects in cladding of the test fuel rods were made before the start of irradiation in the MIR reactor. Different MIR tests included variations of fuel burnup, type of fuel pellets (either hollow or solid) and axial location of the defect in cladding (at the level of the fuel stack or in the plenum). The test fuel rods were irradiated in course of 1-3 MIR cycles (each cycle is ~ 20 days long). Average LHGR was 10-20 kW/m (peak local LHGR was about 40% higher than the average value). In total, 9 tests were performed. But none of them led to secondary hydriding of the cladding.

This finding may be attributed to the fact that due to the presence of the artificial defect in cladding water filled the test fuel rods when they were put into the reactor loop – well before the irradiation started. Another reason is that the irradiation was interrupted by power drops between the subsequent MIR cycles. It is possible that each of these factors contributed to prevention of secondary degradation of the test fuel rods.

Nevertheless, it should be also mentioned that some contribution to the absence of secondary hydriding in the MIR tests could be made by rather short length of the test fuel rods.

2.3 Operational data from NPPs

A practical example from the nuclear industry which gives some evidence of the beneficial effect of power reduction after a fuel failure may be inferred from the case at Balakovo NPP with leaking U-Gd fuel rod[8] in one of the fuel assemblies (FAs). This FA operated one 18-month fuel cycle up to average fuel burnup of ~ 24 MWd/kgU. The U-Gd fuel rod failed in ~ 100 days after beginning of the cycle (BOC). Now of a primary failure its LHGR was about 8 kW/m, and the pellet-to-cladding gap was filled with water. During the cycle, while the gadolinia poison isotopes burnt out, the heat generation rate in the leaking U-Gd rod gradually increased. The last ~ 150 days its average LHGR was considerable – above 18 kW/m. In total, the leaking U-Gd fuel rod operated ~ 370 days after the failure.

Post-irradiation examination (PIE) in hot cells showed that hydrogen uptake by the cladding of the leaking U-Gd fuel rod did not differ markedly compared to that of adjacent intact fuel rods. No severe cladding hydriding was observed.

However, all the leaking WWER fuel (that was examined so far in hot cells) demonstrated secondary cladding degradation if it was operated at similar (16-18 kW/m) or higher LHGRs after the failure. Analysis of the PIE results for leaking WWER fuel and simulations with the RTOP-CA code made the basis to derive a criterion of severe secondary hydriding [17, 18]. This criterion correlates the LHGR after the primary failure and a time needed to severely hydride the cladding. According to this correlation, severe hydriding is possible in ~ 70 days after the primary failure if the leaking fuel operates at 18 kW/m.

Should the criterion [17, 18] be applied to the above-mentioned leaking U-Gd fuel rod, then its cladding should have inevitably experienced secondary degradation by the end of the cycle (EOC). But the observed

[8] Current design of U-Gd and UO_2-fuel rods for Russian WWERs-1000 is the same besides the different chemical composition of the fuel pellets.

hydrogen pickup in it was low. It could happen because of low LHGR and filling of the pellet-to cladding gap with water immediately after the failure had occurred.

3. ANALYSIS OF PHYSICAL PROCESSES INVOLVED IN SECONDARY CLADDING DEGRADATION

3.1 Current understanding of secondary degradation phenomena

A general sequence of processes leading to severe hydriding of zirconium-based fuel cladding is well known [19, 20]. After ingress of coolant inside a leaking fuel rod, water is heated up and evaporated. Generated steam oxidizes UO_2-fuel pellets and inner surface of cladding. Oxidation leads to accumulation of hydrogen. Inside a leaking fuel rod, there may be locations with limited access of new portions of steam and slow outflow of generated hydrogen. In such places hydrogen may become the dominant gas. If the threshold ratio of hydrogen-to-steam pressure is exceeded, then after some incubation period the oxide film on the inner cladding surface loses its protective properties and does not prevent any more from intensive local penetration of hydrogen into the fuel cladding [21, 22].

However, detailed mechanisms and quantitative characteristics of these processes as well as their dependence on different factors (defect size and axial position, fuel rod design, operation conditions) are still not enough understood.

For example, the value of the threshold ratio of hydrogen-to-steam pressure needed for initiation of severe hydriding is the subject of debate, so far. Out-of-pile experiments demonstrate the high rates of hydrogen uptake by zirconium-based cladding only if the ratio of hydrogen-to-steam content in the gas phase is very high: 10^3–10^5 (at temperatures of 300-400°C [9]) [22]. But analysis of in-reactor tests and allowance for irradiation damage of the oxide film by high energy fission fragments suggest that intensive hydriding during operation may initiate at much lower hydrogen content – about 0.1–1 of steam concentration [9]. Regular secondary hydriding of cladding in WWER fuel rods with coarse primary debris-defects [24] confirms the latter point of view.

To find optimal parameters of the short-term power drop, it is necessary to understand the mechanism which is responsible in this case for prevention of severe secondary degradation. It is also important to know how this mechanism depends on fuel rod parameters and irradiation conditions. Available data are scarce and sometimes incomplete. This limits the room for such an optimization at present time. Under these circumstances, the better understanding of secondary degradation phenomena may be achieved by numerical simulations of separate physical processes in leaking fuel rods. Some results of such simulations with the RTOP-CA code are presented below.

3.2 Release of hydrogen from a leaking fuel rod during power drops

The available theoretical concepts and experimental data were analyzed to reveal possible mechanisms that may suppress severe secondary degradation in leaking fuel rods due to the short-term reduction of reactor power. Some simulations with the RTOP-CA code were used for this purpose as well.

After a failure, hydrogen starts to accumulate inside the leaking fuel rod due to oxidation of fuel pellets and the inner cladding surface. Power reduction should lead to release of hydrogen into coolant. A positive effect of the power drop could be attributed primarily to this fact. Therefore, the first step in analysis was focused on the dynamics of hydrogen content in leaking fuel rods.

Analysis has shown that the rate of hydrogen generation and total amount of hydrogen gas (for typical size of the primary debris-defects) are mostly affected by LHGR and oxygen potential of fuel pellets. For the uranium oxide fuel, oxygen potential is governed by the initial non-stoichiometry of UO_{2+x}. Oxygen potential of U-Gd fuel increases along with gadolinium content in fuel pellets. The higher the initial oxygen potential of fuel is, the lower hydrogen concentration would be generated inside a fuel rod in case of a failure.

Hydrogen accumulation inside the leaking fuel rod is described by the three stages (Fig. 1). Peak concentration of hydrogen gas is reached about 2-4 hours after the primary failure (higher LHGR entails higher peak hydrogen content). The main source of hydrogen during this period is oxidation of fuel pellets. Then the rate of hydrogen release begins to dominate over the rate of its generation and hydrogen concentration sufficiently decreases during ~ 2-3 days. It is worth noting that despite the deviation x from UO_{2+x} stoichiometry in most part

[9] The higher threshold ratio of hydrogen-to-steam pressure corresponds to lower temperature.

of the fuel stack is below 1%, the mass of fuel pellets is big enough to make their oxidation the major source of hydrogen at the first stages of the process. In course of the subsequent irradiation (stage III), hydrogen concentration remains practically constant. Hydrogen is generated mainly due to oxidation of the inner surface of fuel cladding (made of E110 alloy in WWER fuel rods). Formation of new portions of hydrogen is balanced by its release from the leaking fuel rod and, partially, by hydrogen uptake by cladding.

Removal of hydrogen during the power drop will raise the oxygen potential of the gas phase inside the leaking fuel rod. After the power is restored, the level of fuel pellets oxidation will appear to be insufficient for the new environment. It will lead to rapid additional oxidation of fuel pellets and recovering of hydrogen content. The corresponding growth of hydrogen concentration will stop when the new stoichiometry of fuel pellets will come in equilibrium with the new hydrogen-to-steam pressure ratio. Since accumulation of new portions of hydrogen demands additional fuel oxidation (which corresponds to higher oxygen potential), than the new hydrogen content will be always below its value before the power drop.

The level to which H_2 content is restored depends on the stage when hydrogen is removed from the leaking fuel rod. If power is dropped at the initial stage (stage I in Fig. 1), when hydrogen content is high, recovering of H_2 concentration will need significant additional oxidation of fuel pellets. So, oxidation will stabilize at noticeably lower content of hydrogen than before the power drop. At later stages (stage II and III in Fig. 1), recovering of hydrogen concentration will need a limited extent of additional fuel oxidation. So the restored hydrogen content will be close to that before the power drop.

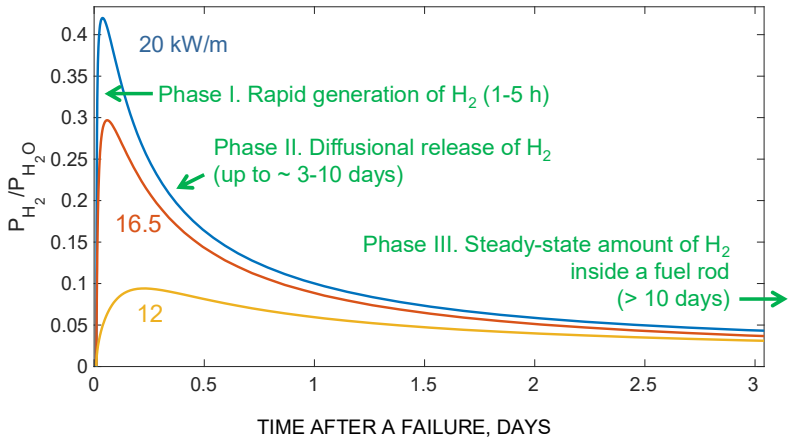

FIG. 1. Dynamics of maximum hydrogen-to-steam pressure ratio inside a fuel rod after a failure. The RTOP-CA simulation for WWER-1000 fuel rod of low burnup, defect in cladding is 1 mm in diameter located 90 cm above the lower end of the fuel stack.

Fig. 2 shows an example of simulated dynamics of hydrogen inventory inside a leaking fuel rod during the power drop and subsequent return to the previous LHGR level. The failure was simulated in the leaking fuel rod in a FA at its 2nd 18-month cycle (see section 0). The power was assumed to be dropped 1 hour after the failure. Fig. 2 demonstrates that total amount of hydrogen is quickly recovered to much extent after restart of irradiation. However, the maximum hydrogen-to-steam pressure ratio decreases noticeably. It is due to release of helium during the power drop and its substitution by steam.

Simulations showed that the release of hydrogen from the leaking fuel rod due to power drop provides a temporary effect. Hydrogen is rapidly accumulated again as soon as reactor returns to full power after the power transient. Maximum hydrogen content inside the leaking fuel rod appears to be somewhat (no more than 2-3 times) lower than that prior to the power drop.

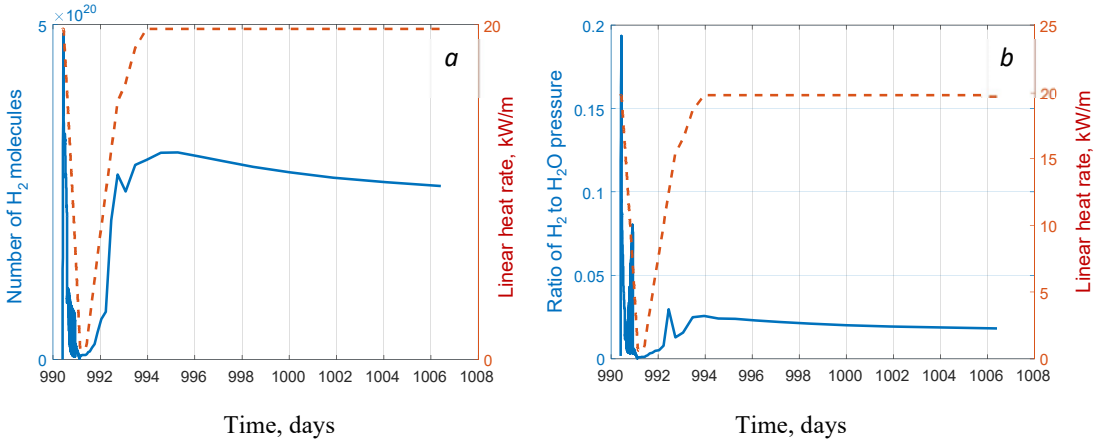

FIG. 2. Dynamics of hydrogen content in a leaking fuel rod failed at the beginning of the fuel cycle, power drop 1 hour after the failure: a – total number of H_2 molecules, b – maximum hydrogen-to-steam pressure ratio.

3.3 Additional factors potentially preventing severe hydriding

As shown in simulations, hydrogen removal from the leaking fuel rod during the power drop hardly is the only factor preventing cladding from severe secondary degradation. So, besides decrease in hydrogen-to-steam pressure ratio there should be some additional processes that evolve at power reductions and suppress secondary degradation. These processes include [6]:

— Possible formation of a very protective oxide film on the inner surface of cladding due to presence of water and its radiolysis by fission fragments in the pellet-to-cladding gap.
— Washing out fission products adsorbed at inner cladding surface by water filling the leaking fuel rod (it is argued that attack by fission products – halogens and cesium – may destroy the protectiveness of the oxide film and facilitate penetration of hydrogen into the cladding).
— Possible additional oxidation of fuel pellets in water while lhgr is low during the transient.
— Rapid helium release from the leaking fuel rod and its substitution by steam (this entails a decrease in the hydrogen-to-steam ratio in the gas phase).

In the latter case helium release may lead to condensation of a water film on cooler areas of the inner cladding surface after return to full power. It is possible due to increase of steam partial pressure. The water film may be an extra barrier between hydrogen and the cladding. But it should be noted that effect of the water film needs more accurate and comprehensive analysis. Hampering penetration of hydrogen into cladding in one place, it may lead to higher hydrogen concentration in other places due to convective mass transfer induced by flowing down of the water film.

The above effects are insufficiently studied and therefore are modeled with large uncertainties. Thus, power reductions should be currently considered as solely an empirically demonstrated means to prevent secondary degradation. Additional experiments would be beneficial for a detailed study of the mechanisms that hamper secondary degradation during power drops. These studies would be also helpful in finding the optimal amplitude and duration of power drops at NPPs.

4. MODEL SCENARIOS OF POWER TRANSIENT

The amplitude and duration of power reduction are not the only important parameters of the power transient. Power maneuvers may cause high mechanical stress in fuel cladding. Mechanical properties of cladding in leaking fuel rods degrade due to hydrogen pickup. Thus, it is crucial to determine the preferable rates of power reduction and subsequent return to the previous power level. Limitations on the rates of power changes could avoid high mechanical stress in leaking fuel and the risk of severe cladding degradation.

Several scenarios were selected for the analysis of thermal and mechanical behavior of leaking fuel during power transients (see Fig. 3).

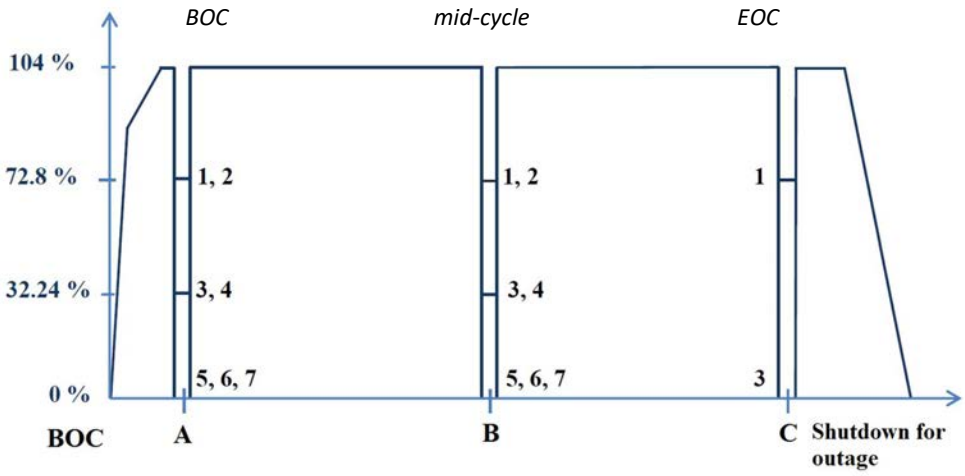

FIG. 3. A scheme of power transient scenarios.

Scenarios in Fig. 3 considered present regulatory limitations and current practices of power maneuvers at WWER-1000 power units. Operational data for one of the 18-months cycles at Rostov NPP-1 was utilized for the basic fuel irradiation history. Three moments of time were selected for the power transient: BOC, mid-cycle and EOC (about 20 days before the shutdown for the planned refueling outage). Various magnitudes and rates of power changes were considered (see Fig. 4 and Table 1).

Pin-by-pin neutronic calculations were performed with the certified SVC code for each scenario. During power transient, axial power profiles in fuel rods are distorted. The LHGR value may increase at some axial locations (see Fig. 5). Hoop stress in cladding increases in such places.

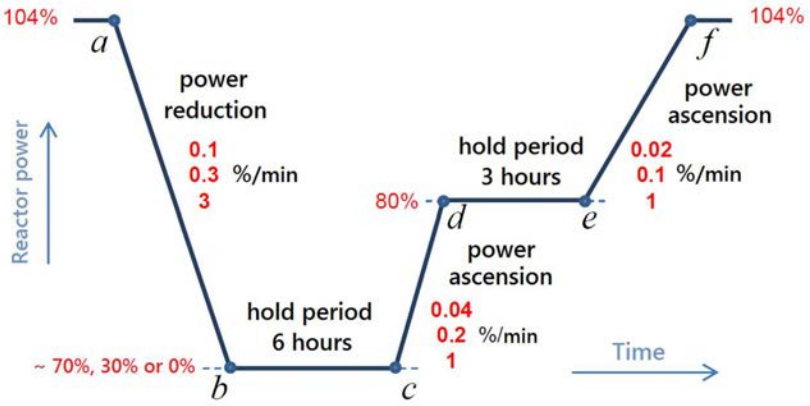

FIG. 4. A scheme of power changes during the transient.

TABLE 1. PARAMETERS OF THE POWER TRANSIENT AT DIFFERENT STAGES (ACCORDING TO THE SCHEME SHOWN IN FIG. 4)

Scenario #	The lowest power during the transient (%N_{nom})	Rate of power change, %/min			Time, h					
		ab	*cd*	*ef*	*ab*	*bc*	*cd*	*de*	*ef*	total
A1	70	0.3	0.2	0.1	1.9	6	0.8	3	4	15.7
A2	70	3	1	1	0.2	6	0.2	3	0.4	9.8
A3	32	0.3	0.2	0.1	4	6	4	3	4	21
A4	32	3	1	1	0.4	6	0.8	3	0.4	10.6
A5	0	0.1	0.04	0.02	16.8	6	32.1	3	20	77.9
A6	0	0.3	0.2	0.1	5.6	6	6.4	3	4	25
A7	3	3	1	1	0.6	6	1.3	3	0.4	11.3
B1	70	0.3	0.2	0.1	1.9	6	0.8	3	4	15.7
B2	70	3	1	1	0.2	6	0.2	3	0.4	9.8
B3	32	0.3	0.2	0.1	4	6	4	3	4	21
B4	32	3	1	1	0.4	6	0.8	3	0.4	10.6
B5	3	0.1	0.04	0.02	16.8	6	32.1	3	20	77.9
B6	3	0.3	0.2	0.1	5.6	6	6.4	3	4	25
B7	3	3	1	1	0.6	6	1.3	3	0.4	11.3
C1	70	0.1	0.04	0.02	5.6	6	4.2	3	20	38.8
C3	3	0.1	0.04	0.02	16.8	6	32.1	3	20	77.9

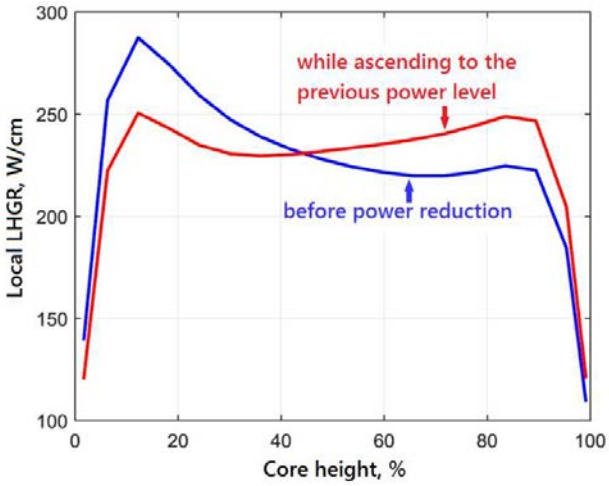

FIG. 5. An example of neutronic calculations: evolution of the axial power profilein one of the fuel rods during power transient shortly before the EOC.

5. DEGRADATION OF CLADDING PROPERTIES IN LEAKING FUEL RODS

After a primary failure, the rate of hydrogen uptake by cladding increases. This entails degradation of cladding mechanical properties and increases the risk of its fracture while mechanical loading.

According to the available PIE data, both ductile and brittle fracture may occur in hydrided cladding made from E110 alloy.

In a conservative approach, it can be assumed that cladding fracture is brittle at hydrogen concentrations above 200 ppm. In this case fracture occurs if stress exceeds ~ 100 MPa.

The ductile fracture happens at hydrogen concentrations below 200 ppm. In the ductile area, the effect of hydrogen content on the mechanical properties and plasticity can be divided in two stress ranges: when stress is much lower than the yield stress and when it is close to the yield stress.

If the stress value is far from the yield stress, strain evolves due to creep of the material. Conservative lower estimate for the failure strain of gas-filled tubes of irradiated fuel claddings made from Zircaloy is 2.0%, according to the numerous test results.

In the high strain region, when stress value is close or exceeds the yield stress, the ductile fracture occurs when plastic strain reaches the value of ~ 1.5 %.

6. EFFECTS OF POWER TRANSIENT PARAMETERS ON BEHAVIOR OF LEAKING FUEL RODS

The RTOP-CA cod was used to study the influence of power transients on behavior of leaking fuel rods. The following issues have been analyzed.

- How does the amplitude of power reduction affect the condition of leaking fuel rods?
- How does the time ($\Delta\tau$) between the moment of a primary failure and the beginning of power reduction influence the level of cladding hydriding and the peak stress-strain in fuel cladding?
- What is the effect of axial position of the defect in cladding?

6.1 Effect of the amplitude of power reduction

Currently, it is believed that secondary failures can be prevented by covering of the fuel stack inside the rod with water [6, 11]. Therefore, it can be assumed that the major aim of power reduction is to provide sufficient water ingress inside a leaking fuel rod (at least sufficient for filling the pellet-to-cladding gap).

Simulations with the RTOP-CA code have shown that filling of the leaking fuel rod with water is practically independent from the time period $\Delta\tau$ between the moment of the primary failure and the beginning of power reduction. It is also insensitive to the axial position of the defect in cladding. So, the key parameters for water ingress are the basic LHGR of a fuel rod and the power reduction amplitude.

If reactor power is reduced down to 70% of the nominal value (N_{nom}), a small fraction of the pellet-to-cladding gap along the fuel stack is filled with water in the leaking fuel rods with high LHGR. If reactor power is reduced to 30%, the pellet-to-cladding gap may not be fully filled with water in the uprated fuel rods (see an example in Fig. 6).

Complete filling with water, including high power rods, takes place if reactor power is dropped down to approximately zero level. The time period when the fuel rod remains filled with water depends on the duration of the power transient. This time period is longer for scenarios with low rates of power reduction and ascension.

Power transients with power drops down to ~ 0–3%N_{nom} lead to complete filling with water not only for the pellet-to-cladding gap. The central channel in the fuel stack is filled with water as well (almost completely). This may be a supplementary positive effect on suppressing secondary degradation due to additional oxidation of fuel pellets. Higher stoichiometry of uranium dioxide results in lower rates of hydrogen generation after the leaking fuel rod returns to full power.

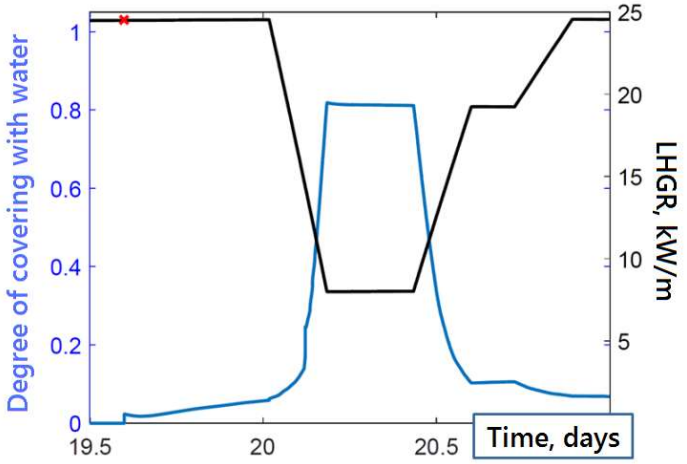

FIG. 6. Fraction of the pellet-to-cladding gap along the fuel stack filled with water in a high-power rod. An example for reactor power drops down to 30% at the BOC (scenarios A3, A4), ✖ denotes the moment of the primary failure.

6.2 Hydrogen content in cladding at the start of power reduction

After the fuel failure, the rate of hydrogen pickup by cladding increases. It is important to acknowledge how much hydrogen has been accumulated in cladding and how much its mechanical properties degraded to the start of the power transient.

The RTOP-CA simulations demonstrate that hydrogen uptake by cladding after the fuel failure feebly depends on fuel burnup and axial position of the defect in leaking fuel rod. Hydrogen uptake is governed by the instant fuel LHGR, and the time elapsed after the primary failure. In all the considered scenarios, hydrogen content in cladding does not exceed 200 ppm by the end of the power transient (see Fig. 7). This hydrogen content does not noticeably affect mechanical properties of E110 cladding in comparison to that of intact fuel rods.

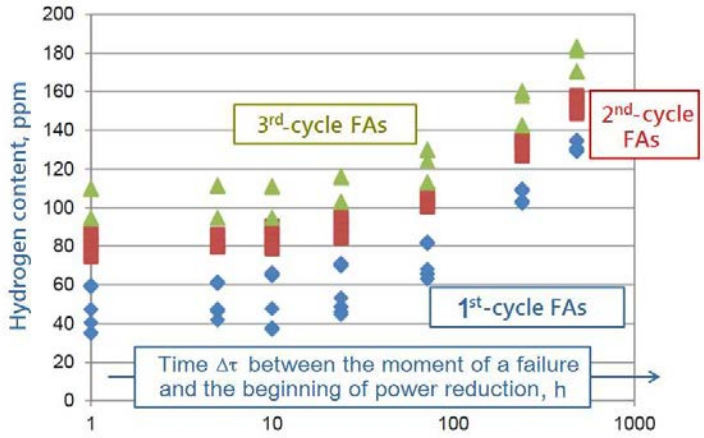

FIG. 7. Hydrogen content in cladding as a function of time ($\Delta\tau$) between the moment of a primary failure and the beginning of power reduction.

6.3 Thermal mechanics of leaking fuel rods during power transient

The greatest mechanical loads on cladding are achieved in high power rods with significant increment of local LHGR when tensile stresses are present in cladding prior to the beginning of the transient due to pellet-to-cladding interaction (PCI).

The magnitude of the hoop stress in cladding grows with increasing time interval $\Delta\tau$ between the fuel failure and the beginning of the reactor power drop. Peak hoop stress in cladding during the considered power transients does not exceed 120-140 MPa, if reactor power starts to decrease no later than 72 hours after the primary failure (see Fig. 8).

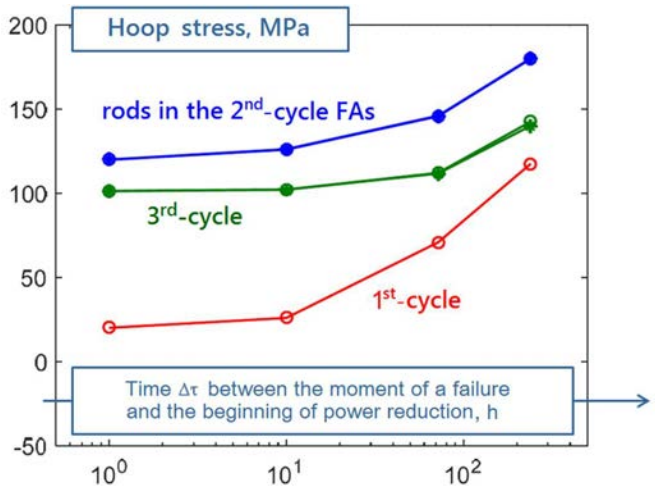

FIG. 8. Peak stress in fuel cladding. Example of simulations for scenario C3.

The highest stress is achieved when maximum increment of LHGR due to the power transient coincides in location with the maximum of LHGR axial profile, and the defect in cladding is located in this zone as well. Peak values of LHGR itself and LHGR increment may be reached at different axial coordinates. In this case, the highest stress is realized if the defect in cladding is located between these coordinates (in the considered scenarios – closer to the zone of maximum local power). At a distance from the zone between the peak values of local power and LHGR increment, the stress in cladding feebly depends on the defect axial position.

The relative strain of cladding is small in all the considered scenarios. During the power transient, it accumulates in the range of ~ 0.15%. In general, it can be concluded that the threshold conditions for cladding fracture are not reached in all the considered scenarios.

6.4 Effect of the rate of power changes on stress in cladding

Analysis has shown that in the considered operational modes, the stress-strain state of cladding in leaking fuel rods does not directly depend on the rate of power changes. The stress and strain in cladding are determined by the basic fuel LHGRs (it is the characteristic of the core loading pattern), and the degree of distortion of power axial profiles in the transient mode (local power increments). Distortion of the power axial profile in fuel rods depends on an algorithm of control actions that the plant operator undertakes to change the reactor power.

In the present study it was assumed that changes in the reactor power were driven by gradual motion of the working group of control rods. During the intermediate hold periods at a given power level, an adjustment of the boric acid concentration in primary coolant was performed. These control actions, firstly, lead to higher LHGR increments in fuel rods during scenarios with faster changes in reactor power. Secondly, the magnitude of LHGR increments depends on how much time elapsed from the BOC before the power transient. The LHGR increments at the very beginning of cycle are generally lower than those at the mid-cycle (see Fig. 9). At the EOC, due to excitation of xenon oscillations, only the "slowest" scenario C3 (power ascension rate 0.02 $\%N_{nom}$/min applied from 80 to 104% of reactor nominal power) satisfies the safety design criteria that impose limitations on local LHGR depending on burnup and axial coordinate in fuel rods.

The magnitude of the local LHGR increments (δLP) may depend on the hold time at the minimum power level and on the intermediate hold time at 80% N_{nom} during the power ascension. The present study has shown that δLP ~ 20-25 W/cm does not bear any risk of cladding rupture. These δLP values may be ensured by different control actions; power transient parameters may also be varied. So, it is possible to make an additional optimization of the considered scenarios in order to provide a more convenient response of the plant operator to fuel failure by a short-term drop of reactor power.

Maximum increments of hoop stress in claddings in different scenarios of the power transient are shown in Fig. 10.

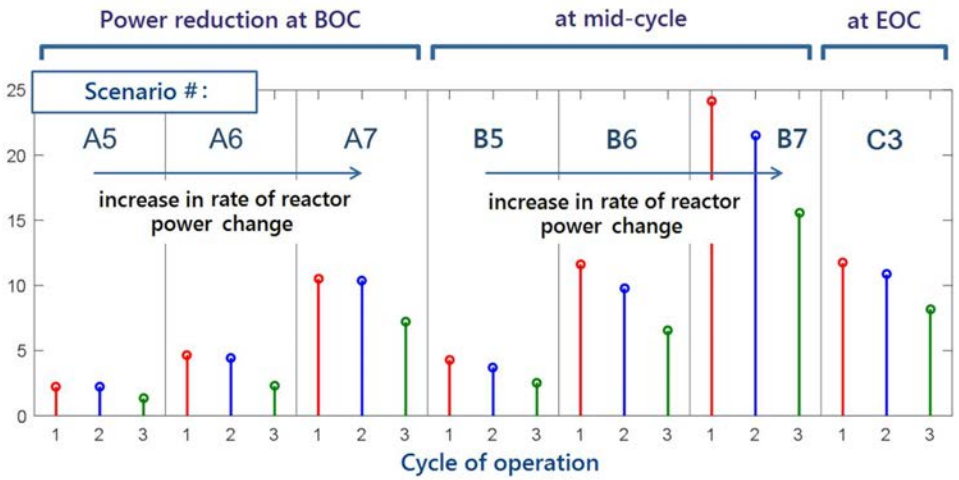

FIG. 9. Maximum LHGR increments (W/cm) in fuel rods during power transients according to different scenarios (see Table 1).

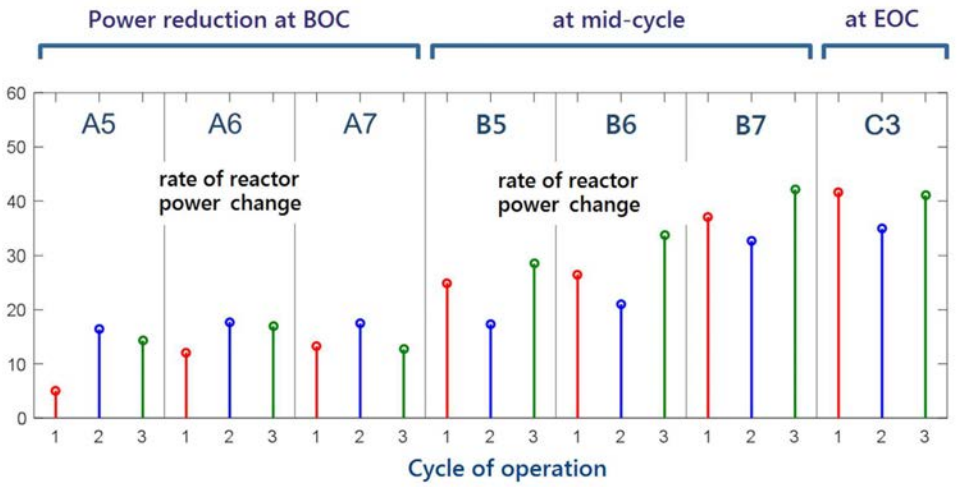

FIG. 10. Maximum increment of mean hoop stress (MPa) in fuel rods during power transients according to different scenarios (see Table 1).

7. PRELIMINARY RECOMMENDATIONS ON WWER POWER REGULATION AFTER DETECTION OF A FUEL FAILURE

In the first half of the fuel cycle, the following basic scenario may be adopted: after a short-term drop of reactor power down to ~ 0-3%, the rate of power ascension should be limited by the value of 0.1 $\%N_{nom}$/min in the range of 80 to 104$\%N_{nom}$. In the second half of the fuel cycle, the rate of power ascension should be limited by 0.02 $\%N_{nom}$/min.

Additional neutronic calculations could provide fewer conservative limitations for the rate of power change in the second half of the fuel cycle. It may be determined when the rate of power ascension should become less than 0.1 $\%N_{nom}$/min. Furthermore, the second half of the fuel cycle can be divided into intervals with different limitations on the rate of power ascension for each interval.

An upper limit for the time between the moment of primary failure and the start of the reactor power reduction could be preliminarily recommended as 3 days (72 hours). The fact of fuel failure can be detected within 3 days at most of the operating WWER units (even when they are not equipped with the on-line system for monitoring and analysis of primary coolant activity).

8. CONCLUSIONS

Currently, the most promising way to reduce the risk of severe secondary degradation of leaking fuel seems to be a short-term power reduction after detection of a failure. The aim of the present study was to estimate the appropriate values for the amplitude and the rate of reactor power changes. Parameters of the power transient were chosen in such a way as, on the one hand, to reduce the risk of severe secondary degradation, and, on the other hand, to eliminate fracture of cladding in leaking fuel rods due to enhancement of mechanical load. The effect of different parameters on the behavior of leaking fuel rods during the power transient was studied using simulations with the RTOP-CA code based on 18-month fuel cycle at WWER-1000 power units.

At present time it may be supposed that an important factor contributing to prevention of severe secondary degradation is filling of the leaking fuel rod with water at low power. The simulations show that meeting this requirement for the uprated fuel rods needs high amplitude of the power reduction. By the preliminary estimate, the thermal power of WWER-1000 reactors is to be dropped down below 30% of the nominal value (N_{nom}). It is shown that if the lower power level is 0-3% it is sufficient for filling with water entire pellet-to-cladding gap in any kind of leaking fuel rod regardless its burnup. The actual value of the lower power level (between 0% and 30%) for achieving the same objective may be specified more accurately by additional simulations.

Since hydrogen uptake by fuel cladding may be quite intensive, the power drop would be more effective if it is carried out as soon as possible after the failure. This fact is a challenge for NPPs to use the on-line systems for monitoring of coolant activity which are capable of prompt automatic detection of a fuel failure occurrence. On the basis of simulations and current understanding of phenomena in leaking fuel rods, the power drop may be preliminary recommended no later than 72 hours after the failure. In this case, uniform hydrogen uptake does not lead to embrittlement of WWER fuel cladding.

Return to full power after a short-term power drop may cause additional tensile stress in cladding. The increment of tensile hoop stress is higher if the power transient takes place during the latter stages of a fuel cycle. To assure lower mechanical loads on the leaking fuel cladding it may be preliminary recommended to limit the rate of power escalation above 80% N_{nom} by the value of 0.1 %N_{nom}/min.

Of course, the best thing would be defining a ‘safety domain’ based on the cladding resistance limits, so that operators whould know they do not take any risk in this “safety domain”. But the current knowledge on different aspects involved into secondary fuel degradation has quite enough blind spots. So, some additional research would be helpful including both simulations and additional small-scale experiments for better mechanistic understanding of phenomena inside fuel rods after occurrence of the failure during reactor operation.

REFERENCES

[1] EDSINGER, K., CHENG, B., *et al.*, Zero by 2010 and recent U.S. fuel reliability experience, Proc. Water Reactor Fuel Performance Meeting (TopFuel), Chengdu, China, Sept.11-14, 2011, paper T2-41.

[2] MAZURKIEWICZ, S., BRETTING, C., *et al.*, Meeting the Industry Challenge to Achieve Leak Free Performance, (AREVA), LWR Fuel Performance Meet. (Top Fuel 2016), Boise, Idaho, USA, 11-16 September 2016, pp.1405-1414.

[3] MOLCHANOV, V., Project «Zero failure level»: status, problems, tasks for the future, Proc. 12th Int. Conf. on WWER fuel performance, modelling and experimental support, Nesebar, Bulgaria September 18-22, 2017.

[4] DESHON, J., WHITESIDE, K., Establishing and Sustaining a Technical Program to Achieve Zero Fuel Failures, (EPRI, INPO), IAEA Tech. Meet. “Achieving Zero Fuel Failure Rates: Challenges and Perspectives,” Nessebar, Bulgaria, 1-2 October 2015.

[5] LOCKE, D.H., The behaviour of defective reactor fuel, Nucl. Eng. Des. **21** (1972) 318-330.

[6] CLAYTON, J.C., Internal hydriding in irradiated defected zircaloy fuel rods, ASTM STP 1023 (1989) 266-288.

[7] OLANDER, D.R. and VAKNIN, S., Secondary hydriding of defected zircaloy-clad fuel rods, EPRI TR-101773 (1993).

[8] KIM, Y.S. and KIM, S.K., Kinetic studies on massive hydriding of commercial zirconium alloy tubing, J. Nucl. Mater. **270** (1999) 147-153.
[9] EVDOKIMOV, I.A. and LIKHANSKII, V.V., In-pile criteria for the initiation of massive hydriding of Zr in steam-hydrogen environment, ASTM STP 1505 (2009) 193-204.
[10] LIMBÄCK, M., DAHLBÄCK, M., HALLSTADIUS, L., *et al.*, Test-Reactor Study of the Phenomena Involved in Secondary Fuel Degradation, Proc. 2004 Int. Meeting on LWR Fuel Performance (TopFuel-2004), Orlando, Florida, September 19-22, 2004, paper 1045, pp.55-68.
[11] WRIGHT, J., TVERBERG, T., YAGNIK, S., LIMBÄCK, M. and SCHRIRE, D., Summary of test reactor experiments to simulate secondary fuel degradation and its mitigation, 2017 Water Reactor Fuel Performance Meeting (TopFuel-2017), September 10-14, 2017, Ramada Plaza Jeju, Jeju Island, Korea.
[12] SOROKIN, A., LIKHANSKII, V., BORISOV, A., ILYENKO, A., GORYACHEV, A. Validation of the enhanced version of the RTOP-CA code designed for modeling the fission products release from failed fuel rod to the primary circuit of WWER, Proc. 13th Intern. Conf. "WWER Feul Performance, Modelling and Experimental Support", 2019, Nesebar, Bulgaria.
[13] SOROKIN, A., LIKHANSKII, V., EVDOKIMOV, I., *et al.*, Capabilities of the RTOP-CA code to simulate leaking fuel behavior and release of radioactive fission products into primary coolant of light-water reactors, Proc. Tech. Meet. Fuel Failure in Normal Operation of Water Reactors: Experience, Causes and Mitigation, IAEA Headquarters, Vienna, Austria, 14–17 December 2020.
[14] KALINICHEV, P.M., EVDOKIMOV, I.A., LIKHANSKII, V.V., A technique for detection of WWER fuel failures by activity of Xe radionuclides during reactor operation, Nuclear Energy and Technology **4** 4 (2018) 263-270.
[15] KALINICHEV, P.M., EVDOKIMOV, I.A., LIKHANSKII, V.V., Experience in detection of WWER fuel failures by activity of ^{133}Xe and ^{135}Xe during reactor operation, Proc. Tech. Meet. Fuel Failure in Normal Operation of Water Reactors: Experience, Causes and Mitigation, IAEA Headquarters, Vienna, Austria, 14–17 December 2020.
[16] CLAYTON, J.C., Internal hydriding in irradiated defected Zircaloy fuel rods: A review, Bettis Atomic Power Lab., West Mifflin, PA (USA), 1987, WAPD-TM-1604.
[17] EVDOKIMOV, I.A., LIKHANSKII, V.V., SOROKIN, A.A., *et al.*, Software in support of fuel operation in WWERs, Proc. 10th Int. Conf. on WWER fuel performance, modelling and experimental support, Sandanski, Bulgaria, 7-14 September 2013.
[18] LIKHANSKII, V.V., EVDOKIMOV, I.A., ALIEV, T.N, *et al.*, Criteria for removal of defective fuel rod from fuel assembly under repair without cladding rupture, Proc. WRFPM 2014 (TopFuel 2014), Sendai, Japan, Sep. 14-17, 2014, paper No. 100073.
[19] ALVAREZ, L., DANIELS, T., *et al.*, Review of Fuel Failures in Water Cooled Reactors, IAEA Nuclear Energy Series, No. NF-T-2.1, IAEA, Vienna, 2010.
[20] RUDLING, P., *et al.*, Secondary degradation mechanisms – a theoretical approach to remedial actions, SKI Report No.00:32, Sweden, April 2000.
[21] UNE, K., Kinetics of reaction of zirconium alloy with hydrogen, J. of the Less Common Metals, **57** 1 (1978) 93-101.
[22] KIM, S.Y., *et al*., High-pressure hydriding of Zircaloy, J. Nucl. Mater. **240** 1 (1996) 27-31
[23] EVDOKIMOV, I.A., LIKHANSKII, V.V., ALIEV, T.N., *et al.*, Secondary Hydriding Criteria Under Irradiation Conditions, Nuclear Eng. and Design **241** (2011) 1414-1420.
[24] MARKOV, D., *et al.*, Integration of post-irradiation examination results of failed WWER fuel rods, Proc. 5th Int. Conf. on WWER fuel performance, modelling and experimental support, Albena, Bulgaria (2003) 273-277.

CAPABILITIES OF THE RTOP-CA CODETO SIMULATE LEAKING FUEL BEHAVIOR AND RELEASE OF RADIOACTIVE FISSION PRODUCTS INTO PRIMARY COOLANT OF LIGHT-WATER REACTORS

A.A. SOROKIN, I.A. EVDOKIMOV, K.E. ULIBYSHEV, A.V. BORISOV, E.Yu. AFANASIEVA
SRC RF TRINITI,
Troitsk, Russian Federation

V.V. LIKHANSKII, O.V. KHORUZHII, V.G. ZBOROVSKII
NRC "Kurchatov Institute",
P.N. Lebedev Physical Institute,
Moscow, Russian Federation

S.A. ILYENKO, Yu.S. KUDRIN, I.V. KISSELEVA, A.V. GORYACHEV, E.A. ZVIR
SSC RIAR,
Dimitrovgrad, Russian Federation

Abstract

The area of application of the RTOP-CA code is simulation of leaking fuel behavior and release of fission products into primary coolant of a WWER power unit. The RTOP-CA code implements a mechanistic approach to modeling the behavior of a leaking fuel rod, based on detailed simulation of physical processes. The code self-consistently takes into account changes in the thermo-physical properties of fuel pellets and cladding due to fuel failure, release of radionuclides from fuel pellets, transfer of fission products and hydrogen to the defect in cladding, change in geometric characteristics of fuel pellets and cladding, thermal behavior of a fuel rod, and release of radionuclides into coolant. The main mechanisms of mass transfer in a leaking fuel rod are associated with the effective diffusion of the components of the steam-gas mixture along the fuel rod, as well as convective transfer due to evolving pressure difference between the leaking fuel rod and primary coolant. Additional mass transfer in fuel rod is possible due to the flowing down of a water film condensed in the pellet-to-cladding gap under the action of gravity and its flashing into steam in the hot regions of the fuel rod. The paper presents a brief description of the RTOP-CA code and some results of its validation. The RTOP-CA code was validated on experimental data for test fuel rods with artificial defects in cladding irradiated in the MIR research reactor. Validation also included the operational data on fission products activity at WWER power units and post-irradiation examinations of leaking WWER fuel.

1. INTRODUCTION

The problem of 'fuel failures 0' in WWERs is associated with assurance of efficient and safe operation of nuclear fuel. Formation of a through-wall defect in fuel cladding leads to release of fission products into primary circuit. The maximum allowed level of coolant activity is limited by safety regulations. Success in operation of nuclear utilities depends on the number and severity of fuel failures. One of the ways to ensure better reliability of nuclear fuel is studying of leaking fuel behavior and release of fission products into the primary circuit. These studies for WWER fuel include experiments [1] in the MIR research reactor with the test fuel rods having an artificial defect in cladding, as well as numerical simulations of fission products release from leaking fuel rods. In experiments at the MIR reactor, behavior of leaking WWER fuel rods of both hollow and solid pellet design was studied. Activities of fission products in coolant of the MIR loop facility were measured during irradiation. The experiments also included post-irradiation examinations of the test fuel rods. The obtained experimental data were used to validate the RTOP-CA code (**R**eac**T**or **OP**eration – **C**oolant **A**ctivity).

The RTOP-CA code was developed to simulate release of radioactive fission products into primary coolant and behavior of fuel rods before and after the failure. The RTOP-CA code is owned by Russian fuel vendor – TVEL Fuel Company. The RTOP-CA code [1] belongs to the class of mechanistic fuel performance codes. It is based on a consistent and detailed physical description of the elementary processes that govern behavior of a leaking fuel rod, as well as interrelations between different processes. The phenomenology implemented in the RTOP-CA code includes changes in properties and operational characteristics of fuel rods before and after the

failure, fission products release from fuel pellets, different mechanisms of radionuclides transfer and release into primary circuit.

The first version of the RTOP-CA code was developed based on the RTOP fuel performance code [4], designed for modeling of thermal behavior of intact fuel rods. The RTOP-CA code was certified in Russia in 2009 for modeling of activity of fission products in WWER primary coolant after a failure of fuel rods of 'traditional' design – with fuel pellets bearing a central hole (also called 'hollow' or 'annular' pellets). At present, fuel with improved economic and technical characteristics is available for WWERs. Higher economic indicators are associated with transition to longer fuel cycles and an increase in the reactor power up to 104–107%. To achieve such indicators, higher fuel enrichment in ^{235}U is applied; fuel loading into the core as well as the number of U-Gd fuel rods are increased. One of the modifications of the WWER fuel design is characterized by the absence of a central hole in fuel pellets ('solid' pellets), a reduced thickness of cladding wall and initial pellet-to-cladding gap of smaller width. Fuel with solid pellets is also planned to be used for 'TVS-KVADRAT' fuel assemblies intended for operation at PWR power units. Currently, a new extended version of the RTOP-CA code has been developed, which includes capabilities for modeling behavior of leaking WWER fuel of different design (hollow/solid pellets, U-Gd fuel rods, fuel rods with blankets[10]). One of the possibilities of the extended version of the RTOP-CA code is simulation of mechanical behavior of fuel rods before and after the failure.

The paper is an overview of capabilities of the extended version of the RTOP-CA code and results of its validation. The second section provides a brief description of the models for release of fission products from fuel pellets and their transport inside a leaking fuel rod. The third section is devoted to validation of the RTOP-CA code based on experimental data from the MIR research reactor, as well as operational data on primary coolant activity from WWER power units.

2. MASS TRANSFER IN LEAKING FUEL RODS

The RTOP-CA code is based on the phenomenology which consolidates available experimental findings and theoretical concepts for both intact and leaking fuel behavior. Validation of the RTOP-CA models was focused (but not limited to) on the data of post-irradiation examinations (PIEs) of WWER fuel from commercial power units. The specific features of the fission products release from leaking fuel rods as well as changes in fuel characteristics due to a fuel failure were validated against the data from the MIR research reactor.

Immediately after the failure, the pressure inside and outside the fuel rod is equalized due to ingress of the coolant into the fuel rod. Under operating conditions, the most part of incoming water flashes into steam. In addition to steam, a fuel rod can also contain considerable amounts of helium, hydrogen, and fission gas. After release from the fuel pellets, fission products (FPs) are transferred to the defect in cladding through a system of channels including the central channel in the fuel stack and the pellet-to-cladding gap. These two main pathways for FPs are interconnected to each other by the net of inter-pellet gaps and cracks in the fuel pellets.

The key mechanisms of mass transfer in the fuel rod are related to effective diffusion and convective transfer along the fuel stack. The effective diffusion is a consequence of a periodical fluid flow in the central channel of the fuel stack arising due to coolant pressure pulsations. Pressure pulsations are caused by operation of circulation pumps and coolant turbulence in the reactor core. Both molecular diffusion and pulsating convective transport can be described in a unified manner by introducing an effective diffusion coefficient. Pulsations of the primary coolant pressure also provide mass transfer between the leaking fuel rod and the coolant under steady-state operating conditions. In a leaking fuel rod with solid pellets, pulsation fluid flows along the fuel rod do not develop due to higher hydraulic resistance. In this case, mass transfer is reduced to molecular diffusion.

In areas of inner cladding surface with a lower temperature, steam can be condensed into a water film. If the fuel heat rate is close to the average value (~ 17 kW/m for WWERs-1000), a water film is formed only in the lower part of the pellet-to-cladding gap. With a decrease of the linear heat generation rate (LHGR), the volume fraction of the liquid phase increases. The presence of the condensed coolant in the fuel rod can lead to convective transfer due to water flowing down under the action of gravity, its contact with hot regions of the fuel pellets and evaporation.

Additional mass transfer in a leaking fuel rod is also caused by mechanisms which lead to violation of the pressure balance between the fuel rod and the primary coolant. Under irradiation conditions, the balance may be

[10] Blankets are sections made from natural uranium in the upper and lower end of the fuel stack.

disturbed by, e.g., evolution of linear heat rate or its axial profile in the fuel rod, increase in the fuel temperature due to degradation of UO_2 thermal conductivity, intensive release of fission gas from fuel pellets, and hydrogen uptake by cladding. In case of imbalance, the pressure inside the leaking fuel rod tends to equalize with the external pressure inducing additional transfer of fluid inside the fuel rod. The most intensive FPs release by this mechanism can be observed during power transients and reactor shutdown.

The behavior of leaking fuel is governed by many interrelated processes: transport of hydrogen, helium and fission gas, oxidation of fuel pellets and cladding inner surface, condensation, or evaporation of portions of water. The conditions for condensation of water in the pellet-to-cladding gap are determined by the steam partial pressure which can vary depending on the local content of hydrogen, helium, and fission gas. Components of the gas mixture are distributed along the fuel rod depending on the mass transfer (including convective transport caused by the water film flowing down in the pellet-to-cladding gap). Fuel oxidation is one of the major sources of hydrogen. The rate and the level of fuel oxidation depend on the hydrogen-to-steam ratio. Changes in fuel stoichiometry led to an increased mobility of fission products in the fuel grains, degradation of UO_{2+x} thermal conductivity and higher temperature. As a result, the rate of FPs release from the fuel rod can significantly increase.

2.1 Release of radionuclides from fuel pellets

The source-term for simulations of FPs transport in the fuel rod is governed by release of radionuclides from fuel pellets. The buildup of radioactive FPs by fission occurs in the form of transmutation chains. The radiological environment at NPPs is mainly influenced by relatively 'long-lived' isotopes (decay constants $\lambda \approx 10^{-6}$-10^{-2} s^{-1}) at the end of the chains. In the RTOP-CA code, when describing the production of nuclides, a simplified shortened notation of the chain of nuclear transmutations is used neglecting all the very short-lived precursors. The transmutation chains accounted for by the code can be represented in the form of pairs: the precursor and its daughter isotope.

The main release mechanisms for FPs under consideration are recoil [5] and diffusion [6] through the open surface of the fragmented fuel pellets. When calculating release by recoil, the pressure and composition of gas adjacent to the surface, as well as the geometry of voids in the fuel rod, are taken into account. The geometric parameters of fuel pellets and cladding are calculated when modeling thermal and mechanical behavior of a fuel rod.

Accumulation of radioactive FPs in the fuel grains is limited due to decay. As a result, the release of the radioactive FPs from the fuel pellets occurs mainly from its free surface. So, evolution of the free fuel surface during irradiation needs to be modeled. The rate of FPs release depends on whether it is the geometric surface of the fragmented pellet or the open surface of as-fabricated and irradiation-induced intergranular pores. To determine the diffusional release of the precursor-daughter pair, a system of coupled diffusion equations within a UO_2 grain is solved in a one-dimensional spherical geometry:

$$\begin{aligned} &\frac{\partial C_p}{\partial t} = y_p \dot{F} - \lambda_p C_p + D_p \Delta C_p \\ &\frac{\partial C_i}{\partial t} = y_i \dot{F} + \Lambda_{p\to i} \lambda_p C_p - \lambda_i C_i + D_i \Delta C_i \\ &C_{p,i}(R_{grain}) = 0; \quad \frac{\partial C_{p,i}}{\partial r}(0) = 0 \end{aligned} \tag{1}$$

Here $\lambda_{i,p}$, $C_{i,p}(r)$ are the decay constants and intragranular distribution of the i^{th} isotope and its precursor concentration, respectively; $\dot{F}$ is the fission rate per unit volume, y_i is the fission yield; $\Lambda_{p\to i}$ is the fraction of the decays $p \to i$, $D_{p,i}$ is the diffusion coefficient of radioactive FPs in the UO_2 grain.

FPs are released from that part of the grain boundaries which belongs to the free surface (the geometric surface of fragmented pellets and open porosity). Release of radionuclides through intergranular porosity is modeled with considering the time of their delay in porosity, which depends on the size of intergranular pores and the rate of fission gas release into them. Parameters of the gas pores are determined in the RTOP-CA code when modeling the behavior of fission gas.

The diffusion coefficients of FPs in the fuel grain are calculated taking into account thermally activated diffusion D_T [8], additional diffusion due to uranium vacancies D_V [10] generated during irradiation, and an athermal irradiation-induced diffusion D_A [8]:

$$D = D_T + D_V + D_A \tag{2}$$

Experimental data [6] from research reactors were used to validate the model of radioactive FPs release from UO_2 fuel. In experiments [6], fuel specimens with specified geometric parameters were irradiated in a ventilated capsule in the DIDO reactor (Harwell). In experiments [7], the behavior of intact PWR fuel rods with low fuel burnup (Bu = 0.44 MW·d/kgU) was studied. The fuel rods were irradiated in a high-pressure reactor loop. During the experiments, the linear heat rate was maintained at the constant value 25 kW/m. The centerline temperature of the fuel was measured using a thermocouple; its value was T = 965°C. Fig. 1 shows a comparison between the calculated and measured release-to-birth rate ratio (R/B) for radioactive FPs [7].

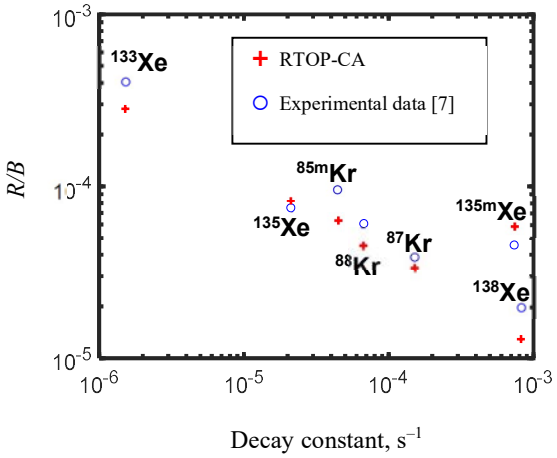

FIG. 1. Release to birth rate ratio for nuclides with different decay constants.

2.2 Fission product distribution in the leaking fuel rod

Radionuclides released from the fuel pellets are mixed with the ambient gas and also can interact with surfaces and water inside a leaking fuel rod. Volatile nuclides (I, Br, Cs, Te) can be partially 'deposited' inside the fuel rod on the surface of pellets and on the cladding inner surface. The adsorbed nuclides do not directly participate in the transport inside the fuel rod. Formation of water condensate in the fuel rod leads to the distribution of nuclides between the steam and the liquid phase. Under operating conditions, the condensate can form in the pellet-to-cladding gap, as well as in pellet cracks and in inter-pellet gaps at the fuel pellets periphery.

The mass transfer is modeled in the RTOP-CA code in a one-dimensional approximation. It is assumed that the transfer occurs along the fuel rod through the generalized channel which includes the central channel in the fuel stack (for hollow pellets design), the pellet-to-cladding gap, pellet cracks, inter-pellet gaps as well as the plenum. The one-dimensional transport model assumes a relatively fast distribution of the components across the fuel rod due to diffusion. Within the framework of the one-dimensional transport model, the distribution of the i^{th} component (i = radioactive FPs, hydrogen, helium, fission gas) along the axial coordinate is described by the concentration $n_i(z)$ averaged over the cross-section (free from fragmented pellets). The average $n_i(z)$ concentration includes components of the coolant gaseous and liquid phases as well as components adsorbed on surfaces inside the fuel rod. The rate of radioactive FPs transfer along the axial coordinate and the rate of their release to the coolant depend on the distribution of radionuclides between the water and steam, the surface area of the fuel and the cladding. Equilibrium steady-state radial distributions of nuclides in the steam and liquid phases of the coolant have the form:

$$n_i^{gas}(r,z) = \frac{K_i^D}{K_{s,i}^{eff}} \frac{n_i(z)}{T(r,z)} \frac{T_{cond}(z) \int dV}{K_i^D T_{cond}(z) \int_{gas} \frac{dV}{T(r,z)} + \int dV \left(1 - g(z)\right)} \tag{3}$$

$$n_i^L(z) = \frac{1}{K_{s,i}^{eff}} \frac{n_i(z) \int dV}{K_i^D T_{cond}(z) \int_{gas} \frac{dV}{T(r,z)} + \left(1 - \delta_g(z)\right) \int dV} \tag{4}$$

Here, integration over the volume of the gas phase is carried out within the axial zone having the coordinate z; $T(r,z)$ is the temperature distribution in the rod; $\delta_g(z)$ is the volume fraction of steam phase. The steam

condensation temperature $T_{cond}(z)$ is determined by the partial pressure of steam in a given axial zone of the rod. The distribution of nuclides between water and steam is characterized by the distribution constant K_i^D [12]:

$$K_i^D = \frac{n_i^{gas}(r_L,z)}{n_i^L(z)}, \tag{5}$$

where r_L is the radial coordinate of the boundary of the steam and liquid phases of the coolant, $n_i^L(z)$ is the concentration of the component in the liquid phase of the coolant. The model assumes that the concentration of components in water is uniform along the radius of the fuel rod. The effective sorption parameter $K_{s,i}^{eff}$ is equal to the ratio of the total number of atoms of the i^{th} nuclide to the total number of its atoms in water and steam:

$$K_{s,i}^{eff}(z) = \frac{N_i^{gas}(z)+N_i^L(z)+N_i^S(z)}{N_i^{gas}(z)+N_i^L(z)} \tag{6}$$

Here i = *I, Xe, Kr, Br, Cs,* $N_i^{gas}(z)$, $N_i^L(z)$, $N_i^s(z)$ is the number of atoms in the steam and liquid phases of the coolant and adsorbed on surfaces, respectively. The equilibrium values of the parameters $K_{s,i}^{eff}$ are calculated taking into account the distribution of nuclides between the liquid and steam phases of the coolant, sorption on surfaces in the rod, as well as the ratio of the surface area of the fuel and cladding to the free volume [13].

2.3 Mass transfer in the leaking fuel rod

To determine the rate of radioactive FPs release to the primary coolant, the RTOP-CA code models diffusion and convective mass transfer along the fuel rod. Apart from radioactive FPs, the components accounted for in transport modeling include hydrogen, helium, and fission gases (xenon, krypton). These gases can be contained in the fuel rod in quantities that are noticeable in comparison with the steam concentration. They affect the conditions for the formation of water condensate. The rate of mass transfer in a leaking fuel rod and the rate of mass exchange with the coolant can change significantly when the water film is formed on the cladding inner surface.

The transfer of radioactive FPs, hydrogen, helium and fission gases is described by the equation:

$$\frac{\partial n_i}{\partial t} = \frac{1}{S}\frac{\partial}{\partial z}\left(\bar{D}_i(z)Sn_V^{tot}\frac{\partial}{\partial z}\left(\frac{n_i}{K_{s,i}n_V^{tot}}\right)\right) - \frac{1}{S}\frac{\partial}{\partial z}\left(\frac{v_v}{K_{s,i}}Sn_i\right) - \omega_i(z)n_i + Q_i(z) \tag{7}$$

Index i refers to a nuclide or fission gas (H_2, He, Xe, Kr). At the lower and upper end of the fuel rod, the following boundary conditions are used:

$$\left.\frac{\partial n_i}{\partial z}\right|_{z=0} = \left.\frac{\partial n_i}{\partial z}\right|_{z=L} = 0 \tag{8}$$

Here $n_V^{tot}(z)$ is the total number of particles per unit volume of the gas phase, determined by the pressure in the primary coolant and the temperature of steam averaged over the cross section; L is the channel length; v_v is the velocity of convective transfer of the steam phase of the coolant; $\bar{D}_i(z)$ is the diffusion coefficient of the component averaged over the cross section of the effective channel. The diffusion coefficient is averaged over the cross-sectional area of the generalized channel considering the radial distribution of the component concentrations (3), (4) and the local diffusion coefficient:

$$\bar{D}_i(z) = \frac{\int D_i(r,z)n_i(r,z)dS}{\int n_i(r,z)dS} \tag{9}$$

The local diffusion coefficients are calculated considering the distribution of the water and steam phases of the coolant, as well as an additional transfer mechanism caused by effective diffusion due to the pulsating flow of the steam-gas mixture in the central channel of the fuel stack. An additional transport mechanism in the central channel of the fuel stack is caused by the diffusion of the component along the radius of the central hole in fuel pellets due to the radial concentration gradient. The inhomogeneity of the component concentrations along the radius of the central hole during the pulsating flow is caused by the inhomogeneity of the flow velocity.

The function $\omega(z)$ in Eq. (7) describes the loss of the components in the fuel rod due to decay (for radioactive FPs) and release to the coolant. The release rate of each component of the gas mixture is considered proportional to its local concentration in the area near the defect.

$$\omega_i(z) = \lambda_i + \mu(z) \tag{10}$$

$$\mu(z) = \delta\left(z - z_{def}\right)\left(\frac{\mu_P^{eff} + \mu_c}{S}\right) \tag{11}$$

Here μ_P^{eff} is the effective rate of mass exchange with primary circuit (m^3/s), caused by the coolant pressure pulsations; $\delta(z - z_{def})$ is the delta function; z_{def} is the defect axial position.

Processes occurring in a leaking fuel rod can lead to a change in the pressure of the steam-gas mixture inside the fuel rod. In this case, in different axial zones of the fuel rod, there may be a lack or excess of pressure in comparison with the primary coolant pressure. The resulting pressure gradients in the fuel rod will lead to the transfer of the steam-gas mixture. The steady-state pressure distribution along the axial coordinate depends on the hydraulic resistance of the fuel rod. In the current version of the RTOP-CA code, the hydraulic resistance of a fuel rod is neglected when solving the convective transfer task. It is assumed that the pressure inside the leaking fuel rod is invariant along the fuel stack and equal to the pressure in the primary circuit. The equality of the pressures at each axial coordinate to the pressure in the coolant is realized in the calculations by the convective transfer of the steam-gas mixture and mass exchange with the primary circuit. The constant μ_c in Eq. (11) characterizes the release rate to the coolant in the case of an excessive number of particles of the steam-gas mixture inside the fuel rod.

The rate of mass transfer due to pressure difference between the fuel rod and primary coolant is given by:

$$\mu_c = \begin{cases} q, & q \geq 0 \\ 0, & q < 0 \end{cases} \tag{12}$$

where q is the rate of steam ingress to the defect area from both sides of the fuel rod

$$q = S\left(z_{def}\right)\left(v_c\left(z_{def}^{-}\right) - v_c\left(z_{def}^{+}\right)\right) \tag{13}$$

$v_c(z)$ is the profile of the convective transfer velocity of the steam phase due to the pressure difference between the fuel rod and the coolant. The velocity values $v_c\left(z_{def}^{-}\right)$ and $v_c\left(z_{def}^{+}\right)$ are taken from the bottom and top sides of the defect, respectively.

In fact, FPs and hydrogen are produced with different rates in each radial cell of a pellet. The effective source $Q_i(z)$ accounts for a contribution of each radial cell at a given axial coordinate. For radioactive FPs the source is the sum of the release rate from the fuel and the rate of decay of the precursor. The source of hydrogen includes its production due to oxidation of the fuel and the cladding inner surface and penetration of hydrogen into the cladding.

The steam concentration in the fuel rod is calculated based on the given total pressure (equal to coolant pressure in the primary circuit) and the distribution of non-condensable gas (H_2, He, Xe, Kr).

In the RTOP-CA code, the gas phase transfer velocity in the leaking fuel rod has two components which are the velocity v_f related to the flow in the water film in the gap and the mass transfer velocity v_c related to the pressure difference between the fuel rod and the coolant:

$$v_v(z) = v_f(z) + v_c(z). \tag{14}$$

The flow in a water film is due to the action of gravity. Under operating conditions of the leaking fuel rod, an amount of the coolant condensate inside the fuel rod is determined by the partial pressure of steam and the temperature distribution in the fuel rod. Under typical WWER conditions, the formation of condensate on the cladding inner surface occurs in the lower part of the rod. The downward flow of the coolant condensate is accompanied by a counter flow of the steam-gas mixture. The steam phase transfer rate is evaluated from the equality of the molar flow rates corresponding to the flow in the water and in the steam-gas mixture.

Changes in fuel temperature and a condensate amount in the fuel rod led to additional transport which is described by the convective velocity component $v_c(z)$. Significant changes in the temperature in the fuel rod, affecting the transport, occur due to the dynamics of the linear heat rate. Several factors can be noted that determine the dynamics of linear heat rate in the rod. First, this is a gradual change in the heat rate during the cycle, due to the burnup of fissile materials and redistribution of the heat generation field in the core. In this case, there is a gradual increase in linear heat rate at the upper and bottom end of the fuel rod and, as a result, partial drying of the volume in the fuel rod. Changes in the linear heat rate are more significant for the mass transfer in a leaking fuel rod. These changes are realized in transient conditions when the characteristic times of the linear heat rate variations can be from several minutes to several hours. An additional contribution to mass transfer can be made by the intensive release of fission gas from the fuel pellets and penetration of hydrogen into the cladding. Also, in

the RTOP-CA code, when calculating the convective transfer velocity, the pressure change in the primary circuit is taken into account.

The rate of mass transfer μ_P^{eff} due to pulsations of the coolant is calculated considering the hydraulic resistance of the fuel rod. In a failed rod, the area adjacent to the defect can be flooded with water. The presence of the liquid phase of the coolant in the defect under nominal operating conditions depends on the value of the local linear heat rate. Accumulation of water near the defect is typical when the breach in cladding is located at the level of the lower fuel blanket, as well as when the U-Gd fuel rod fails at the beginning of operation. A relatively low local linear heat rate can lead to the fact that the entire gap and partially the areas of cracks and inter-pellet gaps will be filled with water. The release of fission products to the coolant due to pressure pulsations in this case will be carried out through the removal of the liquid phase. In this case, the rate of nuclide release will depend on their amount in the liquid phase $n_i^L(z_{def})$ (4). The rate of mass transfer μ_P^{eff} due to pulsations of the coolant is:

$$\mu_P^{eff} = \frac{\rho_v}{K_s^{eff}(\rho_L-\rho_v)} \frac{\mu_P^{gas} S(z_{def})}{K_i^D T_{cond}(z_{def}) \int_{gas} \frac{dS}{T(r,z_{def})} + S(z)\left(1-\delta_g(z_{def})\right)}. \quad (15)$$

Here ρ_L, ρ_v are the densities of the coolant in the liquid and steam phases near the defect. The factor $\frac{\rho_v}{(\rho_L-\rho_v)}$ allows taking into account that in the presence of fluctuations in the coolant pressure, a change in the pressure inside the fuel rod occurs due to a change in the volume of the steam phase, as well as a change in the number of particles in the steam phase due to evaporation/condensation of the coolant. To calculate the value μ_P^{gas}, the hydraulic resistance of the effective channel is calculated. The flow of gas in the system of channels in the failed fuel rod is described by using an equivalent electrical scheme.

3. VALIDATION OF THE RTOP-CA CODE

The extended version of the RTOP-CA code can model the thermal/mechanical behavior of a fuel rod before and after the failure and activity of fission products in WWER primary coolant. The thermo-mechanical options of the code were validated against the PIE data for intact and leaking WWER fuel. The release of fission products was validated on the data from the MIR research reactor, as well as on the operational data on primary coolant activity in WWER power units.

3.1 The experiments in the MIR reactor

The main objective of the experiments in the MIR research reactor was studying the release of radioactive fission products from WWER leaking fuel. The experiments were carried out in the PV-1 loop facility of the MIR reactor under controlled irradiation conditions and known parameters of the artificial defects in cladding of the test fuel rods (1 m fuel stack length). The experiments included irradiation of the test fuel rods, monitoring of activity of different radionuclides (I, Kr, Xe, Cs) in the coolant of the loop facility, and PIEs of the test fuel rods. The mass of the coolant in the loop facility was about 0.25 tons. Coolant activity in the loop due to release of FPs from the test fuel rod was limited only by radioactive decay (coolant purification systems were not used).

To compare the MIR data to the data of activity monitoring in WWER power units, it is necessary to consider the following. The mass of the primary coolant in WWER-1000 reactor is 214 tons. The nominal coolant purification rate is about $2.5 \cdot 10^{-5}$ s^{-1}. This leads to decrease of the steady state ^{131}I activity in the primary coolant by ~ 27 times. The background level of coolant activity in WWERs depends on the amount of tramp uranium (fuel deposits) in the core.

The test fuel rods were irradiated in the MIR reactor in course of 1-3 cycles (about 20 days each). Typically, linear heat rate, temperature and coolant pressure were kept approximately constant during each cycle. Significant changes in these parameters occurred at the beginning of irradiation, as well as in the intervals between subsequent cycles.

The aim of the first series of experiments (Series I) was studying the behavior of leaking WWER fuel at high burnup (up to 66 MW·day/kgU). Uranium dioxide fuel with increased burnup is characterized by low thermal conductivity, developed gas porosity and open surface. A high burnup structure (rim-layer) with high concentration of gas pores is formed at the periphery of fuel pellets. A change in the microstructure and thermo-physical

properties of the fuel pellets at high burnup contributes to the higher rate of FPs release from the fuel pellets. On the other hand, collapsed pellet-to-cladding gap and low linear heat rate during the later periods of operation tend to decrease the FPs release rate and mass transfer in a leaking fuel rod. Two MIR experiments were performed with different axial positions of the artificial defect – in the plenum and in the middle of the test fuel rod (at the level of the fuel stack). The experimental data on coolant activity in the MIR loop facility were used to validate the RTOP-CA code regarding the release of radioactive FPs from leaking WWER fuel of hollow pellet design. The PIE data after MIR irradiation were also used to validate other models. E.g., the data on radial profiles of plutonium content in fuel pellets were found to be in a good agreement with predictions by the RTOP-CA model of plutonium buildup and fuel burnup [14].

The second series of the MIR experiments (Series II) was mainly aimed at studying the release of radionuclides from leaking WWER fuel rods of solid pellet design. One experiment was also carried out with fresh U-Gd fuel rod having an artificial defect in cladding at the level of the fuel stack. The WWER fuel rods of solid pellet design has thinner cladding and more coarse grain size in fuel pellets. Thinner cladding accelerates the collapse of the pellet-to-cladding gap due to irradiation-induced creep. Mass transfer in fuel rods without central channel in the fuel stack is more sensitive to evolution of the pellet-to-cladding gap. Coarse UO_2 grains affect formation and opening of the intergranular porosity and, therefore, the release rate of radionuclides from fuel pellets.

Experiments in the MIR reactor with leaking fuel of solid pellet design were carried out for various fuel burnup, linear heat rate and axial position of the artificial defect. In experiments No. 1 and 2, fuel burnup was about 40 MWd/kgU, the defect in cladding was in the plenum and at the level of the fuel column, respectively. By fuel burnup ~ 40 MWd/kgU, fuel pellets are in contact to cladding and the rate of mass transfer through the pellet-to-cladding gap is limited. Consequently, the rate of FPs release into coolant is low.

Experiment No. 3 was carried out with a fresh U-Gd fuel. The main feature of this experiment and, in general, of U-Gd fuel behavior at the beginning of irradiation is low linear heat rate due to absorption of thermal neutrons by gadolinium isotopes ^{155}Gd, ^{157}Gd. Under these conditions, the pellet-to-cladding gap in leaking U-Gd fuel rods is filled with water.

In experiments No. 4, 5, fresh fuel of solid pellet design was irradiated. In experiment No. 4, the defect was drilled in the plenum. In experiment No. 5, the defect was located at the level of the fuel stack. Due to very low burnup, the pellet-to-cladding gap in the test fuel rods was open during experiments No. 4, 5, and accelerated mass transfer led to more intensive release of the radioactive FPs to the coolant.

Experiments 6, 7 studied the release of radioactive FPs from high burnup (60 MWd/kgU) leaking fuel of solid pellet design. Description of the MIR test parameters is presented in Table 1.

TABLE 1. PARAMETERS OF EXPERIMENTS IN THE MIR REACTOR

Series	Experiment number	Fuel type	Fuel burn-up, MWd/kgU	Defect position	LHGR, kW/m	Subsection
Series I	1	hollow pellets	66	Plenum region (1)	12-13	3.2.1
	2		66	Opposite to fuel pellets (2)	11	
Series II	1	solid pellets (U, Gd) O_2	40	(1)	11	
	2		40	(2)	11	
	3		0	(2)	3-6	3.4.2
	4		0	(1)	5-15	3.3
	5	solid pellets	0	(2)	18-20	
	6		58	(1)	10	3.5
	7		58	(2)	10-11	3.6

3.2 Release of the fission products from WWER fuel rods of hollow pellet design

3.2.1 Release of the radionuclides in experiments in the MIR reactor

In the first experiment (Series I), an artificial defect in the form of a round hole was drilled in the plenum. The test fuel rod was irradiated during one MIR cycle at a constant heat rate. The average fuel burnup in the test fuel rod was 58.4 MWd/kgU. Fig. 2 shows irradiation conditions for this experiment and an example of comparison between the measured and calculated activity of 131I and 85mKr in the coolant. In the second experiment, the defect was made in the form of a longitudinal slot (14 mm long) at the level of the fuel stack. The central part of the slot was located opposite to the inter-pellet gap. The linear heat rate history included three MIR cycles of about 20 days each. The second experiment provided data for steady-state release of radionuclides from leaking fuel, as well as release during transients caused by changes in the linear heat rate, coolant temperature and pressure. Some results of the RTOP-CA code validation against the data of the second experiment are presented in Section 3.5.

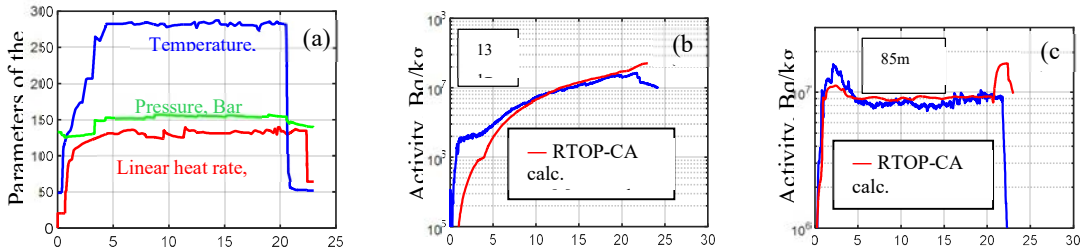

FIG. 2. MIR experiment 1, Series I (artificial defect in the central part of the plenum): (a) – linear heat rate, coolant pressure and temperature, (b) – ^{131}I activity, (c) – ^{85m}Kr activity.

3.2.1.1 Activity data from a commercial WWER

Fig. 3 shows an example of validation against NPP data on activity monitoring. One fuel rod failed after ~ 400 days of 18-month cycle with a significant increase in ^{131}I activity. The leaking fuel assembly was identified and shipped for post-irradiation examinations. The PIEs showed that it was a debris-failure by foreign material in the region of the lower blanket of the fuel rod.

The rise of ^{131}I activity at the time of about 500 days was due to switch-off of the coolant purification system. The observed increase in ^{131}I activity was about 5 times lower than the value that could be expected due to the purification switch-off. Calculations using the RTOP-CA code showed that the reduced increase in activity after the 500th day is explained by a gradual decrease in the linear heat rate in this time interval (Fig. 3): more water condensed in the lower part of the fuel rod and, consequently, the rate of convective transfer of radionuclides away from the defect increased.

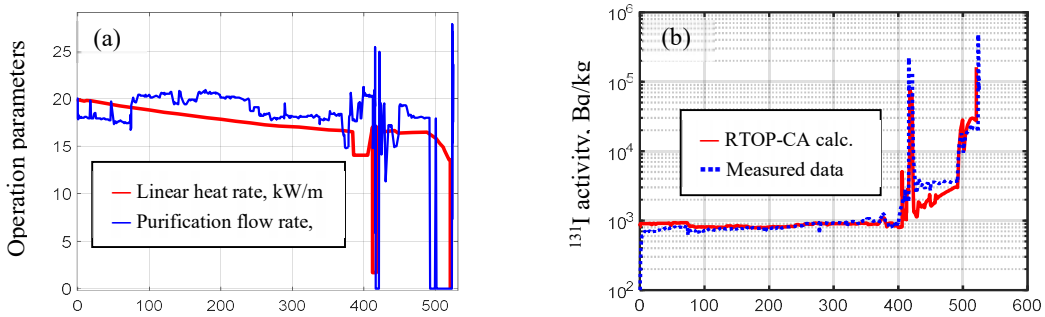

FIG. 3. (a) – Linear heat rate and the rate of coolant flow for the purification system, (b) 131I activity in the primary coolant of the WWER-1000 reactor.

3.3 WWER fuel with solid pellets

The main features characterizing fission products release from a failed fuel rod with solid pellets are associated with mass transfer. Mass transfer proceeds along the pellet-to-cladding gap, as well as along cracks in the fuel pellets. A change in the geometric parameters of the fragmented fuel pellets and the cladding during irradiation leads to a change in the conditions for the mass transfer in the fuel rod. As an example, Fig. 4 shows some data of experiment No. 4, as well as some comparison with the predicted activity of ^{131}I and ^{85m}Kr in the coolant. Experiments No. 4, 5 studied behaviors of the leaking fuel of solid pellet design at low burnup. During the experiment, the pellet-to-cladding gap was open, and the mode of accelerated mass transfer was realized leading to intensive release of radionuclides into coolant. The accelerated mass transfer was due to the flow of condensate on the inner cladding surface under the action of gravity and evaporation in hot regions of the fuel stack.

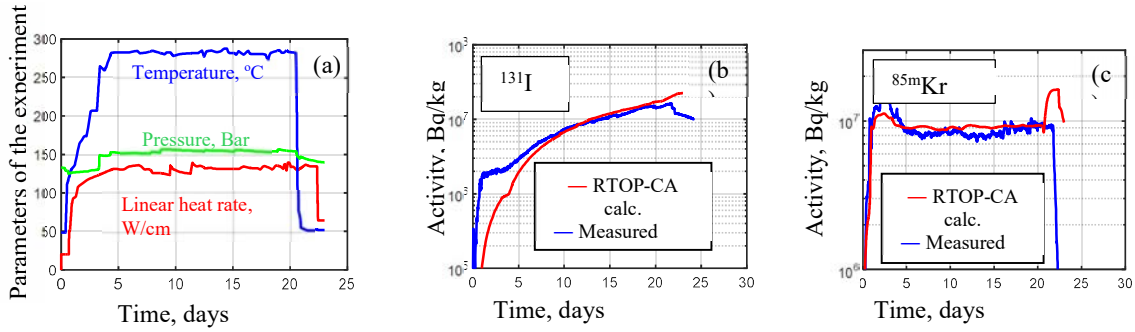

FIG. 4. MIR experiment 4, Series II (artificial defect in the central part of the plenum): (a) – linear heat rate, coolant pressure and temperature, (b) – ^{131}I activity, (c) – ^{87}Kr activity.

The mode of accelerated mass transfer between the fuel rod and the coolant in experiment № 4 led to decrease in hydrogen content in the fuel rod and, consequently, to an increase in the rate of UO_2 oxidation. Due to increase in the oxygen content in the fuel, the mobility of xenon atoms in the UO_2 matrix increased. This led to a reduction of the concentration of xenon dissolved in the fuel in the hot regions of the pellets and formation of intergranular pores (Fig. 5).

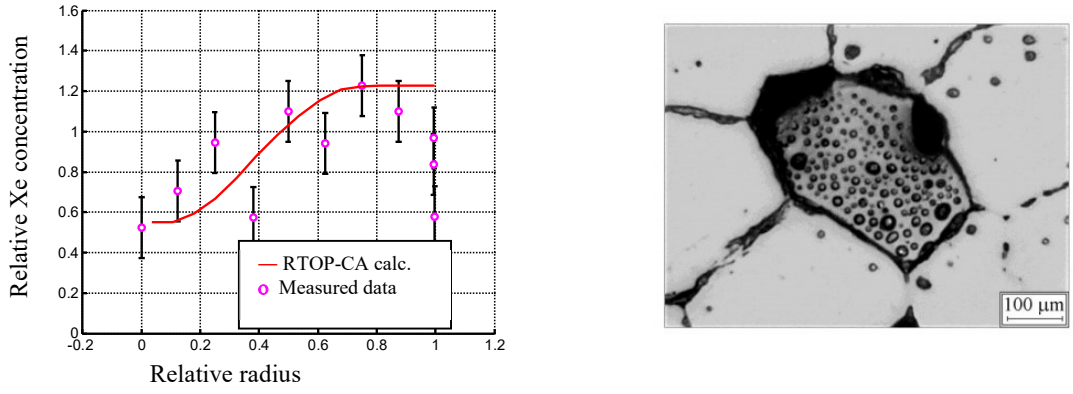

FIG. 5. MIR experiment 4, Series II: Left – Radial distribution of Xe dissolved in fuel pellets; Right – grain-boundary pores in the central part of the pellet.

3.4 Modeling of U-Gd fuel

3.4.1 Burnup of gadolinium isotopes and evolution of heat rate in U-Gd fuel rods

One of the possibilities of the extended version of the RTOP-CA code is simulation of the behavior of fuel rods with a burnable absorber based on Gd_2O_3. The main features that are taken into account in the RTOP-CA code when simulating the behavior of $(U,Gd)O_2$ fuel rods are: reduced linear heat rate at the initial stage of irradiation, inhomogeneity of radial heat rate distribution, as well as decrease of thermal conductivity of fuel pellets with higher gadolinium content [15]. The radial heat rate inhomogeneity in U-Gd fuel rod is due to the high macroscopic cross sections of thermal neutron absorption by ^{155}Gd and ^{157}Gd isotopes.

The most detailed and complete modeling of the burnup of absorbing materials in the core is possible with neutron codes. Fuel performance codes generally use simplified approaches to avoid large computational costs. The RTOP-CA code implements an approach with a simplified description of the neutron spectrum, and an algorithm for direct modeling of neutron trajectories, which is typical to neutron codes. The model takes into account four energy groups: a group of thermal neutrons and 3 groups of epithermal neutrons corresponding to resonances for ^{235}U, ^{155}Gd, and ^{157}Gd. The model assumes that the fluxes of epithermal neutrons corresponding to the resonance peaks for ^{235}U, ^{155}Gd, and ^{157}Gd do not overlap each other. Fig. 6 shows the validation results for the model of burnup of gadolinium isotopes and heat rate in a fuel rod using data [17] obtained by the HELIOS neutron code.

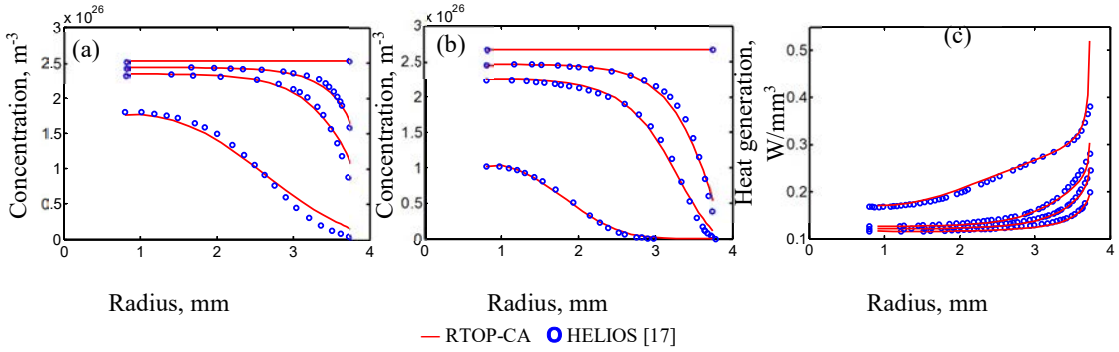

FIG. 6. Burnup dynamics of gadolinium isotopes ^{155}Gd (a), ^{157}Gd (b) and distribution of heat generation rate (c) in the $(U,Gd)O_2$ fuel rod. The presented plots correspond to fuel burnup bu = 0, 0.4, 0.8, 3.1 MWd/kgU.

If U-Gd fuel rod fails in the initial periods of operation, an increased content of liquid water may be observed inside due to the reduced heat rate. Condensation of water can occur in the pellet-to-cladding gap, inter-pellet gaps and cracks. In the lower part of the fuel rod, condensation is possible even in the central hole of fuel pellets. The rate of FPs transfer along the fuel rod through the liquid phase is much lower than in a steam environment. The distribution of fission products between the liquid and gas phases and the rate of FPs transfer depends on the inventory of water in the fuel rod.

3.4.2 MIR experiment with a leaking U-Gd fuel rod

The behavior of a leaking fuel rod was studied during experiment No. 3 in the MIR reactor (Series II). The defect in the cladding was made in the form of an axial slot 14×1.4 mm, located at a height of 150 mm from the lower end of the fuel stack. The mass content of gadolinium oxide was 5%. Fig. 7 shows a comparison of the RTOP-CA predictions with the data on ^{131}I activity in the MIR loop facility.

Experiment No. 3 showed a significantly reduced release of radionuclides from a leaking fuel rod. The low level of FPs activity in the coolant is explained by the reduced linear heat rate in the (U, Gd) O_2 fuel during the experiment. The maximum linear heat rate in the fuel rod during irradiation increased from approximately 3 to 6 kW/m. In the area of the artificial defect, the increase in the linear heat rate was approximately from 2 to 3 kW/m.

The calculations showed that, due to the relatively low linear heat rate, there was high amount of water inside the test fuel rod which led to a significant decrease in the rate of diffusional transfer of radionuclides.

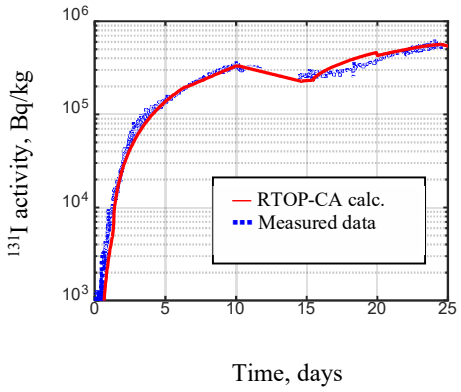

FIG. 7. 131I activity during MIR experiment 3 (Series II) with leaking (U, Gd) O_2 fuel rod.

3.4.3 Fission product release from a full-scale leaking U-Gd fuel rod

Data on iodine activity in WWER-1000 primary coolant were used to validate the RTOP-CA models for leaking U-Gd fuel rod. Fig. 8 shows a comparison of ^{131}I and ^{135}I activity as predicted using the RTOP-CA code and measured at NPP. At the end of fuel cycle, one leaking fuel assembly was found in the core, which had completed one fuel cycle. Post-irradiation examinations have shown that the fuel assembly contained one leaking $(U,Gd)O_2$ fuel rod (Bu = 17 MW·day/kgU). Fuel failure was caused by debris. Near the upper end of the fuel stack there was a through-wall defect about 10 mm long. The width of the defect in the main part was approximately 1 mm. No secondary hydriding in the cladding was found. The data of activity monitoring and PIE data were used to validate the RTOP-CA code.

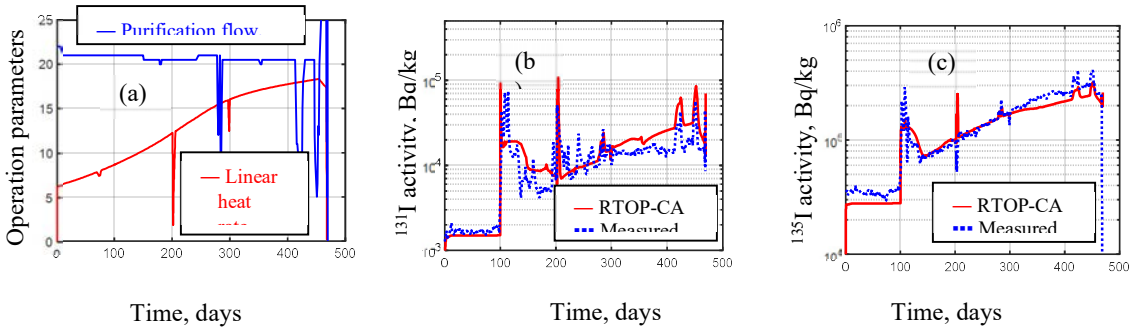

FIG. 8. Operation parameters (a) and activity of ^{131}I (b), ^{135}I (c) in WWER-1000 primary coolant from the leaking U-Gd fuel rod.

Simulations with the RTOP-CA code showed that during the first ~ 100 days from the beginning of the cycle, iodine activity corresponded to release of fission products from fuel deposits in the core. A further sharp rise in radioactive FPs activity was caused by fuel failure. The activity levels observed for about 50 days after the failure were due to the intensive release from the fuel rod by means of convective transfer. During of the fuel cycle, the pellet-to-cladding gap in the leaking U-Gd fuel rod remained open. In the area of the fuel stack located below the defect, steam condensed on the cladding inner surface. The flow in the condensed layer under the action of gravity led to the convective transfer of the steam-gas mixture from the lower part towards the defect. Accelerated delivery of radionuclides to the defect due to convective transfer led to an intensive release of radioactive FPs to the coolant. Due to the increase with time in the linear heat rate and hydrogen generation, the thickness of the water film on the cladding inner surface decreased. This led to a weakening of the convective transport of radionuclides and to a decrease in the activity of radioactive FPs in the coolant. The subsequent (after about 150 days from the start of

the cycle) gradual increase of the iodine activity in the coolant was due to washout of fuel particles into the primary circuit.

3.5 Modeling of FPs release under transient conditions

The application area of the RTOP-CA code includes calculations of the radioactive FPs release to the primary circuit when a leaking fuel rod is irradiated under a steady-state heat rate, as well as in load-follow modes. Under operating conditions in WWERs, power transients take place between fuel cycles. Also, temporary shutdowns or partial reduction of the heat rate during fuel cycles are possible. Load-follow modes of operation are also considered. With a change in the linear heat rate, temperature and pressure of the coolant, an accelerated release of radionuclides to the coolant can be observed, due to the excess of pressure in the failed fuel rod over the pressure in the primary circuit.

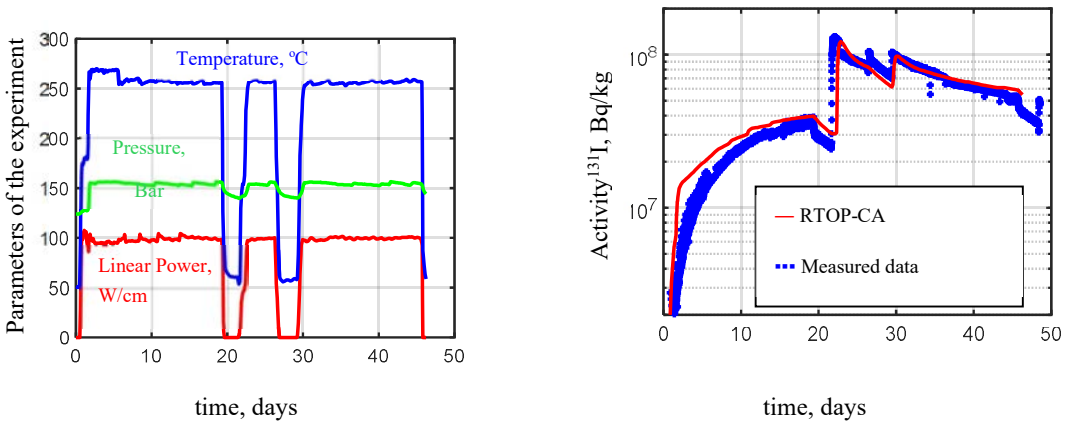

FIG. 9. Time dependence of the parameters of experiment № 6 (left) and activity of ^{131}I (right), in the coolant of the PV-1 loop in experiment № 6 in the MIR reactor with a leaking WWER fuel rod with solid pellets.

The peak values of coolant activity characterize the content of radionuclides in the leaking fuel rod at the time moment before the power transient. If the release rate is high during steady-state operation (for example, in experiments No. 4.5), a relatively small content of radioactive FPs may remain inside the fuel rod. Under such conditions, a change in the mass transfer mode with a change in the heat rate may not affect the value of radionuclide activity observed in the coolant. Among the reference radionuclides of iodine, the release of long-lived iodine ^{131}I is most noticeable.

In experiments in the MIR reactor, peak release of fission products during transients between MIR cycles was observed in an experiment with 'traditional' WWER fuel (hollow fuel pellets), as well as in two experiments with solid pellet design. Fig. 9 shows an example of RTOP-CA simulations compared to the data of experiment No. 6. An intensive release of fission products was observed when power was turned on after a short MIR outage.

3.6 Simulation of the thermo-mechanical behavior of failed fuel rods

Simulation of fuel behavior before and after the failure needs calculation of the fuel temperature, behavior of fission gas in polycrystalline fuel pellets, changes in the microstructure of the fuel and the geometric parameters of the fuel rod, as well as other parameters. In the RTOP-CA code, the basic characteristics of a fuel rod are calculated for the stages before and after the failure. Validation of the parameters affecting the release of radionuclides to the primary circuit was carried out on the results of post-irradiation examinations of intact and leaking WWER fuel rods and on data obtained at research reactors.

The failure leads to a change in the basic characteristics of the fuel rod. The ingress of the coolant inside the fuel rod leads to an increase in the fuel temperature due to a decrease in thermal conductivity in the pellet-to-

cladding gap and in fuel pellets. The decrease in the thermal conductivity of UO_{2+x} is associated with the oxidation of the pellets. Under conditions of higher temperature and oxygen content in uranium dioxide, accelerated gas swelling of pellets can be observed. Another reason for the increase in the pellet size is the precipitation of the U_3O_8 phase near the surface of the fragmented pellets. In a leaking fuel rod, an accelerated collapse of the pellet-to-cladding gap and more intensive mechanical interaction between fuel pellets and cladding can be observed. The mechanical interaction of the fuel and the cladding determines the dimensional changes of the fuel rod after the gap collapse.

Fig. 10 (left picture) shows the results of validation of thermomechanical models of the RTOP-CA code based on the data of PIE of a leaking fuel rod during experiment No. 7 in the MIR reactor. In experiment No. 7, the behavior of a leaking fuel rod with solid fuel pellets was studied. An artificial defect in the cladding was made at the level of the fuel stack. The test fuel rod was manufactured from a full-scale fuel rod of TVSA-5M with an average fuel burnup of 59.4 MWd/kgU. The test fuel rod was irradiated during one 'long' MIR cycle for about 40 days. The maximum local linear heat rate was about 15 kW/m. As can be seen, during the tests there was a significant increase in the cladding diameter due to the increase in the fuel pellets volume. The peak diameters measured at the level h = 0.15 m can be associated with deformation of the cladding due to the application of an artificial defect in this area.

Fig. 10 (right) also shows a comparison of the calculated profilometry of the fuel rod irradiated in a commercial WWER with PIE data. The average fuel burnup in a full-scale fuel rod with blankets was about 55 MWd/kgU. As can be seen, in the central part of the fuel rod, there is a significant backward displacement of the cladding associated with mechanical interaction with the fuel pellets.

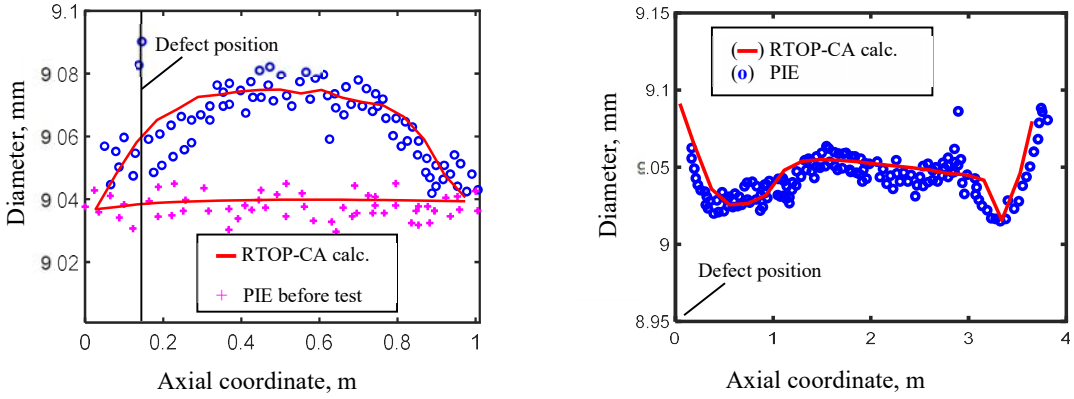

FIG. 10. Axial profile of cladding diameter in the test fuel rod before and after irradiation in the MIR reactor (left) and profilometry (right) of the leaking full-scale fuel rod with blankets (average fuel burnup is 55 MW·d/kgU).

4. CONCLUSIONS

The paper presents the capabilities of the extended version of the RTOP-CA code for simulations of leaking fuel behavior and release of fission products into the WWER primary coolant. The extended version is capable of simulating the behavior of WWER fuel of both hollow and solid pellet design, including U-Gd fuel. The RTOP-CA code implements a mechanistic approach based on detailed modeling of physical processes. Within the framework of this approach, a self-consistent calculation is performed including:

— Parameters of the thermomechanical behavior of a fuel rod.
— Changes in the thermo-physical characteristics of the fuel.
— Behavior of fission products in fuel.
— Changes in the microstructure of UO_2.
— Release of radionuclides from fuel pellets.
— Oxidation of fuel and cladding.
— Cladding hydriding.
— Transport of fission products, hydrogen, and helium in the leaking fuel rod.

— The content of liquid water inside the fuel rod.
— Mass transfer between the leaking fuel rod and the coolant.

Models related to the FPs release from the fuel pellets and transport along the leaking fuel rod are briefly described. To determine the radioactive FPs release from UO_2, the behavior of radionuclides in the fuel grain is simulated. The mass transfer inside the failed fuel rod is simulated considering the effective diffusion, convective transfer, and condensation of the coolant in relatively cold regions of the fuel rod.

The validation of the extended version of the code was carried out based on the results of experiments in the MIR reactor with the test fuel rods having an artificial defect in cladding. Experiments in the MIR reactor were carried out under controlled conditions for irradiation and defect parameters. Experiments included monitoring of coolant activity in the MIR loop facility and post-irradiation examinations of the test fuel rods. Also, when validating the code, the results of PIEs of WWER fuel and WWER operational data on primary coolant activity were used. The approaches implemented in the RTOP-CA code make it possible to adequately simulate the change in the parameters of the leaking fuel and the release of fission products into the primary circuit.

REFERENCES

[1] INTERNATIONAL ATOMIC ENERGY AGENCY, Review of Fuel Failures in Water Cooled Reactors (2006–2015), Nuclear Energy Series No. NF-T-2.5, IAEA, Vienna (2019).

[2] SOROKIN, A., LIKHANSKII, V., EVDOKIMOV, I., ZBOROVSKII, V., VILKHIVSKAYA, O., TOKAREV, S., ULIBYSHEV, K., Modeling in support of experiments in the MIR reactor for justification of fission product release from failed fuel of advanced design and from (U,Gd)O_2 fuel, Proc. 11th Intern. Conf. WWER Fuel Performance: Modelling and Experimental Support, 26 September-03 October 2015, Golden Sands Resort, Bulgaria, Vol. II, pp.564-570.

[3] SOROKIN, A., LIKHANSKII, V., BORISOV, A., ILYENKO, A., GORYACHEV, A. Validation of the enhanced version of the RTOP-CA code designed for modeling the fission products release from failed fuel rod to the primary circuit of WWER, Proc. 13th Intern. Conf. WWER Feul Performance, Modelling and Experimental Support, 2019, Nesebar, Bulgaria.

[4] DOBROV, B.V., KANUKOVA, V.D., KHORUZHII, O.V., KOURCHATOV, S.Yu., LIKHANSKII, V.V., SAKHAROV, B.B., The Development of a Mechanistic code on Fission Product Behavior in the Polycrystalline UO_2 Fuel, Nucl. Eng. and Design **195** (2000) 361-371.

[5] WISE, C., Recoil Release of Fission Products from Nuclear Fuel, J. Nucl. Mater., **136** (1985) 30-47.

[6] TURNBULL, J.A., FRISKNEY, C.A., FINDLAY, J.R., JOHNSON, F.A., WALTER, A.J., The Diffusion Coefficients of Gaseous and Volatile Species during the Irradiation of Uranium Dioxide, J. Nucl. Mater. **107** (1982) 168-184.

[7] CHARLES, M., CHENEBAULT, P., MELIN, P.H., Mechanisms of Fission Gas Release from Different Types of Fuel Rods during Normal Operation: Results and Analysis of CONTACT Experiments, *Light Water Reactor Fuel Performance*, Orlando, Florida, April 21-24, 1985.

[8] ROSSITER, G., WHITE, R., The Fission Gas Diffusion Coefficient in Irradiated Oxide Fuel: An Analysis of Current Experimental Data, Proc. Enlarged Halden Programme Group Meeting, Storefjell, Gol, Norway, 8-13 September 2002.

[9] DAVIES, D., LONG, G., The Emission of Xenon 133 from Lightly Irradiated Uranium Dioxide Spheres and Powders, AERE Report No.4347, Atomic Energy Research Establishment, 1963.

[10] KIM, Y.S., Fission Gas Release from UO_{2+x} in Defective Light Water Reactor Fuel Rods, Proc. Intern. Topical Meeting LWR Fuel Performance, Park City, Utah, USA, April 10-13, 2000.

[11] LIDIARD, A.B., Self-Diffusion of Uranium in UO_2, J. Nucl. Mater. **19** (1966) 106.

[12] The International Association for the Properties of Water and Stream, Kyoto, Japan, September 2004.

[13] KONYASHOV, V.V., KRASNOV, A.M., Radioactive Fission Product Release from Defective Light Water Reactor Fuel Elements, Nucl. Techn. **138** (2002) 1-16.

[14] LIKHANSKII, V., KHORUZHII, O., KURCHATOV, S., SOROKIN, A., Modeling with the RTOP code of radial profiles of heat generation rate and Pu buildup in UO_2 fuel of high burnup, Atomic Energy **92** (2002) 317-324.

[15] FUKUSHIMA, S. *et. al.*, The Effect of Gadolinium Content on the Thermal Conductivity of Near-Stoichiometric (U, Gd) O_2 Solid Solutions, J. Nucl. Mat. **105** (1982) 201-210.

[16] HIRAI, M., ISHIMOTO, S., Thermal Diffusivity and Thermal Conductivity of UO_2-Gd_2O_3, J. Nucl. Sci. Technology, **28** (1991) 995-1000.

[17] IEREMENKO, M., OVDIIENKO, I., Cross-checking of the TRANSURANUS burn-up model for Gd-doped UO_2 WWER-1000 fuel based on results of HELIOS code, 10th Intern. Conf. WWER Fuel Performance, Modelling and Experimental Support. 9-13.09.2013, Sandanski, Bulgaria.

MODELLING OF RADIOACTIVE FISSION GAS RELEASE FROM DEFECTIVE PWR FUEL ROD BY MFPR/R CODE

V.I. TARASOV, V.D. OZRIN
Nuclear Safety Institute (IBRAE),
Russian Academy of Sciences,
Moscow, Russian Federation

M.S. VESHCHUNOV
International Atomic Energy Agency (IAEA),
Vienna, Austria

Abstract

A program package was elaborated by coupling the mechanistic fuel performance code MFPR/R with a recently developed advanced model of mass exchange in defected fuel rods, to simulate release of radioactive gaseous fission products to coolant during thermal reactor operation. To simulate UO_2 fuel oxidation, the processes of the vapor dissociation and radiolysis in the rod free volume were additionally considered. The package was validated by calculation of the release of krypton, iodine, and xenon isotopes to the coolant from defected rods under irradiation in the pressurized light water loop of the NRX reactor at Chalk River Nuclear Laboratories.

1. INTRODUCTION

When water-cooled nuclear reactors are operating with the presence of defected fuel rods, the high-pressure coolant can enter the fuel-to-sheath gap causing fission products (FPs) to escape into the primary coolant. The generalized diffusion model of Lewis et al. [1, 2] was developed by unification of the diffusion model for axial mass transport in the gap (characterized by the fission gas diffusivity) and the phenomenological first-order kinetic model for fission gas (FG) release into the coolant (characterized by the phenomenological escape rate constant, ε). Further advancement of this approach by consideration of additional mechanisms of mass exchange in defective fuel rods, allowing explicit evaluation of the escape rate constant, was proposed recently [3].

In the present paper the advanced model [3] is coupled with the mechanistic fuel performance MFPR/R code to simulate release of radioactive gaseous FPs to coolant from defective fuel rod during normal operation of a water-cooled nuclear reactor. The MFPR code (Module for Fission Product Release) designed for mechanistic modelling of irradiated UO_2 fuel, was developed by IBRAE in collaboration with IRSN (Cadarache) [4, 5] (IBRAE: models and code development and maintenance; IRSN: code application to interpretation of FP behaviour and benchmarking). The code originated from the critical analysis of the VICTORIA code [6] and inherited advantages of mechanistic modelling, first of all, concerning a realistic consideration of FP behaviour based on physically grounded parameters. It self-consistently describes FP transport in fuel and release to open porosity, evolution of fuel microstructure (point defects, such as vacancies and interstitials, and extended defects, such as gas bubbles, sintering pores and dislocations, their nucleation, evolution, and interactions), fuel multi-phase thermochemistry including FP distribution over various molecular and phase states. Being grounded on the physics-based models, the code provides enhanced predictive capability in comparison with a simplified engineering approach. Since 2011 IBRAE is developing its own version MFPR/R implementing new models and refining existing models and numerical schemes. The code was recently extended to modelling of radioactive FP generation, transmutations, and transport [6, 7], fuel densification, pore biased migration and grain edge porosity evolution [8], large pores coalescence in the High Burnup Structure (HBS) at the fuel pellet periphery (rim zone) [9].

The MFPR/R serves as a fuel module in fuel performance and integrated codes. In 2011 the MFPR/R was coupled with the thermomechanical code SVECHA/QUENCH (S/Q) developed in collaboration with KIT (Karlsruhe) [10, 11] to form the fuel performance and safety code SFPR for mechanistic modelling of the single fuel rod behaviour under various regimes of LWR reactor operation (normal and off normal, including severe accidents) [12]. SFPR code is presently under implementation into precision program complex "Virtual NPP with VVER", which is jointly elaborated by VNIIAES (All-Russian Research Institute for Nuclear Power Plants

Operation) and IBRAE [13]. Besides, a modified version of MFPR/R (module RELEASE) is the constituent part of the integrated code SOCRAT for numerical analysis of the behaviour of LWR at various stages of design extension conditions [14]. Recently MFPR/R was extended to mixed oxide (U, Pu) O_2 and nitride (U, Pu) N fuels in Fast Reactors (FRs) and was included in a new mechanistic fuel performance code BERKUT [15], the constituent part of the multi-physics integrated code EUCLIDE [16] developed for safety justification of Gen-IV NPP within the Russian Federal Targeted Program "Nuclear Power Technologies of the New Generation for 2010-2015 and until 2020".

To implement the new model [3] in MFPR/R, firstly the stand-alone computational tool for calculation of FP release from defective fuel rod to the coolant was developed and combined with MFPR/R code, the later providing mechanistic evaluation of the source term (FP release from fuel to the rod free volume). The purpose of this paper is to test the ability of the combined approach to simulate the release of radioactive isotopes of krypton, iodine, and xenon from defect fuel element to the coolant under conditions of steady state irradiation in the pressurized light water loop of the NRX reactor at Chalk River Nuclear Laboratories [17]. After validation of the developed stand-alone module, it is planned to extend it to consideration of transient conditions and to implement the upgraded MFPR into the fuel performance codes.

2. MODEL

2.1 Model suppositions

Simplified rod geometry simulates the fuel column, lower and upper plenums and fuel-to-sheath gap, Fig. 1. The defect is located at axial coordinate z_0.

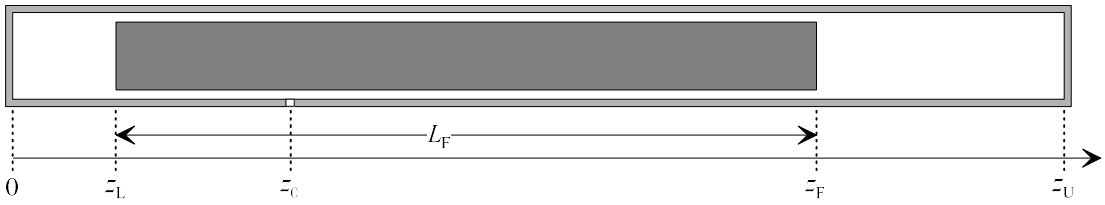

FIG. 1. Schematic geometry of fuel element.

It is assumed that the rod free volume is filled with the non-condensable gas and (after the defect formation) vapor. The non-condensable gas is considered as a mixture of filling gas (He), gaseous FPs (isotopes of Kr, I, Xe), which are generated by fission and released from fuel to the rod free volume; and hydrogen generated due to fuel and cladding oxidation, vapor dissociation and radiolysis. The gas components are well mixed with water vapor in the gap free volume shortly after formation of the defect, in accordance with recent CFD calculations [18]. Experimental data and calculation estimates [1, 2] on the irradiation conditions relate only to some averaged values For this reason, the rod geometry, the fission rate, the fuel and sheath temperatures were considered to be independent on time and axial position in relatively short experimental rods (following calculations [2], see below), the gas temperature in the rod free volume, T_{gap}, was set equal to a half-sum of temperatures at the external pellet surface and at the internal sheath surface.

2.2 Diffusion problem formulation

Under above assumptions the diffusion equation for concentration, $c_0(z,t)$, m^{-3}, of stable non-condensable gas in the rod free volume takes the form:

$$\frac{\partial}{\partial t} S_{\text{free}}(z) c_0 = \frac{\partial}{\partial z} D_0 S_{\text{free}}(z) \frac{\partial}{\partial z} c_0 + q_0, \tag{1}$$

where $S_{\text{free}}(z)$, m^2, is the cross-section area of the rod free volume, q_0, $m^{-1}s^{-1}$, is the linear density of the gas flux to the rod free volume. For simplicity the gas was considered as a homogeneous mixture of gas components with the diffusivity D_0 calculated by Fuller's formula [19]. This supposition and Eq. (1) assume quick gas mixing in

radial direction. This is a good approximation for the gap region but somewhat underestimates diffusion time in the plenum volume.

The boundary conditions correspond to zero gas fluxes at both ends of the rod, whereas the boundary condition at the defect location takes the form [3]:

$$-\frac{\partial}{\partial z}c_0\Big|_{z=z_0-0}+\frac{\partial}{\partial z}c_0\Big|_{z=z_0+0}=\frac{1}{\delta}(c_0(z_0)-c_0^*) \tag{2}$$

where

$$\delta=\frac{d_{\text{clad}}S_{\text{free}}(z_0)}{S_{\text{def}}} \tag{3}$$

d_{clad} and S_{def} being respectively the sheath thickness and the defect area.

For each radioactive FP isotope, the diffusivity D is calculated by Blanc's formula [19] for multi-component gas mixture (with the Fuller's parameterization of binary diffusivities), and the additional term $-\lambda S_{\text{gap}}c(z,t)$, is added in the right side of Eq. (1), where λ is the decay constant, whereas the boundary condition at the defect location is formulated as [3]:

$$-\frac{\partial}{\partial z}c\Big|_{z=z_0-0}+\frac{\partial}{\partial z}c\Big|_{z=z_0+0}=\frac{1}{\delta}(1-\frac{c_0^*}{c_0(z_0)})c(z_0) \tag{4}$$

According to [3], the gas venting from the rod free volume to the coolant commences when the non-condensable gas concentration at the defect location becomes greater than the critical concentration, c_0^*, calculated as:

$$c_0^*\equiv\frac{P_{\text{cool}}-P_{\text{H}_2\text{O}}^{(\text{eq})}(T_{\text{clad}}^{(\text{ext})})}{kT_{\text{gap}}} \tag{5}$$

where P_{cool} is the coolant pressure, $P_{\text{H}_2\text{O}}^{(\text{eq})}(T_{\text{clad}}^{(\text{ext})})$ is the equilibrium steam pressure for the temperature at the external sheath surface$T_{\text{clad}}^{(\text{ext})}$, and k is the Boltzmann constant.

2.3 Source terms

2.3.1 Fission products

In the MFPR/R code the diffusion transport of gaseous FPs in fuel is considered as the three-stage process including [8]:

— FP diffusion within the fuel grains (taking into account FP interaction with the intragranular bubbles and other extended defects);
— FP accumulation in the grain face bubbles and their venting to the grain edge gas-filled channels.
— release from the grain edge channels to the open porosity.

In the first stage, the release-to-birth ratio, $(R/B)_{gr}$, for radioactive FP follows a well-known law:

$$(R/B)_{\text{gr}}=3\sqrt{\frac{D_{\text{gr}}}{\lambda R_{\text{gr}}^2}}\left(\coth\sqrt{\frac{\lambda R_{\text{gr}}^2}{D_{\text{gr}}}}-\sqrt{\frac{D_{\text{gr}}}{\lambda R_{\text{gr}}^2}}\right)=3\sqrt{\frac{D_{\text{gr}}}{\lambda R_{\text{gr}}^2}}\left(1-\sqrt{\frac{D_{\text{gr}}}{\lambda R_{\text{gr}}^2}}+\cdots\right) \tag{6}$$

where D_{gr} is the FP diffusivity in the fuel matrix, which depends on temperature, fission rate and fuel stoichiometry, R_{gr} is the effective grain radius; the second equality presenting two first terms of the series expansion with respect to $D_{\text{gr}}/\lambda R_{\text{gr}}^2$. This dependence is modified by FP interaction with intergranular defects as well as by diffusion of mother nuclides (so called precursor effect). For the two other stages, delay in FP intergranular transport additionally modifies the square root law, Eq. (6), so that the overall release-to-birth ratio, $(R/B)_{\text{bulk}}$, due to diffusion mechanism from the fuel bulk takes the form:

$$(R/B)_{\text{bulk}}=f_{\text{dif}}(\lambda)\left(\frac{R}{B}\right)_{\text{gr}} \tag{7}$$

where the factor $f_{\mathrm{dif}}(\lambda)$ can be rather small [8].

For this reason, the other FP release mechanisms can be essential. In this paper we consider the surface FP release mechanism due to recoil[11], for which the corresponding ratio, $(R/B)_{\mathrm{rec}}$, does not depend on λ [20]:

$$(R/B)_{\mathrm{rec}} = \frac{2\xi_{\mathrm{rec}}\mu_{\mathrm{f}}}{R_{\mathrm{pel}}} \tag{8}$$

where μ_{f} is the fission fragment range in the fuel, $R_{\mathrm{pel}}$is the pellet radius. The probability, ξ_{rec}, for fission fragment to stop in the gas-filled interspace can be estimated as [1]:

$$\xi_{\mathrm{rec}} = \frac{d_{\mathrm{gap}}}{2\mu_{\mathrm{gas}}} \tag{9}$$

where d_{gap} is the pellet-sheath gap width and the fragment range μ_{gas} in the gas phase can be estimated as:

$$\mu_{\mathrm{gas}} = \mu_{\mathrm{gas}}^{(0)} \frac{\rho_{\mathrm{H_2O}}^{(0)}}{\rho_{\mathrm{H_2O}}} \tag{10}$$

where $\rho_{\mathrm{H_2O}}$ is the vapor density in the gap, the upper indexes '0' mark the reference values. Our SRIM calculations for the reference vapor density $\rho_{\mathrm{H_2O}}^{(0)}$ =0.035 g/cm^3 (which corresponds to the vapor number density of $c_{\mathrm{H_2O}}^{(0)}$ = 1.17×10^{27} m^{-3}) resulted in $\mu_{\mathrm{gas}}^{(0)}$ = 19 μm.

Another release mechanism is the FP diffusion from the fuel grains in the near-surface pellet region directly to the rod free volume avoiding FP trapping by the intergranular porosity. The corresponding release-to-birth ratio can be estimated as:

$$(R/B)_{\mathrm{surf}} = \frac{S_{\mathrm{tot}} d}{V}(R/B)_{\mathrm{gr}} \tag{11}$$

where S_{tot} and V are respectively the total area and volume of the fuel sample, d is the effective thickness of the near-surface layer of the pellet (which is slightly less than the geometrical thickness, due to FPs leaving the layer due to recoil).

It is supposed that the FP diffusion release takes place mainly from the butt ends of the pellets (with subsequent venting through the gas-filled interspaces in the pellet stack) whereas the release from the pellet side surface is very small due to low temperature. The geometrical thickness of the near-surface layer is assumed to be of order of fuel grain size, d_{gr}, which is also comparable to the fission fragment range in the fuel. As shown in [12], for the layer of that width, 1/4 of the fission fragments generated in the layer leave it by recoil. Therefore, the effective thickness is ≈ 3/4 of the geometrical layer thickness[12].Therefore Eq. (11) takes the form:

$$(R/B)_{\mathrm{surf}} = \frac{3\xi_{\mathrm{surf}} d_{\mathrm{gr}}}{2h_{\mathrm{pel}}}(R/B)_{\mathrm{gr}} \tag{12}$$

where h_{pel} is the pellet height and ξ_{surf} is the ratio of total pellet surface to the geometrical one. The latter value is generally poorly defined and can be much greater than 1 due to surface roughness and small cracks in the pellet. In these calculations we adopted for ξ_{surf} the value of 20, estimated by Lewis [21] for CANDU fuels.

2.3.2 Hydrogen

Shortly after water enters the rod free volume, hydrogen generation becomes the dominant mechanism for accumulation of stable non-condensable gases in the gap and attainment of their critical concentration, c_0^*, Eq. (5), necessary for gas venting from the rod free volume to the coolant [3]. The important processes of hydrogen generation under irradiation conditions are steam dissociation accompanying the fuel oxidation and radiolysis with the corresponding chemical reactions:

---

[11] Contribution of another surface fission FP mechanism, knockout, can be neglected [21].

[12] In the general case of an arbitrary width, d, of near-surface layer one derives the fraction, f_{rec}, of fission fragments escaping the layer by recoil:

$$f_{\mathrm{rec}} = \begin{cases} \frac{1}{2} - \frac{d}{2\mu}, & d < \mu \\ \frac{\mu}{4d}, & d \geq \mu \end{cases}$$

$$H_2O \rightarrow H_2 + O_{(s)}$$
$$2H_2O \rightarrow H_2O_2 + H_2 \quad (13)$$
$$H_2O_2 \rightarrow H_2O + O_{(s)}$$

where $O_{(s)}$ denotes oxygen adsorbed by the fuel matrix. The rate of the hydrogen generation is described by equation:

$$\frac{d}{dt} c_{H_2} = q_{ox} + q_{H_2}^{(radio)} \quad (14)$$

where c_{H_2} is the hydrogen linear density, q_{ox} and $q_{H_2}^{(radio)}$ are the linear densities of H_2 flux generated respectively by fuel oxidation and radiolysis. The first term in the right-hand side of this equation is described by the surface-exchange model developed in [22]:

$$q_{ox} = k_{ox}(1 - \sqrt{p_{O_2}^{(eq)}/p_{O_2}}) \quad (15)$$

where k_{ox} is the temperature dependent adsorption constant, p_{O_2} is the oxygen pressure in the gap, and $p_{O_2}^{(eq)}(x)$ is the equilibrium oxygen pressure over nonstoichiometric UO_{2+x}. Lewis [2] estimated rates of these processes and demonstrated that radiolysis became the main source of hydrogen under irradiation of experimental rods during a few days. The linear densities of H_2 and H_2O_2 generation rates, $q_{H_2}^{(radio)}$ and $q_{H_2O_2}^{(radio)}$, $m^{-1}s^{-1}$, can be represented in the form:

$$q_{H_2}^{(radio)} = q_{H_2O_2}^{(radio)} = \lambda^{(radio)} c_{H_2O} \quad (16)$$

where c_{H_2O} is the steam concentration, and

$$\lambda^{(radio)} = \frac{\pi R_{pel} \Lambda G N_{H_2}^{(0)}}{c_{H_2O}^{(0)}} \quad (17)$$

Here Λ is the average range of the fission fragment in the fuel-to-sheath gap (which is estimated as the double gap width d_{gap} [23]), R_{pel} is the pellet radius, G is the fission rate, and $N_{H_2}^{(0)}$ is the effective number of H_2 molecules generated in steam with the density $\rho_{H_2O}^{(0)}$:

$$N_{H_2}^{(0)} = Y_{H_2} \Sigma_i \gamma_i \mu_i \frac{dE_i^{(0)}}{dx} \quad (18)$$

where γ_i, μ_i and $dE_i^{(0)}/dx$ are respectively independent yield by fission, range in fuel and stopping power in steam with the density $\rho_{H_2O}^{(0)}$ of fission product *i.* Using data presented in [24] one estimates that $N_{H_2}^{(0)} \approx 1.6 \times 10^5$.

Lewis [25] conservatively assumed that the formed H_2O_2 is completely consumed by the fuel oxidation reaction, basing on the experimental observation of rapid oxidizing UO_2 fuel even in excess H_2. However, the reverse reaction, $H_2O_2 + H_2 \rightarrow 2H_2O$, might essentially suppress this estimate (as noted also in [17]). For this reason and considering the current level of uncertainty for the complex radiation chemistry of water vapour, we consider $\lambda^{(radio)}$ as a fitting parameter in Eq. (16) to get a reasonable value for the fuel oxidation rate (see below Section 3.6).

Sheath oxidation is an additional hydrogen source in the rod free volume. Our calculations with the S/Q cladding oxidation model [10], [11] have demonstrated that this process notably contributed to the hydrogen production only in the initial stage of irradiation, in agreement with Lewis' conclusion [2] (this resulted in somewhat earlier commencement of the gas release to the coolant but made negligible contribution to the final results). On the other hand, radiolysis can essentially change the gas composition in the fuel free volume so that applicability of the model is questionable. Therefore, considering the current level of uncertainty for the complex radiation chemistry of water vapour and avoiding additional uncertainties to the calculations we excluded sheath

oxidation from further consideration. This also correlates with observations of no massive hydriding or deterioration of the sheath in the simulated test [2].

2.4 Analytical estimates

It is instructive to analyse properties of solution of the above presented equations and estimate the key parameters of the model.

2.4.1 Solution for stable gases

In the case of constant coefficients in Eqs (1) and (2) the quasi-stationary solution takes the form:

$$c_0(z) = c_0^* + \frac{q_0 \delta L_F}{D S_{gap}} + \frac{q_0}{2 D S_{gap}} \begin{cases} (z_0 - z_L)^2 - (z - z_L)^2, & z_L \le z \le z_0 \\ (z_F - z_0)^2 - (z_F - z)^2, & z_0 \le z \le z_F \end{cases} \quad (19)$$

Concentration at the defect location is calculated as

$$c_0(z) = c_0^* + \frac{Q_0 \delta}{D S_{gap}} = c_0^* + \frac{Q_0 d_{clad}}{D S_{def}} \quad (20)$$

where

$$Q_0 = q_0 L_F \quad (21)$$

is the total gas flux to the gap (and further to the coolant).

For the escape rate parameter, $\tilde{\varepsilon}$, defined in [3] as

$$\tilde{\varepsilon} = \frac{Q_0}{c_0(z_0) V_{free}} \quad (22)$$

one finds in the quasi-stationary approximation:

$$\tilde{\varepsilon} = \frac{Q_0}{(c_0^* + \frac{Q_0 d_{clad}}{D S_{def}}) V_{free}} \quad (23)$$

In particular, it follows from this equation that $\tilde{\varepsilon}$ is proportional to S_{def} for very small defect area ($S_{def} \ll Q_0 / c_0^* V_{free}$). In the opposite case $\tilde{\varepsilon}$ does not depend on S_{def}, as derived in [3]:

$$\tilde{\varepsilon} = \frac{Q_0}{c_0^* V_{free}} \quad (24)$$

in a qualitative agreement with experimental observations.

2.4.1.1 Solution for radioactive isotopes

For the case of general rod geometry, the quasi-stationary solution has a rather cumbersome form. If there are no plenums, the concentration for $z < z_0$ can be represented in the form:

$$c(x) = \frac{q}{\lambda S_{gap}} \left(1 - \frac{1}{1 + d(\tanh x_0 + \tanh(x_f - x_0))} \frac{\cosh x}{\cos \quad_0}\right) \quad (25)$$

where $x = z / l_{dif}$, $d = \delta / \gamma l_{dif}$, $l_{dif} = \sqrt{D\tau}$. The similar equation is valid for interval $z > z_0$ with the substitution $x \to x_0$ in the numerator.

The flux to coolant is evaluated as:

$$Q_i = q_i \sqrt{D\tau_i} \frac{\sinh x_f}{\cosh x_0 \cosh(x_f - x_0) + d \text{si} \quad x_f} \quad (26)$$

and ratio of the release rate to coolant to the birth rate, $(R/B)_{cool}$, has the form:

$$(R/B)_{cool} = \frac{1}{x_f \cosh \quad_0} \frac{\sinh x_f}{\cosh(x_f - x_0) + d \sinh \quad x_f} (R/B)_{gap} \quad (27)$$

In particular case of the defect location at the rod mid-length, this value reduces to the form:

$$(R/B)_{cool} = \frac{\tanh x_0}{x_0} \frac{1}{1 + 2d \tanh \quad x_0} \quad (R/B)_{gap} \quad (28)$$

similarly, to the relation earlier derived by Lewis, e.g., see [2].

In the case of $S_{\text{def}} \gg Q_0 d_{\text{clad}}/Dc_0^*$ parameter d is evaluated as $d \approx S_{\text{gap}} c_0^* \sqrt{D\lambda}/Q_0$. In addition, if $x_0 < 1$ then one derives a simple relation between isotope fluxes to the coolant and to the rod free volume:

$$(R/B)_{\text{cool}} = \frac{1}{1+\lambda/\tilde{\varepsilon}} \ (R/B)_{\text{gap}} \tag{29}$$

As seen from this equation, if $\lambda \ll \tilde{\varepsilon}$ (long-living isotopes) then $(R/B)_{\text{cool}} \approx (R/B)_{\text{gap}}$ and therefore FP release to coolant follows the square root law, Eq. (6). In the opposite case, for the short-living isotopes,

$$(R/B)_{\text{cool}} = \frac{\tilde{\varepsilon}}{\lambda} \ (R/B)_{\text{gap}} \tag{29}$$

3. CALCULATION RESULTS

In this section the program package performance is illustrated by an example of simulation of a defective CANDU-type fuel element irradiated at the National Research Experimental reactor in the framework of experimental program carried out at Chalk River Nuclear Laboratories from 1975 to 1983 [17]. Failed elements with various degrees of sheath damage were investigated in separate tests. In this paper we present calculation results for FDO-681 fuel element with well-defined defect parameters (drilled 1 mm hole in the sheath at the rod mid-length of the artificial defect).

3.1 Input data

A brief summary of the fuel-operating parameters and fuel element design are given in Tables 1 and 2.

TABLE 1. IRRADIATION CONDITIONS

Defect size/area, mm/mm^2	Average linear power, kW/m	Burnup (initial / final), MWh/kgU	Full power days
1.2/1.1	48	0/20	24

TABLE 2. FUEL ROD AND LOOP CHARACTERISTICS

Fuel	
UO_2 density, kg/m^3	10.72
Enrichment, UO_2%	4.52
pellet diameter, mm	13.61
pellet length, mm	18.0
fuel stack length, mm	168
Sheath	
Outside diameter, mm	15.16
Wall thickness, mm	0.71
Clearance diametral, mm	0.11
Clearance axial, mm	1.07
Loop parameters	
Inlet temperature, ºC	247
Water pressure, MPa	10.5

In absence of temperature measurements, their values were adopted from Ref. [2] where they were estimated with the ELESIM fuel performance code for irradiation conditions similar to those for FDO-681 fuel element, Table 3. The gap thickness was set to be 0.13 mm in those calculations.

For the given temperature in gap, the gas diffusivity was near 10^{-5} m^{2}s^{-1}.

As for isotope inventory for FDO-610 fuel element, the experimental data on release-to-birth ratios are available for ^{85m}Kr, ^{87}Kr, ^{88}Kr, ^{131}I, ^{133}I, ^{133}Xe, ^{133m}Xe, ^{135}Xe, ^{138}Xe, e.g., see [26].

TABLE 3. FUEL ELEMENT TEMPERATURES, K

T_{pel} (centerline)	T_{pel} (surface)	T_{sheath} (inside)	T_{gap}
2231	867	591	729

3.2 Results

At first, the model free parameter $\lambda^{(radio)}$, introduced in subsection 2.3.2 to calculate hydrogen and oxygen generation rate in the rod free volume, was fitted to provide the fuel stoichiometry UO_{2+x} to the end of irradiation in agreement with experimental observations. Unfortunately, there were no direct data for FDO-681, therefore we adopted the value $x = 0.1$ on the base of estimates and available data for other fuel elements [2], [21]. The value $\lambda^{(radio)} = 5.1\times10^{-5}$ s was found to provide the target stoichiometry deviation of 0.0988. Note that this result for $\lambda^{(radio)}$ is only ~10% of the radiolysis reaction rate, consistently with the assessment obtained in [3] from other considerations. With this value of $\lambda^{(radio)}$ the escape rate parameter, calculated using Eq. (22), turned out to be $\tilde{\varepsilon} = 4.0 \times 10^{-5}$ c^{-1}. This is in a reasonable agreement with Lewis' estimates [1], obtained by fitting $\tilde{\varepsilon}$ to experimental FP releases in different CANDU fuel samples and ranged from 0.7×10^{-5} to 4×10^{-5} c^{-1}.

In MFPR, the gas diffusivity in fuel matrix is parameterized using Killeen-Turnbull correlation for the hyper-stoichiometric UO_{2+x} [28]. This leads to a strong dependence of the fission gas diffusivity on the stoichiometry deviation as demonstrated in Fig. 2. It is seen that the fission gas diffusivity increases in hyper-stoichiometric fuel by two and a half orders of magnitude to the end of irradiation in FDO-681. The large values of the FG diffusivity in fuel result in considerable gas release from the fuel grains to intergranular porosity at later stages of irradiation with the release-to-birth ratio varying from 0.3 to 0.6 for the isotopes under consideration, in a qualitative agreement with measurements in some other tests [29]. However, for a ralatively low burnup, when the open porosity channels are not yet formed, release of both stable and radioactive gas isotopes from fuel to the rod free volume is strongly suppressed, as explained in sub-section 2.3.1. Therefore, at the beginning of irradiation almost all the release is due to recoil, whereas at a later stage of irradiation, the diffusional release from the near-surface layer becomes the dominant mechanism, providing 70-80% of the total release into gap for all stable and radioactive isotopes (with except of the short-lived ^{89}Kr and ^{133}I for which diffusional and recoil mechanisms are comparable). For iodine, the release is additionally suppressed by formation of the condensed phases such as CsI so that the recoil is dominant during all irradiation campaign.

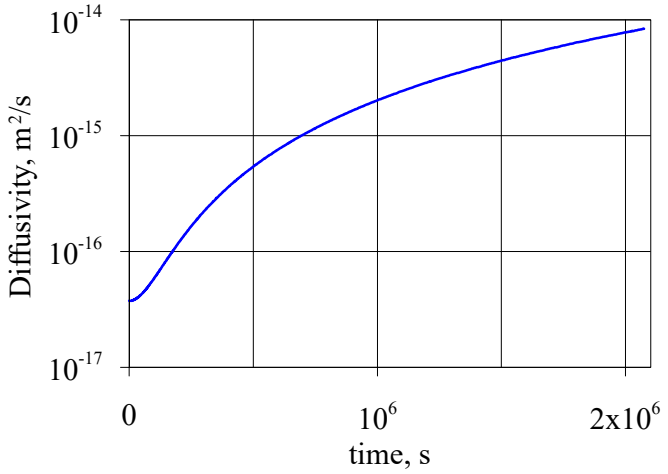

FIG. 2. Time dependence of fission gas diffusivity in UO_2 pellet center in simulation of FDO-681 under irradiation.

The calculated concentration profiles in the steady state are plotted in Fig. 3. It is seen that the concentration profiles are almost flat, slowly varying along z-axis. The concentration of mixture of stable non-condensable gases at the defect location almost coincides with the critical concentration c_0^*, Eq. (5), exceeding it by 0.02%, in agreement with quasi-stationary estimate, Eq. (20).

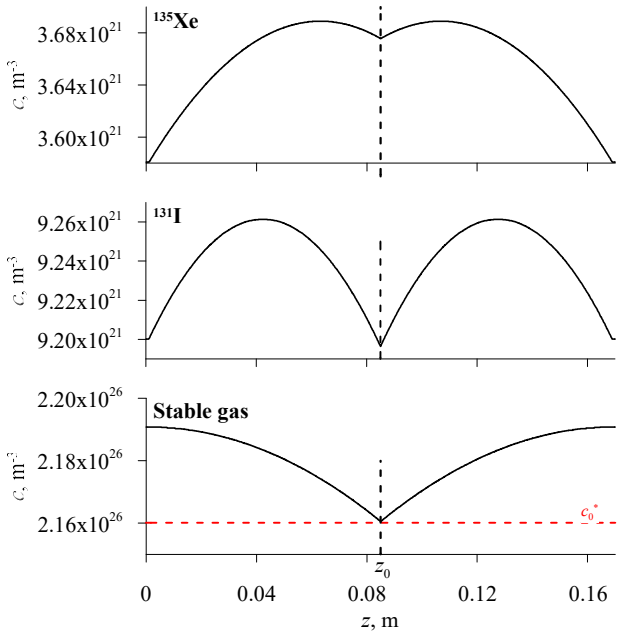

FIG. 3. Calculated concentration profiles for gas mixture and Xe-135 and I-131 in the FDO-691 to the end of irradiation; the red dotted line corresponds to the boundary concentration, Eq. (5).

The calculated release-to-birth ratios are plotted in Fig. 4 for the above listed isotopes.

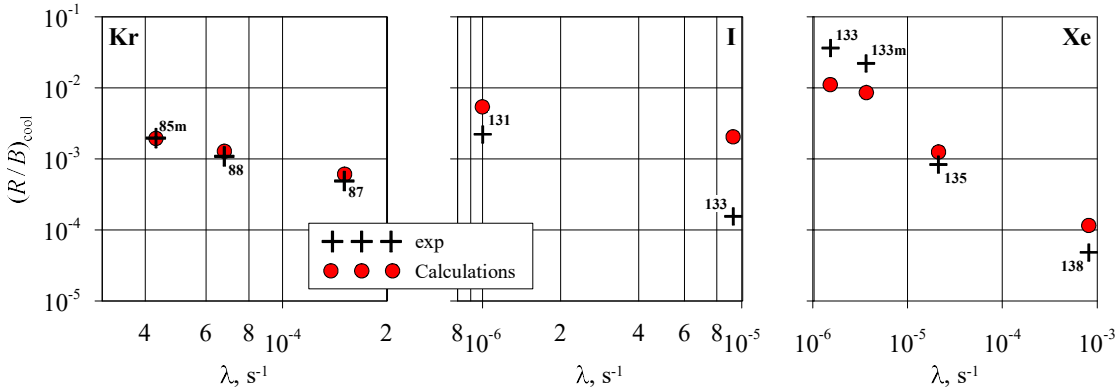

FIG. 4. Release-to-birth ratio vs decay constant.

It is seen that a reasonable agreement with measurements takes place for isotopes of the noble gases, especially for krypton. Some discrepancy takes place for xenon isotopes: underestimation by a half order of magnitude for the comparatively long-living isotopes ^{135}Xe and ^{133m}Xe and overestimation for the short-living ^{138}Xe. This leads to a slightly underestimated slope in the overall dependence of the release-to-birth ratio on the decay constant.

As for iodine, the release-to-birth ratio is overestimated for both the isotopes, especially for ^{133}I (by an order of magnitude). Following [30], this discrepancy can be somewhat reduced taking into consideration that a portion of iodine in the rod free volume deposits on the cladding surface and thus only some fraction, x_I, remains in the gas phase. Figure 5 illustrates change in $(R/B)_{\text{cool}}$ assuming that x_I = 0.2.

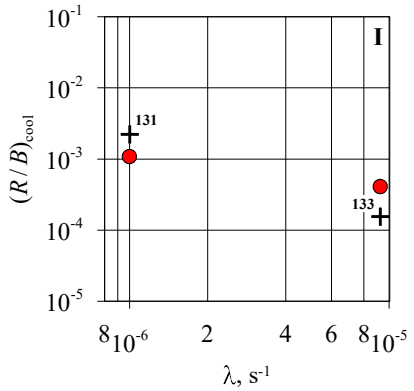

FIG. 5. Release-to-birth ratio vs decay constant for Iodine isotopes assuming $x_I = 0.2$

4. CONCLUSIONS

The advanced model for mass exchange in defected fuel rods [3] was implemented in the mechanistic fuel performance code MFPR/R to simulate release of radioactive gaseous fission products to coolant from defected fuel rods during thermal reactor operation. In this approach, hydrogen generation becomes the dominant mechanism for accumulation of stable non-condensable gases in the free volume of defected fuel element and attainment of their critical concentration, necessary for gas venting from the rod free volume to the coolant. To simulate hydrogen generation under reactor irradiation conditions, the conservative phenomenological model of steam dissociation and radiolysis from the literature [2] was used for calculation of the oxidation rate of UO_2 fuel.

The upgraded MFPR/R code was validated against the test FDO-681 under irradiation in NRX reactor at CRNL [17]. It was shown that a reasonable level of fuel stoichiometry (measured in similar experiments) is achieved by reducing the conservatism of the hydrogen generation model under the assumption that only 10% of hydrogen peroxide formed during radiolysis reacts with the fuel (due to the reverse reaction, $H_2O_2 + H_2 \rightarrow 2H_2O$, neglected in the conservative approach). On this basis, the total hydrogen production rate (due to radiolysis and fuel oxidation) was evaluated, which resulted in a reasonable prediction for the escape rate constant.

Considering the release of radioactive isotopes from a defected fuel element, it was evaluated that the main contribution to the release from the fuel into the rod free volume is made by their diffusion in the near-surface layer of the fuel pellet with a thickness comparable to the grain size. Considering the high diffusivity of gas atoms in the oxidized hyper-stoichiometric fuel, this leads to a considerable radioactive fission gas release from the fuel pellet and, consequently, its weak dependence on the isotope lifetime. Therefore, the dependence of the radioactive fission gas release into the coolant on the lifetime is almost completely determined by the transport delay in the free volume of the fuel rod. The calculated dependence of the release-to-birth ratio on the lifetime turned out to be in excellent agreement with measurements for krypton isotopes, but somewhat weaker for xenon isotopes, while for iodine isotopes the discrepancy was more significant.

To improve the results, additional studies are required, first of all, the elimination of uncertainties in the temperature and geometry of the fuel element during irradiation, a more accurate consideration of iodine deposits on the inner cladding surface, and more realistic modeling of the kinetics of fuel oxidation due to radiolysis, which are foreseen in the near future.

ACKNOWLEDGEMENTS

Mr. P. Polovnikov (IBRAE, Moscow) is acknowledged for his assistance in numerical calculations by SRIM code.

REFERENCES

[1] LEWIS, B.J., A generalized model for fission-product transport in the fuel-to-sheath gap of defective fuel elements, J. Nucl. Mater. **175** (1990) 218-226.

[2] LEWIS, B.J., MacDONALD, R.D., IVANOFF N.V., IGLESIAS F.C., Fuel performance and fission product release studies for defected fuel elements, Nucl. Technol. **103** (1993) 220-245.

[3] VESHCHUNOV, M.S., Mechanisms of fission gas release from defective fuel rods to water coolant during steady-state operation of nuclear power reactors, Nucl. Eng. Des. **343** (2019) 57-62.
[4] VESHCHUNOV, M.S., OZRIN, V.D., SHESTAK, V.E., TARASOV, V.I., DUBOURG, R., NICAISE, G., Development of the mechanistic code MFPR for modelling fission products release from irradiated UO_2 fuel. Nucl. Eng. Des. **236** (2006) 179-200.
[5] VESHCHUNOV, M.S., DUBOURG, R., OZRIN, V.D., SHESTAK, V.E., TARASOV, V.I., Mechanistic modelling of urania fuel evolution and fission product migration during irradiation and heating, J. Nucl. Mater. **362** (2007) 327.
[6] HEAMES, T.J., et al., VICTORIA: A mechanistic model of radionuclide behavior in the reactor coolant system under severe accident conditions. NUREG/CR-5545 SAND90-0756 Rev 1 R3, R4, 1992.
[7] TARASOV, V. I., Modeling the diffusion yield of radioactive fission products from uranium dioxide fuel, Atomic Energy **106** (2009) 395-408.
[8] TARASOV, V. I., VESHCHUNOV M. S., Models for fuel porosity evolution in UO_2 under various regimes of reactor operation, Nucl. Eng. Design **272** (2014) 65-83.
[9] TARASOV, V.I., POLOVNIKOV P.V., SHESTAK V.E., VESHCHUNOV M.S., Development of the MFPR/R code for characterization of the rim zone and high burnup structure evolution in UO_2 fuel pellets, J. Nucl. Mater. **517** (2019) 214-224.
[10] HOFMANN, P., et al., Report FZKA 5846, Karlsruhe, Germany, 1997.
[11] HOFMANN, P., e.a., Report FZKA 6208, INV-COBE (98)-D018, Karlsruhe, Germany, 1999.
[12] VESHCHUNOV, M.S., BOLDYREV, A.V., OZRIN, V.D., SHESTAK, V.E., TARASOV, V.I., A New Mechanistic Code SFPR for Modeling of Single Fuel Rod Performance under Various Regimes of LWR Operation, Nucl. Eng. Des. **241** (2011) 2822–2830.
[13] BOLSHOV, L.A., New generation codes for NPP safety justificationб Transactions of the 9-th International scientific and technical conference "Safety assurance of NPP with WWER", Podol'sk (Russian Federation) 19-22 May 2015.
[14] BOLSHOV, L.A., DOLGANOV, K.S., Kiselev, A.E., Strizhov, V.F., Results of SOCRAT code development, validation and applications for NPP safety assessment under severe accidents, Nucl Eng. Design **341** (2019) 326-345.
[15] BOLDYREV, A.V., Chernov, S.Yu., Dolgodvorov, A.P., Dolinsky, I.O., Ozrin, V.D., Tarasov, V.I., BERKUT – best estimate code for modelling of fast reactor fuel rod behaviour under normal and accidental conditions. In: Proc. Int. Conf. FR-17, Ekaterinburg (2017), paper IAEA-CN245-363.
[16] MOSUNOVA, N.A., Coupled calculations for the fast reactors safety justification with the EUCLID/V1 integrated computer code. In: Proc. Int. Conf. FR-17, Ekaterinburg (2017), paper IAEA-CN245-184.
[17] HASTINGS, I. J., HUNT, C. E. L., LIPSETT, J. J., Release of Short-Lived Fission Products from UO_2 Fuel: Effects of Operating Conditions, J. Nucl. Mater. **130** (1985) 407-417.
[18] DONG, B., LI C., LI L., YIN, J., WANG, D., CFD study on mechanisms of fission gas burst release from defective fuel rods of a typical PWR, Annals of Nuclear Energy **140** (2020): 107089.
[19] POLING, B.E., PRAUSNITZ, J.M., J'CONNELL, The properties of gases and liquids, 5-th edition, McGRAW-HILL, New York (1976).
[20] OLANDER, D.H., Fundamental Aspects of Nuclear Reactor Fuel Elements. Technical Information Center, Office of Public Affairs Energy Research and Development Administration, 1976.
[21] LEWIS, B.J., Fission product release from nuclear fuel by recoil and knockout, J. Nucl. Mater. **148** (1987) 28–42.
[22] DOBROV, B.V., LIKHANSKII, V.V., OZRIN, V.D., SOLODOV, A.A., KISSANE, M.P., MANENC, H., Kinetics of UO_2 oxidation in steam atmosphere, J. Nucl. Mater. **255** (1998) 59.
[23] MARKOWITZ, J.M., Internal zirconium hydride formation in zircaloy fuel element cladding under irradiation, WAPD-TM-351, Bettis Atomic Power Laboratory (May 1963).
[24] LEWIS, B.J., Fundamental aspects of defective nuclear fuel behaviour and fission product release. J. Nucl. Mater **160** (1988) 201-217.
[25] LEWIS, B.J., Fuel oxidation and thermal conductivity model for operating defective fuel rods. J. Nucl. Mater. **306** (2002) 30-43.
[26] LEWIS, B.J., PHILLIPS, C.R., NOTLEY, M.J.F., A model for the release of radioactive krypton, xenon, and iodine from defective UO_2 fuel elements. Nucl. Technol. **73** (1986) 72-83.
[27] LEWIS, B.J., GREEN, R.J., CHE, W.T., A Prototype Expert System for the Monitoring of Defected Nuclear Fuel Elements in Canada Deuterium Uranium Reactors, Nucl. Technol. **98** (1992) 307-321.
[28] KILLEEN, J. C., TURNBULL J. A., An experimental and theoretical treatment of the release of from hyperstoichiometric uranium dioxide, Proc. Workshop Chemical Reactivity of Oxide Fuel and Fission Product Release, Gloucestershire, England, April 7-9, 1987, p. 387.

[29] UNE, K., AMAYA, M., IMAMURA, M., KOREI Y., Fission gas release from defective BWR fuels, J. Nucl. Mater. **226** (1995) 323-326.
[30] BESLU, P., LEUTHROT, C., FREJAVILLE, G., PROFIP CODE: A model to evaluate the release of fission product from a defected fuel in PWR specialists meeting "The behaviour of defected zirconium alloy clad ceramic fuel in water cooled reactors", Chalk River Nuclear Laboratories, Chalk River, Canada, 17-21 September 1979, p.23-28.

LIST OF ABBREVIATIONS

CANDU	CANada Deuterium Uranium (Canadian pressurized heavy-water reactor)
FA	Fuel Assembly
IAEA	IAEA Coordinated Research Project (CRP) on Fuel Modelling in Accident Conditions
FUMAC	
INPO	Institute of Nuclear Power Operations
MTR	Material Test Reactor
NEA	NucleaR Energy Agency
NPP	Nuclear Power Plant
OE	Operational Excellence
OECD	Organisation for Economic Co-operation and Development
PCI	Pellet-Cladding Interaction
RCCA	Rod Cluster Control Assembly
WANO	World Association of Nuclear Operators
WWER	Water-cooled Water-moderated Power Reactor (Russian pressurised light water reactor)

LIST OF PARTICIPANTS

Amer, H.	Egyptian Nuclear Radiological Regulatory Authority (ENRRA) 3 Ahmed El-Zomor Street, PO Box 7551, Nasr City, Cairo, Egypt Email: Hanyamer11@gmail.com
An Na	Hainan Nuclear Power Co., Ltd. Hainan Chanjiang Nuclear Power Plant Hainan Province, Changjiang, China Email: anna@cnnp.com.cn
Arimescu, V.I.	Framatome Inc. Richland, Wa 99354 United States of America Email: ioan.arimescu@framatome.com
Arsenina, O.	National Nuclear Energy Generating Company (Energoatom) 3, Nazarivska Str., 01032, Kyiv, Ukraine Email: e.arsenina@direkcy.atom.gov.ua; arsenina@direkcy.atom.gov.ua
Ayati, S.F.	Atomic Energy Organzaton of Iran End of North Kargar Ave, P.O. Box: 14155-1339, Teheran, Iran Email: fayati@aeoi.org.ir
Bednarova, A.	State Office for Nuclear Safety (SÚJB) Senovazne namesti 9, Prague 1, Czech Republic Email: alzbeta.bednarova@sujb.cz
Carling, K.	Ringhals NPP, Ringhals AB SE-43285 Väröbacka, Sweden Email: karin.carling@vattenfall.com
Da Silva Lapa, N.	Brazilian National Nuclear Energy Commission (CNEN) Rua Gal. Severiano, nº 90/418, CEP 22290-901, Rio de Janeiro, Brazil Email: nlapa@cnen.gov.br
Dethioux, A.	Tractebel Engie S.A. Boulevard Simon Bolivar 34-36, 1000 Brussels, Belgium Email: adrien.dethioux@tractebel.engie.com

Elhefnawy, A.H.M.E.	Egyptian Atomic Energy Authority Madinat Nasr, Cairo, Egypt Email: Ahmed.helmy.elhefnawy@gmail.com
Ernst, D.	Temelín Nuclear Power Plant 1-2; CEZ, a. s. 373 05 Temelín, Czech Republic Email: daniel.ernst@cez.cz
Evdokimov, I.A.	SRC RF TRINITI ul. Pushkovykh, vladenie 12, 108840 Moscow Region, Troitsk, Russian Federation Email: evdokimov@triniti.ru
Faragalla, M.M.M.	Nuclear Power Plants Authority El-Nasr Avenue, Nasr City, P.O. Box 8191, 11371 Cairo, Egypt Email: faragallah.mohamed@yahoo.com
Faulkner, C.	Institute of Nuclear Power Operations Suite 100, 700 Galleria Parkway, SE, Atlanta, GA United States of America Email: faulknercs@inpo.org
Fu, P.	China Nuclear Power Technology Research Institute Co., Ltd. 27/F Science and Technology Building, No. 1001, Shangbuzhong Rd, Shenzhen, China Email: fupengtao@cgnpc.com.cn
Girchenko, A.	National Research Center "Kurchatov Institute" 1, Akademika Kurchatova Pl., Moscow, Russian Federation Email: Girchenko_AA@NRCKI.ru
Godun, O.	National Nuclear Energy Generating Company (Energoatom), Subdivision "Scientific and Technical Centre" Hoholevska str. 22-24, 1109 office, 01601 Kyiv, Ukraine Email: o.godun@ntc.atom.gov.ua
Grant, W.A.	Canadian Nuclear Safety Commission 280 Slater St, P.O. Box 1046, Station B Ottawa, OK, K1P 5S9, Canada Email: Wade.Grant@Canada.ca
Gusev, A.	TVEL JSC 49, Kashirskoe shosse Moscow, Russian Federation Email: AleStGusev@tvel.ru
Hao, T.	Sanmen Nuclear Power Co., Ltd. Sanmen County, Zhejiang, China Email: haotf@cnnp.com.cn

Jacquemain, D.	Nuclear Energy Agency 46, quai Alphone Le Gallo, 92100 Boulogne-Billancourt, France Email: didier.jacquemain@oecd-nea.org
Kalinichev, P.	SRC RF TRINITI ul. Pushkovykh, vladenie 12, 108840 Moscow Region, Troitsk, Russian Federation Email: kalinichev@triniti.ru
Kang, C.	Nuclear Power Institute of China No. 328, Changshun Avenue, Sichuan Province, Chengdu City, China Email: 766718286@qq.com
Lewis, B.	Royal Military College of Canada, Department of Chemistry and Chemical Engineering PO Box 17000, Kingston, ON K7K 7B4 Email: lewibre@gmail.com
Lewis, R.	Bruce Power 123 Front Street, Ontario, M5J 2M2, Canada Email: ross.lewis@brucepower.com
Li, C.	Nuclear Power Technology Research Institute Co., Ltd. Room 2202, Shenzhen Science Technology Building, No. 1101, Shangbu middle Road, Futian District, Shenzhen China Email: lichangzheng@cgnpc.com.cn
Lu, Z.	China Nuclear Power Technology Research Institute Co., Ltd. Room 1605, Science and Technologgy Building, No. 001, Shankbuzhong Road, Futian District, Guangdong Province, Shenzhen, China Email: 240503622@qq.com
Ma, Y.	Fujian Fuqing Nuclear Power Co., Ltd. Qianxue village, Fuqing City, China Email: fqhd-wjsf@cnnp.com.cn; mayc@cnnp.com.cn
Mecir, V.	Temelín Nuclear Power Plant 1-2; CEZ, a. s. 373 05 Temelín, Czech Republic Email: vaclav.mecir@cez.cz
Moatti, M.	EDF DCN Cap Ampère, 1 Place Pleyel, 93282 Saint-Denis Cedex, France Email: marie.moatti@edf.fr

Nemec, T.	Slovenian Nuclear Safety Administration (SNSA) Litostrojska cesta 54, 1000 Ljubljana, Slovenia Email: tomaz.nemec@gov.si
Pasandi, A.	Atomic Energy Organizaton of Iran, TAMAS CO., Chamran Building, 24rd Street, Kargar Shomali, Tehran, Iran Email: pasandi55@gmail.com
Perez, E.	French Nuclear Safety Authority (ASN) 15 rue Louis Lejeune, 92129 Montrouge Cedex, France Email: etienne.perez@asn.fr
Raindl, J.	ČEZ, a. s. - NPP Temelín 37305 Temelín, Czech Republic Email: jakub.raindl@cez.cz
Saqib, A.	Directorate of Nuclear Power Engineering - Reactor (DNPER), PAEC N-Block, PAEC HQ, P.O. Box 3140, Islamabad, Pakistan Email: Ahsaan_222@yahoo.com
Secor, M.	Canadian Nuclear Safety Commission 280 Slater Street, P.O. Box 1046, Station B, Ottawa, ON, K1P 5S9, Canada Email: marcus.secor@canada.ca
Sorokin, A.	SRC RF TRINITI ul. Pushkovykh, vladenie 12, 108840 Moscow Region, Troitsk, Russian Federation Email: Sorokin@triniti.ru
Tarasov, V.	Nuclear Safety Institute of the Russian Academy of Sciences (IBRAE RAN) Bolshaya Tulskaya 52, 115191 Moscow, Russian Federation Email: tarasov@ibrae.ac.ru
Vardanyan, V.	Haykakan Atomayin Electrakayan CJSC Armenian Nuclear Power Plant Metsamor 0910, Armavir Marz, Yerevan, Armenia Email: vrdn_vardanyan@yahoo.com
Veshchunov, M.	International Atomic Energy Agency (IAEA) Vienna International Centre (VIC), PO Box 100, 1400 Vienna, Austria Email: m.veshchunov@iaea.org
Vilkhivskaya, O.	SRC RF TRINITI ul. Pushkovykh, vladenie 12, 108840 Moscow Region, Troitsk, Russian Federation Email: vilkhiv@triniti.ru
Waeckel, N.	105 Rte de St Fortunat 69450 St Cyr Au Mont Dor, France Email: nicolas@waeckel.fr

Wolter dos Reis Nery, R.

ELETROBRAS TERMONUCLEAR SA - ELETRONUCLEAR
Rua Candelária 65 - 7th Floor, CEP 20091-906, Rio de Janeiro, Brazil
Email: wolter@eletronuclear.gov.br

Zareidoost, A.

Atomic Energy Organization of Iran
Public Relations Department
North Kargar Street, Tehran 14155-1339, Iran
Email: azareidoost@aeoi.org.ir

CONTRIBUTORS TO DRAFTING AND REVIEW

Arimescu, V.I.	Framatome Inc., United States of America
Evdokimov, I.A.	SRC RF TRINITI, Russian Federation
Lewis, R.	Bruce Power, Canada
Waeckel, N	EDF, France
Veshchunov, M.	International Atomic Energy Agency

Technical Meeting

Vienna, Austria: 14–18 December 2020

Consultancy Meeting

Vienna, Austria: 13 – 14 April 2021

IAEA
International Atomic Energy Agency

No. 26

ORDERING LOCALLY

IAEA priced publications may be purchased from the sources listed below or from major local booksellers.

Orders for unpriced publications should be made directly to the IAEA. The contact details are given at the end of this list.

NORTH AMERICA

Bernan / Rowman & Littlefield

15250 NBN Way, Blue Ridge Summit, PA 17214, USA
Telephone: +1 800 462 6420 • Fax: +1 800 338 4550

Email: orders@rowman.com • Web site: www.rowman.com/bernan

REST OF WORLD

Please contact your preferred local supplier, or our lead distributor:

Eurospan Group

Gray's Inn House
127 Clerkenwell Road
London EC1R 5DB
United Kingdom

Trade orders and enquiries:

Telephone: +44 (0)176 760 4972 • Fax: +44 (0)176 760 1640
Email: eurospan@turpin-distribution.com

Individual orders:

www.eurospanbookstore.com/iaea

For further information:

Telephone: +44 (0)207 240 0856 • Fax: +44 (0)207 379 0609
Email: info@eurospangroup.com • Web site: www.eurospangroup.com

Orders for both priced and unpriced publications may be addressed directly to:

Marketing and Sales Unit
International Atomic Energy Agency
Vienna International Centre, PO Box 100, 1400 Vienna, Austria
Telephone: +43 1 2600 22529 or 22530 • Fax: +43 1 26007 22529
Email: sales.publications@iaea.org • Web site: www.iaea.org/publications

22-02653E

International Atomic Energy Agency
Vienna